doi: 10.3289/geomar_rep_72_1998

FS SONNE
FAHRTBERICHT SO131
CRUISE REPORT SO131
SINUS

SEISMIC INVESTIGATIONS AT THE NINETY EAST RIDGE OBSERVATORY USING SONNE AND JOIDES RESOLUTION DURING ODP LEG 179

KARACHI - SINGAPORE
04.05. - 16.06.1998

Edited by
Ernst R. Flueh and Christian Reichert
with contributions of cruise participants

GEOMAR
Forschungszentrum
für marine Geowissenschaften
der Christian-Albrechts-Universität
zu Kiel

Kiel 1998

GEOMAR REPORT 72

GEOMAR
Research Center
for Marine Geosciences
Christian Albrechts University
in Kiel

Redaktion dieses Reports:	Ernst R. Flüh and Christian Reichert	Editors of this issue:	Ernst R. Flüh and Christian Reichert
Umschlag:	GEOMAR Technologie GmbH	Cover:	GEOMAR Technologie GmbH

GEOMAR REPORT
ISSN 0936 - 5788

GEOMAR REPORT
ISSN 0936 - 5788

GEOMAR
Forschungszentrum
für marine Geowissenschaften
D-24148 Kiel
Wischhofstr. 1-3
Telefon (0431) 600-2555, 600-2505

GEOMAR
Research Center
for Marine Geosciences
D-24148 Kiel / Germany
Wischhofstr. 1-3
Telephone (49) 431 / 600-2555, 600-2505

TABLE OF CONTENT

1.1 SUMMARY

SONNE cruise SO-131 (SINUS = Seismic Investigations at the Ninetyeast Ridge Observatory using SONNE and JOIDES RESOLUTION) was originally conceived as a two-ship experiment combining basic research to study the structure and composition of the Ninetyeast Ridge and the adjacent oceanic basins, as well as conducting a high resolution quasi-3D survey providing necessary information for an effective and reliable operation of the future oceanic seismological obseratory at ODP site 1107. A number of different geophysical methods and acquisition arrangements were employed for this approach.

Misguided freight for JOIDES RESOLUTION and adverse weather conditions disabled coincident two-ship operations due to severe time delays in the JOIDES RESOLUTION schedule. Accordingly, slight changes in the scientific programme of SONNE were made providing some compensation by deploying two Ocean Bottom Hydrophones (OBHs) in very close position to the ODP site 1107 before conducting two circular profiles with 2 and 6 nm radius around the ODP site.

A total of 1,360 nm (2,520 km) of profile length were acquired with seismic refraction/wide-angle and seismic reflection methods including the deployment and successful recovery of 108 OBH and OBS (Ocean Bottom Seismometer) stations and the use of a 3-channel seismic mini-streamer. Along these lines as well as along additional some 700 nm (1,300 km) of hydroacoustic and magnetic data were collected, providing about 3800 km of magnetic total field measurements. The kernel was a network of profiles in an area approximately 30 nm by 60 nm per side around the ODP site and a roughly 330 nm long E-W running traverse through its center. Along all profiles bathymetry data with HYDROSWEEP multiple beam sonar and sediment echography data (4.0 Khz PARASOUND) were acquired. After completion of the work in the main target area an adjacent region over the Ninetyeast Fracture Zone in the east was bathymetrically surveyed.

Three piggy-back experiments were included: First, the test of a new seismic energy source deployed at the sea floor making use of imploding glass spheres. All five spheres that were deployed successfully imploded and the seismic signals were clearly detected. This test was enabled by JOIDES RESOLUTION who kindly supplied the required dynamite caps. Second, a new 1200 m long vertical array of hydrophones was deployed for the first time. Third, a small array consisting of 4 VLF airguns with a total volume of 3.2 ltr. was tested.

Despite the disadvantageous weather conditions with strong winds predominantly around 12 m/s and periods of more than 18 m/s and high sea state, average to fair data quality was achieved throughout the entire survey, and no accidents occurred. The quasi-3D profile network alone yielded some 220,000 seismic traces. Theoretical binning models calculated in advance enabled an optimal arrangement of ocean bottom instruments and profile locations leading to a more or less well balanced coverage in the most important area giving values of up to 60-fold.

A portion of the tremendous total data set was processed to an advanced stage during the cruise. Along major profiles ray-tracing models were calculated. One of the first results is that the oceanic crust with usual thicknesses around 7 — 8 km in the adjacent deep sea basins thickens significantly beneath the Ninetyeast Ridge to about 25 km. Upper crustal velocities seem to be reduced compared to the adjacent basins, and rather high middle and lower crustal velocities are encountered. A rather prominent sub-Moho reflection, associated with a velocity increase from about 8.2 to 8.5 km/s, is found at a depth of approximately 35 km below the Ninetyeast Ridge. This interface can be followed on both sides to depths of about 20 km.

While the Ninetyeast Ridge is gently dipping to the west into the Indian Ocean Basin, it has a remarkably steep escarpment of more than 2.500 m to the east. Here the adjacent seafloor of the Wharton Basin shows a prominent deformation pattern, suggesting substantial strike slip movement and possible transfer of crustal material away from the Ninetyeast Ridge into the basin. This may also explain the slightly thickend crust here. The top of the Ninetyeast Ridge is rather smooth, but several

small seamounts were found. Two of them were investigated in detail and tentatively called Monte Sinus and Monte Cosinus. They seem to be remnants of the latest active volcano chimneys, that were more resistant to coastal erosion when the ridge subsided below sealevel.

Preliminary seismic modelling of the data collected across the Ninetyeast Fracture Zone shows a prominent crustal thickening. This thickening is mainly to accomodate the addition of low velocity upper crustal material.

The 3-channel seismic reflection data show in great detail the layered sedimentary cover which is a few hundred meters thick. The top of the basement is clearly imaged as well. The oceanic crust thereunder or the volcanic extrusions show only sparse and weak reflections respectively. The Moho could not be detected at zero offset, although it is recognized in the wide-angle/refraction data as a prominent reflection at nearly all stations.

The magnetic data, though recorded by a single magnetometer without corrections regarding diurnal variation, show only slight differences of a few nT compared to double recorded profiles and close parallel lines. Thus, corrections derived from the manifold crossings are believed to produce reliable values.

The SINUS project was conducted in co-operation by GEOMAR, BGR, WHOI and IFG-Hamburg. It was funded by the German Federal Ministry of Education, Science, Research and Technology.

1.2 Zusammenfassung

Die SONNE-Fahrt SO-131 (SINUS = Seismic Investigations at the Ninety East Ridge Observatory using SONNE and JOIDES RESOLUTION) war ursprünglich als Zweischiffs-Experiment konzipiert, um sowohl Struktur und Aufbau des Ninetyeast Ridge (NER) und der benachbarten ozeanischen Becken zu untersuchen als auch um eine hochauflösende quasi-3D Studie durchzuführen. Letztere hat eine große Bedeutung für den effektiven und erfolgreichen Betrieb des zukünftigen ozeanischen seismologischen Observatoriums an der ODP-Site 1107. Eine Reihe verschiedener geophysikalischer Methoden und Aufnahmeverfahren wurde eingesetzt, um diese Ziele zu erreichen.

Fehlgeleitete Fracht für das ODP-Bohrschiff JOIDES RESOLUTION und widrige Wetterbedingungen verhinderten die Durchführung simultaner Zweischiffsarbeiten durch schwerwiegende Verzögerungen im Zeitplan der JOIDES RESOLUTION. Dementsprechend wurden Änderungen im Programm von FS SONNE vorgenommen, die eine gewisse Kompensation durch das Absetzen von zwei Ozeanboden-Hydrophonen (OBHs) sehr nahe bei ODP-Site 1107 und die anschließende Durchführung von zwei Kreisprofilen mit 2 bzw. 6 sm Radius um die ODP-Site ermöglichten.

Insgesamt wurden 1.360 sm (2.520 km) Profillänge refraktions- und reflexionsseismisch vermessen, wobei 108 OBH- und OBS- (Ozeanbodenseismometer-) Stationen erfolgreich besetzt und abgeborgen wurden, sowie ein Dreikanal-Ministreamer zum Einsatz kam. Längs dieser Strecke sowie weiteren etwa 700 sm (1.300 km) Profillänge wurde das magnetische Anomalienfeld vermessen. Den Kern der Arbeiten stellten ein Netzwerk von Profilen auf einer etwa Fläche von ca. 30 x 60 sm im Quadrat um die ODP-Site und eine etwa 330 sm lange Ost-West-Traverse durch deren Zentrum dar. Längs aller Profile wurden bathymetrische Messungen mit dem HYDROSWEEP-Fächerecholot und sedimentechographische Aufnahmen mit dem PARASOUND-System (3,5 Khz) durchgeführt. Nach Beendigung der Arbeiten im Hauptuntersuchungsgebiet wurde eine östlich benachbarte Fläche über die Ninetyeast-Bruchzone bathymetrisch vermessen.

Drei Nebenexperimente wurden durchgeführt: Erstens der Test einer neuartigen seismischen Energiequelle, die auf dem Meeresboden abgesetzt wird und die Schallwellen implodierender Glaskugeln ausnutzt. Alle fünf Glaskugeln implodierten wie geplant, und die ausgesandten seismischen Signale konnten klar erkannt werden. Dieser Test wurde durch die Unterstützung der JOIDES RESOLUTION

ermöglicht, die die benötigten Sprengzünder zur Verfügung stellte. Zweitens wurde zum ersten Mal ein 1.200 m langes Hydrophon-Vertikalarray eingesetzt. Drittens wurde ein ein kleines Array mit 4 VLF-Luftpulsern mit einem Gesamtvolumen von 3,2 l erprobt.

Trotz der ungünstigen Wetterbedingungen mit vorherrschendem Starkwind von 12 m/s und stürmischen Perioden von mehr als 18 m/s sowie starkem Seegang wurde eine mittlere bis gute Datenqualität während der gesamten Messungen erzielt. Es traten keine Unfälle auf. Mit dem quasi-3D Profilnetzwerk wurden etwa 220.000 seismische Spuren gewonnen. Theoretische Überdechungsberechnungen, die vorher erarbeitet worden waren, ermöglichten eine optimale Anordnung der Ozeanbodeninstrumente und der Profilführung, wodurch eine mehr oder weniger ausgeglichene Überdeckung mit Werten bis zu 60-fach im wichtigsten Teilgebiet erreicht wurde.

Ein Teil des riesigen Gesamtdatensatzes wurde bereits an Bord bis zu einem weit fortgeschrittenen Stadium bearbeitet. Längs der bedeutenderen Profile wurden Strahlenmodelle berechnet. Eines der ersten Resultate ist, daß sich die ozeanische Kruste von üblichen Mächtigkeiten um 7 bis 8 km in den benachbarten Tiefseebecken auf bis zu etwa 25 km Mächtigkeit unter dem Ninetyeast Ridge verdickt. Die Geschwindigkeiten der Oberkruste scheinen im Vergleich zu den benachbarten Becken verringerte Geschwindigkeiten aufzuweisen, und ziemlich hohe Geschwindigkeiten werden in der mittleren und unteren Kruste angetroffen. Eine recht auffällige Reflexion unterhalb der Moho, verbunden mit einem Geschwindigkeitsanstieg von etwa 8,2 auf 8,5 km/s wurde in einer Tiefe von ungefähr 35 km unter dem Ninetyeast Ridge festgestellt. Diese Grenzfläche kann nach beiden Seiten hin bis in Tiefenbereiche um 20 km verfolgt werden.

Während der Ninetyeast Ridge nach Westen sanft zum Indischen Ozeanbecken hin einfällt, weist er im Osten eine bemerkenswert steile Abbruchkante mit mehr als 2.500 m Versatz auf. An dieser Stelle zeigt der benachbarte Meeresboden des Wharton-Beckens ein auffälliges Verformungsmuster, das auf bedeutende Scherbewegungen und einen möglichen Transfer von Krustenmaterial weg vom Ninetyeast Ridge in das Becken hinweist. Dies könnte auch die verdickte Kruste an dieser Stelle erklären. Die Oberfläche des Ninetyeast Ridge ist ziemlich glatt, es wurden jedoch einige kleine Meeresbodenkuppen gefunden. Zwei von ihnen wurden im Detail untersucht und vorläufig Monte Sinus und Monte Cosinus benannt. Es scheint sich um Reste spät-aktiver Vulkanschlote zu handeln, die der Küstenerosion mehr Widerstand entgegensetzten, als der Ridge unter den Meeresspiegel versenkt wurde.

Erste seismische Modellierungen der Daten von der Ninetyeast-Bruchzone zeigen eine deutliche Krustenverdickung. Sie wird hauptsächlich erzeugt durch zusätzliches Material mit geringerer Geschwindigkeit in der Oberkruste.

Die seismischen Dreikanal-Reflexionsdaten stellen die geschichtete sedimentäre Bedeckung von ein paar hundert Metern mit großer Auflösung dar. Die Oberkante des Basements wird ebenfalls gut abgebildet. Die ozeanische Kruste darunter, bzw. die vulkanischen Extrusiva zeigen nur wenige und schwache Reflexionen. Die Moho konnte in den Steilwinkeldaten nicht erkannt werden, obwohl sie bei fast allen weitwinkel-/refraktionsseismischen Stationen als deutliche Reflexion hervortritt.

Die Magnetik-Daten, obwohl sie mit einem Einzelmagnetometer aufgenommen und hinsichtlich der täglichen Variation nicht korrigiert wurden, zeigen beim Vergleich doppelt vermessener Profile oder engabständiger Parallelprofile nur geringe Unterschiede von wenigen nT. Deshalb dürften mit Korrekturen, die aus den vielzähligen Profilkreuzungen abgeleitet werden können, zuverlässige Daten erzeugt werden können.

Das SINUS-Projekt wurde in Kooperation von GEOMAR, BGR, WHOI und IFG-Hamburg durchgeführt. Es wurde vom Bundesministerium für Bildung, Wissenschaft, Forschung und Technologie finanziert.

2. Introduction

(E. Flueh, C. Reichert, I. Grevemeyer, M. Perez)

The Ninetyeast Ridge was chosen by the international scientific community for the installation of the first seismic International Ocean Network (ION) station, known as NERO (Ninety East Ridge Observatory). The borehole to be drilled during ODP Leg 179 will be instrumented on a later re-entry cruise with broadband seismometers to monitor teleseismic earthquakes. The schedule for both the JOIDES RESOLUTION and the R/V SONNE made it possible to meet at NERO and conduct an Offset Seismic Experiment (OSE) using a borehole seismometer. The main objective of Cruise SO131 is to investigate the local and regional crustal structure around NERO.
The Ninetyeast Ridge was first recognized by Sewell (1925) and further charted by Stocks (1960). It was named by Heezen and Tharp (1965) for it´s position close to the 90°E meridian. The bathymetry of the Indian Ocean is, based on gravity derived predictions and the GEBCO charts (Smith and Sandwell, 1997) shown in Figure 2.1., with all geographical names used.
Early interpretations suggested the Ninetyeast Ridge to be a horst structure resulting from compression initiated by relative motion between the Australian and Indian plates (Francis and Raitt, 1967; Le Pichon and Heirtzler, 1968). Sclater and Fisher (1974) interpreted the ridge as extrusive lavas along a leaky transform fault. It is now generally accepted as a hotspot trace connecting the Rajmahal trap basalts from India and Bangladesh to the Kerguelen Hotspot. The Rajmahal traps represent the 117 m.a. plume head (e.g. Morgan, 1981; Duncan, 1991; Kent et al., 1997). The northward motion of the Indian plate can be reconstructed through the age progression of lavas along the Ninetyeast Ridge as the hotspot track.

2.1 Plate Tectonic Framework of the Indian Ocean

Since Eocene times the generation of oceanic crust in the Indian ocean eastwards of the Rodriguez triple junction occurs along the Southeast Indian Ridge. Beside this spreading axis major structural features of that part of the Indian Ocean are the Ninetyeast Ridge, and the Broken Ridge northwards of the spreading centre, and the Kerguelen Plateau to the south. These features are thought to be created by a single hotspot since India, Australia, and Antarctica broke apart in the Cretaceous around 117 m.a. (e.g. Peirce, 1978; Morgan, 1981; Duncan, 1981; 1991; Royer et al., 1991).

The Ninetyeast Ridge is a major aseismic ridge that can be traced for about 5000 km from latitude 30°S northward into the Bay of Bengal, where it is buried beneath the Bengal Fan. This remarkably linear and nearly meridional ridge varies in width from 100 to 200 km and is elevated about 2 km compared to the Central Indian Basin to the West and the Wharton Basin to the East. Sclater and Fisher (1974) divided Ninetyeast Ridge into three major domains. North of 5°S the ridge is wide and formed by discontinuous blocks; south of 5°S to Osborne Knoll near 14.5° S the ridge becomes narrow, linear, and continuous, and south of Osborne Knoll it becomes significantly wider and less linear. In total, the volume of magmatic products of Ninetyeast Ridge is estimated to be about 24 x 10^6 km^3 (Schubert and Sandwell, 1989) which corresponds to an average magmatic output rate of about 1.5 km^3/yr over the last 40 m.a.

Paleontological, paleomagnetic, and radiometric analysis of rock samples from DSDP legs 22 and 26 and ODP leg 121 indicate that the basement ages become older in the northward direction from approximately 38 m.a. at DSDP site 254 near the southern terminus of the ridge to 80-82 m.a. at the most northerly ODP site 758 (Royer et al., 1991; Duncan, 1991; Peirce, 1978). The general northerly increase in age relates the Ninetyeast Ridge and the 117 m.a. Rajmahal traps onshore eastern

India / Bangladesh to a long-lived hotspot that progressively built Rajmahal traps and Ninetyeast Ridge on the Indian plate as the plate drifted northwards (e.g. Luyendyk and Rennick, 1977; Morgan, 1981; Duncan, 1981; 1991; Royer et al., 1991; Kent et al., 1997). Basement paleolatitudes from most DSDP and ODP sites provided evidence that the hotspot plume remained at a constant paleolatitude near 50°S, the present location of the Kerguelen hotspot, beneath the Kerguelen archipelago (Royer et al., 1991; Peirce, 1978). Indeed, in terms of isotopic analysis of volcanic rocks the most likely hotspot that created the ridge is the Kerguelen plume, however, the basalts do not represent a simple mixing of a Kerguelen plume and Southeast Indian Ridge mantle (Saunders et al., 1991; Weis and Frey, 1991). Therefore, mantle processes forming Ninetyeast Ridge are not fully understood. A third component, the St. Paul hotspot, may explain the genesis of Ninetyeast Ridge lavas, especially those erupted on the southern portion of the ridge (Weis and Frey, 1991). Nevertheless, the 50°S paleolatitude of the mantle plume clearly indicates that the ridge was attached to the Indian plate which has drifted rapidly northwards since the Late Cretaceous.

A line of evidence suggests that at least the southern part of Ninetyeast Ridge resulted from excess volcanism on the edge of the Indian plate. A small-amplitude gravity anomaly over the ridge implies a locally compensated structure (Bowin, 1973), suggesting that the ridge was emplaced in a near or on-axis environment. This issue is clearly supported by geochemical and isotopic studies of basalts drilled at the Ninetyeast Ridge. The tholeiitic, iron-rich, and voluminous character of basalts is typical of oceanic islands associated with hotspots on or near mid-ocean ridges (Saunders et al., 1991). These observations are consistent with marine magnetic data which show that the ridge and the lithosphere of the adjacent Central Indian Basin are approximately contemporaneous (Royer et al., 1991). However, to keep the Southeast Indian Ridge in the vicinity of the hotspot several southward ridge jumps must have occured (Royer and Sandwell, 1989; Royer et al., 1991). Consequently, parts of the mirror images of Ninetyeast Ridge on the Antarctic plate were transfered on the Indian plate, representing parts of the middle portion of Ninetyeast Ridge between 2.5°S to 15°S (Royer et al., 1991). Nevertheless, the paleolatitude of the mantle plume and its location relative to the spreading axis indicate that the Southeast Indian Ridge has migrated northwards since the Late Eocene. In Figure 2.1.1 plate tectonic reconstructions after Kent et al. (1997) are shown and the known identified magnetic anomalies are seen in Figure 2.1.2 (Royer et al., 1991).

In the Wharton Basin, eastwards of Ninetyeast Ridge, Lui et al. (1983) and Geller et al. (1983) identified an abandoned spreading centre that became extinct in the middle Eocene when the Southeast Indian Ridge separated Kerguelen Plateau from Broken Ridge (Royer and Sandwell, 1989). A set of nearly meridional fracture zones devided the fossil ridge into distinct segments. These fracture zones are clearly recognized in both bathymetric and magnetic data. One of them is following the 90°E meridian and therefore named the Ninetyeast Fracture Zone. The occurence of symmetric sets of spreading anomalies suggests that the northern Wharton Basin was part of the Indian plate, while the southern part belonged to the Australian plate. Northwards of 5°S, magnetic data indicated that the Ninetyeast Ridge is slightly oblique relative to the fracture zone pattern, suggesting that the northern ridge may have formed in an intraplate setting (Royer et al., 1991). Plate tectonic reconstructions of Royer and Sandwell (1989) show that while the Southeast Indian Ridge jumped southwards the Wharton Basin spreading ridge migrated northwards. Thus, a new fracture zone bounding the Ninetyeast Ridge was established in the Early Tertiary at 88.5°E extending from ~12°S to Broken Ridge. Consistently, the voluminous southern part of the ridge was emplaced along a transform plate boundary.

In terms of the interpretations of Royer et al. (1991) summarized above, the three distinct structural domains defined by Sclater and Fisher (1974) are controlled by

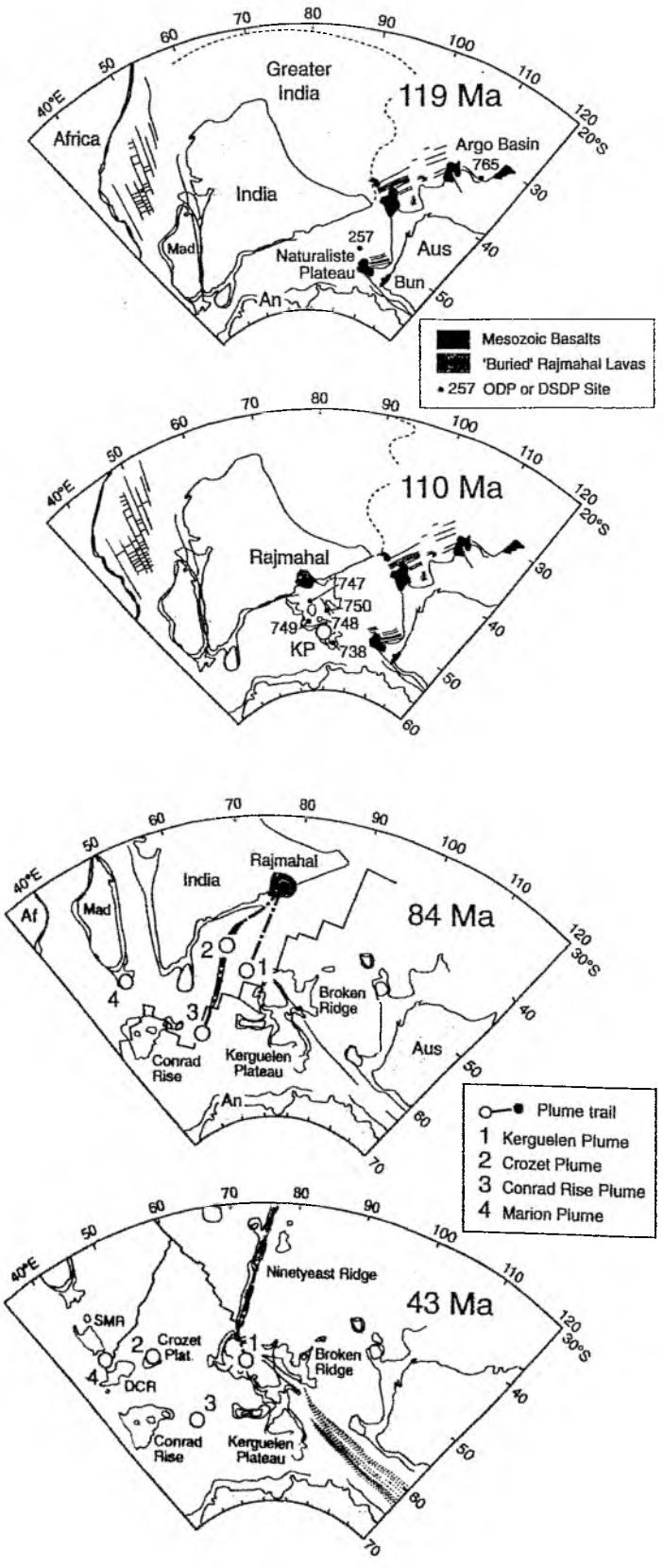

Figure 2.1.1: Plate tectonic reconstruction of the Indian Ocean (Kent et al., 1997).

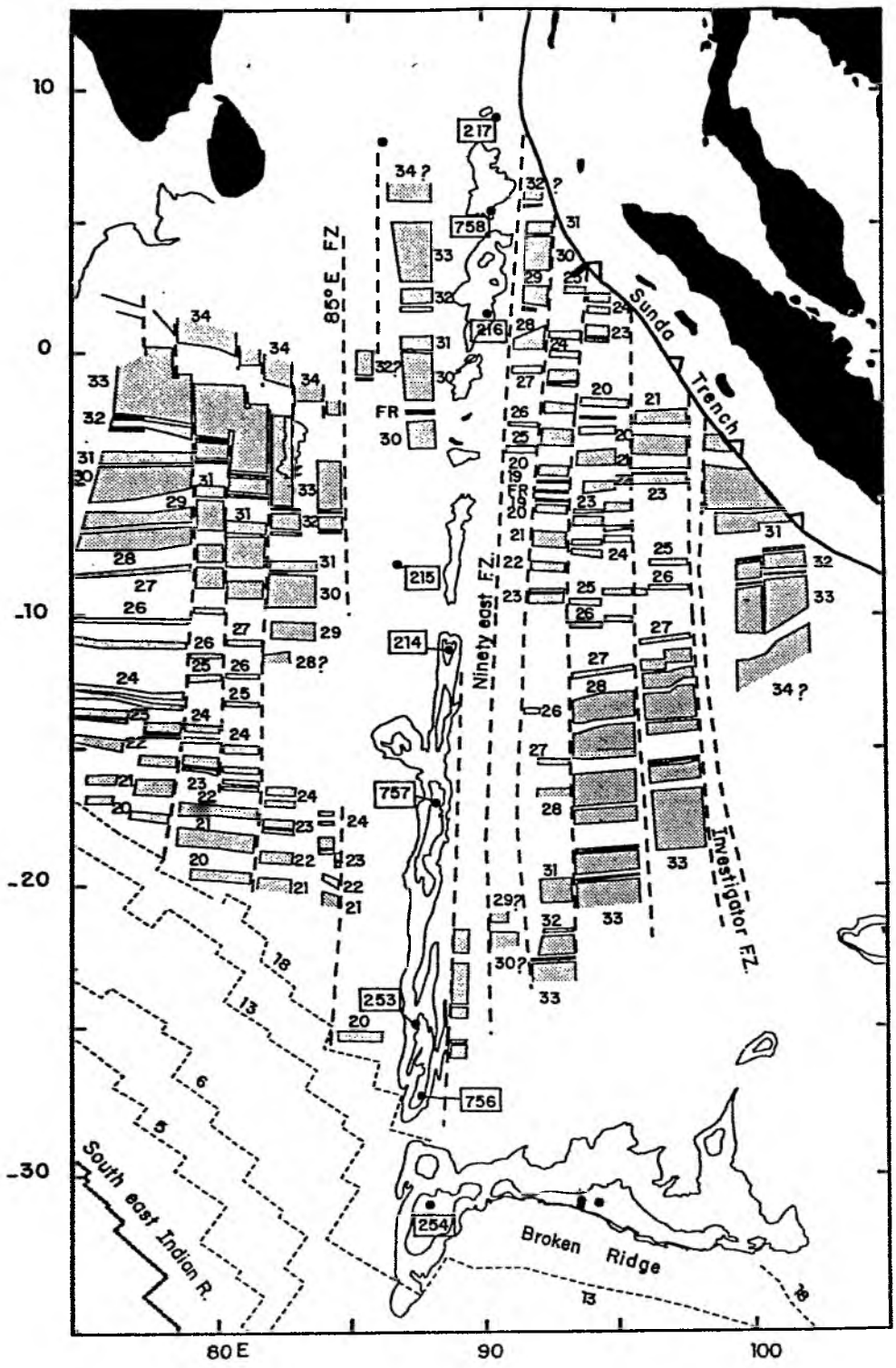

Figure 2.1.2: Magnetic spreading anomalies identified in the Indian Ocean (Royer et al., 1991).

the location of the hotspot with respect to India, Australia and Antarctica. The northern domain (north of ~5°S) where the ridge is wide corresponds to the portion that was generated in the middle of the Indian plate; the narrow and continous domain between 5° to 15°S was emplaced at the boundary between Antarctic and Australian plates; and the southern domain (south of 15°S) was emplaced near the new fracture zone separating Indian and Australian plates. Consequently, the age of the oceanic crust increases to the North in the Indian Basin and on Ninetyeast Ridge. In the Wharton Basin, however, crustal ages increase to the south. At roughly 19°S identical ages of about 52 m.a. face Ninetyeast Ridge (Müller et al., 1997).

2.2 Results of DSDP and ODP Drilling on the Ninetyeast Ridge

DSDP legs 22 (von der Borch, Sclater et al., 1974) and 26 (Davies, Luyendyk et al., 1974) and ODP leg 121 (Pierce, Weissel et al., 1989) all visited Ninetyeast Ridge and adjacent Broken Ridge. The location of these sites is shown in Figure 2.2.1 (after Pierce, Weissel, et al., 1989). These sites allowed the age progression to be determined in detail and all indicate that the ridge has been generated from subaerially erupted lavas near 50°S at the present Kerguelen Hotspot. However, DSDP and ODP drilling also provided new evidence on the structure and geology of the ridge (e.g. Peirce, Weissel, et al., 1989). The sedimentary sequences of the three sites drilled during leg 121 – site 756 at about 27°S, site 757 at about 17°S, and site 758 at about 5.5°S – are all similar in lithology. Nannofossil ooze with varying amounts of foraminifers grades down into chalks at site 757 and 758 and over lies basalt at site 756 and ash/tuff sequences at sites 757 and 758. At greater depth at sites 757 and 758, basaltic basement was sampled. With increasing basement age the thickness of sediment increases from 150 m at site 756, over 370 m at site 757, to 500 m at the most northerly site 758. The volcanic basemet itself is composed of tholeiitic basalts. The absence of recovered alkalic suites is inconsistent with an intraplate setting such as the Hawaiian Islands and the Kerguelen Island. Thus, the geochemical data strongly support the idea that the ridge was erupted on or very close to an active spreading axis. Loading of young and consistently weak lithosphere suggest an Airy-type compensation mode of the topograhy. Therefore, Ninetyeast Ridge is characterized by a small free-air gravity anomaly (Bown, 1973) and a low geoid/topography ratio (Sandwell and Mackenzie, 1989).

A characteristic of six of the seven DSDP and ODP sites is the high abundance of basaltic ash overlying the basement lava flows. These ashes formed in a shallow marine environment as subaerial volcanic centres emerged and subsided. At site 757, for example, the eruptive centre was at or near sea level. The resultant magma-water interaction caused large surtseyan-type eruptions that created hydroclastic accretionary lapilli and thick fine-grained ash deposits. At site 758 turbidity flows and air falls persisted after the production of local lavas had ceased. These ash layers could be the distal facies of large surtseyan or volcanic eruptions, like those sampled at site 757. Distal ashes cover much of Ninetyeast Ridge. Apparently, Ninetyeast Ridge was constructed by discrete, subaerial volcanic centres. Between those volcanic centres, volcanic activity was limited to deep-water pillow and sheet flows, as recoverd at site 758. At any time during the history of Ninetyeast Ridge these different types of volcanic activity were occuring simultaneously on different parts of the ridge. However, at the locations of volcanic centres on the ridge there was a succession from deep-water submarine flows to phreatic eruptions to subaerial flows followed by a second phase of phreatic eruptions as the mature volcano subsided when moving away from the hotspot source.

2.3 Presite Surveys at Site 757

Before site 757 was drilled during leg 121, a site survey was carried out aboard the R/V Conrad as part of cruise RC2707 in August 1986 (Newman and Slater, 1988). Geophysical equipment on this cruise consisted of a single channel streamer and two 80 cubic inch waterguns as sources. Four sonbuoy refraction profiles were collected, and additionally the magnetic and gravity field were observed. Figure 2.2.1 shows the locations of the lines together with the bathymetry around site 757 (after Pierce, Weissel, et al., 1989).

The seismic data were made available to us in digital format from Lamont Doherty Geological Observatory ODP database, and reprocessing of parts of the data was successfully done. Two adjacent East-West lines and two North-South lines are shown in Figures 2.2.2 and 2.2.3. Data processing included spiking deconvolution , frequency filtering, and water velocity migration. The statistical spiking deconvolution was carried out using a 240 ms long Wiener optimum filter, computed for every single trace in a 2 seconds window starting at the sea bottom. The frequency filter had a pass-band between 7 to 50 Hz. For migration a finite difference algorithm was used with a constant velocity of 1500 m/s. For display purposes a normalization of the amplitude was applied to every single trace. The best of the four sonobuoy lines (dropped at shotpoint 6790) is shown in Figure 2.2.4. No improvement compared to the original data presented by Newmann and Sclater (1988) is evident.

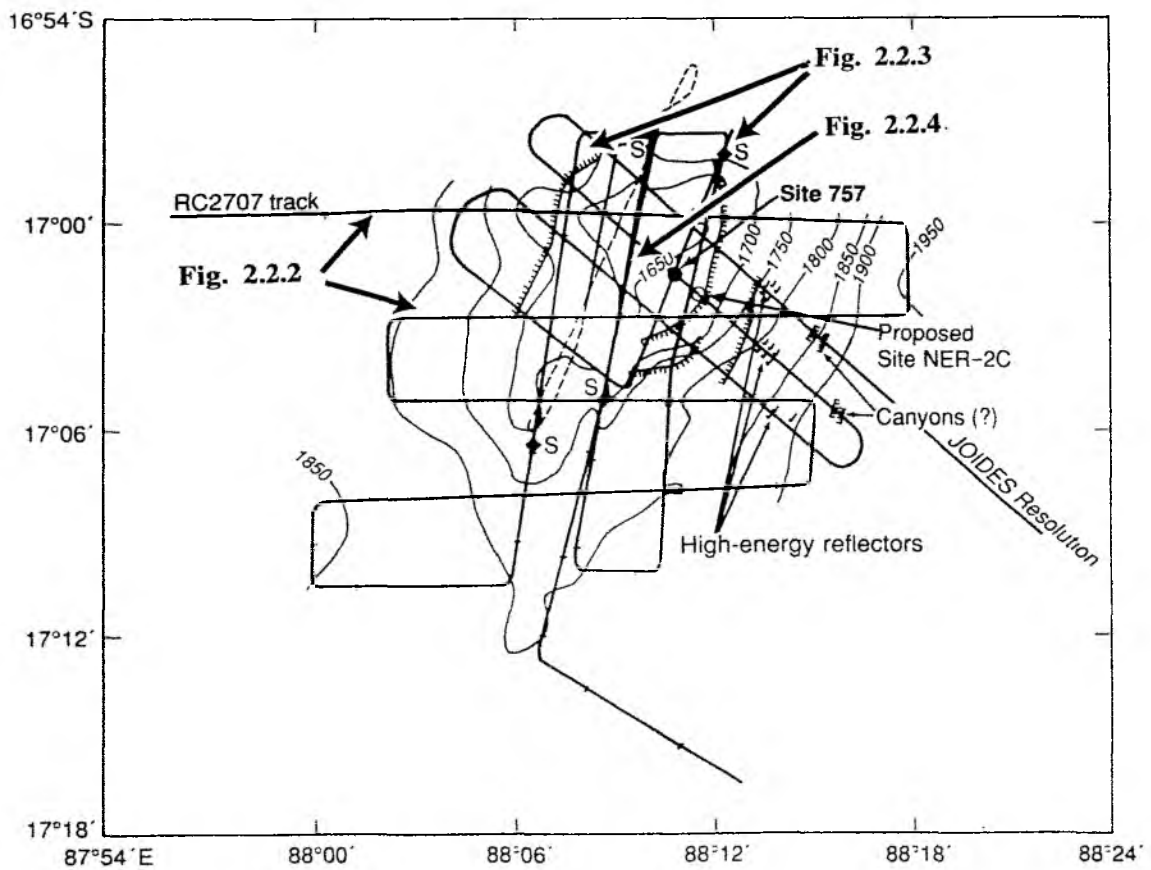

Figure 2.2.1: Bathymetric chart showing the single streamer data collected during the RC2707 cruise in 1986 abord the R/V CONRAD. The reprocessed lines and the suonoboy data, that are shown in Figures 2.2.3 to 2.2.5 , are marked with arrows.

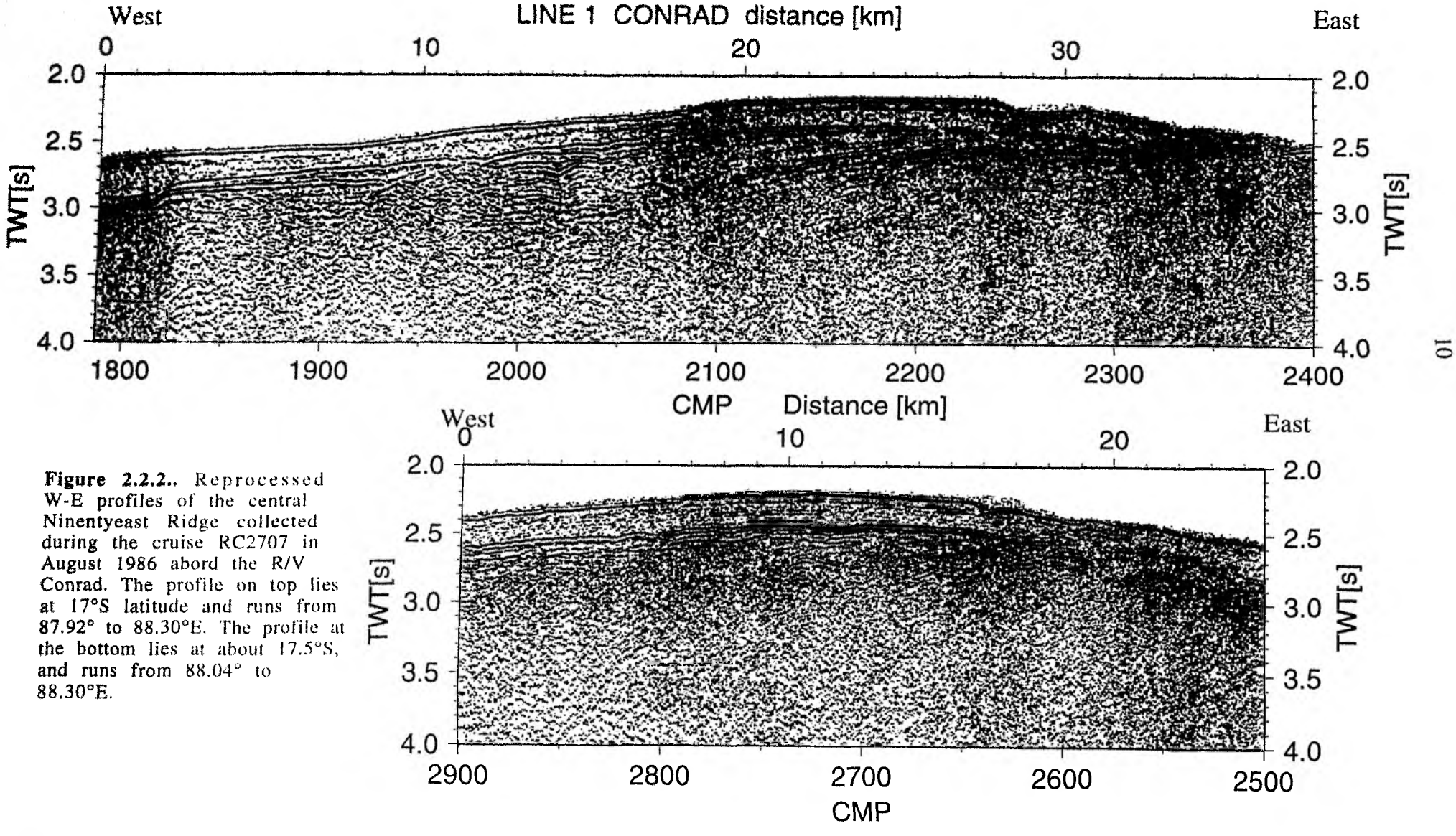

Figure 2.2.2.. Reprocessed W-E profiles of the central Ninentyeast Ridge collected during the cruise RC2707 in August 1986 abord the R/V Conrad. The profile on top lies at 17°S latitude and runs from 87.92° to 88.30°E. The profile at the bottom lies at about 17.5°S, and runs from 88.04° to 88.30°E.

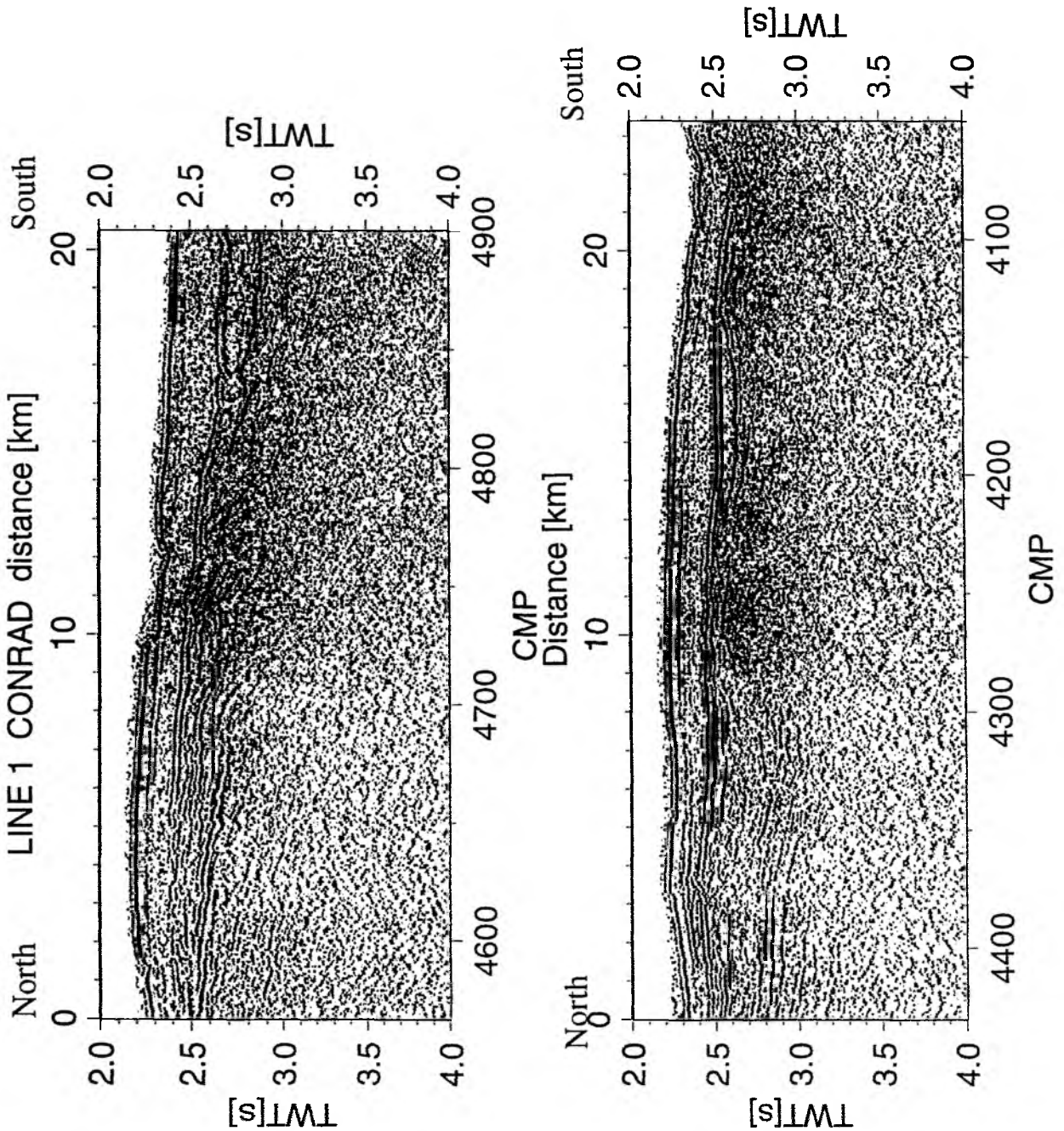

Figure 2.2.3.. Reprocessed N-S profiles of the central Ninentyeast Ridge collected during the cruise RC2707 in August 1986 abord the R/V Conrad. Both profiles run from 16.95°S to 17.17°S latitude approximately. The profile on top lies at about 88.17°E, while the one at the bottom lies at 88.11°E.

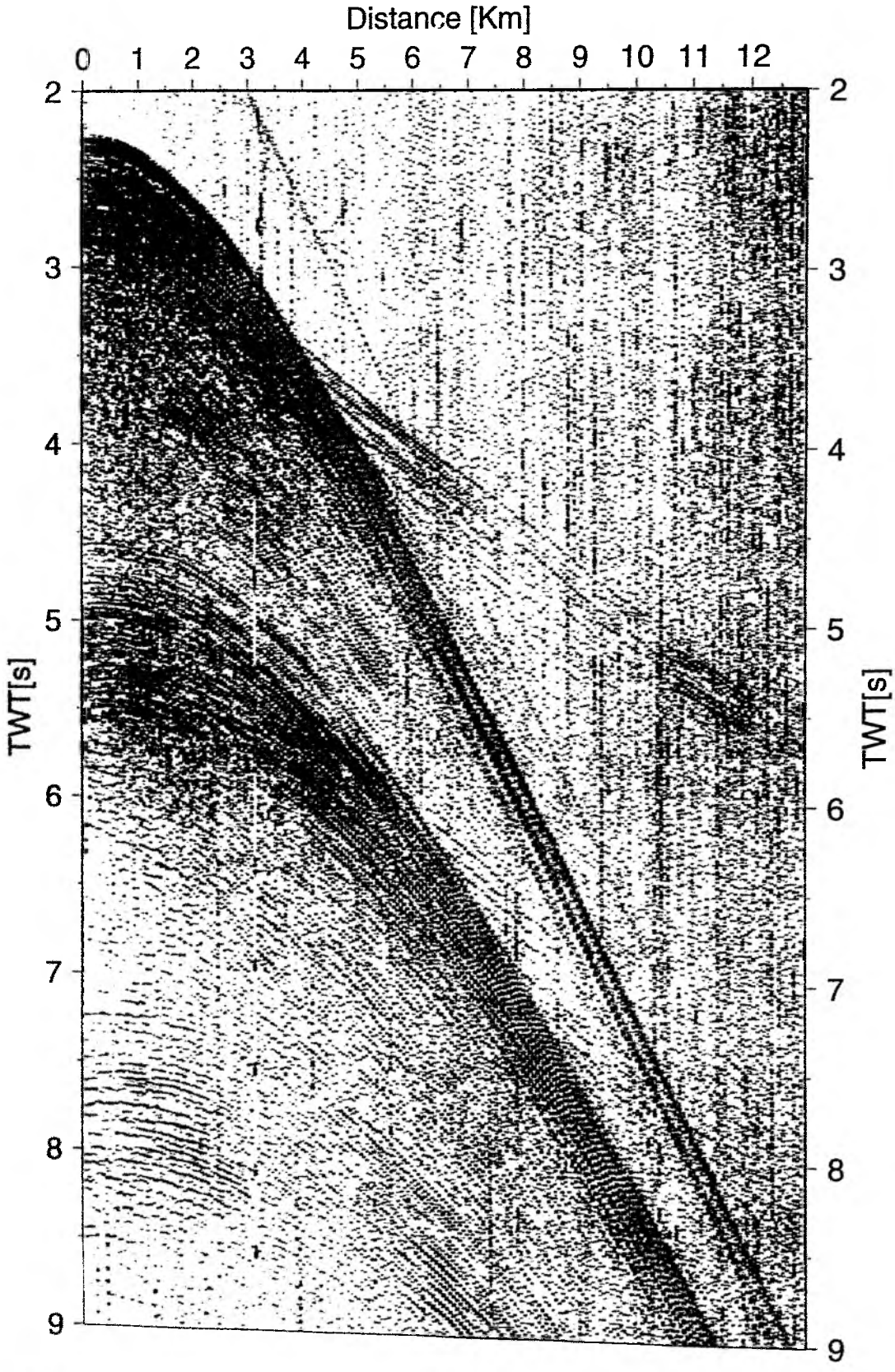

Figure 2.2.4.. Air gun sonobuoy record registered during the cruise RC2707 in August 1986 abord the R/V Conrad, at shot point 6790, 88.15°E, 17.08°S.

The magnetic and gravity data collected around site 757 both show considerable scatter and large anomalies, which can partly be explained by poor navigation and missing corrections for daily variations, but in part also reflect the highly variable basement topography, as noted by Newmann and Sclater (1988).

2.4 Aims of the Survey

The main focus of cruise SO131-SINUS was to investigate the crustal structure in the vicinity of site 757 in a local and regional survey, since this site had been chosen to host the first ION (International Ocean Network) site to be drilled during ODP leg 179 and to be occupied by a broadband seismometer later in 1999. Little knowledge is available on the crustal structure of the Indian ocean following the pioneering work of of Francis and Raitt in 1967. As is common for most hotpsot traces, the crustal structure and thus the amount of extrusively and intrusively added material is poorly constrained. In order to reliably interpret seismic signals to be recorded at the ION site later, a good knowledge of the crustal structure and its lateral variability in velocity, attenuation and anisotropy is a prerequisite. We also hope to be able to identify converted shear-waves, which can be used to quantify the density and alignment of faults and fractures in the oceanic crust.

2.4.1 ODP Leg 179

Leg 179 was originally planned as a technology leg devoted to hammer drill testing and the installating of the borehole for the ION site. The availability of R/V SONNE at the same time in the area around site 757 made a seimic two-ship experiment a scientifically interesting goal and thus two days for a specially designed OSE (Offset Seismic Experiment) with SONNE as the shooting ship and JOIDES RESOLUTION as a receiver ship with a three-component borehole seismometer deployed was also scheduled. These shots should also be recorded by an aerial array of ocean bottom hydrophones (OBH) and seismometers (OBS).

2.4.2 The ION-Site

Digital, broadband seismic networks have successfully been used to tomographically image the earth´s deep interior and the resulting models are key elements for geodynamic studies of the earth´s interior. During the past ten years, our knowledge of the processes within the deep earth has been greatly expanded by the development of new generations of global monitoring networks in seismology, geodesy, and the continuation of long term observations in geomagnetism. However, the existing seismic networks suffer from an uneven distribution on the earth´s surface, with the majority of stations on continents in the northern hemisphere. Combined with the concentration of large earthquakes to the active tectonic regions, large regions of the earth´s interior are not sampled adequately and will remain incomplete unless instruments are deployed on the ocean floor. Especially the upper mantle beneath the southern oceans is practically unexplored (Wysession, 1996).
Recent advances in technology (e.g. Montagner et al., 1994) have demonstrated, that the installation of fully functioning seafloor observatories can be a reality. Therefore, the Ninetyeast Ridge has been chosen as the first site towards an International Ocean Network (ION). Installing a reentry cone and casing down to basement will be the first step towards a Geophysical Ocean Bottom Observatory (GOBO). The NERO site will not only fill a global gap, it will also improve understanding some of the complexity within the Indian Ocean on a regional scale. NERO is ideally located on the Ninetyeast Ridge, where it is surrounded by active earthquake regions and also by some of the highest intraplate earthquake activity.

The porposed location is close to site 757 of ODP leg 121, where 370 m of sediment were encountered above basement. The drilling conditions were excellent and thus the installation of the borehole, its casing to basement and a reentry cone should be a straightforward matter.

2.4.3 SO131 - SINUS

In order to study the crustal structure around site 757 a number of regional seismic refraction and wide angle profiles and a detailed 3-D survey in the immediate vicinity of the NERO site were planned. The regional network should consist of four north-south oriented lines, one in the Indian Basin, one on the ridge crest, and two to the east in the Wharton Basin in between the two morphologically evident fracture zones, as outlined in Figure 2.4.3.1. A 300 mile long east-west dip-profile connecting the north-south strike-lines was also planned. For the 3-D survey area we planned the deployment of up to 30 ocean bottom recorders and shooting along a regular grid with azimuthally separated cross lines and along circles with different radii around the borehole during the operation of a three component borehole seismometer aboard JOIDES RESOLUTION (see also chapter 6.3.4.7).

Minor components of the cruise SO131 were test of a newly constructed vertical array and of implosive seabottom shots (see chapters 5.2.4 and 5.3.3), which were successfully carried out.

3. PARTICIPANTS

3.1. SCIENTISTS

Ernst R. Flüh, GEOMAR, chief scientist
Christian Reichert, BGR, co-chief scientist
Jörg Bialas, GEOMAR
Hajnal Borus, KI
Hans Dohmann, BGR
Urte Domaschk, GEOMAR
Olaf Exner, HB
Ingo Grevemeyer, GEOMAR
Eric J. Haase, WHOI
Rolf Herber, HH
André M. Hojka, GEOMAR
Dirk Kläschen, GEOMAR
Christian Kopp, GEOMAR
Heidrun Lelgemann, GEOMAR
Marta Perez-Gusine, GEOMAR
Klaus Puskeppeleit, BGR
Detlef Roß, KI
Joachim Sievers, BGR
Klaus-Peter Steffen, GTG
Detlef Sturm, BGR
Wilhelm Weinrebe, GEOMAR

3.2. CREW

Henning Papenhagen	Master
Michael Oberländer	Chief-Officer
Norbert Ladewich	1st Officer
Wolfgang Köthe	Radio-Officer
Dagmar Gran	Surgeon
Andreas Martin	Chief-Engineer
Peter Uwe Schade	2nd Engineer
Werner Guzman-Navarrte	2nd Engineer
Rudolf Freitag	Electrician
Rainer Duthel	Electrician Engineer
Helmut Vöhrs	Electronic Engineer
Jens Grigel	System-Operator
Andreas Klein	System-Operator
Anton Unterberger	Fitter
Werner Sosnosky	Motorman
Hermann Rademacher	Motorman
Gerhard Paul	Motorman
Uwe Nagelberg	Motorman
Klaus Hermann	Chief-Cook
Wilhelm Wieden	2nd Cook
Johann Bronn	Chief-Steward
Hans-Jürgen Prechtl	2nd Steward
Andreas Wege	2nd Steward
Karl-Heinz Hartwig	Boatswain
Siegfried Becker	Able Bodied Seaman
Norbert Bosselmann	Able Bodied Seaman
Karsten Bosselmann	Able Bodied Seaman
Alwin Basner	Able Bodied Seaman
Eugenios Dracopoulos	Able Bodied Seaman
Götz vom Berg	Able Bodied Seaman

3.3. ADDRESSES OF PARTICIPATING INSTITUTIONS

GEOMAR: GEOMAR
Forschungszentrum für
marine Geowissenschaften der
Christian-Albrechts-Universität zu Kiel
Wischhofstraße 1-3
24148 Kiel
Germany
Tel. (++49) +431-600-2972
Fax. (++49) +431-600-2922
e-mail: nn@geomar.de

BGR: Bundesanstalt für Geowissenschaften und Rohstoffe
Stilleweg 2
Postfach 510153
30631 Hannover
Germany
Tel. (++49) +511-643-0
Fax. (++49) +511-643-3663
e-mail: nn@bgr.de

GTG: Geomar Technologie GmbH
Wischhofstraße 1-3
24148 Kiel
Germany
Tel. (++49) 431-7209-610
Fax (++49) 431-7209-699
e-mail: gtg@geomar-gtg.de

WHOI: Woods Hole Oceanographic Institute
Department of Geology and Geophysics
Woods Hole, MA 02543
United States of America
Tel.: (++1) 508-289-2626
Fax.: (++1) 508-457-2150
e-mail: ehaase@gannet.whoi.edu

HH: Institut für Geophysik, Universität Hamburg
Bundesstr. 55
20146 Hamburg
Germany
Tel.: (++49) +40-4123-2973
Fax.: (++49) +40-7718-4101
e-mail: herber@dkrz.de

HB: Universität Bremen
FB5, Geowissenschaften
Postfach 330440
28334 Bremen
Tel. (++49) +421-218-4985
Fax. (++49) +421-218-7163
e-mail: exner@dkrz.de

KI: Institut für Geophysik, Universität Kiel
Olshausenstr. 40-60
24098 Kiel
Germany
Tel. (++49) +431-880-3913
Fax.: (++49) +431-880-4432
e-mail: nn@uni-kiel.de

4. AGENDA OF THE SONNE CRUISE SO131

(E. Flueh)

SONNE cruise SO131 started on 04. May 1998 in Karachi, Pakistan. After loading three containers of geophysical equipment and installation of the laboratories, Sonne left the pier at 11:00 05. May 1998 for an 11 days transit to the working area on the Ninetyeast Ridge near 17°S. The equipment to be installed consisted of the two airgun arrays and their trigger system, 25 ocean bottom hydrophones (OBH), a ministreamer, magnetometer, and several workstations and PC´s for data acquisition and processing.

Since the sea was very calm some initial instrument tests were performedduring the night 05/06 May. The streamer was tested for waterdepth and noise conditions. Two different acquisition systems for the streamer were tested along three short profiles (SO131-01,02,03) and compared to the signals recorded by one ocean bottom hydrophone (OBH01) deployed at waterdepth of about 800 m. Our transit continued in perfectly calm seas with moderate southerly currents, so that partially SONNE could steam at an average rate of more than 13 knots for several days. While within the Pakistani EEZ, hydroacustik data were continuously recorded until 15:00 06. May. On 07. and 11. May we stopped for several hours to test the releaser-systems of the OBH using the geo-cable in water depth of more than 3000 m. All 26 systems worked well. Starting around 10. May the wind and swell increased noticeably, and on 11. May we encountered force 8 winds when crossing the equator at 17:57 local time. Wind and swell would not diminish for most of the remaining part of the cruise. Hydrosweep recording was started on 11. May, after reaching international waters. On 14. May we tested a newly designed 1200 m long vertical array, but found that the buoyancy was insufficient. Also the magetometer was tested for a short time. The average transit speed slowed considerably in the last days of our transit.

The working area was finally reached 16. May and 12 OBH were deployed along the N-S oriented profile SO131-04 in the Indian Basin along 86°40.0´ between 00:00 and 05:20. the line was shot from 10:30 16.05 to 08:00 17.05, with the streamer and magnetometer also deployed. During transit to the start of the shooting line and back to the instruments two magnetic profiles, 101 and 102 were recorded. All OBH except OBH08 were recovered between 15:30 17.05 and 02:00 18:05, and a CTD was run to waterdepth of 4200 m in between.

For Profile SO131-05 25 additional instruments were deployed on the E-W oriented line due east of OBH08 at an average spacing of 3 to 4 nm. OBH37 was deployed at 16:00 18.05, and after magnetic profile 103 was surveyed, shooting started at 22:00 18.05. with 60 s shot interval and terminated at 08:00 20.05., followed by magetic profile 104.

All instruments were subsequently retrieved and redeployed along SO131-06 in continuation of SO131-05. OBH61 was finally deployed at 20:00 21.05. Along magnetic profile 105 strong swell caused the hydrosweep data to be useless, even during shooting along SO131-06 from East to West at 5 knots large parts of the hydrosweep data were erroneous. The shooting had to be detoured slightly at 21:30 on 22.05, when JOIDES RESOLUTION arrived at the NERO Site while SONNE was just shooting across it. Shooting terminated at 06:00 23.05 and after magnetic profile 106 we approached JOIDES RESOLUTION for the exchange of equipment, which was accomplished using a Zodiak. High swell prohibited a planned visit between the scientists, but communication between the two ships was straight forward using the radios.

OBH40 to 61 were recovered between 16:00 23.05 and 09:00 24.05, followed by two magnetic profiles 106 and 107. OBH38 and 39 remained in place to further record the shots from the planned 3-D experiment around NERO.

Another test of the 1200 m long vertical array was successfull, and the array was deployed together with the other instruments (OBH62 to OBH83) between 21:00 24.05 and 12:00 25.05. Another magnetic profile, 109, was run before the starboard array was used to shoot the first line within the 3-D experiment. Strong swell and force 6 to 7 winds allowed only one line to be shot (profile SO131-07) from 15:30 to 22:30. Further increasing winds and swell prohibited the continuation of the shooting, but after magnetic profiles 110 to 113, the next line SO131-08 was shot using one array only from 09:00 to 18:00. Along most of this line the magnetometer was not deployed due to necessary repair work on the winch. Weather had improved slightly and shooting could continue along lines SO131-09 to 17 with both arrays until 12:00 29.05. Along SO131-11 the shot interval was set to 30 s, and 60 s for all other lines. On 29.05

between 14:00 and 18:00 five OBH were recovered (OBH39, 79,80,81, and 83) due to shortage of battery power, and four instruments were redeployed (OBH84 to 87). The last two positions were very close (0.2 nm) to NERO to substitute for the borehole seismometer which the JOIDES RESOLUTION in the end could not deploy due to their tight schedule. JOIDES RESOLUTION left the NERO site 08:00 28.05. Shooting continued at 19:00 29.05 with two circles of 2 and 6 nm radii around Nero (profiles SO131-18 and 19). Inspection of the data retrieved from the recovered instruments suggested that some of the lines should be extended to ensure better coverage of prominent deep reflections. Subsequently lines So131-23 to so131-28 were extended to 30 nm off the Nero site. Several segments near to NERO were shot with a 30 s shot interval, while the remaining parts had a 60 s shotinterval. Shooting terminated at 15:00 01. June on line SO131-28, which partially was coincident with line SO131-16, were a gap in the streamer records was closed. The first instrument to be released was the 1200 m long vertical array. However, despite many successfull release commands it soon become apparent, that the array was not ascending to the surface. It was therefore decided to retrieve all other instruments first. After about half the instruments were recovered, the release command unit failed to acknowledge any further commands, but instruments were still released. All recorders were recovered by 10:00 02. June and an attempt was made to dredge the vertical array. We deployed about 6500 m of wire in a circle around the array which was located at a water depth of 1830 m. A Thayssen dredge hook was attached to the wire, and when pulled tight about 100 m above the hook the lower part of the array was caught. Soon after, the top bouy appeared at surface, but the cable broke and the buoy drifted away. When the cable was finally recovered, the ship moved towards the top buoy and recovered it without any damage. Much to everyones relief, the components were fully recovered and the recorder showed no data loss. It remains unclear, why the anchor got caught in the releaser and bottom hydrophone.

Several profiles for magnetic and hydrosweep and a short seismic line were run the night 02. to 03. June. At 09:00 the SEEBOSEIS experiment began. Six instruments (OBH88 to 93) were deployed in close proximity, and 5 bottom shots were deployed. In addition, airguns were fired along the line using only one subarray. Afterwards, all instruments were successfully recovered by 18:00 03. June. All five shots were successfully recorded by every instrument but one.

Several profiles with hydroacoustics and magnetic were run afterwards trying to image the escarpment of the Ninetyeast Ridge to the east around 88°45.0´.

From 16:00 to 24:00 04. June another 15 OBH (OBH94 to 108) were deployed at 4 nm spacing along the East-West oriented line in continuation of profiles SO131-05 and 06. They covered the region in the Wharton Basin across the Ninetyeast Fracture Zone. Profile SO131-31 was shot from 05:00 05. June to 14:30 06. June with a shot interval of 60 s. Before instrument recovery started, a short high resolution profile SO131-32 was shot across two small hills on the Ninetyeast Ridge, which were discovered from Hydrosweep data and also as side-swipes on previously collected reflection profiles. These 100 to 150 m high mountains were tentatively named Monte Sinus and Monte Cosinus, I accordance with their appearance on the Hydrosweep display.

All OBH were recovered between 06:00 and 18:00 07. June, and subsequently we started a mapping programme along the Ninetyeast Fracture Zone between 16 and 17° S. Increasing winds forced an early departure before completion of the envisioned area to be mapped. At 21:00 08.06. the magnetometer was brought onboard and SONNE headed towards Sunda Strait, fighting force 6 to 8 winds. We passed Cocos Islands (Keeling Islands) in the evening of 10.06, and transit speed of RV SONNE slowed to less than 10.5 knots in heavy winds and swell. On 12.06 winds decreased for several hours, and a test of a four element high resolution airgun array (total volume 3.2 ltr.) was conducted for about one hour. Repair work on the W4 winch was also accomplished on 12.06, and included another CTD measurement. On 13.06 we entered Sunda Strait, and for the first time since May 11 encountered calm seas, which remained smooths for the rest of the transit.

SONNE finally met the pilot in Singapore at 11:00 15.06. after transiting 8300 nm within 42 days at sea, and the scientific equipment was unloaded. A complete trackchart of cruise SO131 is shown in Figure 4.1.

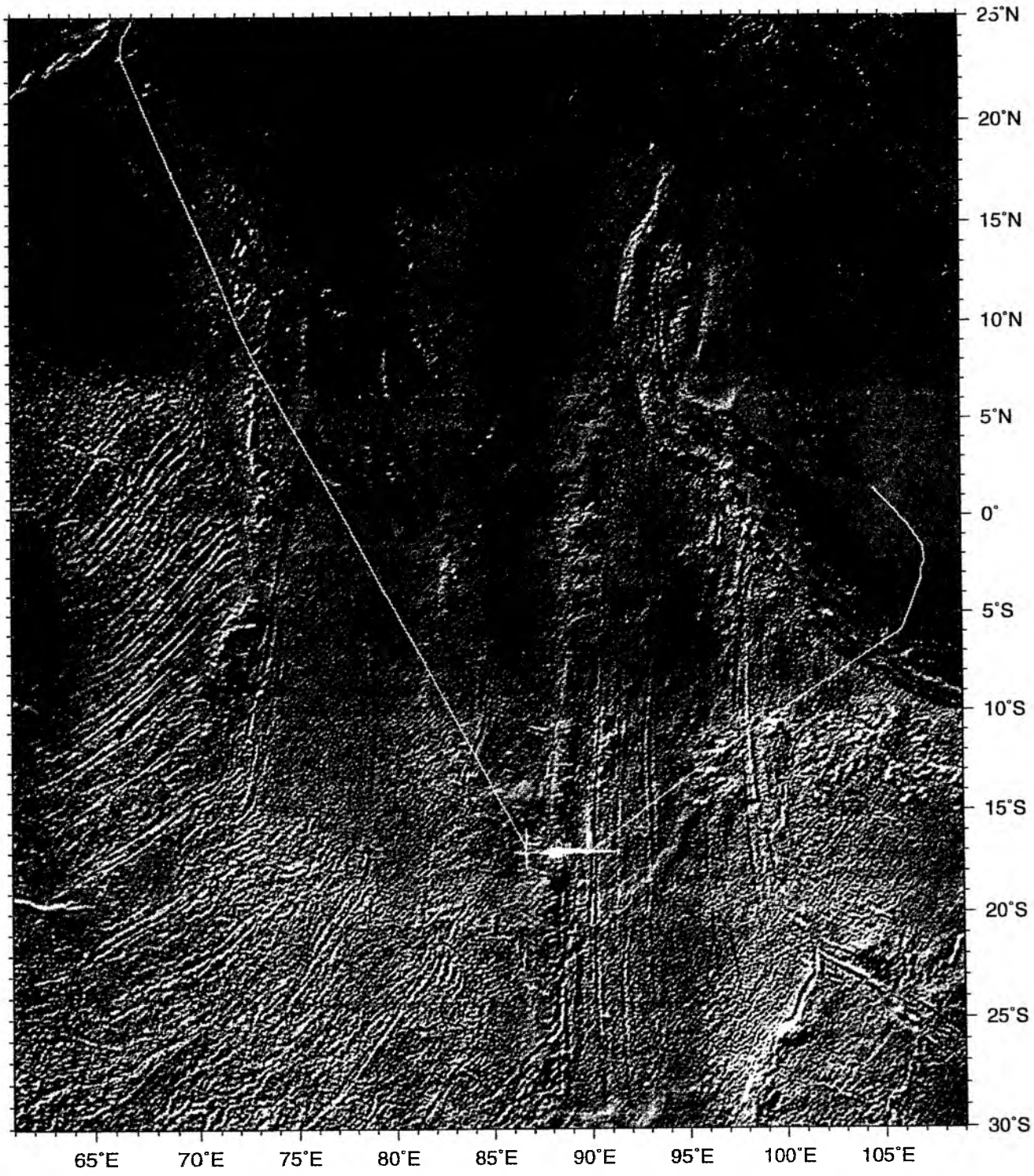

Fig. 4.1: R/V SONNE cruise 131 total track.

5. SCIENTIFIC EQUIPMENT

5.1 COMPUTER FACILITIES

(W. Weinrebe)

The experiments and investigations during SO131 cruise required special computing facilities in addition to the existing shipboard systems. For processing of seismic data and analysis of HYDROSWEEP recordings a workstation cluster was installed onboard comprising

1	"moho"	SUN sparc20	2 CPU, 256 MB memory	22 GB disks, DAT, Exabyte, CD	Sun Solaris 2.5
2	"avalonia"	SUN sparc5	1 CPU, 64 MB memory	13 GB disks, DAT, CD-R, Methusalem	Sun Solaris 2.5
3	"jurassic"	SUN LX	1 CPU, 48 MB memory	12 GB disks, DAT, Methusalem	SunOS 4.1.3
4	"laurentia"	SUN LX	1 CPU, 48 MB memory	9 GB disks	SunOS 4.1.4
5	"baltica"	HP9000-715/50	1 CPU, 48 MB memory	8 GB disks, DAT, CD, MO-disk 1.3 GB	HP-UX 9.0.5
6	"andean"	PC Pentium 133	1 CPU, 64 MB memory	8 GB disks, DAT, CD	Redhat-Linux 5.0

In addition to these workstations three desktop Macintosh computers were installed:

1 PowerMacintosh 8500/120

2 PowerMacintosh 7200/90

3 PowerMacintosh 7100/80

For plotting and printing two HP Postscript Laserprinter were used (papersize A3 and A4), one OYO-11"-thermoplotter as well as the shipboard color plotters.

For recording of magnetic and streamer data and for OBH maintenance two PCs as well as several laptops were used.

The workstation cluster and two of the Macintosh desktops were placed in the magnetic/gravity lab and the Reinlabor.

The workstation cluster was set up according to a "client-server" model, with "moho" being the server. All important file systems from the main server at GEOMAR were duplicated onto the "moho"-disks. Using NFS-, NIS-, and automounter services the computing environment was identical to that at GEOMAR so every user found his/her familiar user interface. All data file systems were mounted on every workstations so that an overall pool of 32 GB disk space was available.

The convenience of network mounted file systems has to be paid for with heavy network load, particularly during playback of OBH-data from tape to disk (c.f.

SO123 cruise report). This required a high-performance network, which was accomplished by a switched twisted-pair ethernet. A 12-port ethernet switching-hub (3COM-SuperstackII 1000) with an uplink connection of 100 Mbps to the server "moho" and dedicated 10 Mbps ports to the client workstations maintained the necessary network performance. In order to keep the shipboard network undisturbed by the workstation cluster, but to allow for communication between them, the server "moho" was equipped with two network interfaces and served as router. This provided additional benefit of a simplified network configuration. Considerable setup work was dedicated to "moho", while the other workstations used the same IP-addresses and network configuration as at GEOMAR.

This network setup showed a reliable and stable performance, and no breakdowns or bottlenecks were observed as compared to the SO-123 cruise (Flueh and Reichert, 1997). The reconfigured shipboard network using twisted-pair technology and "star-"topology instead of BNC-cables along a linear "bus" with hubs in the main labs improved the flexibility to easily hook up systems to the network.

5.2 SEISMIC DATA AQUISITION

5.2.1 THE Mini-Streamer

(J. Bialas)

During this cruise all shots were additionally recorded by a short streamer. It is a three channel unit originally build by Prakla-Seismos, Hannover, Germany for the Deutsches Hydrographisches Institut in 1979.

The system comprises three parts, a 50 m long active length, a 50 m long stretch length and a 150 m long towing cable. The active length is separated into three groups of 16 HHOC type hydrophones. Construction of the first and third group are identical while the middle one has a smaller hydrophone separation. Within group one and three the hydrophones are 1.2 m apart building a 18 m long unit. This selection results in an antenna directivity which is sensitive to high frequency wavefronts impinging from the near vertical. The -3 dB point is found to be at 48 Hz for wavefronts traveling at 90° (measured from the vertical), 66 Hz / 30°, 190 Hz / 11.5° and 380 Hz / 5.7°. The central group is only 6 m long with 16 hydrophones each 0.4 m apart. The -3 dB point is found at 110 Hz / 90°, 220 Hz / 30 °, 550 Hz / 11.5° and 1.1 kHz / 5.7°. Adding all three groups together the total directivity is (-3 dB) 18 Hz / 90°, 36 Hz / 30°, 90 Hz / 11.5°, 180 Hz / 5.7°. At the tail a depth sensor is installed which indicates the actual depth moduulated as frequency changes. With a base frequency of 990 Hz at the surface it increases by 100 Hz per bar (100 Hz per 10 m). The whole unit is stored and operated from a hydraulic winch at the stern of RV SONNE, in between the two airgun arrays (see 5.3).

For recording the data one of the four channel OBH recording units (see 5.2.2) was used. During the SINUS cruise the Marine Broadband Seismic recorders (see 5.2.2) were available, one such unit having with the high frequency license kit installed which enables sampling intervals up to 10 kHz. This unit was choosen to record the streamer signals with 500 Hz sampling interval resulting in a Nyquist frequncy of 250 Hz, which is well above the expected maximum energy of 100 Hz.

For a first test of the floating depth three short profiles were shot with a single airgun as source. During this experiment different weights were attached to the towing cable trying to deepen the active length. At all depths the influence of the wave state to the vertical swelling of the streamer was equal. Therefore it was decided only to add a small weight (10 kg) 60 m in front of the stretch length and a small chain (5 kg) at the end of the 30 m tail rope, both well separated from the hydrophones. With these weights and 120 m towing and lead in cable the streamer floated at 15 m depth during all profiles. In order to suppress the wave state induced low frequency noise (up to 5 Hz) the input impedance of the channel separator was changed to shift the -3 dB point from 3 Hz up to 15 Hz. Together with the use of the standard OBH preamplifiers a suitable signal recording was achieved. An oscilloscope connected to a separate output of the channel separator enables online control of each channel.

The streamer provided usefull information during the cruise and the sedimentary structure was well imaged along all profiles. These data are essential for detailed interpretation of the wide-angle data.

5.2.2 THE GEOMAR OCEAN BOTTOM HYDROPHONE (OBH)

(E. Flueh and J. Bialas)

THE INSTRUMENT

The first GEOMAR Ocean Bottom Hydrophone was built in 1991 and tested at sea in January 1992. A total of 24 instruments were available for SO131. This type of instrument has proved to have a high reliability; in fact during this cruise, the

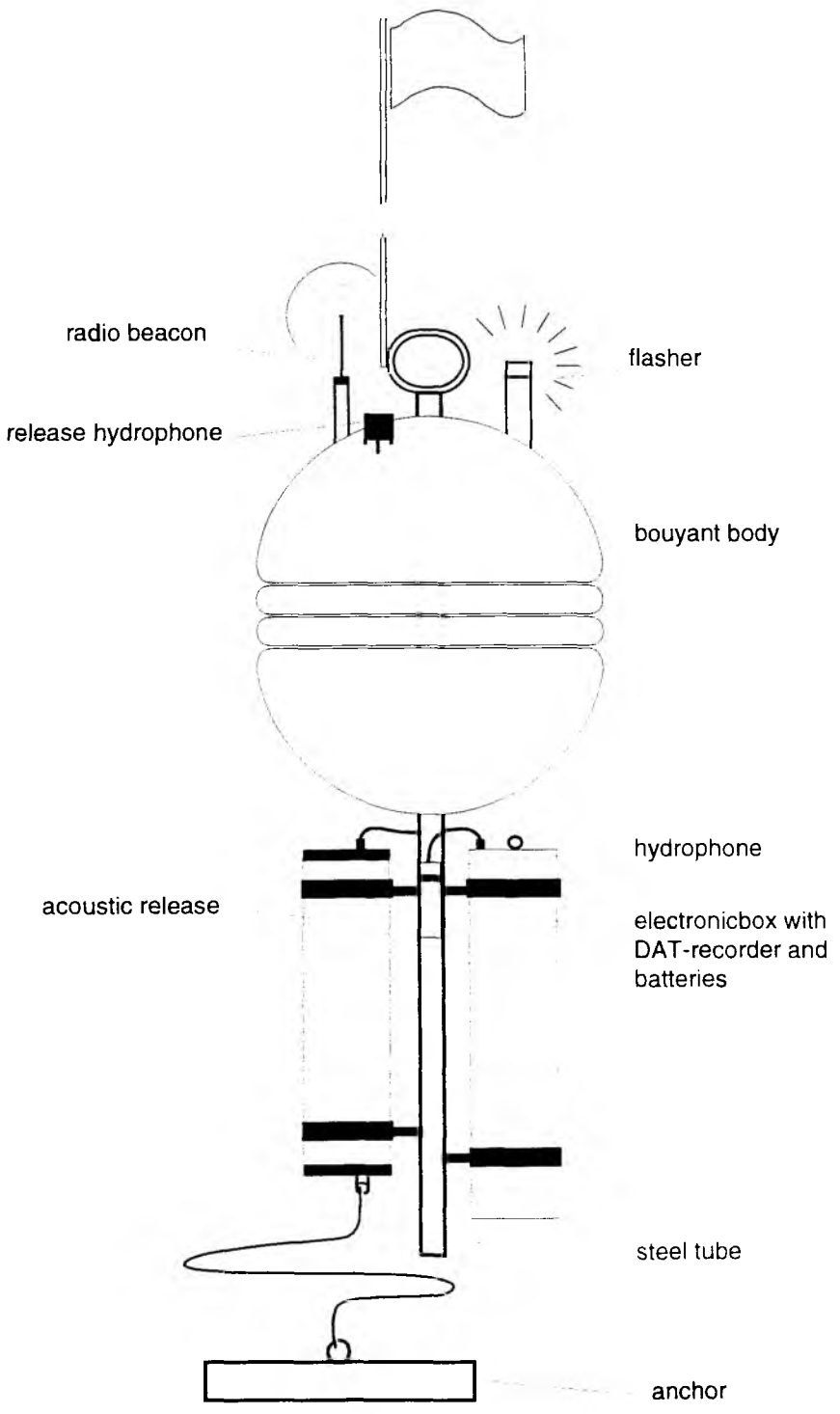

Figure 5.2.2.1: Principle design of the GEOMAR OBH

800th successful deployment was made. Altogether 107 locations were occupied during the SINUS cruise.

The principle design of the instrument is shown in Figure 5.2.2.1, and a photograph showing the instrument upon recovery is seen in Figure 5.2.2.2. The design is described in detail by Flueh and Bialas (1996).

The systems components are mounted on a steel pipe, which holds the buoyancy body on its top. The buoyancy is made of syntactic foam and is rated, as are all other components of the system, for a waterdepth of 6000 m, except for the pressure cylinders, holding the recording electronics. Here various models for variable depth (2500 m, 3000 m, and 6000 m) are available. Attached to the buoyant body are a radio beacon, a flash light, a flag and a swimming line for retrieving from aboard the vessel. The hydrophone for the acoustic release is also mounted here. The release transponder is a model *RT661CE* made by *MORS Technology*. Communication with the instrument can be made through the ships transducer system, and even at maximum speed and ranges of 4 to 5 miles release and range commands are successful. For anchors, we used pieces of railway tracks that weighed about 40 kg each. The anchors are suspended 2 to 3 m below the instrument. The sensor is an *E-2PD* hydrophone from *OAS Inc.*, and the recording device is a *Methusalem* recorder of *DELTA t*, which is contained in its own pressure tube and mounted below the buoyant body opposite the release transponder (see Figure 5.2.2.1). Two alternate hydrophones were also tested during this cruise (see chapter 6.3.4.3). The *Methusalem* consists of a preamplifier (26 dB), a highpass and antialias filter, a 13 bit A/D converter and a core memory of 0.768 MB. Signals are sampled at 800 Hz, and after FIR-decimation filtering, a resolution of 14 to 15 bits is achieved. Data are stored as 16 bit integers on a DAT-cassette, which is run in audio-mode to save power consumption and which can store about 1.1 GB of data. The power supply is from alkaline batteries for long term deployments or from rechargeble lead batteries for short term deployments (up to 3.5 days). The instrument can be programmed before deployment through an RS232 interface. Up to 4 channels with different amplifications and sampling rates can be recorded. A DTCXO (0.05 ppm accuracy) is checked against GPS time before and after deployment. The DAT-cassettes are read from a playback system, which simulates a SCSI-interface, to a workstation for data reduction and analysis (see Chapter 6.3.2).

Marine Broadband Seismic Recorder (MBS)

During this cruise a new recorder was used for the seismic data acquisition. The so called *Marine Broadband Seismic recorder (MBS)* manufactured by *SEND GmbH*, was developed based upon experience with the DAT based recording unit Methusalem (Flueh and Bialas, 1996) over the last years. This new recorder avoids mechanically driven recording media, and use of the PCMCIA technology enable static flash memory cards to be used as unpowered storage media. Read/write errors due to failure in tape handling operations should not occur any more. In addition, a data compression algorithm is implemented to increase the data capacity. Redesign of the electronic layout enables a decreased power consumption of about 25% compared to the *Methusalem* system. Depending on the sampling rate data output could be in 16 to 18 bit signed data. The system was developed to serve a variety of seismic recording requirements. Therefore, the bandwidth reaches from 0.1 Hz for seismological observations to the 50 Hz range for refraction seismic experiments and up to 10 kHz for high resolution seismic surveys. The basic system is adapted to the required frequency range by setting up the appropriate analog front module. Operational handling of the recording unit is similar to the *Methusalem* system. Clock synchronization and drift are checked after recovery and compared with the original GPS units. After recording the flashcards need to be copied to a PC workstation. During this transcription the data are decompressed and data files from a maximum of four flash memory cards (up to 300 Mbyte each) are combined into one data set and formatted according to the PASSCAL data scheme used by the *Methusalem* system. This enables full compatibility with the established processing system. While the *Methusalem* system did provide 16 bit integer data, the 18 bit data resolution of the *MBS* can be fully utilized using a 32 bit data format.

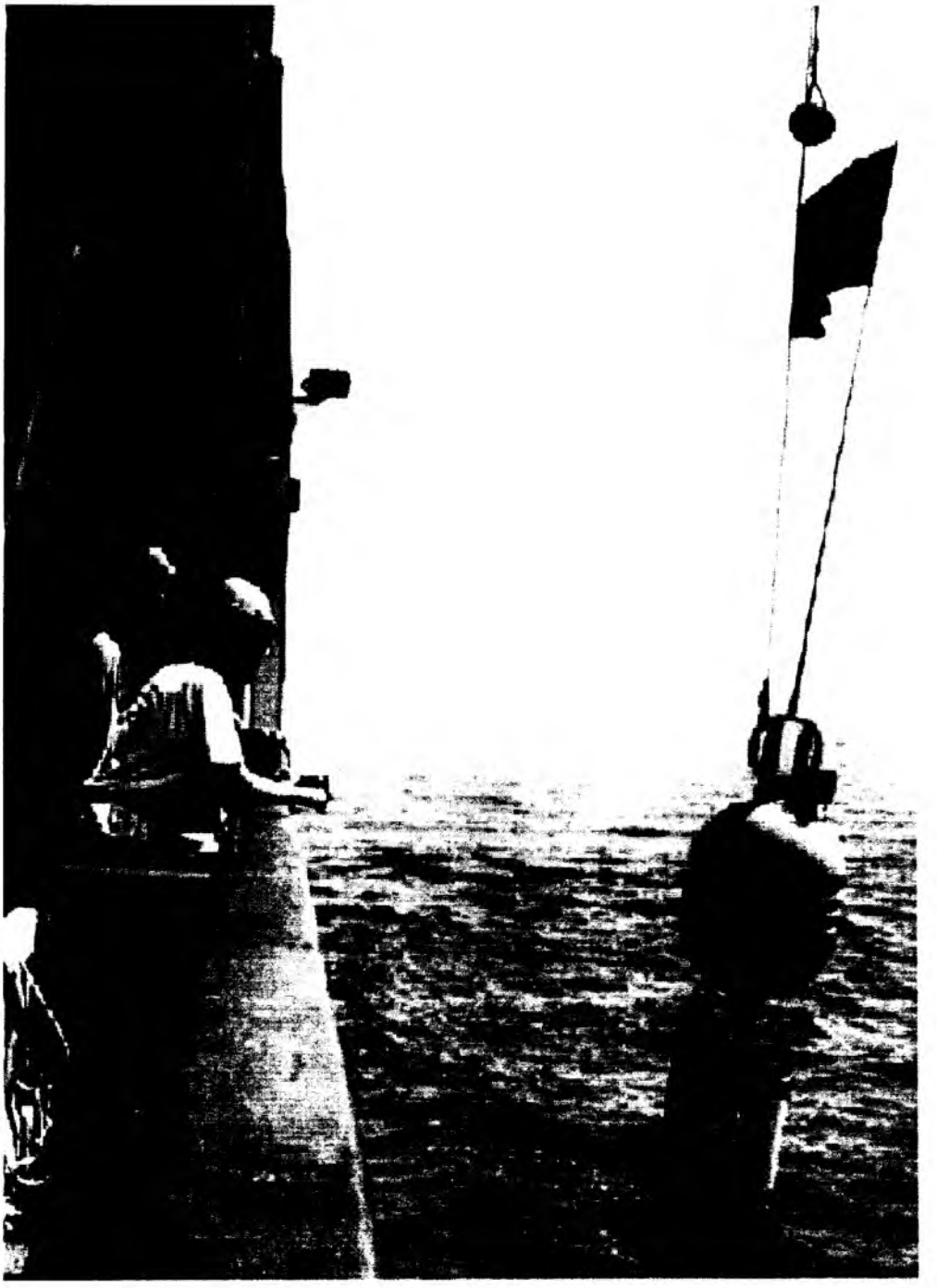

Figure 5.2.2.2: The GEOMAR OBH upon recovery.

During operation of the system it cecame apparent that there were some time shifts at arbitrary intervals in the data. These were detected during routine checks of the seismic sections and could be corrected manually. Discussion by email with the manufacturer could not resolve the problem during the cruise as it seemed that a new ROM design needs to be loaded into the units.

DATA PROCESSING

The OBH data recorded on the *Methusalem* and the *MBS* have to be converted into standard SEG-Y format for further processing. The necessary program structure was mainly taken from the existing REFTEK routines and modified for the OBH requirements and GEOMAR's hardware platforms. Because the GEOMAR OBH works in a continous mode, most of the modifications on the existing program package had to be done in the program parts handling continuous data streams.

A flow chart shown in Figure 5.2.2.3 illustrates the processing scheme applied to the raw data. A detailed description of the main programs follows below:

- **ref2segy**

Downloading the raw data from DAT tape on a harddisk of a SUN workstation is done by the program ref2segy. It will produce a pseudo SEG-Y trace consisting of one header and a continous data trace containing all samples. For each channel (different amplifications) one file will be created. The name of this file contains the start time, the serial number of the *Methusalem* and the channel number. In addition a log and an error file will track the download process. The file size of the data is directly related to the recording time. For example a recording time of one hour sampled with 200 Hz will produce a file size of 1.44 MB per channel. A record with two channels and a recording time of two days will get a total data volume of 70 MB.

- **merge**

If a tape error occured during the download process, the ref2segy program has to be restarted. This will lead to several data files with different starting times. Merging these files into a single file is done by the program merge. The gap between the last the sample and the first sample of the consecutive data trace will be filled up with zeros. Overlapping parts will be cut out.

- **segy2trig**

The trigger signal, which is provided by the airgun controll system, is recorded simultaneously on an additional *Methusalem* during the shoting period. This tape is treated as a regular data tape and downloaded to the harddisk via the ref2segy program. The segy2trig program detects the shot times in the data stream. It determines the shot times by detecting the trigger signal through a given slope steepness, duration and threshold of the trigger impulse. The output is an ASCII table consisting of the shot number and the shot time. The accuracy of the shot time is one of the most crucial matters in seismic wide-angle work. It has to be reproduced with a precision of 5 ms. Due to this demand the shot times have to be corrected with the shift of the internal recorder clock. As additional information the trigger file contains the profil number and the start/end time of the profil and the trigger recording. The shot times are part of the UKOOA file which links the coordinates of the source and the hydrophones with the shot times.

- **ukooa**

The ukooa program is used to establish the geometric data base. It requires the trigger file containing the shot times, the ships navigation and the position of each OBH for input. The ship navigation is stored in a database about every two seconds (see Chapter 5.4.3). The program calculates the coordinates of each shot and creates a file in the UKOOA-P84/1 format as output. This file will be used when creating a SEG-Y section via the dat2segy program.

- **dat2segy**

The dat2segy program produces standard SEG-Y records in a 16 bit integer format by cutting the single SEG-Y trace (from the merged ref2segy file) into

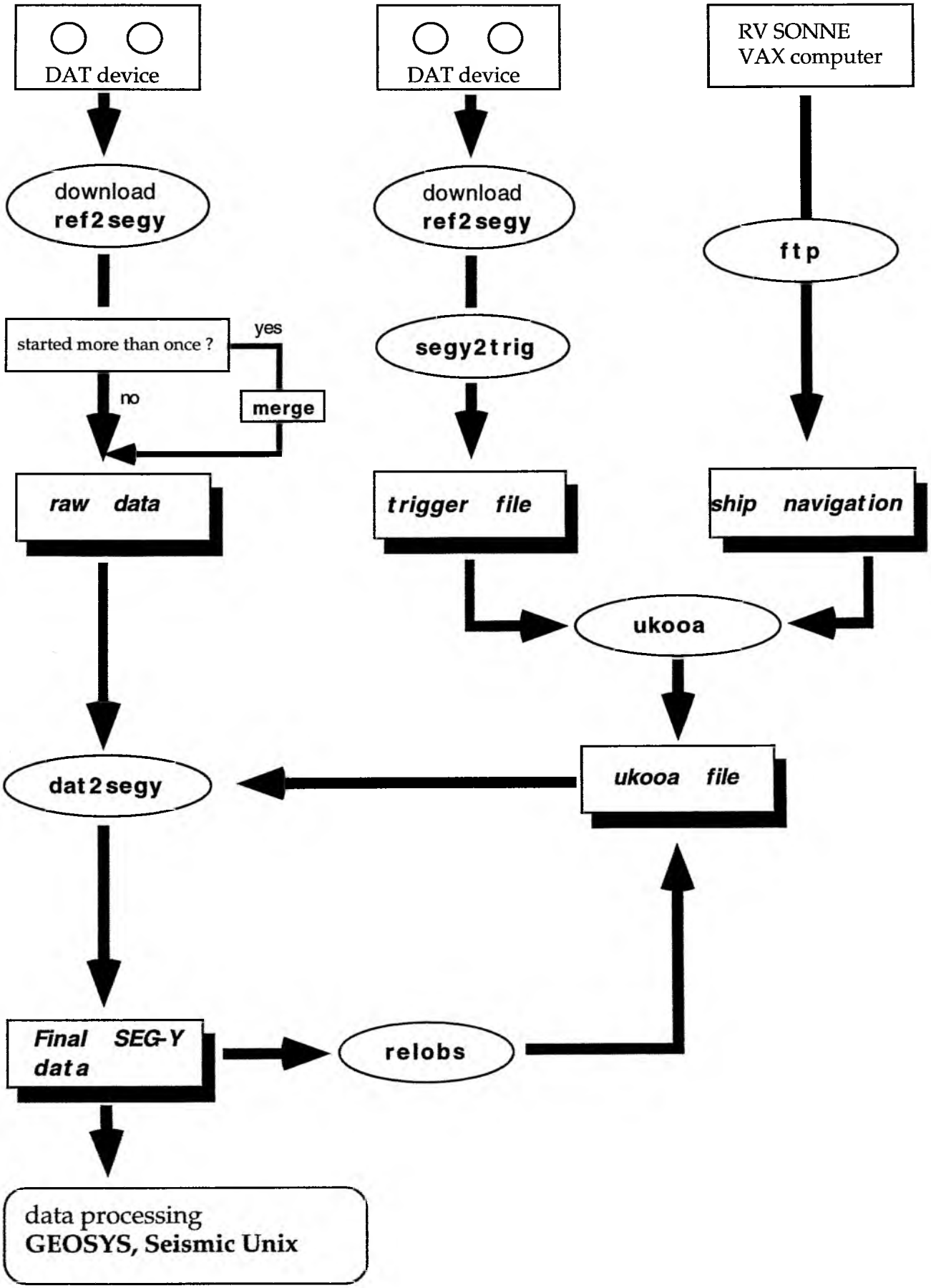

Figure 5.2.2.3: processing flow from raw data to SEG-Y records.

traces with a certain time length. It reads both the ukooa file with the geometry informations and the downloaded raw data as produced with the ref2segy program. In addition the user can use several parameters for controlling the output. These parameters are informations about the profile and the receiver station, number of shots to be used, trace length, time offset of the trace and reduction velocity (to determine the time of the first sample within a record (see Chapter 6.3.2)). Also the clocks drift of the recorder is taken into account and corrected for. The final SEG-Y format consists of the file header followed by the traces. Each trace is built up by a trace header followed by the data samples. The output of the dat2segy program can be used as input for further processing with GEOSYS or Seismic Unix (SU).

Beside these main programs for the regular processing sometimes additional features are needed for special handling of the raw data:

- **divide**

The program divide cuts the raw data stream in traces with a given length without offset and time informations. The output is stored as SEG-Y format. The routine is useful for a quick scan at the raw data or if a timing error has occured.

- **segyhdr**

The routine segyhdr prints all the header values of the raw data on the screen.

- **segyshift**

The program segyshift modifies the time of the first sample, which means that the whole raw data trace can shifted by a given value. This is very useful when shifting the time base from Middle European Time to Greenwich Mean Time or any local time. Because of recording problems, the data sometimes shows a constant time shift, which can be corrected as well with segyshift.

- **castout**

The program castout allows you to cut out a specified time window of the raw data stream. When the shoting window is much smaller than the recording time, one can reduce the data volume by cutting out only the useful informations. This will reduce the demand on diskspace.

- **relobs**

Due to a drift of the OBH during deployment and errors of the ship's GPS-navigation system the OBH-positioning may have a mislocation of up to several 100 m. As this error leads to an asymmetry and wrong traveltime information in the record section it has to be corrected, which is done with the program relobs. As input the assumed OBH-location, shot-locations and the picked traveltimes of the direct wave near to its apex are needed. By shifting the OBH-position relobs minimizes the deviation between computed and real traveltimes using a least mean square fitting algorithm assuming a constant water velocity.

5.2.3 THE GEOMAR OCEAN BOTTOM SEISMOMETER

(J. Bialas, K.-P. Steffen, E. Flueh)

The Ocean Bottom Seismometer (OBS) construction (Fig. 5.2.3.1) is based on the experiences with the GEOMAR OBH. It was built by *GTG*, Kiel, Germany. For system compatibility acoustic release, pressure tubes, and the hydrophone are identical to those used for the OBH. Syntactic foam was used as floatation again but of larger diameter due to the increased payload. Other than the OBH the OBS has three legs around its center post to which the anchor weight is attached. While the OBH is floating about 1 m above the sea bottom, the OBS touches the sea bottom to avoid collision of the the seismometer cable with the anchor. The sensible seismometer is deployed about 1 m to the side of the system once the sea floor is touched. During diving of the system the footplate of this seismometer release lever is about one meter below the base of the anchor and will therefore hit the seafloor at first. During touch down the baseplate forces an upward movement of the lever which

will lay out the seismometer hook until the seismometer anchor is about 0.5 m above the seafloor. At about 45 degrees to the vertical the seismometer is released from its hook and falls to the sea floor from about 1 m height. This should ensure the coupling of the seismometer to the sea floor. At this time the only connection from the seismometer to the instrument is a cable and an attached wire which will take the pull load while rising to the sea surface later. A movement or current on the instrument is thus not transmitted mechanically to the seismometer. All three channels are preamplified within the seismometer housing and recorded by the standard *Methusalem* recorder as used in the OBH units. Parallel to these three channels the standard hydrophone is recorded on the fourth channel.

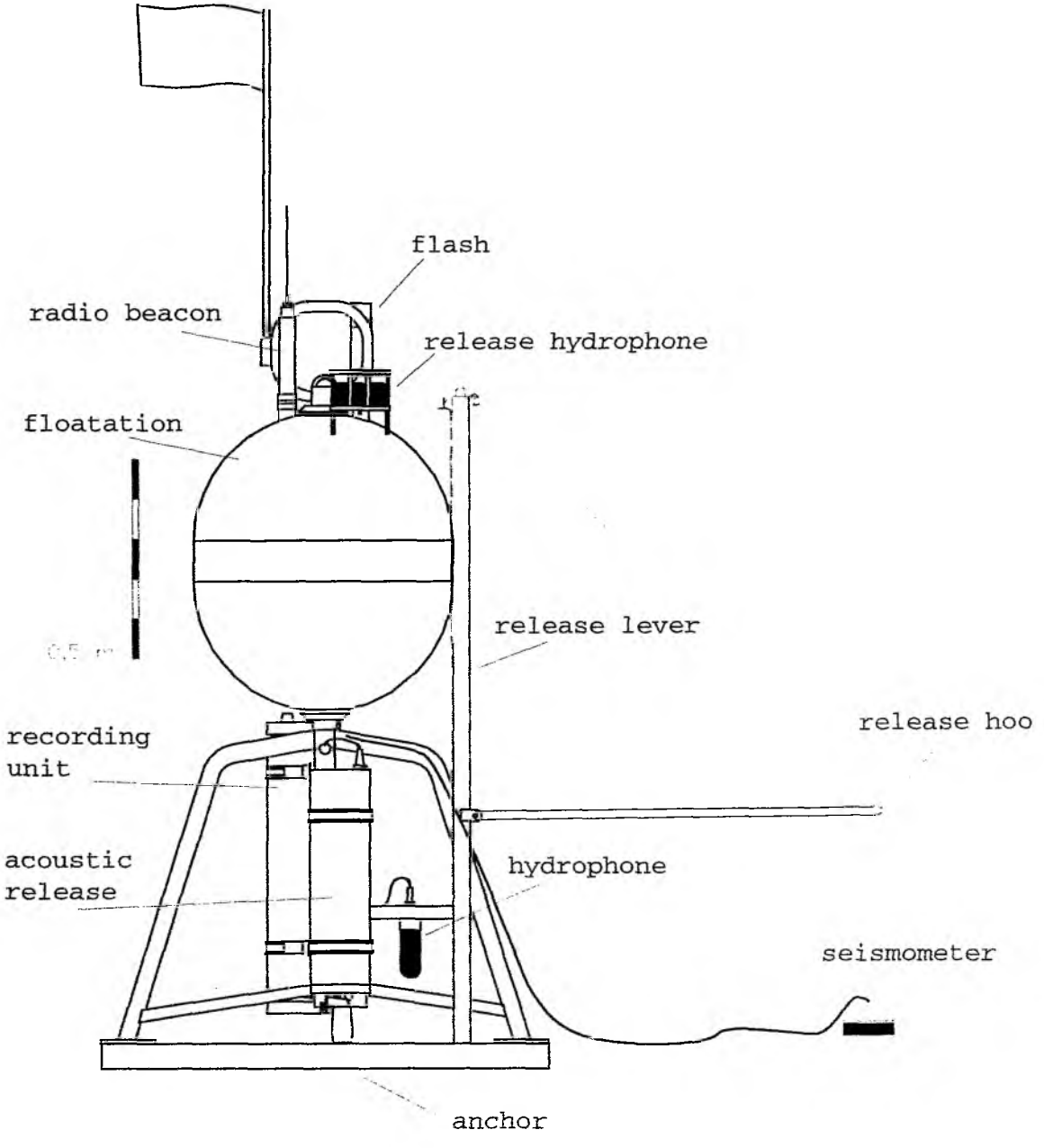

Figure 5.2.3.1: The GEOMAR Ocean Bottom Seismometer.

5.2.4 Vertical Arrays

(J. Bialas, K.-P. Steffen, E. Flueh)

During this cruise we operated two vertical arrays, one of which was used on earlier cruises before (Flueh and Fisher, 1996). That one is a 100 m long cable with four groups of AQ-1 hydrophones manufactured by *BENTHOS*. Each group contains ten hydrophones and a AQ-302 preamplifier. Bouyancy and electronic equipment is the same type as for the OBH system. As a reference, a standard *OAS* hydrophone is attached to the first channel. On previous cruises the array worked well and stacking of the single channels could improve the data quality. During cruise SO131 we encountered severe problems with the connector, which led to an increased signal-to-noise ratio on the array channels. Also, as noted before, the length of 100 m is too short to separate up and down propagating wave fronts.

This processing technique needs to be better adapted to the new array developed at GEOMAR. This array is a 1200 m long cable with 3 channels. An enlarged OBH type float with two disks is used at the top of the cable to carry the electronics pressure cylinder and the recovery aids. Below this, three consecutive 400 m long sections of cable are connected to the bottom where an acoustic release transponder carries the anchor weight. Major components were taken from the OBH system and therefore the individual channels are set up by one *OAS* hydrophone each. Every 400 m a small pressure tube acts as a connector between two cables. The tube houses batteries, a preamplifier, hydrophone and two cable connectors. Each case feeds its hydrophone connection into channel number one and shifts all other channels taken from the cable over by one. This system enables one to install the tube at any position and ensures that the closest hydrophone will always be channel one. Prior to the first deployment floatation tests of the equipment were performed. The first active deployment was done during the 3-D survey close to the NERO site. As the deployment operation takes 30 to 60 minutes, it was done using the large A-frame at the stern of RV SONNE. After deploying the top buoy, SONNE sailed slowly along the profile while the cable was pulled out to sea. This ensures that the system was deployed along the scheduled line although the exact inline position needed to be relocated after recovery. At the time of recovery the release transponder answered promptly and signaled that the anchor had been released. Nevertheless, during frequent ranging the distance readings remained consistantly close to the original water depth. As no sign of the top buoy was recognized at the surface, after half an hour it became clear that the ranging was valid and the system was stuck on the bottom. While sailing slowly across the deployment position the point of closest approach was noted. Later on, a dredge was used to recover the array. Due to the skillfulness of the ships crew this operation was a success.

Playback of the data showed clear signal arrivals for the standard hydrophone and the second channel of the array only. The first and third channel of the vertical array recorded static noise with a frequency of 11 Hz, the origin of which needs further investigation. A first inspection after recovery showed that all units were properly connected.

5.3 SEISMIC SOURCES

5.3.1 THE BGR AIRGUN ARRAY

(C. Reichert, J. Sievers)

The seismic signals were generated by a tuned set of 20 airguns (VLF, Prakla-Seismos) grouped in two identical linear sub-arrays 10 m apart on starboard and port side, respectively (Figure 5.3.1.1). The total volume of the BGR airgun array is 51.2 litres (3,124 cu.in.) filled by pressured air of some 135 bar (1,956 psi). Each sub-array consists of 3 groups each from stern to tail:

- 4 x 3.0 L + 2.5 L
- 2.5 L + 2.3 L + 2.0 L
- 2.3 L + 2.0 L

The total length of each sub-array is 19.6 m starting at 40 m behind the stern. The geometrical airgun centre is 50 m behind the stern and 116 m behind the positioning reference point (satellite antenna on the bearing deck). Three buoys per sub-array keep the airguns at 7 m water depth.

During profiles SO131-01 through -03 one VLF airgun on port-side with 3 L volume, 30 m from stern with air pressure of 130 bar (1,880 psi) was used.

Exact shot timing of the particular airguns is ensured by a microprocessor-controlled airgun-synchronisation unit type Prakla VZAD and VZAC2 with storage oscilloscope. The system start is externally triggered by a Meinberg clock GPS 166 during SONNE cruise SO-131.

The pressured air was provided by SONNE's LMF compressor, manufactured by Leobersdorfer, Austria, with a capacity of 25 cbm/minute. In case of malfunction an identical LMF alternate compressor is available. During profiles SO131-01 through -03 when only one airgun was used and lower capacity was sufficient pressured air was provided by the two available Junkers compressors. The air pressure was in the range 130-133 bar (1,884 - 1,928 psi) when 60 s or 30 s shot interval was applied. When a shot interval of 10 s was used the air pressure was ca. 127 bar (1,841 psi).

Quality control during airgun operation consisted of:

- continuous control of the airgun pressure;
- control of the airgun operation (autopops, misfires, delays) and sensor signal;
- duly maintenance of particular airgun assembly parts during off-times (e.g. gaskets, valves, connectors, umbilicals etc.).

With few exceptions all 20 airguns were properly working throughout the survey. In this regard there was no interruption at all. Because of wear and tear or overstress by bad weather, respectively, particular airguns or accessories failed before regular maintenance was due, and they had to be inactivated. The relative failure of airgun operation amounts some 4%, i.e. the ratio between the number of airguns in malfunction and the nominal number related to the number of shots. In other words, less than one airgun out of 20 was not operating, on average. This implies a total volume loss throughout the survey of also around 4%, i.e. on average 49.2 L were available (see also Appendix 9.1.2).

TIME REFERENCE

The Meinberg clock GPS 166 provides the absolute universal time corrected (UTC) from the GPS system. The minute and second pulses bear an accuracy of < 1 ms. 21 GPS satellites and 3 additional spare satellites are on orbit in 20,000 km altitude with a period of ca 12 h per cycle. This ensures that at least 4 satellites can be received at any time at any location in the world. By positioning with 4 satellites an automatic position dependent traveltime compensation is applied.

This time reference was fed into the shooting PC, into the mini-streamer recording system and into the PC that was used for calibration of the internal quartz clocks installed in the respective OBS/OBH systems. Thus, an identical time base was provided for all seismic systems.

VZAD AND VZAC

The VZAD unit controls synchronisation and triggering of up to 20 airguns. According to external trigger pulses a 20 ms TTL pulse is generated and sent to the VZAC unit. Here, it is transformed to 60 V and sent to the magnetic airgun valves. The valves do open and in the same instant a sensor sends the time break signal to the VZAD. The deviation between this response pulse and the target value (offset) is determined and used for correction of the trigger pulse sent to the airguns providing optimum synchronisation. This procedure automatically compensates for time delay produced by worn-out assembly parts of particular airguns in the course of operation.

SHOOTING PC AND PROGRAMME CODE

The so-called shooting PC keeps control on all systems. It is connected to the VZAD, to the positioning system and - in case of multi-channel seismics - to the recording system. The programme code TIMER22 used to run this PC is an upgrade of an earlier version TIMER21 by J. Adam (Sievers & Adam., 1997). The programme internally generates a series of suitable trigger signals for the VZAD with selectable intervals between 10.000 and 65.535 seconds on the PC quartz clock time base. Simultaneously, a random function can be superposed varying the interval within a range of $\pm$ 300 ms. In combination with multiple coverage seismics and related stacking this is used to suppress the multiple seafloor reflections from previous shots that disturb the current seismic reflection signals.

Alternatively, an external input (e.g. the Meinberg clock GPS 166) can be used. In this mode, TIMER22 generates a series of trigger signals on an absolute time base with selectable intervals between 10.000 and 65.535 seconds. The random function superposition option is inactive in this case. This mode was used for the operation during SO-131.

The trigger signals are sent to the VZAD that fires the airguns with a constant time delay of 73,8 ms due to electronic and mechanical components and returns a time break pulse to the shooting PC. During SO-131 the time break sent to the ministreamer recording system was taken from the sensor of airgun 20 incorporating the said time delay of 73.8 ms.

Simultaneously, via 9 serial RS232 interfaces different data are read and compiled. An 'external header' is generated and saved in a protocol file. The external header comprises the following information:

- shot no, status, GPS time, GPS date, PC date, PC time, actual time, nominal time, half random width
- error, GPS latitude, GPS longitude, course, speed, shot interval
- error, shot no, trigger mode, gun dalay average interval, gun offset
- gun no, status, offset, delay, error
- streamer data (n.a. on SO-131)
- error code, sign, starboard air pressure, label
- error code, sign, port air pressure, label
- error code, latitude, longitude, altitude (position corrected by BGR nav system)
- extension
- software version no

SHOT TRIGGERING DURING SO-131

The shots were triggered in time intervals of 60 seconds on full minute UTC, 30 seconds or 10 seconds, respectively. Thus, the ship's speed of 5 knots over ground yields a shot distance of 154 m, 77 m or 26 m, respectively. For instance, a shot interval of 10 s was used throughout the three profiles SO131-01 through -03 at the Indus fan. A complete documentation is given in Appendix 9.1.2.

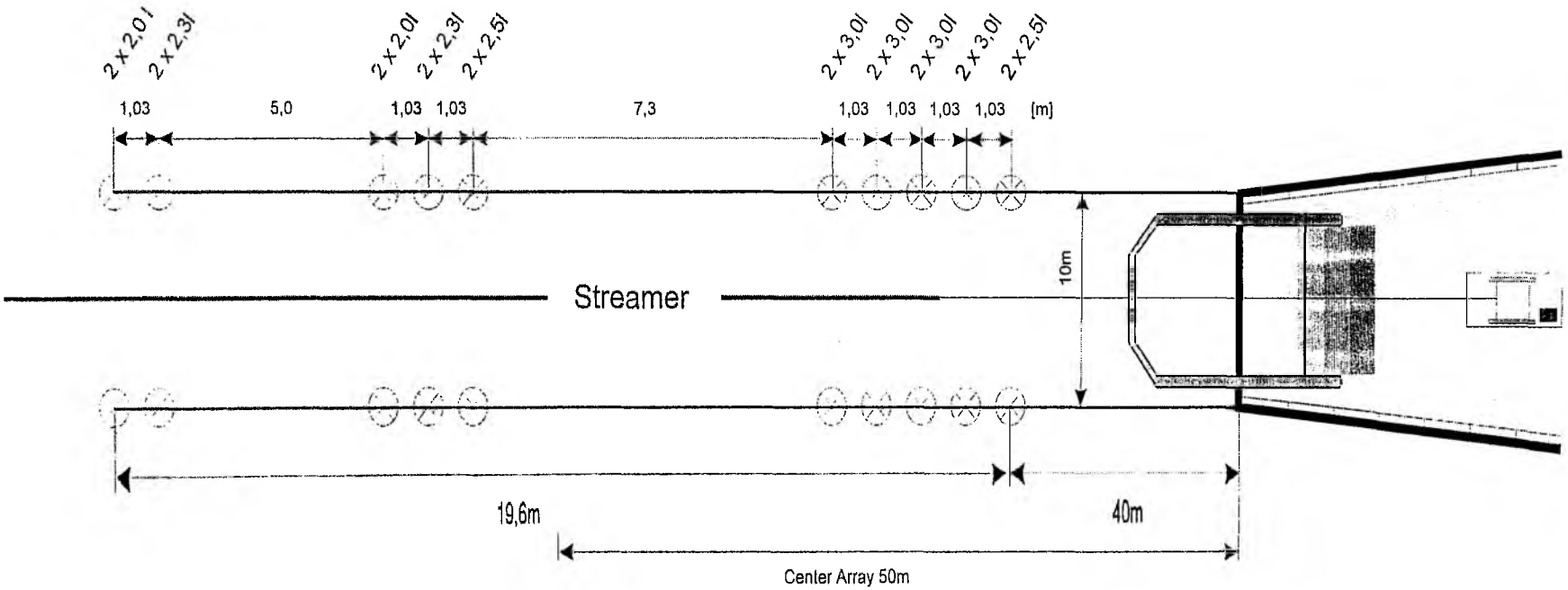

airgun numbering

1	2		3	4	5		6	7	8	9	10	port
11	12		13	14	15		16	17	18	19	20	starboard

Figure 5.3.1 - 1 : Geometry of the BGR airgun array.

5.3.2 THE GEOMAR HIGH RESOLUTION AIRGUN ARRAY

(J. Bialas, K.-P. Steffen)

After shooting the final line of the SINUS experiment the GEOMAR gun array was rigged up ffor initial test. It is comprized of four Prakla-Seismos (now Geco-Prakla) guns built in 1972. Two VLA type guns with 0.3 l volume each and two VLF type guns with 0.6 l and 2.0 l volume. These guns were formerly operated by the Bundesanstalt fuer Seeschiffahrt und Hydrographie (BSH) as single guns only. During transit to Singapore a first test for array operation and functionality was planned. Due to its volume, the array is intended to be used for future high resolution studies.

Carrying frames, separated by 1.5 m, were prepared to fit the SONNE's sliding frame prior to the cruise. As a first test the guns were lined up in order of increasing volume. Pressure pipes and trigger lines were prepared to tow the array about 30 m behind the stern of the vessel and due to the small size of the guns, it was decided to tow them at about 5 m depth. The working air pressure was 130 bar. The 26 year old fire box failed to shoot the guns. Therefore, the trigger lines were hooked onto the BGR shooting box (see chapter 5.3.1). After testing the valves and doing a few test shots onboard the array was ready for its first deployment.

5.3.3. SEEBOSEIS

(R. Herber, O. Exner, I. Grevemeyer)

5.3.3.1. Introduction

In the deep oceans, seismic refraction profiles using sonobuoys or ocean-bottom seismographs are inherently limited in their ability to detect and resolve the velocity structure at or near the seabed. The geometrical constraints of a thick water layer mask many arrivals that turn in the uppermost several hundered meters of the crust. To overcome this problem, Ewing and Purdy (1982) produced a method for determining seafloor velocities and velocity gradients consistent with the first refracted arrival time and apparent velocity of ocean-bottom seismograph or sonobuoy recordings. Nevertheless, in regions where the upper crustal layer is thin, energy propagating solely within the uppermost regions of the crust will be entirely masked by the water wave. Consequently, the technique introduced by Ewing and Purdy (1982) produces artificial velocities at the seafloor.

Seismic velocity determination of uppermost crust took a major leap forward when both the receiver and the source were placed close to the seafloor. Traditional near- or on-bottom seismic experiments utilize explosive charges as acoustical sources (Koelsch et al., 1986; Kirk et al., 1991), though heavy weights dropped onto the seafloor have also been used (Whitmarsh and Lilwall, 1982). Recently, scientists from the University of Hamburg developed a new experimental tool, called SEEBOSEIS, to carry out seismic measurements on the seafloor (Weigel et al., 1996). To generate seismic signals, implosive sources were placed close to the seabed. Each of the sources consisted of a 10 inch Benthos hollow glassphere with 3 g of explosive inside. The small explosive charge was used to destabilize the wall of the glassphere so that the ambient water pressure was able to smash it. A shooting cable connected the ocean-bottom recording systems with the shooting device. So the shot instant could be estimated to within a few milliseconds. First measurements in the Pacific Ocean indicate that the imploding glasspheres can produce strong delta-pulse like signals (Weigel et al., 1996; Essen et al., 1998), however, it turned out that deployment of the tool was a critical issue. In 1997 researchers from the Universities of Hamburg and Bremen joined forces to rebuild SEEBOSEIS. The new tool consists of separate ocean-bottom recording systems and implosive sources (see chapter 5.3.3.2.).

Near-bottom seismic experiments generally allow a determination of P-wave velocity, while S-wave velocity of unlithified and partially lithified marine sediments have been difficult to measure. However, the ability to locate a seismic source at the seafloor also permits the efficient generation of dispersed interface waves (or Scholte waves) that travel along the ocean floor like Rayleigh waves travel along the surface

of the Earth (e.g. Essen et al., 1981; 1998; Nolet and Dorman, 1996). The major goal of the on-bottom seismic experiment at ODP Site 575 on Ninetyeast Ridge was a test of the new SEEBOSEIS tool. A second objective, however, was to assess both the P-wave and S-wave velocities within the uppermost crust using refracted or diving waves and dispersed Scholte modes.

5.3.3.2. The Experimental Tool

The rebuilt SEEBOSEIS system consists of two separated components: the broadband ocean-bottom recording systems and the implosive sources. Both components are operated and controlled individually. The recording unit consists of three components: an audio dat-recorder, a crystal clock and a microprocessor for controlling the recorder.

The technical data of the unit are:

dynamic range:	90 dB
frequency range:	2 Hz - 15 kHz
channels:	2 OBH, 1 time-signal
	4 OBS, 1 time-signal
recording time:	6 h continuously
sensor:	hydrophone E2PD
	geophone 1 Hz Lennartz

The broadband ocean-bottom recording systems can be mounted on any carrier system. For the experiment on the Ninetyeast Ridge we used two pop-up OBHs supplied by Geomar (Flüh and Bialas, 1996) and a Hamburg-OBS (Herber et al., 1984). In general, any OBH or OBS could be used as the carrier or recording unit. However, the high bubble pulse frequency of bottom shots required recording systems with sampling rates of 500 to 1000 Hz or higher. In addition, bottom shots permit the generation of dispersed interface waves, and these wavetrains may have frequencies lower than 1 Hz (Essen et al., 1981; 1998; Nolet and Dorman, 1996). Therefore, broadband recording systems are recommended to sample the entire wave field radiated by bottom shots.

The implosive source used for SEEBOSEIS is attached inside a 10 inch Benthos hollow glassphere with penetrator. In the glassphere, two electrical detonators (about 1g explosives) were placed close to the glasswall. When ignited the detonators will destabilize the glassphere and it will be crushed by the ambient hydrostatic pressure. The shooting time is controlled by an external shooting device (Figure 5.3.3.2.1.). Unfortunately, no independent data or spectral behaviour of our source is available. The work of Essen et al. (1998), however, provides an initial assessment on the source signal. Their work (along with previous work cited by Essen et al., 1998) suggested that the time scale for the implosion is short enough to consider the source pulse a delta function for all practical purposes.

The frequencies generated by the implosive sources range from about 100 Hz up to several kHz. With increasing source depth, the emitted frequency radiated by the source will increase, i.e., the signal frequency is closely related to the source depth. However, measuremets in the Pacific Ocean have shown that imploding glasspheres permit the efficient generation of seismic waves. Moreover, the tests have shown that P-waves and guided waves can be recorded with commonly used hydrophones and/or geophones (Weigel et al., 1996; Essen et al 1997).

The shooting time itself is controlled by an electronic device, which has two main components: the compact electronic device and a high voltage power supply. The electronic device is built completly of HC-MOS technology for low power operation and high speed performance. It has four ports for:

- power supply
- high voltage power supply (photo flashlight)
- blasting caps
- syncroniation with a reference clock.

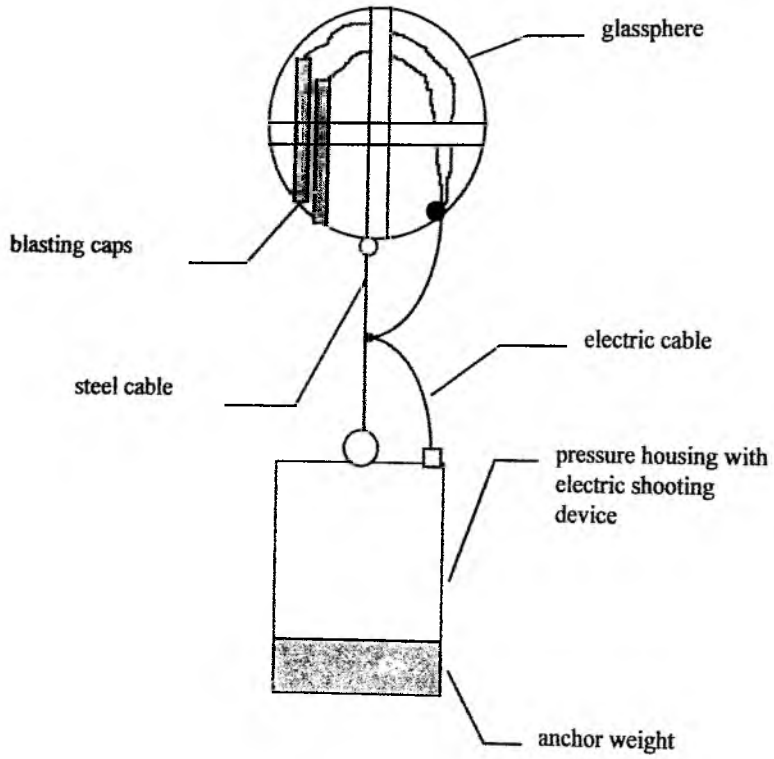

Figure 5.3.3.2.1.: Seismic source with pressure housing and anchor weight.

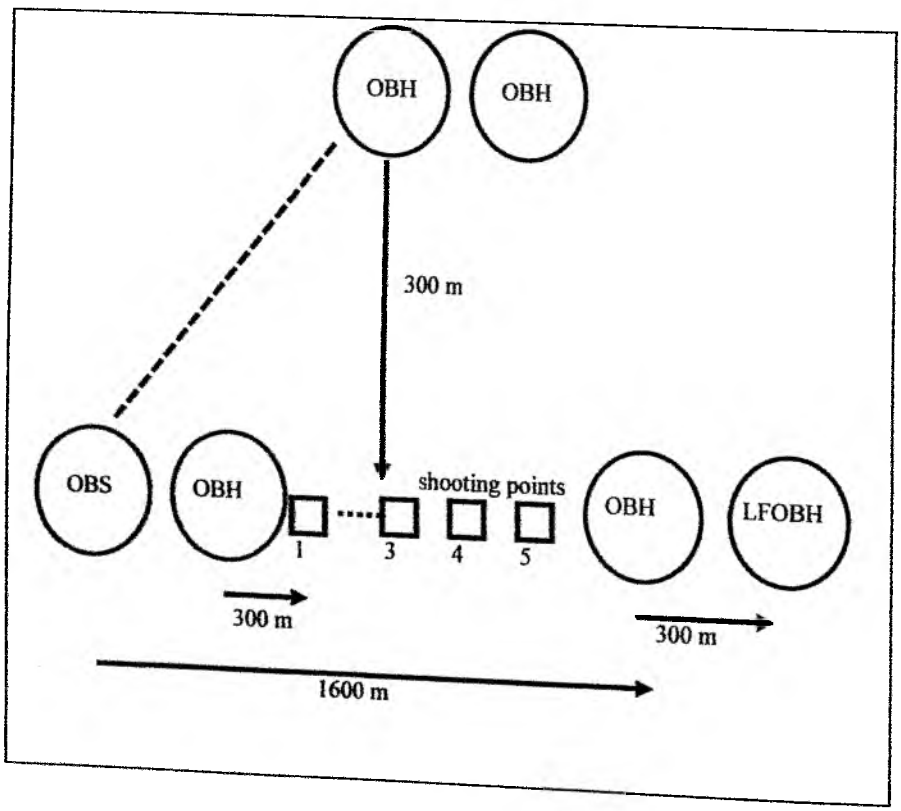

Figure 5.3.3.2.2.: Setup of the SEEBOSEIS - experiment.

The blasting caps require an ignition voltage above 100V DC. We chose a flashlight as a high voltage power supply. The power supply for the electronic device itself are two 9V block batteries which guaranty a minimum of 20 hours operating time. To get an exact starting time, the electronic device must be syncronisized with a reference clock (for example an DCF-signal). Two dipswitches allow the time until ignition to be set between 1 and 65535 seconds. After the countdown stops, a reedrelais switches the voltage from the flashlight to the blasting caps with a time delay of less than one millisecond. To minimize the time drift of the device, we use a programmable quartz oscillator with a frequency variation of f/f0 = 5 ppm. Each electronic device, however, will have a characteristic drift. To determine the drift, we run the devices under temperature conditions of 4°C (i.e. temperature at the seafloor) and 20°C. Condsidering the drift function we can determine the shooting event within about 10 ms.

For the experiment we received 10 blasting caps from D/V JOIDES RESOLUTION, which we used to prepare five glasspheres. Figure 5.3.3.2.2 shows the experimental setup. In addition to the three broadband recording units described above, we deployed two MBS-OBHs and one MBS-OBS supplied and operated by Geomar. The sampling rates of the instruments were 500 Hz, 62 Hz and 1000 Hz, respectively. Four recording systems and the implosive sources were deployed along a ca. 2 km long profile to provide a reversed seismic refraction experiment. Two instruments were placed about 300 m off-line and will be used along with the other systems for an acoustic triangulation to determine the position of the bottom shots. To place constraints on the seafloor position of the receivers the profile was shot with 3 airguns from the BGR array (see also Appendix 9.1.3). Additionally, the shots were recorded by the 3-channel streamer and Parasound was used to image the uppermost sediment cover. Results of the experiment are described in section 6.3.4.2.

5.4 MAGNETOMETER

(J. Bialas)

During cruise SO131 we used a geoMetrics G801/3 Marine Proton Magnetometer which was formerly operated by the Bundesanstalt für Geowissenschaften (BGR), Hannover. This unit comprises a gasoline filled sensor with 350 m marine cable and a control unit. On board RV SONNE the winch was placed on the port side back deck and the sensor was towed to the port side of the vessel. A boom leads the cable some 7 m aside the ship in order to prevent it from being tangled with other equipment (airguns) towed behind the stern of the ship. The measured values of the total intensity magnetic field were displayed at the console and provided as digital output coded in BCD values.

Two software codes logging the magnetometer values were available, one of which also reads the time and coordinates from a GPS unit. Unfortunately this routine failed during the cruise. Therefore, the PC internal clock was set manually to UTC time with an accuracy of 1 s and an alternate software was used to store the magnetic data with a time stamp only. During routine checks the watch-standers discovered that the program did not operate without errors. At the top of the hour the system would hang-up and a restart of the program was necessary. However, this occured not every hour but at unpredictable intervals, so the causing error was not determined during the cruise. Comparison of the system parameters to those from the originally developed unit showed that at the DOS Version on the PC was older than the one used for development, and may have influenced the stability of the code, as some system calls were used. Knowing this, the watch-standers checked the unit at least every hour and could restart the recording within a few minutes if the program hung. After data backup the files were transferred to the sun workstations. Coordinates were then assigned to each magnetic stamp on the basis of the recorded time and displayed using GMT plot routines.

5.5 SHIPBOARD EQUIPMENT

(W. Weinrebe)

5.5.1 HYDROSWEEP

For continuous bathymetric profiling the HYDROSWEEP multibeam system from ATLAS-ELEKTRONIK is available onboard RV SONNE. Using a frequency of 15.5 kHz and 59 beams in a swath of 90° it can map the seafloor with a scanline width up to twice the waterdepth. Range of the central beam is up to 10,000 m with an error of 1% and for the outer beams up to 7,000 m with a precision of about 1% if roll is less than 10° and pitch less than 5°. Corrections for roll, pitch, and heave are automatically applied. Due to the fixed angle between beams, resolution is dependent upon the waterdepth and varies from about 170 m to 200 m in waterdepths of 5,000 m to 6,000 m.

To calculate depths from echo time delays the velocity of sound in the different waterlayers is required. HYDROSWEEP uses a second set of transducers and a calibration scheme with soundings alongtrack to determine an average water sound velocity profile (Schreiber und Schencke, 1990),. Yet in certain areas this algorithm fails (c.f. Flueh and von Huene, 1994). So for better results, direct measurement of sound velocity at different depths using a CTD is required.

Postprocessing of HYDROSWEEP data comprises the merging of navigational data, the calculation of depth and positions of the footprints of the beams, removing artifacts and erreoneous datapoints, and generation of a digital terrain model (DTM). The ATLAS HYDROMAP software, based on the CARIS software package, is available onboard for that purpose. However, for several reasons outlined in Flueh and von Huene (1994) and Weinrebe (1997), the academic software MB-System (Caress and Chayes, 1996) from Lamont-Doherty Earth Observatory is used for HYDROSWEEP data processing.

5.5.2 Parasound

For the geological mapping of the uppermost sedimentary layer the parametric echosounder PARASOUND from ATLAS ELEKTRONIK is available onboard R/V SONNE. This system uses a parametric signal generated by the superposition of two, slightly offset, high frequencies to gain deeper penetration and higher resolution compared to that of ordinary echosounders. One signal is generated with a fixed frequency of 18 kHz, the other can be set to values between 20.5 kHz and 23.5 kHz (at 0.5 kHz increments), thus yielding a parametric signal of 2.5 kHz to 5.5 kHz with a (narrow) beam angle of about 4°. The footprint of a beam ensonifies an area of approximately 7% the waterdepth. Due to the narrow beam, no echos from the seabottom or sedimentary layers will reach the receiver if the seafloor is inclined more than 2°, restricting the application of PARASOUND to relatively flat areas.

5.5.3 NAVIGATION

A crucial prerequisite for all kinds of marine surveys is the precise knowledge of position information (latitude, longitude, altitude above/below a reference level). Since 1993 the global positioning system (GPS) is commercially available and widely used for marine surveys. It operates 24 satellites in synchronous orbits, thus at least 3 satellites are visible anywhere at any moment (Seeber, 1996). The full precision of this originally military service yields positioning accuracies of a few meters, yet this is restricted to military forces and usually unaccesible to commercial users (Blondel and Murton, 1997). For civilian purposes the precision is in the order of 100 meters.

The resolution of GPS can be enhanced with the Differential GPS (D-GPS) scheme (Blondel and Murton, 1997, Knickmeyer, 1996). Using several reference

stations the determination of the ship's position can be corrected in real time and enhanced to a 1 m to 5 m accuracy. Since the cruise SO-109 (1996) D-GPS service is available onboard R/V SONNE. The ASHTEC system gains a validated accuracy of approximately 5 m in the area of the SINUS investigations. However, due to the great distances to reference stations (Singapore, Jakarta, Perth) the radio-transmission of the reference signals is occasionally interrupted for several seconds and the position determination fail. These missing positions are then calculated by interpolation.

Operation on the 3D survey and future tomographic interpretation depends strongly on such an accuracy. Therefore all lines of the 3D area were plotted at a scale that displays each shot as a single point. By careful reading of these maps several minor steps within the plotted ships track were detected. It was known from earlier 3D surveys (CONDOR, off Chile; PACOMAR, off Costa Rica) that such offsets will result into a poor resolution during traveltime inversions. Therefore it was decided to smooth these steps by a projection procedure. For this purpose the project routine of the General Mapping Tool (GMT) software package (Wessel and Smith, 1991) was used. A window with a width of five shots was moved along each profile with an overlap of one shot. This procedure calculates a straight line between first and last shot of the window, where all other positions are projected on. The width of five shots proofed to smooth the observed unconsistencies not only on straight profiles but on the two circles as well.

5.6 Two-Ship Communication

(E. Haase)

5.6.1 Ranging System

For the ship-to-ship experiment a microwave ranging system was employed to achieve precise distance measurements between the vessels. The sytems used onboard the RV SONNE and the JOIDES RESOLUTION were the Trisponder 540 Ranging System manufactured by Del Norte Technology, Inc. of Euless, Texas U.S.A..

The Trisponder 540 System generates a 1000 Watt pulse near 9 GHz and has a maximum range of 80 km. The Distance Measuring Unit, data recording device and master microwave transponder were operated onboard the SONNE utilizing an omni-directional wave guide with a 30° vertical angle. While the remote transponder operated onboard the RESOLUTION used a directional wave guide with a horizontal beam angle of 87°, vertical angle 5°.

The principle of the ranging system requires radio transceivers to be carried aboard each ship, one acting as the master unit and other the remote unit. The master unit transmits a microwave pulse that travels in direct line to the remote unit which, upon receiving the signal, transmits a response pulse back to the master unit. When the master unit receives the return pulse it calculates the two-way travel time, adds delay corrections and determines a range between the transceivers.

Every 2 seconds the master unit on the SONNE interrogated the remote unit on the RESOLUTION for a range. Initial contact was achieved at a distance of over 72 km, but successful readings were sporadic. As the 2 ships converged ranging improved gradually until, at approximately 35 km, the readings were continuous and consistent. This effect may have been due to the types of wave guides used, signal shadowing from the masts of the ships, and/or weather conditions which sometimes caused excessive roll and pitch.

The range measurements are used in a series of calculations to find the distance of each shot point from the airgun array towed by the SONNE to the ocean bottom seismometers (OBS) deployed in the area beneath the RESOLUTION. To make these calculations several parameters must be known: the most important and the one with the greatest margin of error are the ship-to-ship range values. The parameters for the SONNE include distance behind the stern the airgun array is

towed, depths of the airgun array, position of the master transceiver relative to the stern, plus heading, course and speed-over-ground. Parameters for the Resolution include the heading, position of the remote transceiver relative to the port where the drilling string passes through the ship, azimuth and distance of the ship away from the borehole, azimuth and distance of the OBS relative to the borehole, and water depth.

The parameters are used to solve a series of triangulations which calculate a vector from the geometric center of the airgun array to the OBS stations. The resultant data assists in determining seismic velocities by knowing the precise distance between each shot point and OBS.

5.6.2 Data Transmission

As an alternative to costly satellite transmissions, a wireless Local Area Network (LAN) was established between the RV SONNE and the JOIDES RESOLUTION to transfer data files. The equipment on both vessels utilized PCs equiped with wireless ethernet cards manufactured by NCR Corporation. The PCs were connected to all-weather Cushcraft S8964B antennas mounted in prominent positions on the upper decks.

The wireless LAN equipment was originally intended for indoor use and broadcasts a signal of 0.5 Watts through a desktop antenna. Modifications were made so that larger outdoor antennas could be mounted and make the system suitable for use in a marine environment. Both 486 PCs were DOS based with WAVELAN software version 1.01 installed. The antennas were 107 cm conical omni-directional units and transmitted in a spread spectrum of 896 to 960 MHz.

Weather conditions seemed to dictate the range at which a link could be achieved. In good weather initial contact was made at over 5 km. Contact in fair conditions was achieved around 3 km, and in poor weather, under 2 km. Once linked, communication was maintained without interuption until some threshold distance was reached and contact was lost completely.

Both ASCII and binary formats transferred flawlessly in FTP mode. These included text files, image files and GPS data. Excellent examples are Figures 5.6.2.1, 5.6.2.2, and 5.6.2.3. These three images of the SONNE were taken with a digital camera from the RESOLUTION and transferred by the wireless LAN as a single compressed file over 1.43 Mbytes in size. The file was subsequently decompressed and the three color JPEG files printed. Close examination of the large scale images reveals no missing pixels or distortions. As well, no other files FTP'd via the wireless LAN experienced any data corruption. A file being transferred when contact was lost was simply truncated and needed to be transferred again when the ships moved back into range.

A requirement of this arrangement is that one PC has to be set to server mode so the other PC may access it. The PC on the RESOLUTION was the dedicated server and the PC on the SONNE was able to transfer files whenever the conditions permitted. This set-up proved to be a simple, reliable and inexpensive method to transfer data between ships.

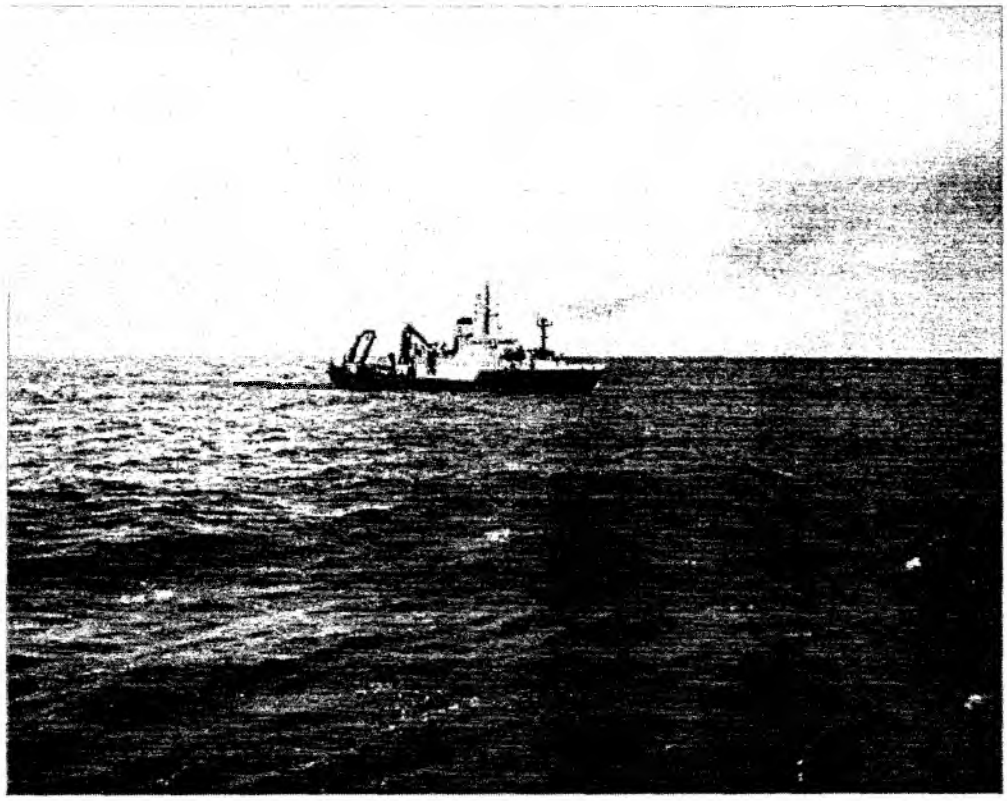

Figure 5.6.2.1: Images (1-3) of the RV SONNE transferred by wireless LAN.

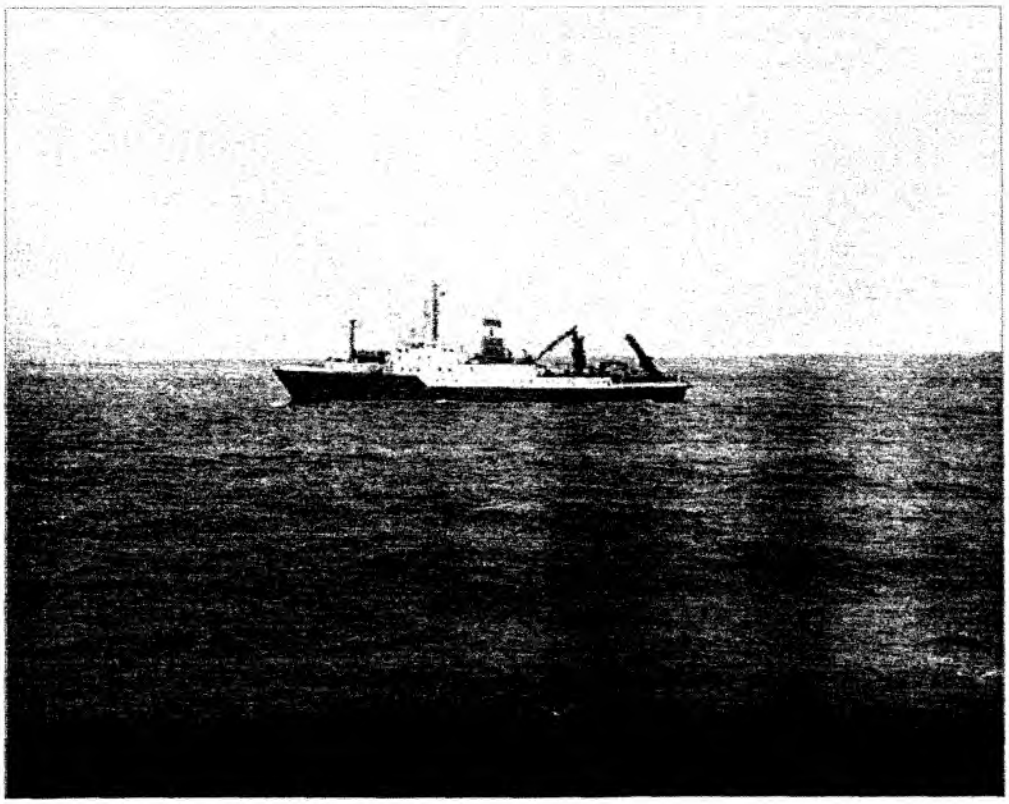

Figure 5.6.2.2

Photocredits: anonymous crew member of the JOIDES RESOLUTION

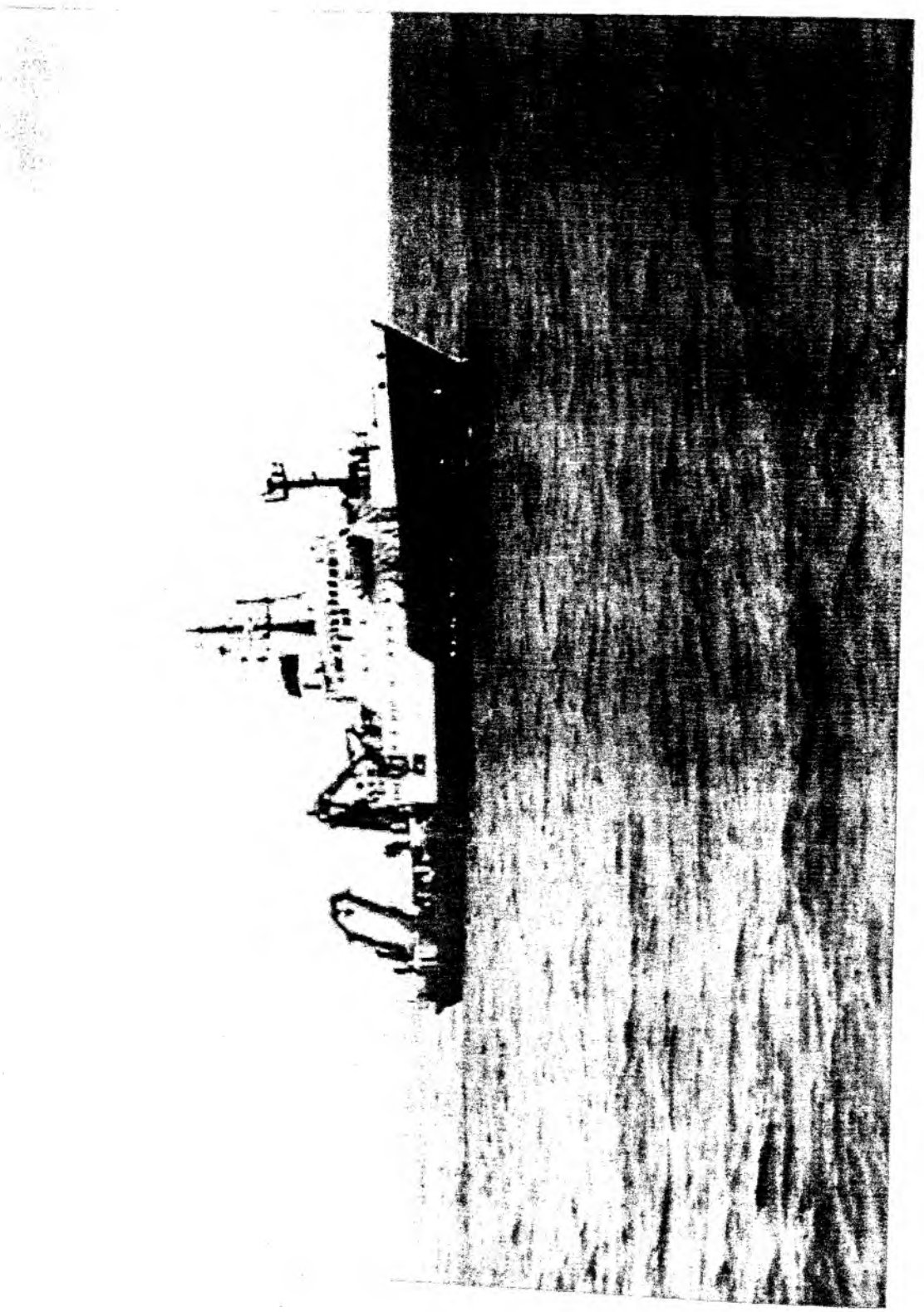

Figure 5.6.2.3

6 WORK COMPLETED AND FIRST RESULTS

6.1 HYDROSWEEP

(W. Weinrebe)

Data from the HYDROSWEEP system were continuously recorded during the whole cruise after leaving the Indian EEZ and until reaching Australian waters near Cocos-(Keeling-) Islands. In total in 740 hours a number of 216026 swaths, i.e. 12745534 beams were recorded. Due to long periods with bad weather conditions data quality was often very poor, there were even periods with no HYDROSWEEP data at all. On average, the amount of usable beams were around 70%, whereas in good weather conditions a rate of more than 90% can be achieved.

The HYDROSWEEP data were processed onboard using the MB-System software developed at Lamont-Doherty Earth Observatory (Caress and Chayes, 1996). A water velocity profile was measured with a CTD at position 16°59.42' S and 86°39.72' E on may, 17, 1998 (Figure 6.1.1). Using this velocity function raw HYDROSWEEP echo time data were converted to depth by complete ray tracing through the different water layers. A second CTD was run later further to the east. The results are rather similar, as can be seen from Figure 6.1.2. Sweeps including all 59 beams were then displayed in profile on a screen and edited to eliminate erratic points. Edited sweeps were then assembled, gridded, and contoured with the GMT software (Wessel and Smith, 1991). No filters were applied to smooth the edited data, thus more small tectonic features, but also more noise, are visible in the maps. However, the viewer can distinguish between small tectonic features and map artifacts.

Only in the areas of the Ninetyeast Ridge Escarpment and the Ninetyeast Fracture Zone a dedicated HYDROSWEEP survey was performed, whereas in the other areas bathymetric mapping was done while seismic profiling, so no complete area coverage but a bundle of tracks were surveyed (Figure 6.3.1). However, at the site of the seismic 3-D survey (NERO site) the number of tracks were sufficient to yield a nearly complete coverage of the area. For these three areas HYDROSWEEP data were processed to generate contour maps of waterdepth and perspective images of the morphology.

THE NERO SITE

An area approcimately 50 km by 50 km was mapped around ODP site 757, the NERO site. The site is situated on top of a small hill with a summit in a waterdepth of 1640 m and a height above the surrounding seafloor of about 300 m (Figures 6.1.3 and 6.1.4). The mountain has an elliptic shape with a long axe about 30 km in length in southwest-northeast direction and a short axe of around 20 km. The the northeast the hill continues into a small ridge with steep slopes, like a panhandle. Whereas the north, west, and south sides of the hill have a gentle slope, the eastern side shows two steep cliffs with heights around 40 m, and a terrace about 2 km wide in between. Several generally east trending canyons are cut in these cliffs. Very peculiar features are several steep piles or needles found particularly in the eastern flank, which were first believed to be erreoneous data points in the HYDROSWEEP data, however, they showed up in several different tracks at identical locations. These peaks with a height up to 180 m and a diameter of approximately 200 m to 300 m were investigated with a dedicated seismic profile and are discussed seperately in 6.3.4.9.

THE NINETYEAST RIDGE ESCARPMENT

The eastern flank of the Ninetyeast Ridge is built by a steep escarpment, the Ninetyeast Ridge Escarpment. A section of this escarpment approximately 80 km by 30 km wide was mapped with the HYDROSWEEP system and extended the surveyed area along profiles p05 and p06. A contour map of the area is shown in Figure 6.1.5, and Figure 6.1.6 displays the area in a perspective, illuminated

image. The north-south trending escarpment is extremely steep with a height of more than 2,000 m. An area about 10 km wide adjacent to the base is essentially flat. The east side of this stripe is bounded by a series of elongated hills with heights of about 700 m, arranged in an en-echelon shape and trending northeast-southwest. A second and a third series of similar but smaller hills are following to the east, resulting from lateral north-south movement along the escarpment. In the southern part, the escarpment is divided by a terrace up to 3 km wide in two parts.

THE NINETYEAST FRACTURE ZONE

At the eastern end of the transect over the Ninetyeast Ridge an L-shaped area about 100 km long and 30 km wide was surveyed with HYDROSWEEP. A contour map is shown in Figure 6.1.7 and a perspective, illuminated image in Figure 6.1.8. Though the fracture zone was not mapped totally the gross structure is clearly visible in the figures. The area is characterized by three sawtooth-like, north-south trending cliffs with steep slopes to the west and moderate slopes to the east. The summit height of these ridges evidently increases from west to east. The westernmost is not very well expressed and shows heights of about 200 m, whereas the other ones are about 800 m to 1,000 m high. These structures were obviously built up by compression in east-west direction. Another peculiar feature are several small elongated ridges trending east-west with lengths up to 20 km. These are found particularly east of the fracture zone.

6.2 PARASOUND

PARASOUND data were collected during the HYDROSWEEP and magnetic surveys and along all seismic lines. In flat areas a penetration up to 100 m into the uppermost sedimentary layers were achieved. Data was recorded on paper plots as well as on tapes with the PARADIGMA system. Processing and interpretation of the data was not attempted onboard.

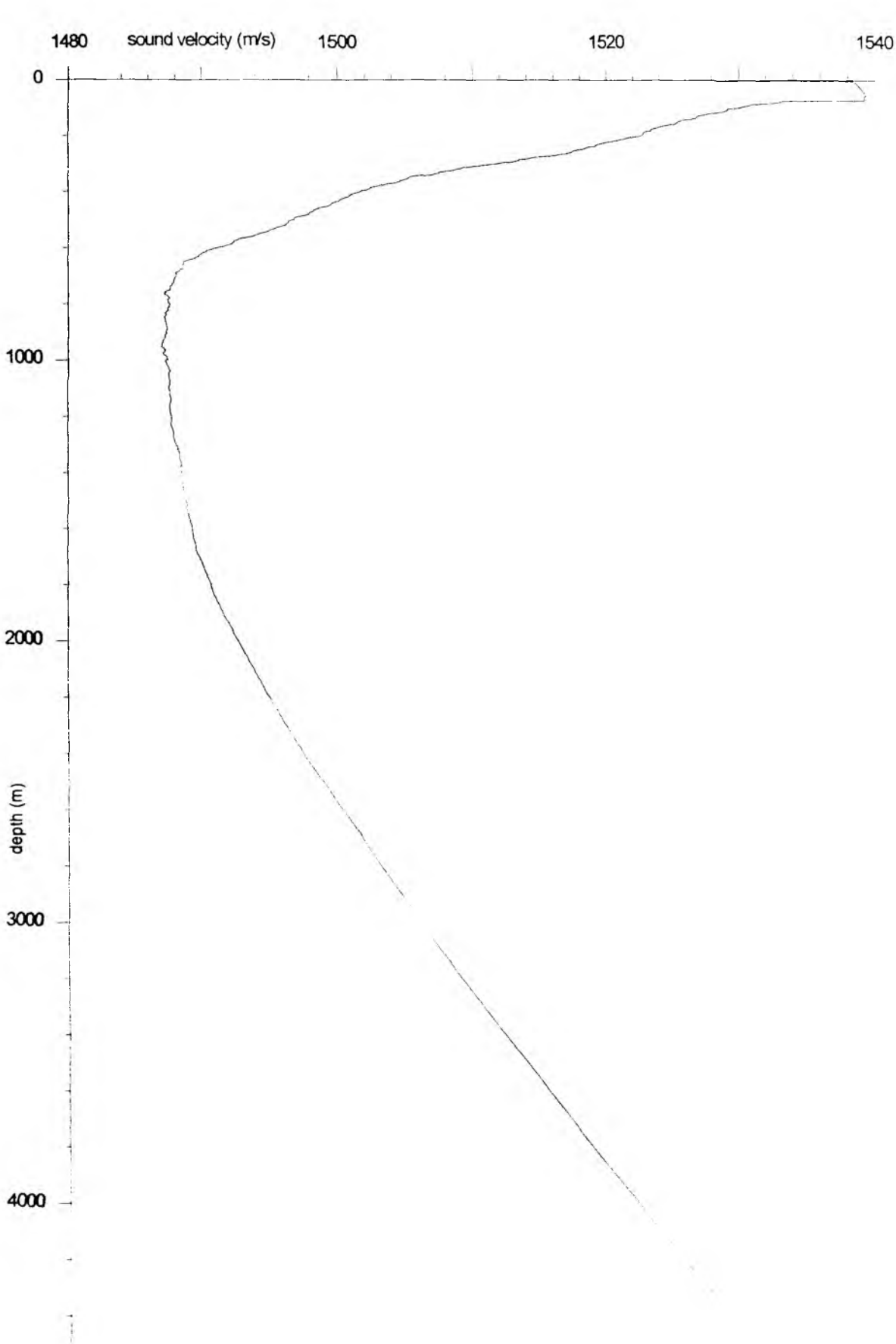

Fig. 6.1.1: Water velocity profile at position CTD-01.

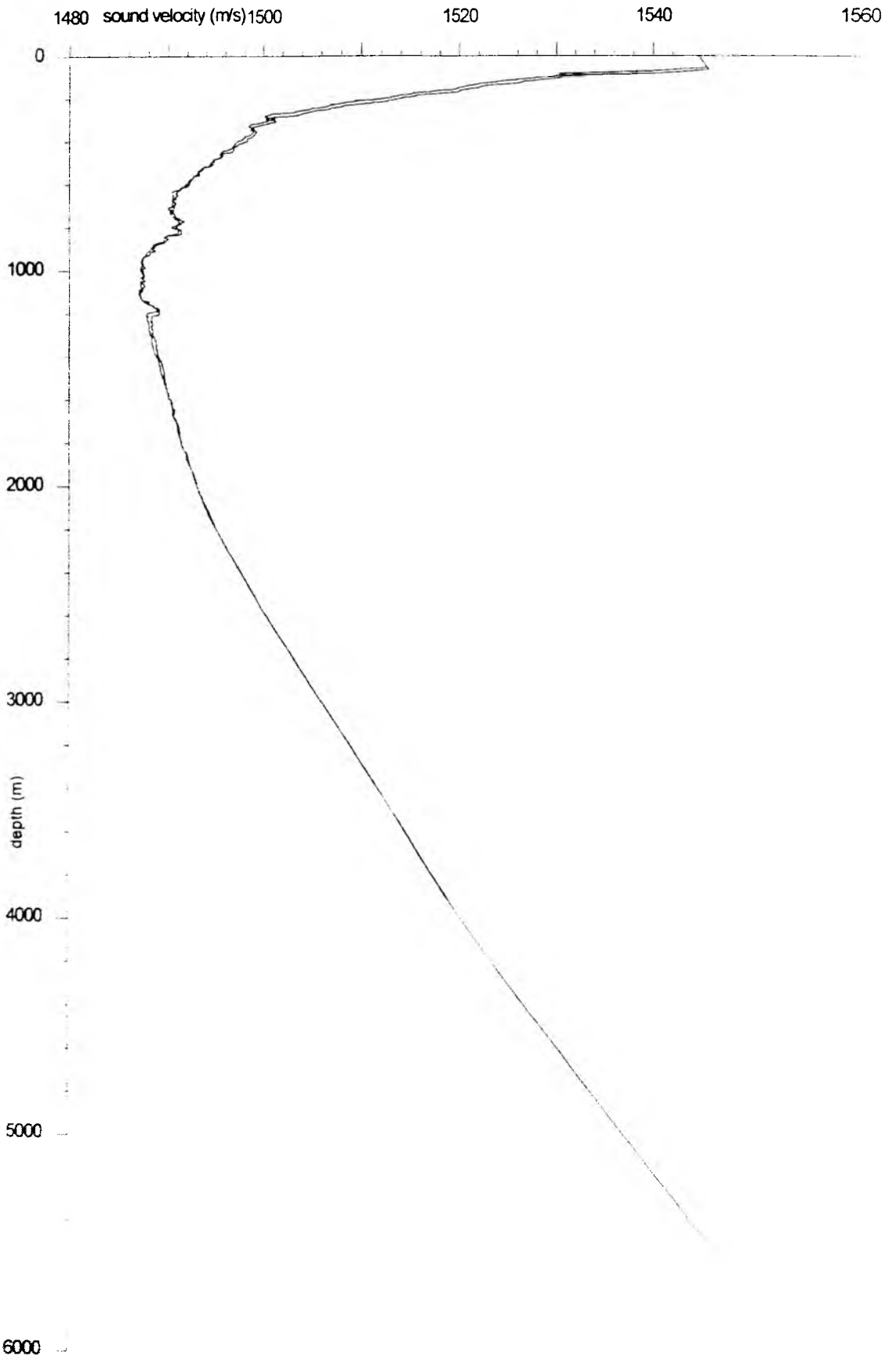

Fig. 6.1.2: Water velocity profile at position CTD-02.

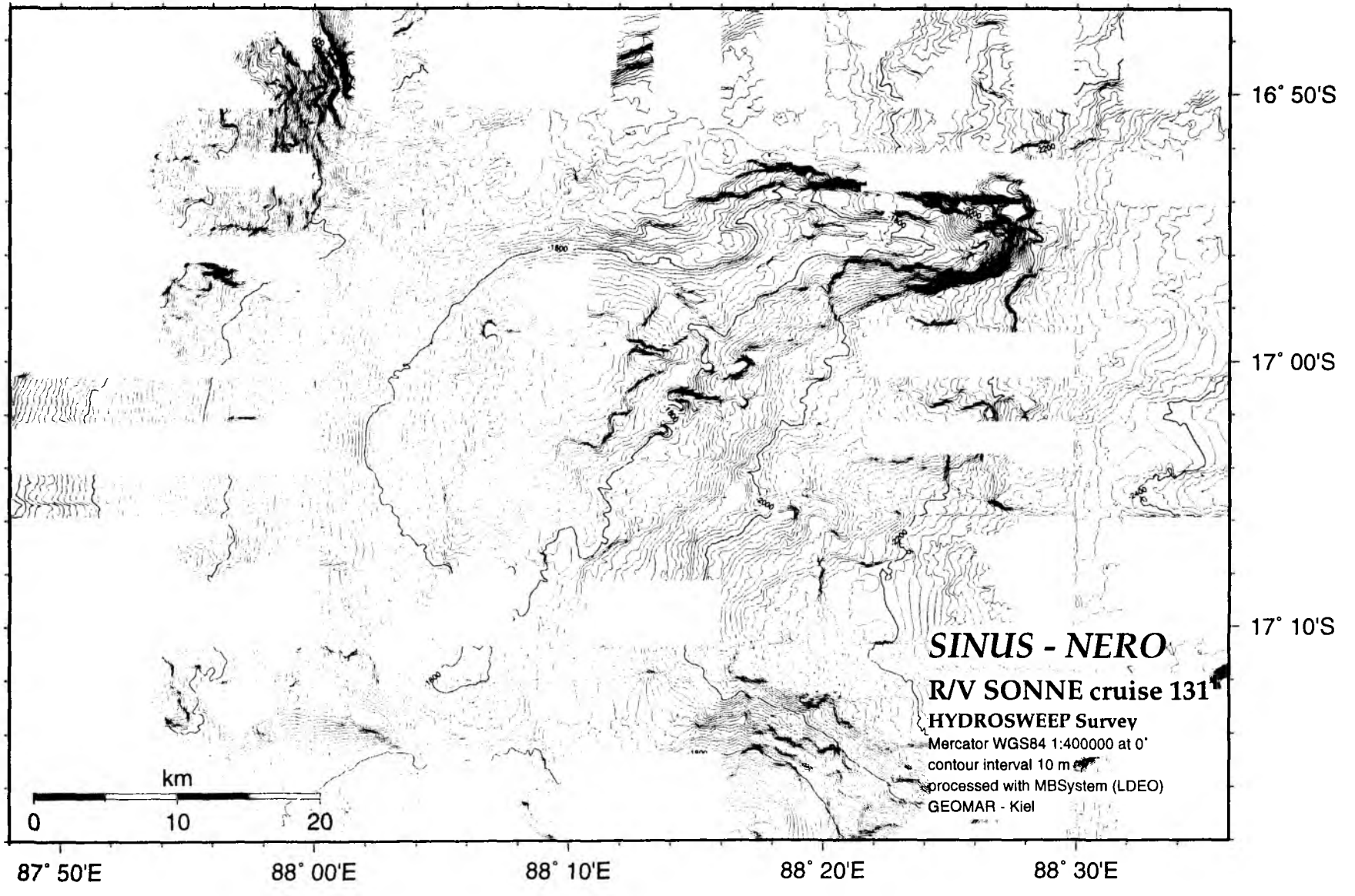

Fig. 6.1.3: Bathymetric map of NERO site.

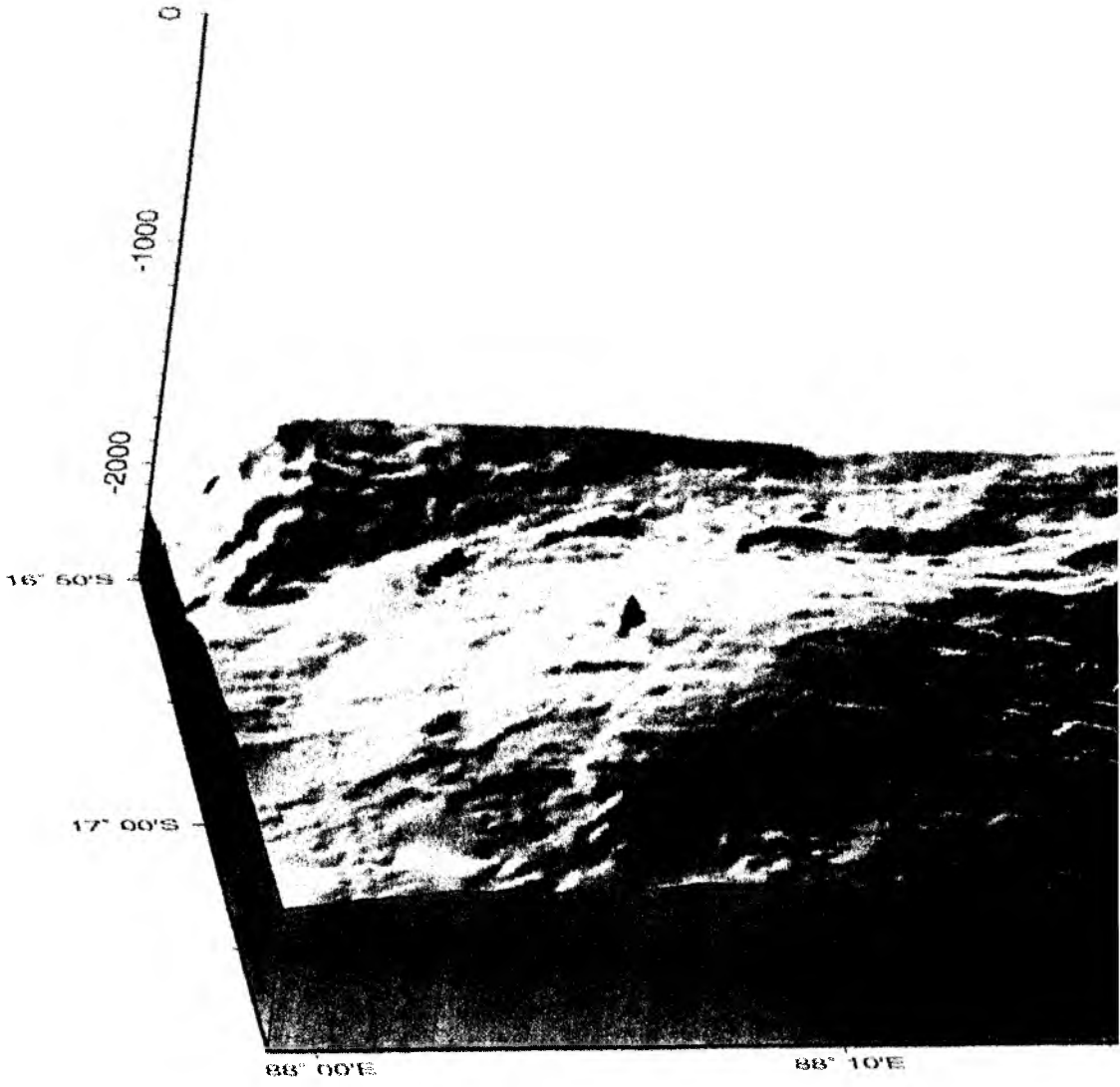

Fig. 6.1.4: Perspective image of NERO area. View from south, illumination f

rom northwest.

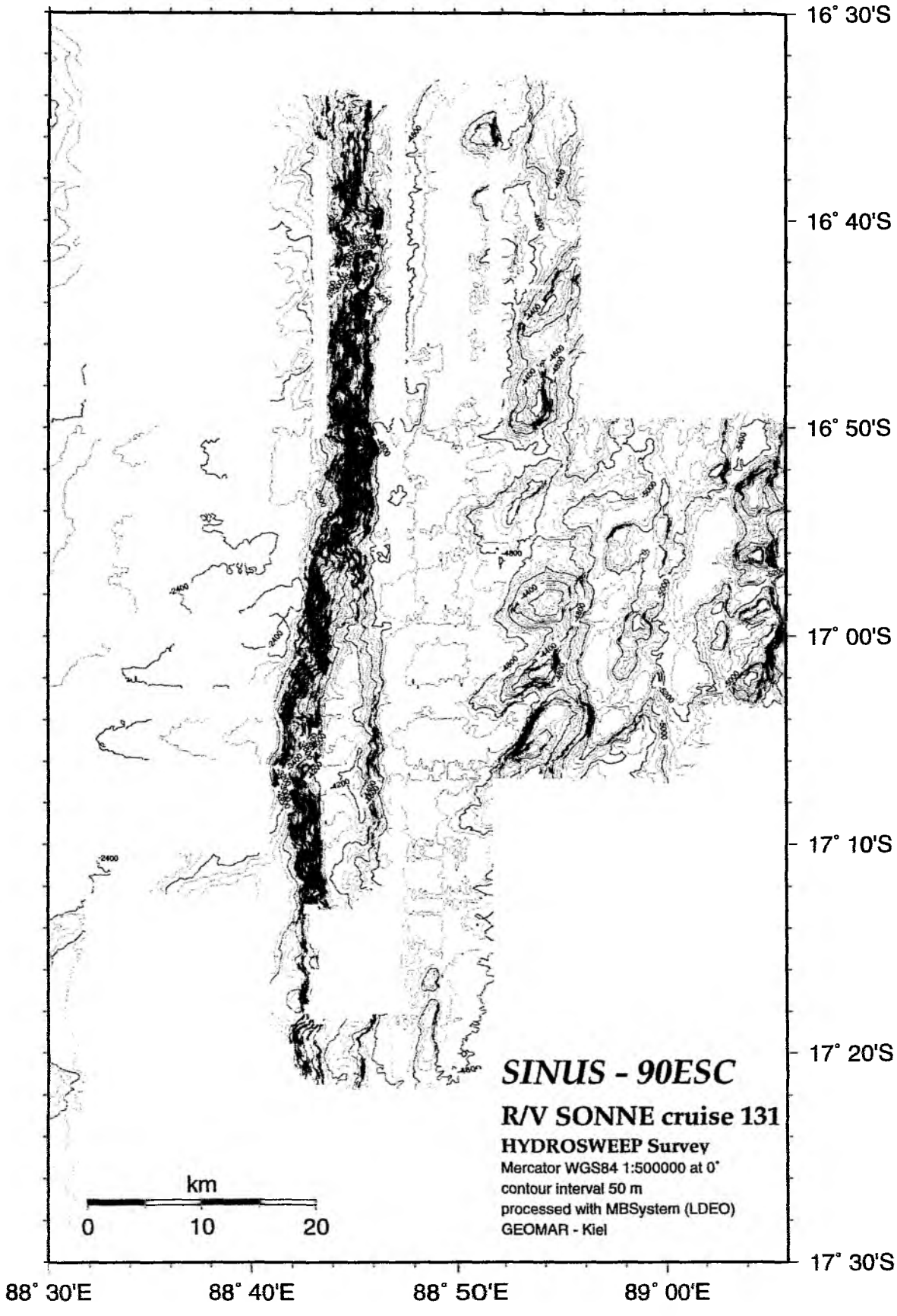

Fig. 6.1.5: Bathymetry of the Ninetyeast Ridge Escarpment.

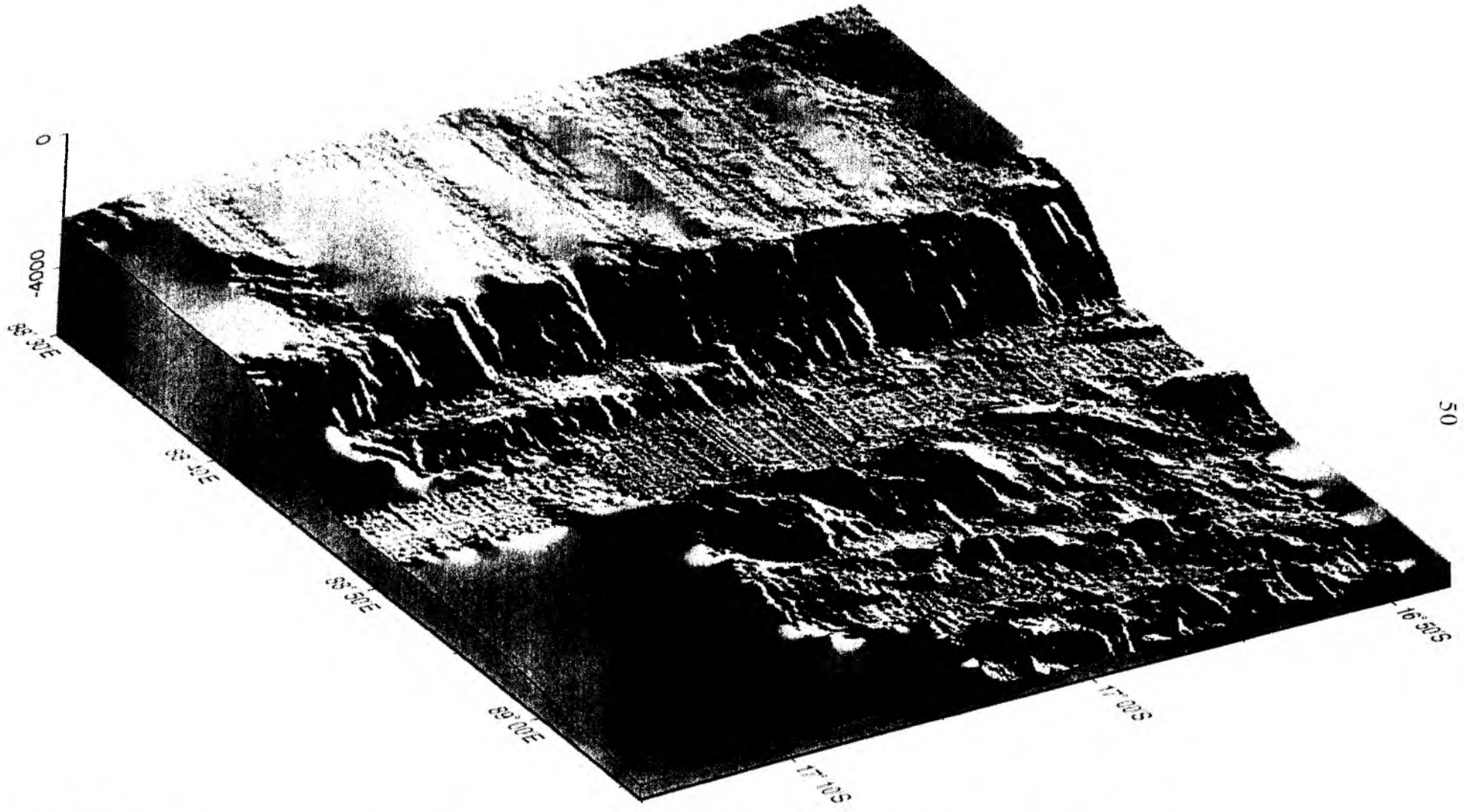

Fig. 6.1.6: Perspective image of Ninetyeast Ridge Escarpment. View from southeast, illumination from northwest.

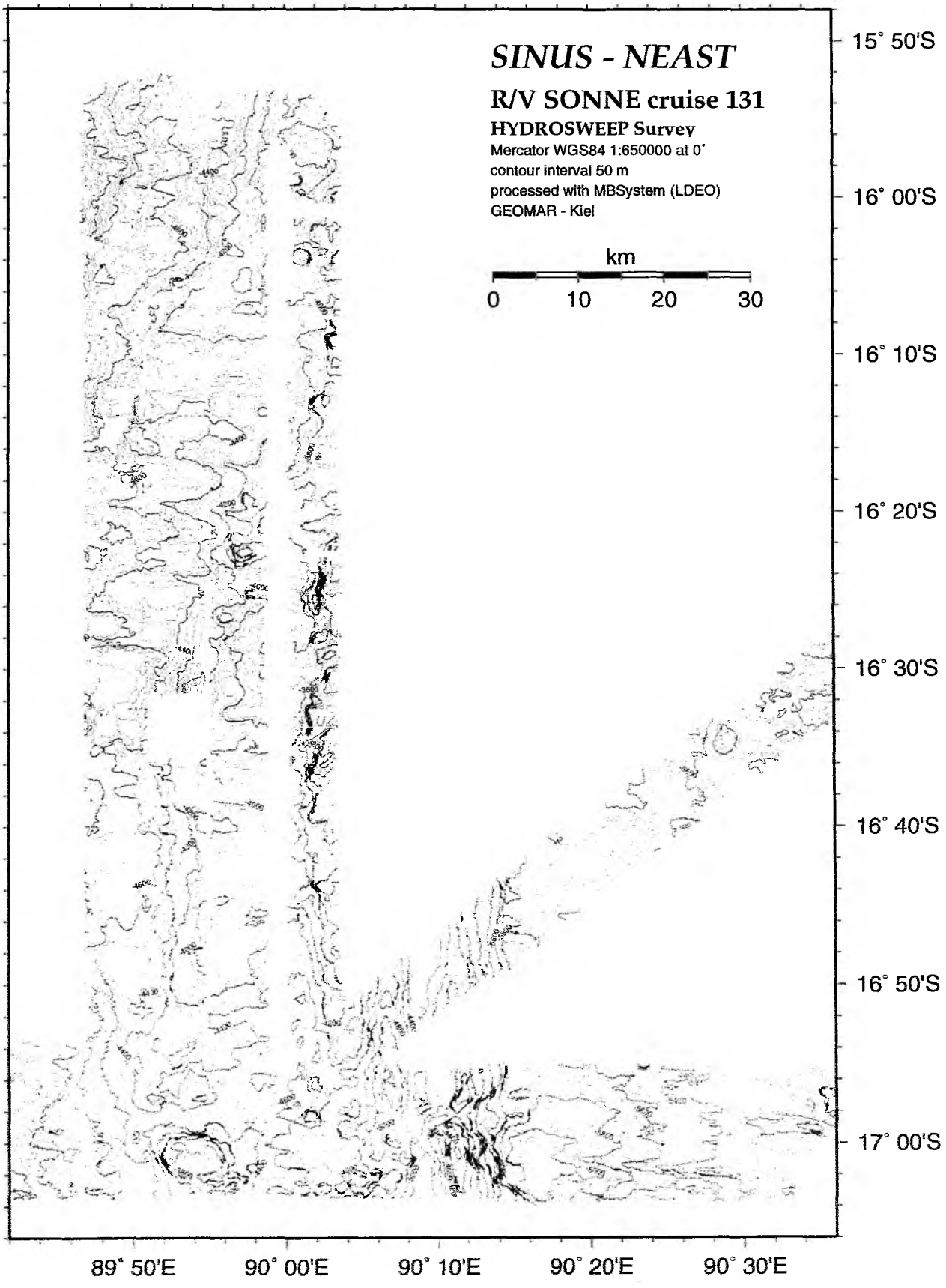

Fig. 6.1.7: Bathymetry of the Ninetyeast Fracture Zone.

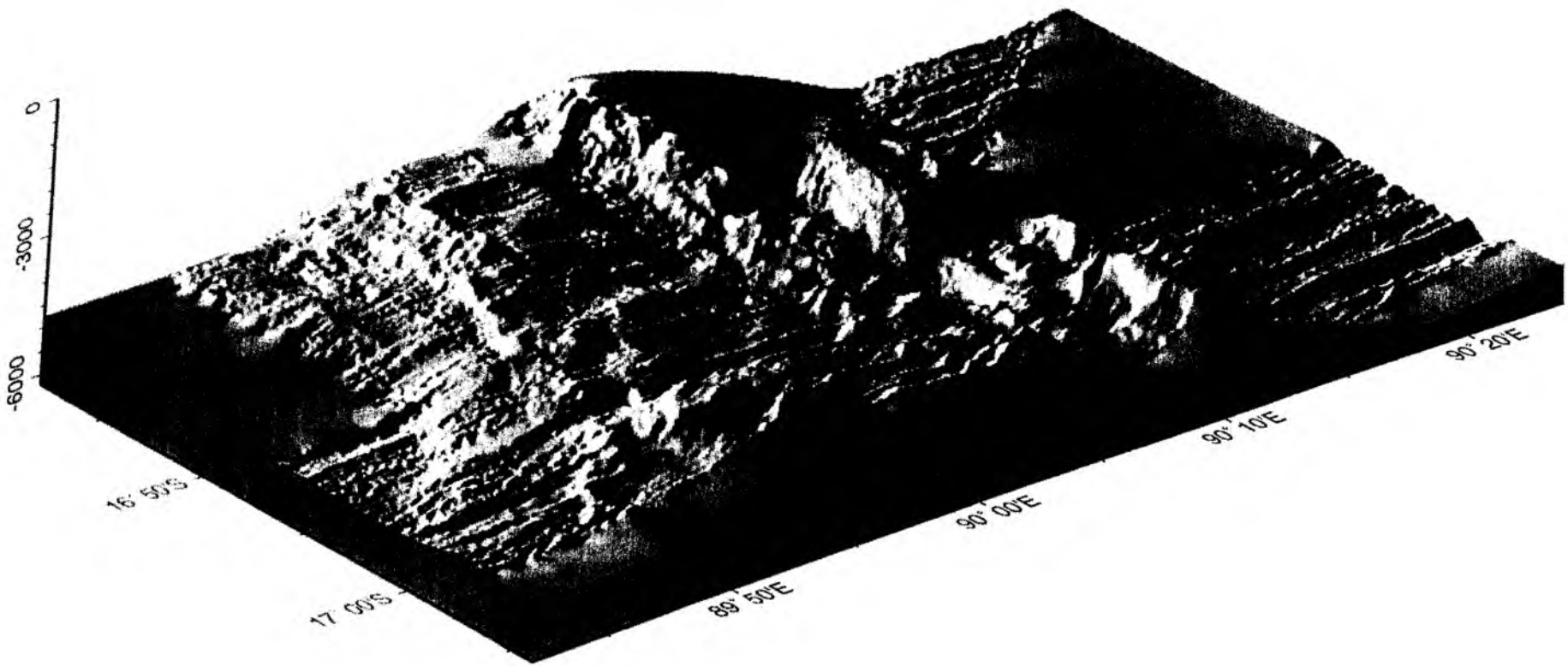

Fig. 6.1.8: Perspective image of Ninetyeast fracture zone area. View from southwest, illumination from northwest.

6.3 SEISMIC WIDE-ANGLE WORK
6.3.1 INTRODUCTION

(E. Flueh)

The central activity during the SO131 - SINUS cruise concentrated on the collection of seismic wide-angle data. Different recording units were used: the are Ocean Bottom Hydrophones (OBH) and one Ocean Bottom Seismometer (OBS) and two Vertical Arrays, as well as a three-channel streamer. In addition for the SEEBOSEIS experiment three recorders of Hamburg University were operated.

A total of 108 deployments were made, and all instruments were safely recovered. In Figure 6.3.1.1 a summary of the profiles and recording sites is shown. The data quality is variable, but mainly excellent. Due to rough topography in the Wharton Basin and near surface volcanics on some sections arrivals can only be traced to intermediate offsets of 30 to 50 km. On other stations however, seismic signals penetrating the upper mantle are clearly seen to distances beyond 200 km to the maximim observation range.

Shooting was made using the well tuned BGR airgun array, and caused no problems or delays. No serious malfunctioning of the guns was ever observed. Details on the profiles with a total number of nearly 22.000 shots along the profiles with a total length of 2.500 km are given in Appendix 9.1.2.

Data from all instruments were played out during the cruise, and written in SEG-Y standard format for data reduction, plotting, processing, interpretation and exchange. Despite the large data volume (about 400 MB per instrument per deployment, totaling 50 GB), this work was accomplished during the cruise, by using the available computerpower during continues 24 hour shifts. However, the full data set of the 3-D experiment could not be converted into SEG-Y during the cruise, but the raw data were saved and copied, and for each instrument a subset of the data was converted into SEG-Y for quality controll. The excellent cooperation between the scientific parties onboard and the ship's crew enabled a rather smooth operation.

A preliminary interpretation could be achieved for most profiles, especially those collected in the first days of the cruise. In the following chapters the processing (Chapter 6.3.2) and modelling techniques (Chapter 6.3.3) applied are described first. This is followed by a description of each profile, which includes the chronology of the experiment (all times given correspond to local time), the most important data and the first results.

6.3.2 SEISMIC PROCESSING AND DATA EXCHANGE

(D. Klaeschen)

6.3.2.1 Mini-Streamer Data

Raw data: As data example, channel 1 for profile SO131-05 is shown in Figure 6.3.2.1.1. For the analysis profile ranges between 31 and 38 km will be studied in detail.

Frequency filter test: To determine the frequencies of the seismic energy filter panels for the profile range 31-38 km corresponding to the shot point numbers 201-250 are shown in Figure 6.3.2.1.2 and Figure 6.3.2.1.3. Below the data the autorrelation function is attached. The amplitude spectra of the Ormsby frequency filter operators are characterised by linear slopes. The filter is described by four corner frequencies:

Lower stop / pass band boundary and upper pass / stop band boundary. The frequencies on the filter panels correspond to the lower and upper pass frequencies. The main energy for the upper sediment structure (300 ms below

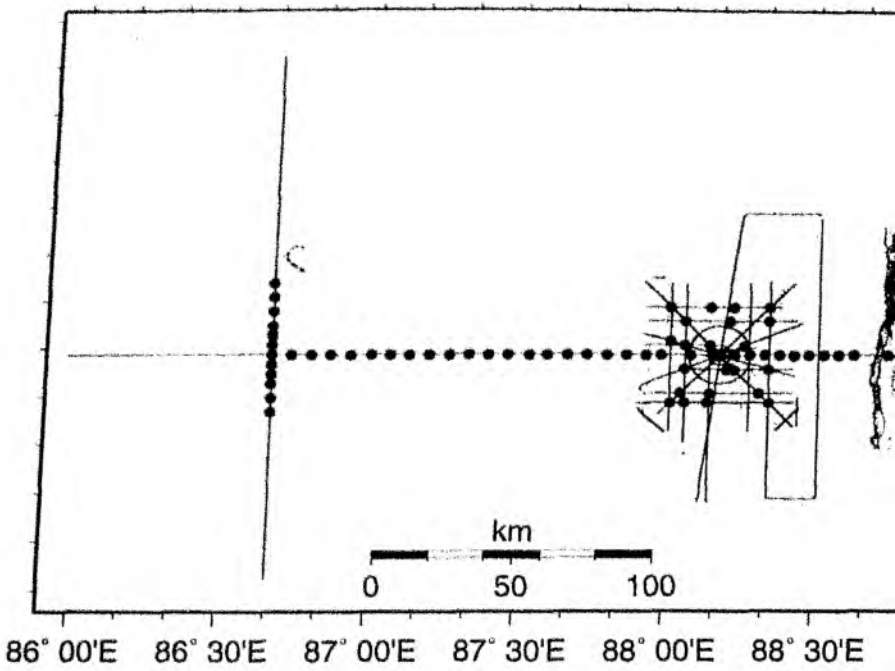

Fig. 6.3.1: SO131 - all Shot and OBH positions.

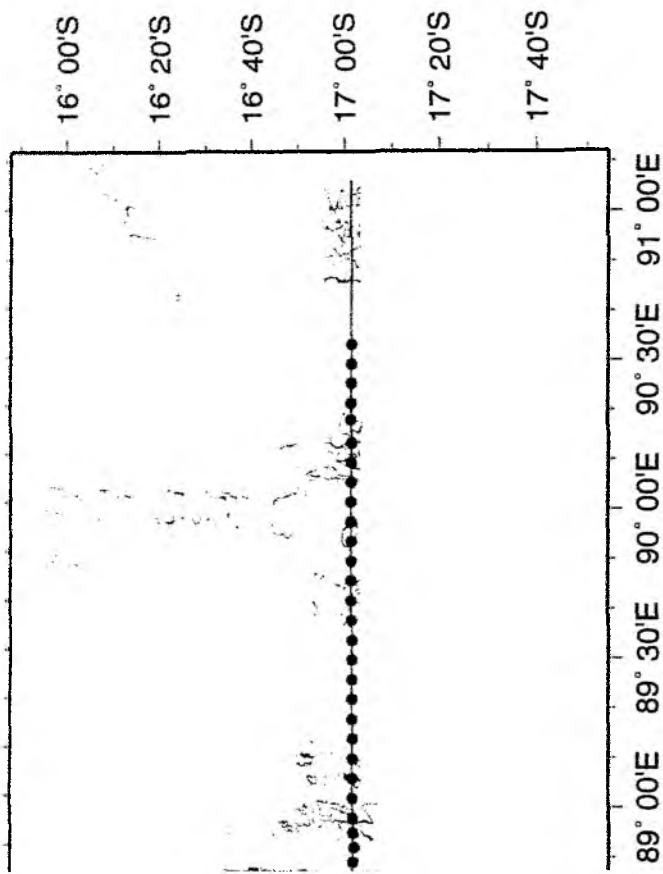
16° 00'S
16° 20'S
16° 40'S
17° 00'S
17° 20'S
17° 40'S
89° 00'E
89° 30'E
90° 00'E
90° 30'E
91° 00'E

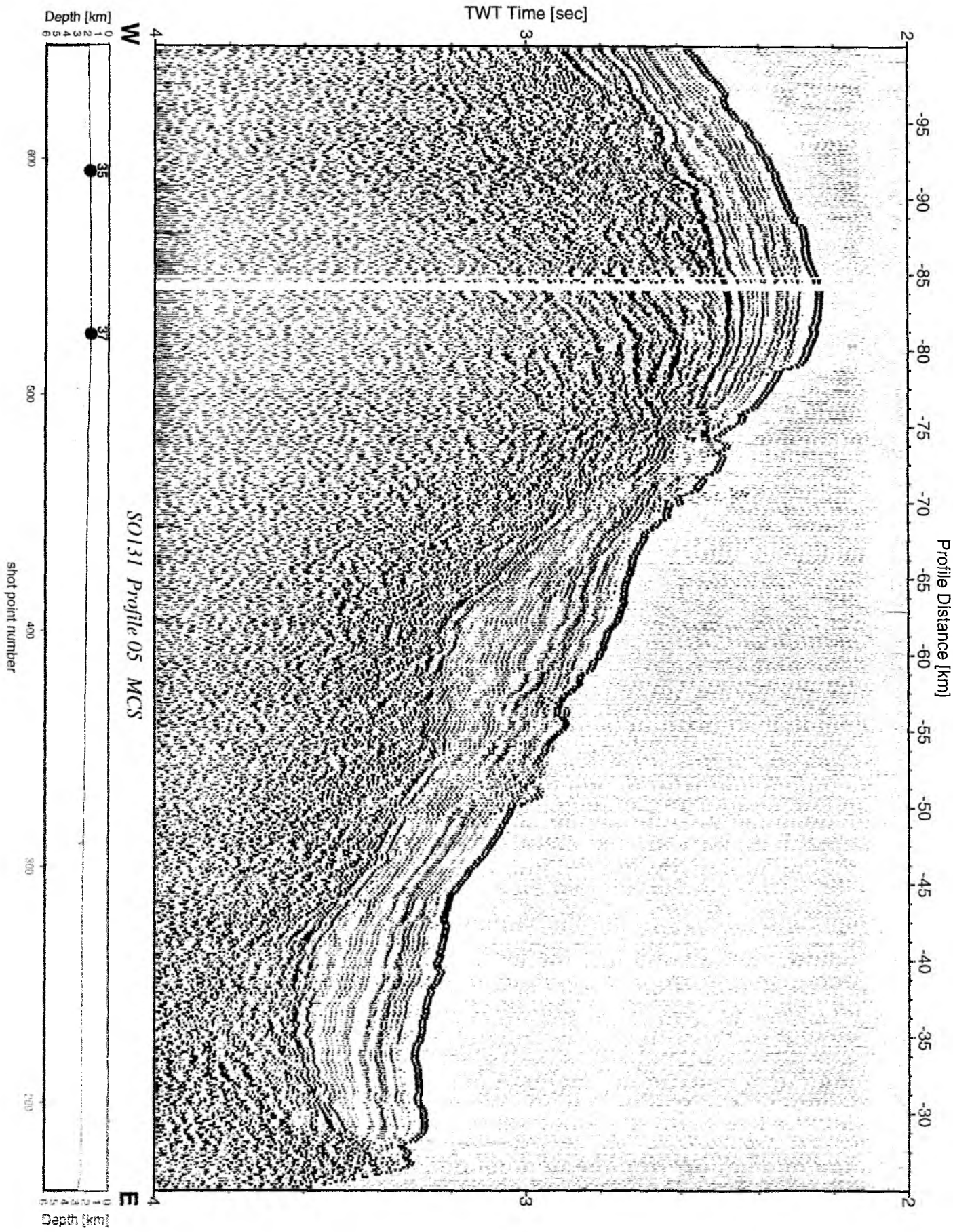

Figure 6.3.2.1.1: Un-processed seismic section from MCS channel 1, Profile 05.

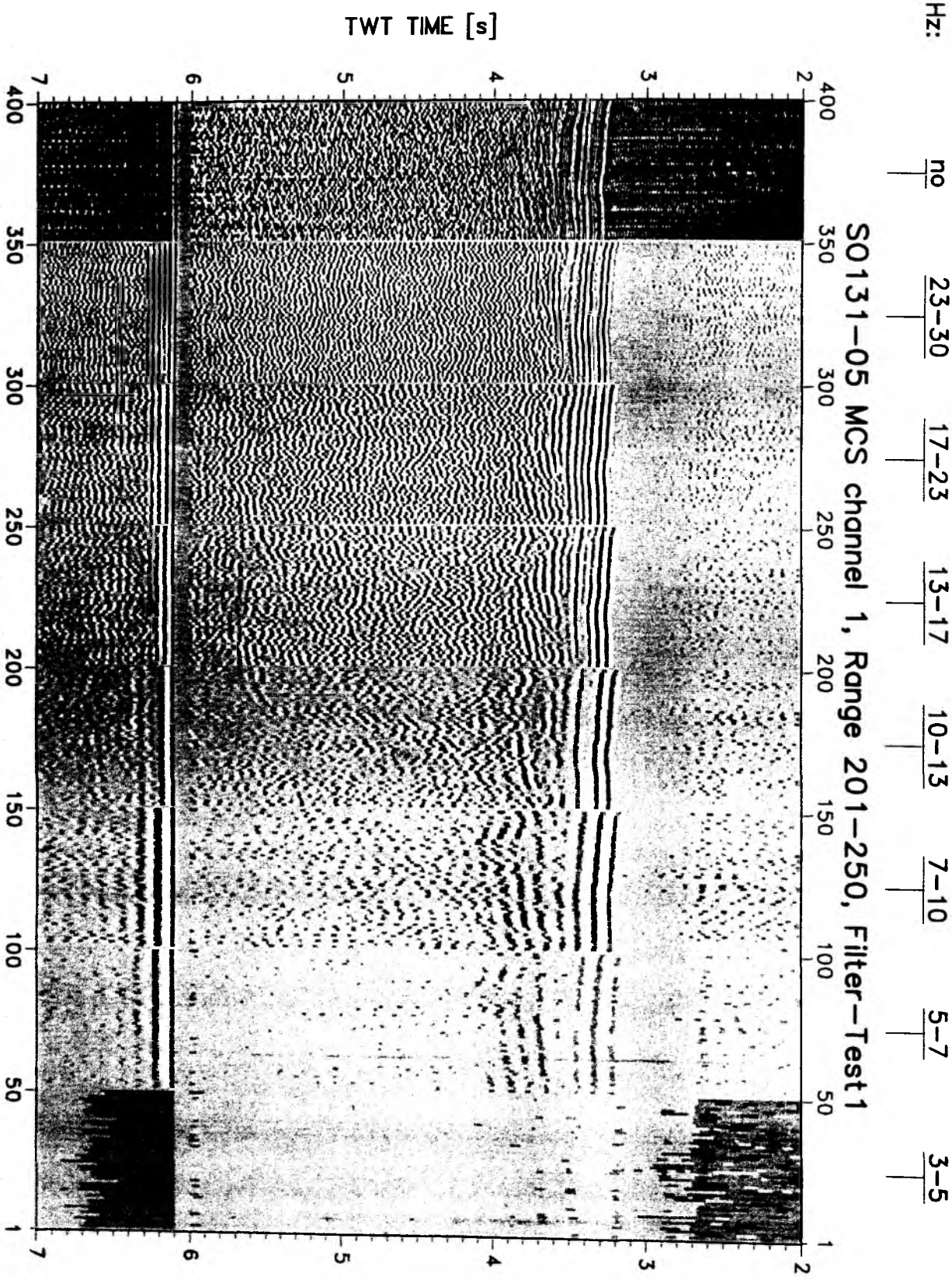

Figure 6.3.2.1.2: Filter test1 panels in the shot point range 201-250.

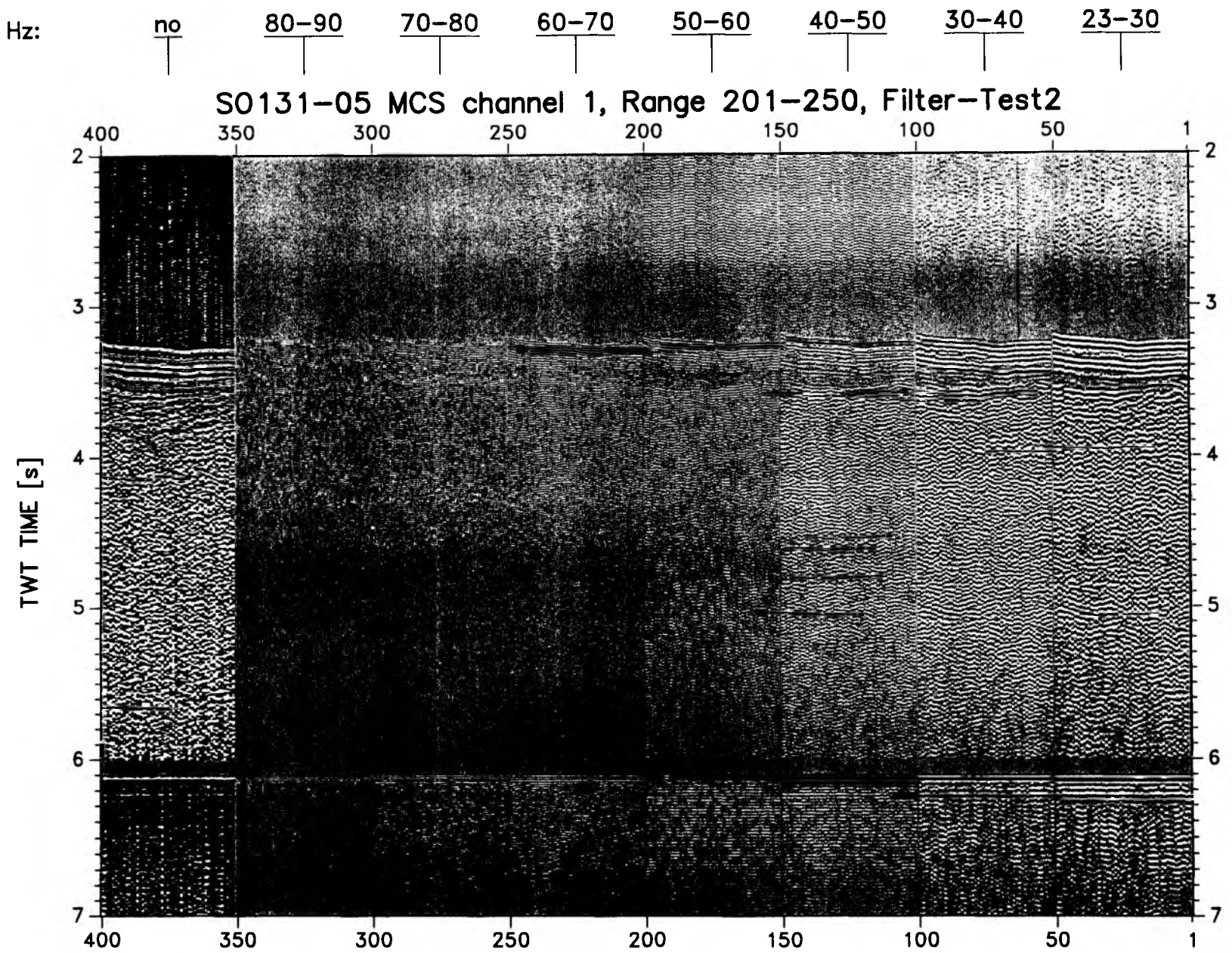

Figure 6.3.2.1.3: Filter test2 panels in the shot point range 201-250.

seafloor) is between 7-90 Hz. Below the sediment structure (2 s below the seafloor) the frequency content decreases to values between 7-40 Hz. As a broad frequency range is contained in the data a time dependent filtering was applied based on the seafloor topography.

Deconvolution test: To improve the temporal resolution of the seismic data a deconvolution is applied to compress the basic seismic wavelet. The recorded wavelet has many components, including the source signature, recording filter, and hydrophone response. Ideally, deconvolution should compress the wavelet components and leaving only the earth's reflectivity in the seismic trace. The deconvolution algorithm which was applied is the Wiener deconvolution in sucessive trace segments which is based on the following assumptions:

1. The earth's reflectivity is 'white'.
2. The wavelet shows the minimum-delay phase behavior.

As in near-vertical data the amplitude spectra of the seismic traces vary with time, the deconvolution must be able to follow these time variations. Each trace is therefore devided into 3 s data gates with 1.5 s overlap, in which time invariant deconvolution operators are computed from the autocorrelation function of the data segments and applied. As the signal to noise ratio is relatively poor especially at later travel times the autocorrelation function is laterally averaged over 11 traces. The overall deconvolved trace results from a weighted merging of the independently deconvolved gates.

The deconvolution test panel is shown in Figure 6.3.2.1.4 for the profile range 31-38 km. Again, below the the data the autorrelation function is attached. A constant operator length of 240 ms and a variation of the predictive length from 0 (spike) to 160 ms is displayed.

On the undeconvolved data in Figure 6.3.2.1.4 a second peak of energy at 120 ms is clearly visible in the autocorrelation function. The best resolution is obtained for a predictive length of 0 ms but with a reduction of signal to noise ratio especially at later travel times. A predictive length of 80 ms was choosen for this data set which is a compromise between temporal resolution and signal to noise ratio.

After deconvolution a time variant Ormsby filter was applied. As the depth of the seafloor changes rapidly along the seismic lines, each trace was staticly corrected to a fictive seafloor travel time of 8 s based on the water depth. This information is available in the trace headers. After applying the time variant filter a spherical divergence correction was used with an interval velocity of 1500 m/s at the seafloor and 6000 m/s 2 s below the seafloor followed by a trace normalization along the seafloor event. After this spatially invarient pre-processing each trace was shifted back again to the original travel times, nmo corrected by water velocity and stacked in bins depending of the pop interval of the shots along the profile. After stacking a Butterworth filter was applied for the final data representation. This filter is showing only a small amount of ringing compared to other filter technics. The Butterworth filter is characterised by a lower and upper corner frequency of 8 and 90 Hz. At these frequencies the amplitudes are reduced by a factor of 0.5.

Processed data: Comparison of the pre-processed data in Figure 6.3.2.1.5 to the un-processed data in Figure 6.3.2.1.1 shows a clear reduction of the high frequency noise at later travel times.

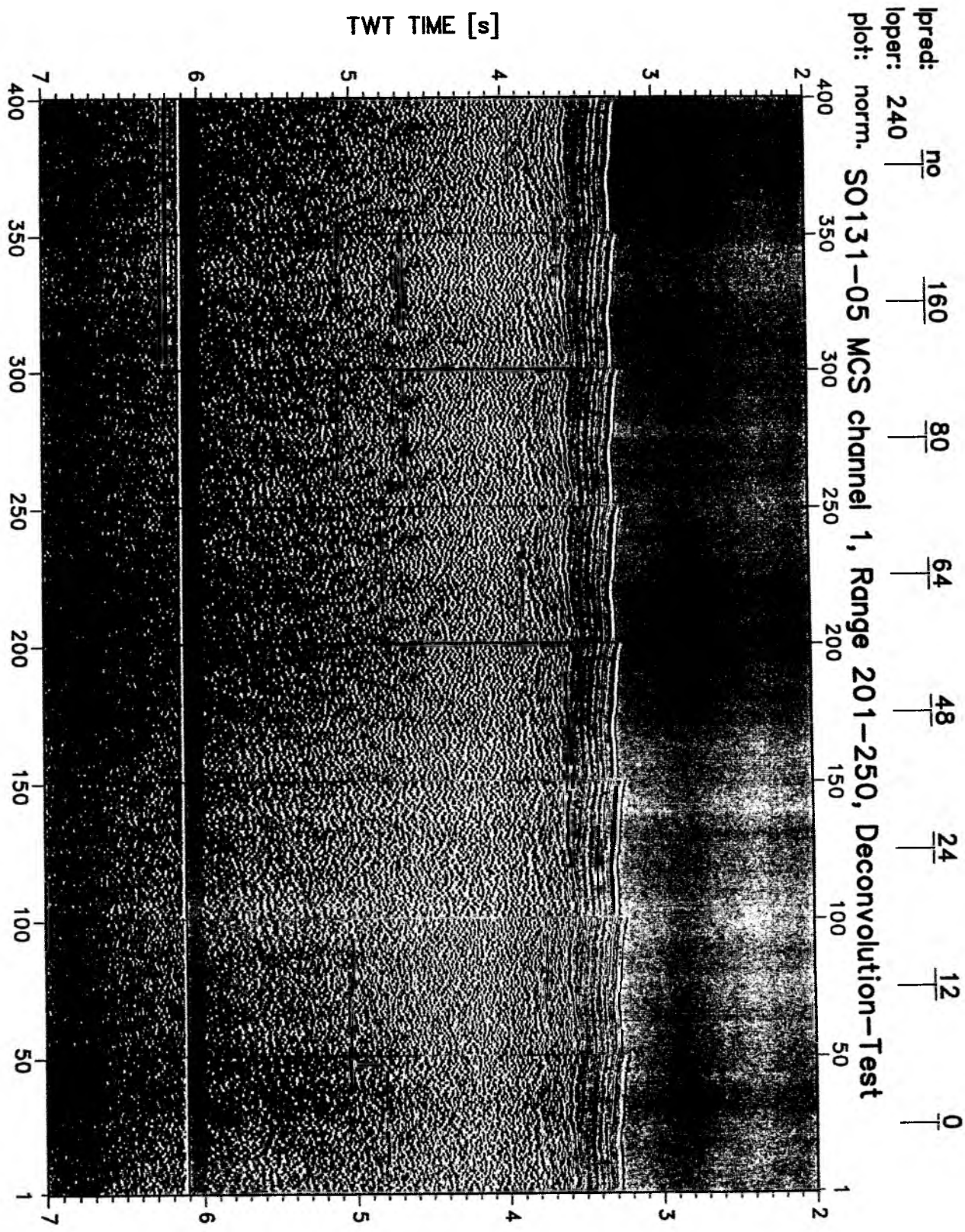

Figure 6.3.2.1.4: Deconvolution test in the shot point range 201-250.

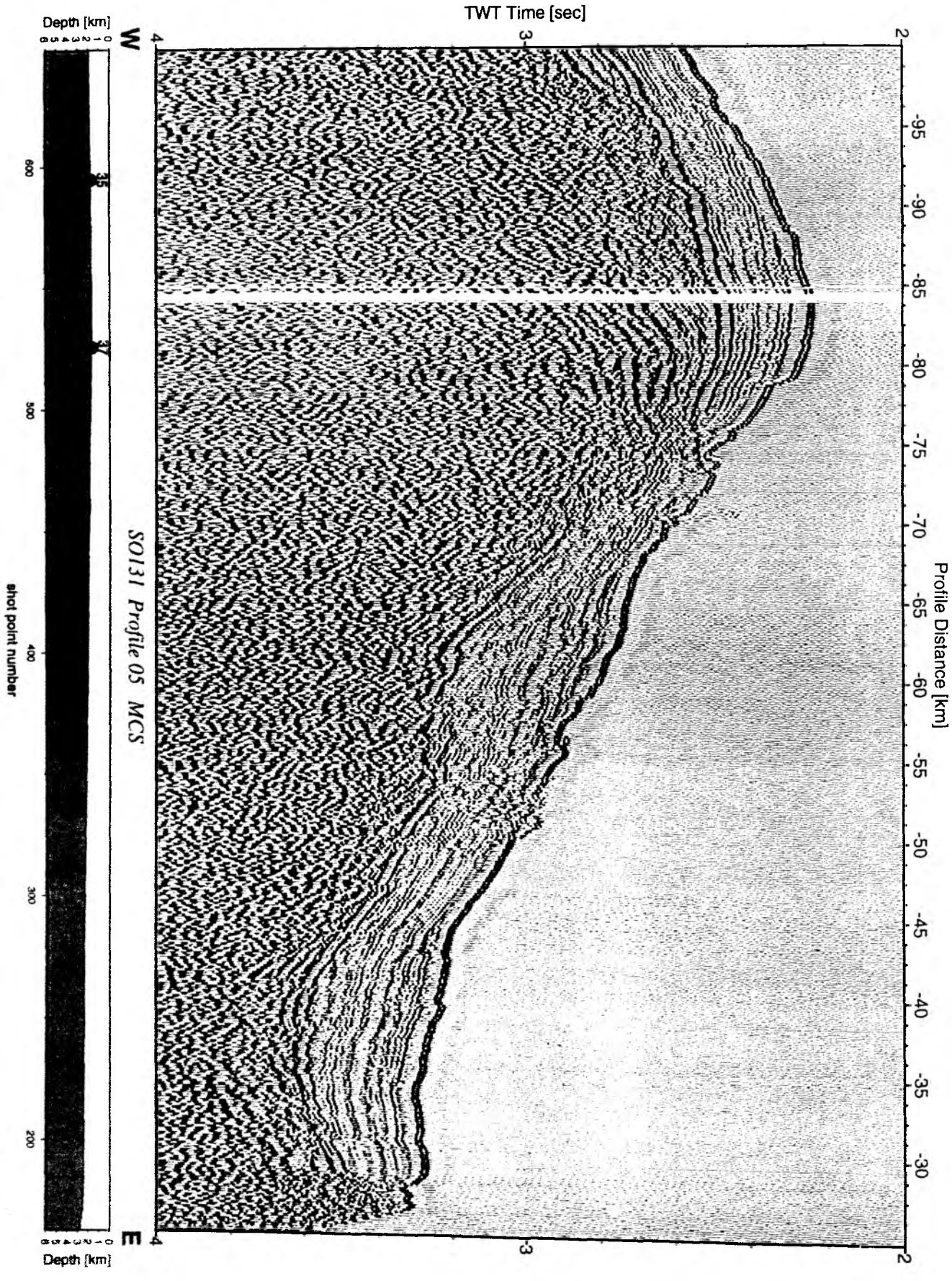

Figure 6.3.2.1.5: Pre-processed seismic section from MCS stack, Profile 05.

Processing sequence:

- Input: SEGY-data, 2 ms sample rate, with complete geometry information
- Ormsby frequency filter with lower stop/pass and upper pass/stop band (Hz)
  5/8 110/125
- resampling to 4ms
- Gated Wiener deconvolution: gate length 3s, overlap 1.5 s, 11 traces for averaging the autocorrelations, operater length 240 ms, prediction interval 80 ms
- static correction to a fictive seafloor travel time of 8 s
- time dependent Ormsby frequency filter (on time shifted traces)

100%-time TWT (s)	lower stop/pass	upper pass/stop band (Hz)
8.3	7/10	90/110
8.6	7/10	50/60
11.0	5/8	30/40

- spherical divergence correction based on interval velocities: 1500m/s at 8s TWT time and 6000 m/s at 10 s TWT time (on time shifted traces)
- trace normalization: 2 s window length with a center time at 8 s TWT time
- static correction to original travel times
- nmo-correction based on water velocity of 1500 m/s
- stacking in offset bins along the profile
- Butterworth frequency filter: 8-90 Hz

- stack bin width (m)	pop interval (s)
150	60
75	30
50	20
25	10

DATA EXCHANGE

For the exchange of the MCS data the SEGY-format on disk in a Sun-tar-format was choosen. The trace length for the raw and processed data is 16 s. The raw data set containes the channel 1 to 3 and the processed data only of the stacked section of channel 1 to 3. The offset in the SEGY-header corresonds to the distance from the first shot point of the profile. The complete geometry information is positioned in the SEGY-trace header:

Information	Receiver No.	Shot No.	Offset	Water Depth
Byte:	13-16	21-24	37-40	61-64

6.3.2.2 OBH/OBS-DATA ANALYSIS AND PROCESSING

Raw data: As data example, the OBH station 03 for profile SO131-04 is shown in Figure 6.3.2.2.1. For the analysis offset ranges between 3.0-10.5 km, 31.5-39 km, and 67.5-75 km south will be studied in detail.

Frequency filter test: To determine the frequencies of the seismic energy filter panels for the offset range 3.0-10.5 km, 31.5-39.0 km and 67.5-75.0 km respectively are shown in Figure 6.3.2.2.2, 6.3.2.2.3 and Figure 6.3.2.2.4. Below the data the autorrelation function is attached. The amplitude spectra of the Ormsby frequency filter operators are characterised by linear slopes. The filter is described by four corner frequencies:

Lower stop / pass band boundary and upper pass / stop band boundary. The frequencies on the filter panels correspond to the lower and upper pass frequencies. The main energy for the phases between 3.5 and 5.2 s in the offset range from 3.0-10.5 km is between 5-30 Hz and for the direct wave more than 30 Hz is obtained. The main energy of the phase between 3.0 and 3.8 s in the offset range

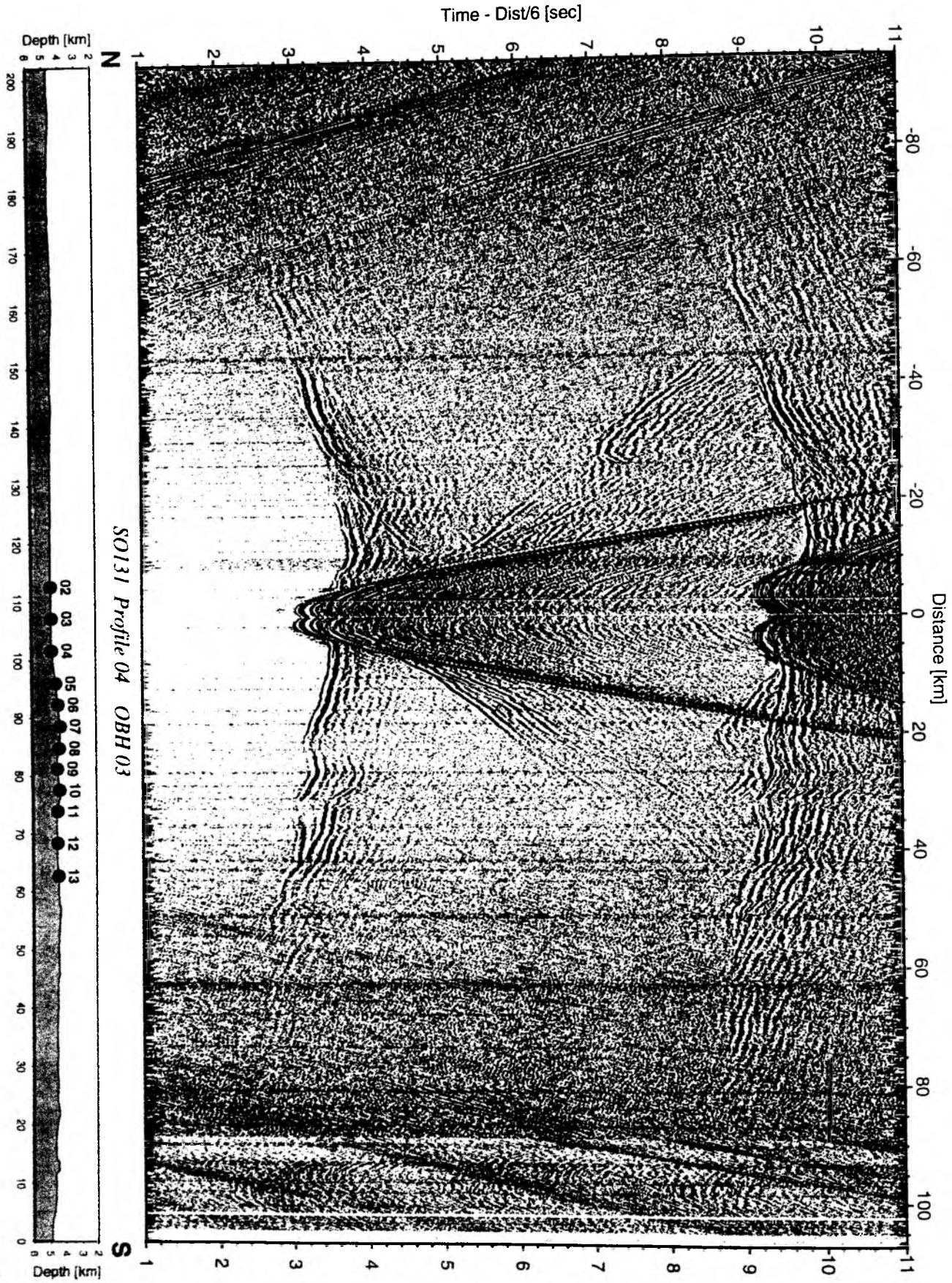

Figure 6.3.2.2.1: Un-processed record section from OBH 03 , Profile 04.

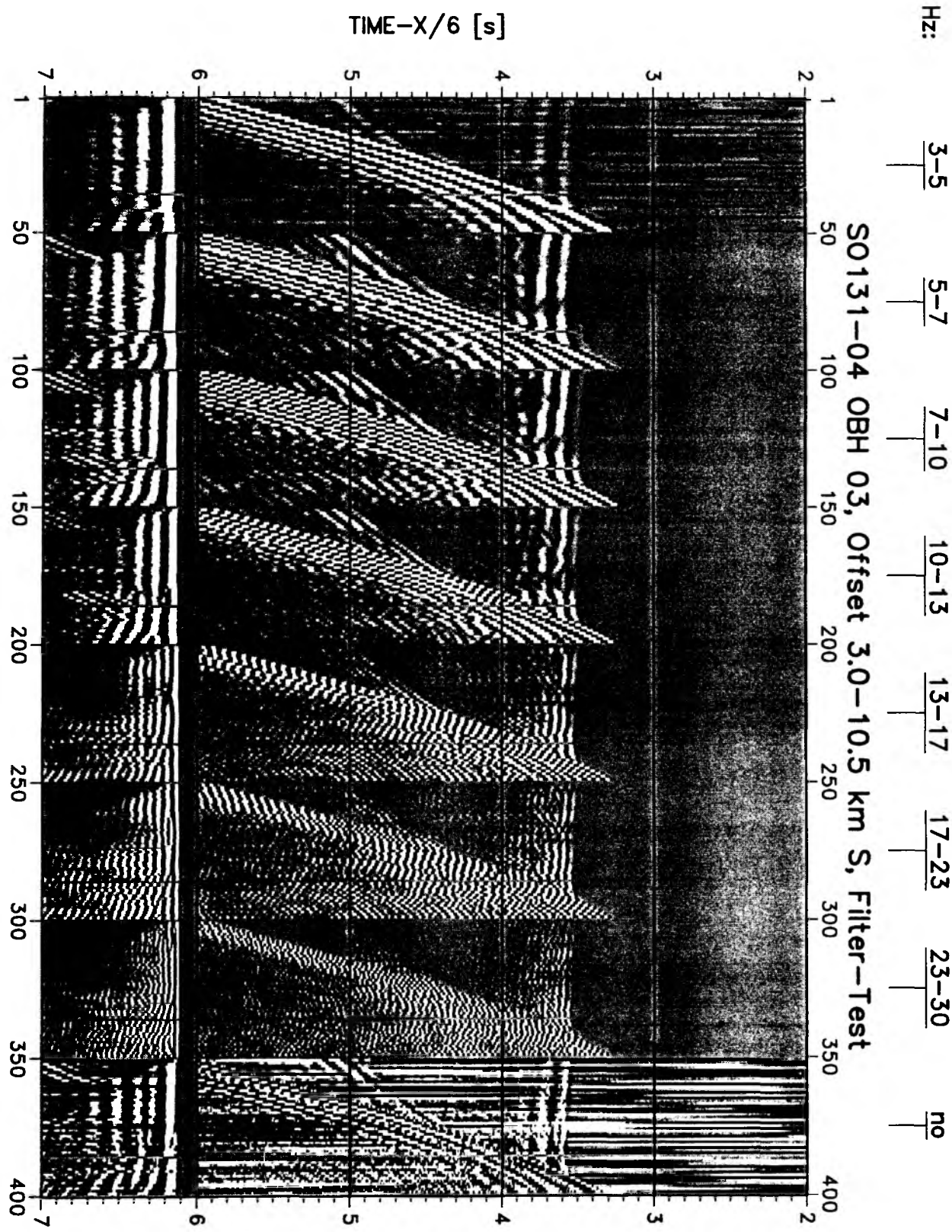

Figure 6.3.2.2.2: Filter test panels in the offset range 3.0-10.5 km South.

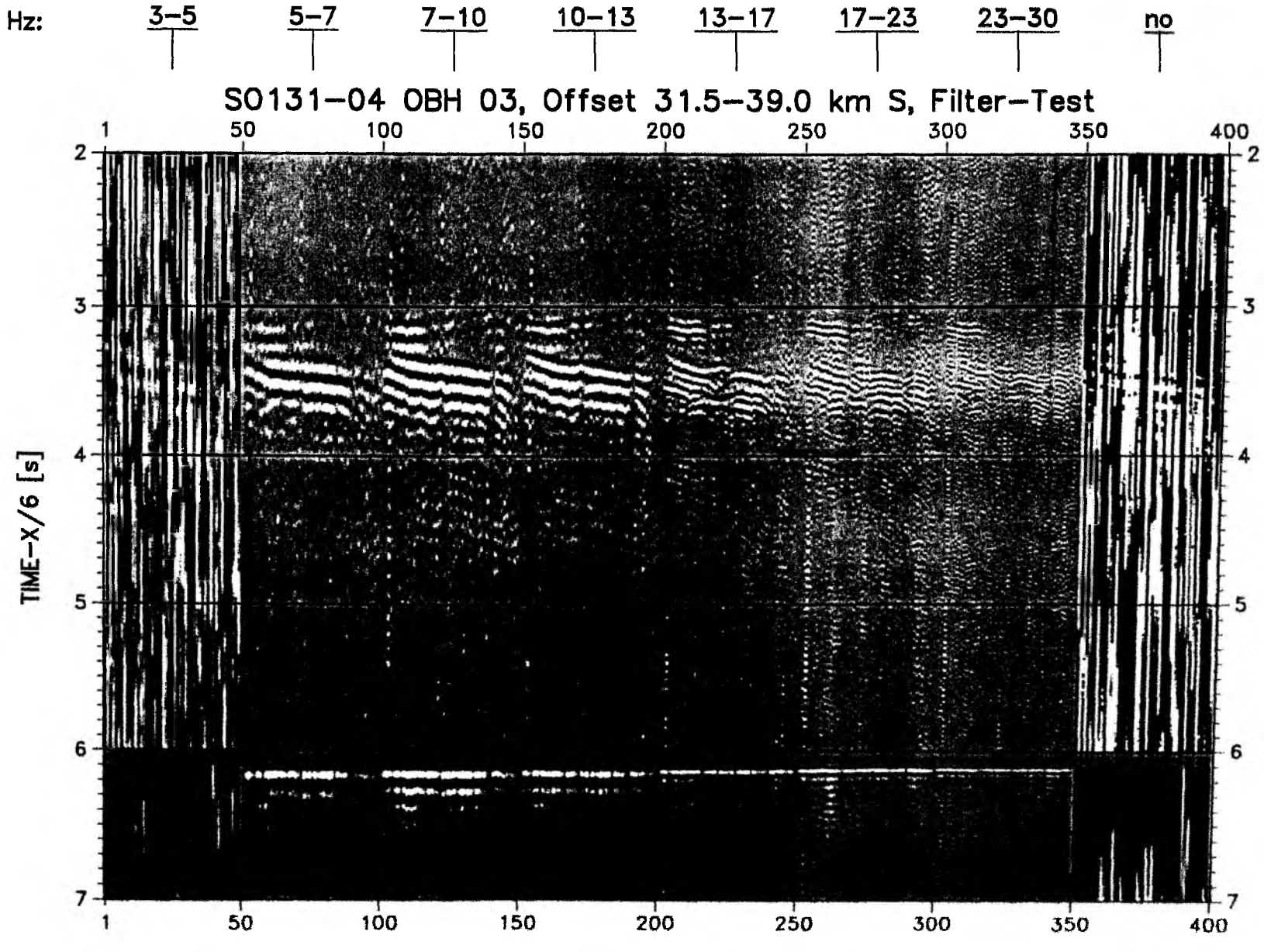

Figure 6.3.2.2.3: Filter test panels in the offset range 31.5-39.0 km South.

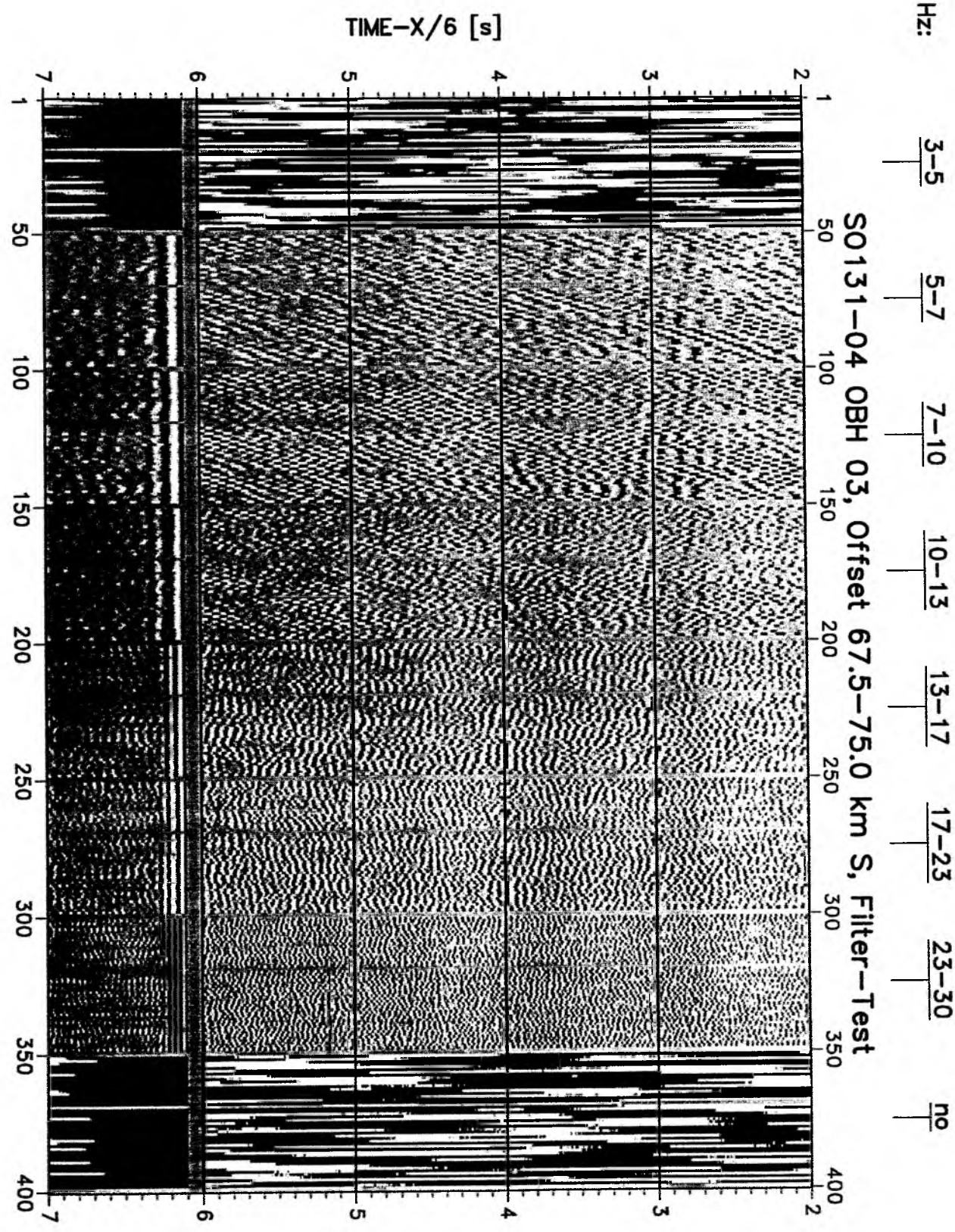

Figure 6.3.2.2.4: Filter test panels in the offset range 67.5-75.0 km South.

from 31.5-39.0 km is between 5-23 Hz and the main energy of the phase between 2.5 and 3.2 s in the offset range from 67.5.-75.0 km is between 5-13 Hz. As a broad frequency range is contained in the data a time and offset dependent filtering was applied.

Deconvolution test: To improve the temporal resolution of the seismic data a deconvolution is applied to compress the basic seismic wavelet.

As in wide-angle data the amplitude spectra of the seismic traces vary with time and offset, the deconvolution must be able to follow these time and offset variations. Each trace is therefore devided into 2 s data gates with 1 s overlap, in which time invariant deconvolution operators are computed from the autocorrelation function of the data segment and applied. The overall deconvolved trace results from a weighted merging of the independently deconvolved gates.

The deconvolution test panels are shown in Figures 6.3.2.2.5, 6.3.2.2.6, and 6.3.2.2.7 for the offset range 3.0-10.5 km, 31.5-39.0 km and 67.5-75.0 km south respectively. Below the data the autorrelation function is attached. A constant operator length of 480 ms and a variation of the predictive length from 0 (spike) to 320 ms is displayed.

On the undeconvolved data in Figure 6.3.2.2.5 strong reverberation from the direct wave is clearly visible in the autocorrelation function. The best resolution is obtained for a predictive length of 0 ms but with a reduction of signal to noise ratio. On the undeconvolved data in Figures 6.3.2.2.6 and 6.3.2.2.7 a second peak of energy at 120 ms is clearly visible in the autocorrelation function. The best resolution is obtained for a predictive length of 0 ms but with a reduction of signal to noise ratio. A predictive length of 80 ms was choosen for this data set which is a compromise between temporal resolution and signal to noise ratio.

After deconvolution a time variant Ormsby filter was applied. As the seafloor time changes rapidly along the seismic lines, each trace was staticly corrected to a fictive seafloor travel time of 6 s based on the water depth. This information is available in the trace headers. After applying the time and offset variant filter which depend on the reduction velocity applied the data were shifted back to their original travel times.

Processed data: Comparison of the pre-processed data in Figure 6.3.2.2.1 to the un-processed data in Figure 6.3.2.2.8 shows a clear reduction of the high frequency noise on the far offset traces and a compression of the wavelet signal. For the picking of events and model building by raytracing both sections were used to keep all the avialable seismic information.

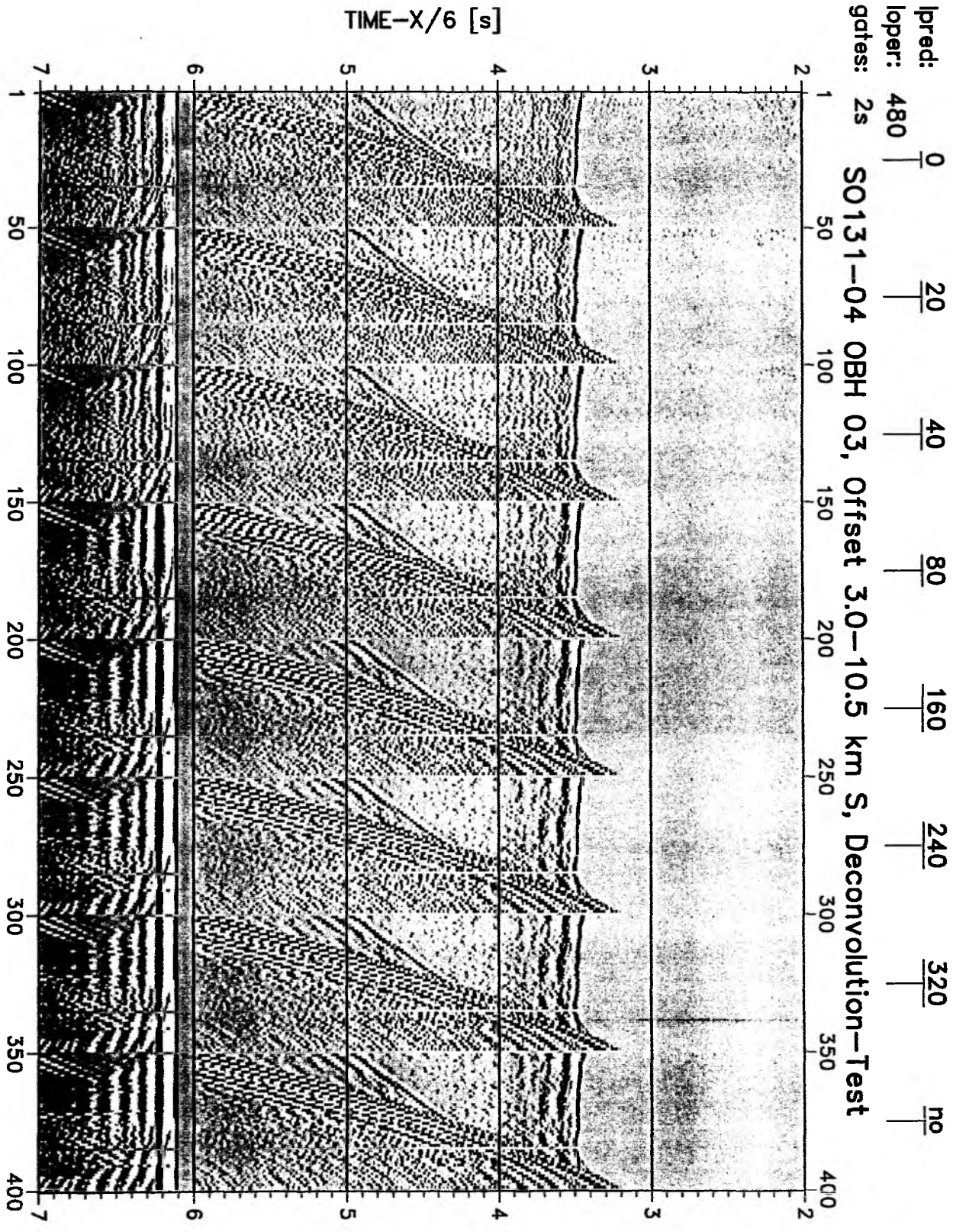

Figure 6.3.2.2.5: Deconvolution test in the offset range 3.0-10.5 km South.

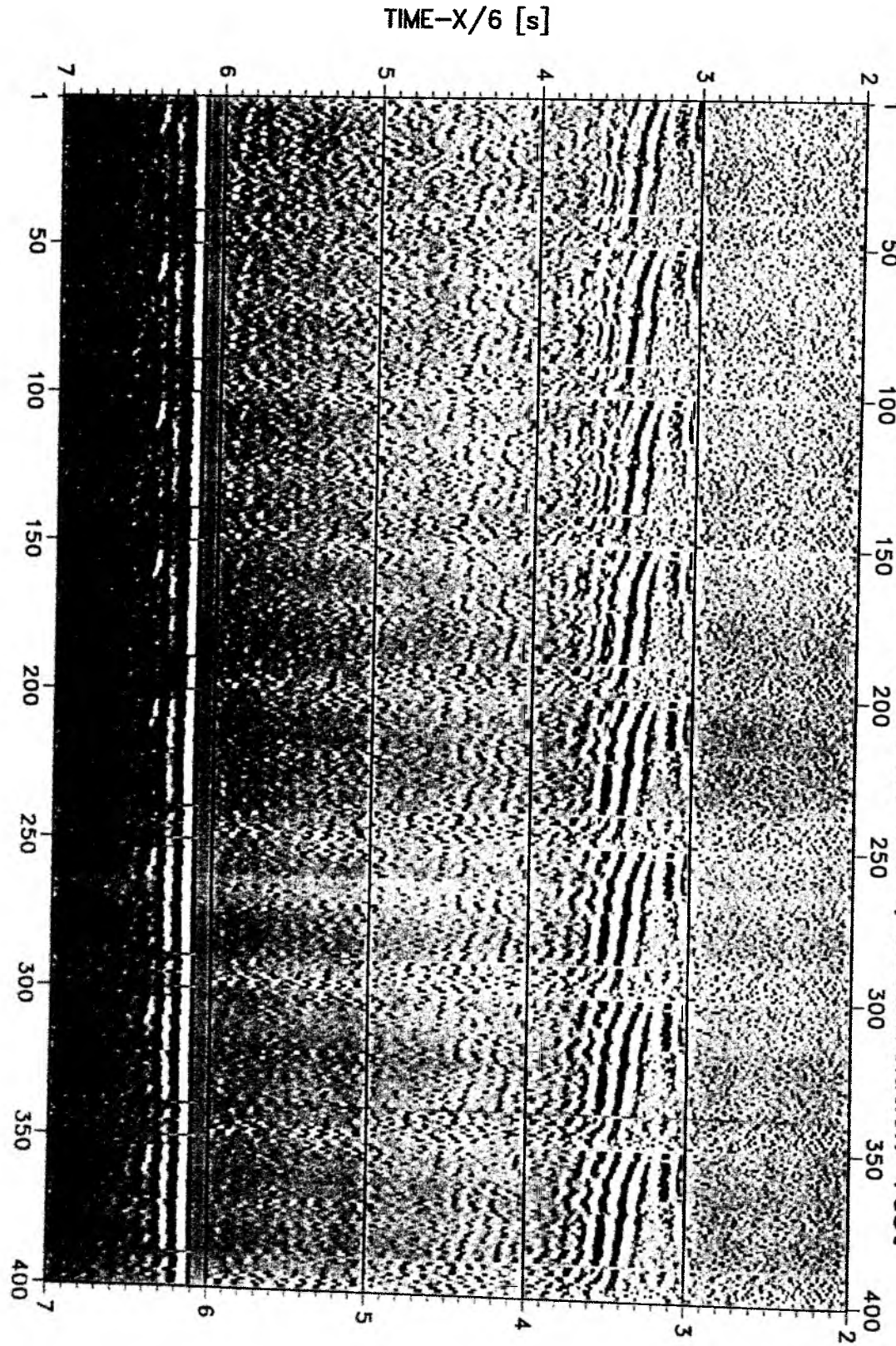

Figure 6.3.2.2.6: Deconvolution test in the offset range 31.5-39.0 km South.

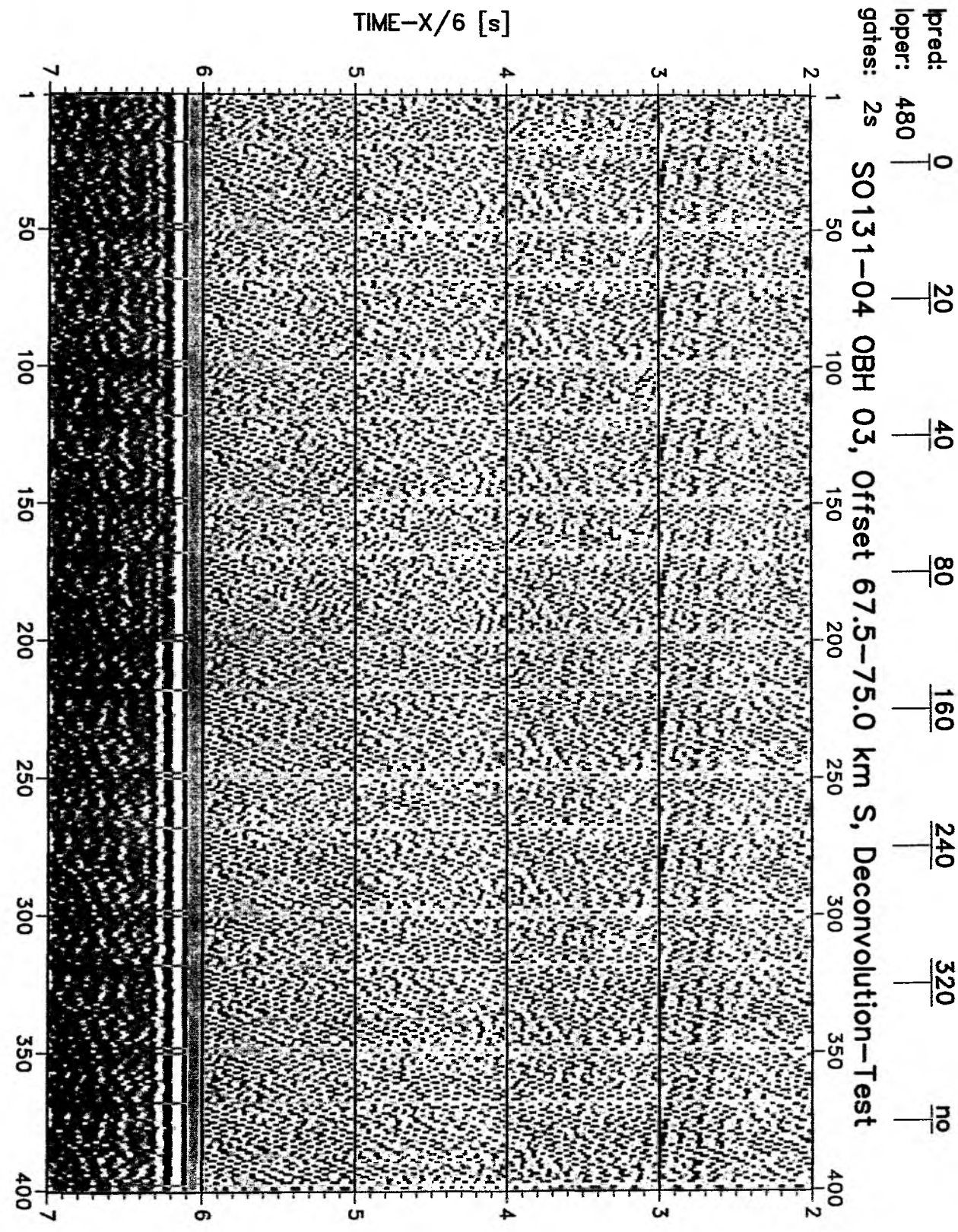

Figure 6.3.2.2.7: Deconvolution test in the offset range 67.5-75.0 km South.

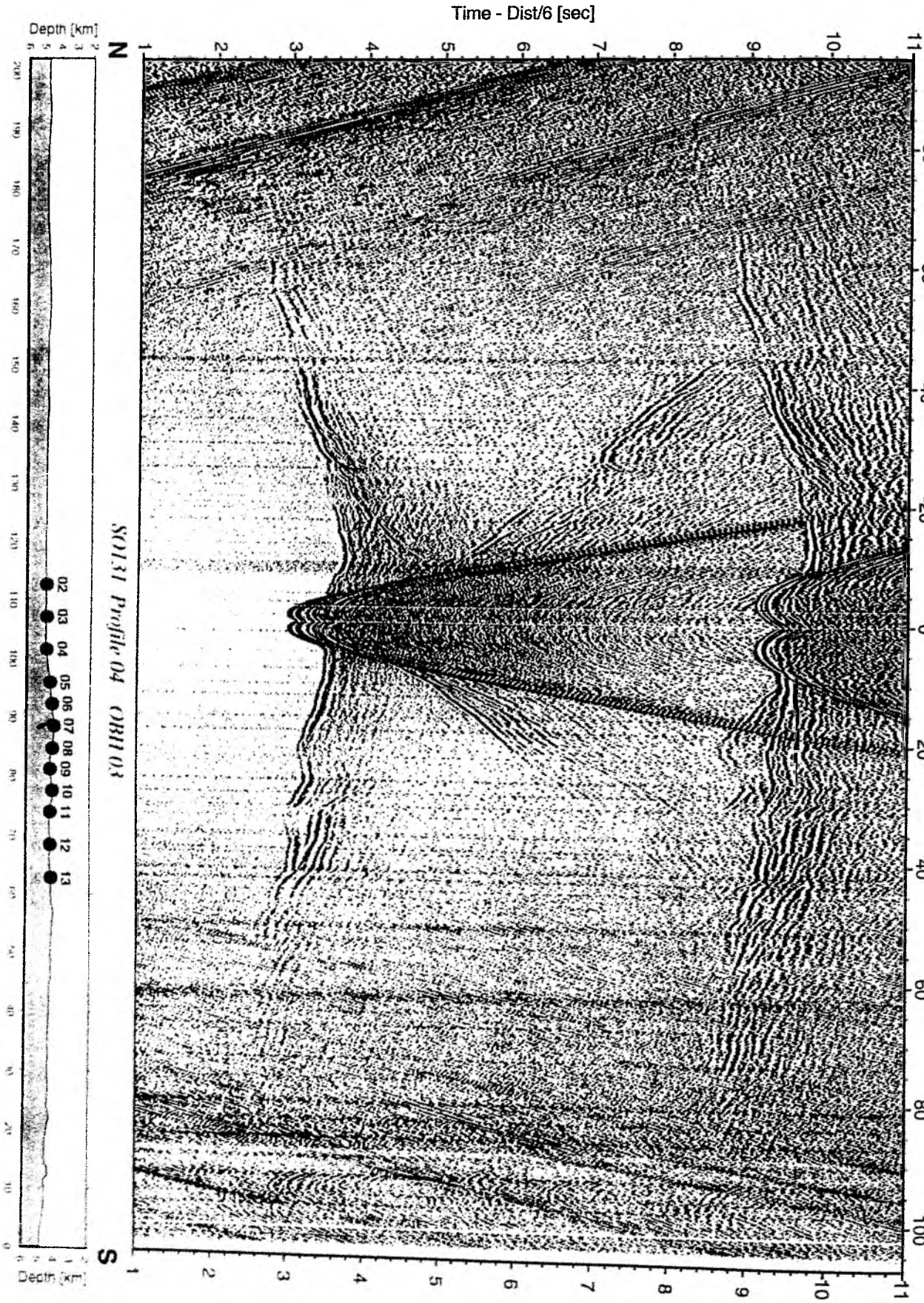

Figure 6.3.2.2.8: Pre-processed record section from OBH 03 , Profile 04.

Processing sequence:

- Input: SEGY-data, 5 or 4 ms sample rate with complete geometry information
- low cut frequency filter 5Hz with 48 db slope
- Gated Wiener deconvolution: gate length 2s, overlap 1 s, operater length 480 ms, prediction interval 80 ms
- static correction to a fictive seafloor travel time of 6 s
- time and offset dependent Ormsby frequency filter (on time shifted traces with a reduced time scale of 6 km/s):

offset (km)	100%-time (s)	lower stop/pass	upper pass/stop (Hz)
0	7.5	3/5	35/50
0	9.5	3/5	20/40
0	11.5	3/5	10/20
30	4.755	3/5	35/50
30	6.755	3/5	20/40
30	8.755	3/5	10/20
60	2.01	3/5	35/50
60	4.01	3/5	20/40
60	6.01	3/5	10/20
90	0.005	3/5	35/50
90	1.265	3/5	20/40
90	3.265	3/5	10/20
120	0.005	3/5	35/50
120	0.01	3/5	20/40
120	0.52	3/5	10/20

- time and offset dependent Ormsby frequency filter (on reduced time scale with 8km/s):

offset (km)	100%-time (s)	lower stop/pass	upper pass/stop (Hz)
0	4.0	3/5	35/55
0	6.0	3/5	20/35
0	8.0	3/5	10/20
40	2.0	3/5	35/55
40	0.5	3/5	20/35
40	1.0	3/5	10/20
60	2.0	3/5	35/55
60	1.0	3/5	20/35
60	0.0	3/5	10/20

- linear time and offset scaling (on unreduced time scale only for plotting).

DATA EXCHANGE

For the exchange of the OBH/OBS data (GEOMAR) the SEGY-format on disk in a Sun-tar-format was choosen. The trace length for the raw and processed data is 20 s. The complete geometry information is positioned in the SEGY-trace header:

Inform.	Receiver No.	Shot No.	Offset	Red. Vel.	Water Depth
Byte:	13-16	21-24	37-40	93-94	61-64

Profile No.	Reduction Velocity (km/s)	Trace Length (s)
03	6	4
04	6	20
05	8	20
06	8	20
07-29 (3D)	6	20
30	6	10
31	8	20
32	8	20

6.3.3 WIDE-ANGLE DATA MODELLING

(The Modelling/Interpretation Group)

The OBH/OBS data have been analyzed for crust and upper mantle velocity structure. The modelling sequence of the wide-angle data involves three different steps:

A) Picking: The traveltimes of the observed phases are picked interactively on the workstation's screen using Seismic Unix Software and Xbuplot (Zelt, 1992). This provides ascii files, containing offsets and traveltimes of phases for each record, which will be used for the modelling.

B) 1-D modelling: A 1-D velocity-depth modelling has been undertaken for some of the record sections. This first approach to determine the velocity structure along the different lines allows to define preliminary velocity-depth models, which are used as the starting point during the 2-D modelling.

The software used for this porpuse is an interactive program „MacR1D„ (J. Luetgert, 1992) for calculating travel-time curves from 1-D velocity-depth functions. The ability to quickly manipulate velocity-depth functions and immediately see the resulting travel-times gives useful insights into the effects of changing gradients, low-velocity zones, etc.

C) 2-D modelling: Models have been created for some of the lines. For the modelling waterdepth is taken from UKOOA-files. The models are capable of predicting the correct offset/time of as many of the observed phases as possible. Two different programs to trace rays in 2-D media have been used: „MacRay„ and „Rayinvr„. Another method for inversion („Raytomorf„) was also applied to find a starting model for detailed forward modelling.

-- „MacRay„ (J. Luetgert, 1992) is an interactive application for calculating travel-time curves from 2-D velocity models. It is based upon RAY84 and RAY86 seismic raytracing programs written for the DEC VAX/VMS environment and adapted to the Apple Macintosh graphical interface for the display and manipulation of the velocity models.

Velocity models are defined by two or more interfaces extending across the model. Any pair of successive interfaces describes a layer, within which the velocity may be defined in terms of the velocity at the top and bottom of the layer. Within any layer the velocity may be inhomogeneous but continuous. First or second order discontinuities in velocity may occur at interfaces. The ray tracing algorithm that is used calculates the propagation of rays within a layer by the stepwise integration of a system of first order differential equations (Cerveny et al., 1977). Lithologic interfaces are represented in the model as first or second order velocity discontinuities. When an interface is encountered in the calculation of a ray, Snell,s law is applied and the calculation is continued. „MacRay„ is very usefull for quickly manipulating velocity models.

-- „Rayinvr„ is a program to trace rays for rapid forward modelling and inversion of refraction and reflection travel times (Zelt and Smith, 1992; Zelt and Forsyth, 1994). The program assumes a 2-D (x,z) isotropic medium and the velocity model is composed of a sequence of layers separated by boundaries consisting of linked linear segments of arbitrary dip. The velocity within a layer is defined by velocity values specified at arbitrary x-coordinates along the top and bottom of the layer. For the purposes of ray tracing, the model is automatically broken up into an irregular network of trapezoids, each with dipping upper and lower boundaries and vertical left and right sides. The velocities at the four corners of the trapezoid are used to interpolate a velocity field between the trapezoid so that the velocity varies linearly along its four sides. Therefore, horizontal as well as vertical velocity gradients may exist within a trapezoid. Raytracing is performed by numerically solving the ray tracing equations for 2-D media using a Runge Kutta method. The partial derivates of travel time with respect to

those model parameters selected for adjustment are calculated analytically during ray tracing; these parameters include velocities and the vertical position of boundary nodes. The traveltime residuals with respect to the observed data are also calculated and are used later to update the model parameters by applying the method of damped least-squares to the linearized inverse problem. The algorithm can include any type of arrival, including multiples and/or converted shear waves.

As a first approach, we have performed velocity-depth modelling through classical forward analysis of arrival times. Finally, an iterative damped least-squares inversion procedure to optimize the velocity and depth values is applied.

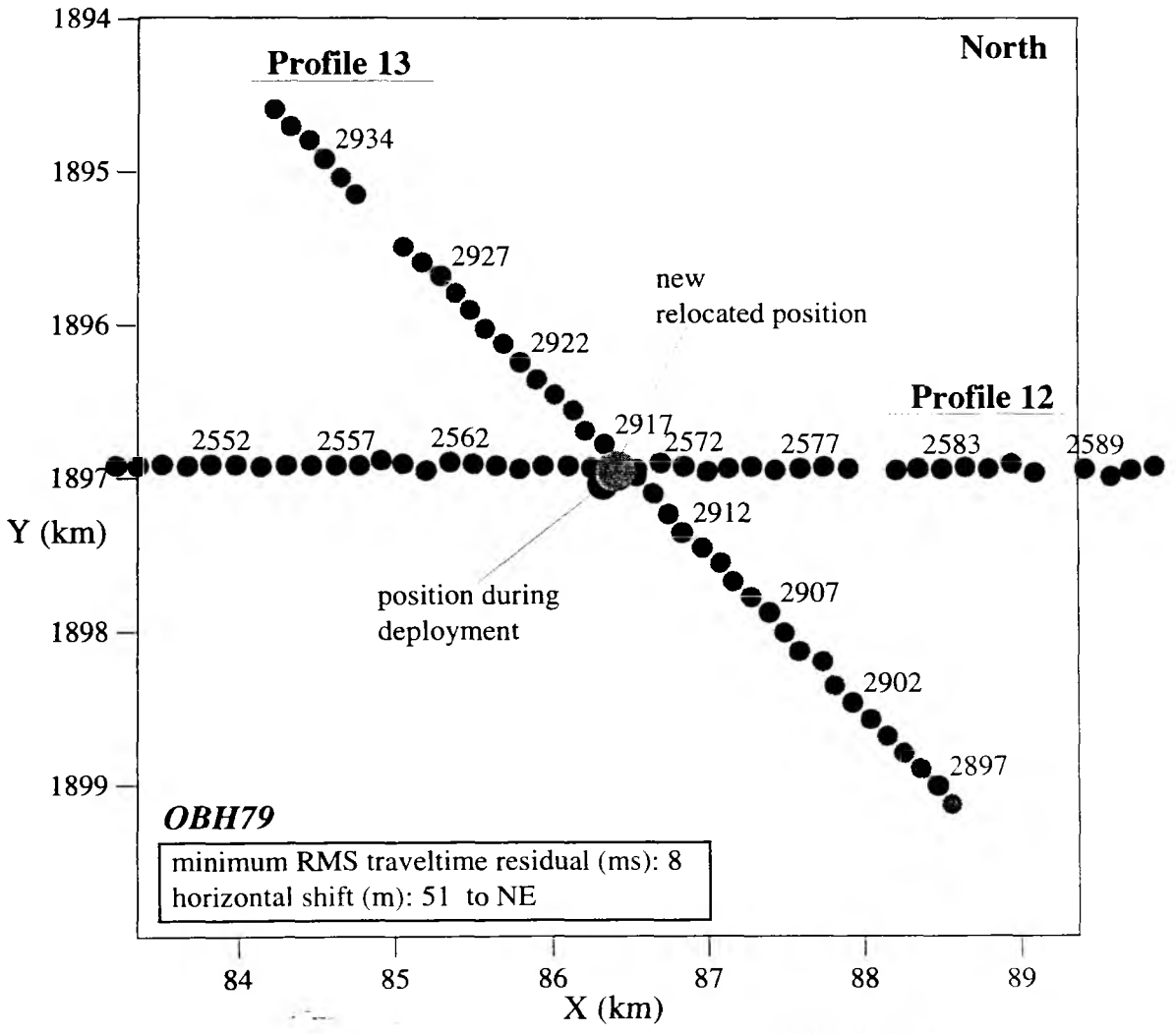

Figure 6.3.3.1: Three dimensional relocation of OBH79 (shot points as small dots).

-- "Raytomorf" is a two dimensional inversion routine based on a finite-difference solution for inversion of the velocity field. The finite-difference algorithm is based on equations developed by Vidale (1988). Based on a gridded velocity field the travel time field is calculated with the use of an expanding square. Starting from a point source fd equations are used to calculate travel times to the neighbouring grid nodes. Selection of the nodes is done according to the scheme of an expanding square where the nodes located on the sides of the square are used. Ammon and Vidale (1993) modified the set of fd equations in order to handle media with strong velocity variations. After determination of the travel time field rays are traced through and ray

length segments are computed for each cell of the velocity model. Then the ray length matrix is inverted for a set of slowness correction values. The inversion of the slowness correction vector can be performed using Singular Value Truncation, Damped Least Squares or Conjugate Gradients (LSQR). Due to the large number of observations the LSQR method was choosen. The code enables to vary the weighting factor for the minimization of the Laplacian smoothness of the slowness correction vector as well as the number of iterations in the LSQR matrix inversion. Application of the program was done within a recursive loop using the last inverted model as the input to the next run.

D) 3-D modelling: In a 3-D survey it is evident that some of the 2-D routines are not sufficient to handle typical problems which may occur in terms of out-of-plane effects, relocation and offline observation. For subsequent 3-D modelling, software was used which take these effects into consideration.

-- "xlocate" (written by C. Zelt) is a useful tool which helps to relocate the OBH position in three dimensions. Therefore, all traces with direct wave travel time picks and the OBH position during deployment need to be transformed into a cartesian UTM grid. The number of profiles crossing the OBH can in theory be between 1 and infinity. When using one profile only, it means that *xlocate* can also be used for 2-D repositioning. Here direct wave traveltimes of inline as well as offline observations may be used. Because of the hyperbolic equation describing the dependency of traveltime versus offset for a given water depth, an OBH can be located into the apex of a hyperboloid. The best projection in the x-y plane (i.e. northing and easting), has to be found by minimizing the deviation between the observed traveltimes and estimated traveltimes provided by the theoretical shape of the hyperboloid. Finally the new x-y location has to be transformed to mercator projection to be consistent with the UKOOA-format. Figure 6.3.3.1 shows the relocation for OBH79. Approximately 40000 UTM coordinates from a 2 km by 2 km wide grid with a 10 m spacing have been tested to find the best possible location. It turned out that OBH79 had to be shifted 51 meters to north-east from its observed position.

6.3.4 SEISMIC PROFILES
6.3.4.1 Test-Profiles SO 131-01, -02, -03

(C. Reichert, D. Klaeschen, A. Hojka)

Introduction

Shortly after the departure from Karachi during the early transit to the Ninetyeast Ridge study area three seismic test profiles (Fig. 6.3.4.1.1) were surveyed on the outer Indus shelf and slope. These tests were performed within the scope of earlier investigations (e.g. von Rad et al., 1995; von Rad & Tahir, 1997) that resulted in an ODP proposal submitted by von Rad et al. in January 1998.

The investigations focus on the stable, mid-depth oxygen-minimum zone (OMZ) between 200 and 1,200 m water depth in the northern Arabian Sea that prevents bioturbation and favours the accumulation of organic carbon (total organic carbon, TOC)-rich, partly laminated or even varved sediment. These conditions offer an excellent opportunity to study the variability of the tropical monsoonal circulation and marine productivity on millenial to annual timescales during the Quaternary in ultra-high resolution. The study area is influenced by

- warm and saline near-surface waters originating from the Persian Gulf
- high fluxes of both eolian and fluviatile (Indus River) terrestrial sediment
- high oceanic (monsoonal) surface water productivity and biogenic fluxes.

During a previous SONNE cruise (SO-90) in 1993 four areas within the OMZ off Pakistan were studied in more detail by taking a number of cores along three transects across the continental margin. Two of these transects are located on either side close to the deeply incised Indus Canyon. The Indus Canyon and its seaward channel-levee system is the major conduit for funnelling riverine detritus from the shelf down to the large Indus Fan. Therefore, the continental slope to its sides is formed by a draping of a sequence of hemipelagic sediment that were not interrupted by any turbidites during the past 50 Ka.

The characteristic sediment cores taken from OMZ water depths at the Indus continental slope reveal a consistent pattern of dark, TOC-rich, partly laminated intervals alternating with light, TOC-poor, pteropod-rich bioturbated intervals (von Rad et al., 1995; Schulz et al., in press; von Rad et al., in press). A strong correlation with the data of the Greenland Ice Core data (GRIP) were found evidencing almost coincident climate variations over large parts of the northern hemisphere (Schulz et al., in press).

High-resolution seismic studies (3.5 Khz) show that the Late Quaternary sedimentation is influenced by fluctuations of productivity, anoxia, fluvial input and delta progradation controlled by sea-level changes (von Rad & Tahir, 1997). Basically, four episodes can be distinguished from Late Pleistocene to present. Slumping and debris flows were triggered at the continental slope during the last glacial maximum. Correlation of acoustic reflectors dated in lower to upper slope cores yields that the sedimentation rates on the upper slope are in the order of 30 - 40 cm/Ka.

During the MAKRAN I survey (SO-122) multi-channel seismic (MCS) data were acquired with 24 traces also in the area of the Indus fan, shelf and slope (Roeser et al., 1997). Profile SO122-16 runs rectangularly to the slope in the NW of the Indus Canyon and crosses the OMZ. The data of that profile show in the upper 400 ms two-way time (TWT) below sea floor (bsf) strong, continuous, subparallel, gently seaward dipping reflectors that are interpreted as progradational prodelta mud sequences. From the sedimentation rates maximum ages between 1 (Mid-Pleistocene) and 2.7 Ma bp (Tertiary/Quaternary boundary) are assessed. The total thickness of the sediment overlying the seismic basement approaches 5 - 6 s TWT (approximately 7 - 10 km).

By bio-, chrono-, chemo- and magnetostratigraphical studies this textbook example of fine-layered, laminated and undisturbed Quaternary sediment it is intended to clarify the paleo-oceanographic and paleo-climatological evolution as well as the variation in paleo-productivity during the past 2 - 3 Ma. Thus, an ODP drilling proposal was submitted that forms part of a group of high-resolution paleo-oceanographic drilling proposals in the northern Arabian Sea: POM-1 (Pakistan Oxygen Minimum) that should reach a subbottom depth of 400 m, i.e. penetrate a time span of 1 - 2.7 Ma maximum. The location was selected on the basis of the SO122-16 MCS profile. However, at the optimum position, there was no profile crossing that could provide the required 3D dip information.

Since our transit to the Ninetyeast Ridge study area runs very close to the POM-1 location we were asked by the ODP proponents to conduct at least one additional underway seismic profile across the POM-1 location rectangularly to SO122-16.

Data acquisition

Since not all pre-conditions could be achieved in due time we were only able to run a set of test profiles checking our instrumentation that was used for the first time in this configuration. However, the results are so encouraging and important that they are presented here.

The position map is presented in Fig. 6.3.4.1.1 along with bathymetric data. The profile data are given in Appendix 9.1.1 and 9.1.2.

Equipment

1 Ocean Bottom Hydrophon (OBH); position SO131-03 at 23° 06,2' N and 66° 27,7' E

1 Mini-streamer with three traces (50 m active length) mid-ships, 120 m lead-in section, 10 m damping section, nearest trace 138 m from stern, tail at approximately 14 m depth.

1 VLF airgun on port-side, 3 L volume, 30 m from stern, pressure: 130 bar (1,880 psi); the trigger unit used for these profiles differs from that described in section 5.3.1. Due to the test character a provisional system was operated that did not use the VCAD and VZAZ units. A simple trigger programme on a PC contolled the shooting intervals and recorded the time breaks with reference to the internal quartz clock of the PC. This clock was calibrated just before commencement of each profile with a GPS reference. As the results demonstrated there was a linear time shift during operation time that can be compensated by an appropriate factor. The time breaks used for processing were referenced to GPS time (UTC) directly.

1 *Methusalem* recording unit on profiles SO131-01 and 03; one *MBS* on profile SO131-02 providing higher frequency resolution by asampling rate of 1 ms.

Parameters

ship's speed 5 kn over ground
shot interval 10 s (ca. 26 m on seafloor)

Processing

The Mini-Streamer and OBH data were processed differently from to the scheme outlined in chapter 6.3.2. The reason was that only one airgun was used for shooting, and the source signal had strong reverberations of 1 s data length. Further was the Mini-streamer recording system (anti alias and low cut filters) not yet optimal tuned for these three profiles.

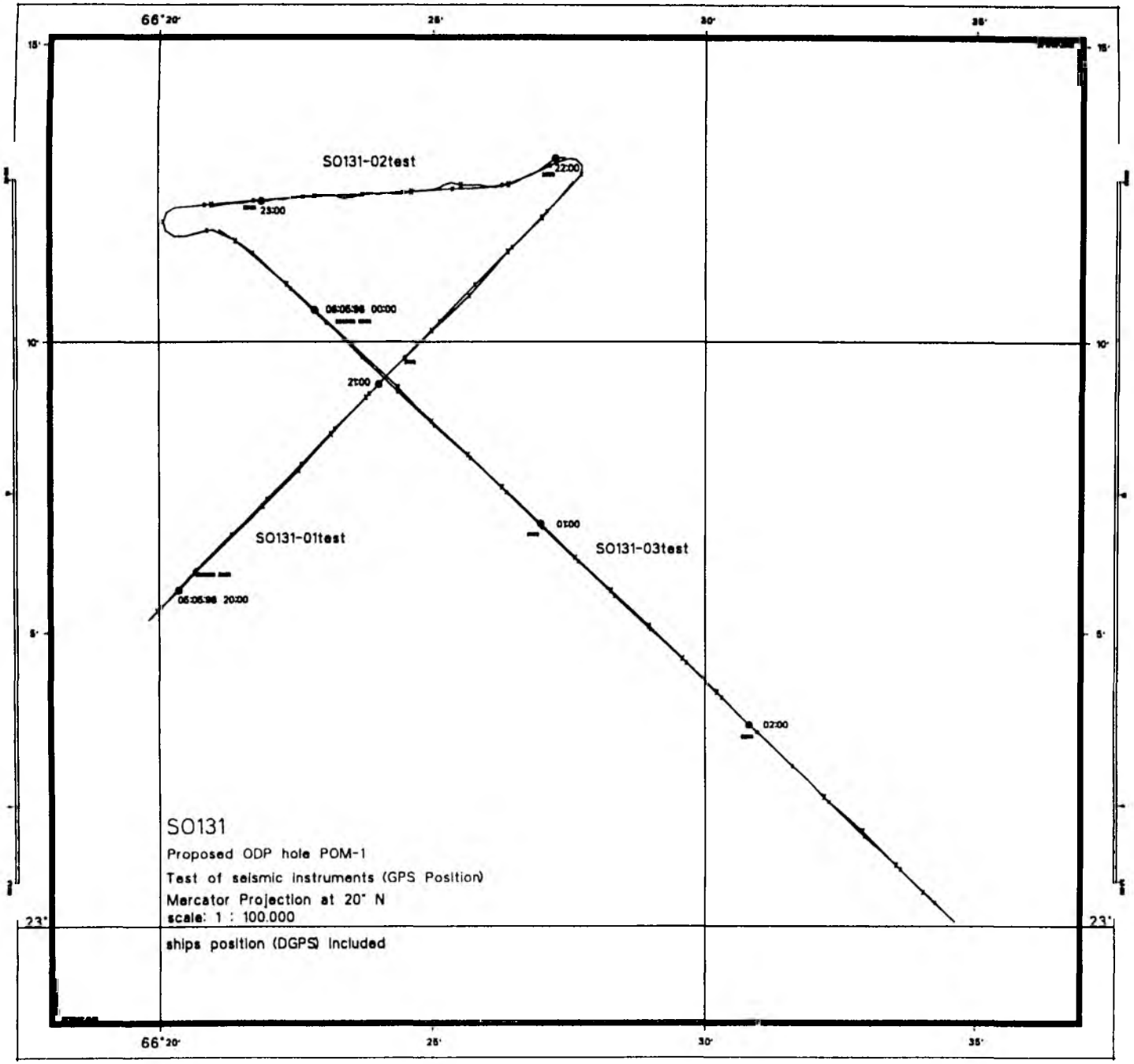

Fig. 6.3.4.1.1: Position map of profiles SO131-01 through -03.

Processing sequence for the Mini-Streamer Data:

- Input SEGY-data:
  Profile 01, 03 with 5 ms sample rate, trace length 4 s, with complete geometry information.
- Profile 02 with 2 ms sample rate, trace length 4 s, with complete geometry information.
- Wiener deconvolution: gate length 0.5 s (0-0.5 s, direct wave), operator length 500 ms, prediction interval 0 ms
- Ormsby frequency filter (minimum delay characteristic) with

	lower stop/pass	and upper pass/stop band (Hz)
Profile 01, 03:	13/17	40/50
Profile 02:	13/17	110/130

- time variant scaling with 2 s window length (agc).
- nmo-correction based on water velocity of 1500 m/s
- stacking in common shot point domain along the profile
- Wiener deconvolution: gate length 3.5 s (0.5-4 s), operator length 500 ms, prediction interval 0 ms
- Ormsby frequency filter (zero phase characteristic) with

	lower stop/pass	and upper pass/stop band (Hz)
Profile 01, 03	13/17	40/50
Profile 02	13/17	110/130

- time variant scaling with 0.25 s window length at 0.25 s and 1.5 s window length at 4 s (time variant agc).

Processing sequence for the OBH-Data:

- Input: SEGY-data, 5 ms sample rate with complete geometry information
- Wiener deconvolution: gate length 12 s (0-12s), 100 traces for averaging the autocorrelations, operator length 1000 ms, prediction interval 0 ms
- Butterworth frequency filter: 3-45 Hz
- Gated Wiener deconvolution: gate length 2s, overlap 1 s, operator length 480 ms, prediction interval 80 ms
- time and offset dependent Ormsby frequency filter as described in chapter 6.3.2.2. (on time shifted traces with a reduced time scale of 6 km/s).

Description of Profiles SO131-01 and -02

Profile SO131-01 runs from SW to NE across the continental middle slope and upper slope scarp. Profile SO131-02 is connected to it in the NE and runs almost exactly westward with an approximate angle of 45° to the slope strike. For the sake of simplification and comparison both data sets are given in one display (Fig. 6.3.4.1.2). The left-hand panel shows SO131-01, and the right-hand panel SO131-02. While profile SO131-02 is connected to -03 in the west a crossing exists between SO131-01 and -03 that is marked in the figure.

According to their strike direction the seafloor in both profiles shows considerable depth variation from 410 m at their junction to 1,200 m in the SW and to 1,050 in the west, respectively. A scarp exists at about 3 km distance on either side of the junction. It is characterized by a number of near-vertical normal faults extending over a range of some 3 km that is characterized by weak folding. The other portions of the profiles show a very smooth seafloor. Underneath an about 400 ms TWT broad band of parallel reflections follows Layer I (L I) that is unconformably separated from the underlying domain by a stronger reflector (R I). The seafloor reflection shows a broad double pulse that is followed after some milliseconds by a weaker signal that has a very similar shape. Since the strong bubble effect due to the use of a single airgun could strongly be discriminated by appropriate deconvolution this must be a superposition effect of the fine layering in the near-bottom strata inferred by von Rad & Tahir (1997) from high-

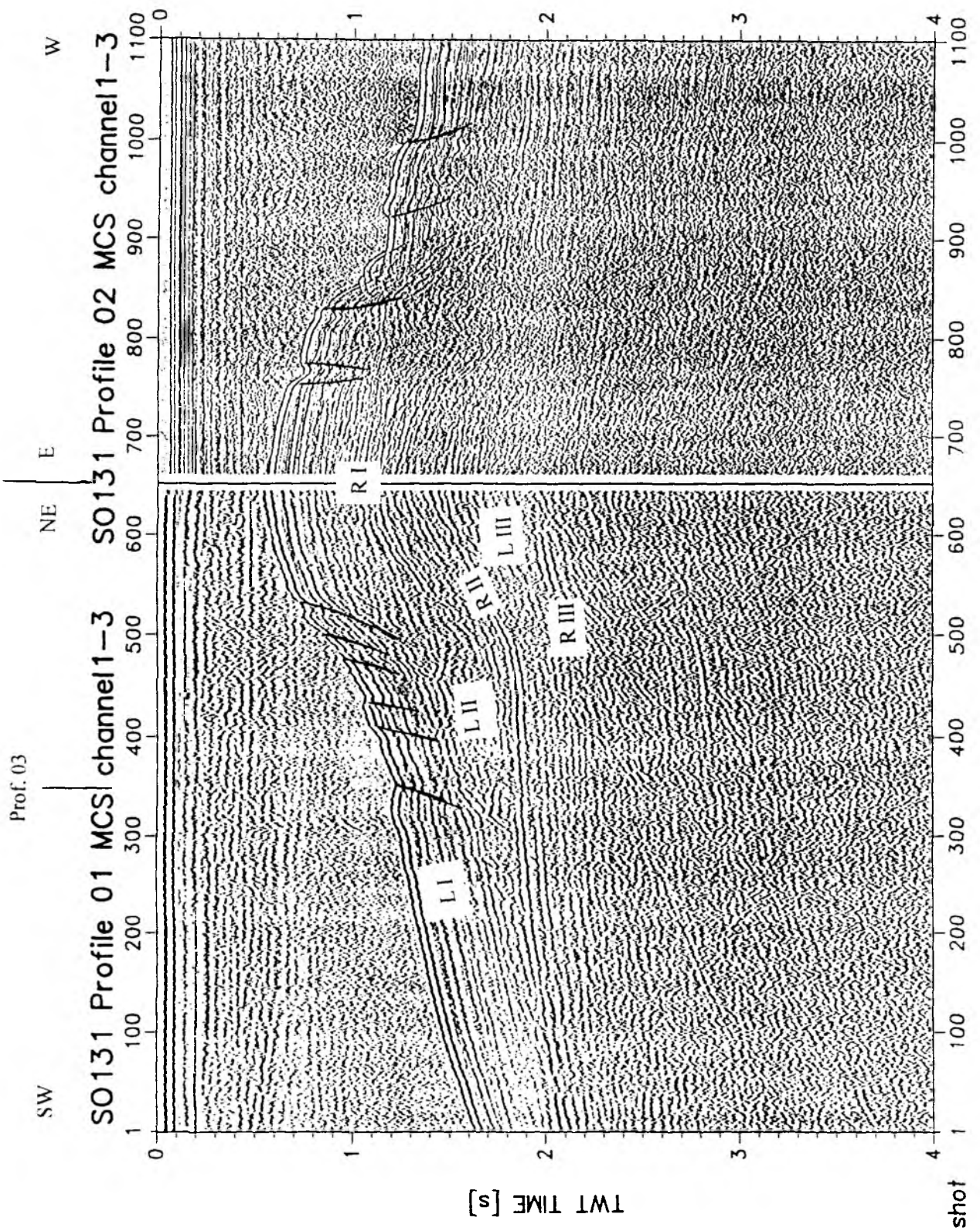

Fig. 6.3.4.1.2: Unmigrated traveltime section of profiles SO131-01 (left-hand panel) and SO131-02 (right-hand panel) with interpretation. The crossing with profile SO131-03 is indicated.

resolution seismics (3.5 Khz) adding up the particular reflections to a low frequency mixed signal. In fact, profile SO131-02 (right-hand panel in Fig. 6.3.4.1.2) that was recorded with a *MBS* recorder enabling a broader frequency band up to higher frequencies clearly shows the very fine structure of L I in great detail. It should be noted that the high frequency content of profile SO131-02 seems to decrease the strength of the reflections.

Layer II (L II) unconformably underlies L I and is represented by an irregular pattern of short reflections that seem to be parallely aligned only beneath the upper slope. The base of L II is represented by a strong and very smooth reflector (R II) that can be followed without interruption over almost the entire length of either profile. L II is thinning considerably in seaward direction. The next layer toward greater depth (L III) is characterized again by clearly subparallel reflection elements that show, however, a greater degree of discontinuity than those of L I. The basis is somewhat uncertain. However, there are indications - particularly in comparison with profile SO131-03 - that the reflection elements (R III) that show only very little greater strength than their surroundings represent an unconformity to the underlying very diffuse pattern of weak reflectivity.

Description of Profile SO131-03

Profile SO131-03 runs NW-SE parallel to the continental slope and crosses profile SO131-01 and the proposed ODP location POM-1. In contrast to the profiles described above, the seafloor morphology is extremely hummocky (Fig. 6.3.4.1.3). A great number of near-vertical normal faults is observed separating domains that are weakly folded. Folding is considerably decreased in the southeastern portion of the profile. The layers and reflectors described previously are clearly developed here and can be traced easily. They fit very well in traveltime and character at the crossing with profile SO131-01. Reflecor I parallels the seafloor morphology in the northwestern portion and deviates considerably in the southeast where it represents a clear unconformity. L II is relatively constant in thickness along the entire profile whereas L III thins remarkably toward SE.

OBH data of station SO131-01

The refraction events observed by OBH station SO131-01 (Fig. 6.3.4.1.4) along profile SO131-03 (Fig. 6.3.4.1.3) show medium to poor quality corresponding to the weak energy source. The data are deconvolved in order to suppress the strong bubble. The signal fades out at 14 km offset, already. The observed first arrival times give the following apparent velocities from top to bottom:

	toward NW	toward SE
•	v1 = 2.5 km/s	v1 = 2,5 km/s
•	v2 = 3.1 km/s	v2 = 2.9 km/s
	v3 = 3.8 km/s	v3 = 3.2 km/s

The velocity of the uppermost layer could not be determined since the related events are concealed by the direct water wave. An assessment of the boundary values yields 1.5 km/s < v0 < 1.85 km/s. The small direction-dependent differences in the velocities indicate only little dip of the corresponding boundaries as it was expected in slope-parallel direction.

Ray-tracing calculations were performed in order to determine the appropriate velocity depth model using the MacRay program from Luetgert (1992; see also section 6.3.3 for detailed description). According to the observations the geometry comprises three layers over a half space. As initial model a depth assessment from the cross-over distance formula was used. The final model that could be elaborated within the available time is given in Fig. 6.4.3.1.5 (observed and calculated travel times in the upper panel; model boundaries and ray paths in the lower panel) and in Fig. 6.4.3.1.6 (velocity model used). All observed phases could be matched by the calculated values within a deviation of 100 ms or smaller.

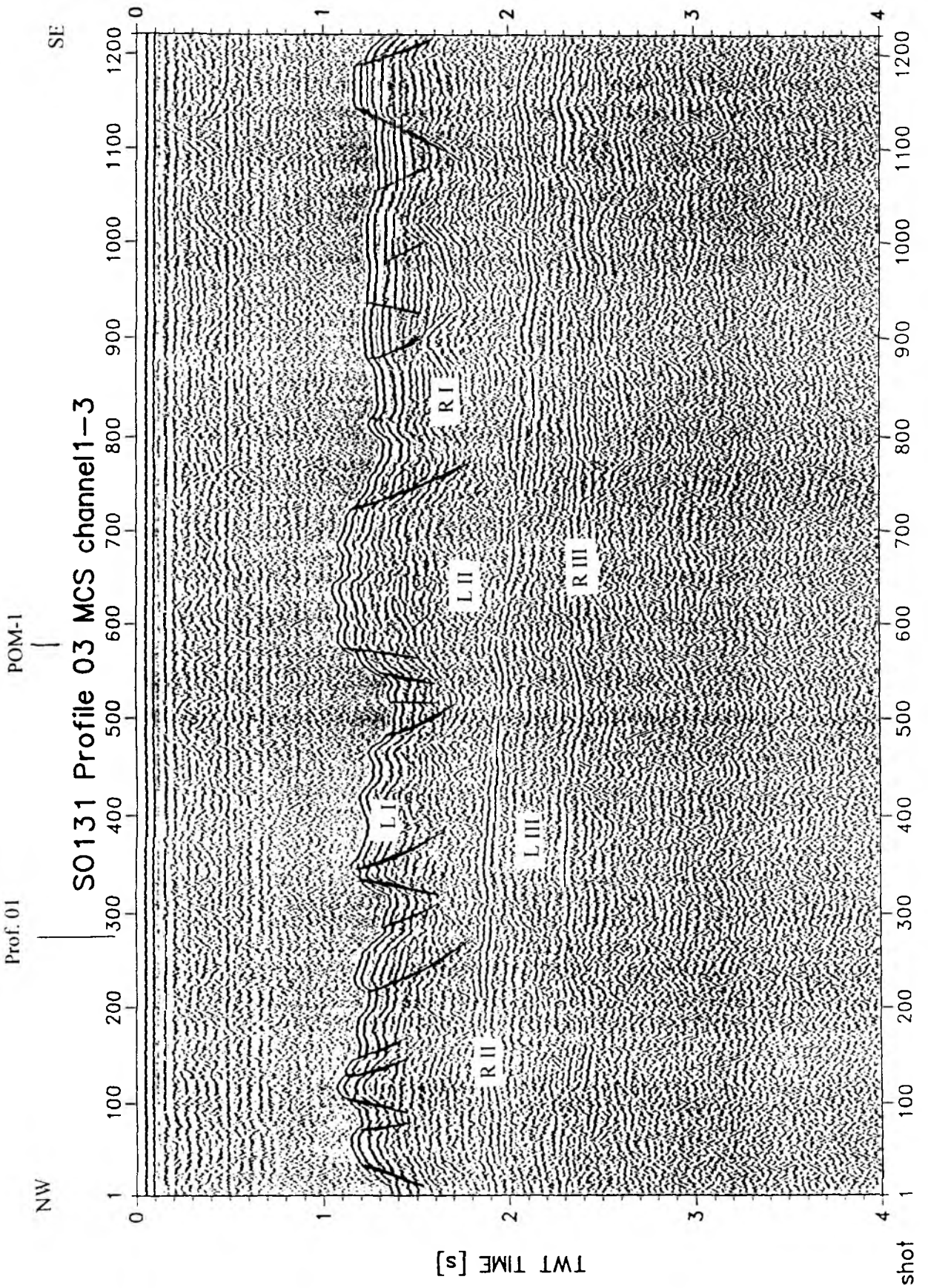

Fig. 6.3.4.1.3: Unmigrated traveltime section of profile SO131-03 with interpretation. The crossing with profile SO131-01 and the location of the proposed ODP drillhole POM-1 are indicated.

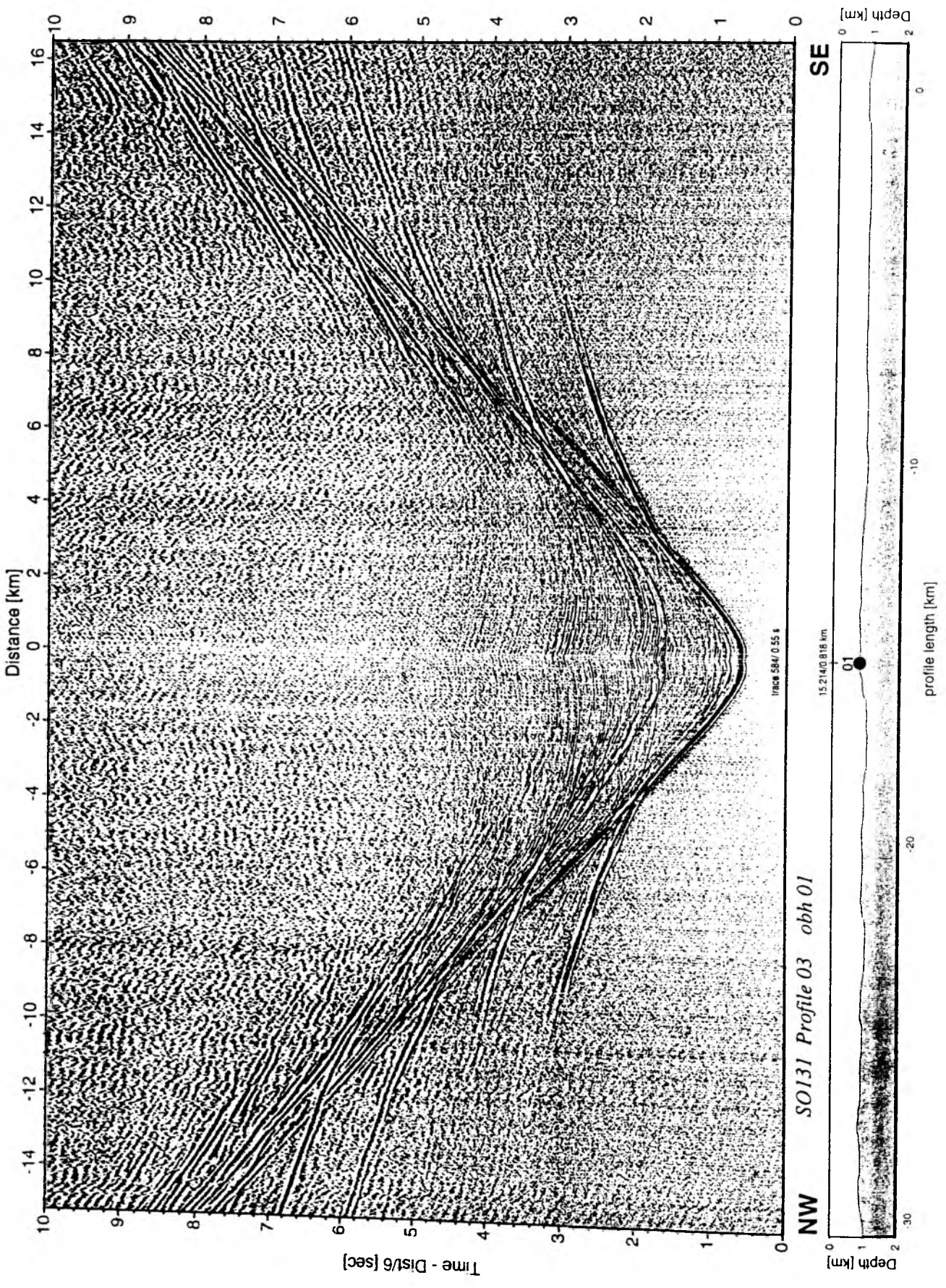

Fig. 6.3.4.1.4: Traveltime section of OBH station SO131-01 on profile SO131-03. The time scale is reduced with a velocity of 6 Km/s.

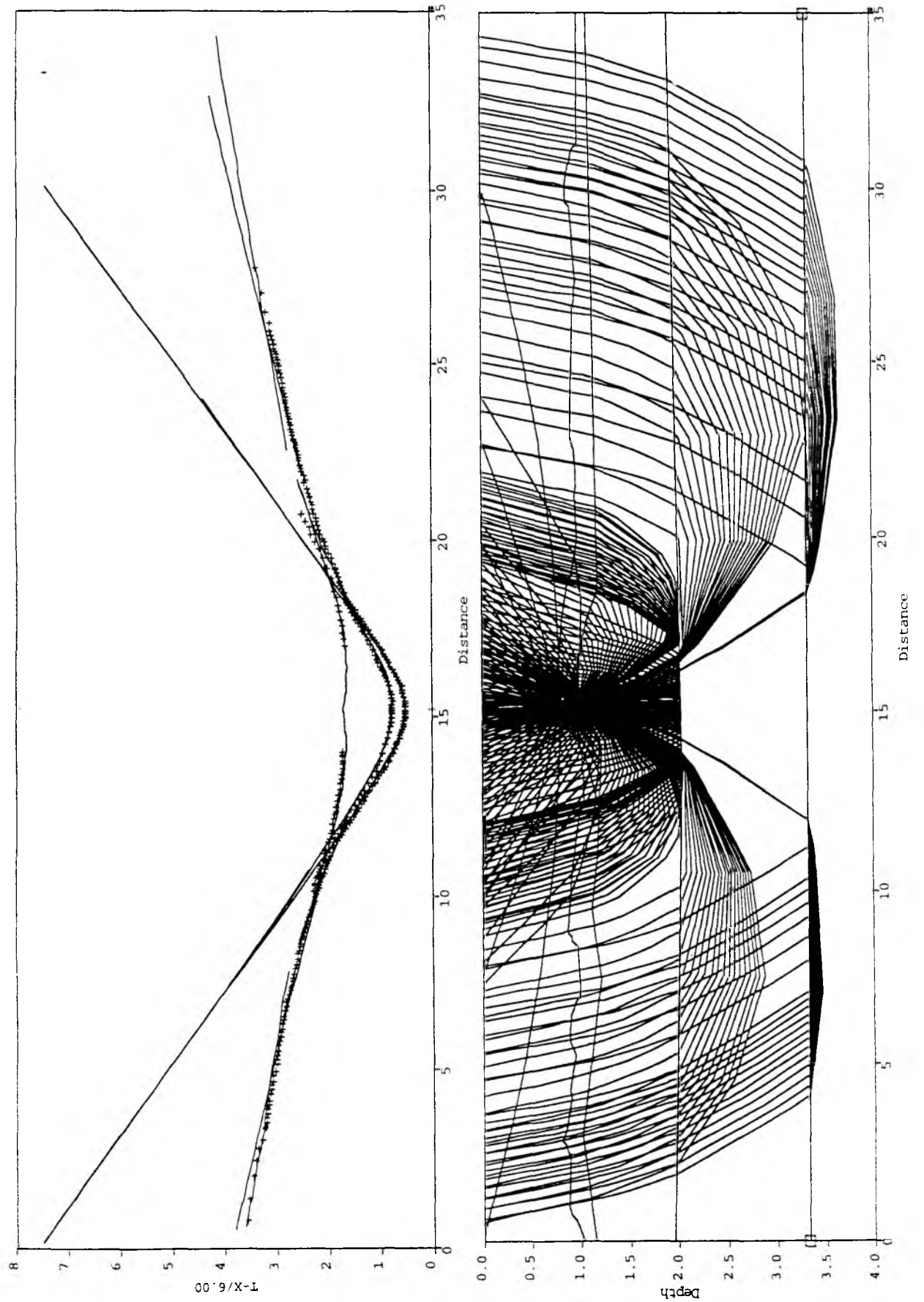

Fig. 6.3.4.1.5: Raytracing for OBH station SO131-01. Upper panel: traveltime picks (crosses) and calculated traveltimes (solid lines). Lower panel: ray paths.

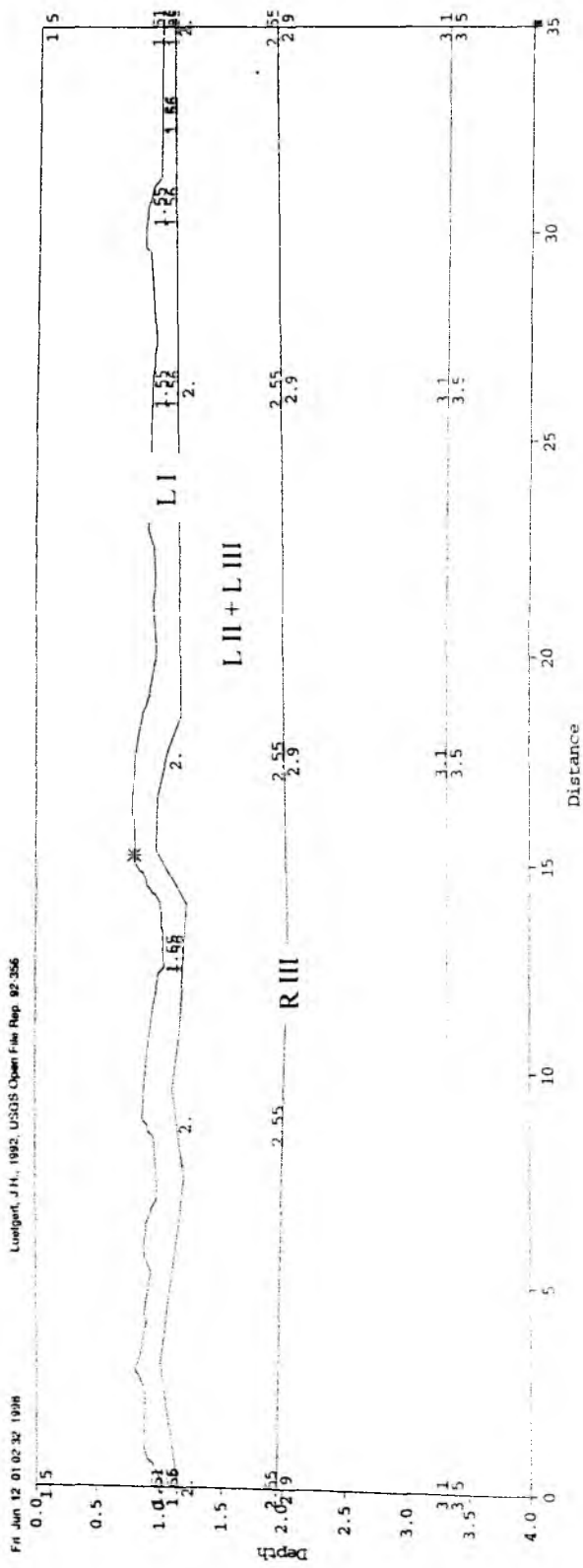

Fig. 6.3.4.1.6: Velocity model for OBH station SO131-01.

The uppermost layer L I bounded by the seafloor and R I follows subparallely the seafloor morphology bearing a thickness of some 260 m at the POM-1 location (= OBH 01 position). It is characterized by velocities of 1.55 km/s close to the water velocity indicating fresh, unconsolidated sediments. It must be emphasized that the ambiguity between thickness and velocity has not been analyzed due to lack of time. However, the almost perfect fit of the underlying layers shows that we are not very far from reality. Below a layer of 1.000 m thickness at POM-1 location. A velocity gradient from 2.0 to 2.55 km/s was modeled. During modeling work it turned out that reflector R II obviously is not represented or visible in the OBH data by a separate travel time branch. It probably does not bear a prominent velocity discontinuity because appropriate modeling was not possible. Thus it appears that reflector R II is hidden in the corresponding curved travel time branch. The normal incidence TWT bottom reflection time of L II corresponds almost exactly with the R III reflector in the near-vertical reflection data and gives 1.2 km bsf at the POM-1 location. Underneath, a 1.3 km thick layer with a small velocity gradient from 2.9 to 3.1 km/s follows. Its corresponding near-vertical reflection time of some 3.0 s cannot be checked in the near-vertical reflection data since no continuous reflector is observed in this domain that is additionally masked by multiples.

Discussion and conclusions

The data acquired during the SO-131 cruise show a strong similarity to the results of profile SO122-16. All three layers and their respective bottom reflectors are recognized again, and they show the same character in all data sets. Also their TWT or depth positions are strongly comparable respective to their relative slope locations. The uppermost layer (L I) is characterized by fine layering and represents hemiplagic sediment in mostly undisturbed sequence of Quaternary age (von Rad & Tahir, 1997) which is supported by the observed low seismic velocities. At particular slope locations, however, they are disturbed probably by slumping and creeping. The thickness of L I varies only little around a few hundred metres.

Near-vertical normal faults are observed dissecting L I close to the upper slope scarp extending downslope by 5 to 8 km. On the profiles rectangular to the slope they clearly indicate gravitational slumping and creeping according to their position at the steepest part. Profile SO131-03, runs parallel to the slope and is located just in this disturbed part. Near-vertical normal faults are observed along the entire line. Here, they could represent transpressional and transtensional structures that form due to the slumping and creeping process taking place in out-of-plane direction and compensate for the downslope movement differences. On the other hand, the observed local depressions of the seafloor could represent small canyons where rapid mass transportation and currents occur as it is suggested by the bathymetric map presented by von Rad & Tahir (1997). However, the clear near-vertical faults at their flanks and the missing levees commonly observed elsewhere are counterarguments. Possibly, both effects are superposing another.

The deeper layers L II and L III are clearly bounded by continuous reflectors obviously representing unconformities. Their nature and age is unclear, yet. Most possibly they are formed by sea level variations. The bondary between them bears no sharp velocity contrast.

Regarding the proposed location of POM-1 it must be emphasized that the presently selected one is very disadvantageous with respect of the intended aims according to our data and the re-inspection of profile SO122-16. In our view a slope position between 700 ms TWT (520 m) and 1.300 ms TWT (980 m) should be avoided. In contrast, according to the data at hand a downslope position or upslope above the upper slope scarp is advisable in order to drill undisturbed sequences. The latter provides the additional advantage that 3D dip control is given at the junction between profiles SO131-01 and -02 if this position would be selected.

6.3.4.2. SEEBOSEIS – First Results

(I. Grevemeyer, O. Exner, R. Herber)

The aim of the on-bottom seismic experiment on Ninetyeast Ridge near ODP site 757 was a test of the rebuilt SEEBOSEIS tool. Nevertheless, SEEBOSEIS was constructed to sample the seismic structure of the uppermost crust or sediment. Therefore, a succesful deployment of the instruments should yield valuable clues about the P-wave and S-wave velocitiy structure within the uppermost kilometre of crust.

The setup of the experiment was described in Chapter 5.3.3.2. All five sources placed along the refraction line imploded. The direct wave traveling along the seabed and several seismic phases were detected by four of the ocean-bottom receivers. The off-line broadband OBH and the low-frequency MBS-OBH (the low sampling rate was chosen to sample guided waves) failed. In addition, the HH-OBS suffers from noise of unknown source, though the hydrophone channel provided data of excellent quality. However, the remaining instruments provided 35 recordings of the five bottom shots, i.e., 20 recordings by hydrophones and 15 recordings from the three components of the MBS-OBS. This database is sufficient to draw some conclusion.

First we have to note that the seabed was relatively plain (Figure 6.3.4.2.1) so that seafloor topography did not affect the recorded wave field significantly. To allow an easier handling of the data from OBH 91 and OBS 93, we resampled those data at 4000 Hz. Figures 6.3.4.2.2 to 6.3.4.2.5 show the first breaks and the direct wave detected by the hydrophones. Most profound, the broadband instruments from the Institute of Geophysics, University of Hamburg (see Chapter 5.3.3.2) were able to detect much high frequencies than the MBS systems from Geomar. Although OBH 90 (sampling rate 500 Hz) has recorded first breaks, there might be aliasing in the data. A comparison of wavetrains recorded by the MBS-OBS (sampling rate 1000 Hz) and OBH 91 and OBS 93 may suggest that 1000 Hz might be sufficient to sample first breaks. Nevertheless, the images of the P-wave field sampled at 4000 Hz are much clearer. We therefore suggest that instruments with sampling rates of more than 1000 Hz are recommended for the detection of bottom shots.

OBS 88, OBH 91 and OBS 93 provided data from a reversed refraction experiment, and OBH 90 provided shots recorded off-line. First breaks from the bottom shots were recorded over a distance of about 2100 m. So the bottom shots will allow us to determine the velocity structure within the uppermost hundred meters. Along with the surface shots recorded by the ocean-bottom receivers (e.g., Figure 6.3.4.2.6) the dataset will allow us to determine P-wave velocities from the seabed down to mid crustal levels.

Previous studies have shown that bottom shots generates dispersed interface or guided waves (called Scholte waves) that travel along the seafloor in the same way Rayleigh waves travel along the surface of the Earth (Essen et al., 1981; 1998; Whitmarsh and Lilwall, 1982; Kirk et al., 1991; Nolet and Dorman, 1996). The propagation of these waves is closely related to S-wave velocity of crust. Therefore, the detection of Scholte modes provided the opportunity to study S-wave velocities of the upper crust. Figure 6.3.4.2.7 shows interface waves recorded by OBH 90 and OBS 88. Wavetrains useful for dispersion analysis, however, were only detected by the vertical geophone. In Figure 6.3.4.2.8 we show all five shots. A striking feature of the figure is that the energy transported by Scholte modes increases from shot no. 1 to shot no. 5. This observation simply depends on the epicentral distance, i.e., shot no. 5 was located much closer to the OBS than shot no. 1. The distance was ~800 m and ~2100 m, respectively. After relocating the shots, dispersion analysis will yield the group velocity as a function of frequency, i.e., the Gabor matrix. The Gabor matrix yields the dispersion curve which can be used to determine the S-wave properties of the structure sampled by Scholte waves (e.g., Essen et al., 1981; 1998).

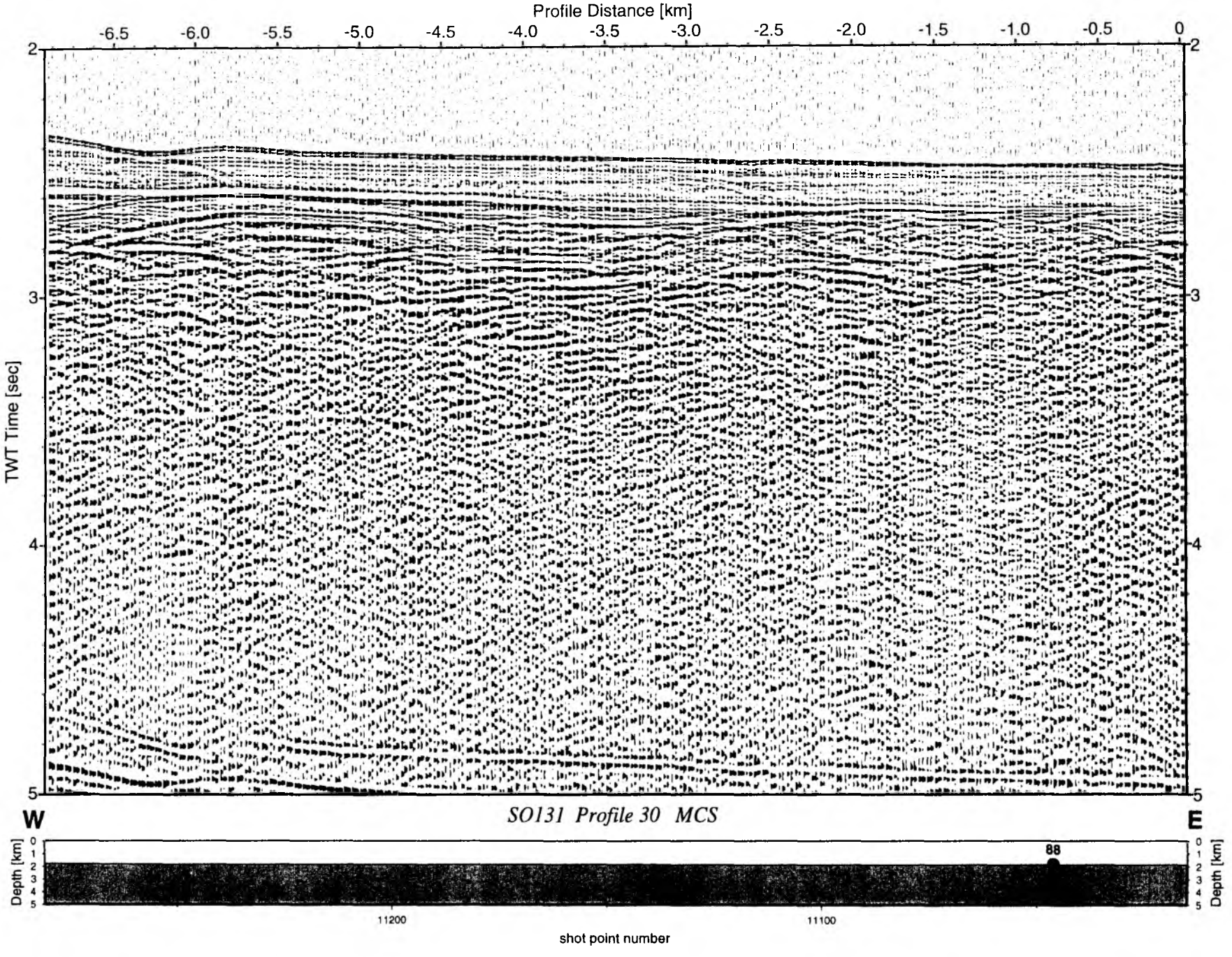

Figure 6.3.4.2.1: Seismic section from MCS stack, Profile 30.

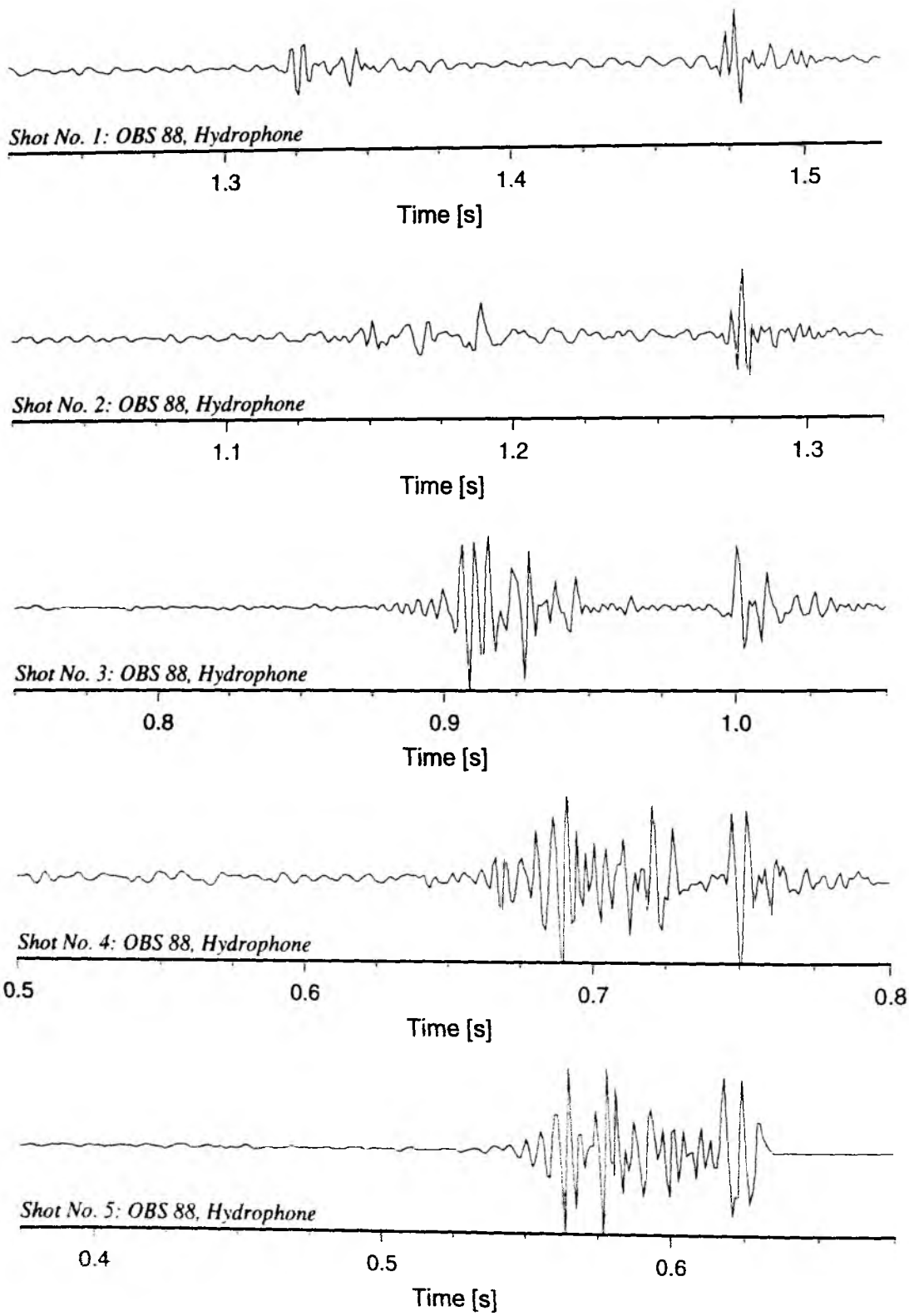

Figure 6.3.4.2.2: Bottom shots recorded on the hydrophone channel of OBS 88.

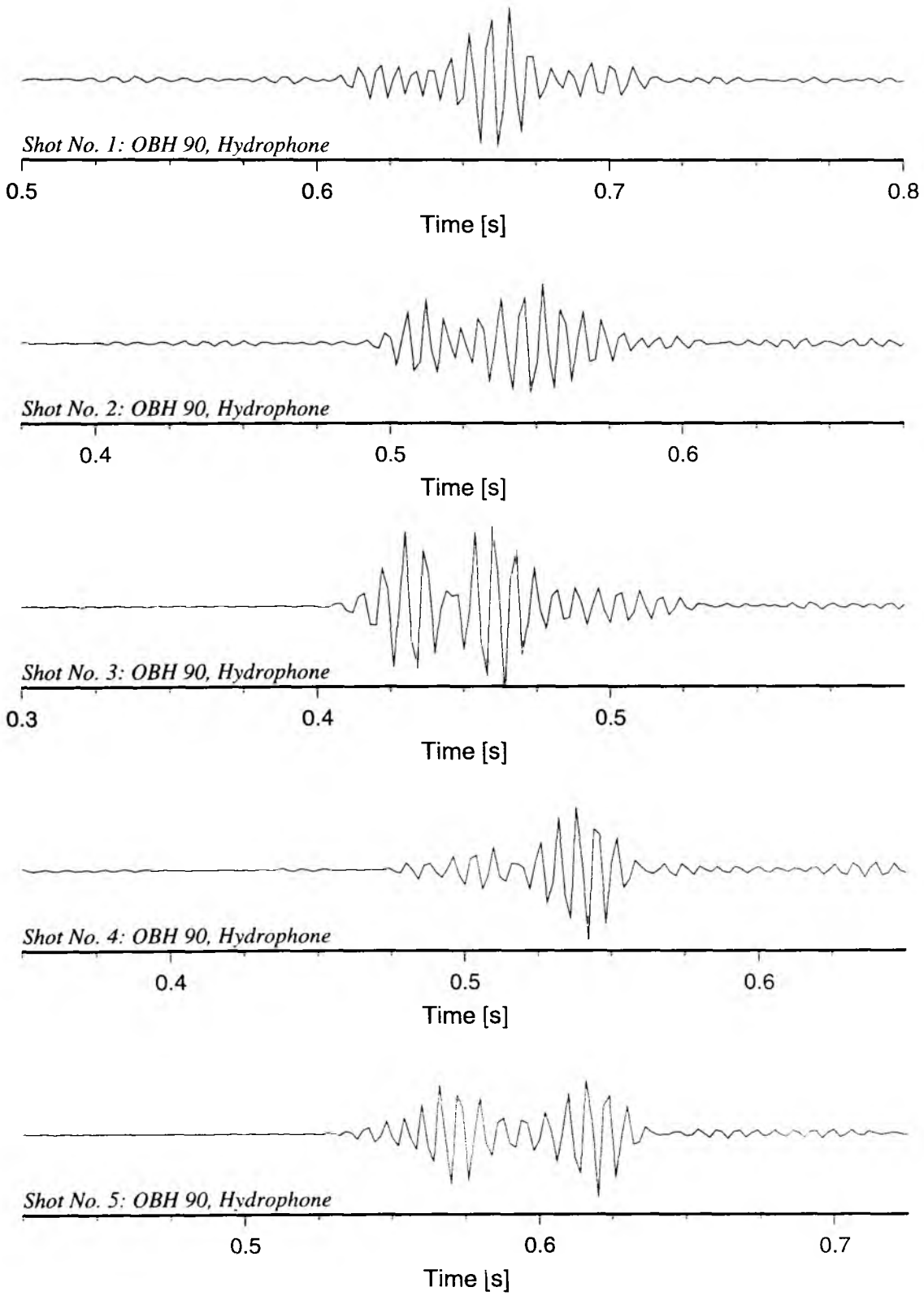

Figure 6.3.4.2.3: Bottom shots recorded on OBH 90.

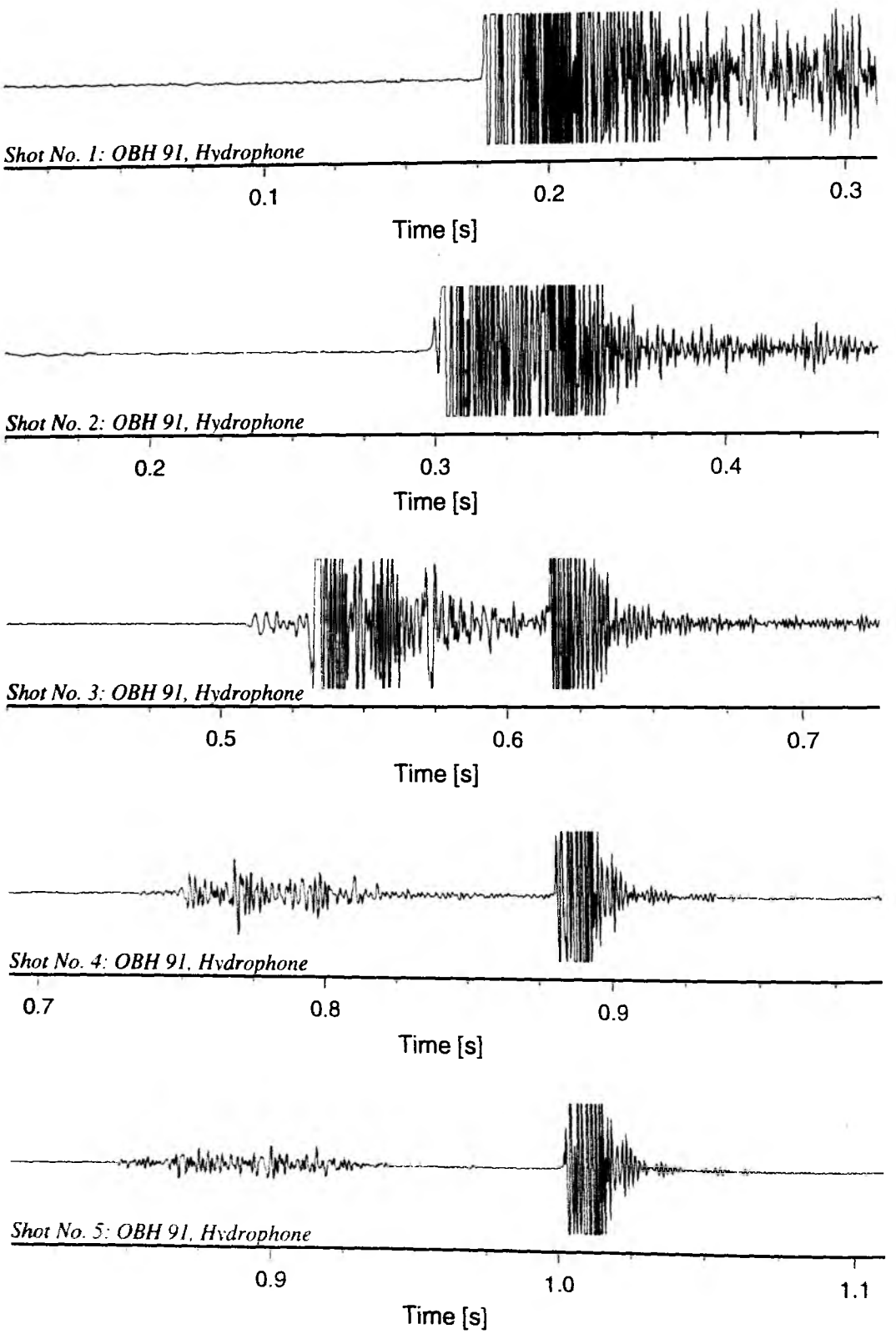

Figure 6.3.4.2.4: Bottom shots recorded on OBH 91.

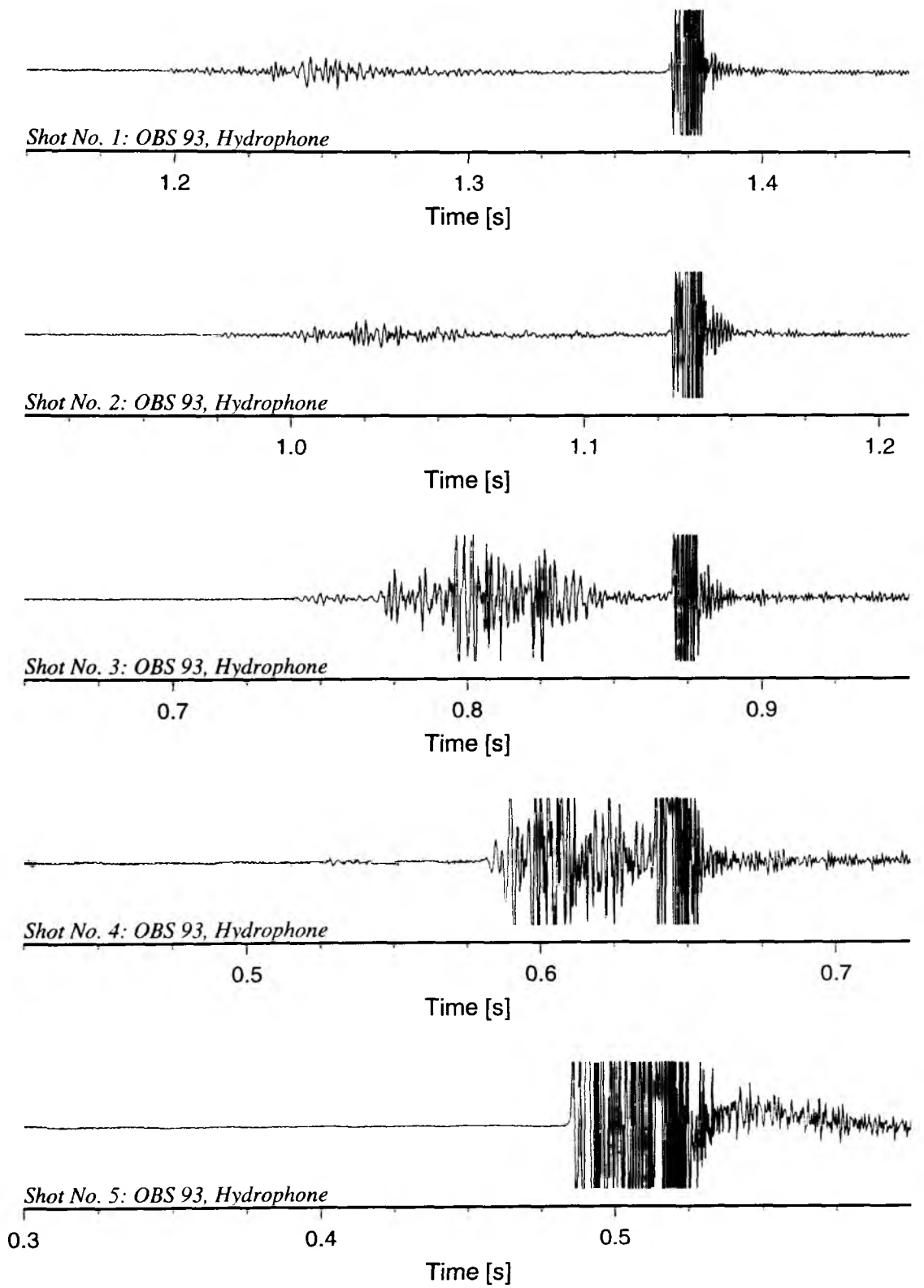

Figure 6.3.4.2.5: Bottom shots recorded on the hydrophone channel of OBS 93.

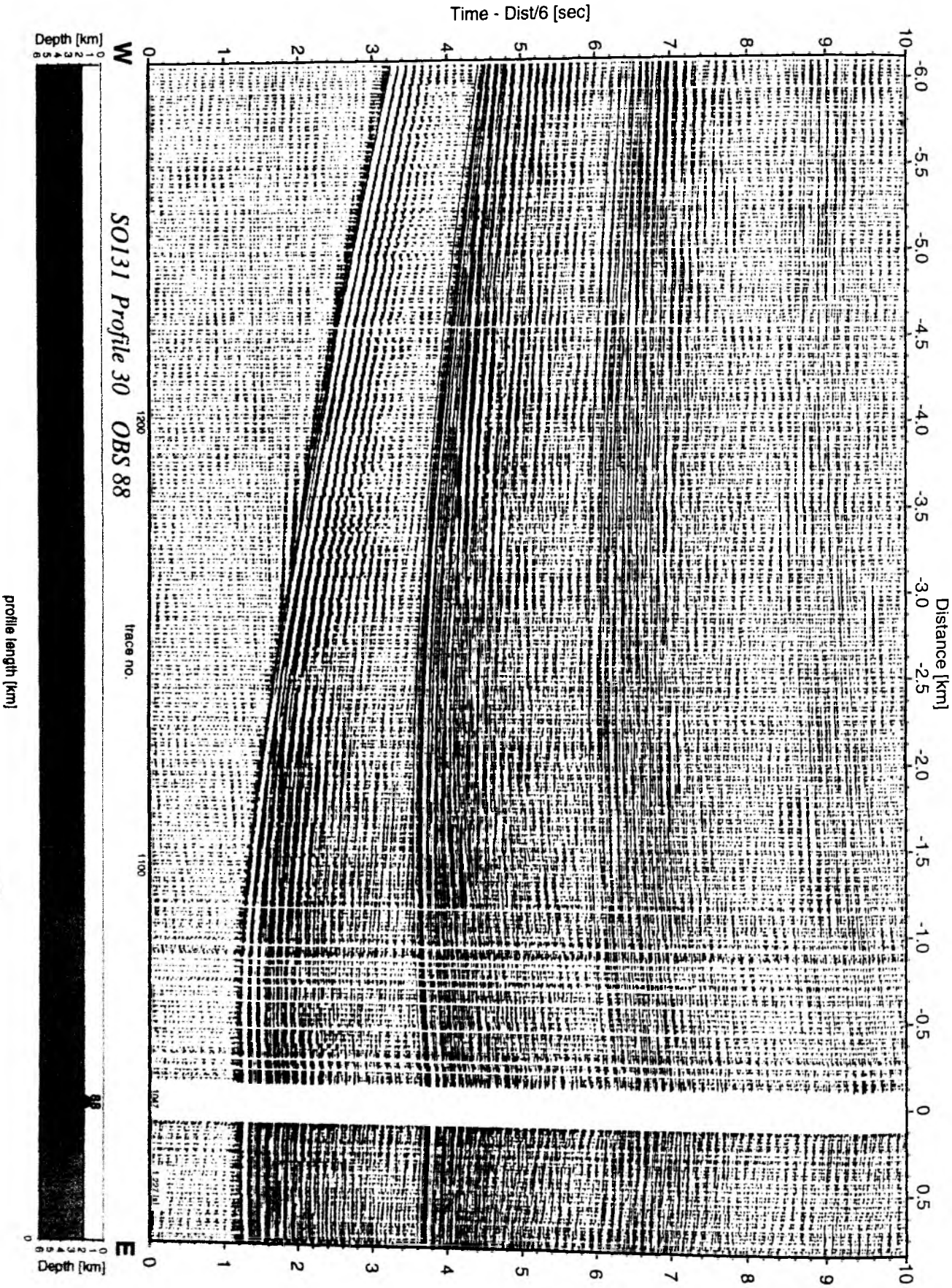

Figure 6.3.4.2.6: Record section from OBS 88 hydrophone, Profile 30.

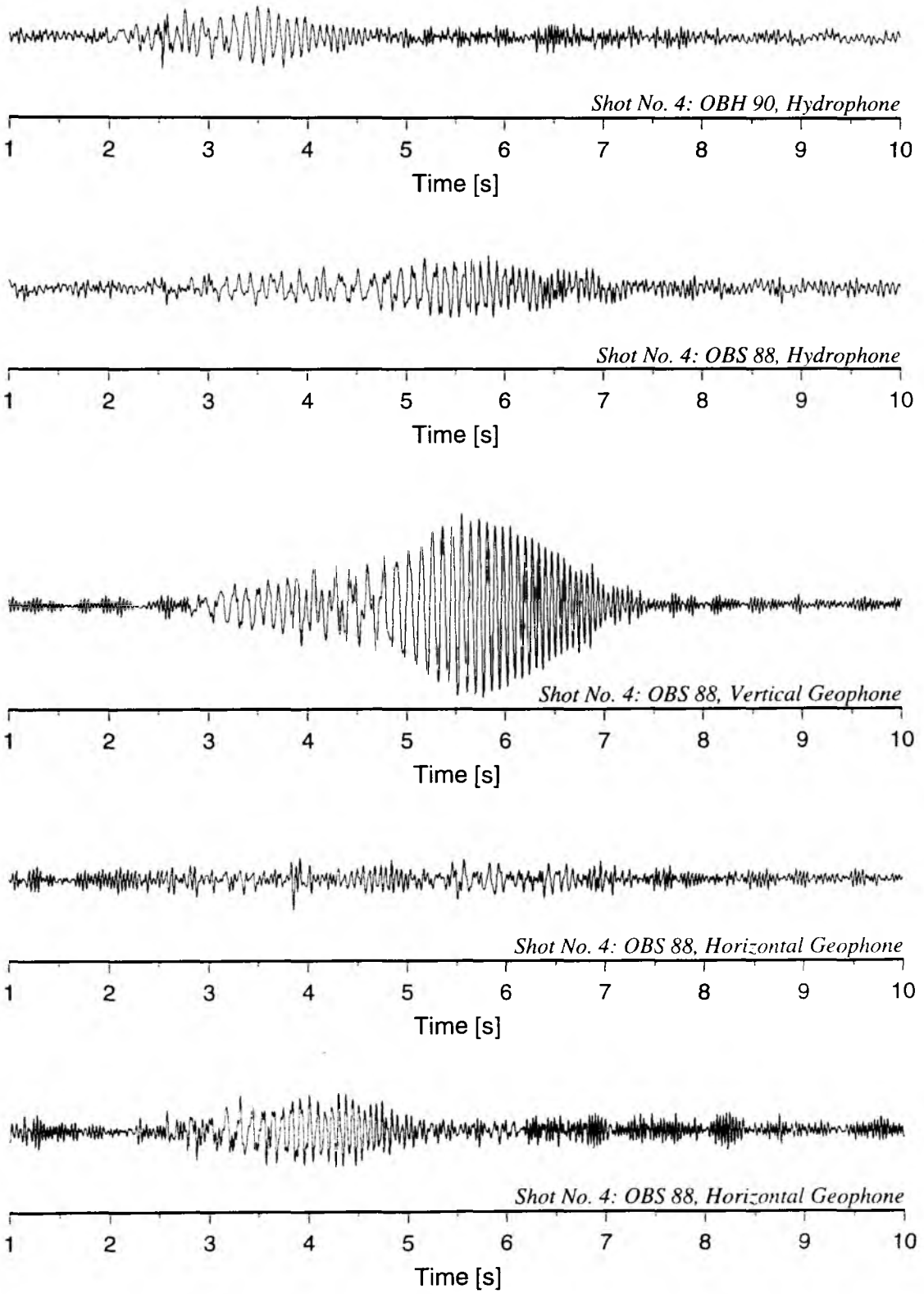

Figure 6.3.4.2.7: Scholte waves from shot no. 4 recorded on OBH 90 and OBS 88.

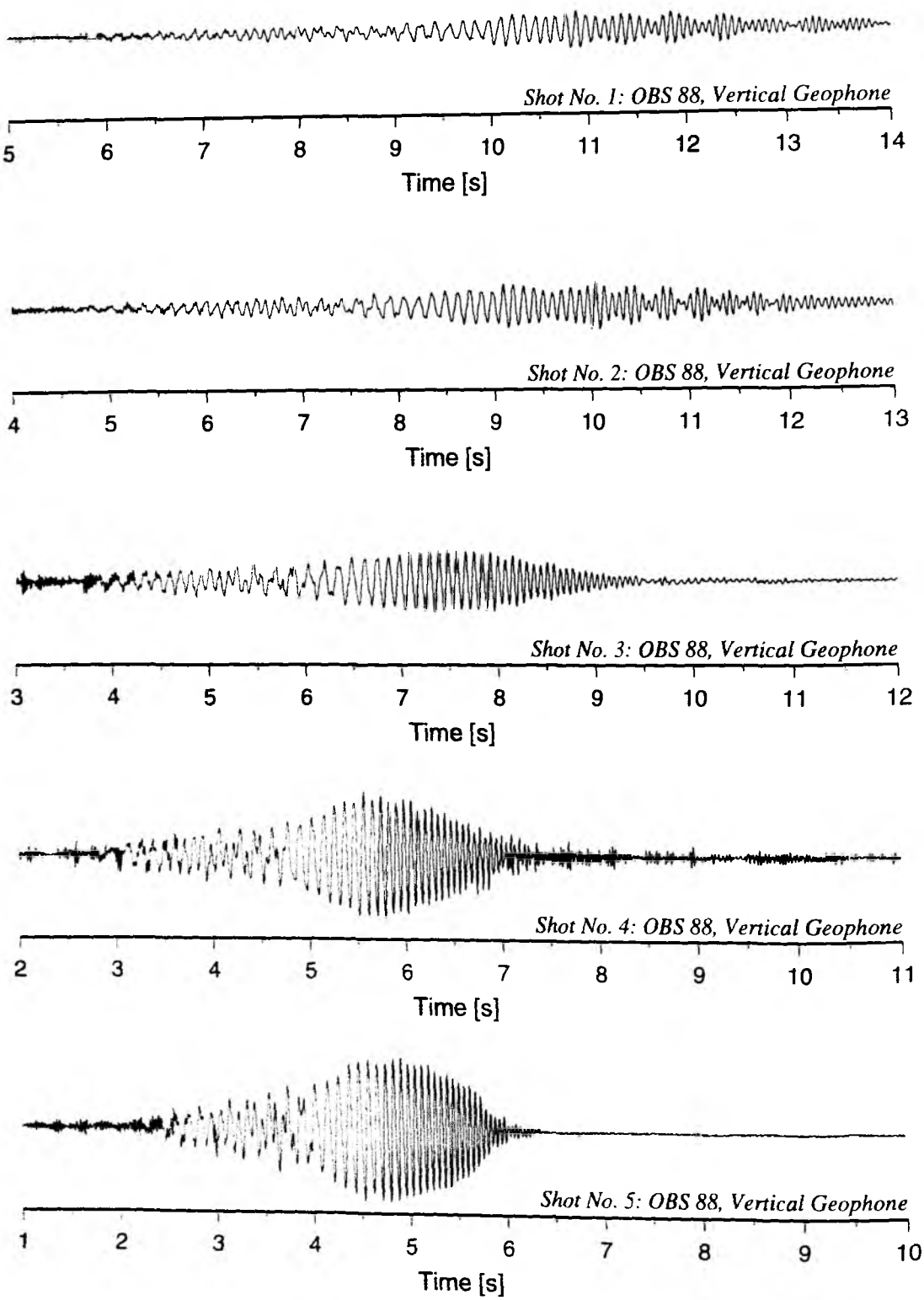

Figure 6.3.4.2.8: Energy transported by Scholte waves versus distance, OBS 88.

6.3.4.3 TEST OF THE GEOMAR HIGH RESOLUTION AIRGUN ARRAY

(J. Bialas, K.-P. Steffen)

After sailing 3 days in rough weather the conditions became smoother on June 12 and the airgun array and the streamer were briefly deployed. After the first few shots one of the o.3 ltr. VLA type guns failed by first producing auto-pops before starting to permanently blow out the air. All other guns operated well for the test. Due to their age the valves of the guns were not equipped with a trigger sensor which would give an exact shot signal. Neither was a depth measurement of the guns nor a near-field signature hydrophone available to control each gun. Due to the considerable swell, the depth apparently varied from shot to shot. Earlier plans to shoot across a set of OBH to study the far-field signature were impossible due to the adverse sea-states. Online observations therefore could only be done through the streamer recordings. We ran two short test lines, one with the three remaining guns, the other with the 2.0 ltr. gun switched off. Due to the great water depth (up to 6000 m) no reflections other than a seabottom arrival was recorded by the streamer, and this reflection was rather weak and scattered.

Detailed examples of a shot signal from the two configurations are shown on Figure 6.3.4.3.1. Shot 85 and its frequency spectrum was generated by the full array, while shot 50 results from two guns only. Both traces are scaled with the same plot parameters to allow comparison of the amplitudes. In both cases a 0.4 sec long signal could be observed. The example from shot 85 with the 0.3 - 0.6 - 2.0 ltr. volume contains higher frequencies up to 55 Hz. A low frequency bubble oscillation is observed at 10 Hz resulting from the sum of the single gun events. It was detected twice, with the primary signal being as large as the first bubble. For the second bubble pulse the amplitude has decayed to 1/2 of the initial event. Higher frequency amplitudes are observed between the primary and the first bubble. During the second test with the 0.3 - 0.6 l volume configuration the bubble oscillation was observed at 15 Hz. The increase may be explained by the remaining small volumes which result in a higher frequency content. Amplitude ratios of primary and bubbles are similar to those of shot 85. The frequency spectrum is limited to about 50 Hz. Although the volume was smaller than for shot 85, probably the water depth was too great for the small volume guns to generate signals at higher frequencies.

The signals obtained from this setup are far from being acceptable. However, given the strict time limitations and the poor weather conditions, it was mainly a functionality test of the guns itself. It also became apparent that the array should preferably be towed at a larger distance from the ship, so it would react less vigorously to the roll and pitch of the vessel. Further tests with different configurations of airgun volumes and distances within the array are necessary to achieve a tuned signal. Theoretical considerations (Dragoset, 1990; Laws et al., 1990) indicate that a primary/bubble ratio of 5:1 could easily be achieved.

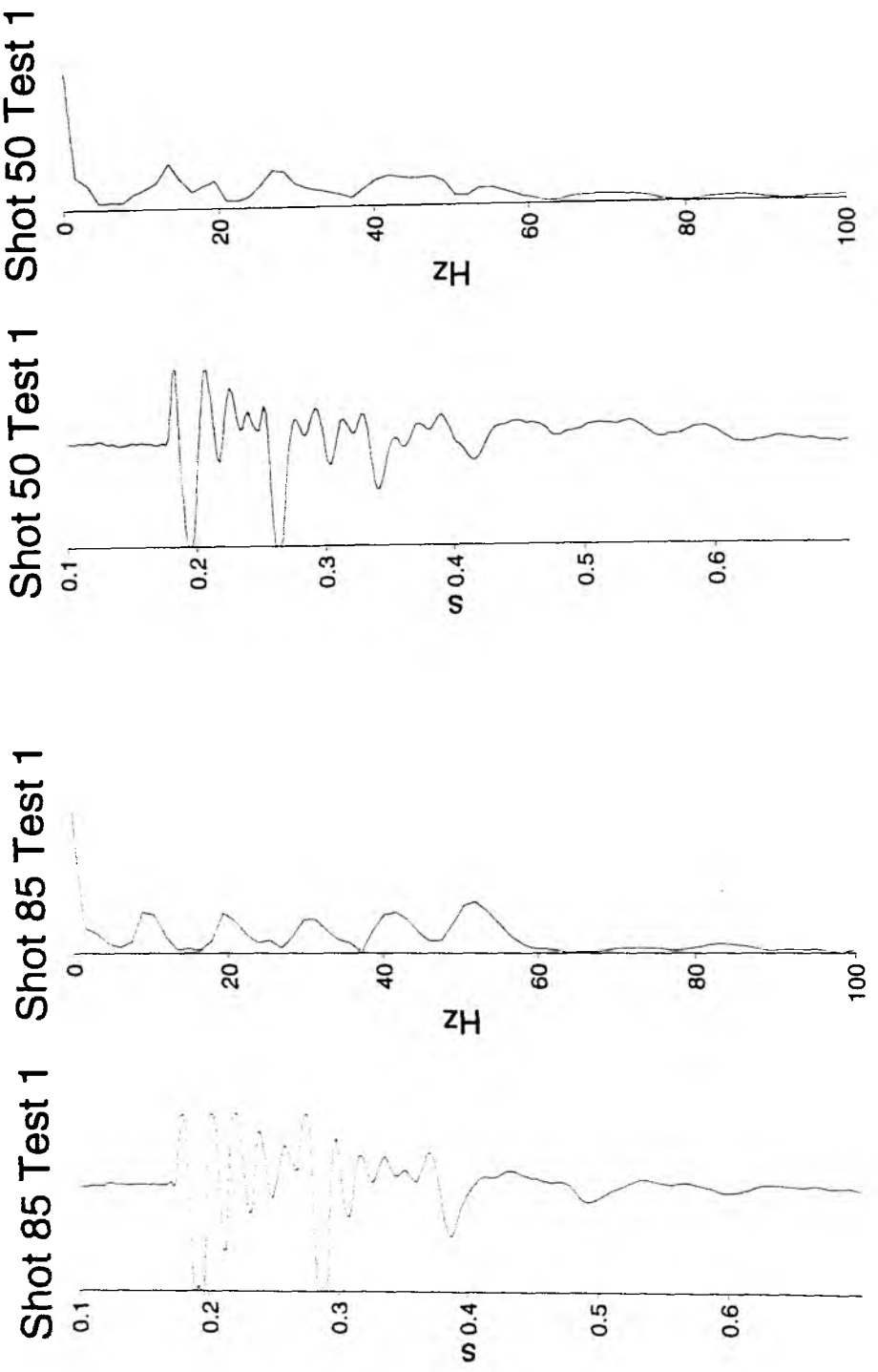

Figure 6.3.4.3.1: Shot signals from the GEOMAR airgun array.
lower half: shot and spectra from 0.3 - 0.6 - 2.0 l gun
upper half: shot and spectra from 0.3 - 0.6 l gun

6.3.4.4 PROFILE SO131-04

(U. Domaschk, C. Kopp, and E. Flueh)

Profile SO131-04 is located west of Ninetyeast Ridge along 86°40.0´ in the Indian Basin. Altogether twelve instruments were deployed in previously unmapped areas between 01:00 and 05:30 16.05. Waterdepth ranged between 4300 and 4800 m and was more variable than anticipated. The distance between instruments was between two and three miles. The main aim of this profile was to determine the velocity structure of the Indian Basin as a reference for the changes expected at Ninetyeast Ridge and in the Wharton Basin. Shooting was done from 10:30 16.05 to 08:00 17.05 at 5 knots with a shot intervall of 60 s except for the first two hours when, due to technical reasons shots were fired every 20 s. All instruments except one (OBH08) were recovered by 04:00 18.05. OBH08 was also used to record the shots along Profile SO131-05 and was subsequently recovered by 20.05. The location of the instruments and the shots together with the surveyed bathymetry are shown in Figure 6.3.4.4.1. During shooting the streamer was deployed and also provided usefull information. The processed section is shown in Figure 6.3.4.4.2. All instruments worked well and the record sections, including the four OBS components, are shown in Figures 6.3.4.4.3 to 6.3.4.4.17. Details on instrumentation can be found in Appendix 9.1.4.

Modelling and interpretation:

The profile was chosen to compare relatively undisturbed oceanic crust of the Indian Basin with crust of the Ninetyeast Ridge. But bathymetry along the profile was much rougher than expected before starting the experiment. The MCS data (Figure 6.3.4.4.2) also show a rough basement topography. The sedimentary cover thickness varies between c. 300 m in small basins to around 0 m at the top of basement outcrops. The basement highs seem to belong to the westernmost edge of the Ninety-East Ridge, whereas the subdued topography in the north is part of the Indian Ocean Basin. No deeper reflections than basement are observed in the reflection line.

The wide-angle sections are of high data quality. A very strong wide-angle PmP is observed on all sections, but only very short Pn-phases can be identified on several stations (OBH02, 03, 04, 05, 07 and 11). The crustal phases suggest a rather continuous increase of crustal P-wave velocity. Only small discontinuities were introduced for modelling. The wide-angle sections also show S-wave arrivels, converted at the basement. Here, velocity discontinuities can be better identified.

Water depth and sedimentary thickness for the model were taken from the navigation data and the MCS data. After an adjustment of picked and calculated phases with *MacRay*, a preliminary model of four gradient layers was used as a starting model for inversion with *raytomorf* (see chapter 6.3.3). A first trial with a 1 km x 1 km grid showed unreliable results, so re-gridding to 250 m x 250 m was necessary. This approach increased the computing time, so only few iteration processes could be completed. Those results were again taken to improve the *MacRay* modelling (Figure 6.3.4.4.21).

Several tests have been done with different smoothing factors. The best model with the best fit was achieved using a smoothing factor of 60. Ten recursive inversions including five internal matrix inversions of *raytomorf* have been calculated. The final RMS error was given with 104 ms. In addition, an

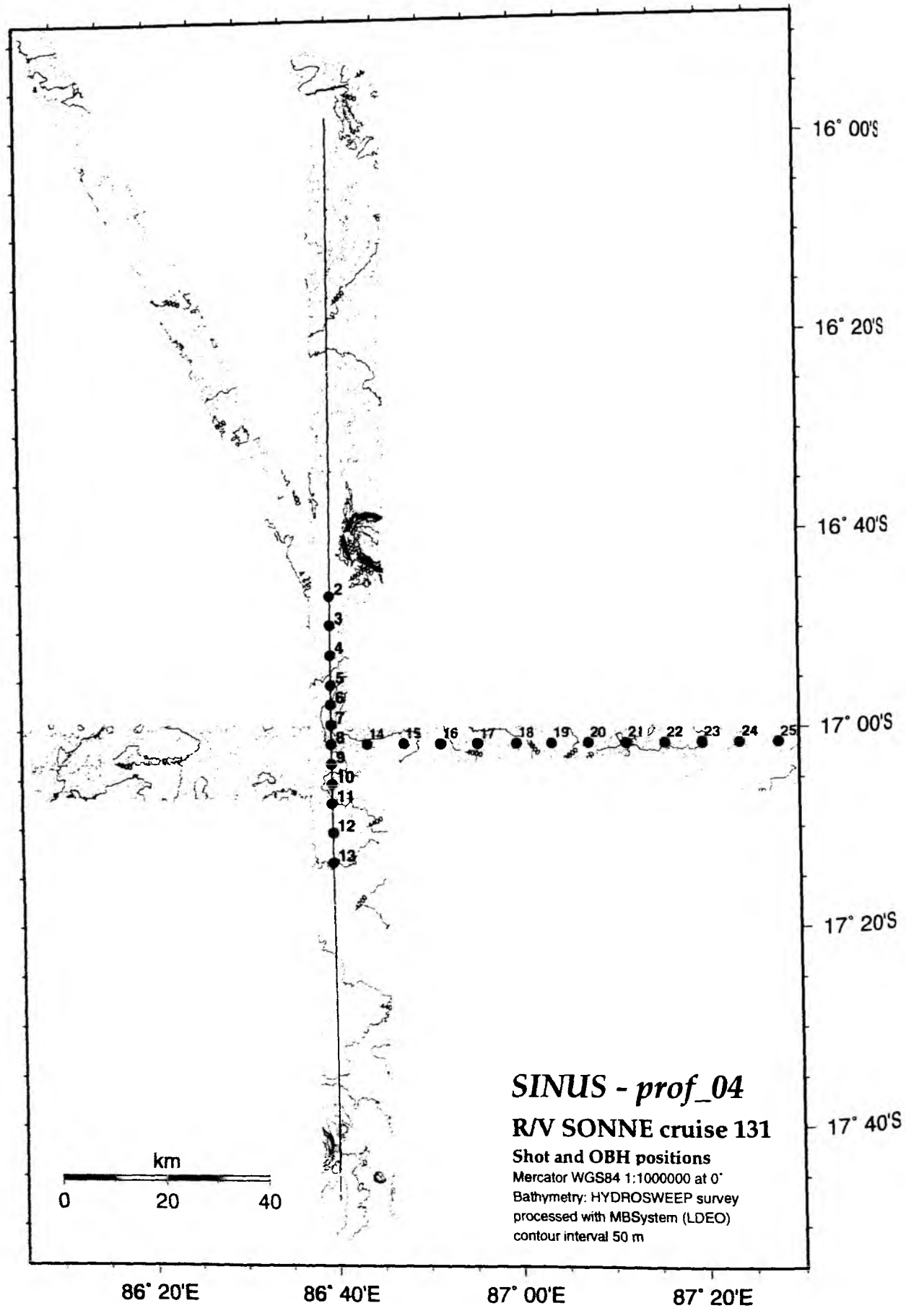

Fig. 6.3.4.4.1: Profile 04 - Shot and OBH positions.

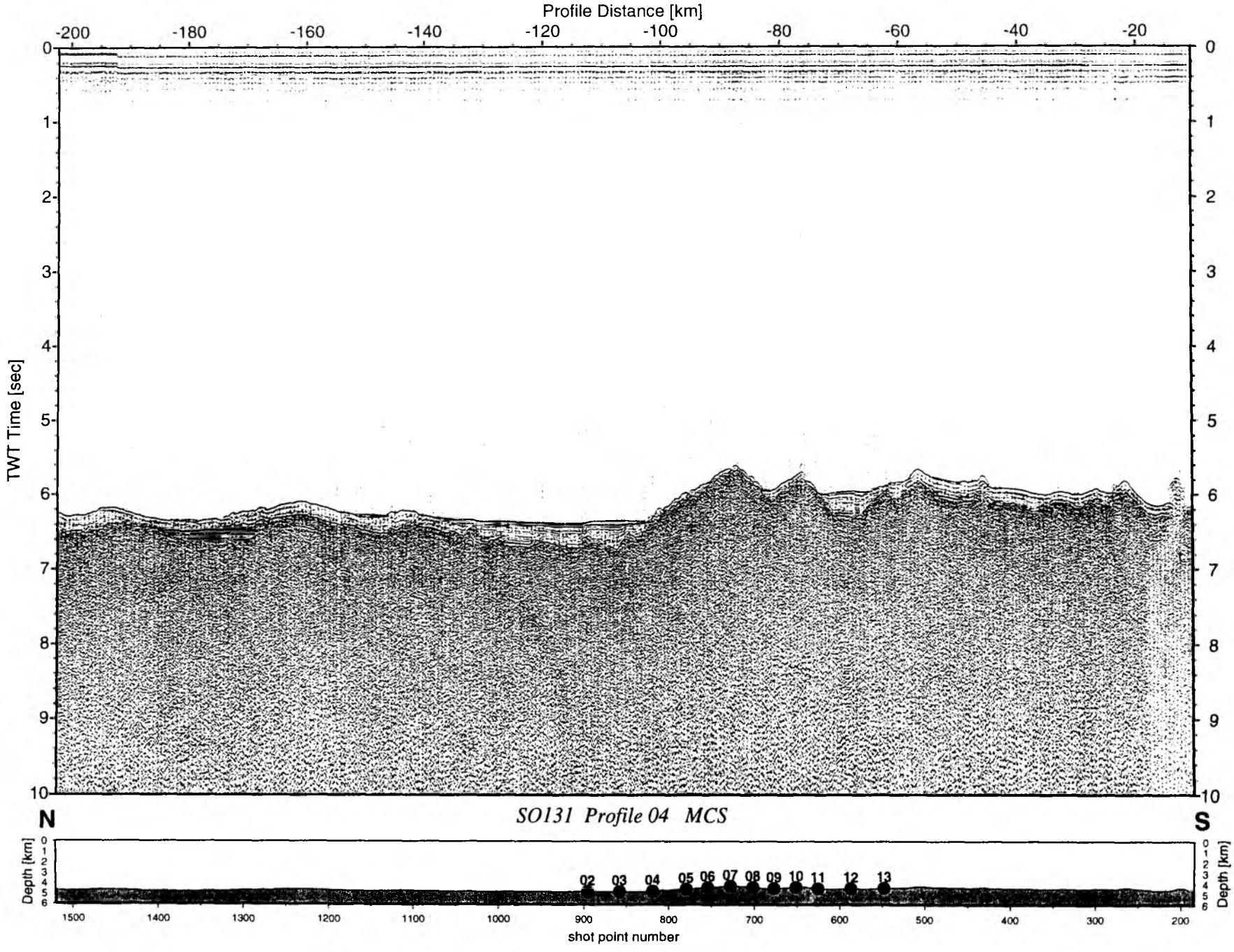

Figure 6.3.4.4.2: Seismic section from MCS stack, Profile 04.

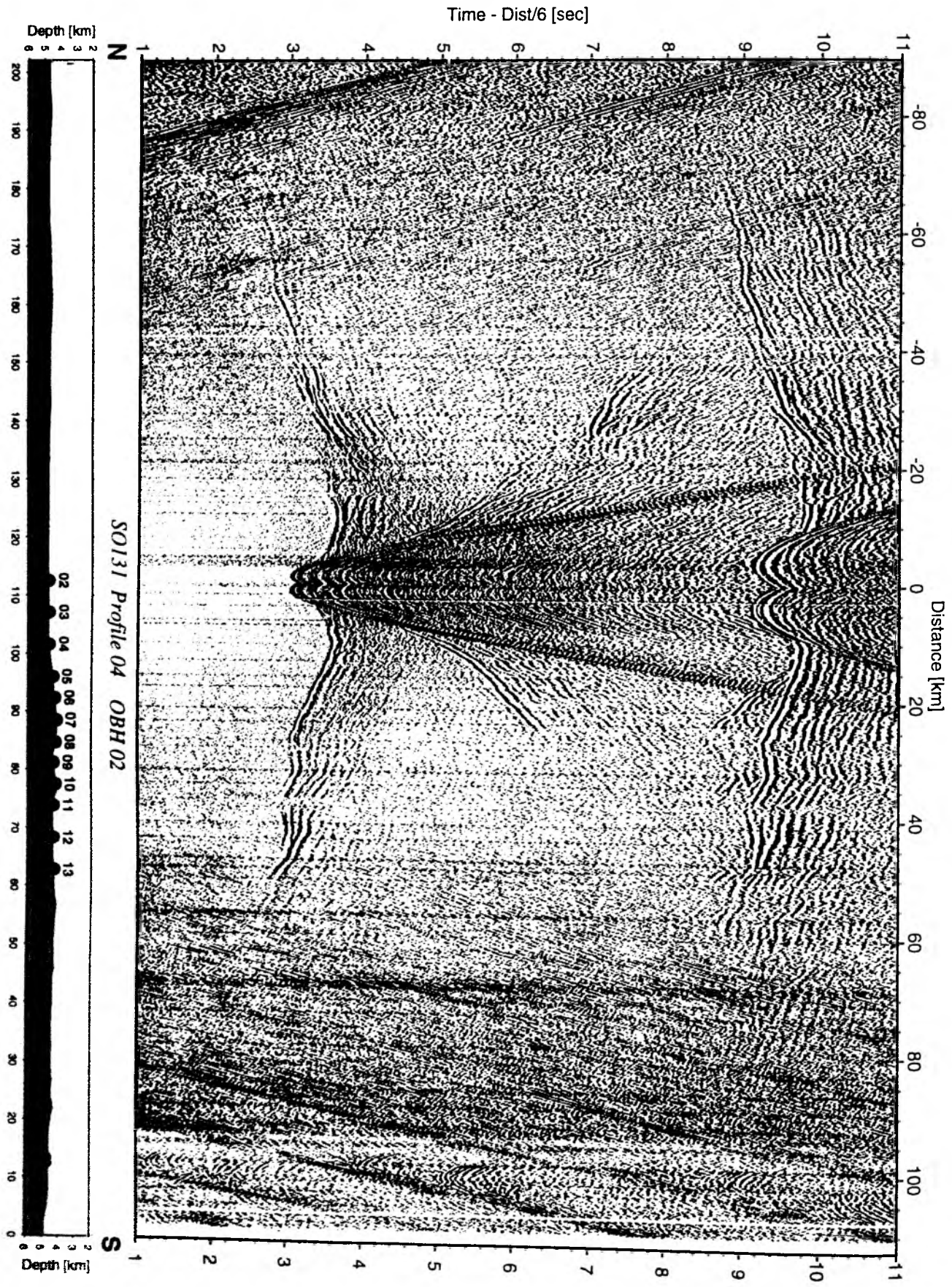

Figure 6.3.4.4.3: Record section from OBH 02, Profile 04.

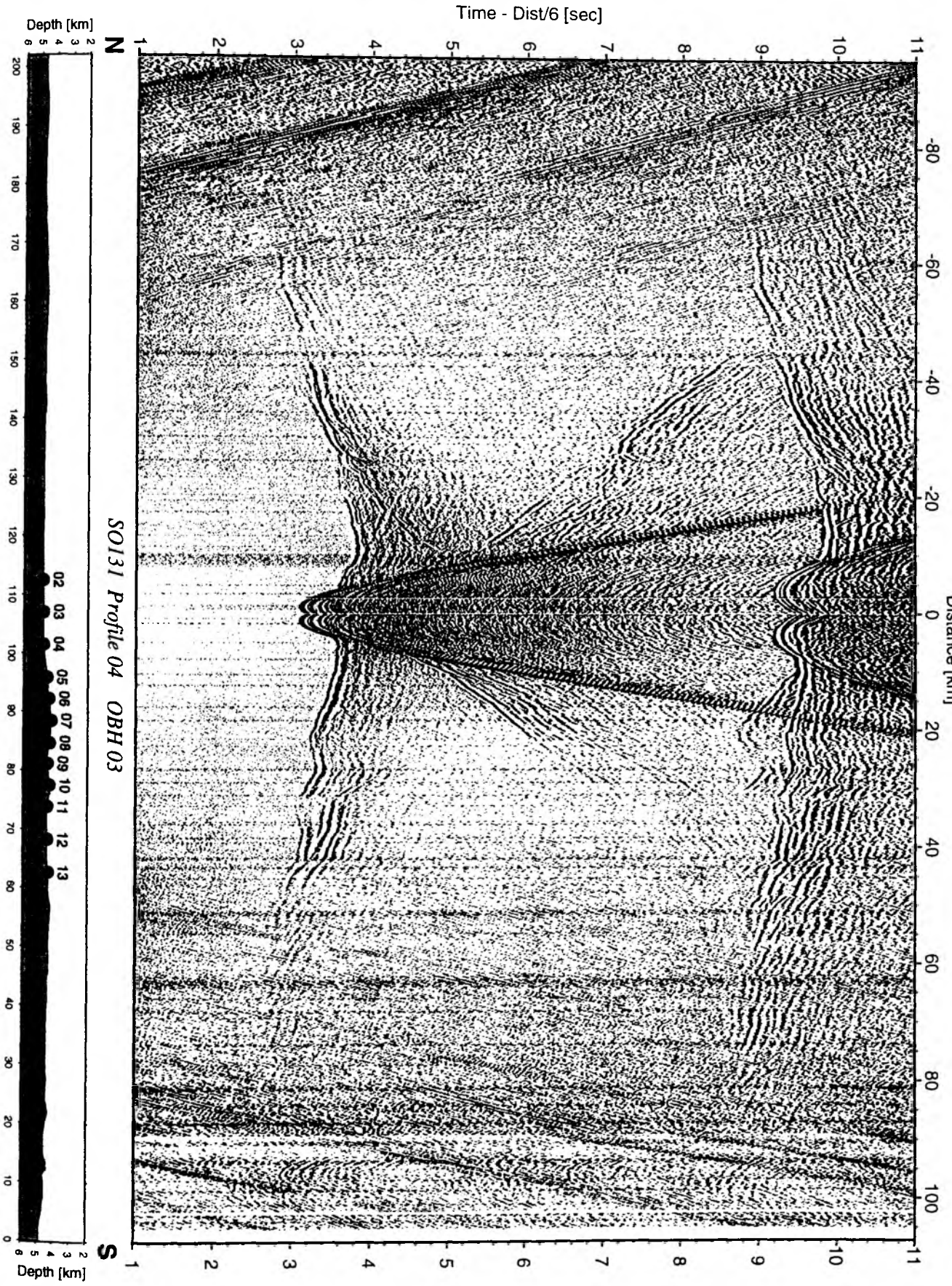

Figure 6.3.4.4.4: Record section from OBH 03, Profile 04.

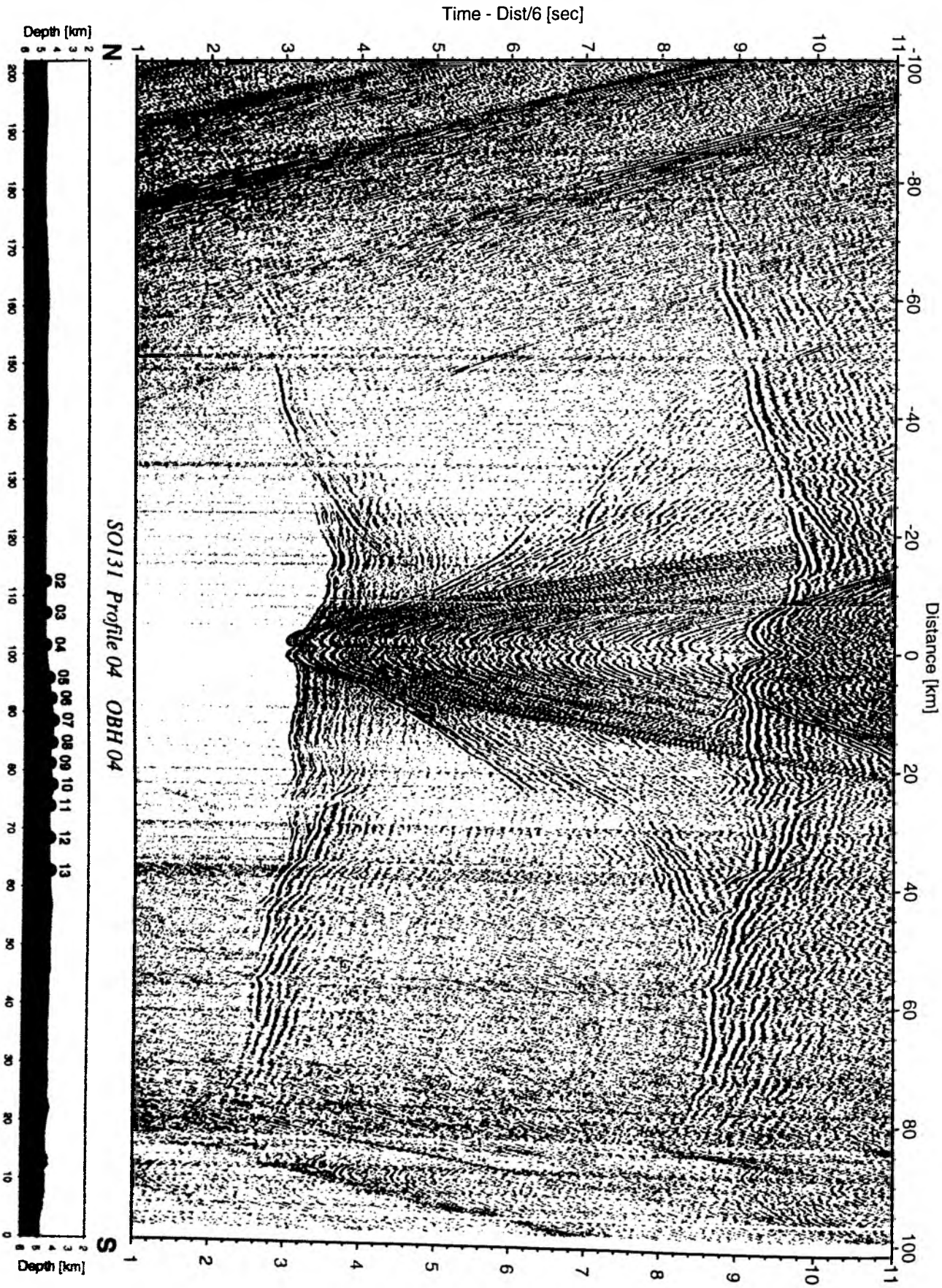

Figure 6.3.4.4.5: Record section from OBH 04 , Profile 04.

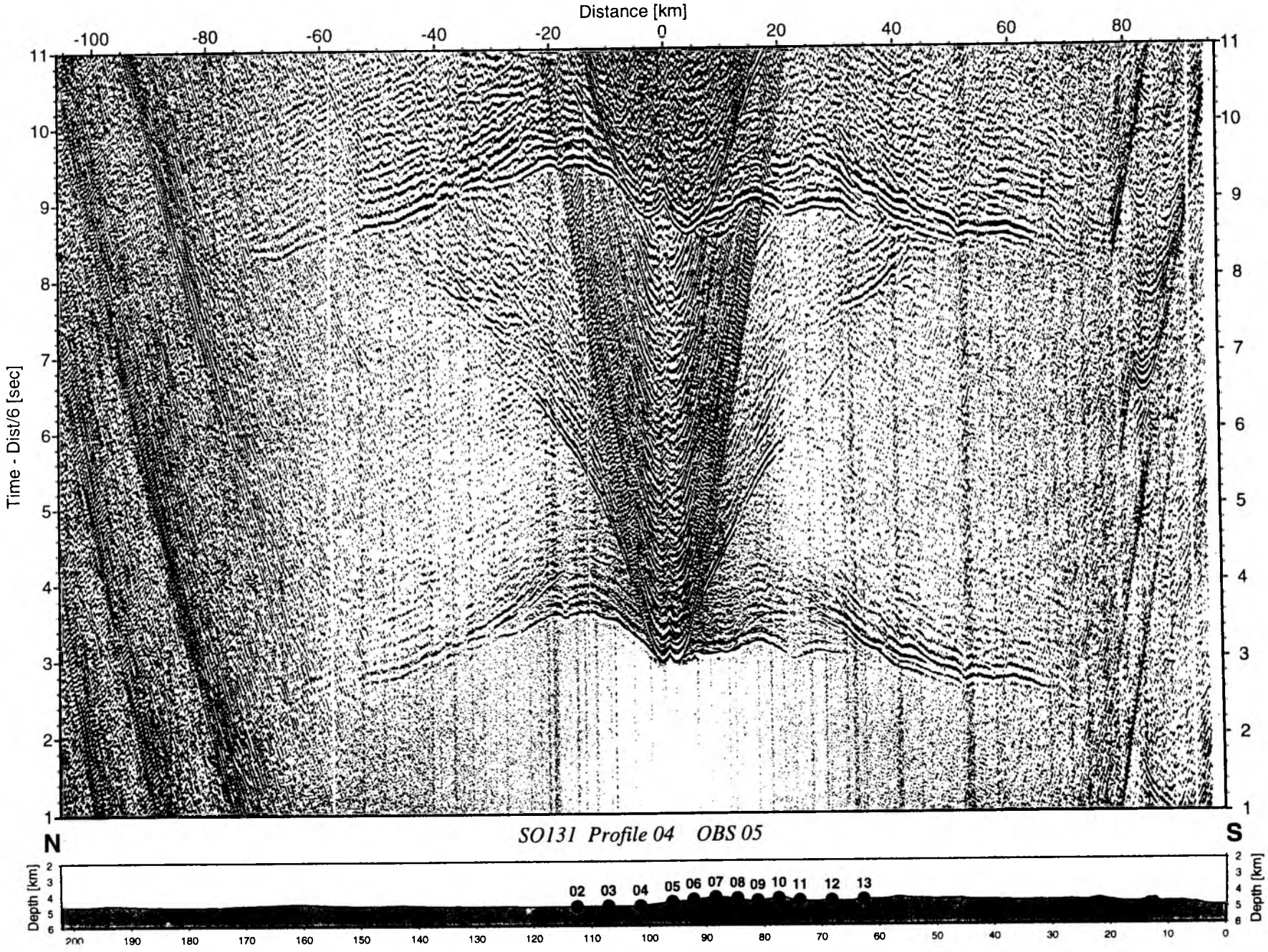

Figure 6.3.4.4.6: Record section from OBS 05 hydrophone, Profile 04.

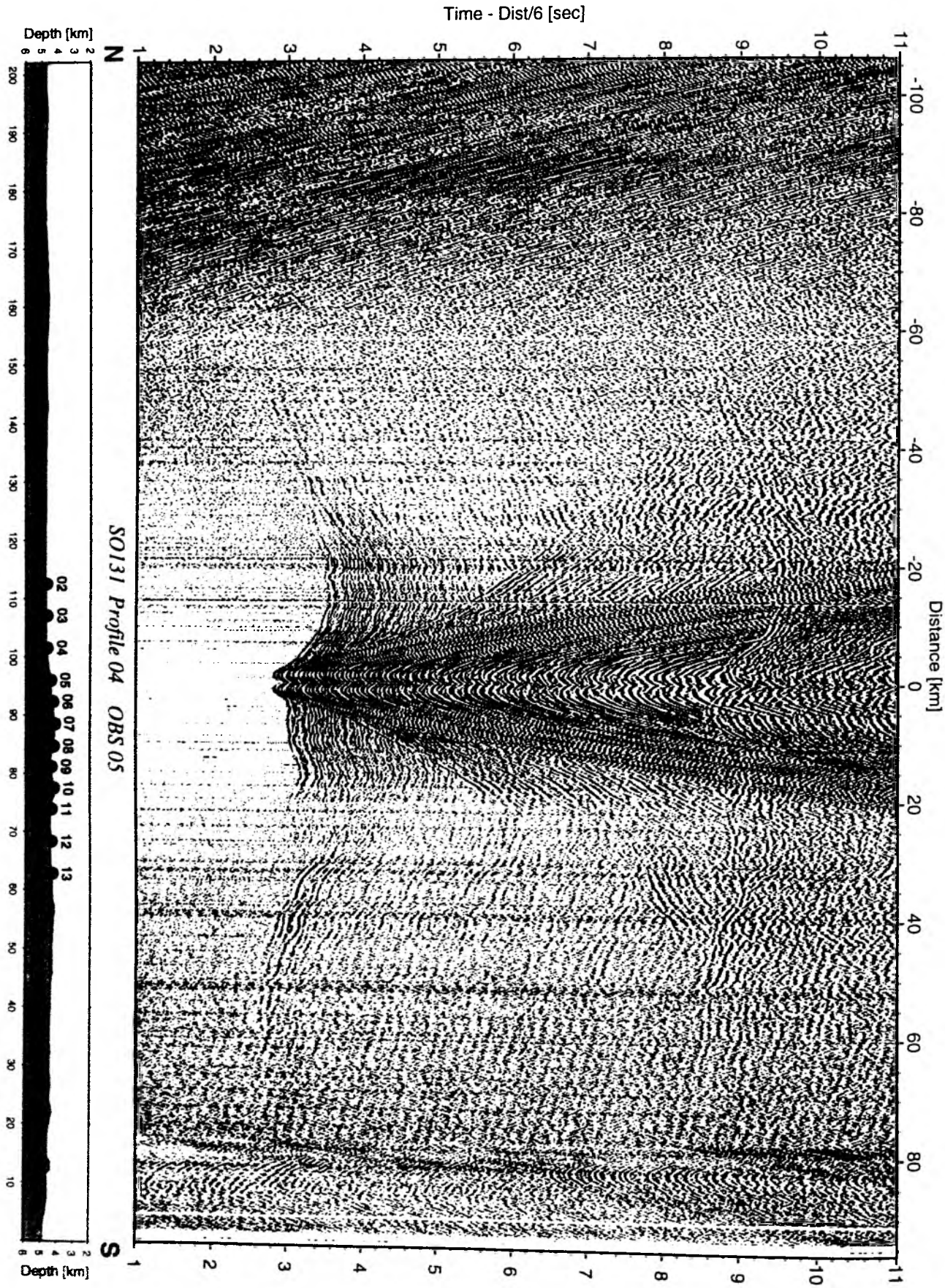

Figure 6.3.4.4.7: Record section from OBS 05 vertical component, Profile 04.

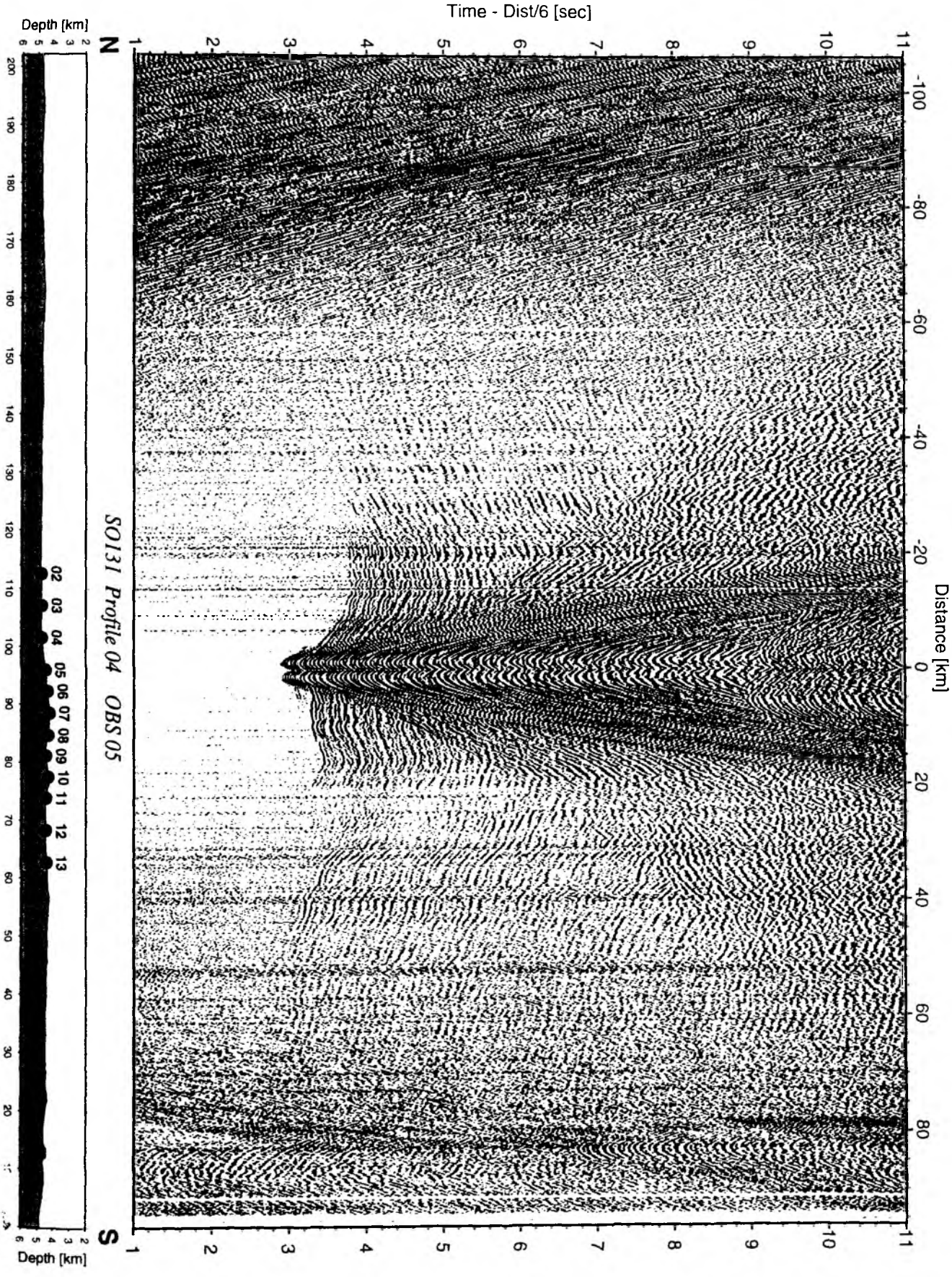

Figure 6.3.4.4.8: Record section from OBS 05 horizontal component 1, Profile 04.

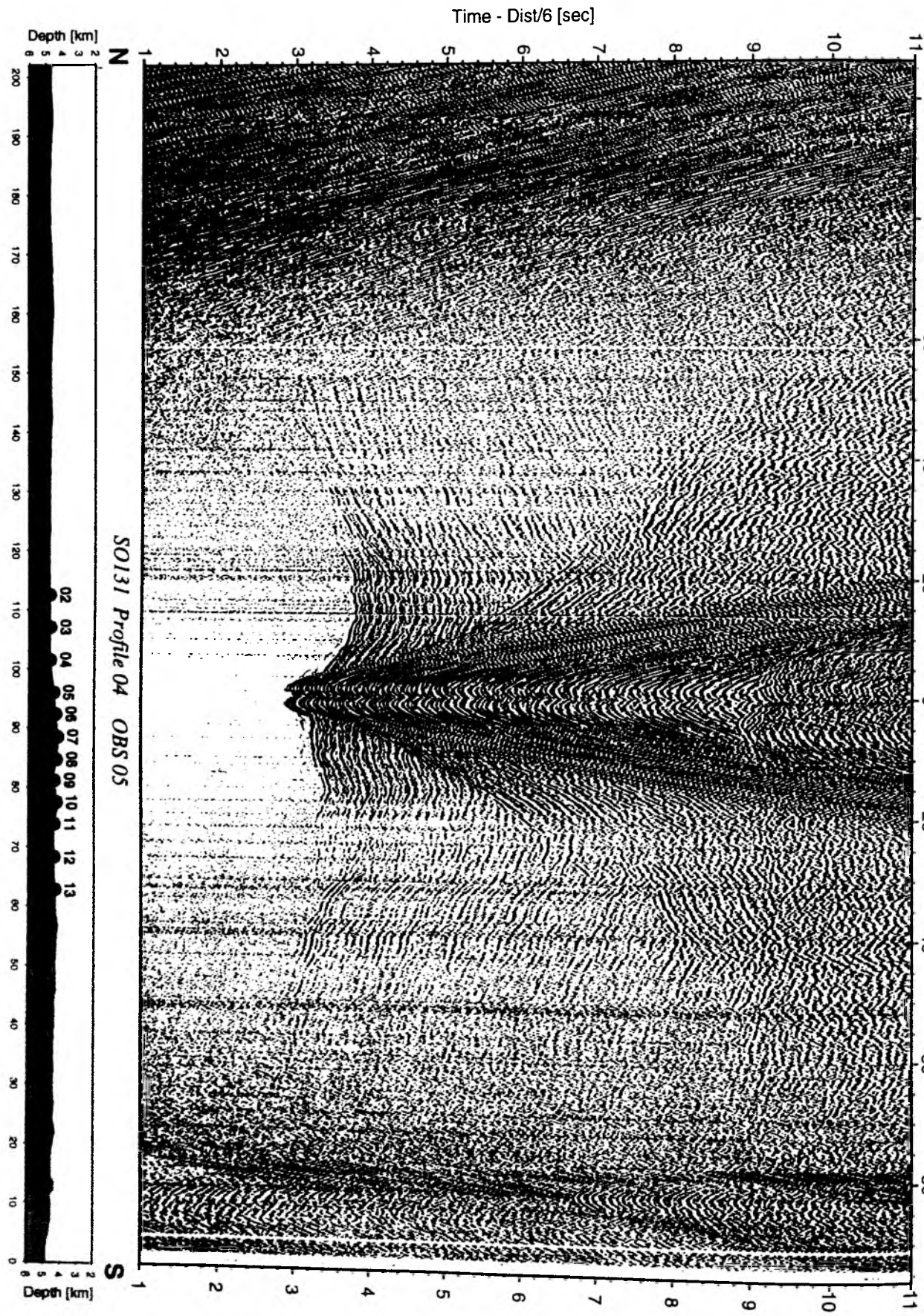

Figure 6.3.4.4.9: Record section from OBS 05 horizontal component 2, Profile 04.

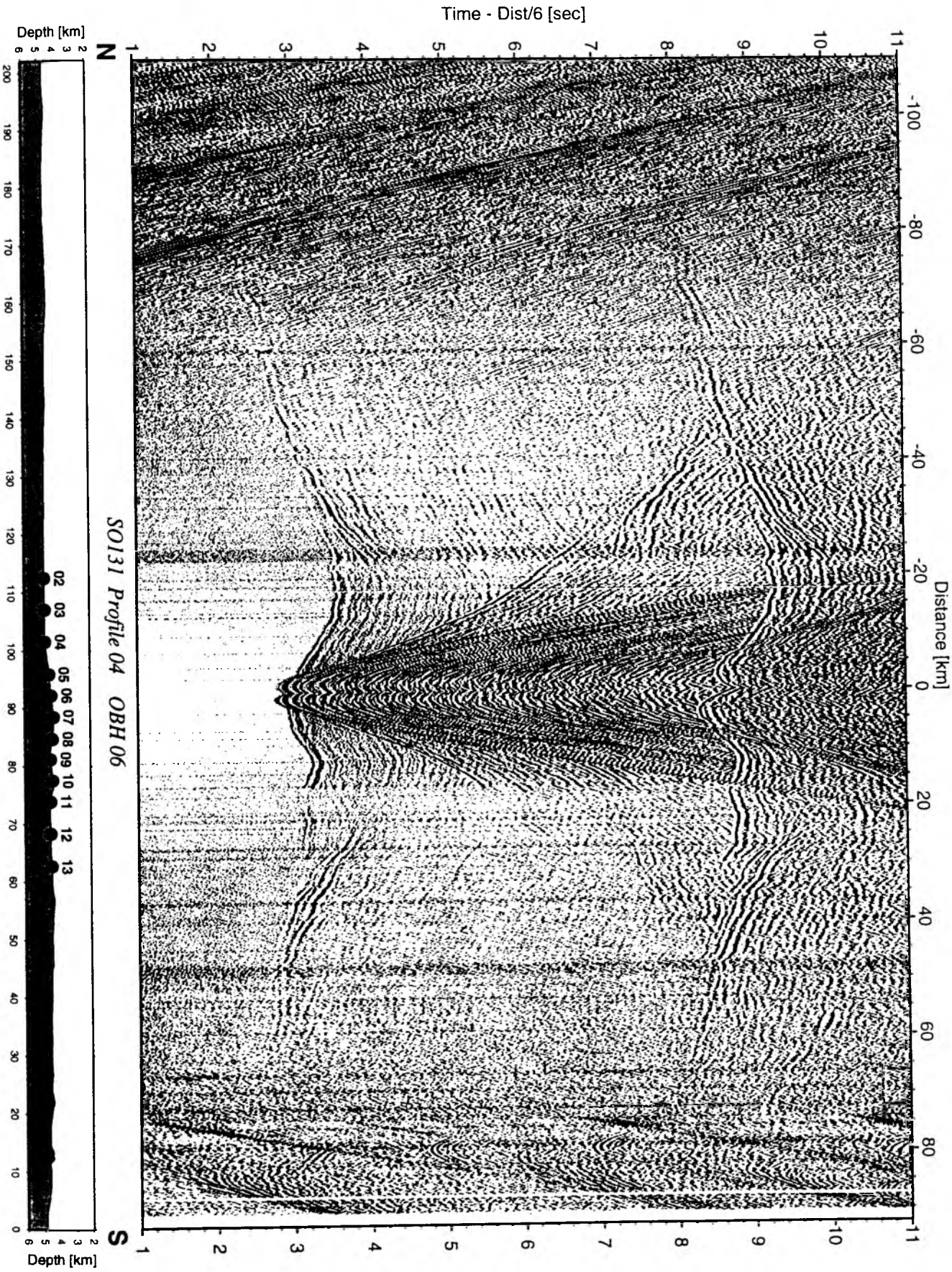

Figure 6.3.4.4.10: Record section from OBH 06 , Profile 04.

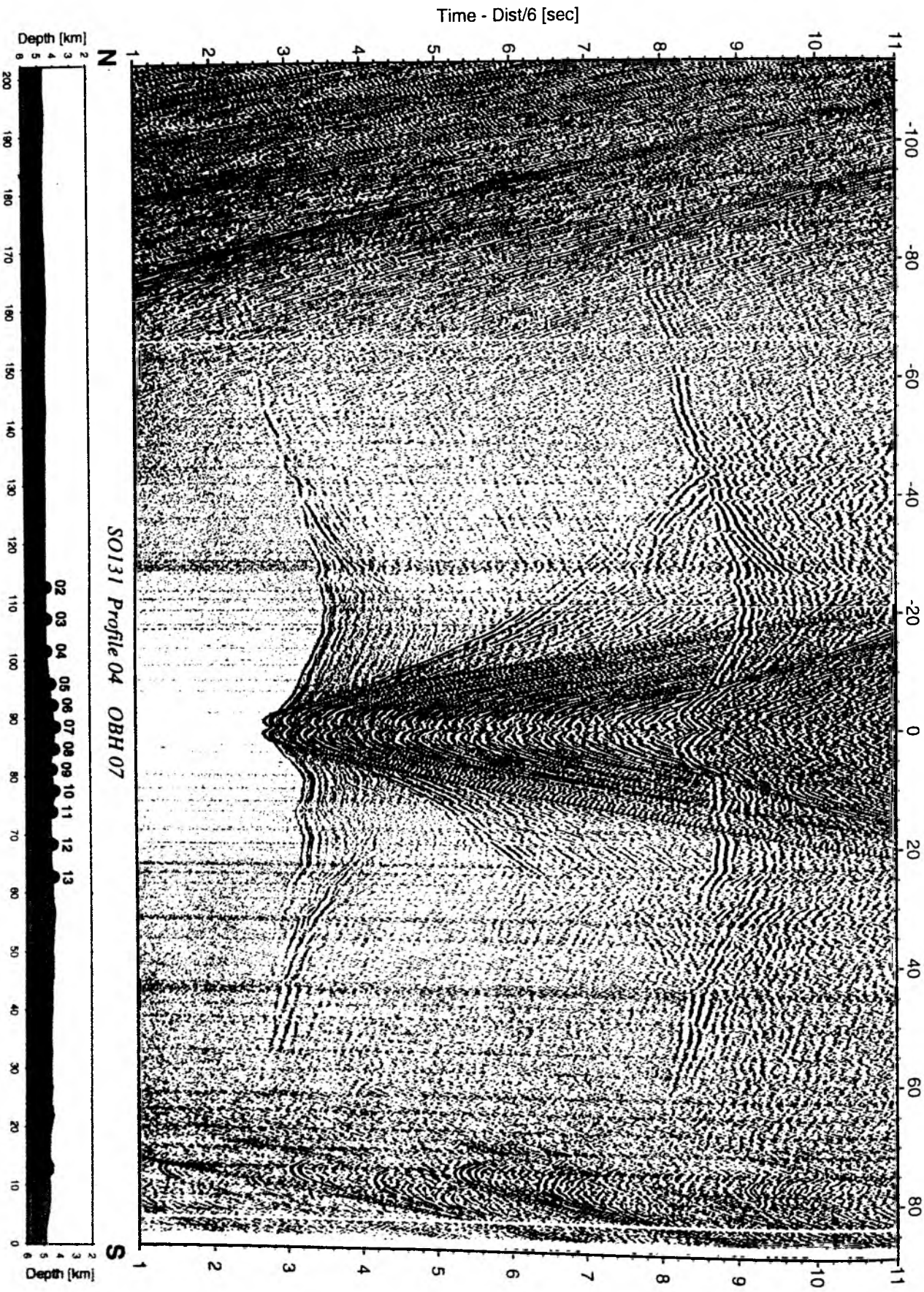

Figure 6.3.4.4.11: Record section from OBH 07 , Profile 04.

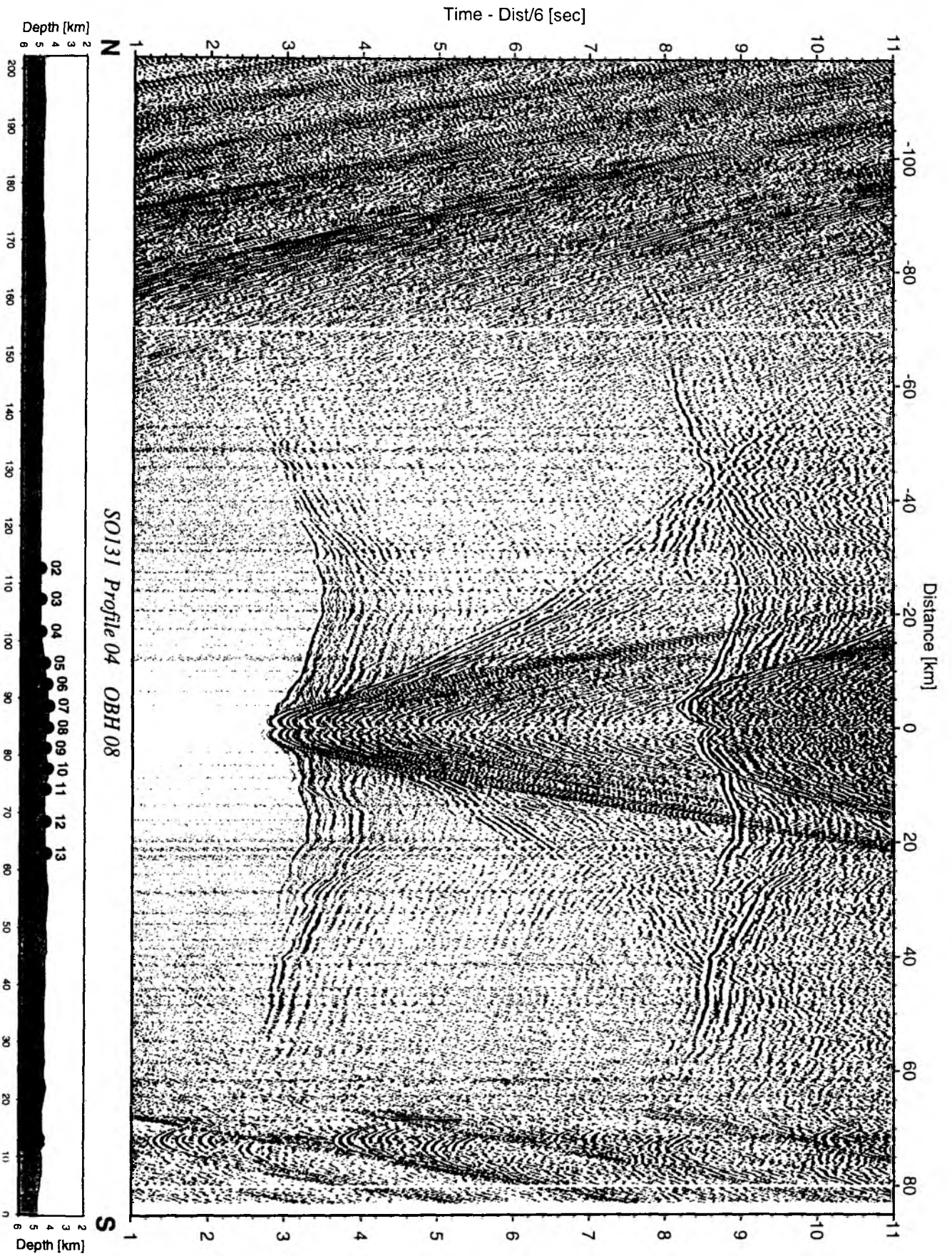

Figure 6.3.4.4.12: Record section from OBH 08 , Profile 04.

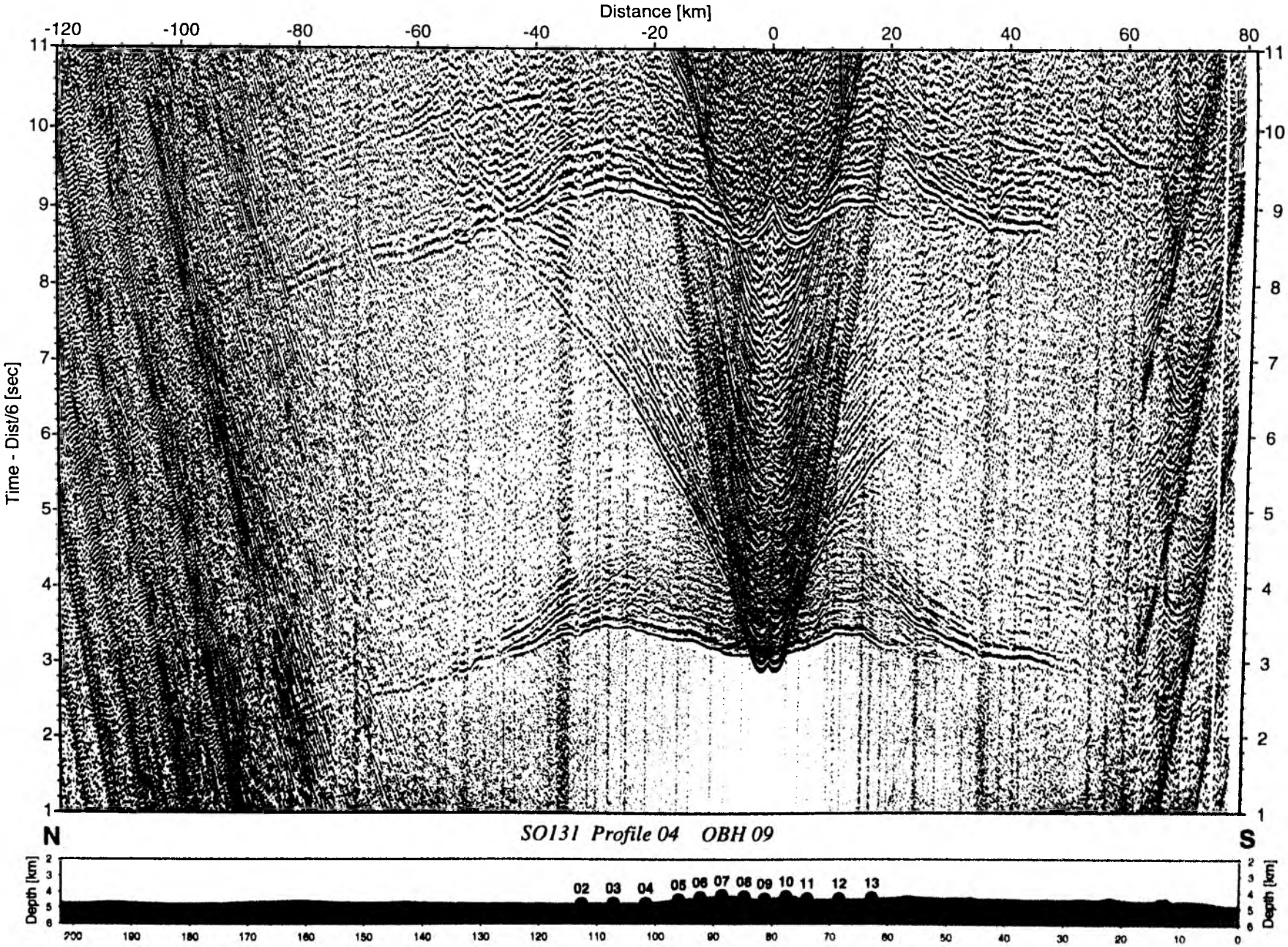

Figure 6.3.4.13: Record section from OBH 09 , Profile 04.

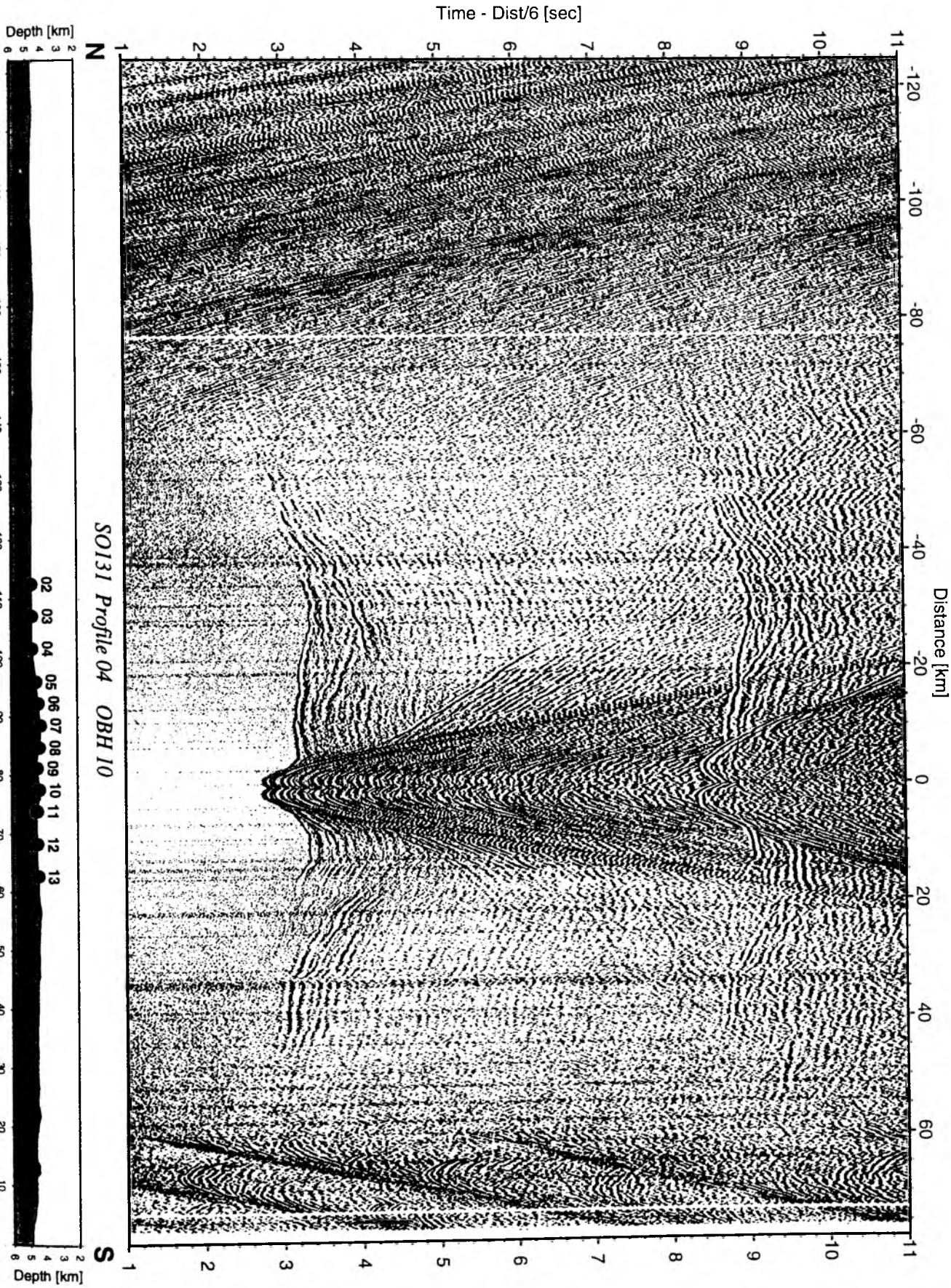

Figure 6.3.4.4.14: Record section from OBH 10 , Profile 04.

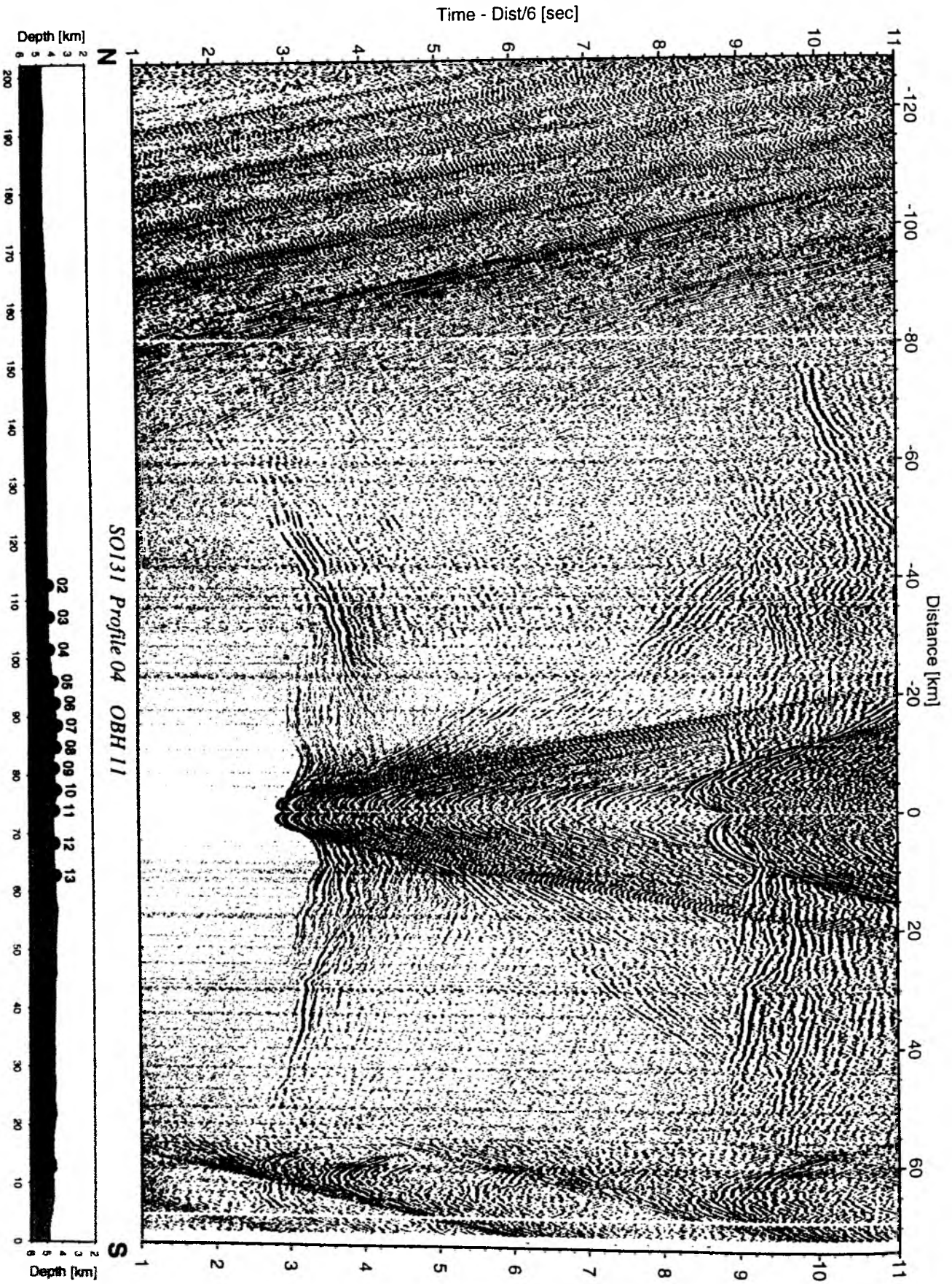

Figure 6.3.4.4.15: Record section from OBH 11 , Profile 04.

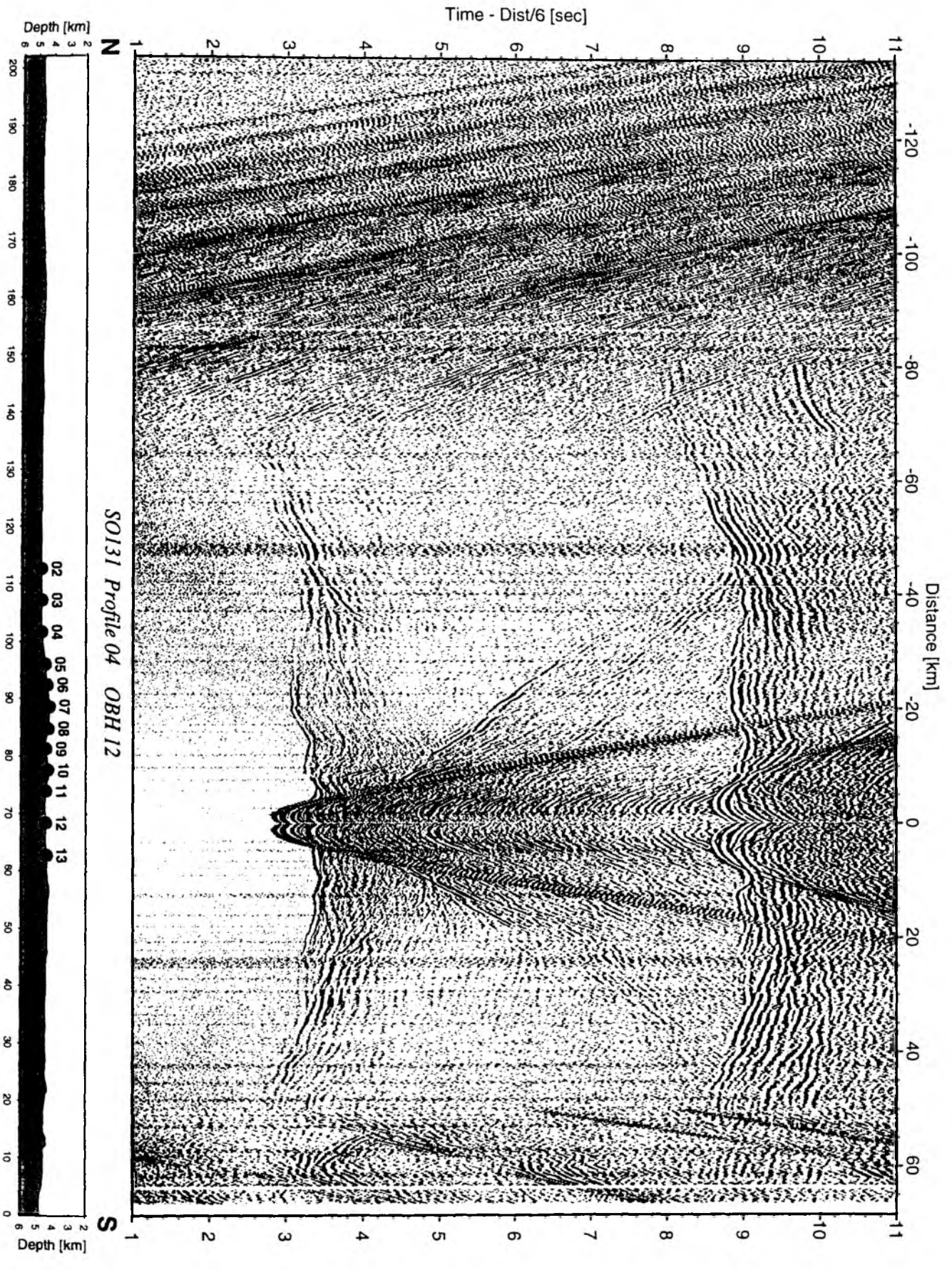

Figure 6.3.4.4.16: Record section from OBH 12 , Profile 04.

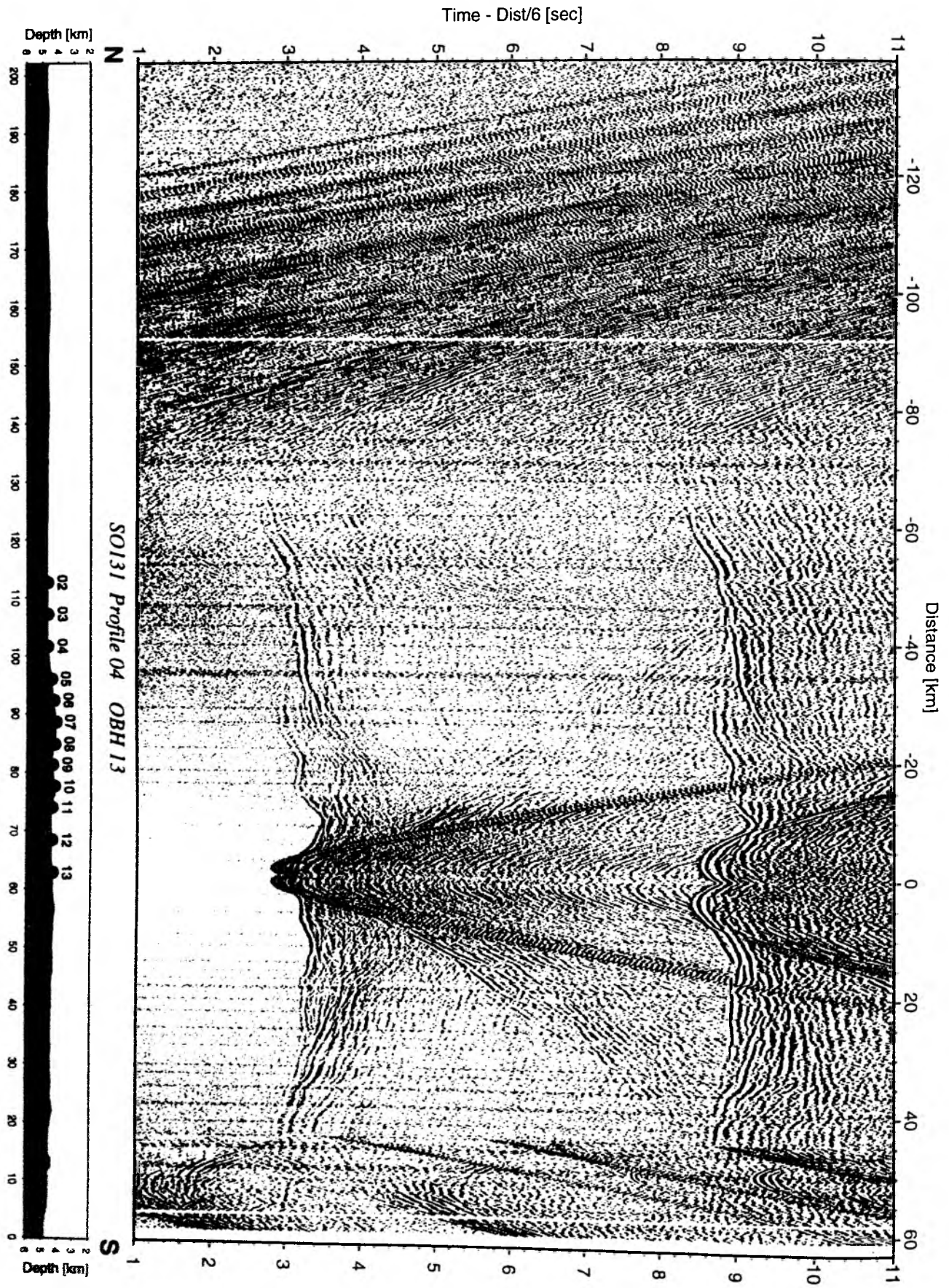

Figure 6.3.4.4.17: Record section from OBH 13 , Profile 04.

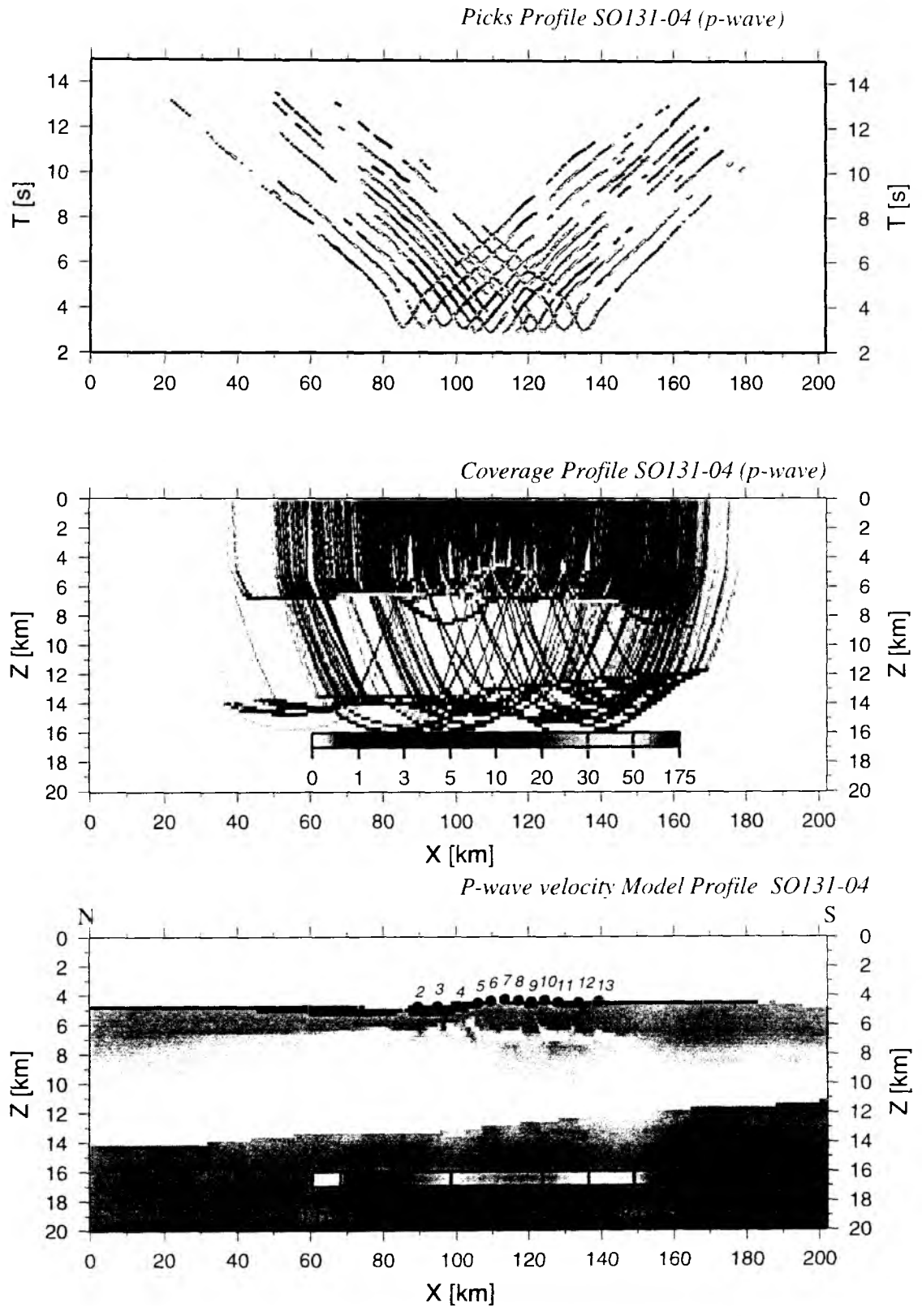

Figure 6.3.4.4.18: RAYTOMORF P-wave velocity Model Profile SO131-04

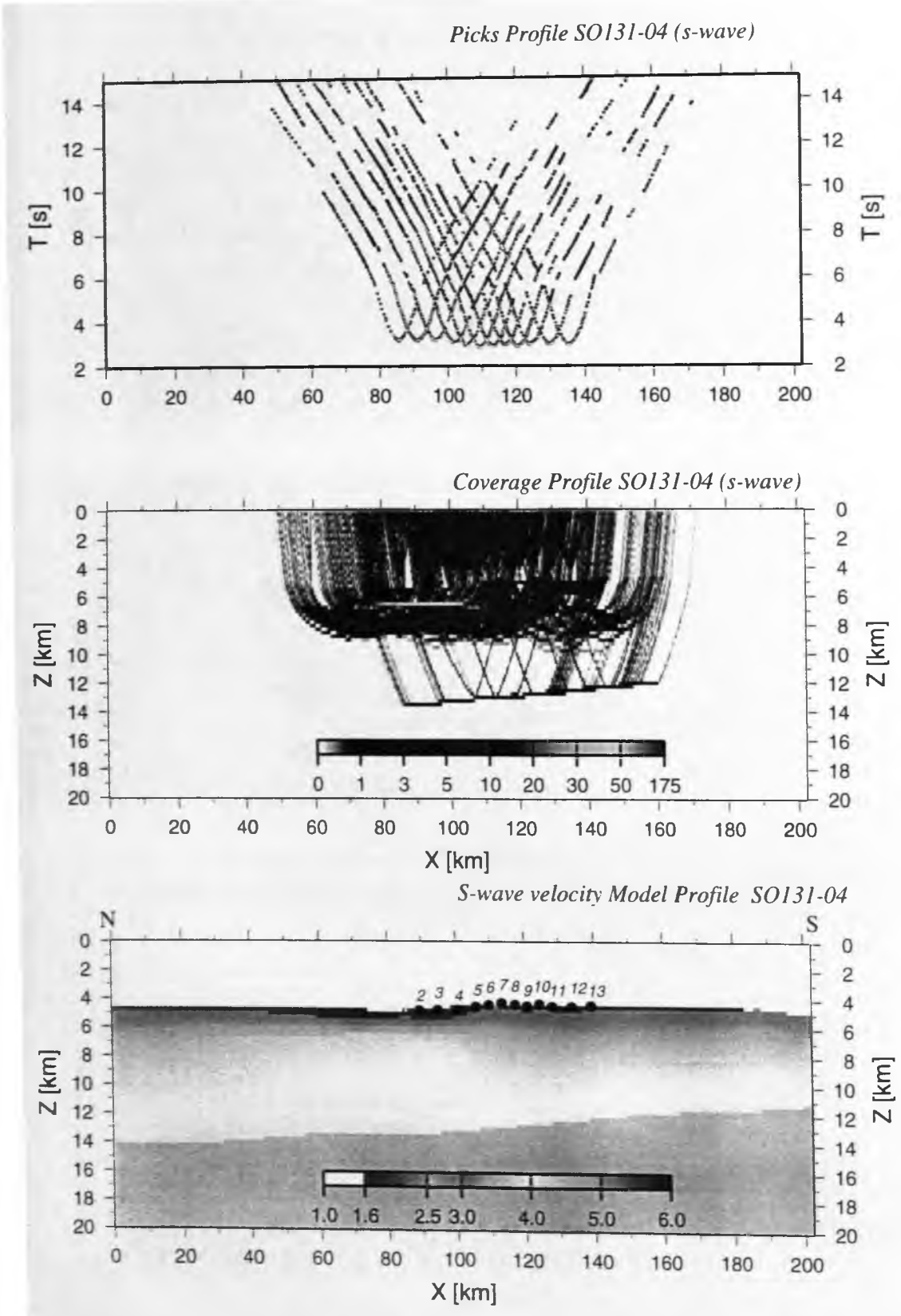

Figure 6.3.4.4.19: RAYTOMORF S-wave velocity Model Profile SO131-04

inversion of the converted S-wave arrivals was applied, with crustal and mantle velocities divided by √3.

Using the same parameters the final RMS error increased to 219 ms. The P-wave inversion shows a high increase of velocities from 5.0-6.5 km/s in the first 1.5 km of the basement. The velocity gradient decreases to 0.1 1/s (6.5-7.2 km/s for the next 7 km down to Moho). Unfortunately the calculated high velocities at lower depth form a low velocity zone beneath, which effectively trap the modelled rays. This effect could be avoided by a more detailed starting model and sacrificing Moho phases. The ray coverage and unreduced picks and calculated first arrivals are shown above the model in Figure 6.3.4.4.18.

The calculated and picked arrivals of the S-wave velocity model (Figure 6.3.4.4.19) do not correspond as well as in the P-wave modelling, especially in the lower parts, possibly caused by picking Moho reflections instead of refracted waves. The upper crustal ray penetration is generally better than in the P-wave model except for the mantle, where only a few rays were traced. Also S-wave velocities show a high gradient in the c. 1.5 km thick upper crust (2.5-3.6 km/s) rather than the in c. 7 km lower crust (3.6-4.1 km/s). The mantle velocities could not be modelled because of poor ray coverage.

The P/S-ratio (Figure 6.3.4.4.20) shows only few variations. Most of them are artifacts, caused by limited ray penetration of the S-waves into the mantle (underneath 12km depth) or the "ray trap" at the transition zone between upper and lower crust. Only the anomaly beneath OBH 03, 04 and 05 seems reliable. Underneath the basement high, a ratio of about 2 is observed, possibly marking a zone of different petrological composition. This structure may be interpreted as a vulcanic crustal addition at the westernmost rim of the Ninetyeast Ridge.

The final raytracing model, based on modification of the *raytomorf* model to include all wide-angle reflections, especially the pronounced PmP-phases, is shown in Figure 6.3.4.4.21. Clearly a crustal thickening by 1 km is indicated in the area where basement crops out. This is again interpreted as additional magmatic input from the Hotspot activity into older Indian Ocean crust.

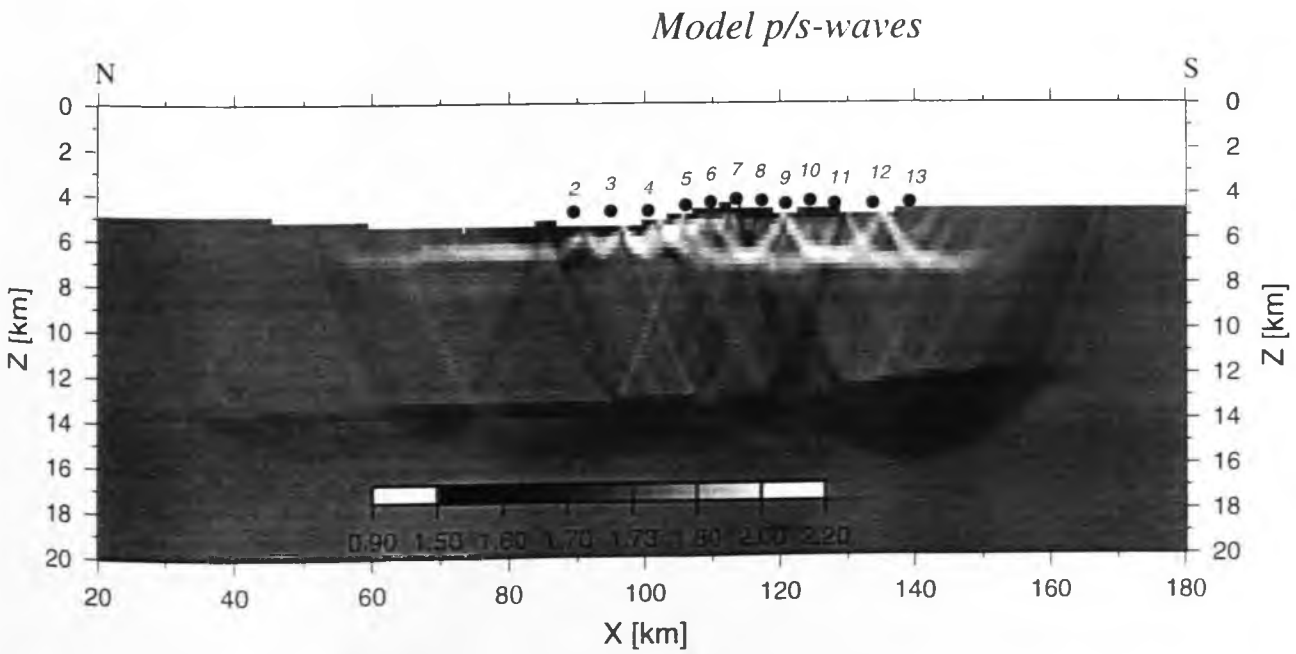

Figure 6.3.4.4.20: P/S-wave ratio Profile SO131-04

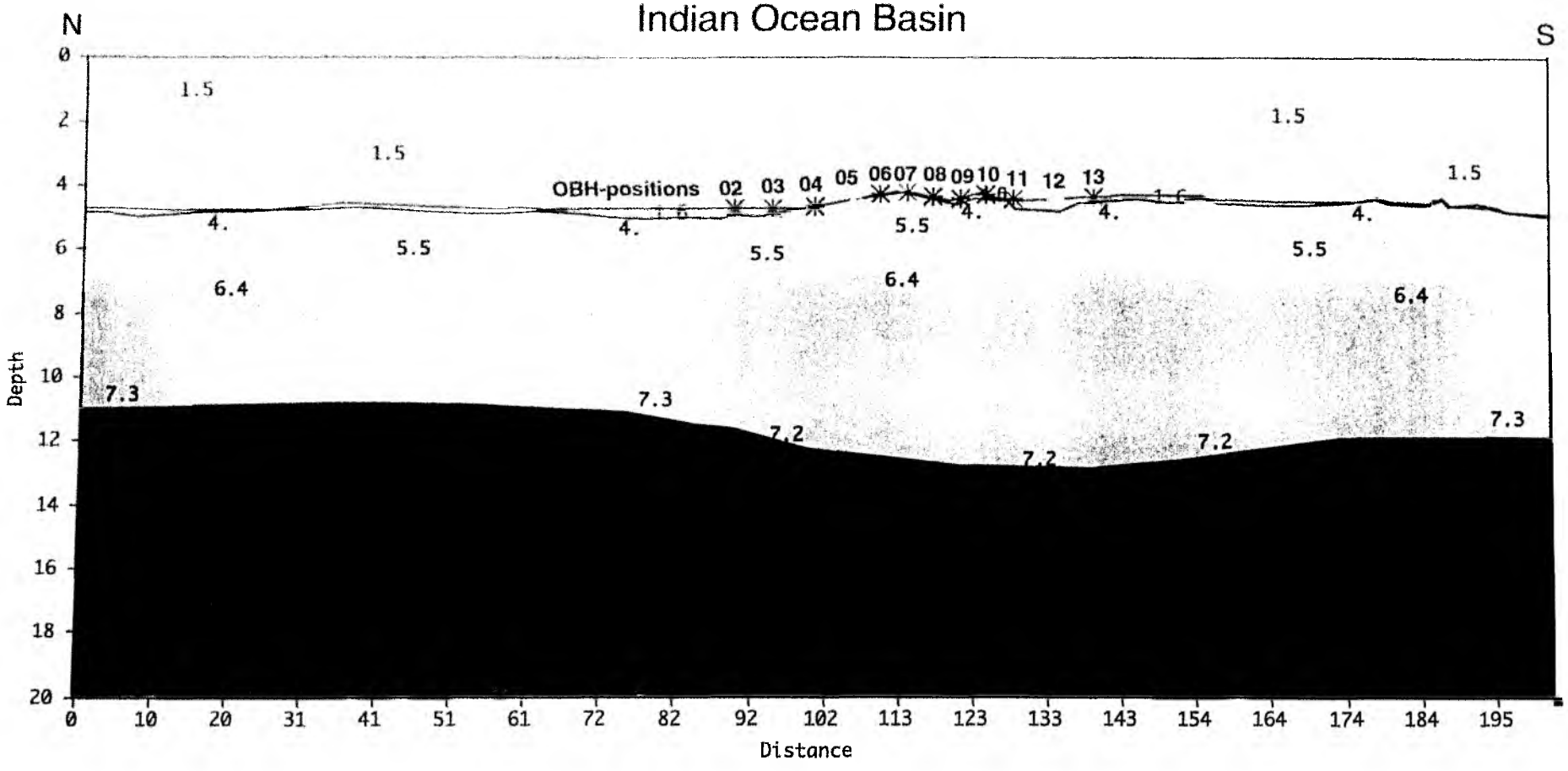

Figure 6.3.4.4.21: P-wave velocity model of profile SO131-04 modelled with MacRay-Software

6.3.4.5 PROFILE SO131-05

(I. Grevemeyer, E. Flueh, A. Hojka, H. Lelgemann)

Profile SO131-05 is an east-west oriented dipline across the Ninetyeast Ridge, that together with profiles SO131-06 and SO131-31 constitutes a more than 500 km long traverse across the ridge. It starts in the Indian Basin and the first OBH-position is coincident with profile SO131-04 (OBH08). Another 24 instruments were deployed further east on 18.05 between 04:00 and 16:00. Among these instruments were also the OBS and the short vertical array. Details on instrumentation can be found in Appendix 9.1.5. Shooting at 60 sec intervalls started at about 22.00, 18.05 and lasted to 08:00, 20.05. The total length of the shooting line is 320 km (see Figure 6.3.4.5.1). The reflection data collected with the streamer during shooting are shown in Figure 6.3.4.5.2. They clearly image the upper layers All instruments were successfully recovered between 14:00 20.05 and 07:30 21.05. Some instruments failed to record data for various reasons. All record sections obtained are shown in Figures 6.3.4.5.3 to 6.3.4.5.31. Most of them are of excellent quality, and arrivals can be seen to distances of nearly 200 km.

Modelling and Interpretation

From the 25 instruments deployed, 23 seafloor receivers provided data for geophysical interpretation. For on board modelling 13 stations (11 OBHs; 1 VAR, channel 1; 1OBS, channel 1) were chosen. In addition, we included four instruments located on profile 06, which approached Ninetyeast Ridge from the East (see Chapter 6.3.4.6.). P-wave arrivals of first breaks and of major wide-angle reflections were picked by eye. A low ambient noise level and the good quality of waveforms made the picking of arrivals relatively straightforward. We interpreted the first breaks in terms of two crustal refraction branches, though some stations on Ninetyeast Ridge show second arrivals which may indicate the existence of three or four crustal layers. Adjacent OBHs, however, often display quite different travel-time curves, which indicates a considerable degree of upper crustal heterogeneity. Uncertainties estimated for crustal arrivals vary from about 20 ms to 80 ms.

In addition to the crustal refraction branches we identified several wide-angle phases and rays turning within the upper mantle. Stations located westward of Ninetyeast Ridge show the typical features of oceanic crust: a clear PmP and Pn phase. Approaching Ninetyeast Ridge, however, OBHs display a second wide-angle reflection from greater depth. In terms of seismic data from large igneous provinces sampled elsewhere (e.g. ten Brink and Brocher, 1987; Caress et al., 1995), we related this phase to a reflection from the base of a subcrustal plutonic body. Moreover, there is a third wide-angle phase from a reflector located within the upper mantle, most pronounced in records from OBH 26 to 30. These instruments are located on the upper apron of Ninetyeast Ridge. Additionally, at an offset of more than 140 km, they show a strong refraction branch from that boundary. This branch is characterized by strong amplitudes and apparent velocities of >> 8 km/s. It's offset and the high velocity suggest that the arrival turned within the upper mantle at depth well below Moho. In accordance with a decreasing signal-to-noise ratio at larger offsets, uncertainties of up to 120 ms were assigned to those mantle phases.

We modelled the travel time data using a two-dimensional ray tracing algorithm (Zelt and Smith, 1992). The travel times were calculated using a 'top-down' approach, modelling velocity and depth to each layer before moving to the next. Each layer is defined by a series of boundary nodes along it's upper surface and velocity nodes along it's upper and lower surface. The starting model was defined by typical oceanic crust (e.g. White et al., 1992; Grevemeyer et al., 1998) and consists of a 2 km thick upper crustal layer 2 and of a 4 km thick layer 3. Seismic velocities are 4.5-6.6 km/s and 6.7-7.1 km/s, respectively. Sediment thicknesses covering igneous crust were derived from the seismic reflection data (Figure

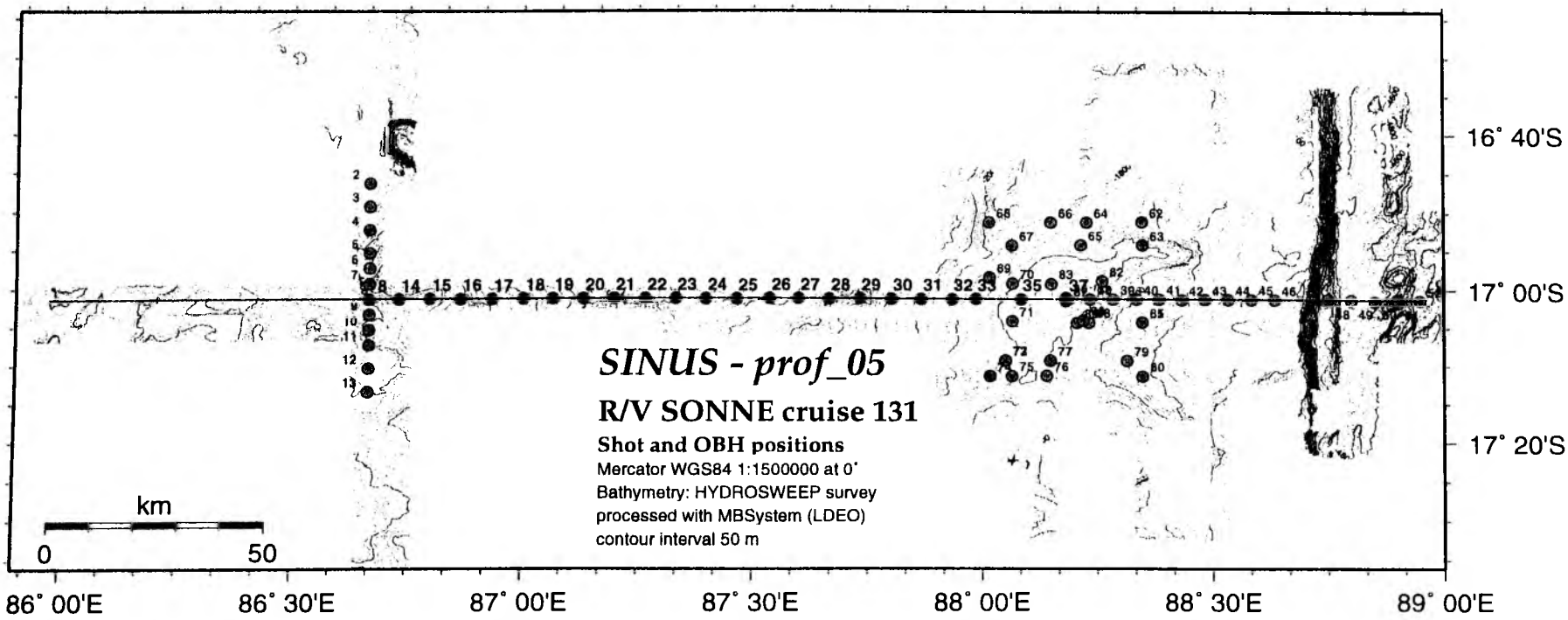

Fig. 6.3.4.5.1: Profile 05 - Shot and OBH positions.

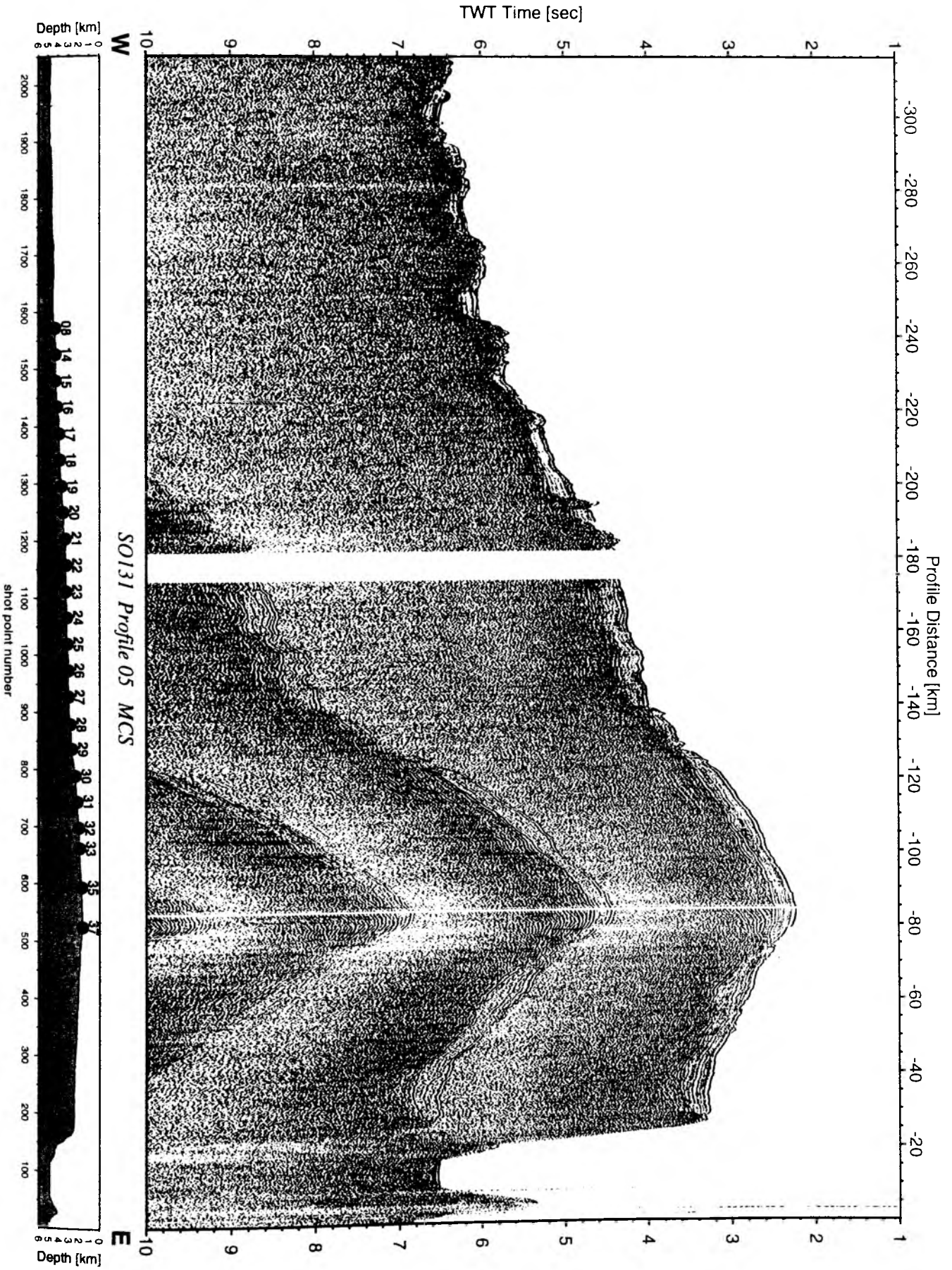

Figure 6.3.4.5.2: Seismic section from MCS stack, Profile 05.

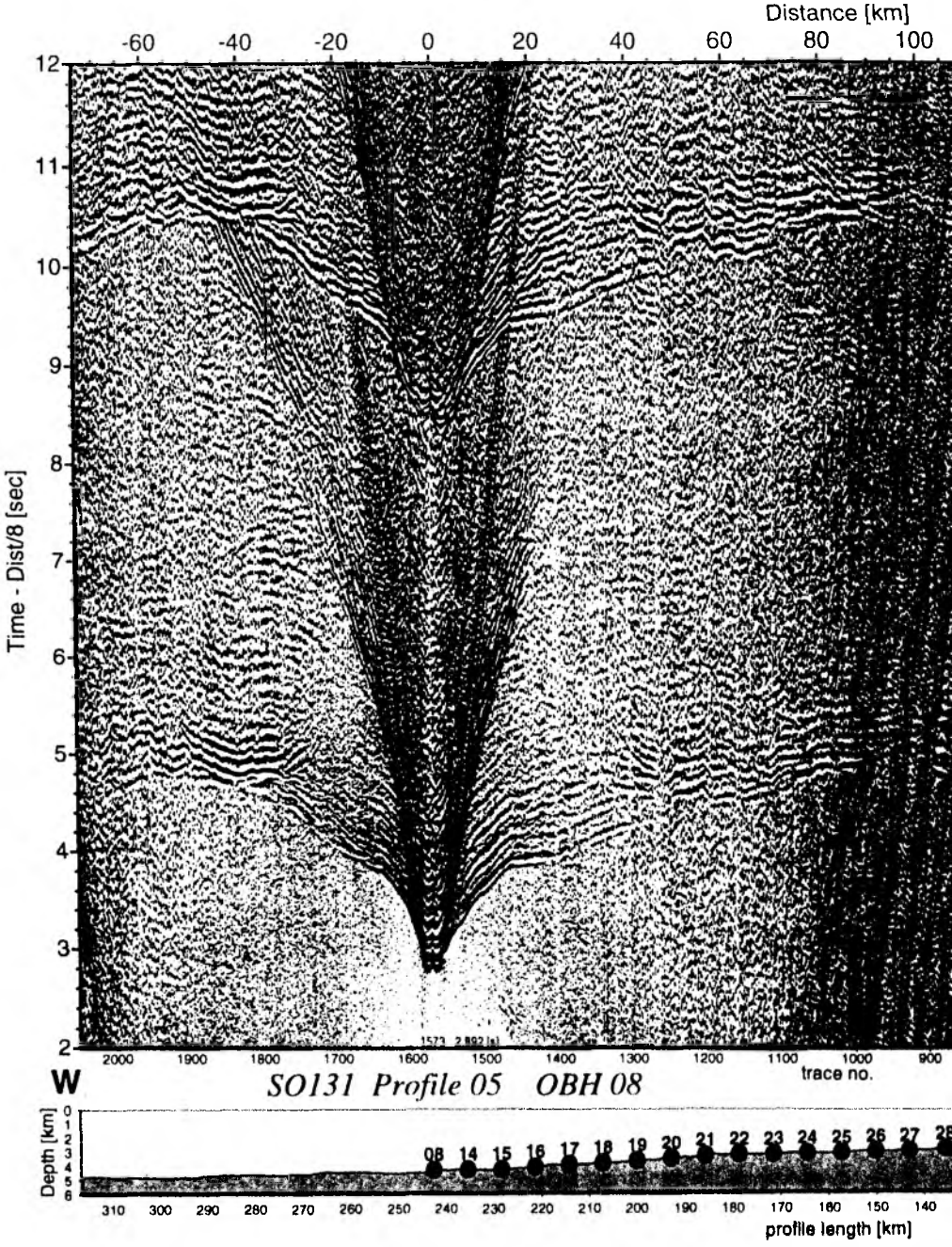
Distance [km]
-60
-40
-20
0
20
40
60
80
100
Time - Dist/8 [sec]
12
11
10
9
8
7
6
5
4
3
2
2000
1900
1800
1700
1600
1500
1400
1300
1200
1100
1000
900
trace no.
W
SO131 Profile 05 OBH 08
Depth [km]
0
1
2
3
4
5
6
08
14
15
16
17
18
19
20
21
22
23
24
25
26
27
310
300
290
280
270
260
250
240
230
220
210
200
190
180
170
160
150
140
profile length [km]

Figure 6.3.4.5.3: Record section from OBH 08 , Profile 05.

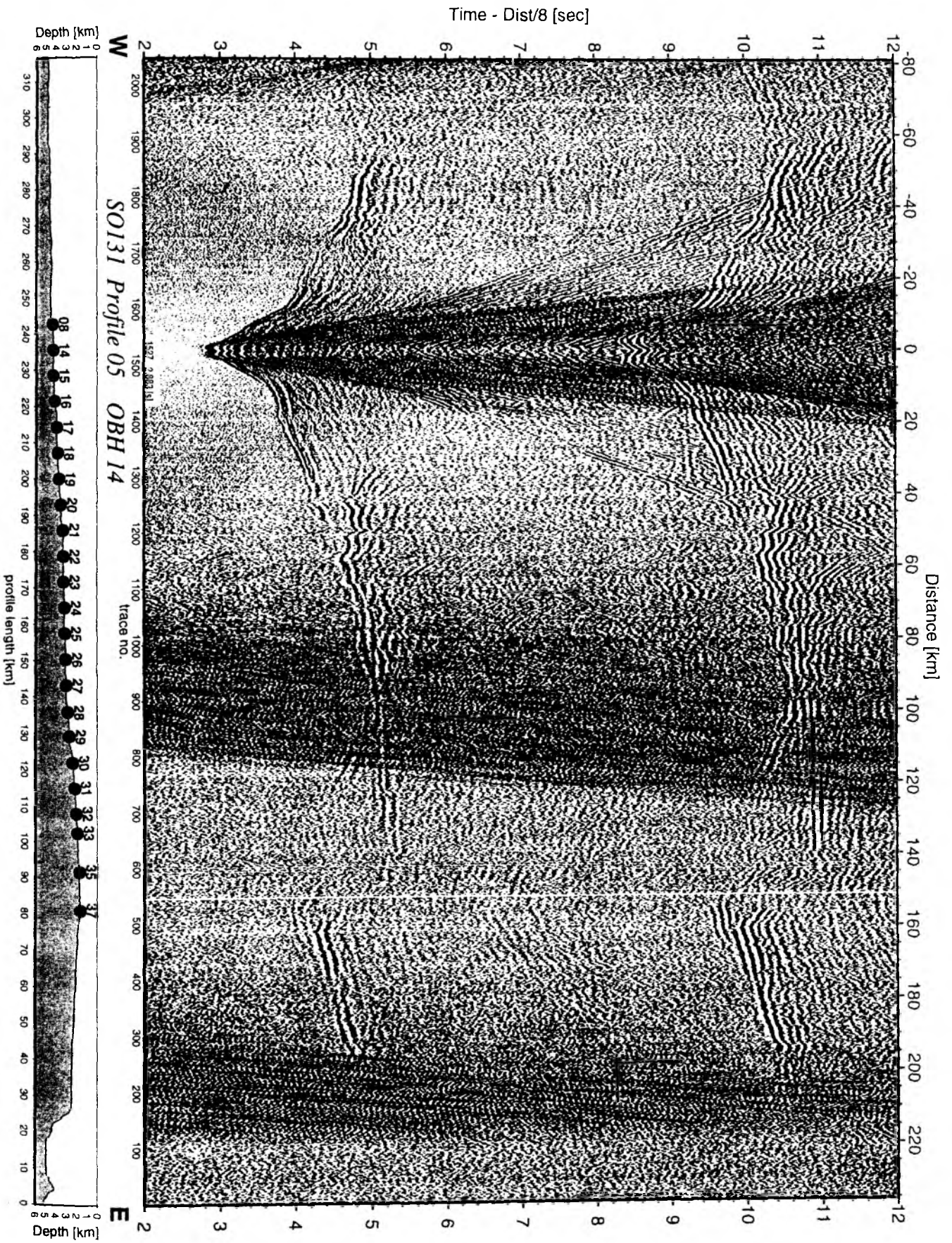

Figure 6.3.4.5.4: Record section from OBH 14 , Profile 05.

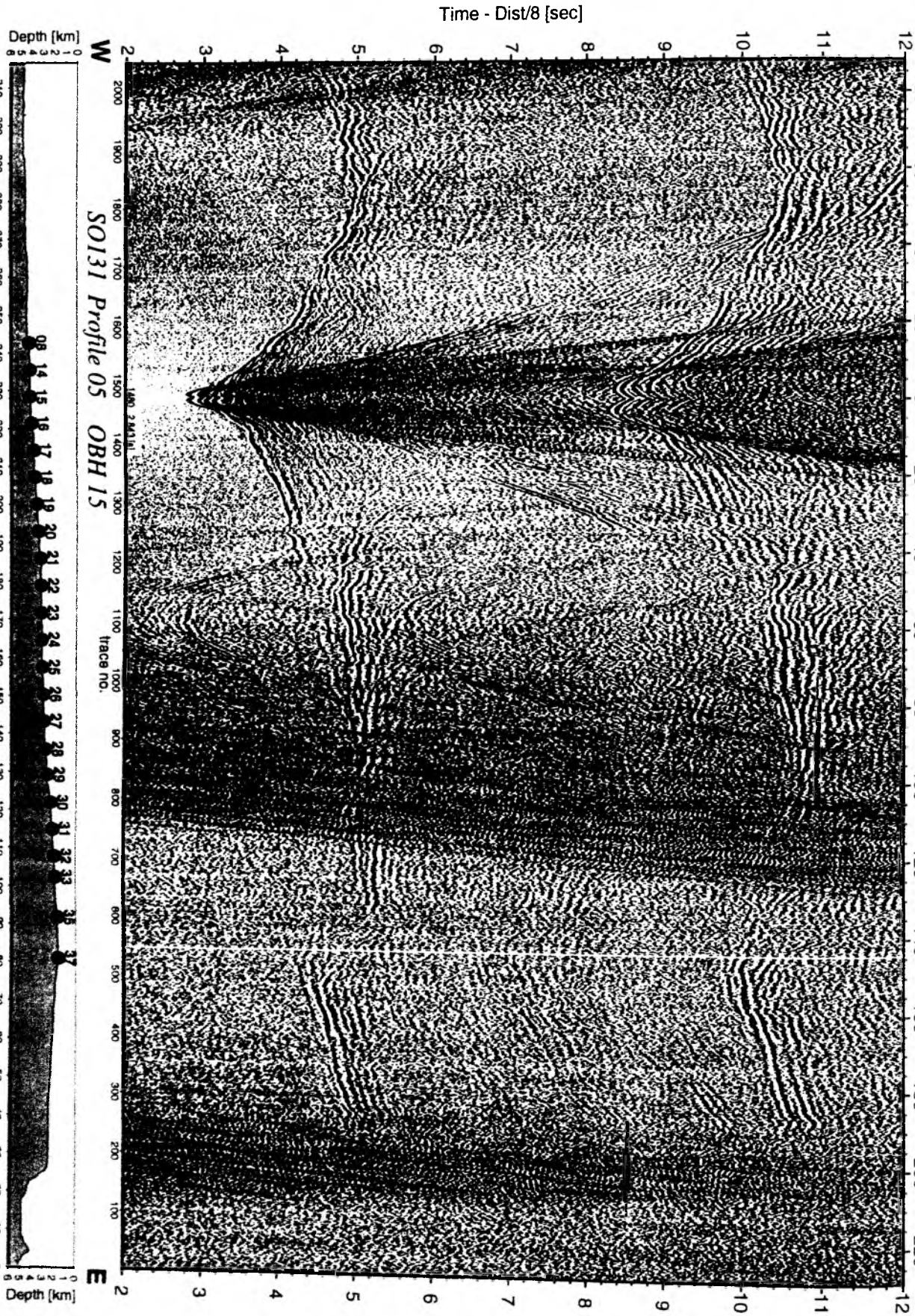

Figure 6.3.4.5.5: Record section from OBH 15 , Profile 05.

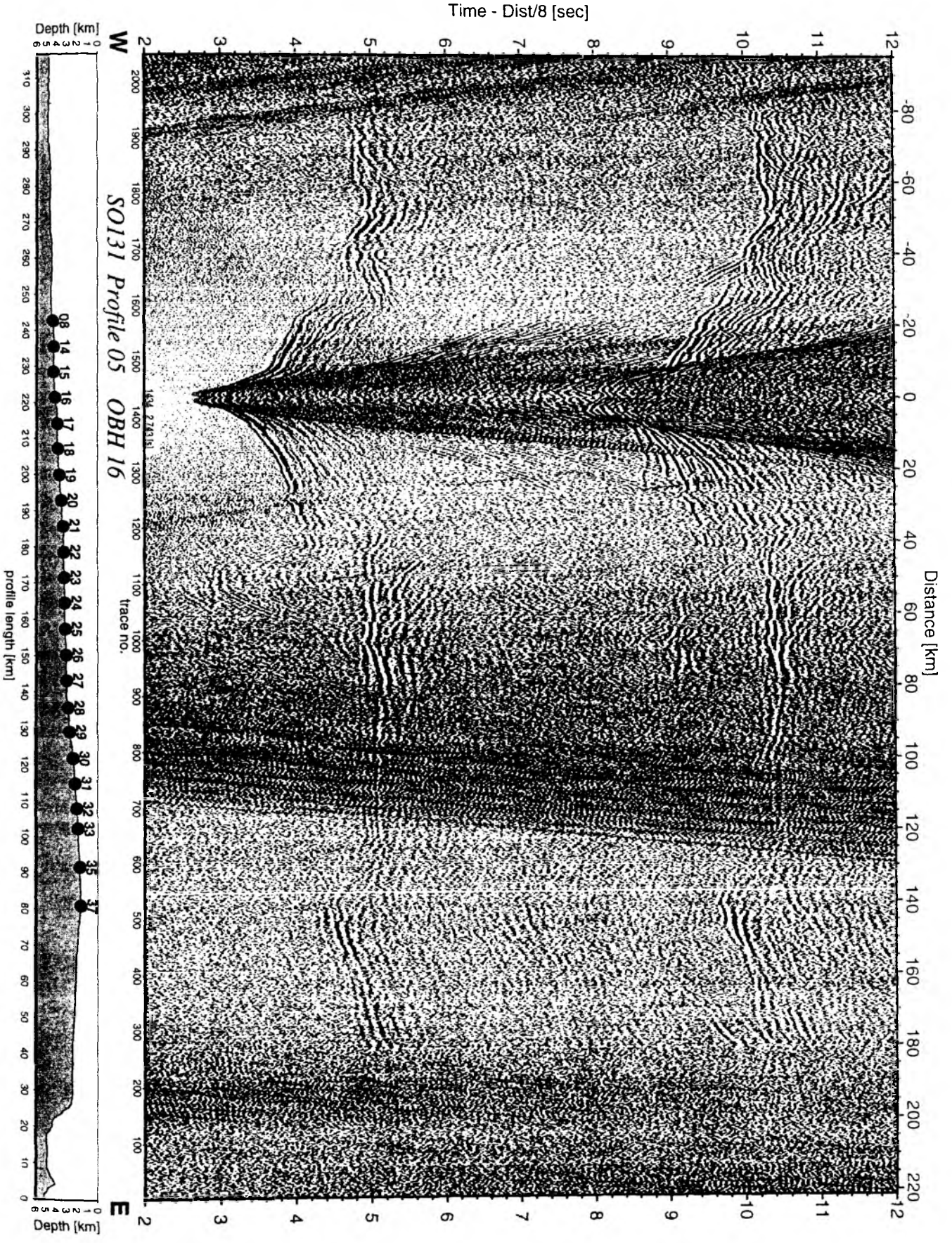

Figure 6.3.4.5.6: Record section from OBH 16 , Profile 05.

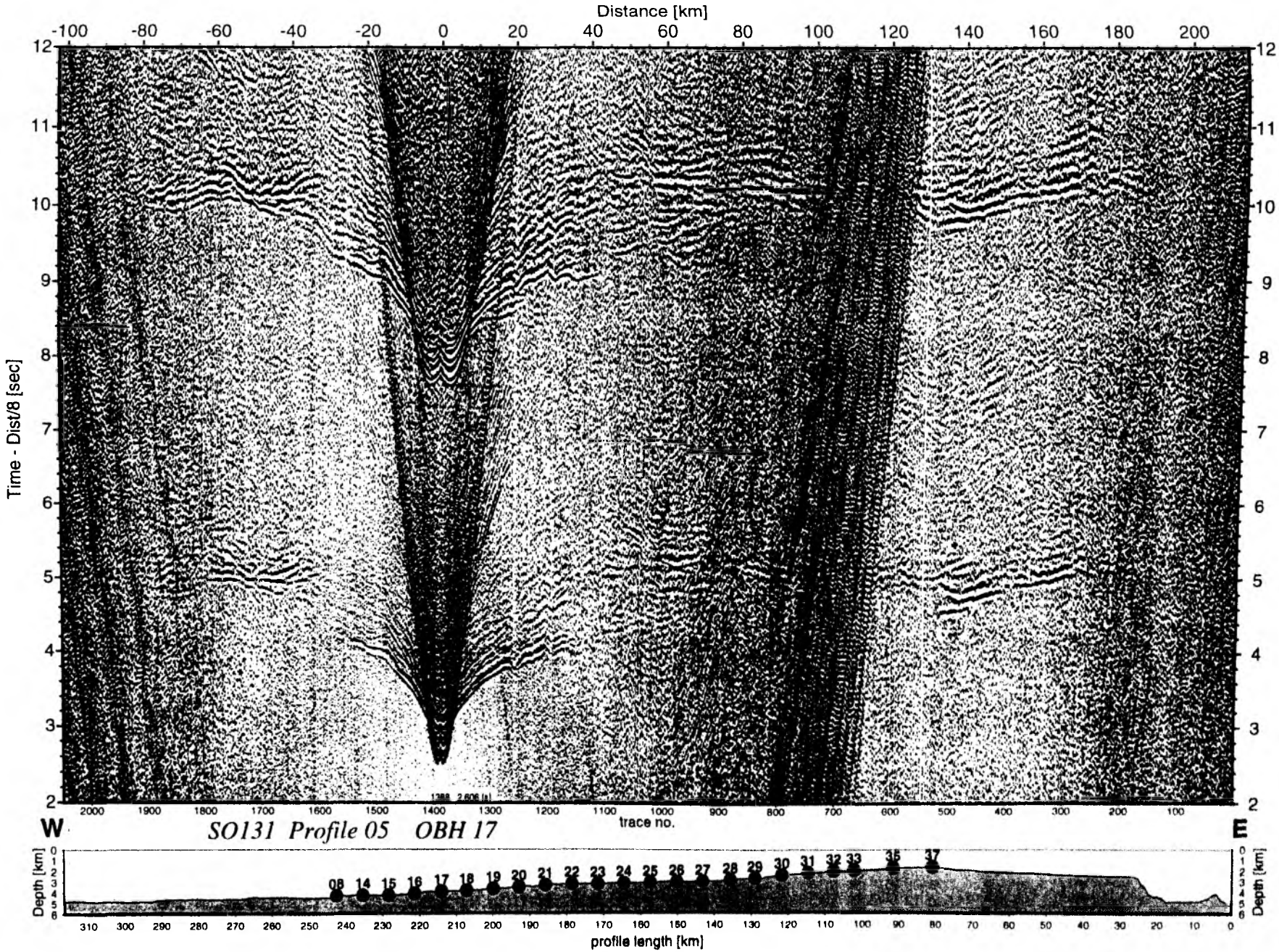

Figure 6.3.4.5.7: Record section from OBH 17 , Profile 05.

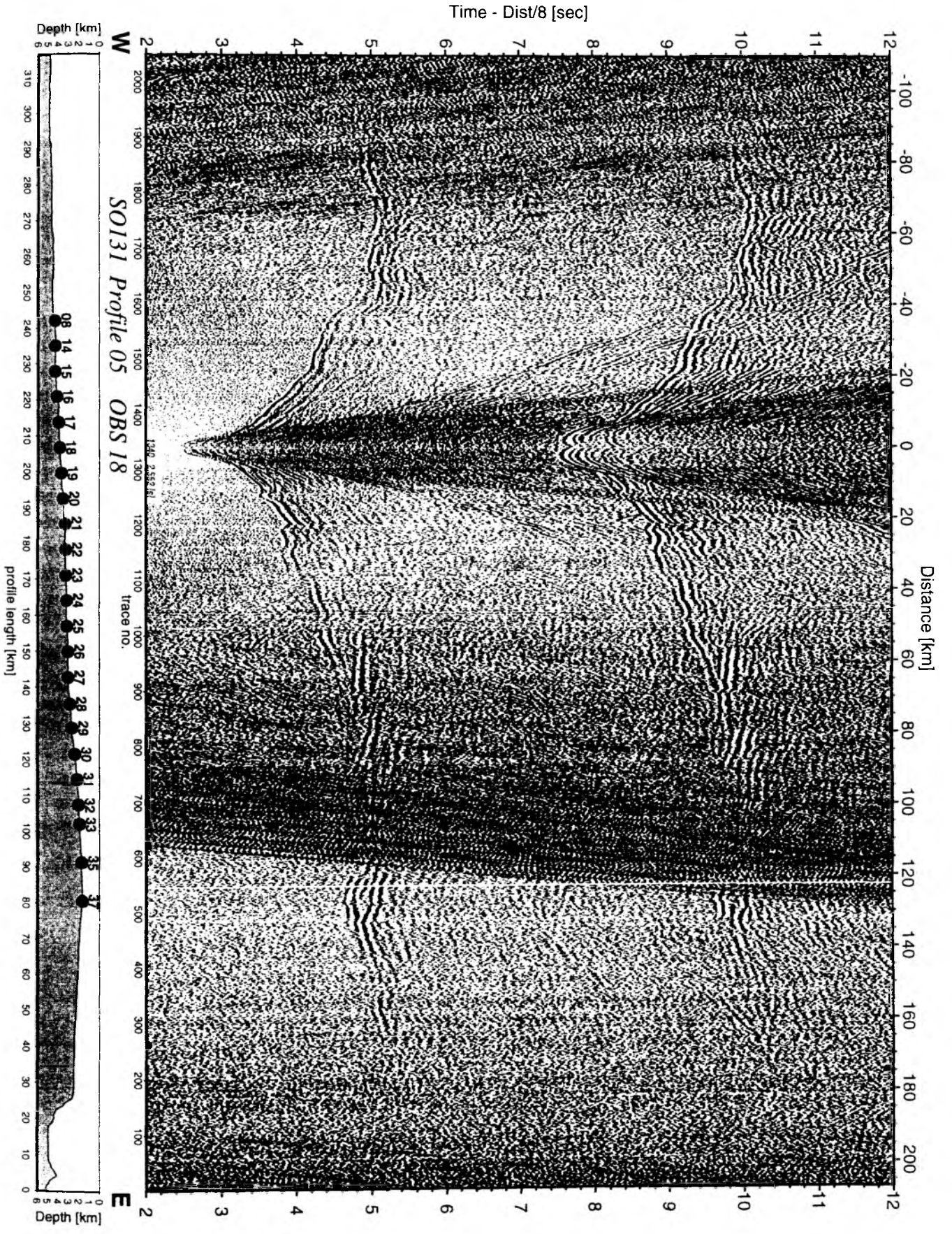

Figure 6.3.4.5.8: Record section from OBS 18 hydrophone, Profile 05.

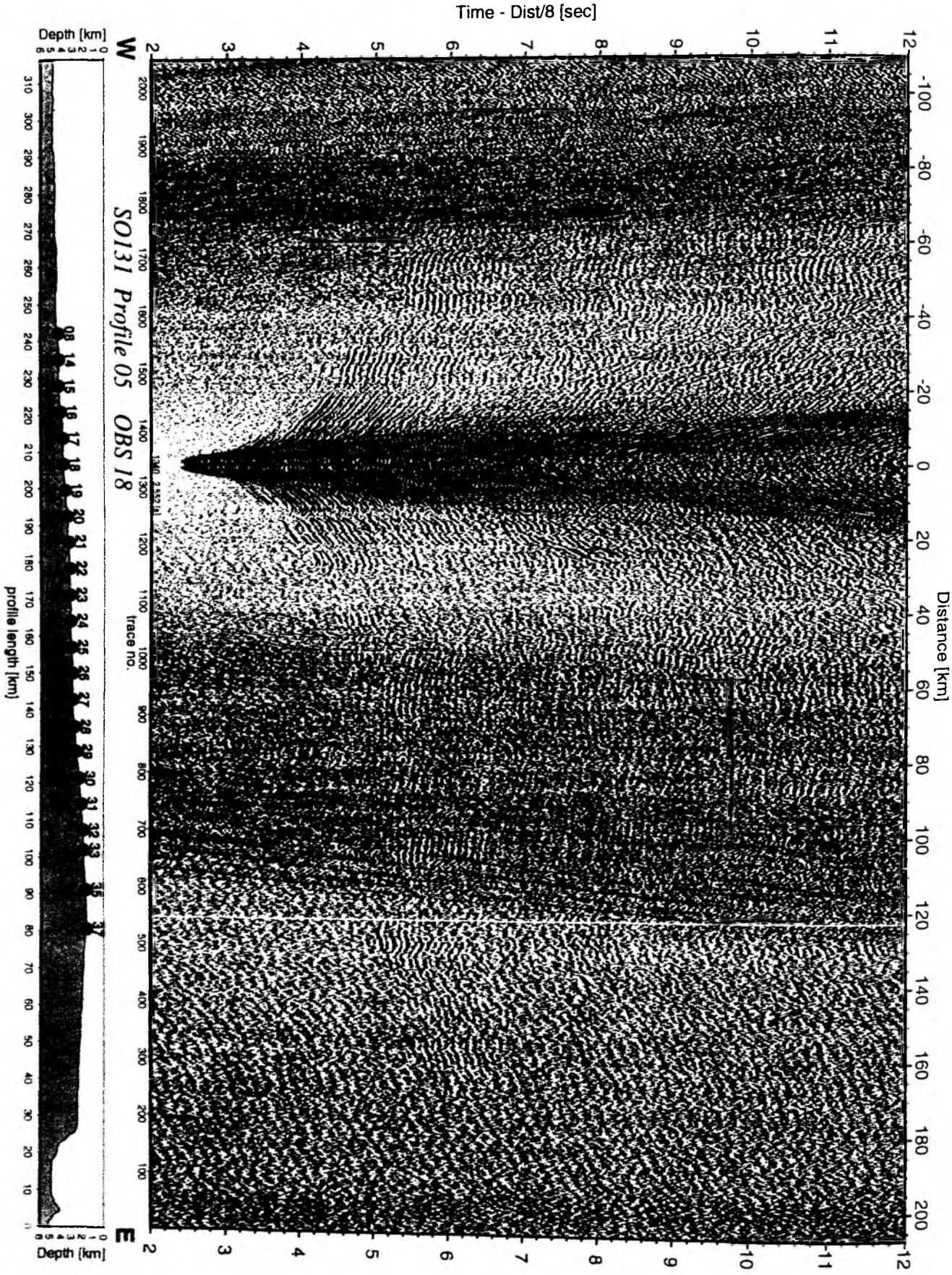

Figure 6.3.4.5.9: Record section from OBS 18 vertical_component, Profile 05.

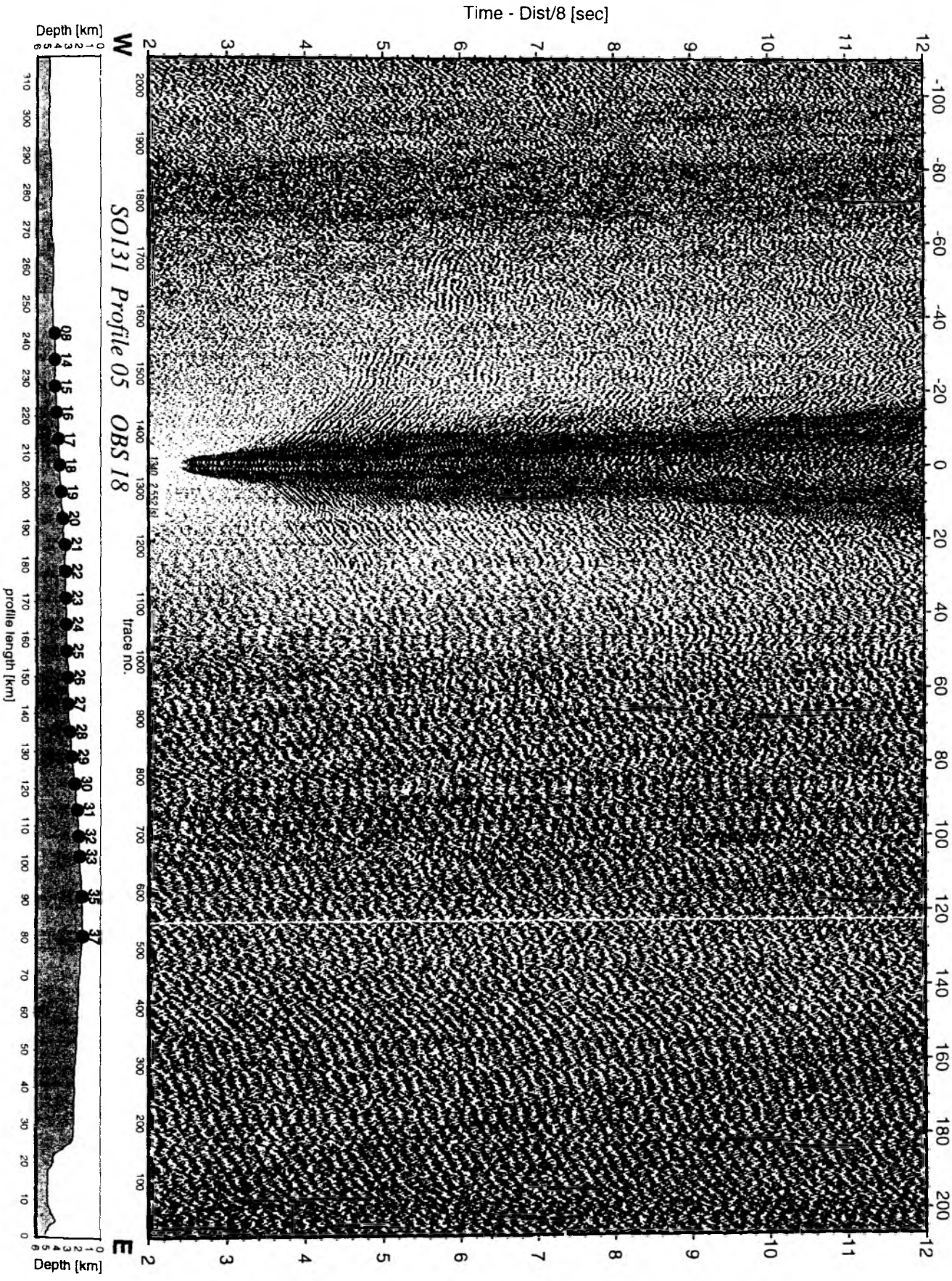

Figure 6.3.4.5.10: Record section from OBS 18 horizontal_component_1, Profile 05.

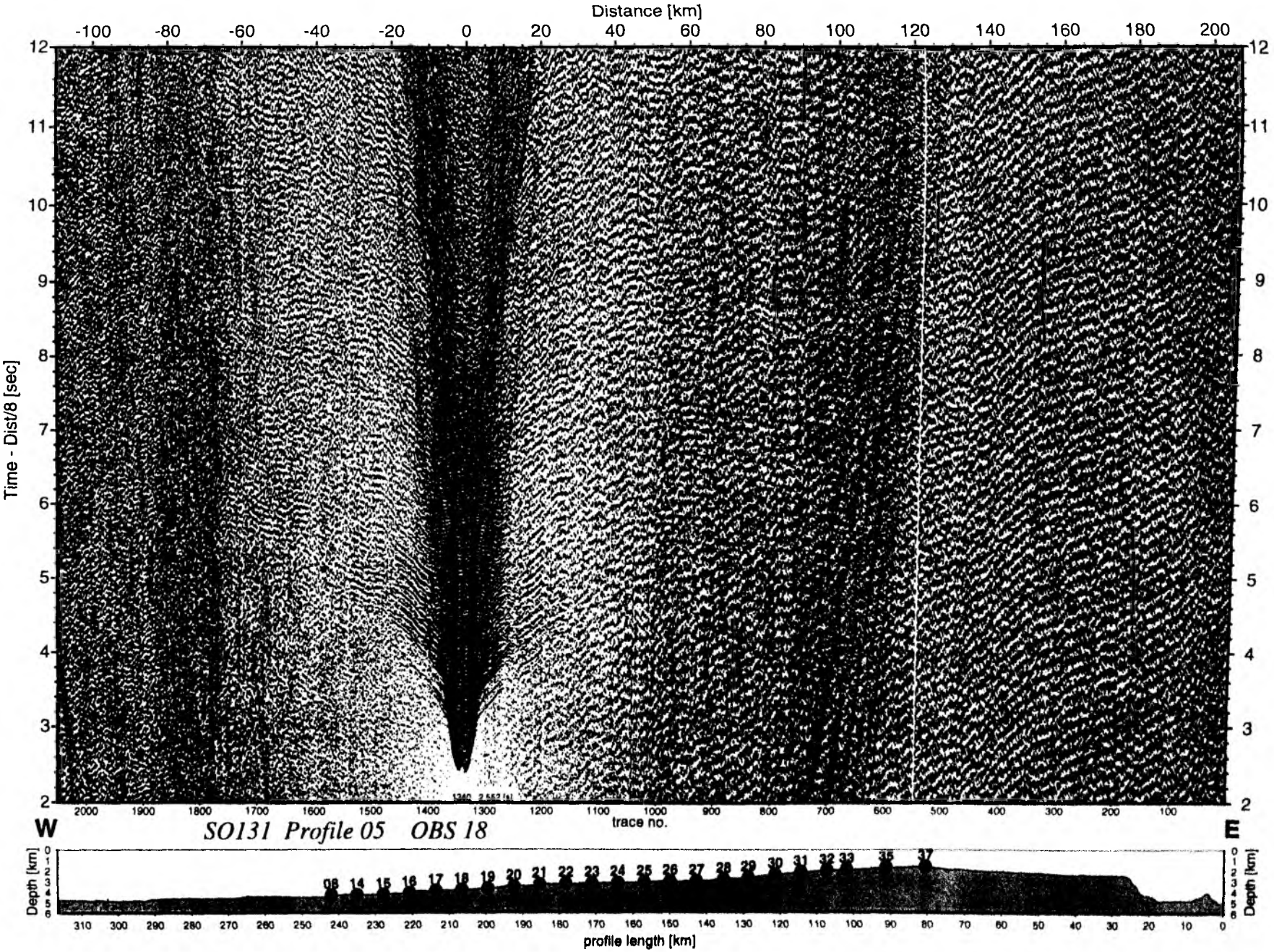

Figure 6.3.4.5.11: Record section from OBS 18 horizontal_component_2, Profile 05.

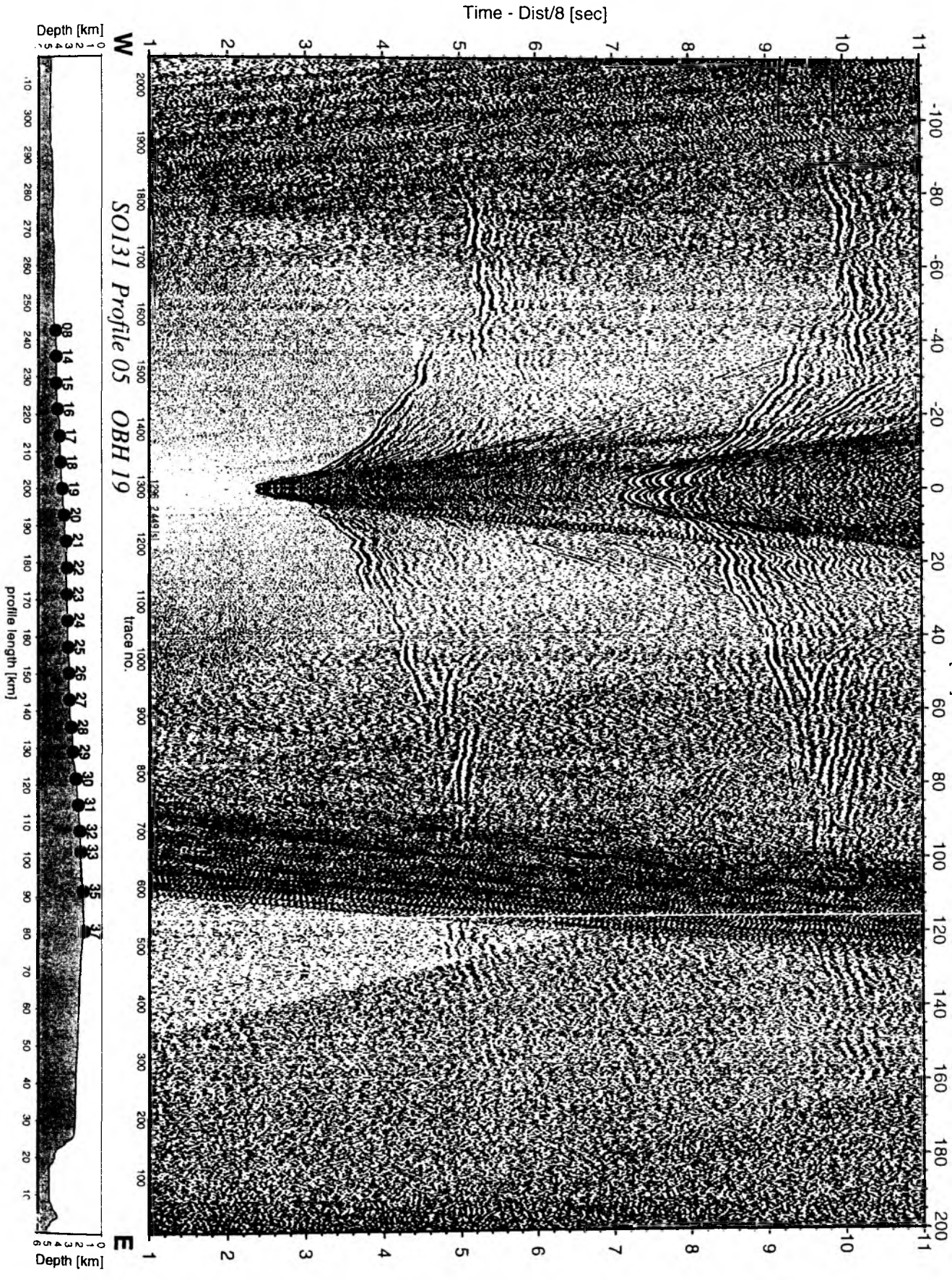

Figure 6.3.4.5.12: Record section from OBH 19 , Profile 05.

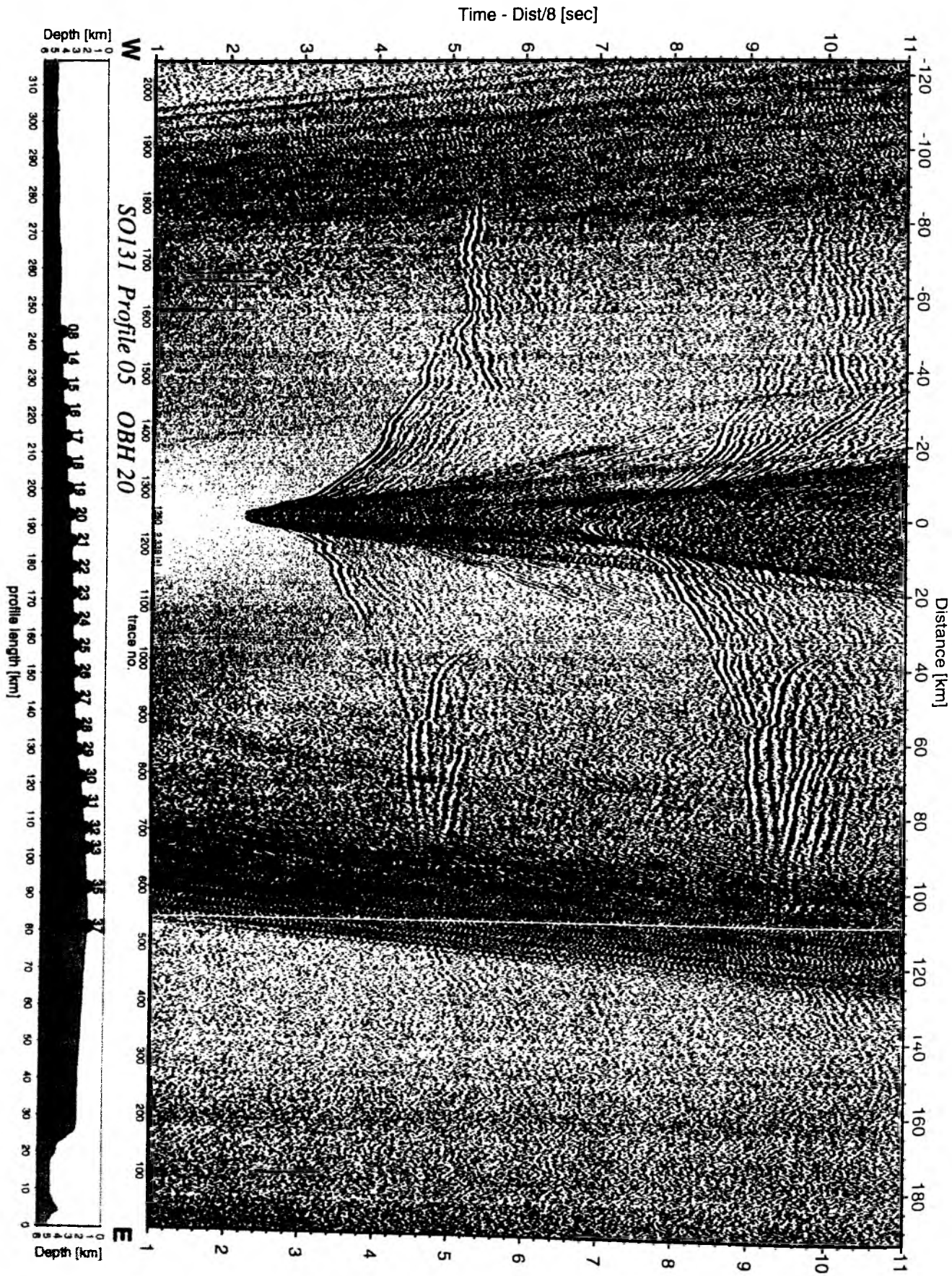

Figure 6.3.4.5.13: Record section from OBH 20 , Profile 05.

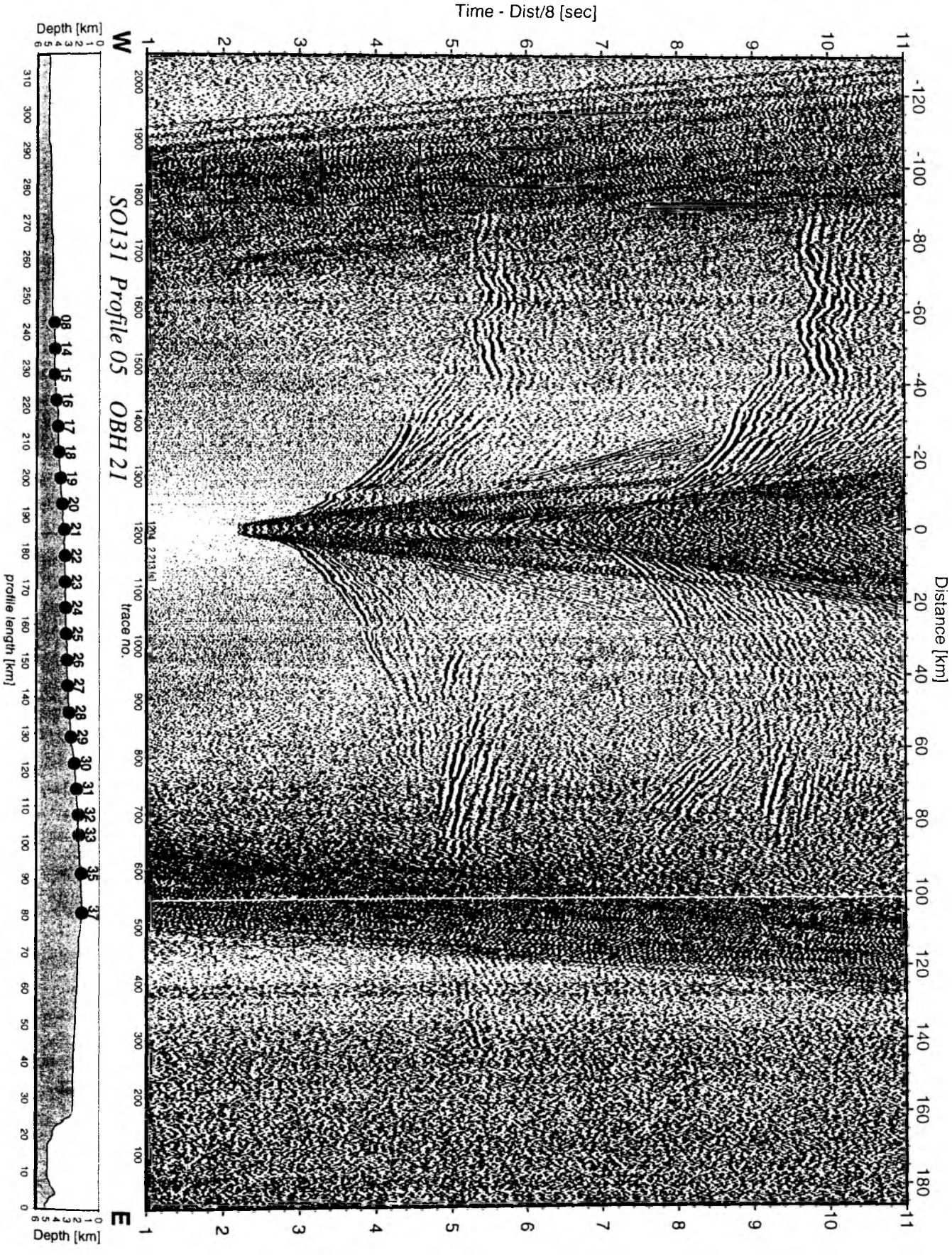

Figure 6.3.4.5.14: Record section from OBH 21 , Profile 05.

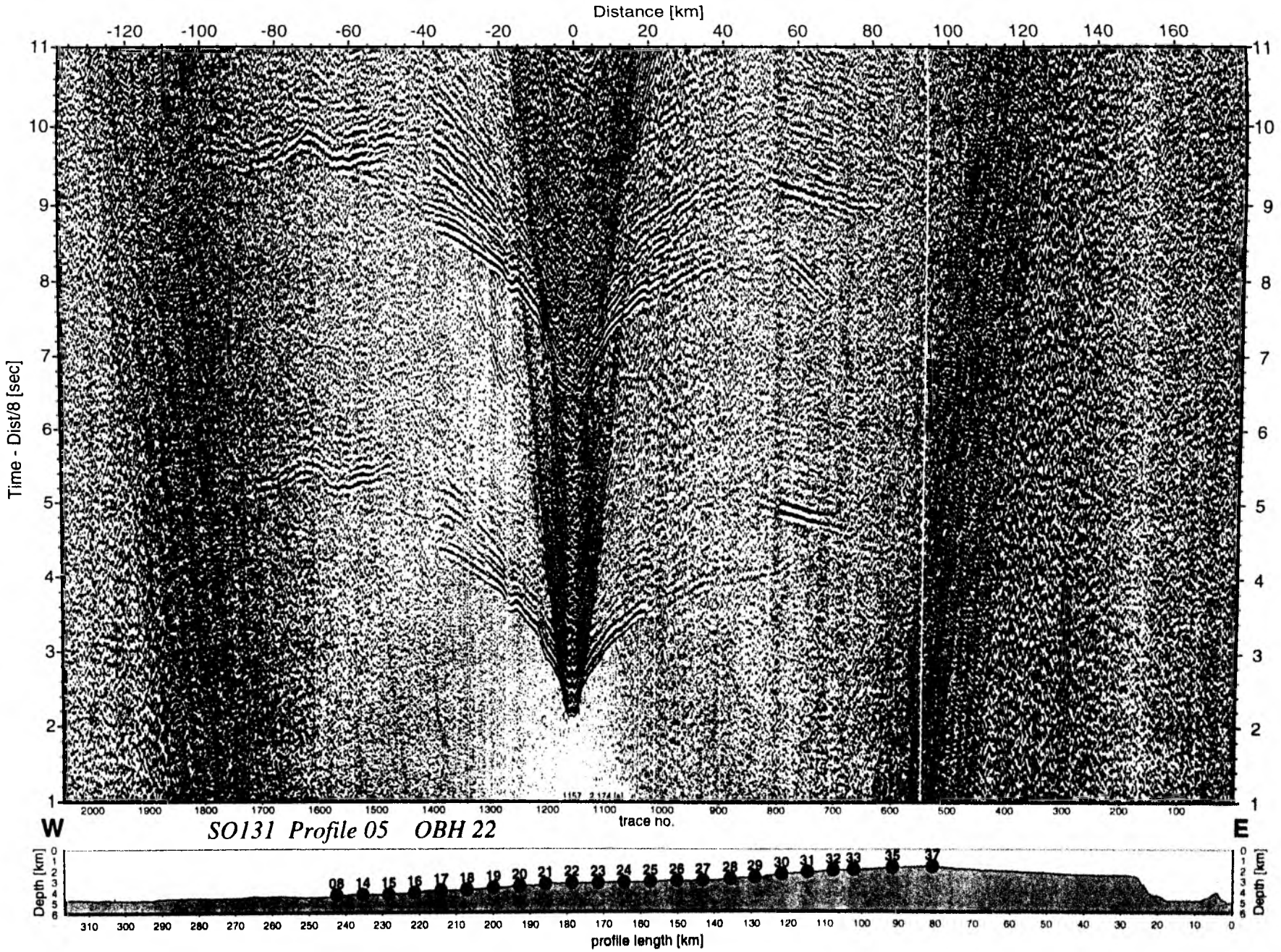

Figure 6.3.4.5.15: Record section from OBH 22 , Profile 05.

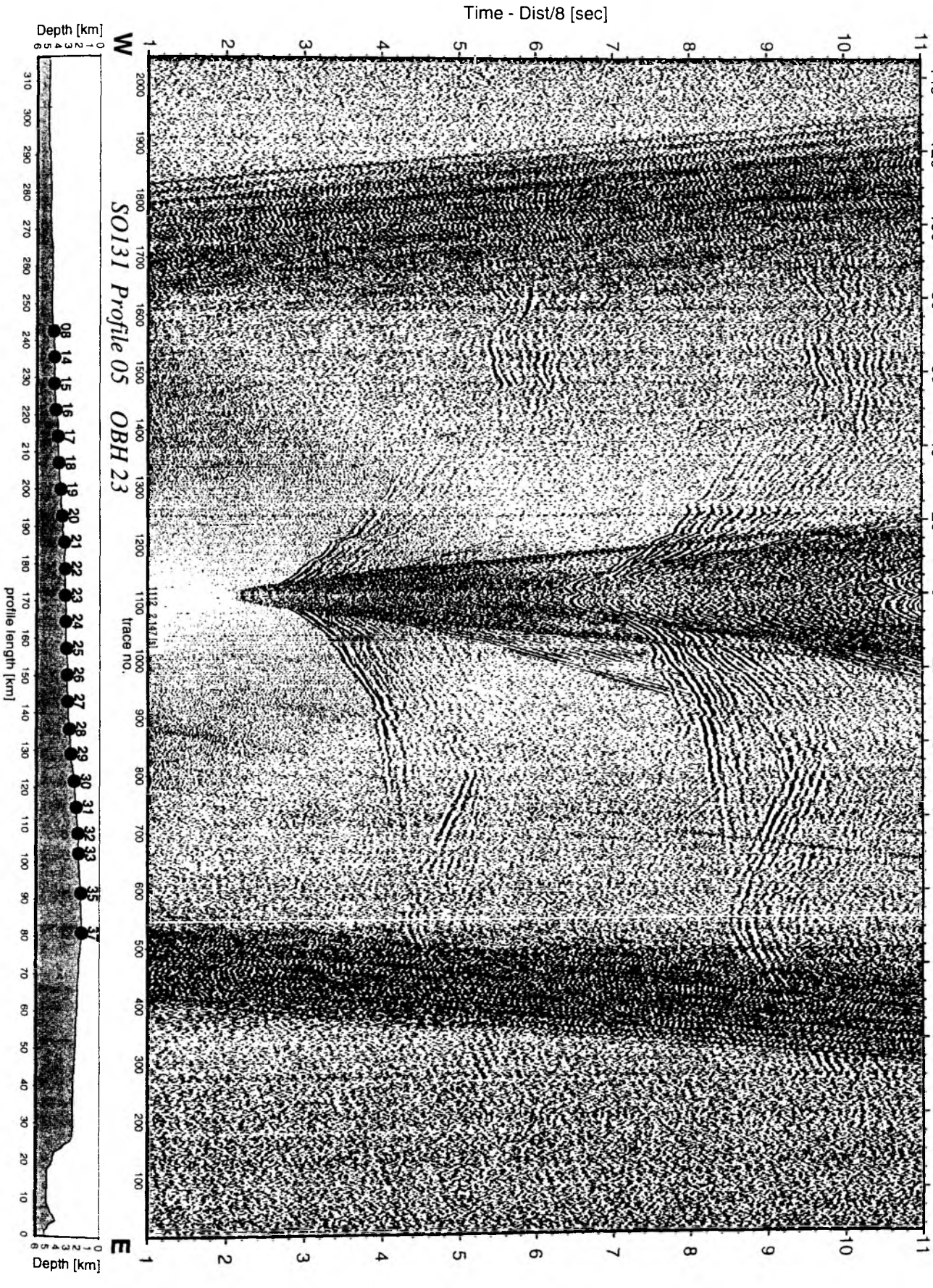

Figure 6.3.4.5.16: Record section from OBH 23 , Profile 05.

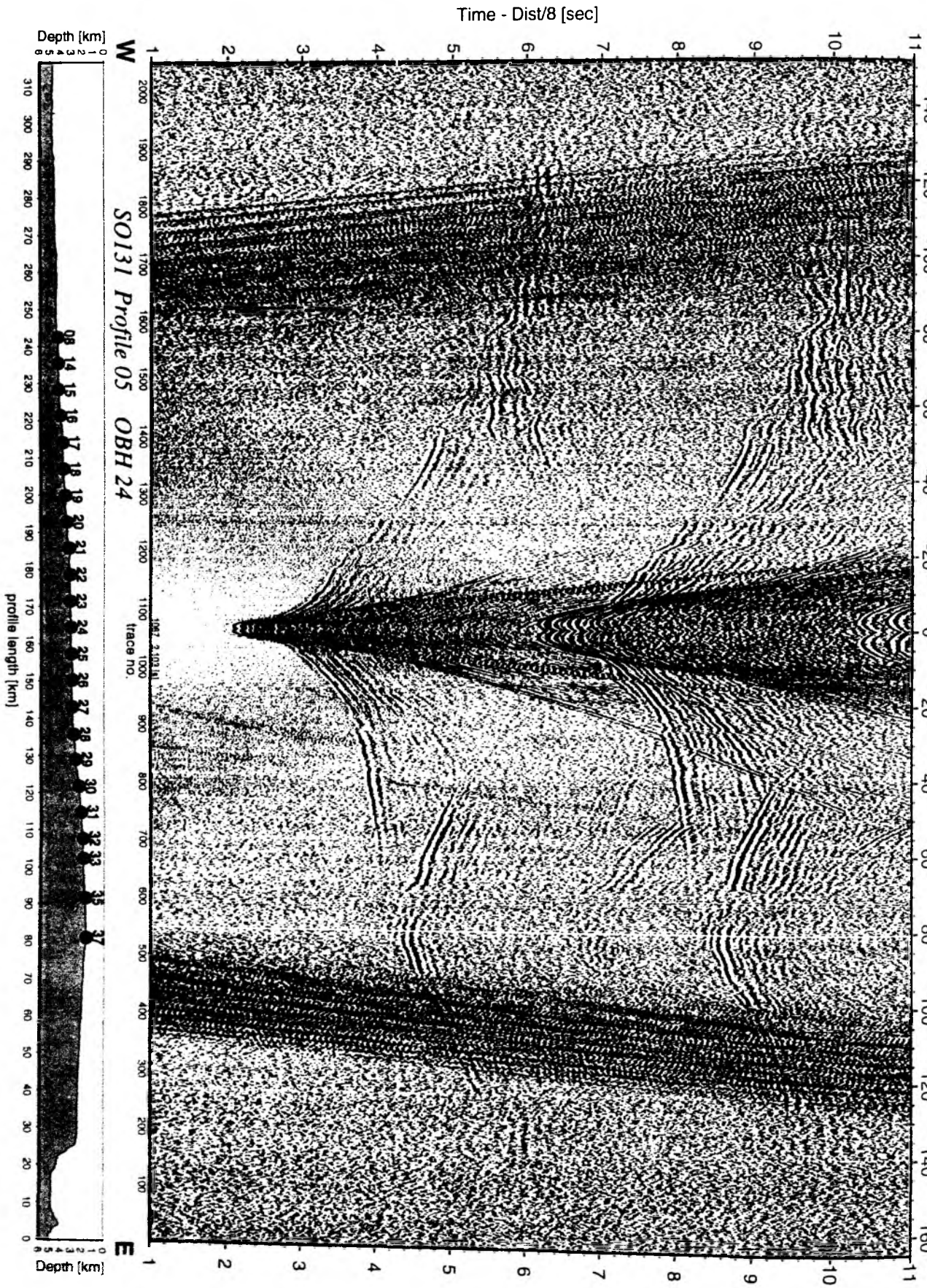

Figure 6.3.4.5.17: Record section from OBH 24 , Profile 05.

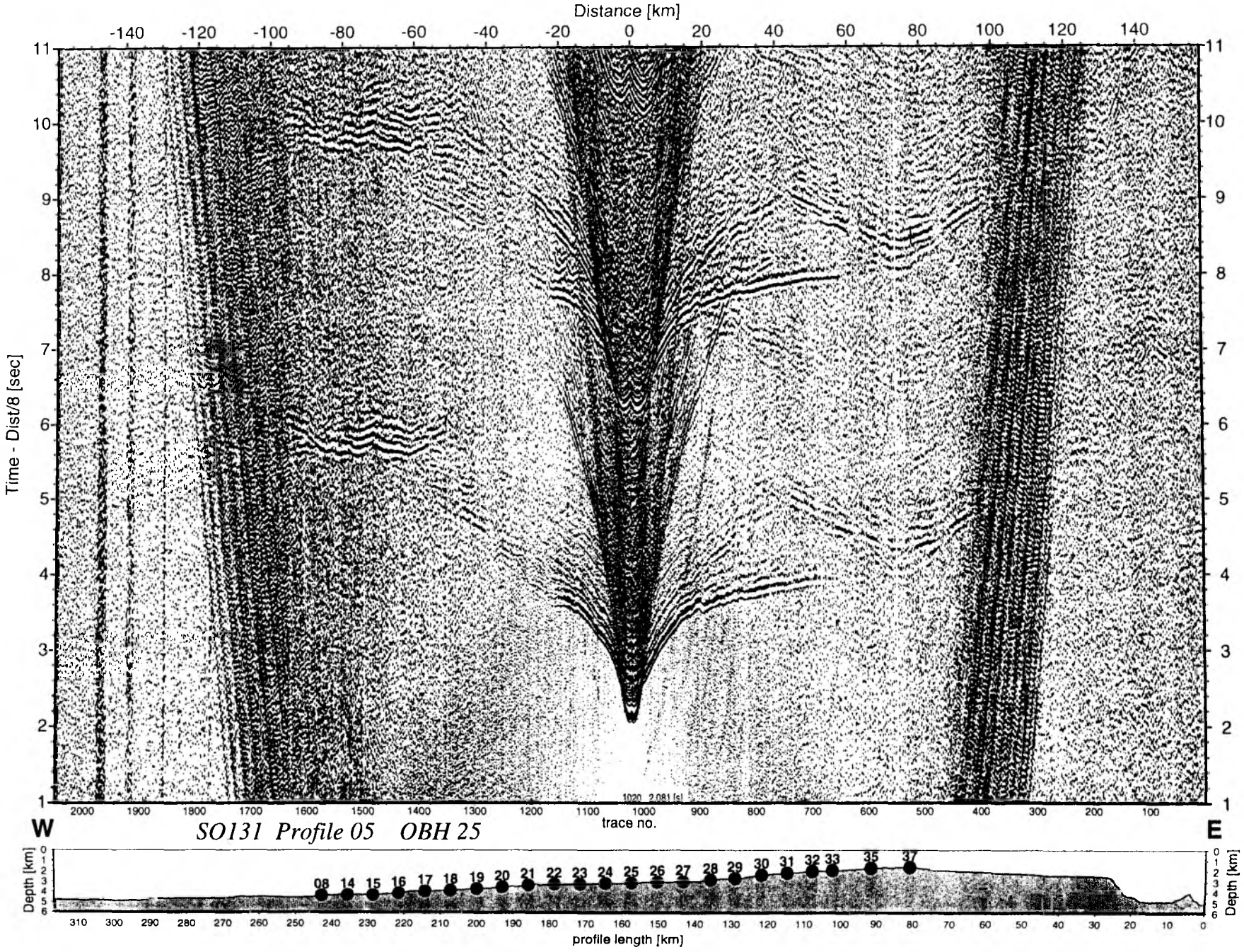

Figure 6.3.4.5.18: Record section from OBH 25 , Profile 05.

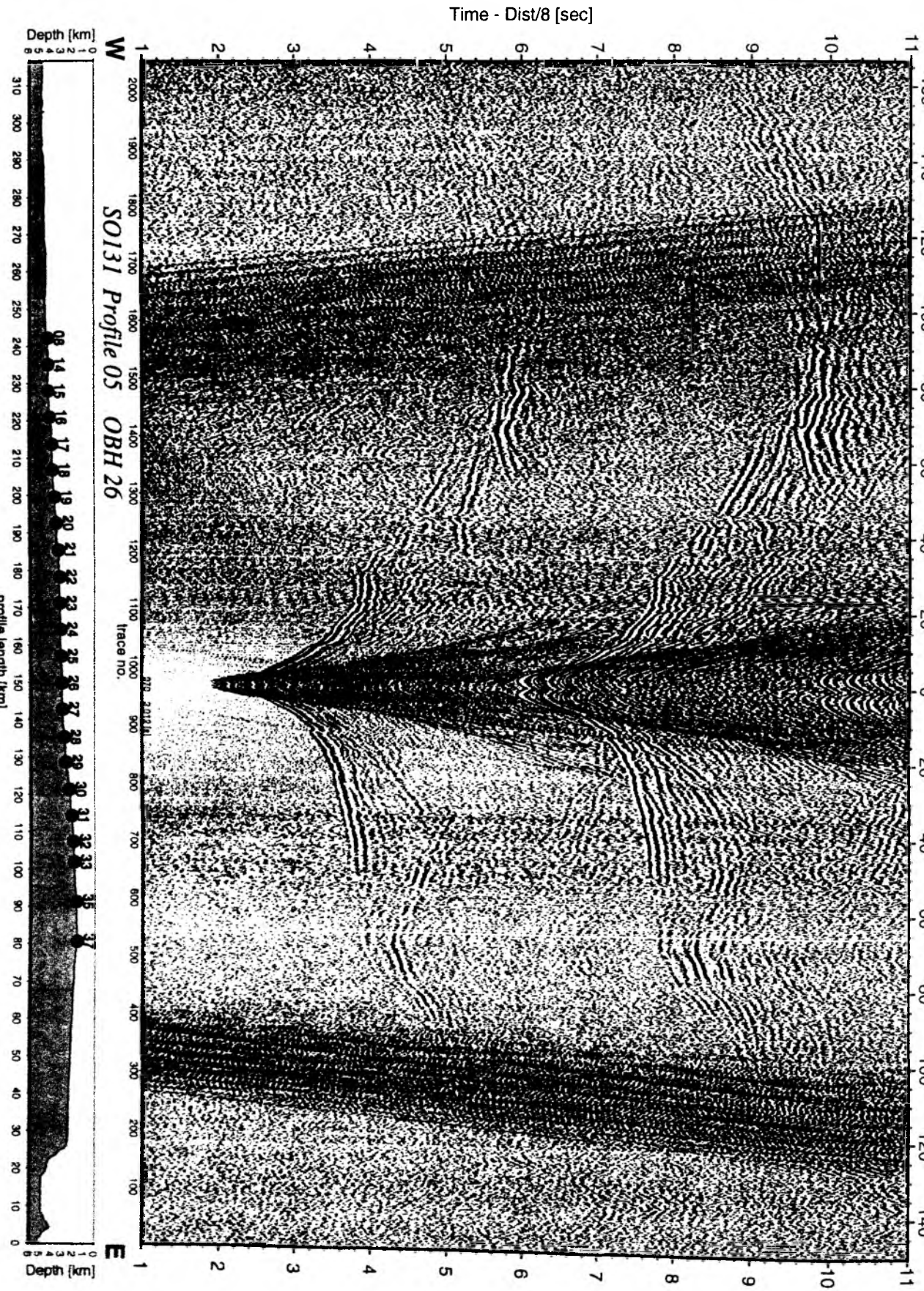

Figure 6.3.4.5.19: Record section from OBH 26 , Profile 05.

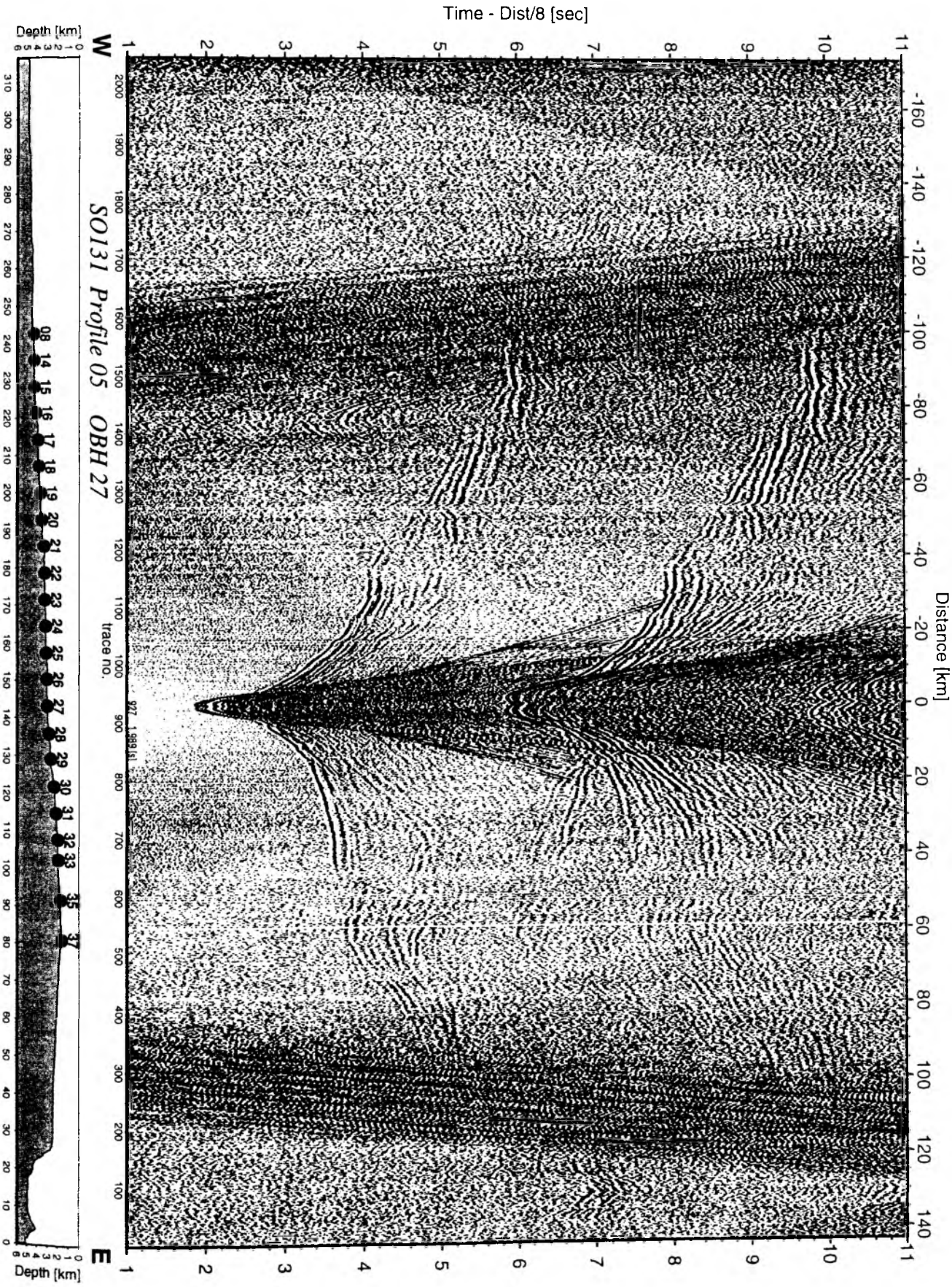

Figure 6.3.4.5.20: Record section from OBH 27 , Profile 05.

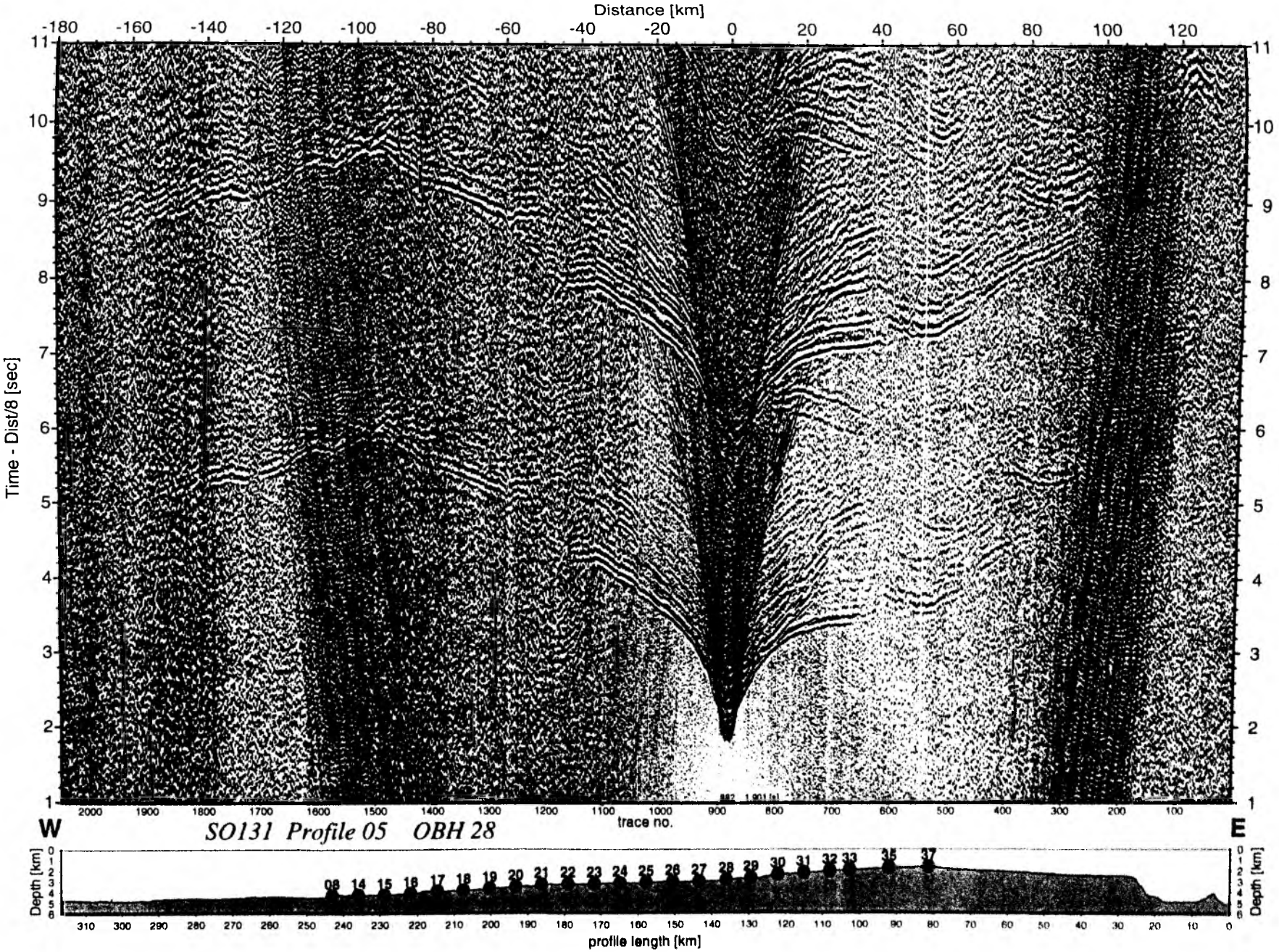

Figure 6.3.4.5.21: Record section from OBH 28 , Profile 05.

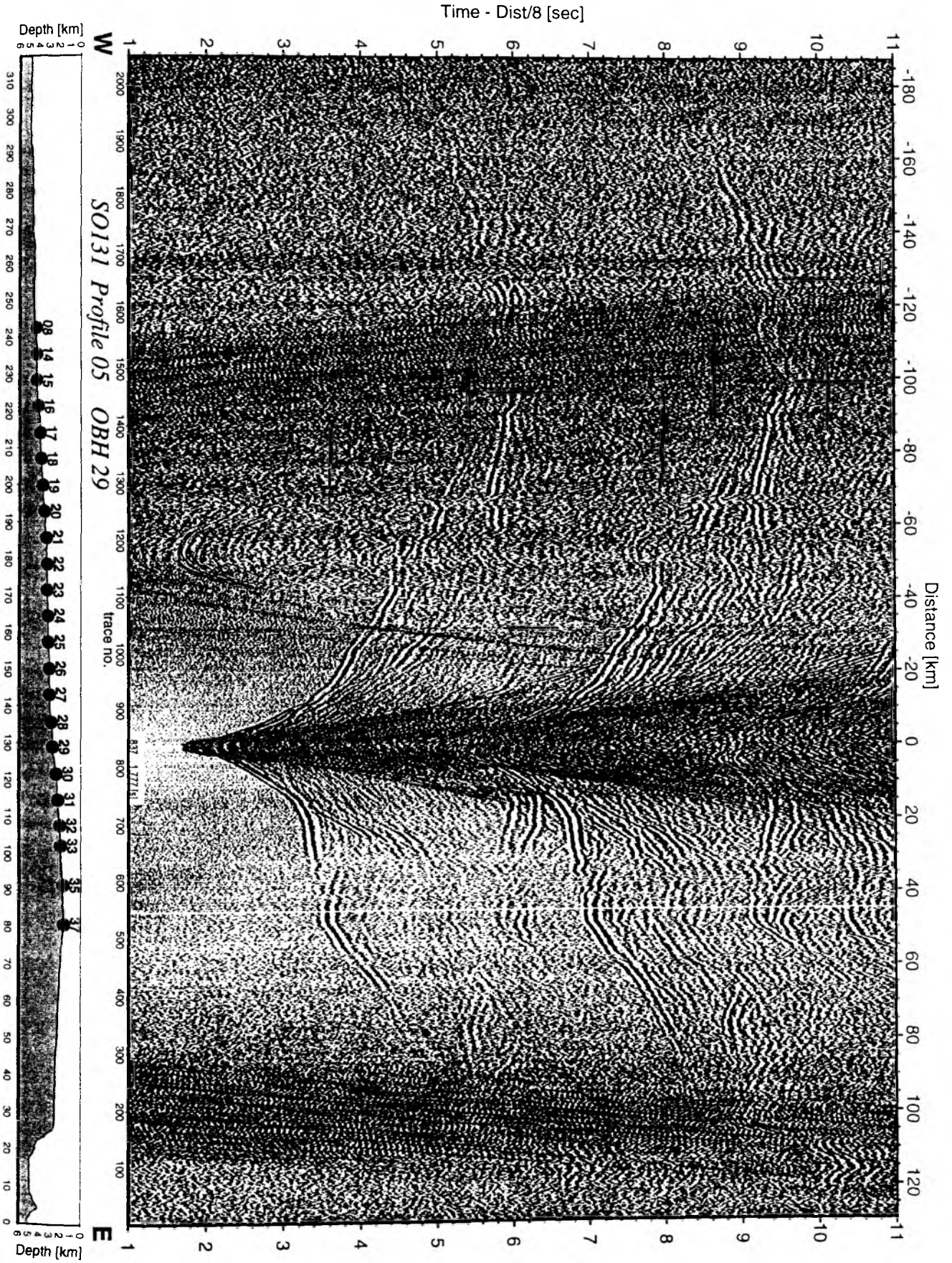

Figure 6.3.4.5.22: Record section from OBH 29 , Profile 05.

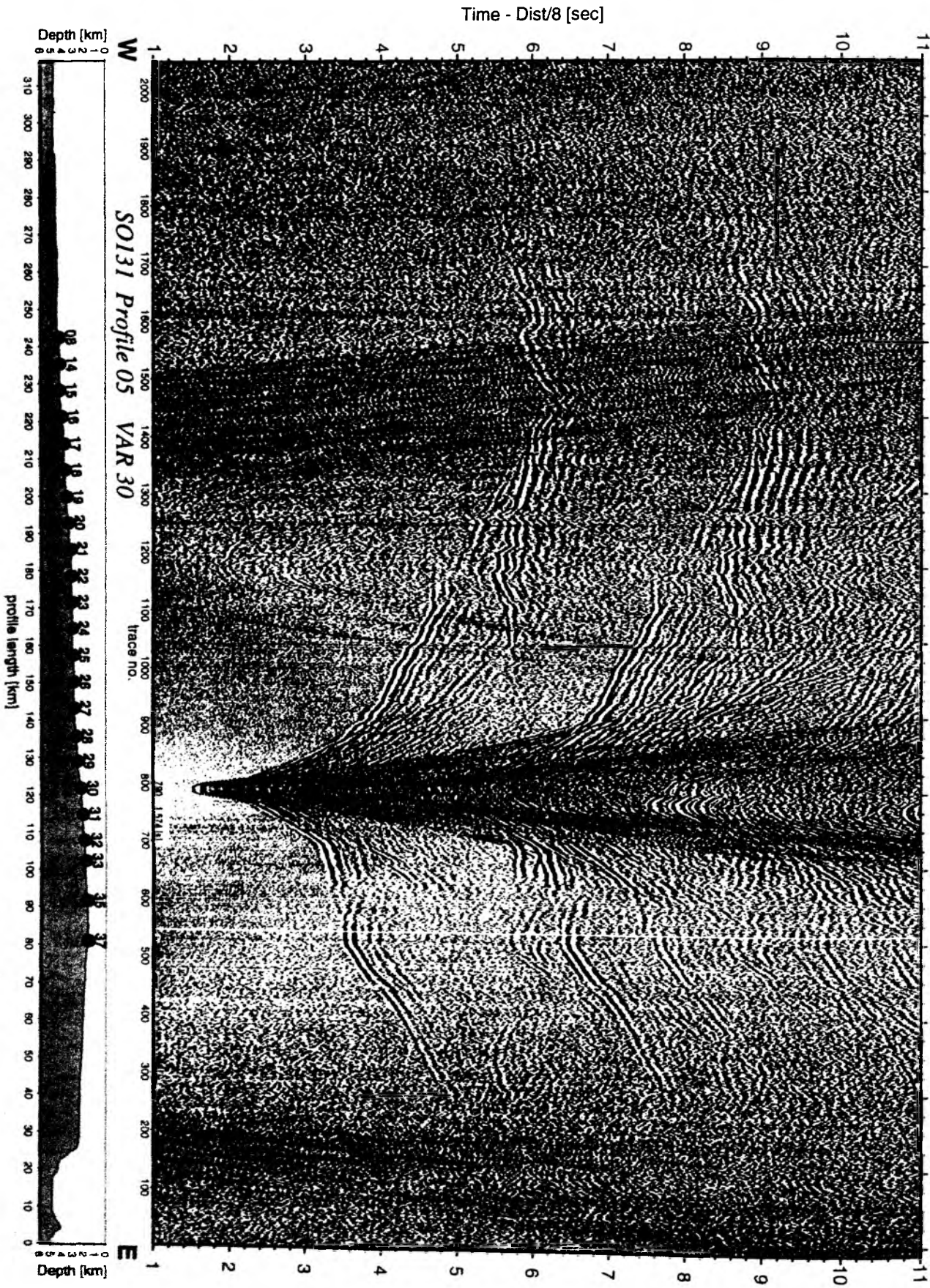

Figure 6.3.4.5.23: Record section from VAR 30 channel_1, Profile 05.

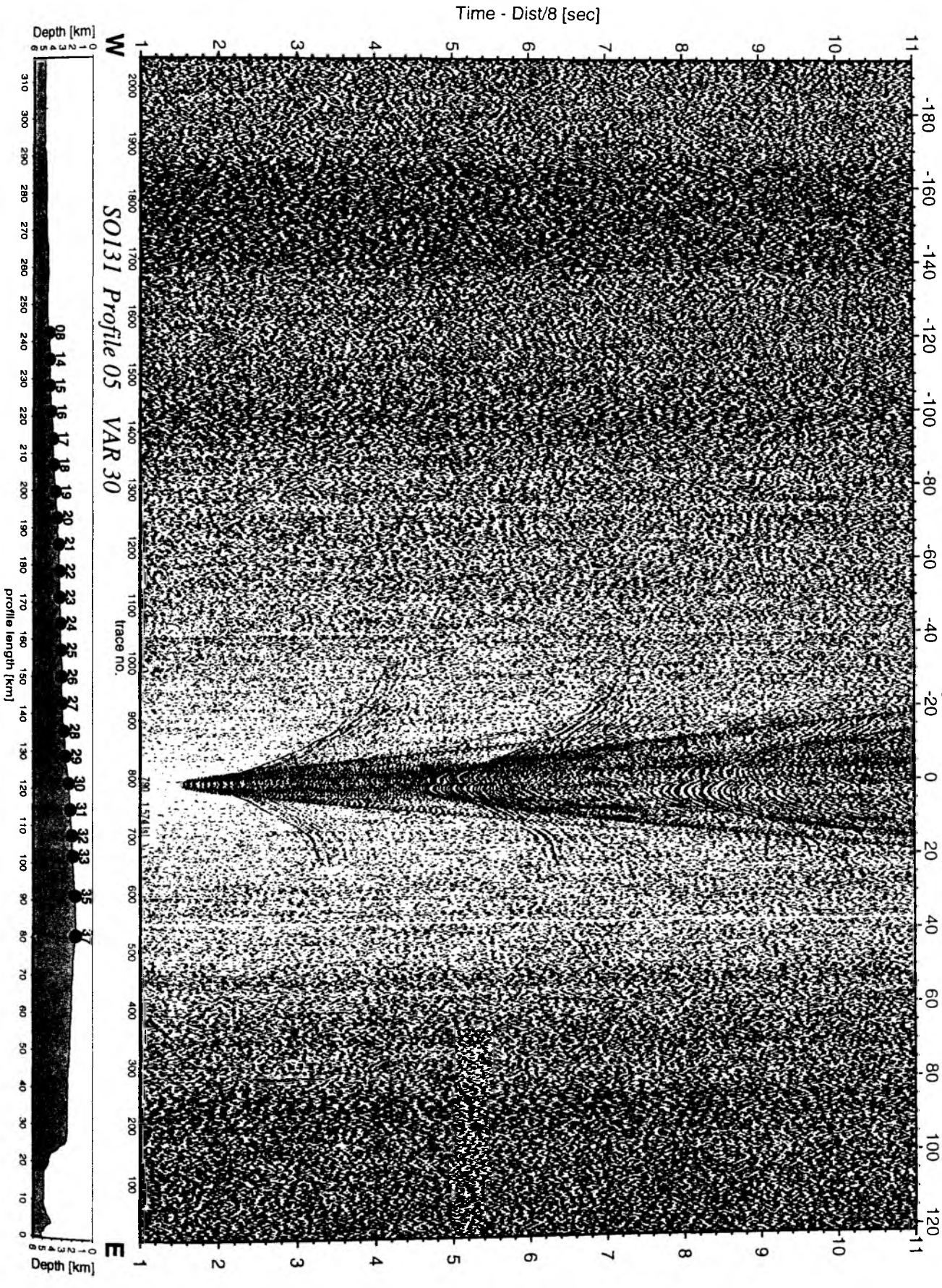

Figure 6.3.4.5.24: Record section from VAR 30 channel_2, Profile 05.

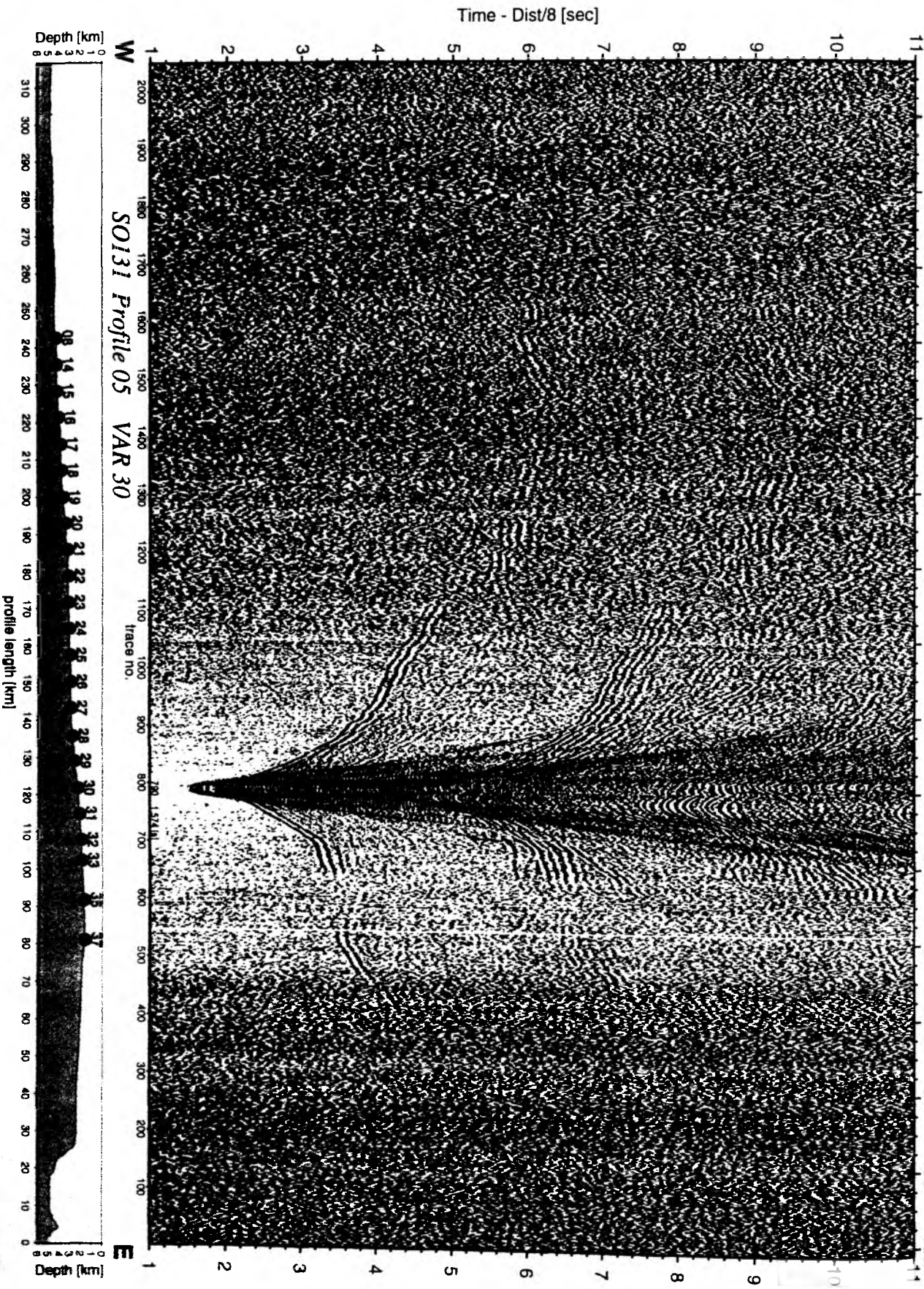

Figure 6.3.4.5.25: Record section from VAR 30 channel_3, Profile 05.

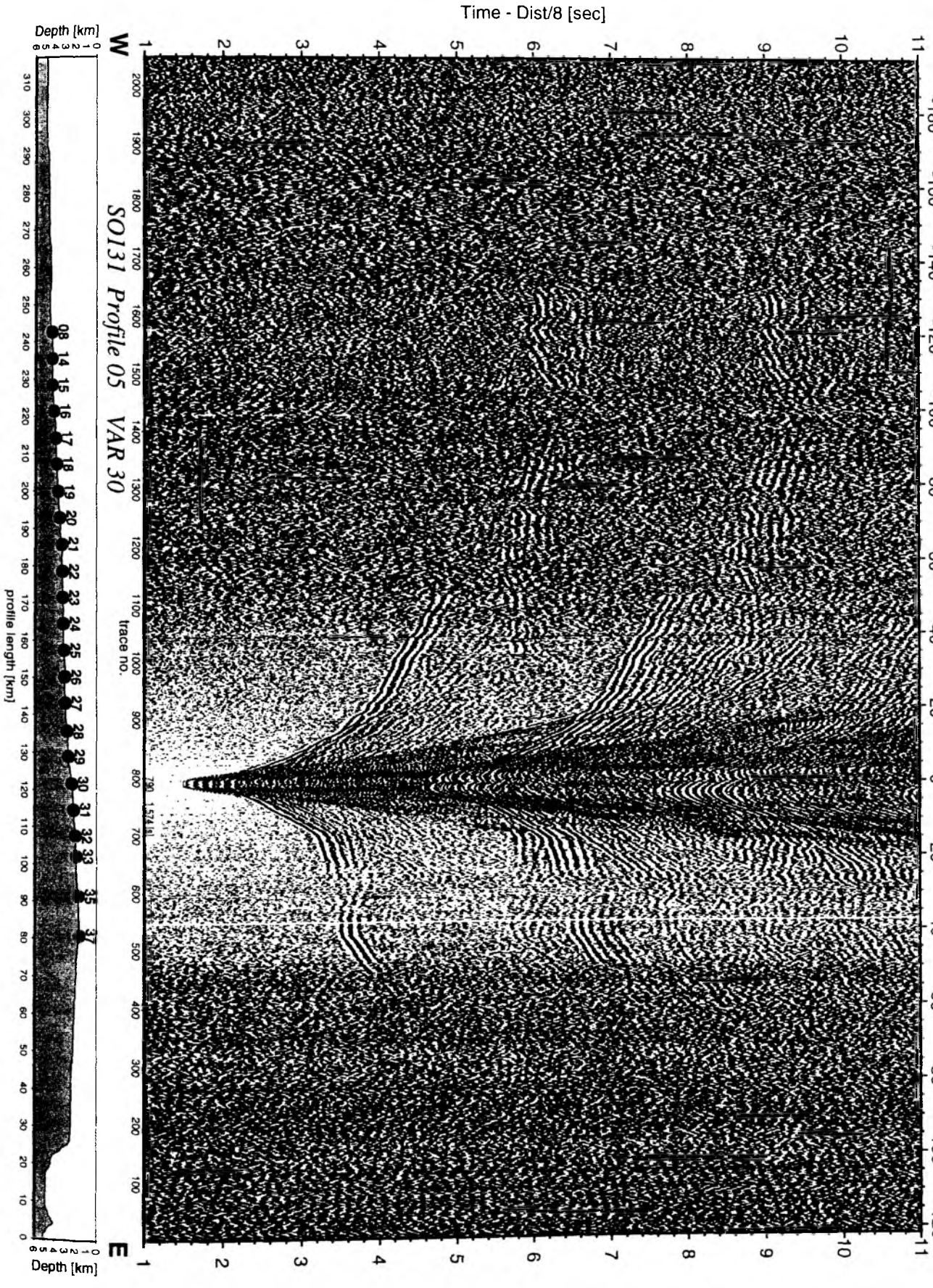

Figure 6.3.4.5.26: Record section from VAR 30 channel_4, Profile 05.

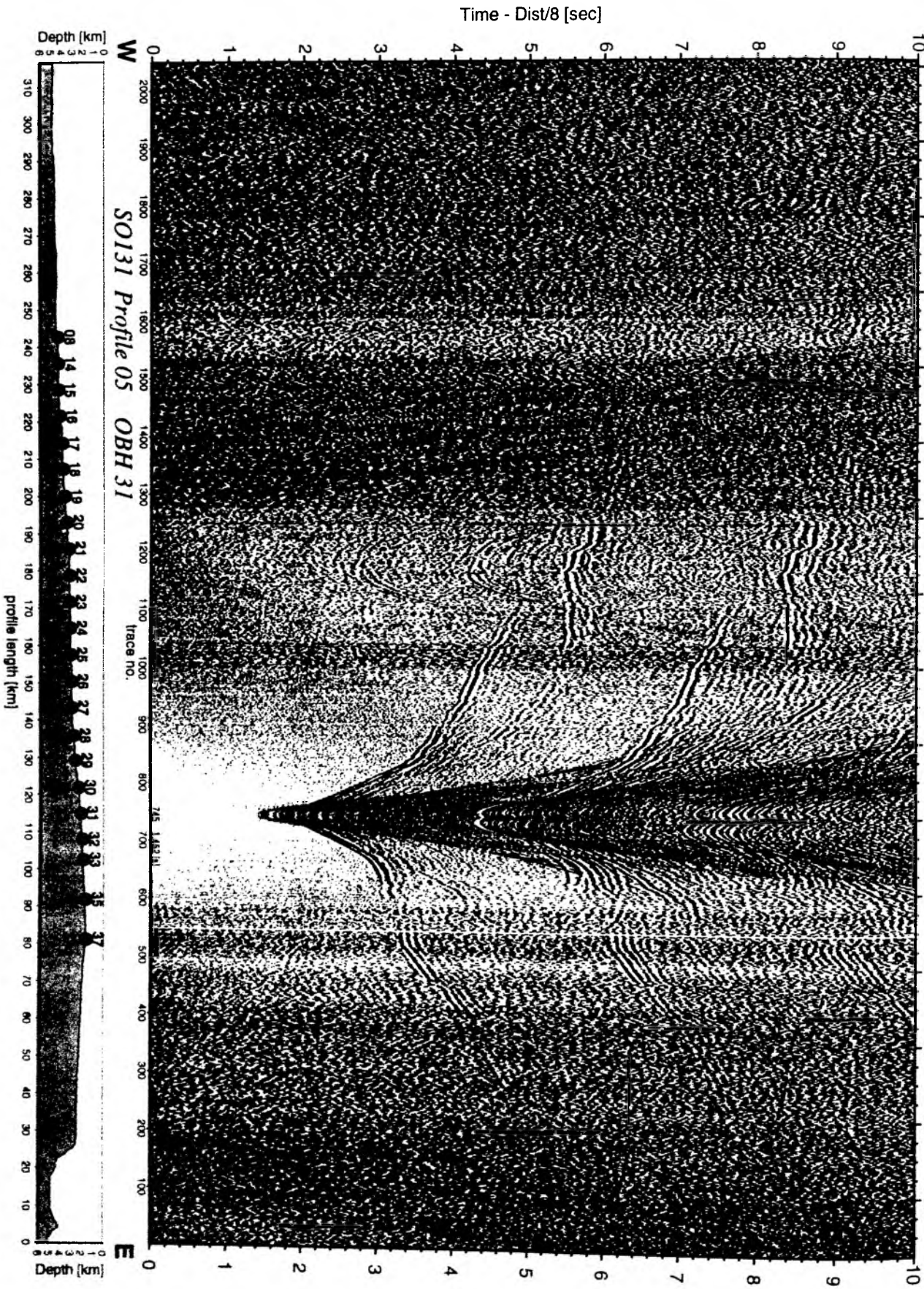

Figure 6.3.4.5.27: Record section from OBH 31 , Profile 05.

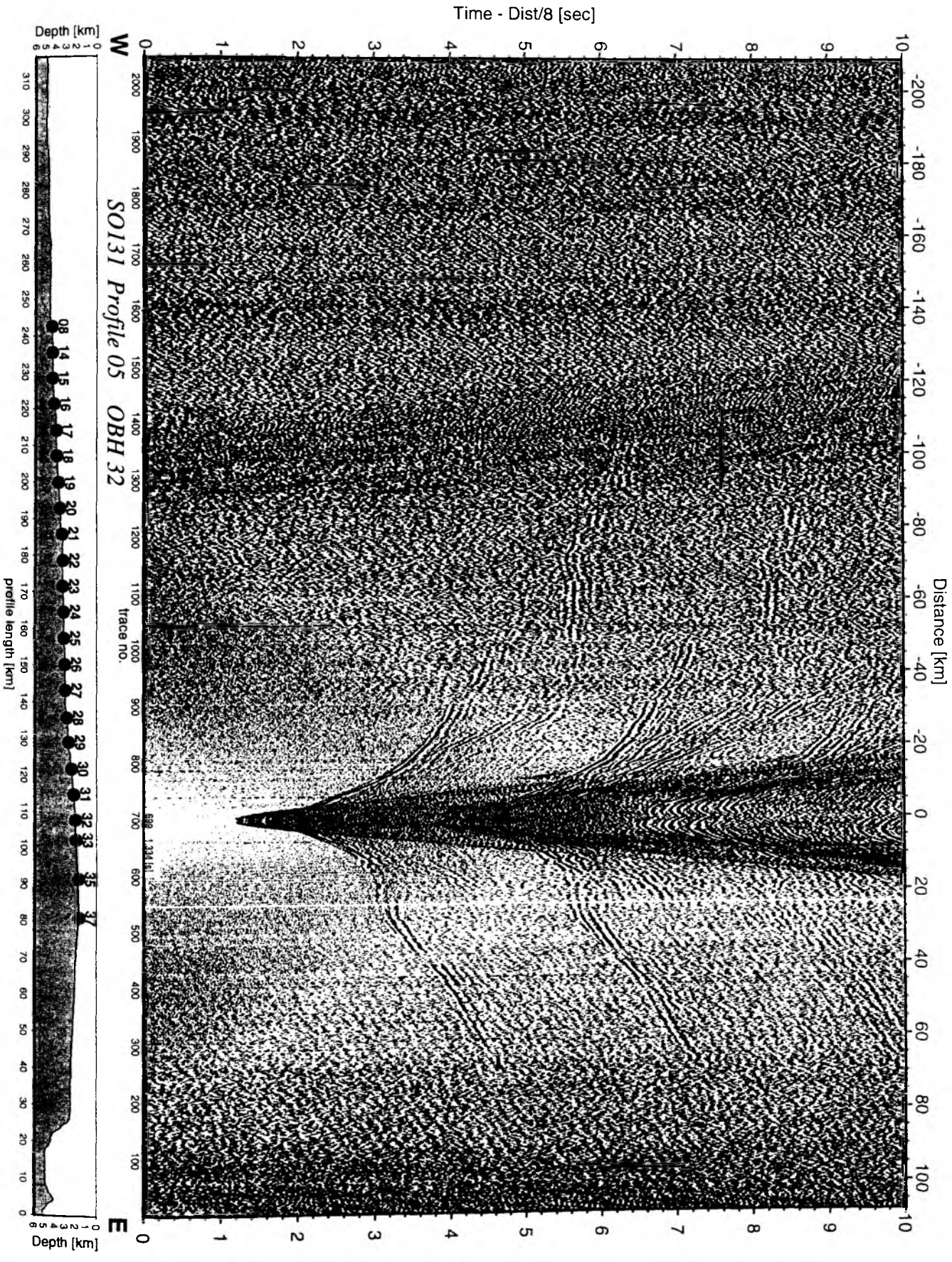

Figure 6.3.4.5.28: Record section from OBH 32 , Profile 05.

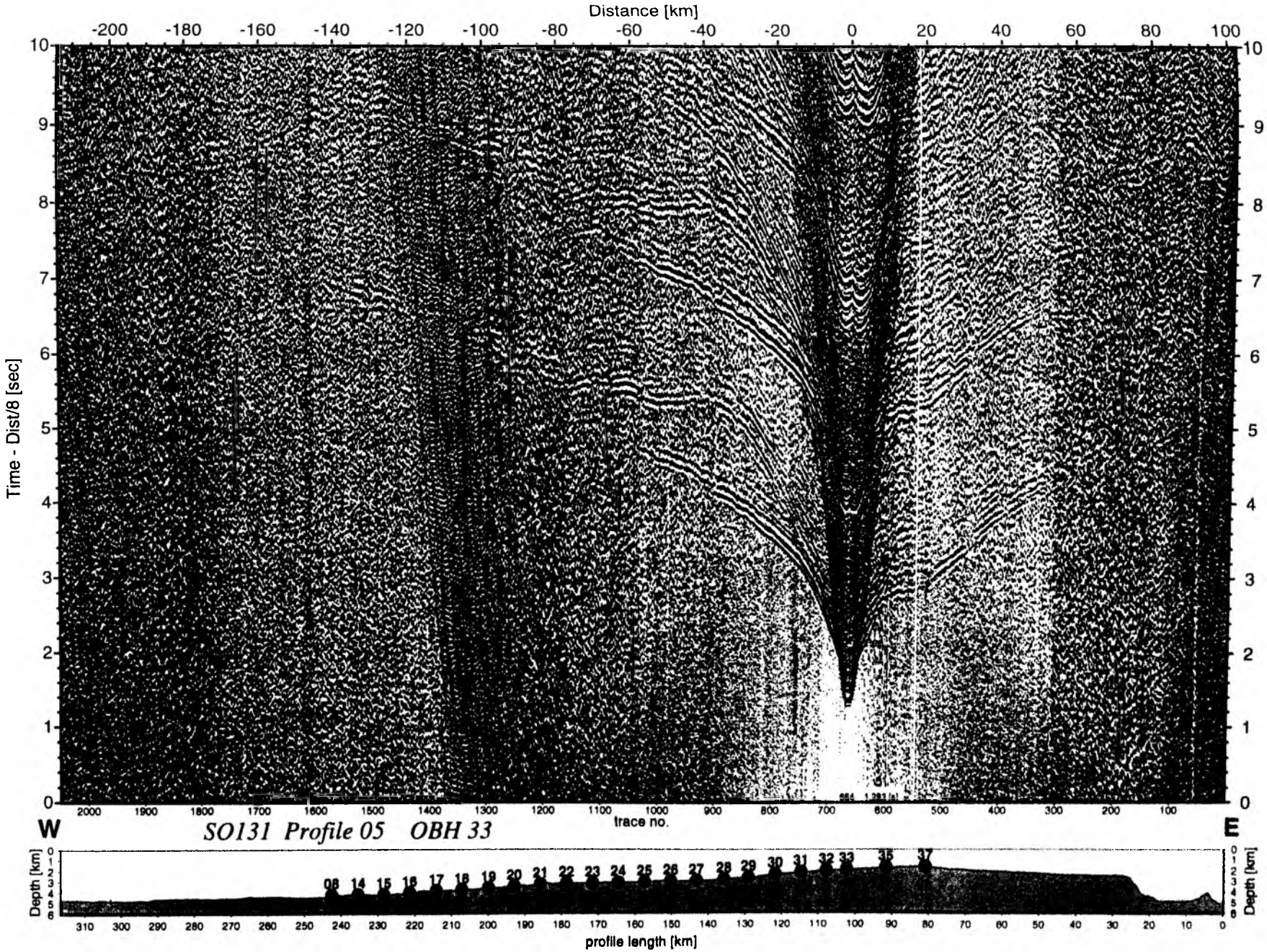

Figure 6.3.4.5.29: Record section from OBH 33 , Profile 05.

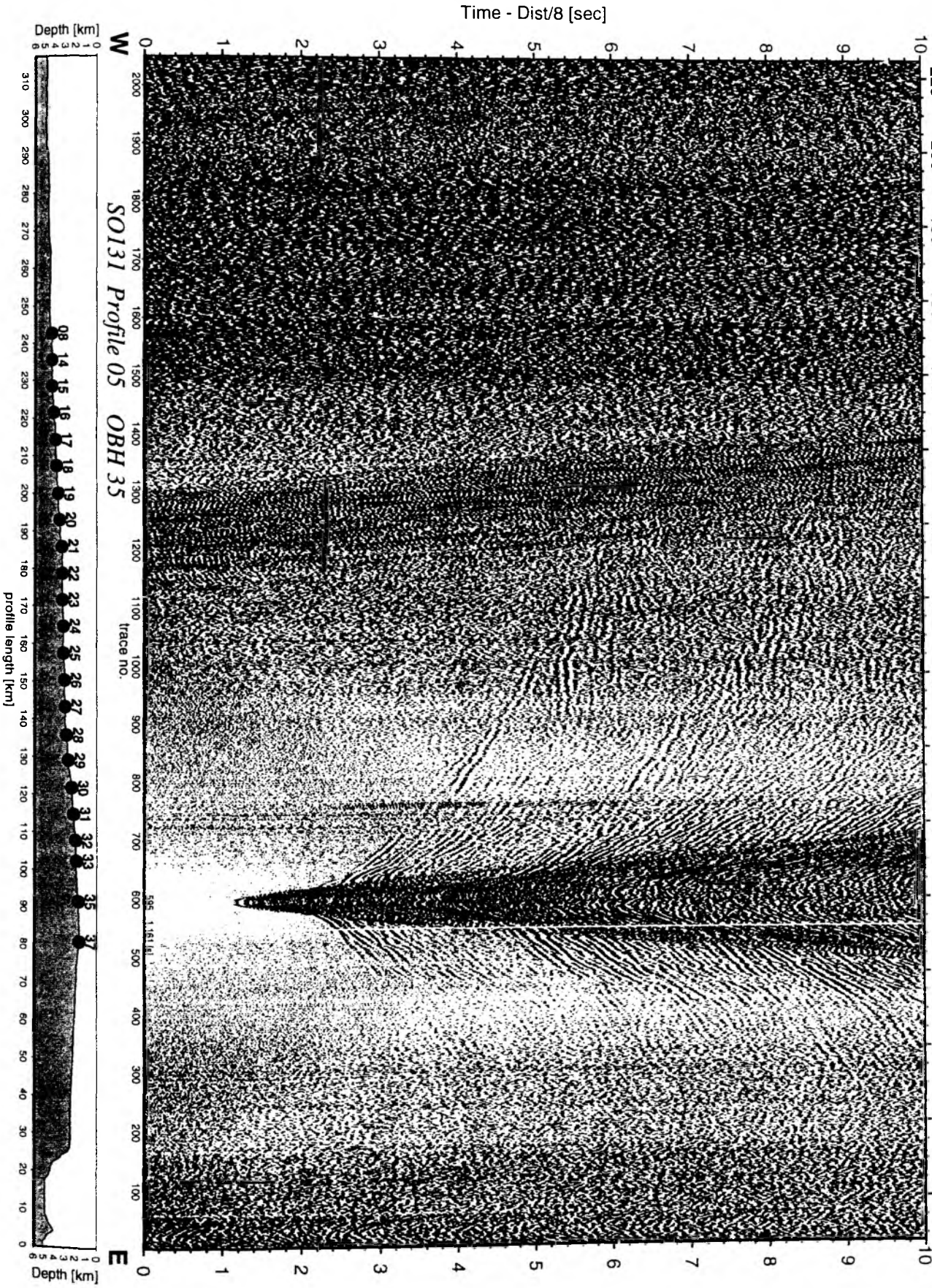

Figure 6.3.4.5.30: Record section from OBH 35 , Profile 05.

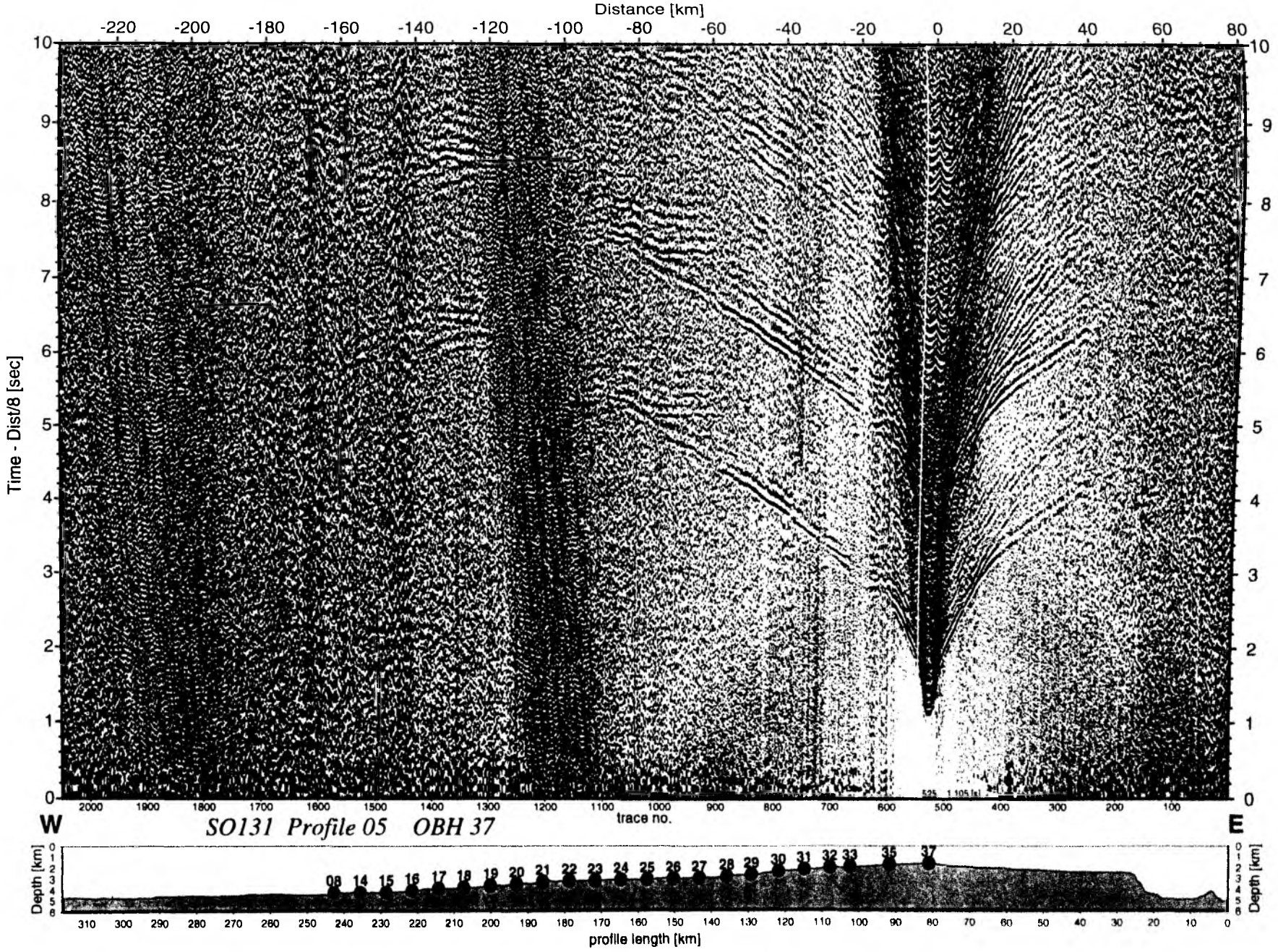

Figure 6.3.4.5.31: *Record section from OBH 37 , Profile 05.*

6.3.4.5.2.). We applied the same velocity structure to Ninetyeast Ridge. However, the gravity field over the Ridge suggested an Airy-type isostatic compensation mode (MacKenzie and Sandwell, 1989). Therefore, we introduced a crustal root, which is clearly supported by the mantle phases discussed above. Figures 6.3.4.5.33 to 6.3.4.5.35 show the ray tracing of those OBHs used to yield the velocity-depth model shown in Figure 6.3.4.5.36.

In the next paragraphs we will compare the structure across Ninetyeast Ridge with typical features of oceanic crust. Therefore, we briefly review the most striking features of oceanic crust. Compared with the continental crust oceanic crust has a nearly uniform thickness. Away from mantle plumes and fracture zones, it's thickness ranges from about 6 to 7 km (Chen, 1992; White et al., 1992; Grevemeyer et al., 1998). However, approaching hotspots crustal thickness increases and decreases close to major fracture zones (White et al., 1992). Another feature of oceanic crust is it's velocity structure. The upper crust (layer 2) is a region of strong velocity gradients while the lower crust (layer 3) is relatively homogeneous, although it does show an increase in velocity with depth (e.g. Spudich and Orcutt, 1980; Purdy, 1983; Grevemeyer et al., 1998). Mature upper crust has at it's top velocities of > 4.5 km/s (Grevemeyer and Weigel, 1996; 1997). Velocities increase with depth and reach about 6.5-6.6 km/s at the base of layer 2. The boundary between layer 2 and 3 primarily shows a decrease in vertical velocity gradient, rather than indicating a rapid change in velocity (Spudich and Orcutt, 1980; Purdy, 1983; Detrick et al., 1994; Grevemeyer et al., 1998). Velocities within layer 3 increase from about 6.7 km/s to 7.1 km/s at the crust/mantle boundary. The layered velocity-depth structure that marine seismologists have derived from seismic refraction experiments is generally related to geological structure in terms of the vertical distribution of lithologies that are found in ophiolite sequences. Therefore, upper oceanic crust is composed of basaltic rocks (Vp < 6.7 km/s) and the lower crust is made of massive gabbro (Vp ~6.7-7.1 km/s). The upper mantle is composed of peridotites (Vp ~ 8.0 km/s).

In the western portion of the profile we would expect oceanic crust. Although there are some deviations in terms of the model described above, the structure is in reasonably good agreement with typical oceanic crust. Layer 2 has velocities ranging from 4.8 km/s at the seafloor to 6.2 km/s at the layer 2/3 boundary, i.e., velocities at the base of layer 2 are comperatively slow. Consequently, velocities at the layer 2/3 boundary increase rapidly by 0.4 km/s. Within layer 3 velocities increase from 6.6 km/s to 7.0 km/s. In the upper mantle, we obtained velocities of 8.05 km/s and crustal thickness is within the range of typical oceanic crust. Similar results, but slightly higher lower crustal velocities were determined along profile So131-04.

Approaching Ninetyeast Ridge the two new wide-angle phases described above support two layers beneath the old oceanic crust. The first layer may represent an underplating body with velocities of about 7.35-7.4 km/s. These velocities are typical of intrusions at the base of oceanic crust found underneath large igneous provinces (ten Brink and Brocher, 1987; White and McKenzie, 1989; Caress et al., 1995). The crust/mantle transition zone was imaged about 24 km beneath sea level. Velocities in the uppermost mantle have velocities of 8.05-8.2 km/s. Nevertheless, the second wide-angle reflection along with it's refraction branch suggested a layered mantle. These phases yielded velocities of about 8.4 km/s. Both layers introduced here generally mimic the topography of Ninetyeast Ridge. We therefore suggest that these features are closely related to the hotspot volcanism which has created Ninetyeast Ridge (see Chapter 2.1.1).

The dense spacing of the seafloor receivers provided good coverage of upper and mid crustal structure. A structural comparison of Ninetyeast Ridge and oceanic crust can be made using the correlation between P-wave velocity profiles of the ridge and oceanic crust sampled in the Central Indian Basin at the western terminus of the profile. Most profound is that the P-wave velocity as a function of subbasement depth within the Ninetyeast Ridge is significantly lower than those in oceanic crust. The low velocities found in uppermost crust beneath the summit and the apron are indicative of low densities and high porosities, consistent with

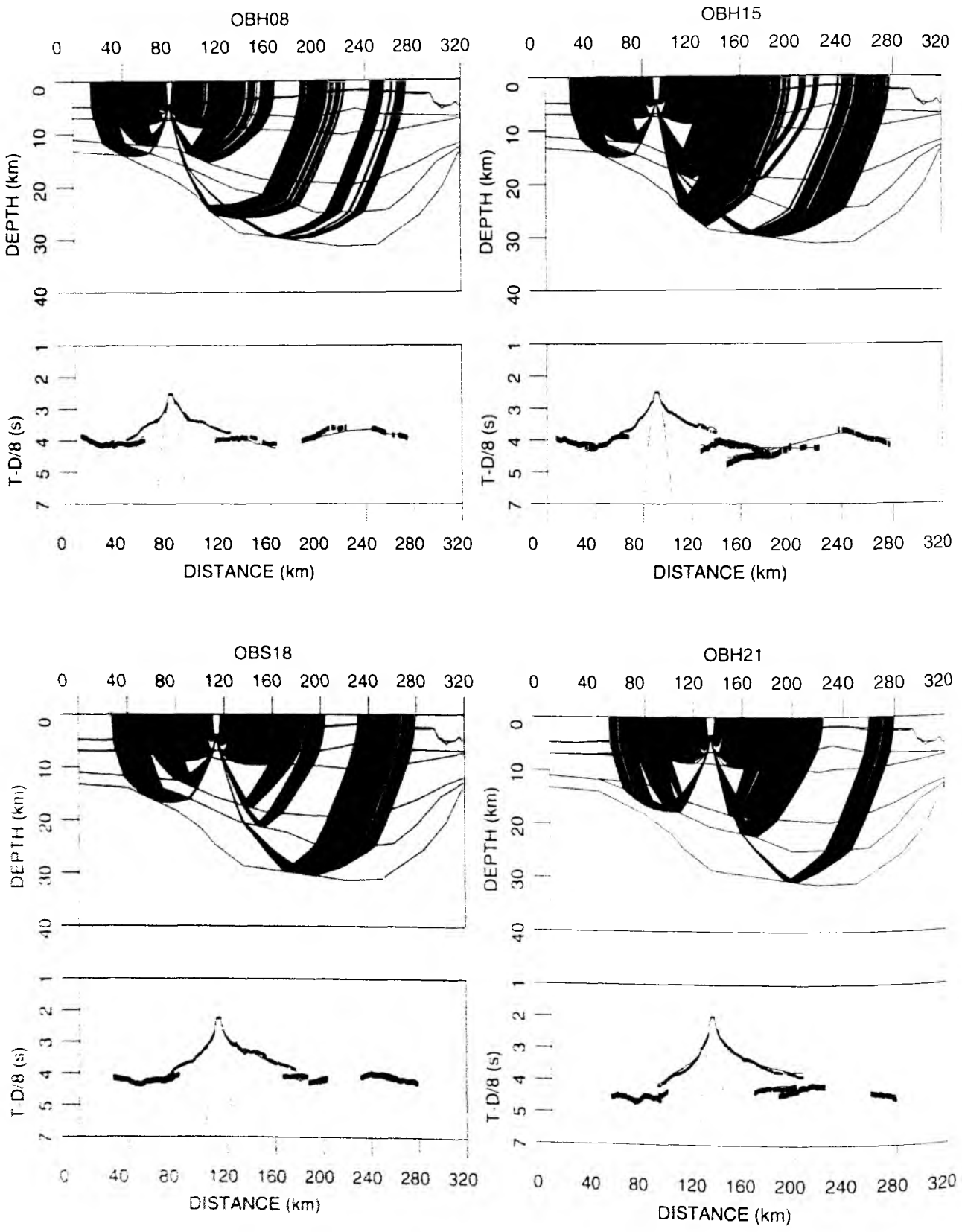

Figure 6.3.4.5.32: Ray tracing of travel times recorded along profile 05.

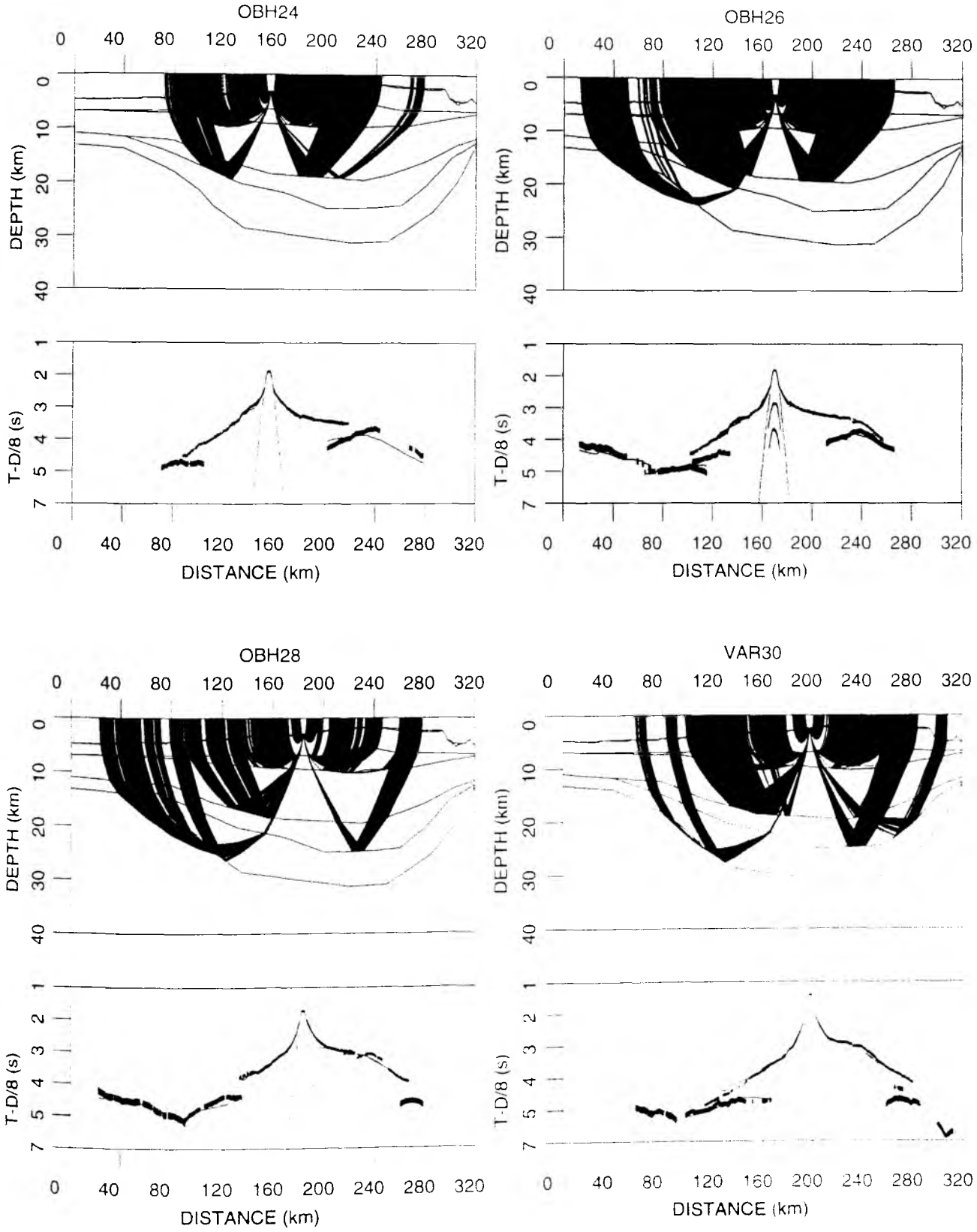

Figure 6.3.4.5.33: Ray tracing of travel times recorded along profile 05.

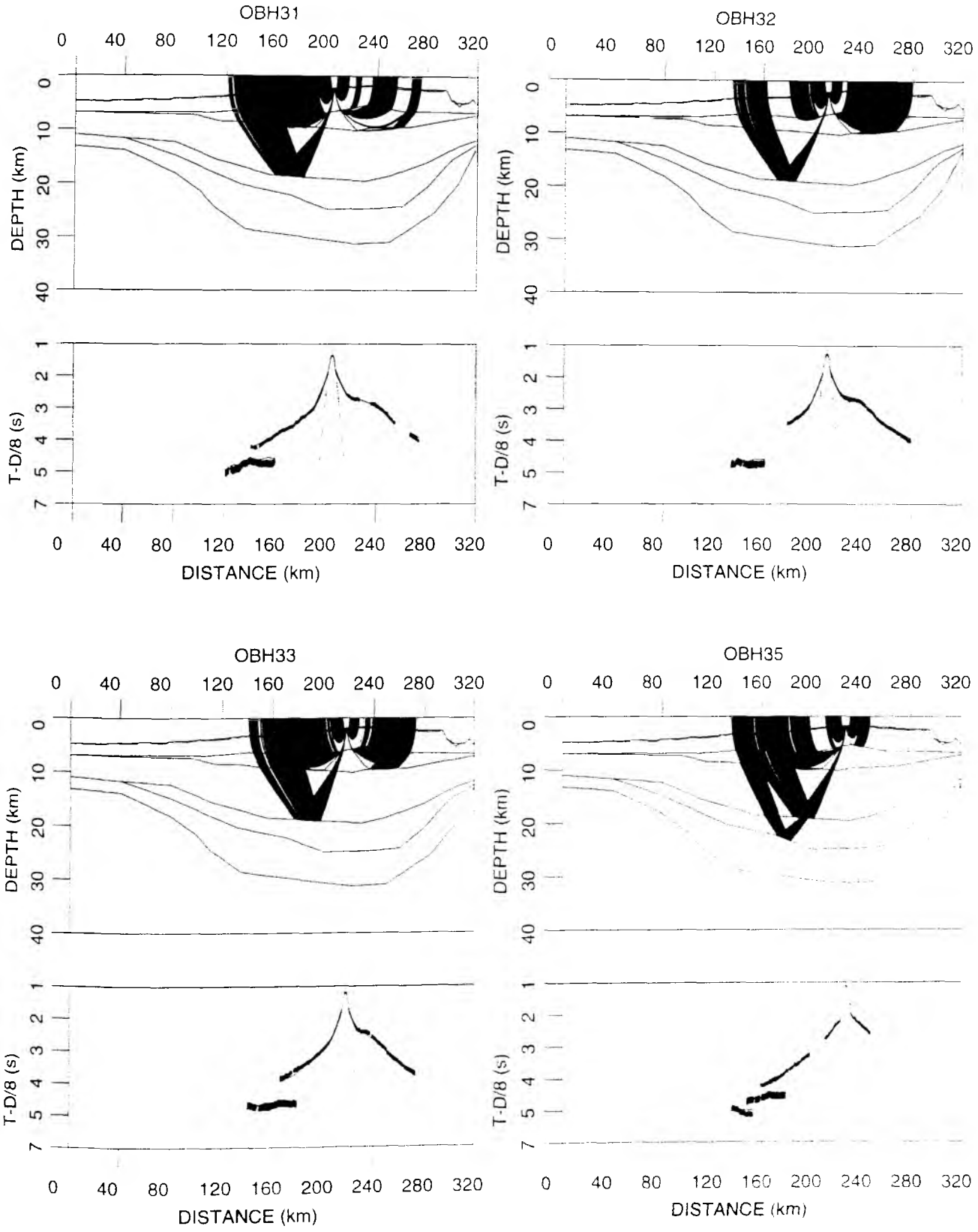

Figure 6.3.4.5.34: Ray tracing of travel times recorded along profile 05.

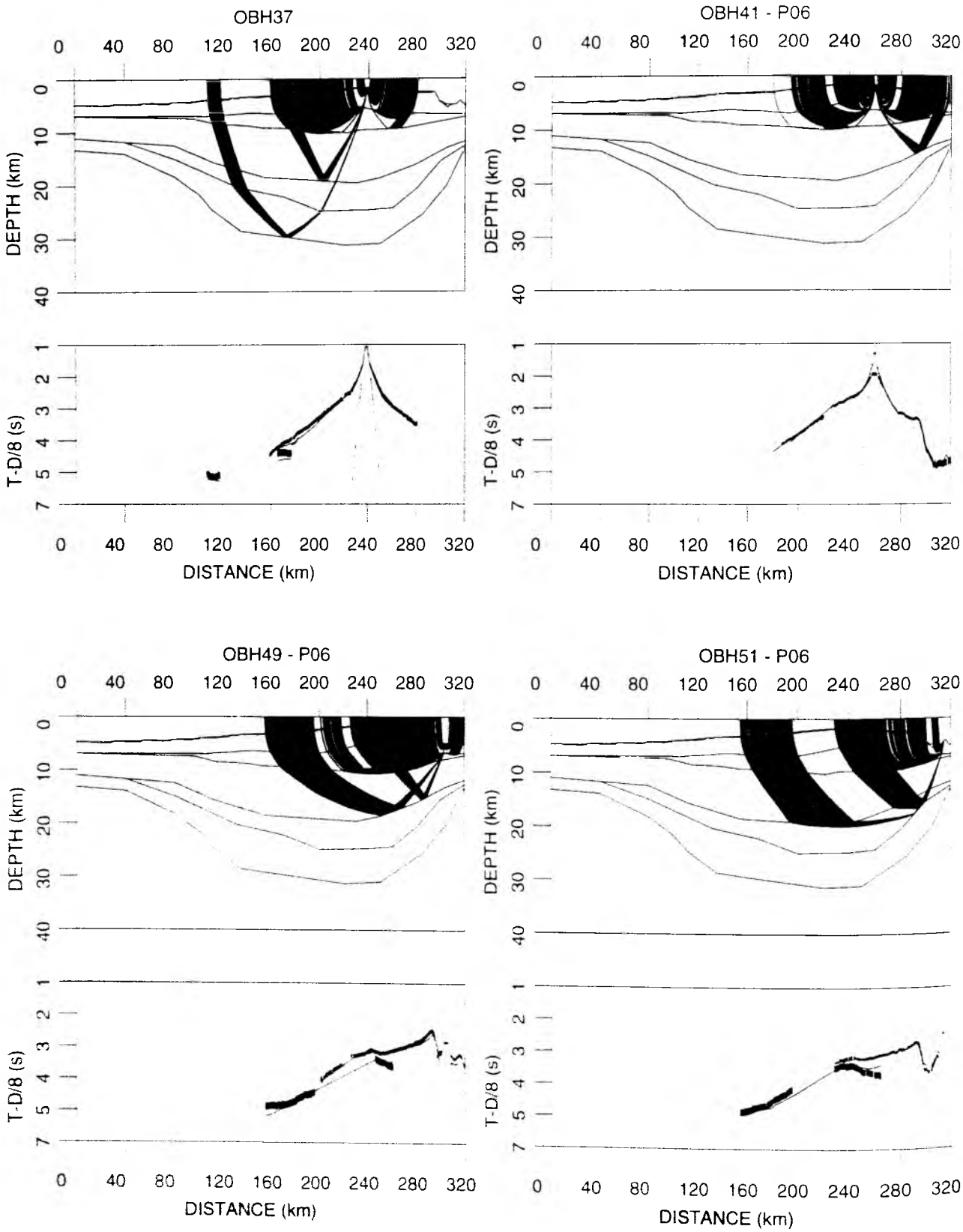

Figure 6.3.4.5.35: Ray tracing of travel times recorded along profile 05 + 06.

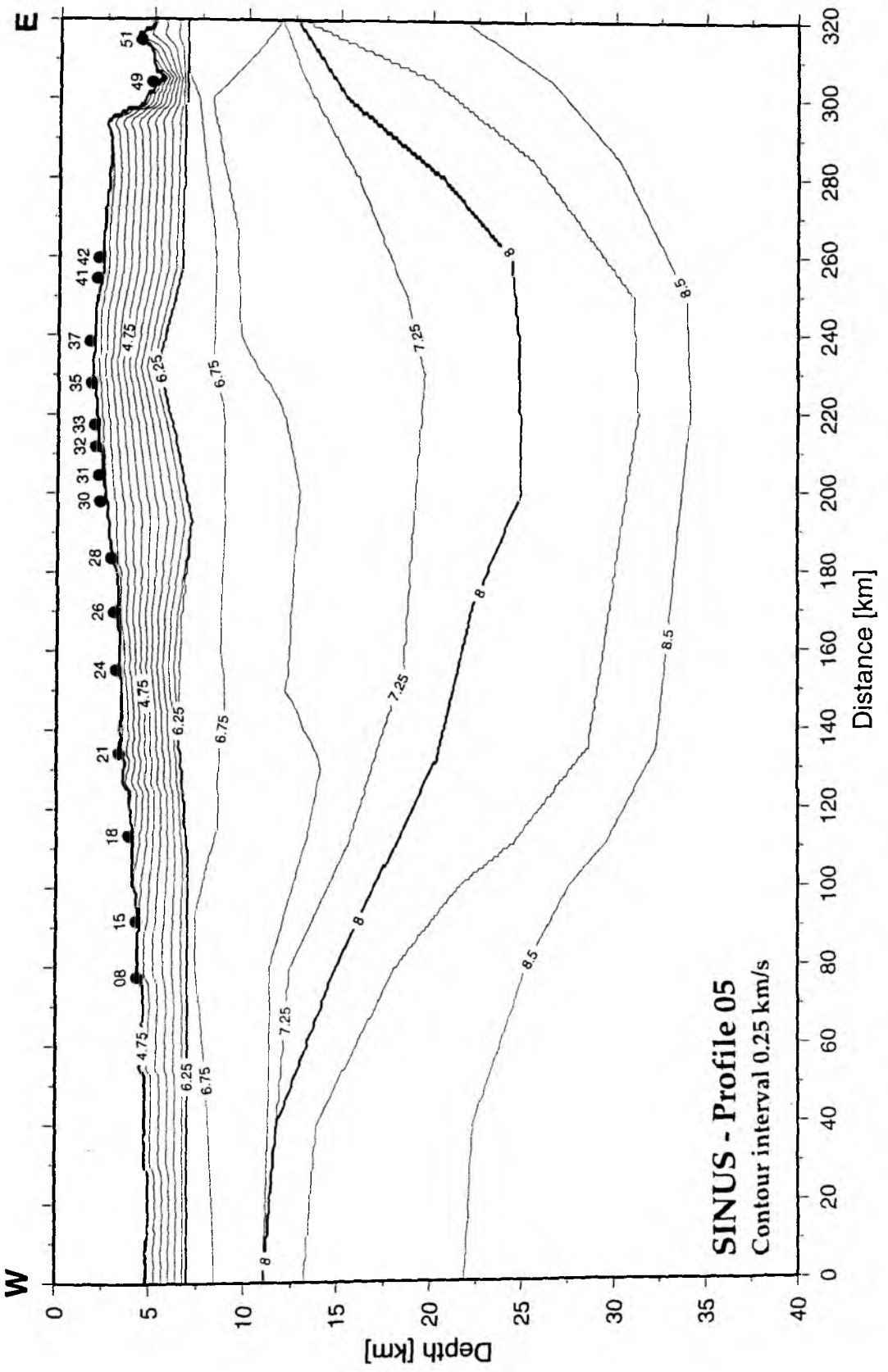

Figure 6.3.4.5.36: Velocity-depth model of profile 05 (dots mark OBHs used for ray tracing).

series of alkali basaltic pillow lavas, hyaloclasties and breccias, sampled on Ninetyeast Ridge and on seamounts emplaced elsewhere (Peirce, Weissel et al., 1989; Staudigel and Schmincke, 1984). In comparision with oceanic layer 2, higher porosities in intraplate seamounts are expected due to eruptions at shallower depth (Peterson and Moore, 1987) and higher lava cooling stresses (Bonatti and Harrison, 1988). Furthermore, as a seamount peak reaches a critical depth for explosive volcanism, clastic processes become more important. Compared to oceanic crust volcaniclastic deposits [i.e., breccias, tephra, slump blocks and local lava flows (Staudigel and Schmincke, 1984)] leave more open void spaces than basalts extruded in deep water and therefore yield lower velocities. Moreover, mass wasting processes may explain the lateral heterogeneous structure of the apron.

At the edifice the transition to P-wave velocities of more than 6 km/s occurs at 3-4 km beneath the summit. These velocities are typical for intrusive rocks. In oceanic crust this transition occurs about 1.5 km beneath the seafloor. Obviously, extrusive volcanism is enhanced at Ninetyeast Ridge. Nevertheless, the same holds for the plutonic section. Rocks with velocities of more than 6.7 km/s occupy a section up to 10 km thick, compared to 4-5 km in oceanic crust. Within the edifice, we have to introduce a transition zone between rocks with velocities typical of basalts and velocities common for gabbros. These transition zones primarily show a decrease in vertical velocity gradient. In terms of seismic velocities the lower crust seems to be relatively homgeneous. This observation is consistent with petrological constraints from the Pliocene seamount series of La Palma, where Staudigel and Schmincke (1984) found a suite of mostly gabbroic and ultramafic rocks. They interpreted their results in terms of a basal plutonic suite. Moreover, seismic studies of Kilauea, Hawaii (Klein, 1981; ten Brink and Brocher, 1987), the Marquesas islands (Caress et al., 1995) and the Great Meteor tablemount (Weigel and Grevemeyer, 1998) provided crustal structure models, which generally show the same features.

To conclude, the structure obtained from our preliminary seismic data analysis is in reasonably good agreement with other structures deduced from geophysical and geological data that are suggested to be of the same origin. Applying commonly used relationships between seismic velocities and crustal lithology, the features could be interpreted in terms of thick oceanic crust. The data also indicate that sub- and intracrustal intrusions present an integral part of intraplate volcanoes. A second model of Ninetyeast Ridge obtained primarily from data recorded on profile 6 (see Chapter 6.3.4.6.) provided only minor differences in crustal structure. Nevertheless, a post cruise data analysis considering all the data obtained along the Ninetyeast Ridge transect (i.e., on profile 5, 6 and 31) will help to constrain (or to disprove) our preliminary results and interpretation.

6.3.4.6 PROFILE SO131-06

(M. Perez, H. Lelgemann)

Profile SO131-06 is another east-west oriented dipline across the Ninetyeast Ridge, in prolongation of SO131-05. It starts immediately east of the NERO site, and 24 instruments were deployed to the east into Wharton Basin, crossing the 89° fracture zone. Instruments were deployed between 01.00 and 20:00 on 21.05. Shooting started at 02:00 21.05 with 60 s shot interval and was terminated at 06:00 22.05. A small detour was made around the NERO site, which during shooting was occupied by the JOIDES RESOLUTION. The location of instruments and shots is shown in Figure 6.3.4.6.1. The streamer was also deployed during shooting, and the near vertical data are shown in Figure 6.3.4.6.2. All instruments except the two westernmost ones (OBH38 and OBH39) were recovered between 16:00 23.05 and 09:00 24.05. Details on instrumentation can be found in Appendix 9.1.6. All instruments except one recorded well, and the record sections are shown in Figures 6.3.4.6.3 to 6.3.4.6.30. Most of them are of excellent quality, especially those located in deeper waters. On the ridge, the shots apparently suffered from scattering at the rough basement, and arrivals are sometimes rather weak. On the contrary, shots fired in the Indian Basin were well recorded at offsets of nearly 250 km by instruments in the Wharton Basin.

Modelling and interpretation:

Profile S0131-06 covers the Ninetyeast Ridge and runs into the Wharton Basin, crossing the 89° fracture zone. A lateral comparison of the thickness of the oceanic crust shows significant variation due to the thickening of the crust underneath the ridge. The crust-mantle boundary rises under the Wharton Basin to a depth of about 10 km. The crustal thickening can still be witnessed under the 89° fracture zone, where the Moho lies in a depth of about 15 km.
About 160 km of profile SO131-05 is also recorded on the stations of profile SO131-06 and vice versa, while profile SO131-31 continues further to the east. The velocity models for all three profiles were combined and are displayed and presented in chapter 6.3.4.8.

Arrivals were picked for all instruments on profile SO131-06 and modelled by raytracing with *MacRay*. All record sections display a high degree of asymmetry, resulting from the bathymetry difference of Ninetyeast Ridge and Wharton Basin as well as from the rough topography of the basin compared to the smoother topography on the ridge. The resulting velocity model for profile SO131-06 is shown in Figure 6.3.4.6.31 (c). S-waves were recorded on some of the sections, though not very strong. Thus modelling of S-waves was not attempted.

The MCS data of profile SO131-06 (Figure 6.3.4.6.2) display a sedimentary cover on the ridge with a thickness varying between 150m and 400m, which was modelled using the refraction data. The slope of the ridge and the rough topography in the Wharton Basin display no sediment except in some smaller basins and on top of the 89° fracture zone. In the preliminary model several layers were employed to trace the upper crustal phases, with velocities ranging from an average of 3.45 km/s to 4.3 km/s to about 5.4 km/s. The lower crust includes an isopach at about 10 km depth representing a velocity step of less than 0.2 km/s. The gradient above this line is 0.33 s^{-1}, while the gradient below is less than 0.02 s^{-1}. The high velocites of 7 km/s at this transition are needed to calculate the lower crustal phases (Figure 6.3.4.6.31 (a), (b) and Figure 6.3.4.6.32. (c)).

Most of the stations in the Wharton Basin (OBS 48, OBH 49-61) show very strong PmP and Pn arrivals (Figure 6.3.4.6.31(b) and Figure 6.2.4.6.32 (a) and (b)) recorded from shots in the Indian Basin at offsets of more than 200 km and displaying high amplitudes. The crust-mantle boundary underneath the Ninetyeast Ridge was modelled at 20-22 km below seafloor (Figure 6.3.4.6.31(c)), rising towards the Wharton Basin. The inclining of the Moho towards the Wharton Basin also becomes evident in the low apparent velocity of the Pn arrival on the stations in the Wharton Basin (e.g. OBH 58, 60, 61). However, the crustal thinning towards the 89° fracture zone is not as dramatic as expected, still displaying a crustal thickness of about 10-12 km here. This suggests that the crustal thickening underneath the Ninetyeast Ridge, which probably resulted from massive lava flows, is not affected by the fracture zone. The thinning continues in the Wharton Basin, resulting in a crustal thickness of only about 5 km. At the crust-mantle boundary a velocity increase from 7.4 km/s to 8.0 km/s is observed. Towards the west, the Moho continues at depths greater than 20km, which also becomes evident on stations of profile SO131-05 (Figure 6.3.4.6.32 (a) and (b)). On the westernmost part of the profile, the Moho reaches a depth of 13 km, which is coincident with the velocity model of profile SO131-04.

On some of the stations of profile SO131-06 (e.g. OBS 48, OBH 49, 57, 60, 61), as well as on stations of profile SO131-05 (Figure 6.3.4.6.31 (a) and Figure 6.3.4.6.32 (a), deeper mantle reflection and refraction phases were recorded. These can be modelled by a boundary within the mantle, which in the model occurs at depths greater than 30 km and marks a velocity increase from 8.2 km/s to 8.5 km/s

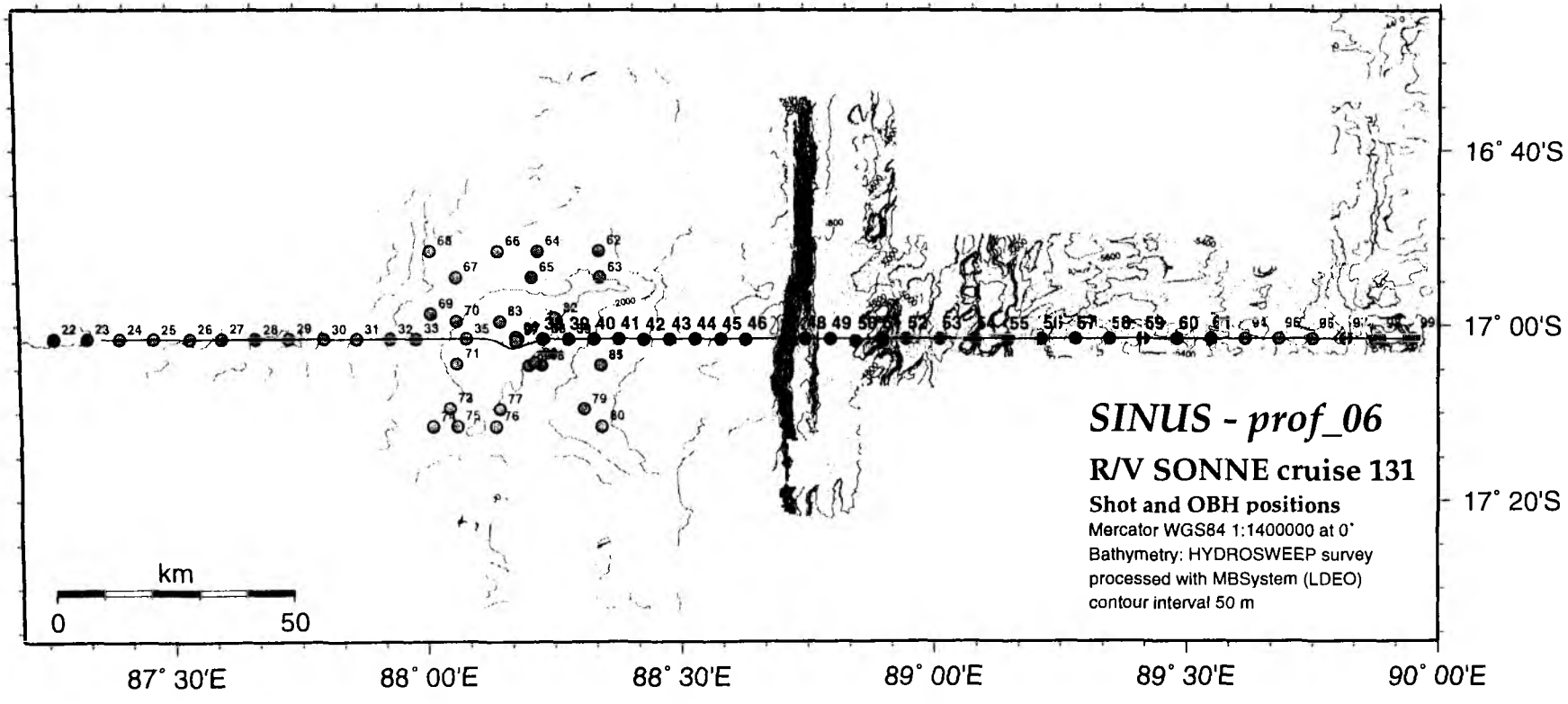

Fig. 6.3.4.6.1: Profile 06 - Shot and OBH positions.

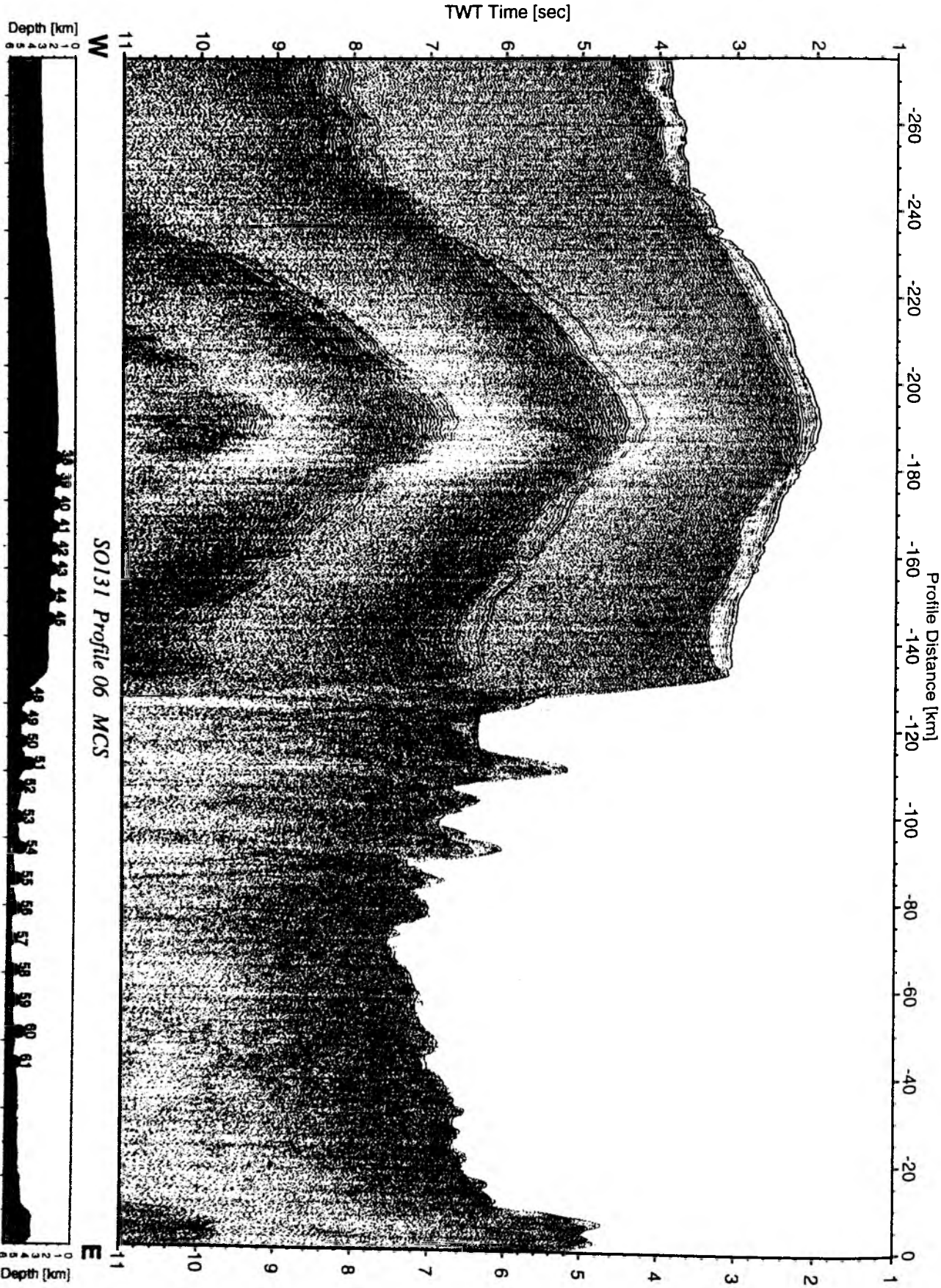

Figure 6.3.4.6.2: Seismic section from MCS stack, Profile 06.

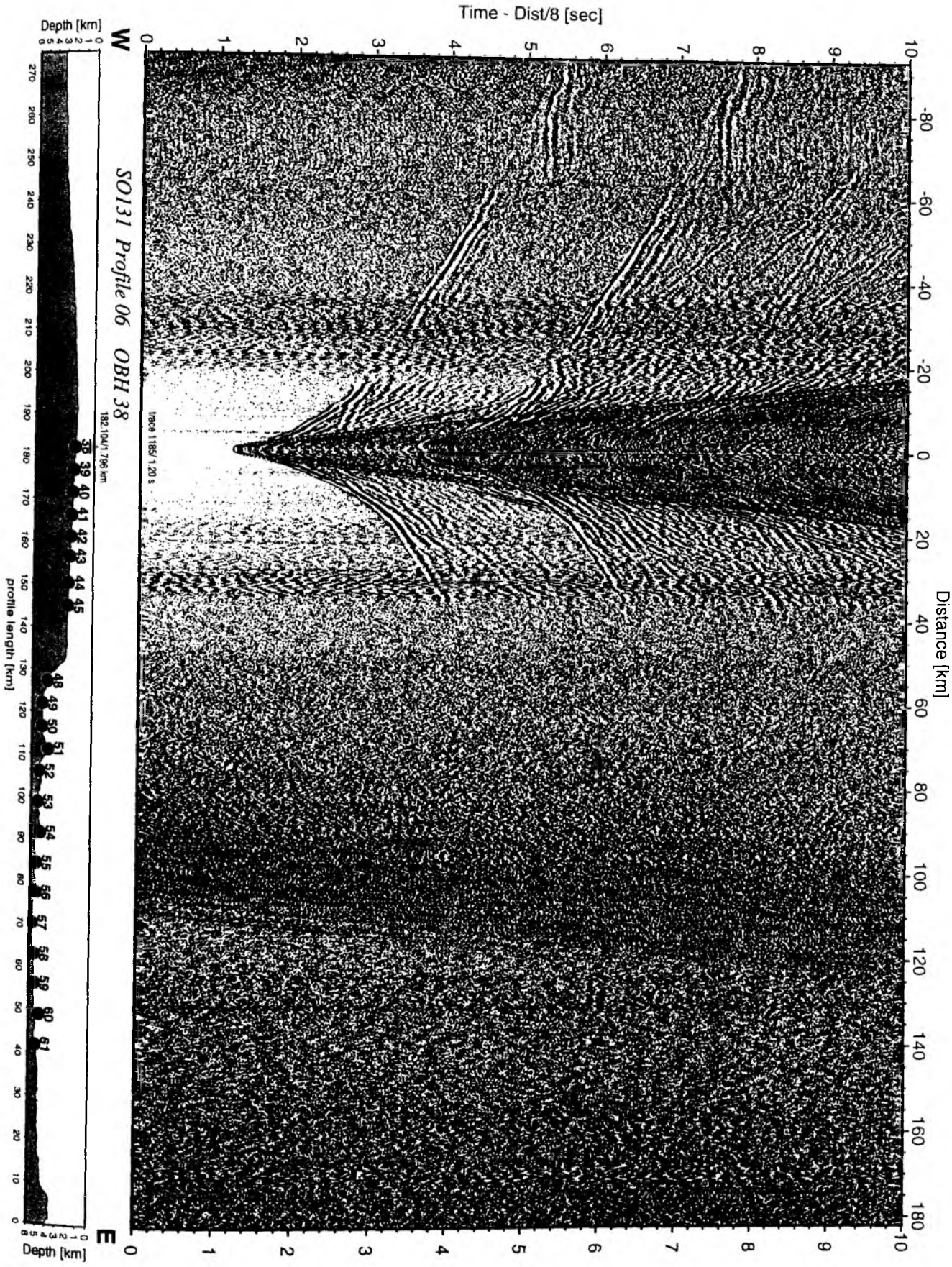

Figure 6.3.4.6.3: Record section from OBH 38 , Profile 06.

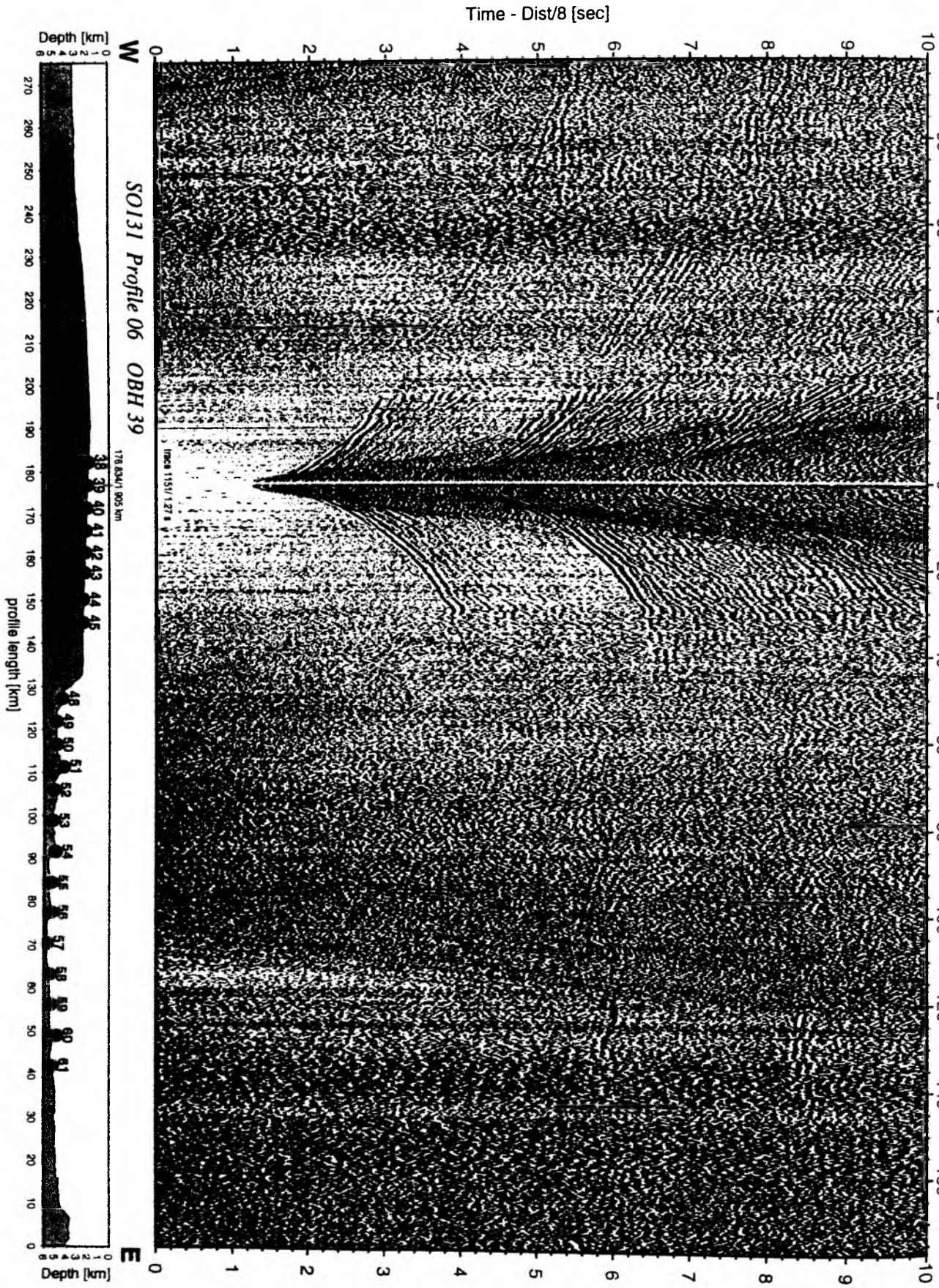

Figure 6.3.4.6.4: Record section from OBH 39 , Profile 06.

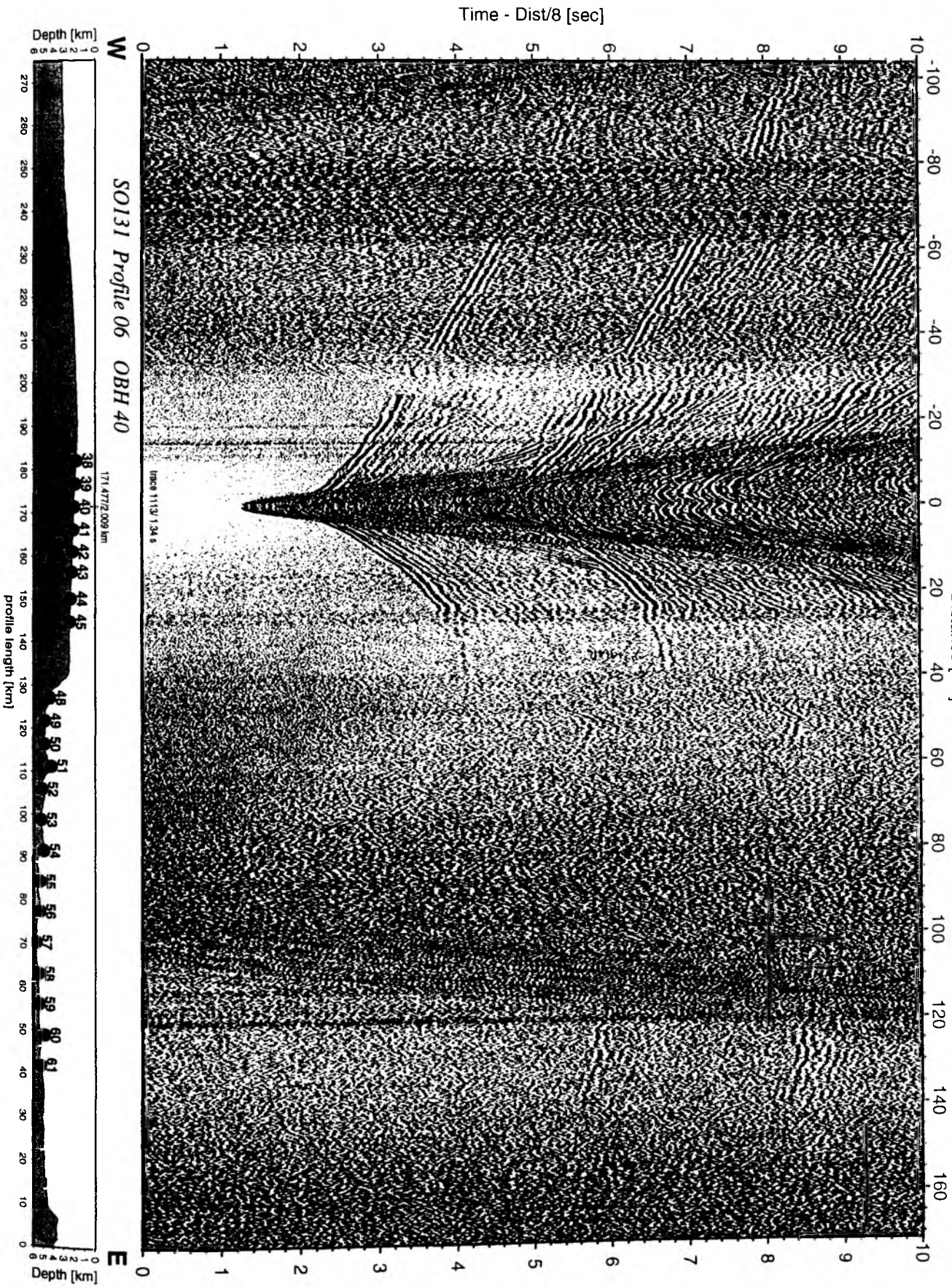

Figure 6.3.4.6.5: Record section from OBH 40 , Profile 06.

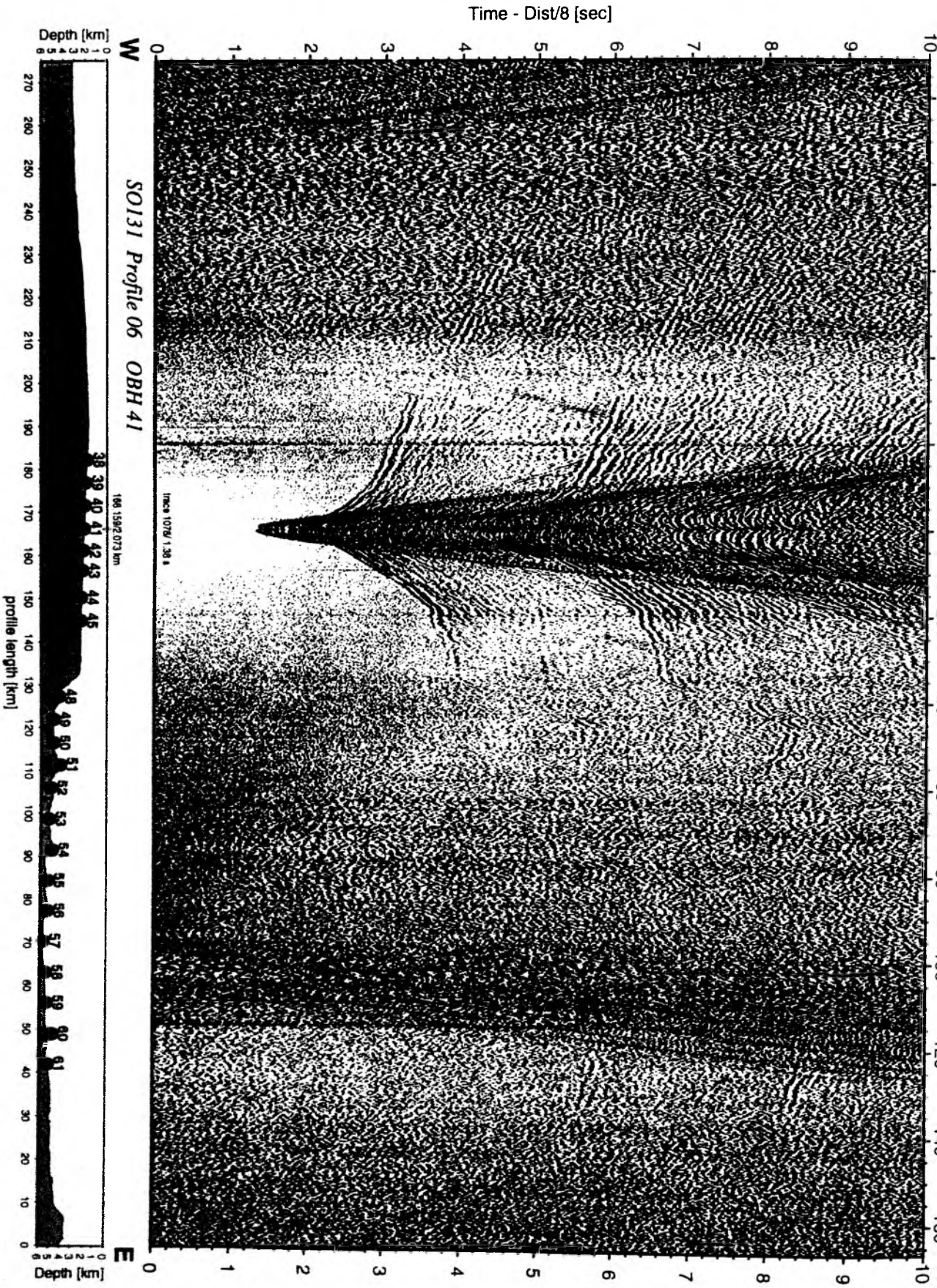

Figure 6.3.4.6.6: Record section from OBH 41 , Profile 06.

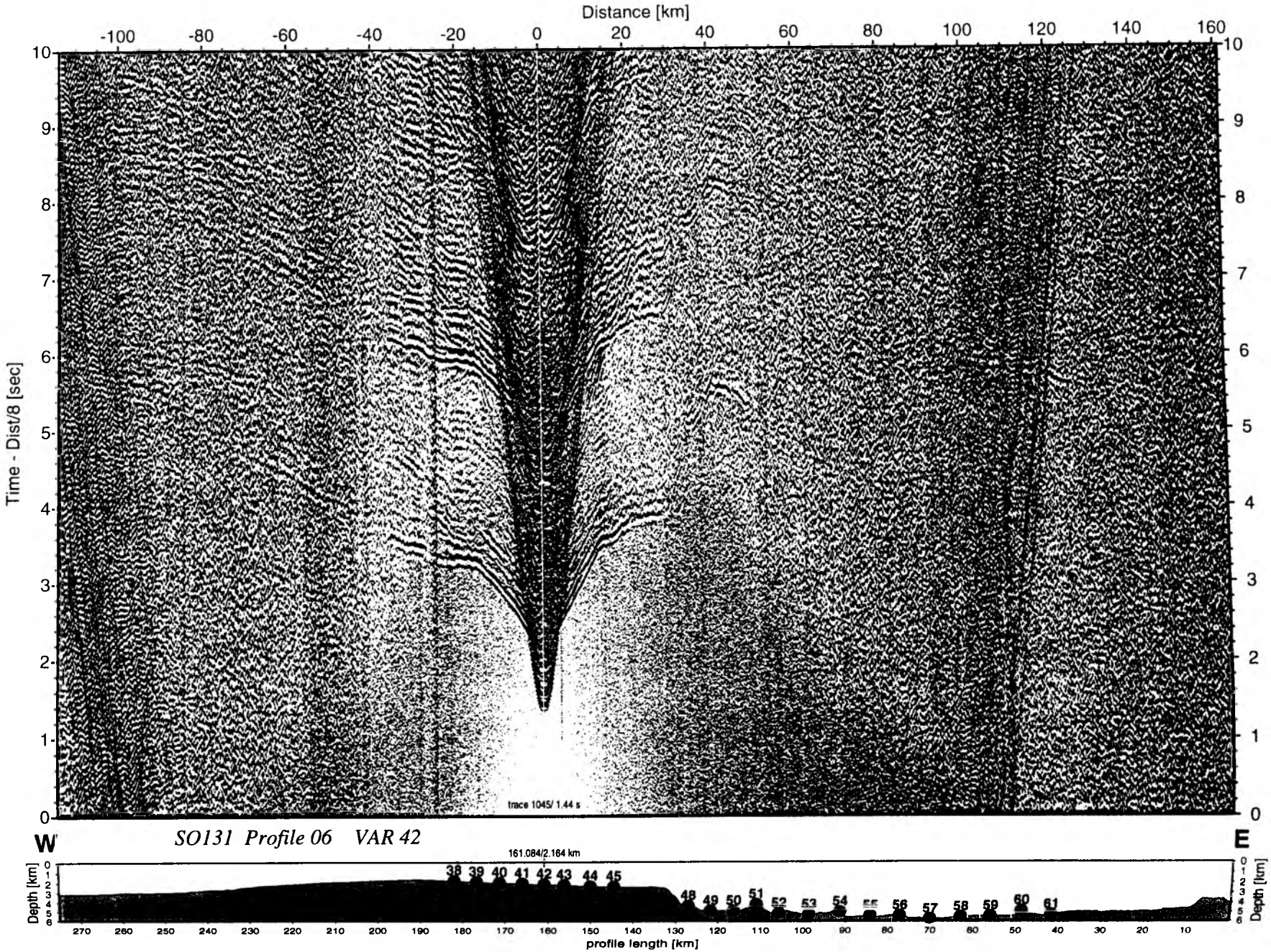

Figure 6.3.4.6.7: Record section from VAR 42 channel_1, Profile 06.

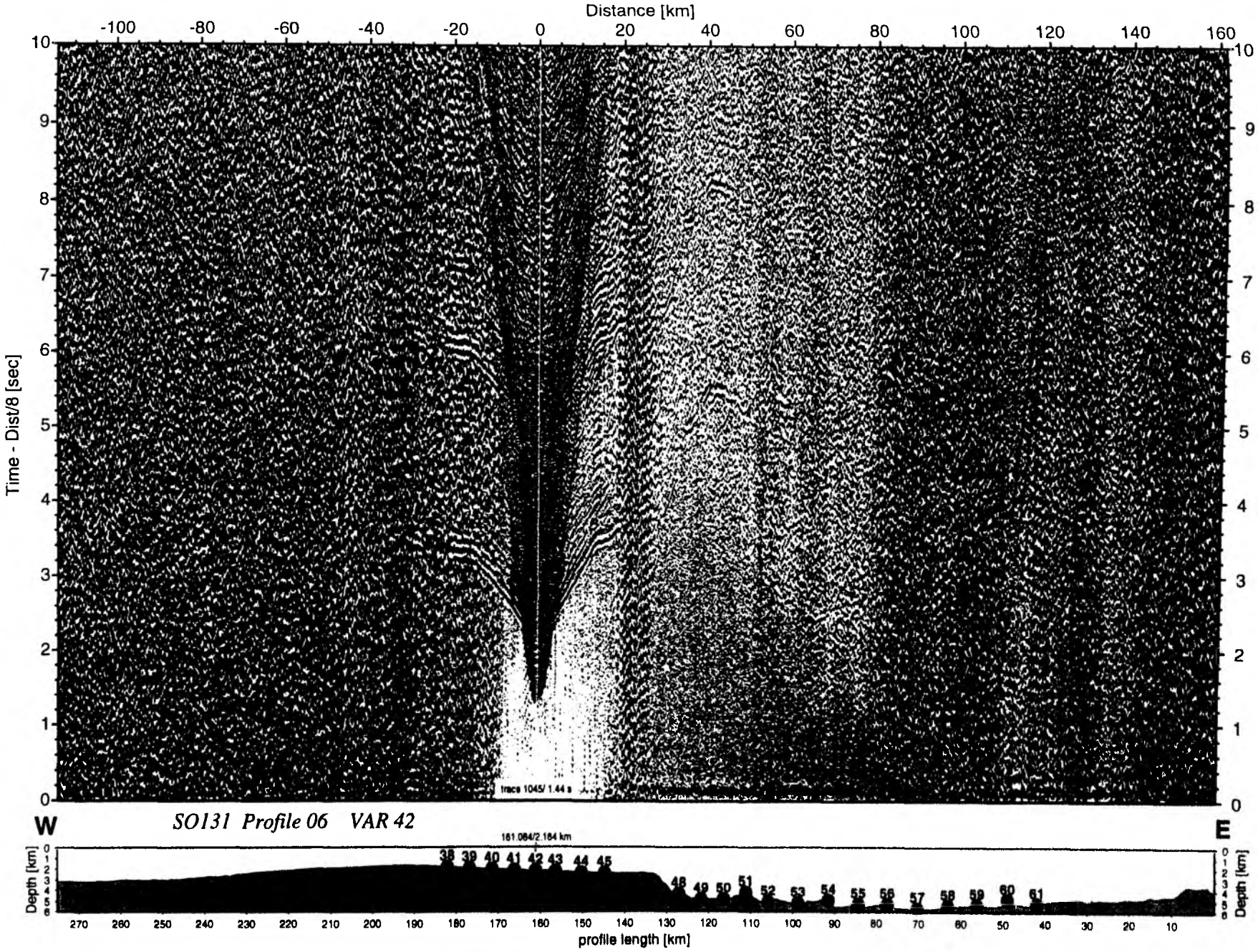

Figure 6.3.4.6.8: Record section from VAR 42 channel_2, Profile 06.

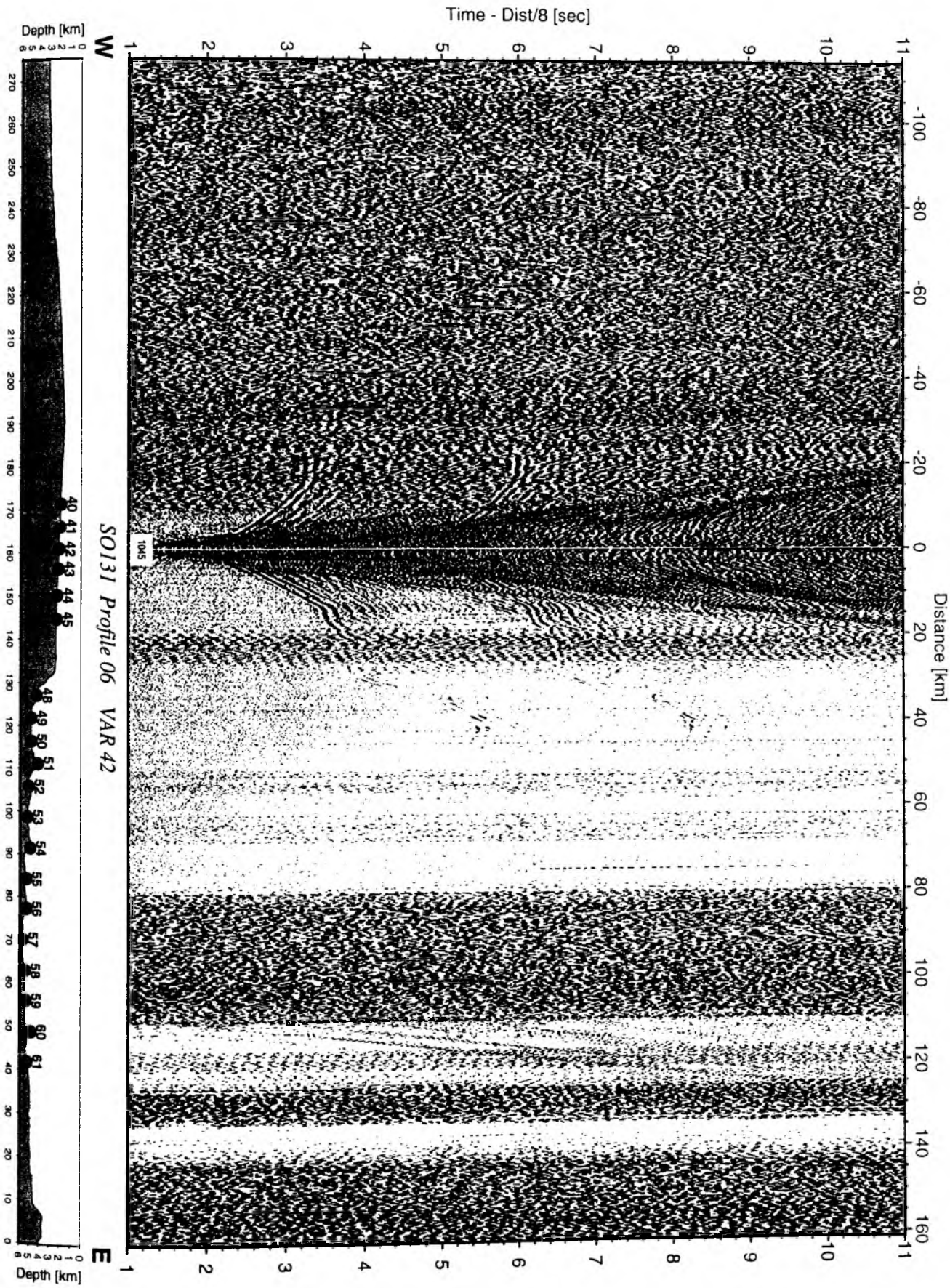

Figure 6.3.4.6.9: Record section from VAR 42 channel_3, Profile 06.

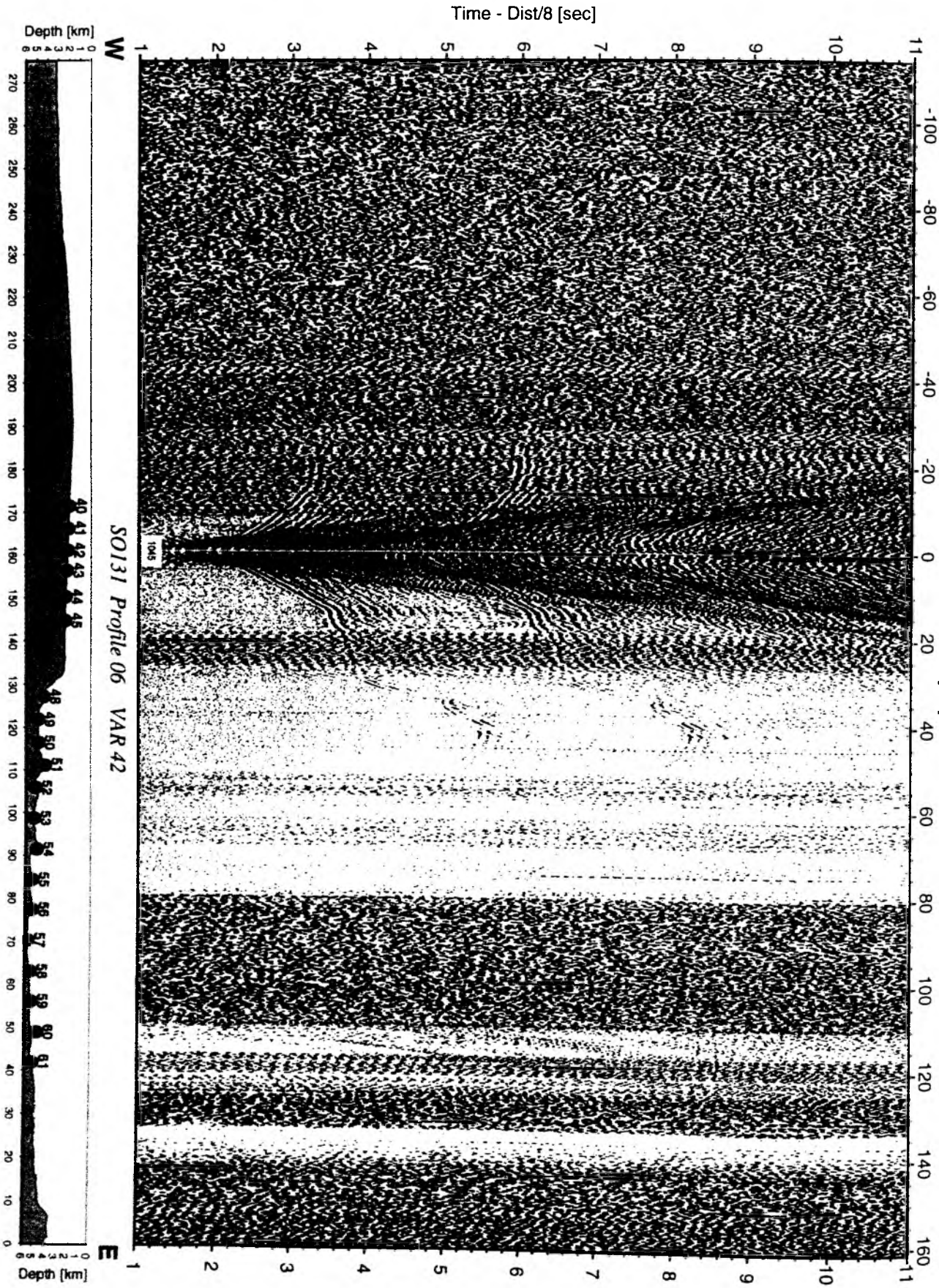

Figure 6.3.4.6.10: Record section from VAR 42 channel_4, Profile 06.

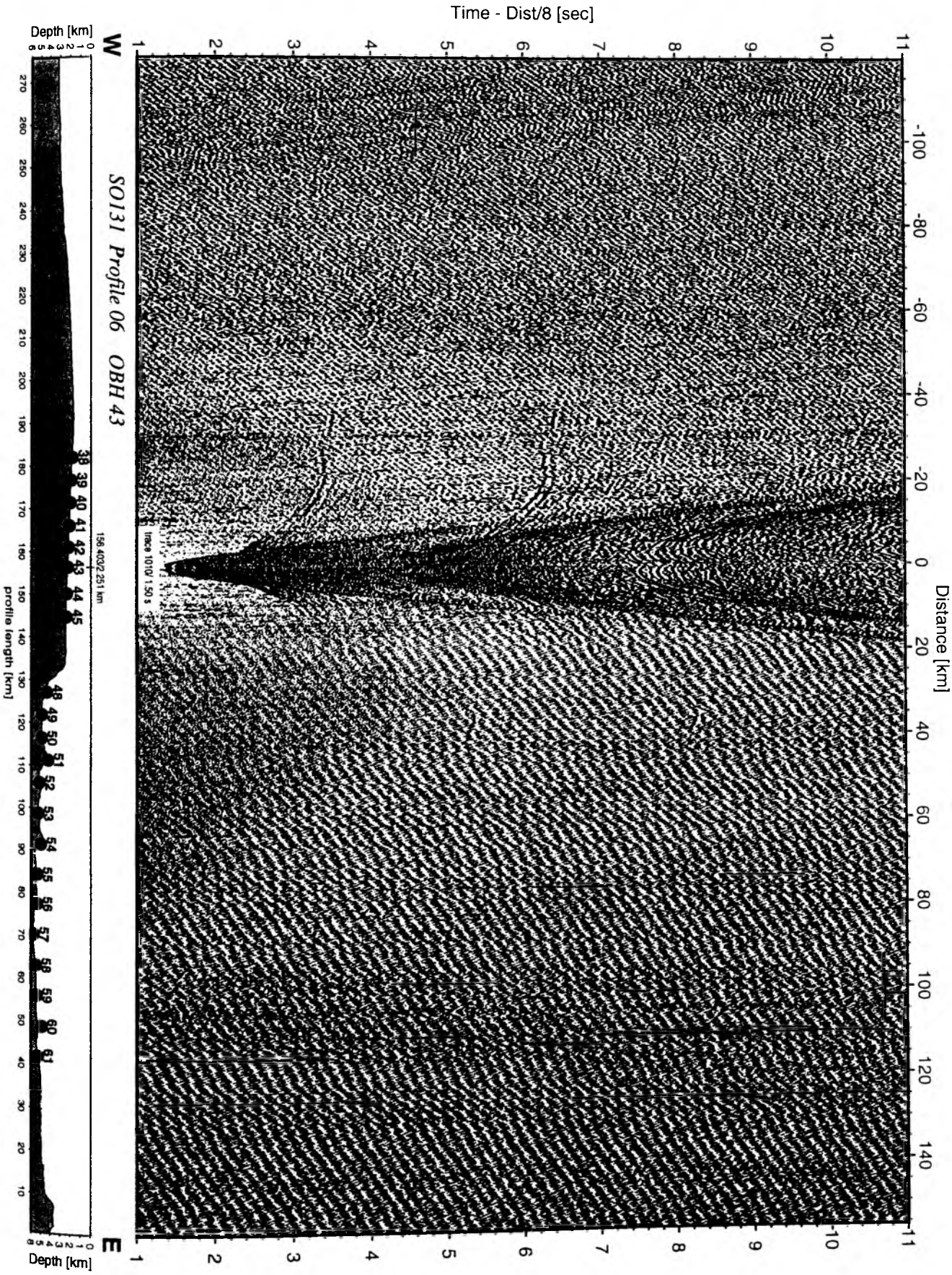

Figure 6.3.4.6.11: Record section from OBH 43 , Profile 06.

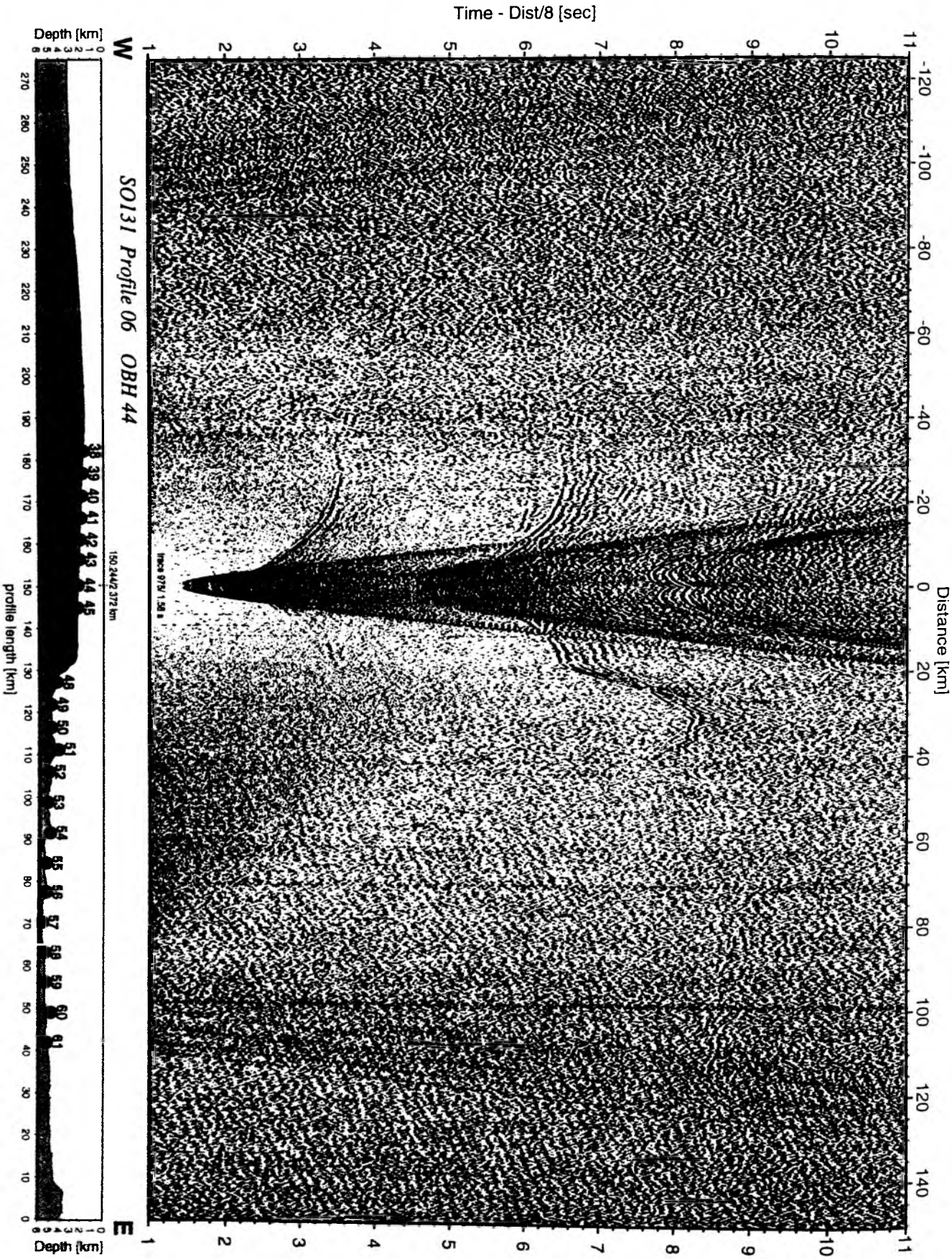

Figure 6.3.4.6.12: Record section from OBH 44 , Profile 06.

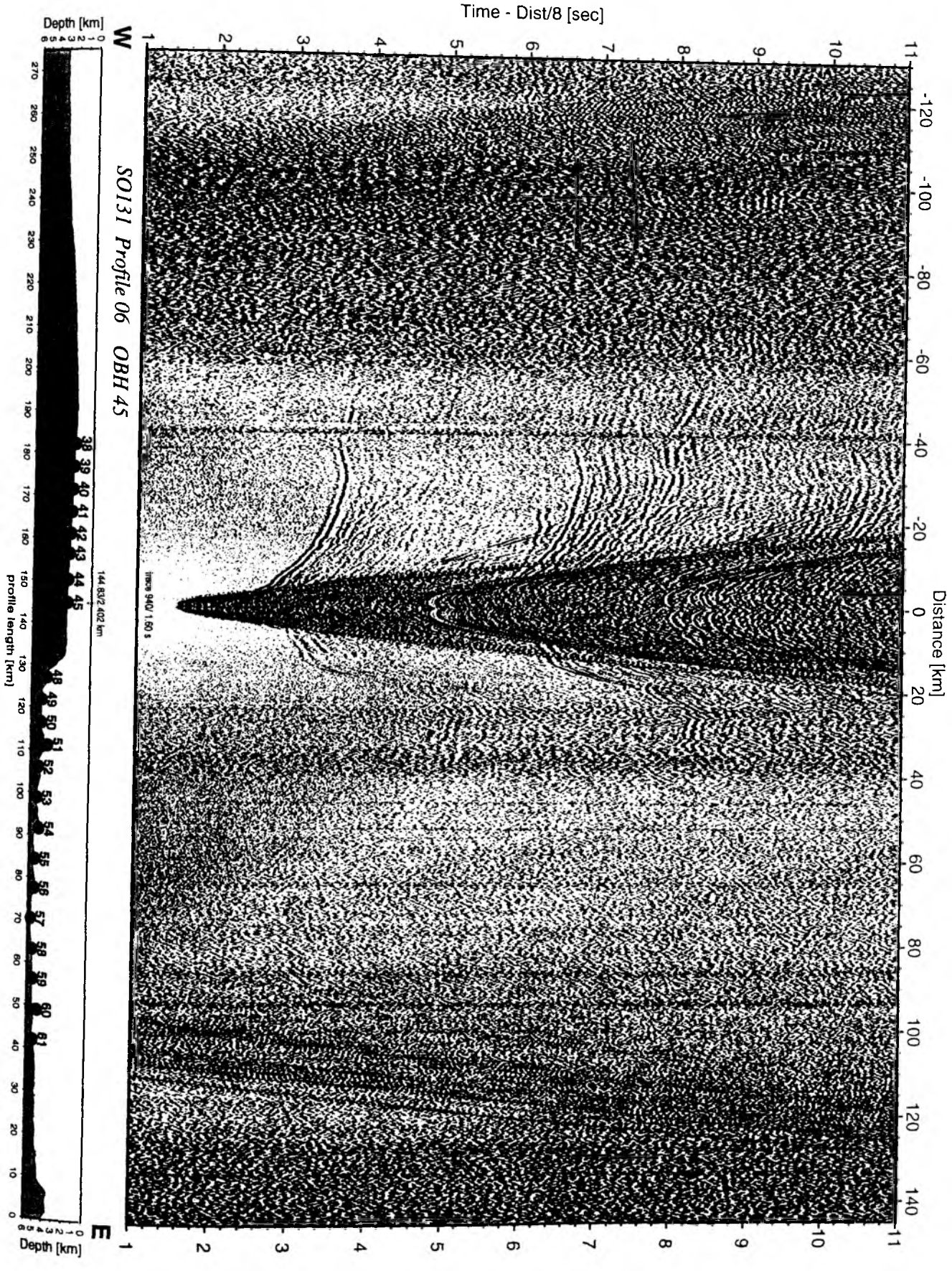

Figure 6.3.4.6.13: Record section from OBH 45 , Profile 06.

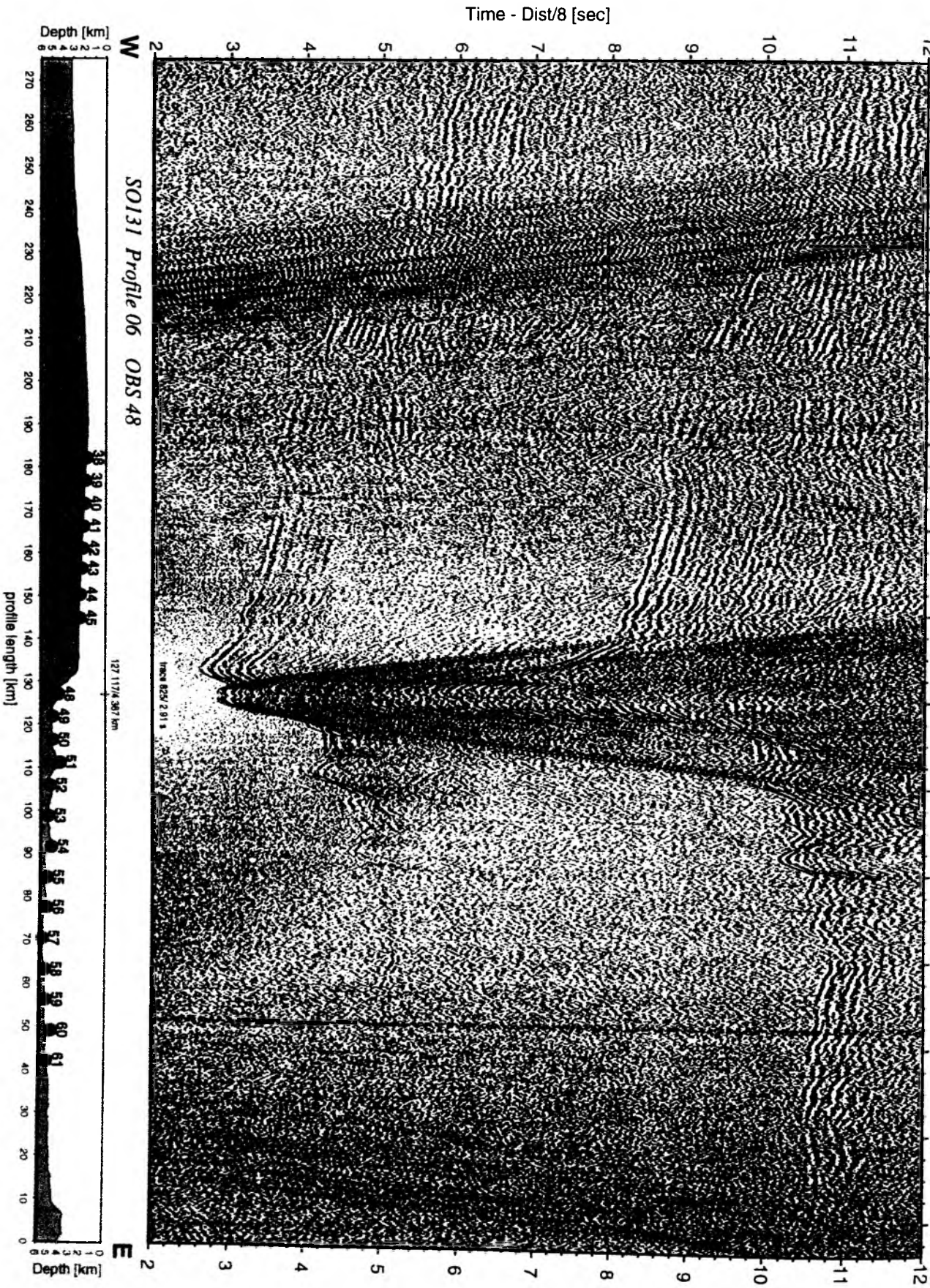

Figure 6.3.4.6.14: Record section from OBS 48 hydrophone, Profile 06.

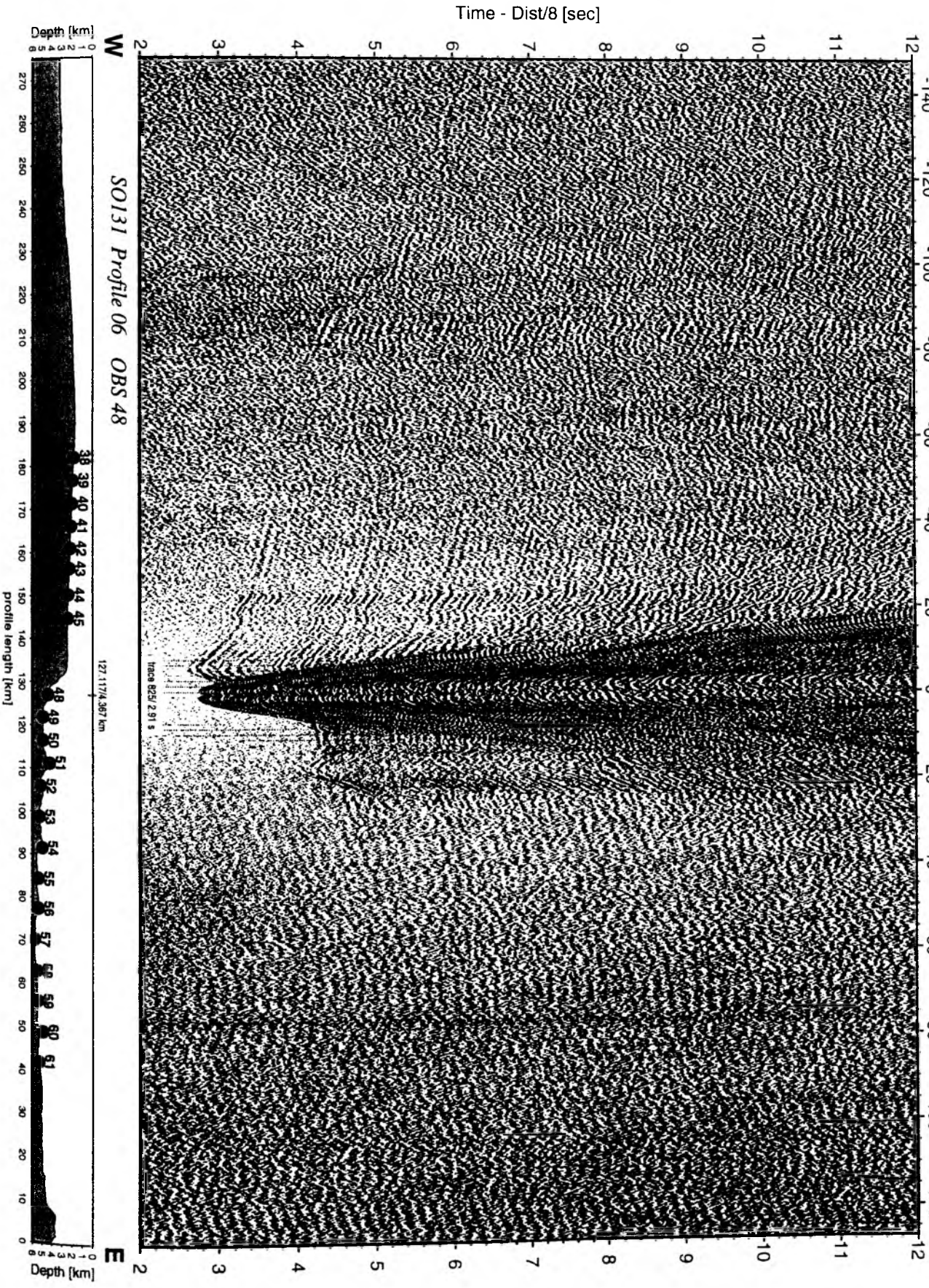

Figure 6.3.4.6.15: Record section from OBS 48 vertical component, Profile 06.

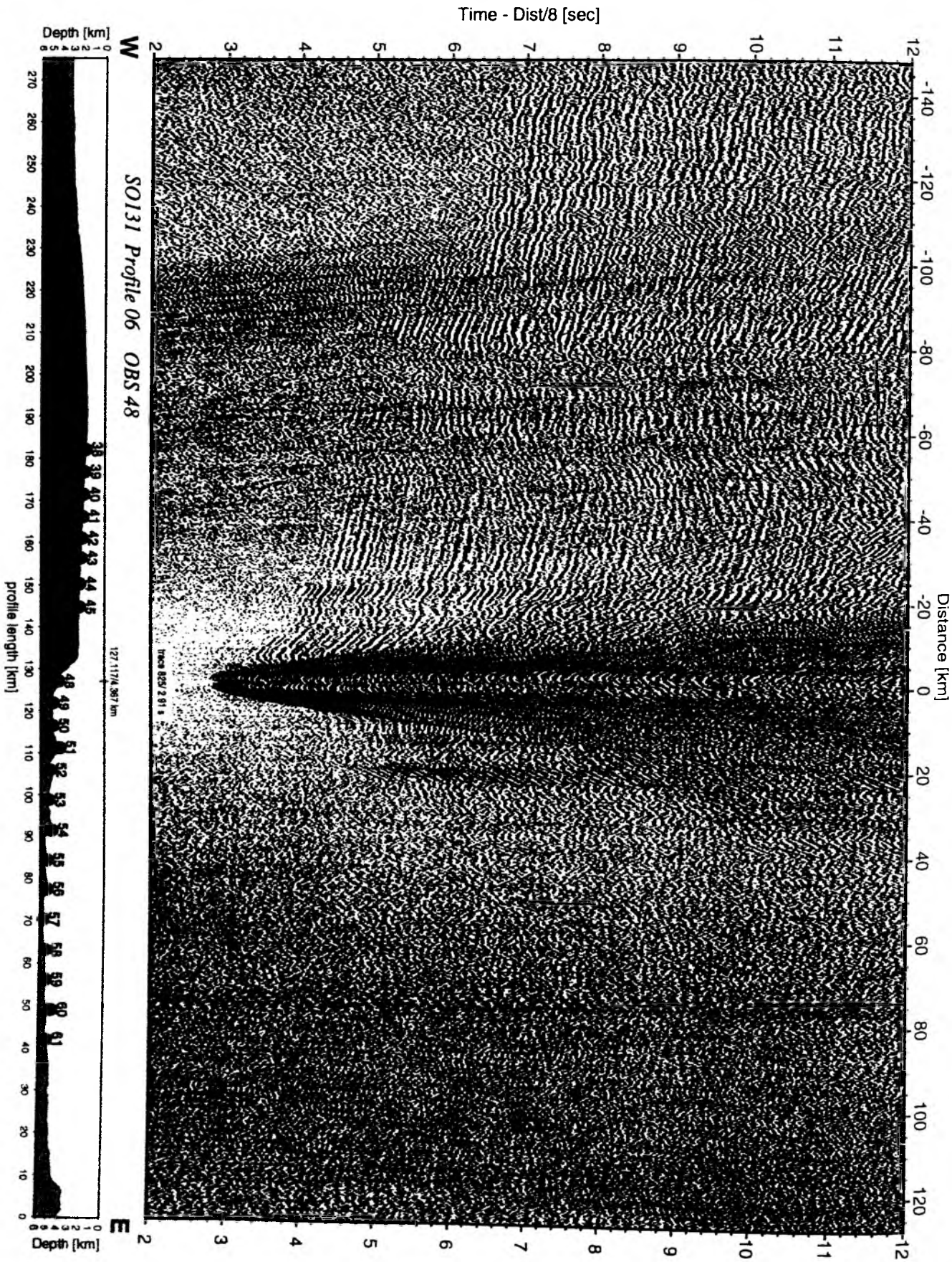

Figure 6.3.4.6.16: Record section from OBS 48 horizontal component 1, Profile 06.

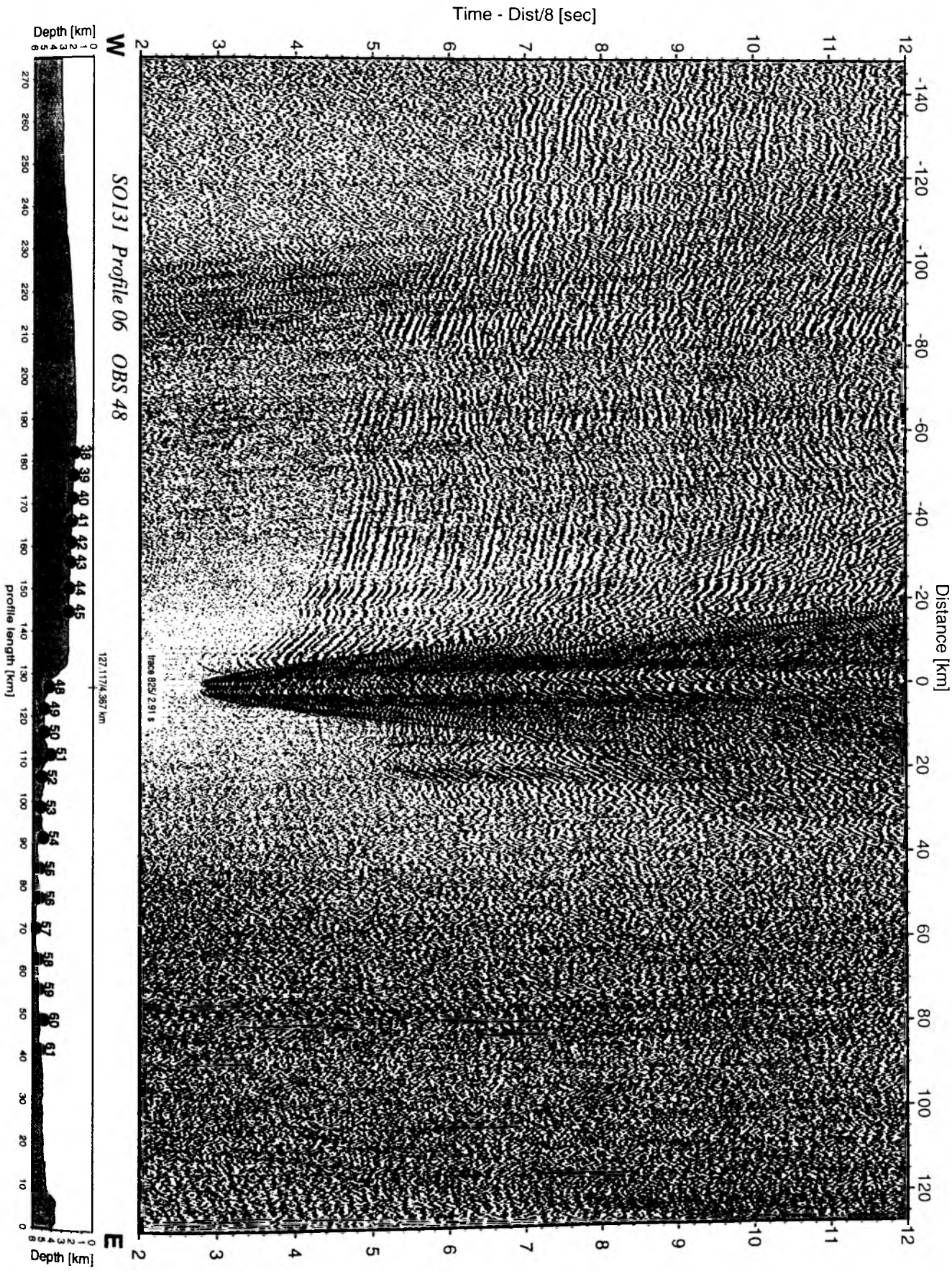

Figure 6.3.4.6.17: Record section from OBS 48 horizontal component 2, Profile 06.

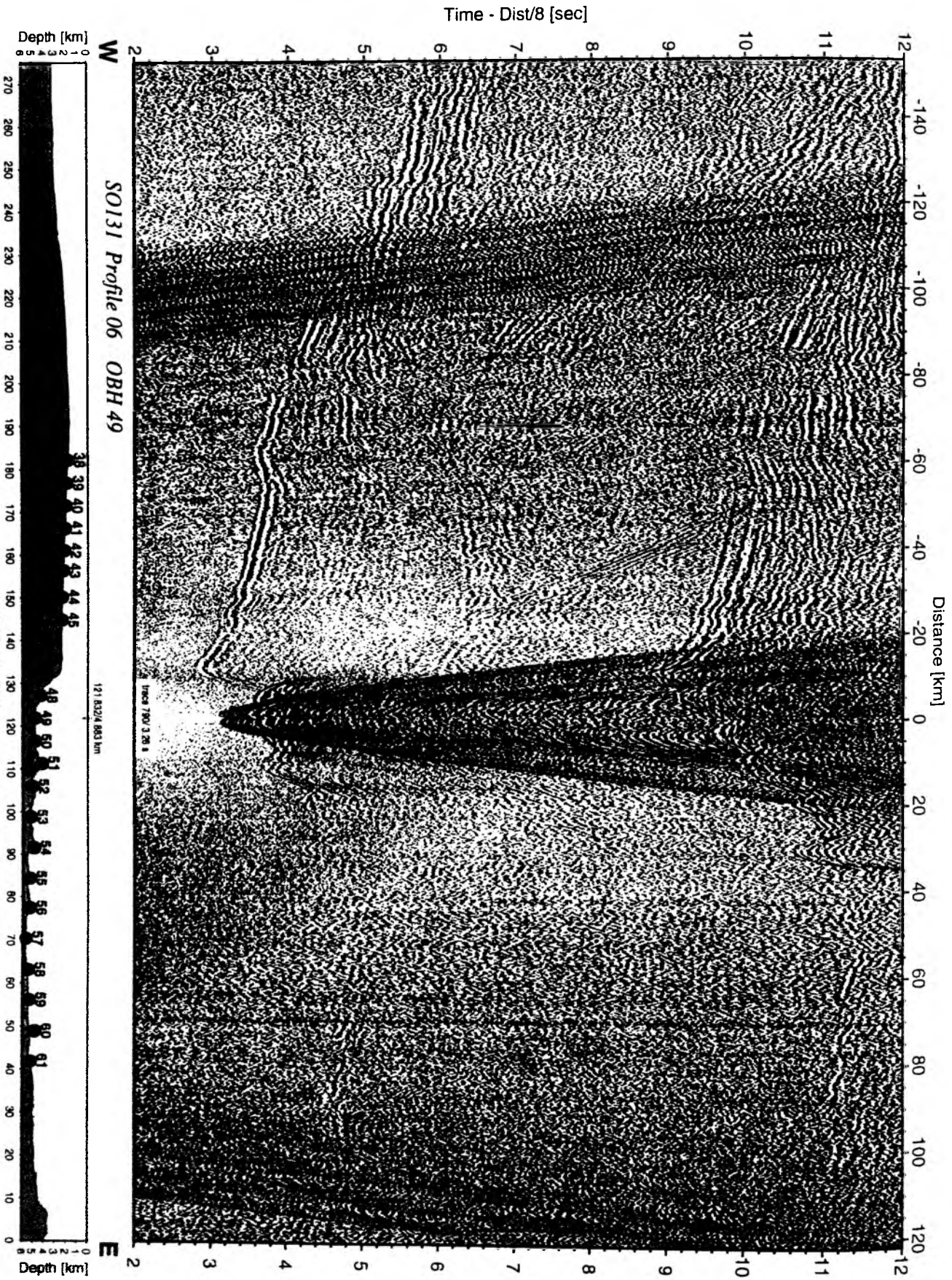

Figure 6.3.4.6.18: Record section from OBH 49 , Profile 06.

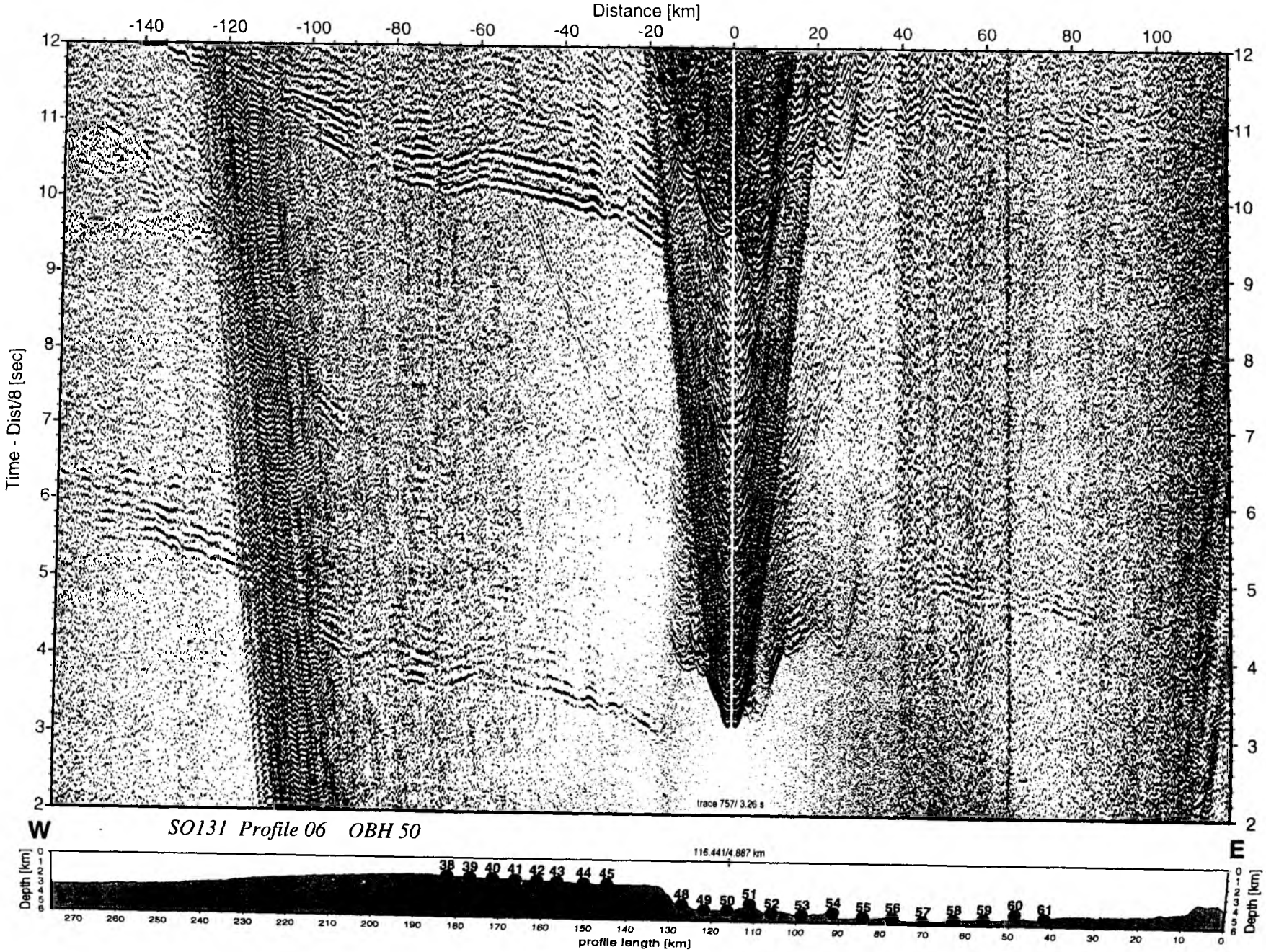

Figure 6.3.4.6.19: *Record section from OBH 50 , Profile 06.*

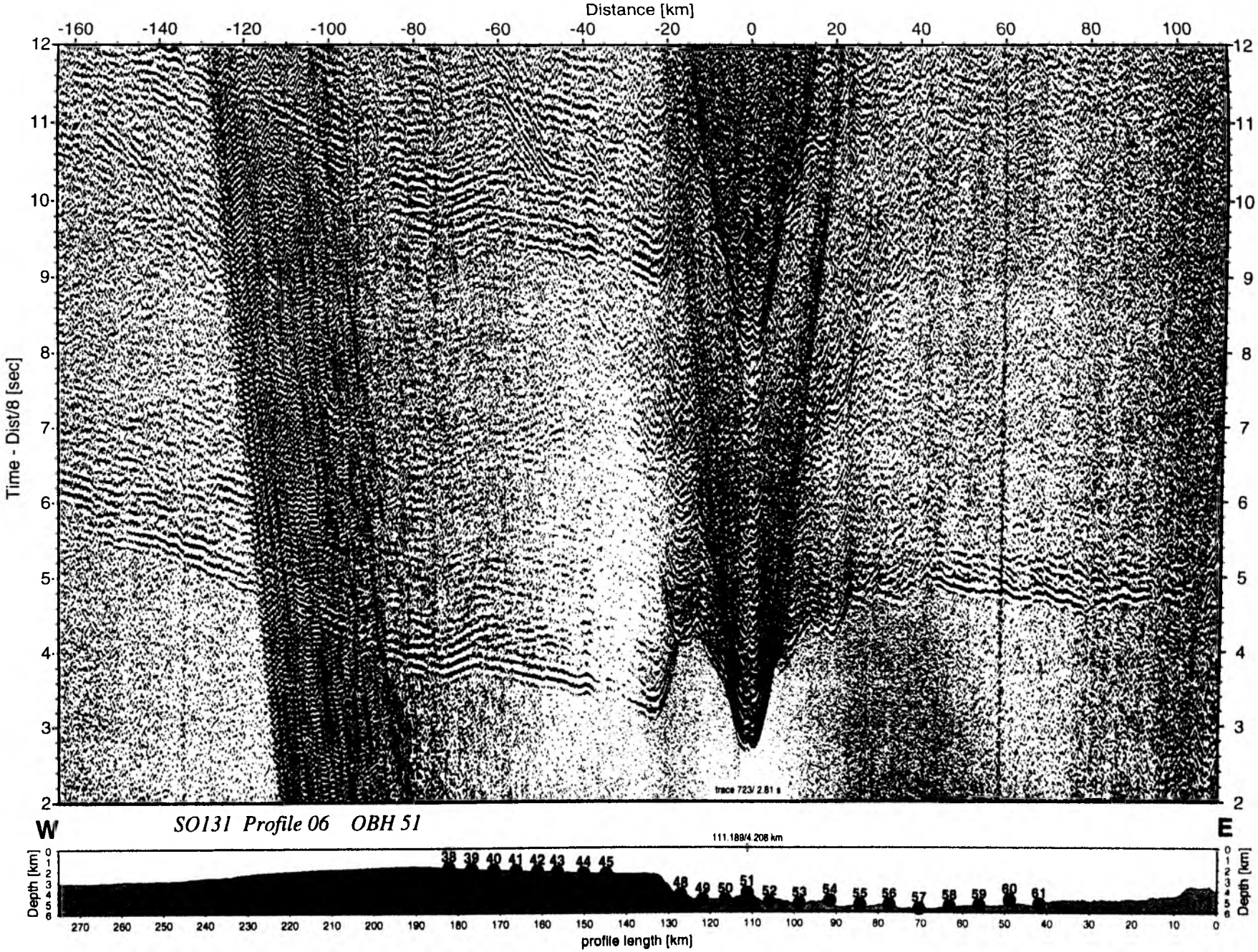

Figure 6.3.4.6.20: Record section from OBH 51 , Profile 06.

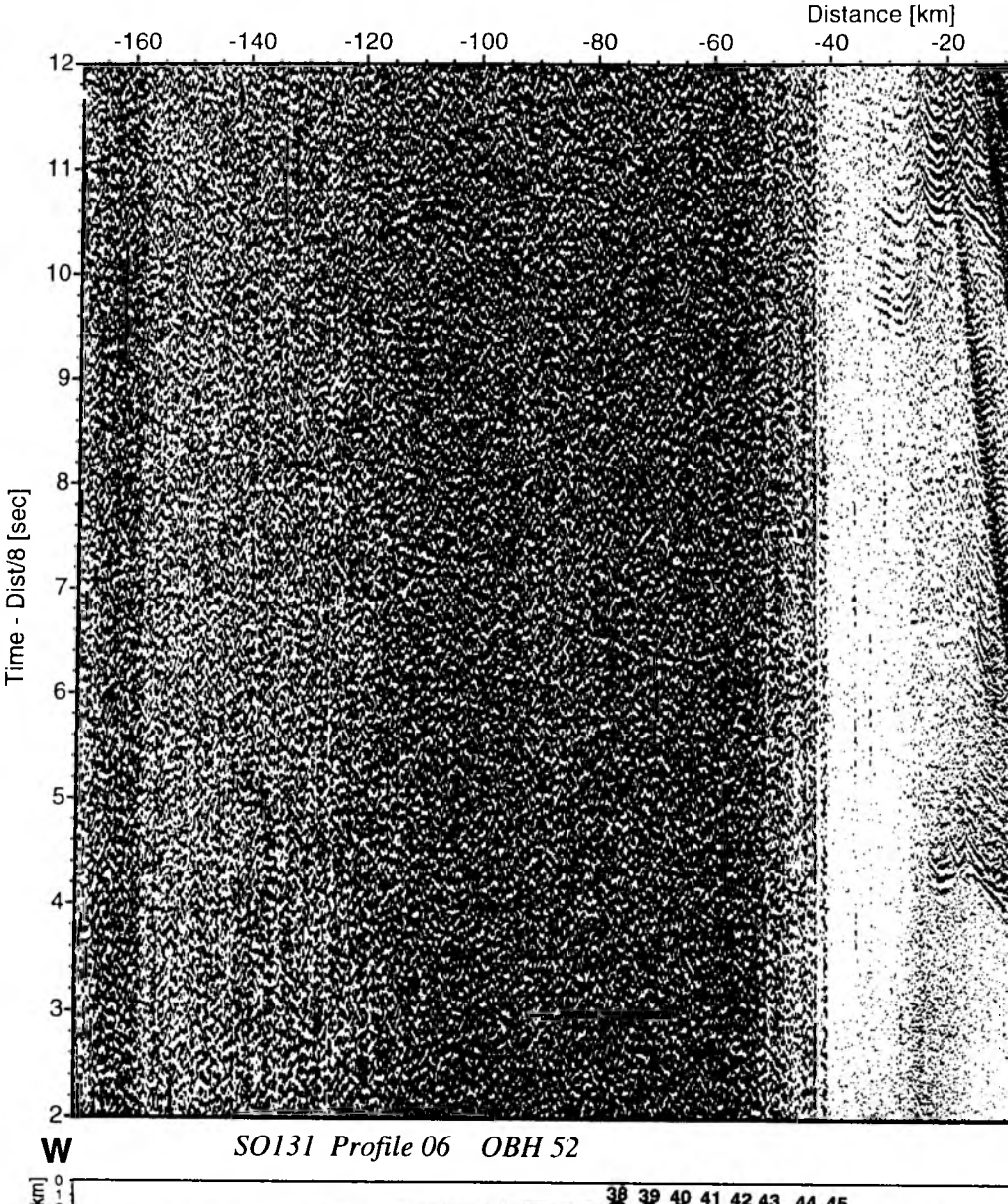
Distance [km]
-160
-140
-120
-100
-80
-60
-40
-20
Time - Dist/8 [sec]
12
11
10
9
8
7
6
5
4
3
2
W
SO131 Profile 06 OBH 52
Depth [km]
0
1
2
3
4
5
6
38
39
40
41
42
43
44
45
48
49
270
260
250
240
230
220
210
200
190
180
170
160
150
140
130
120
profile length [km]

Figure 6.3.4.6.21: Record section from OBH 52 , Profile 06.

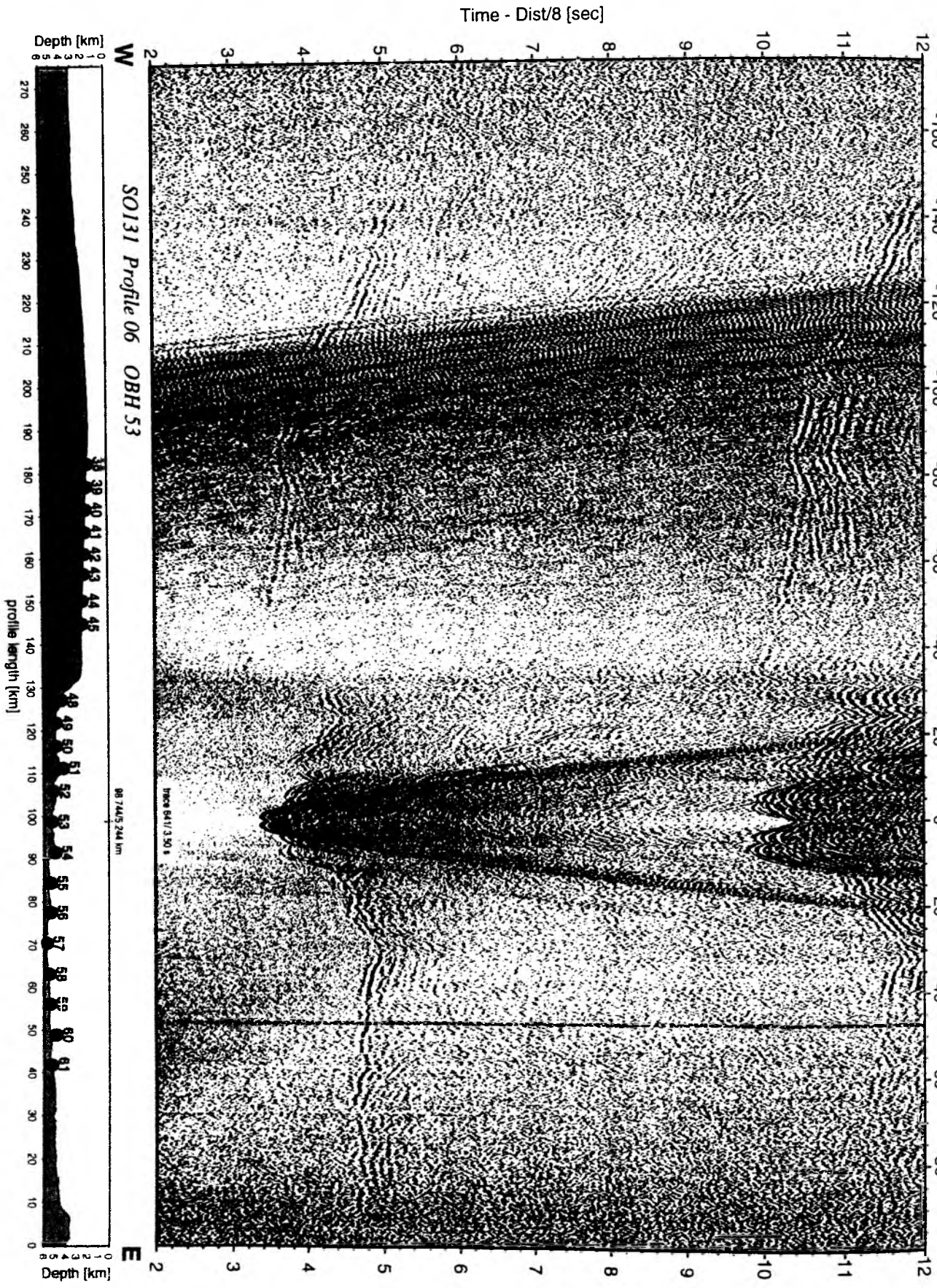

Figure 6.3.4.6.22: Record section from OBH 53 , Profile 06.

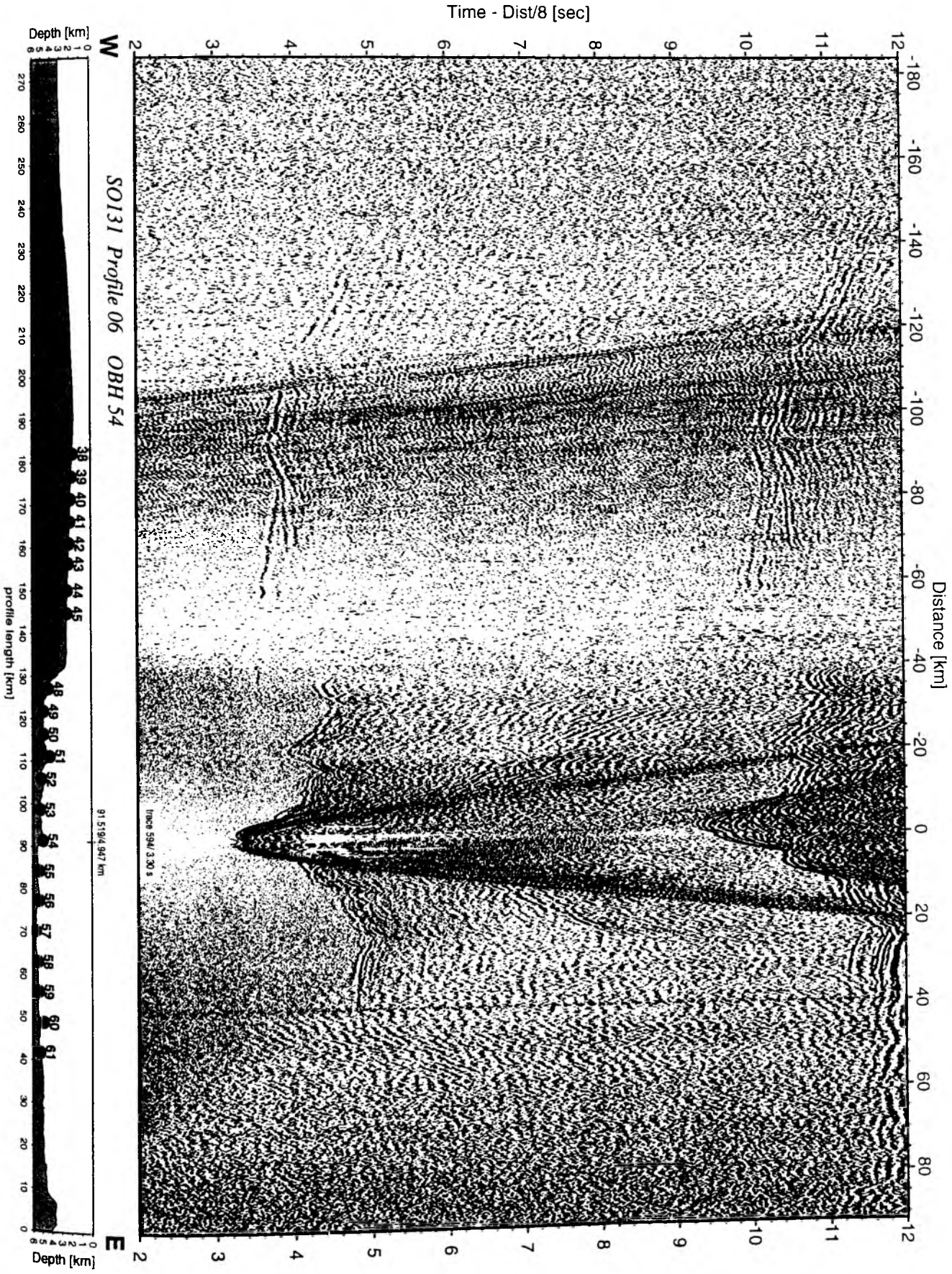

Figure 6.3.4.6.23: Record section from OBH 54 , Profile 06.

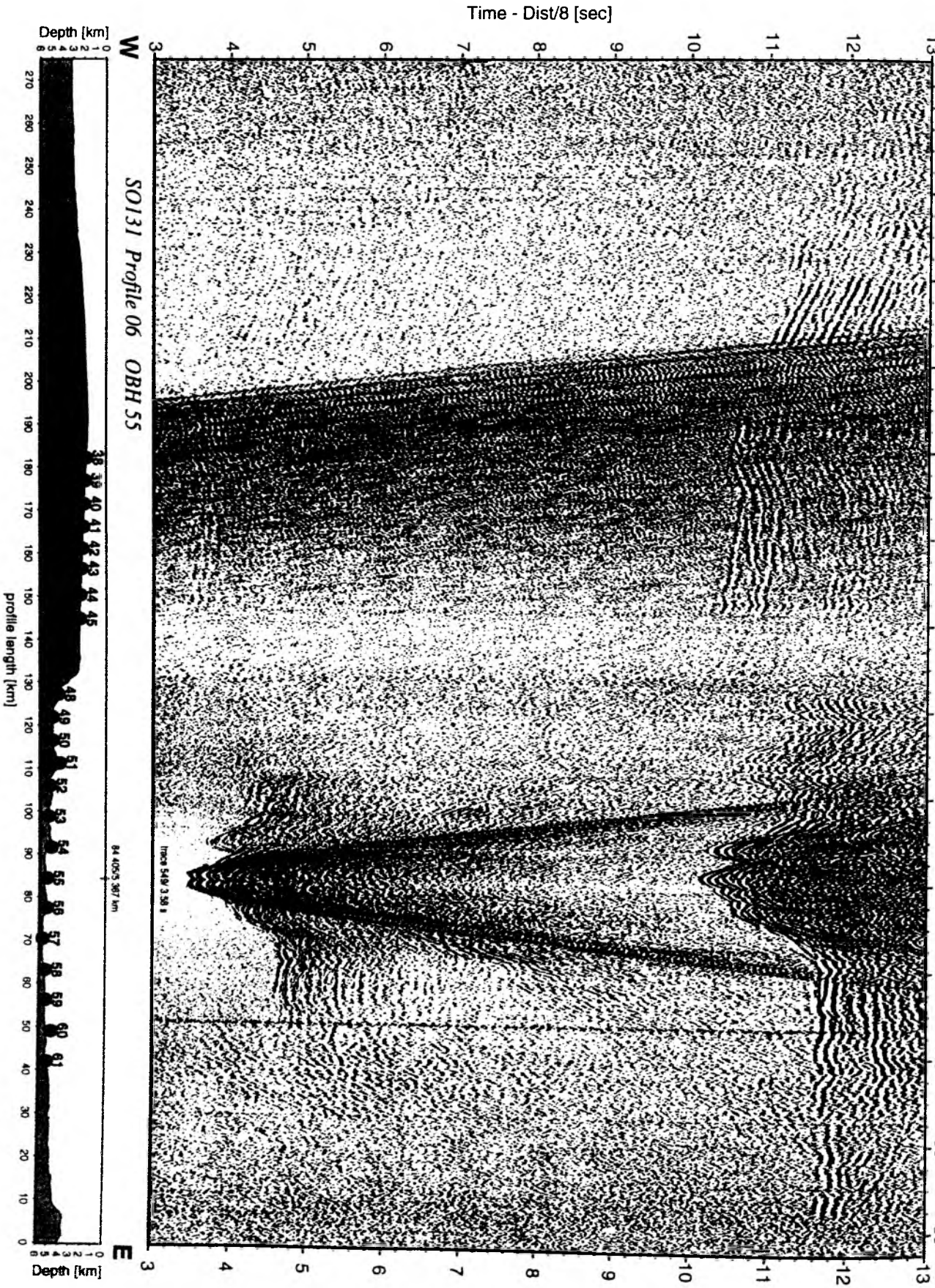

Figure 6.3.4.6.24: Record section from OBH 55 , Profile 06.

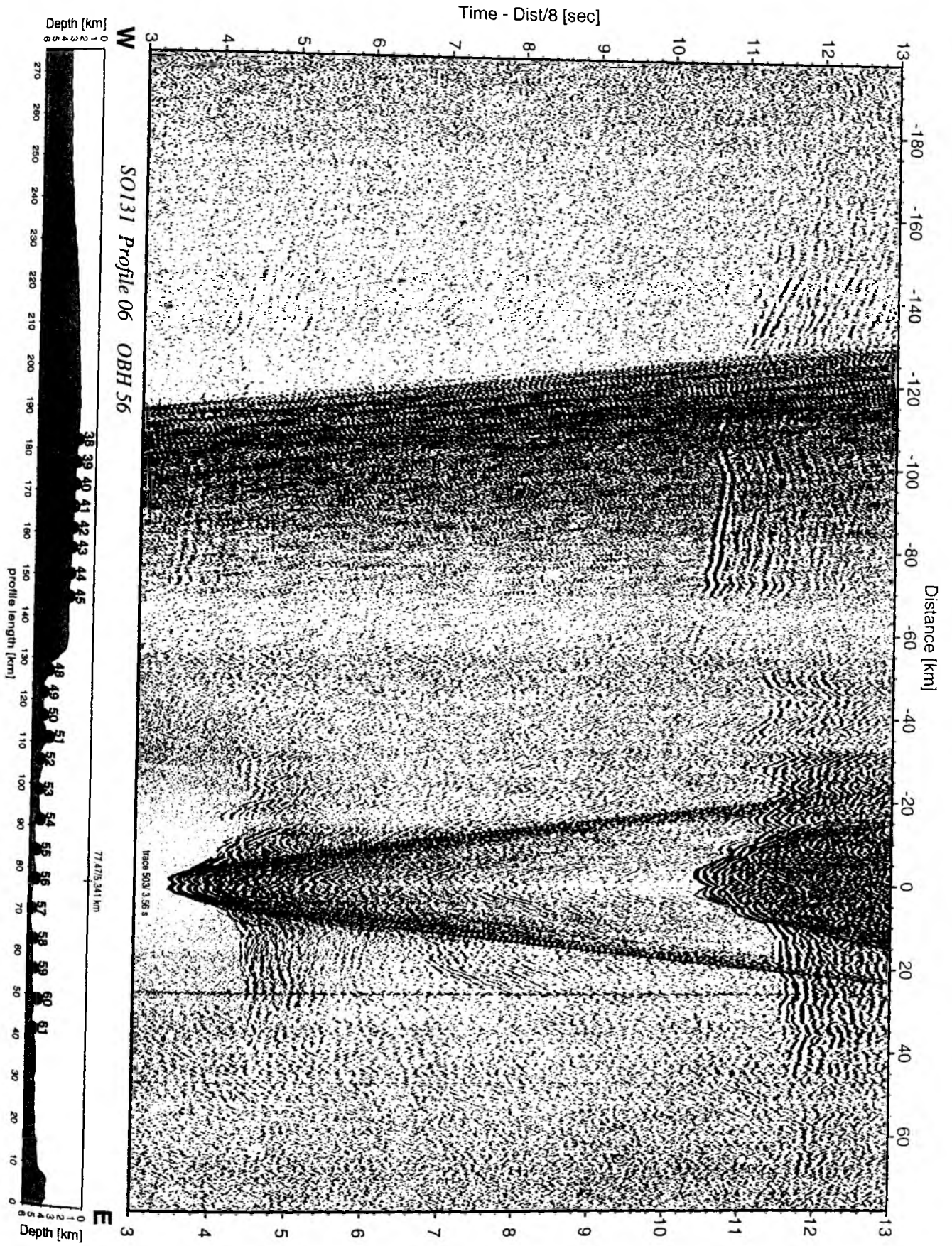

Figure 6.3.4.6.25: Record section from OBH 56 , Profile 06.

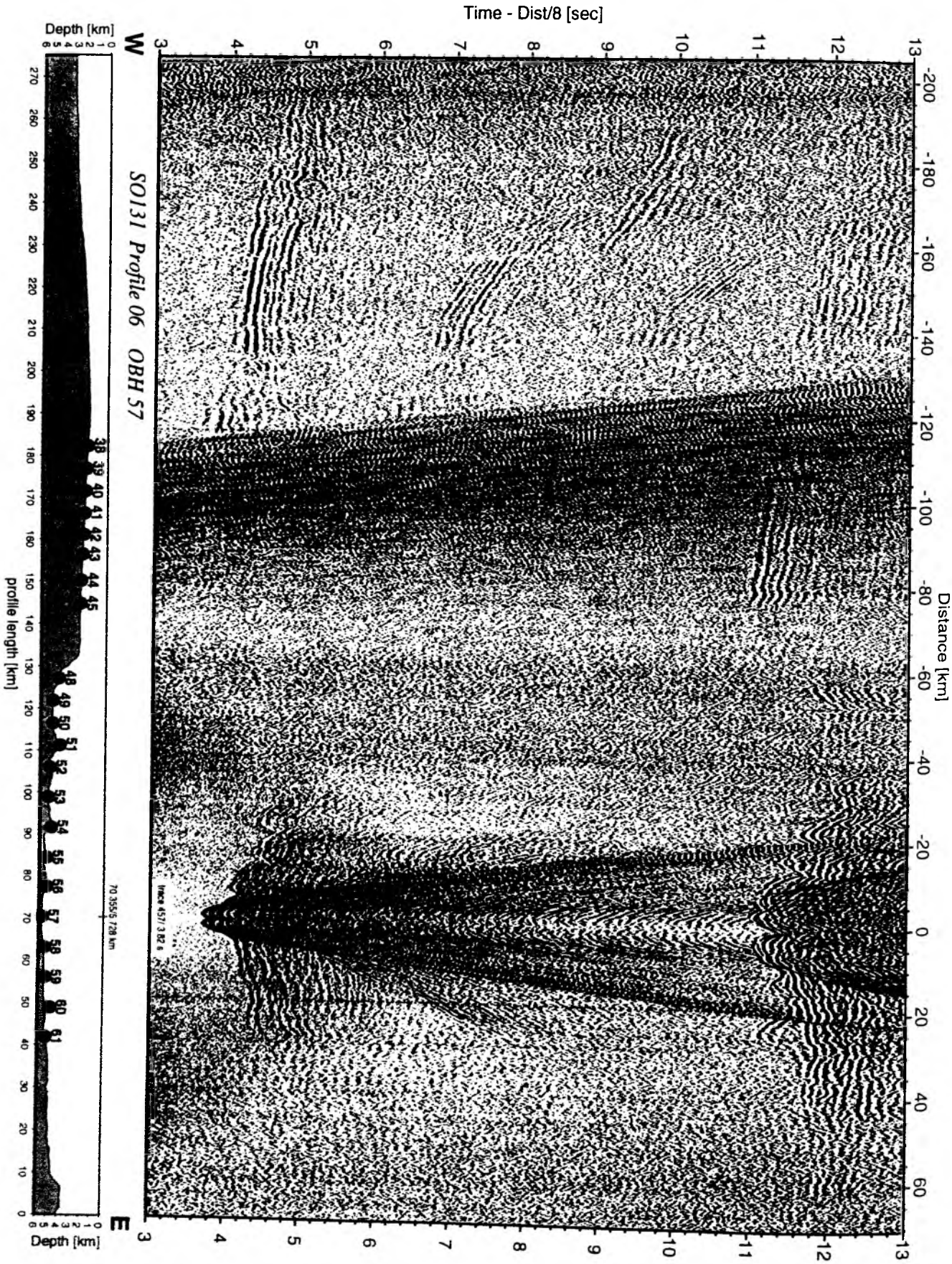

Figure 6.3.4.6.26: Record section from OBH 57 , Profile 06.

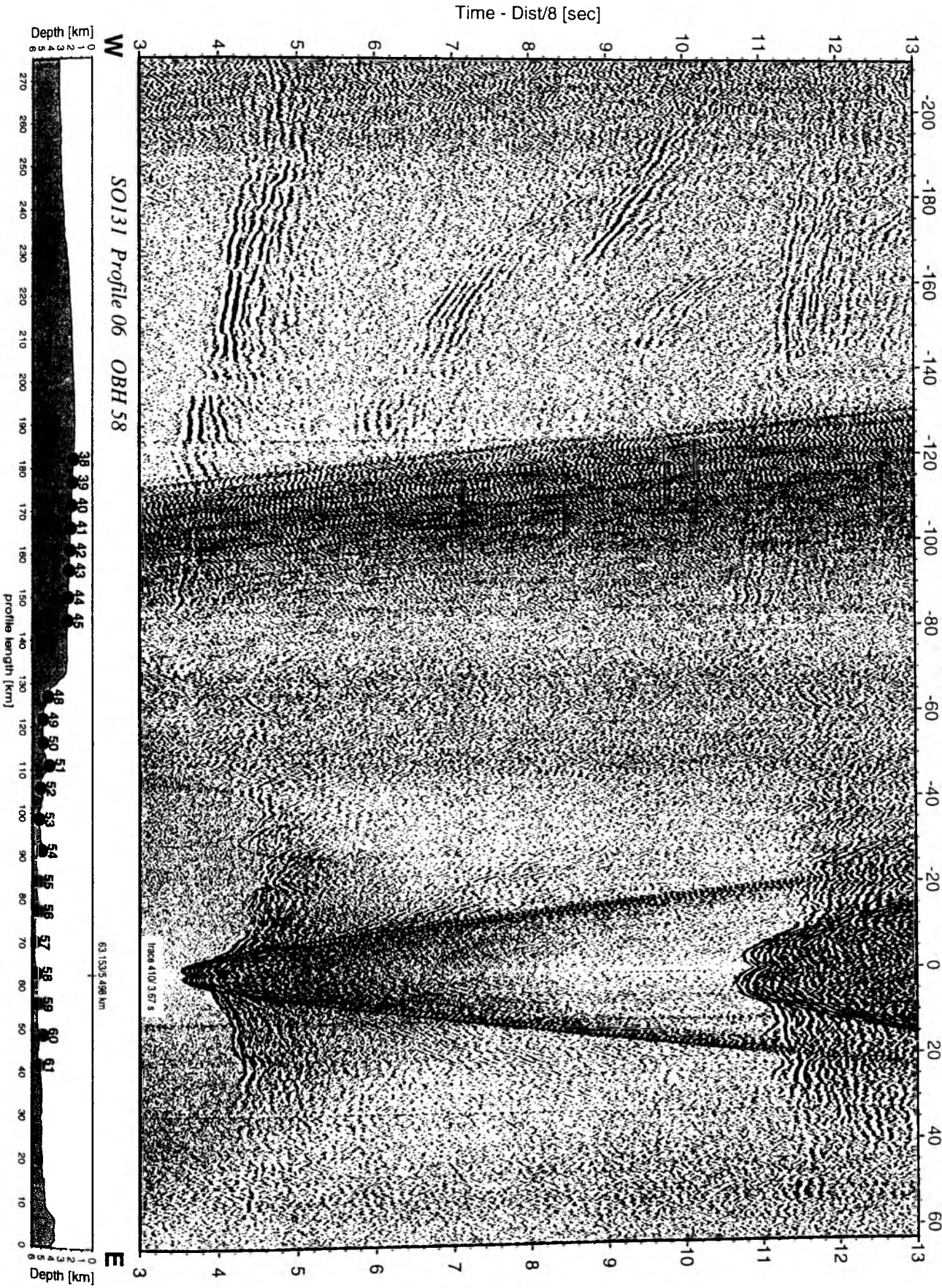

Figure 6.3.4.6.27: Record section from OBH 58 , Profile 06.

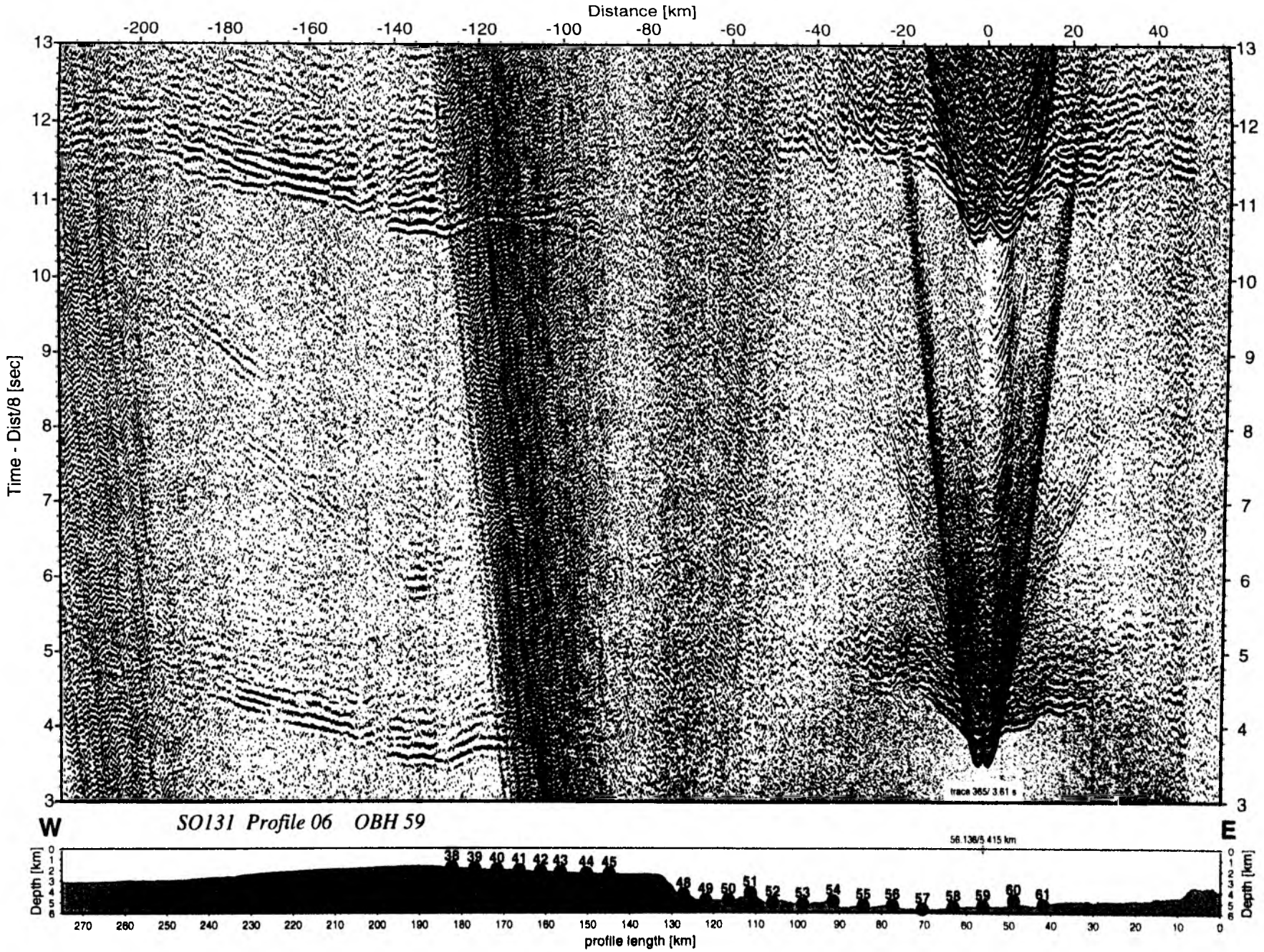

Figure 6.3.4.6.28: Record section from OBH 59 , Profile 06.

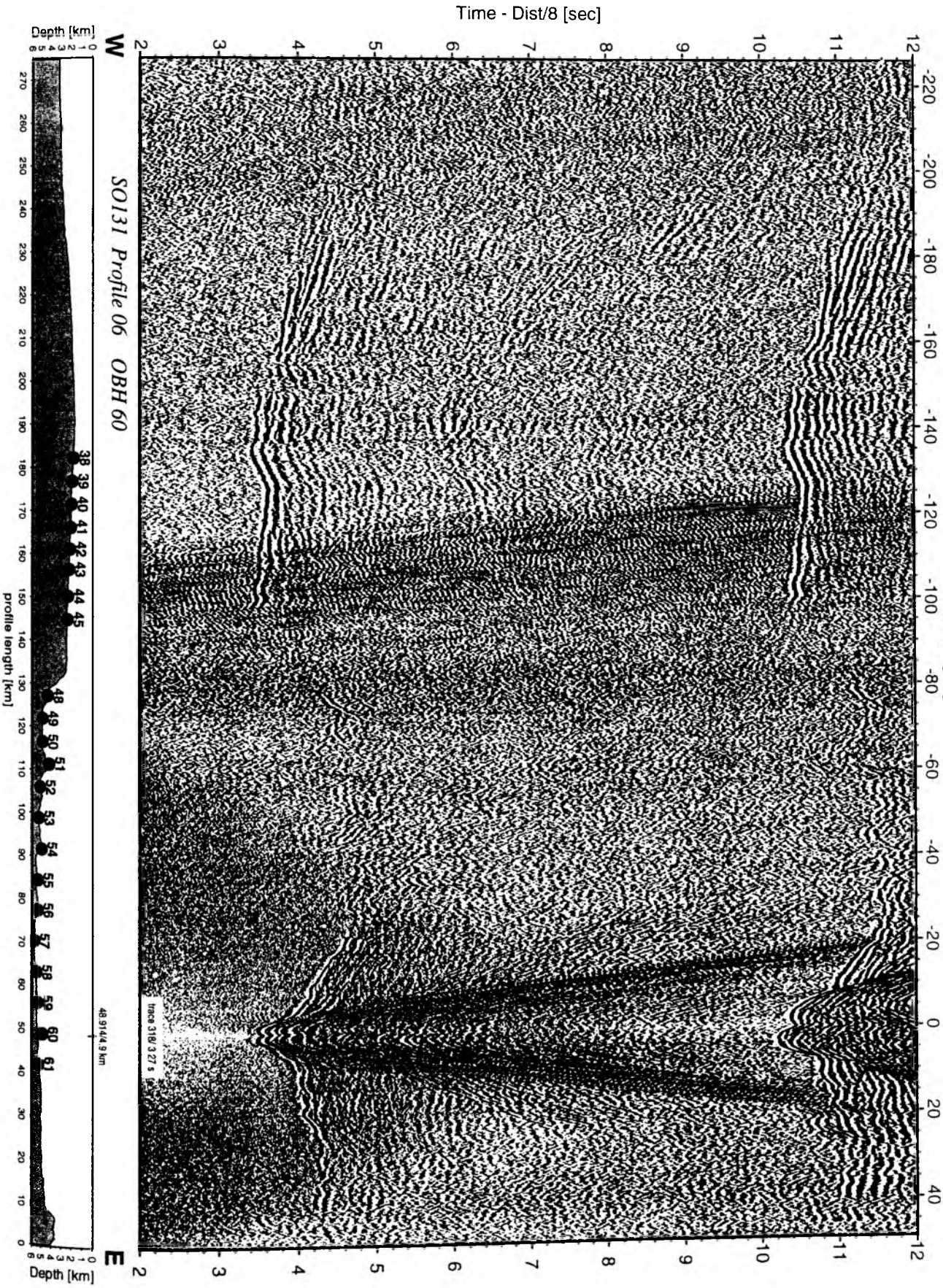

Figure 6.3.4.6.29: Record section from OBH 60 , Profile 06.

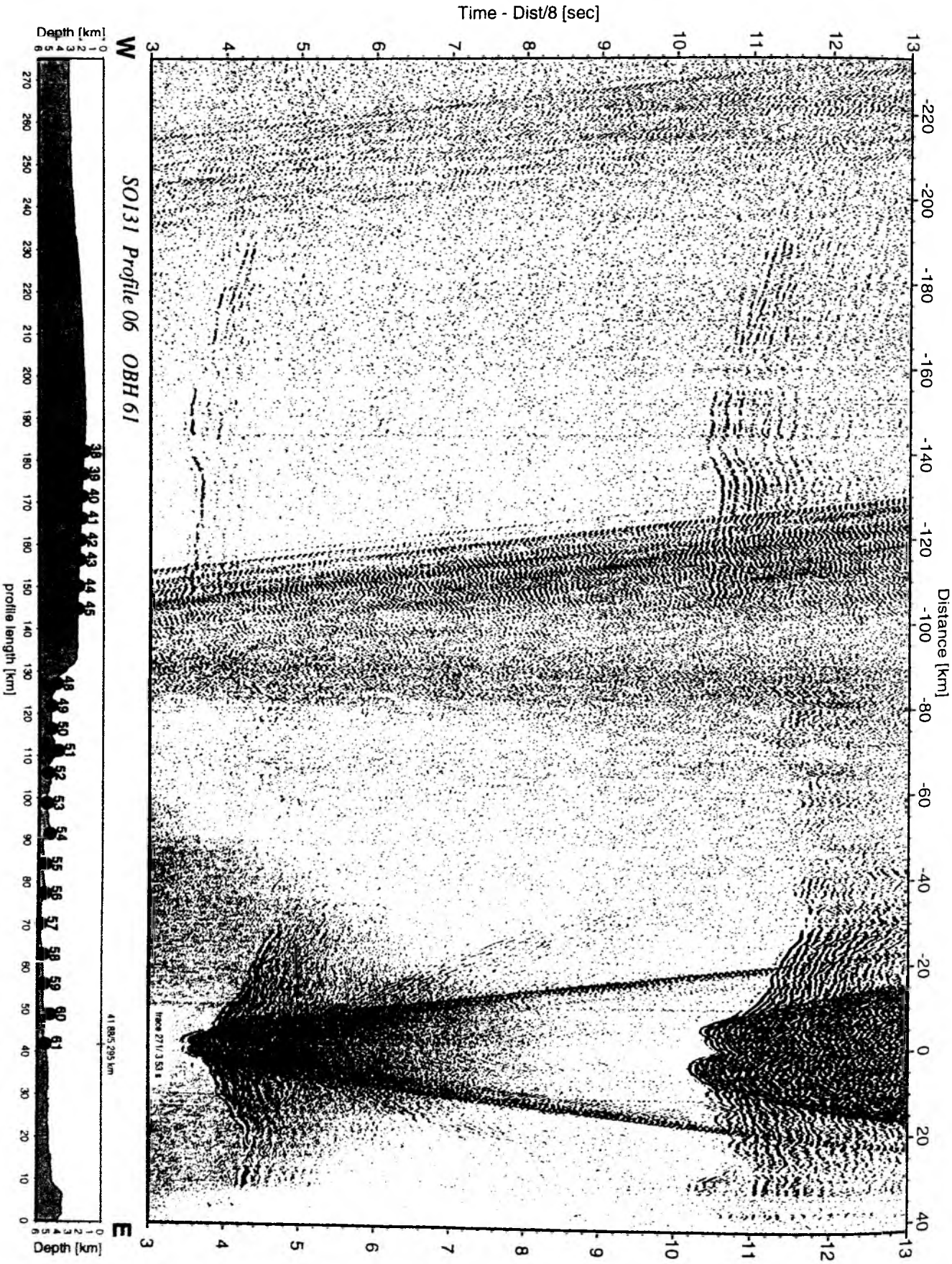

Figure 6.3.4.6.30: Record section from OBH 61 , Profile 06.

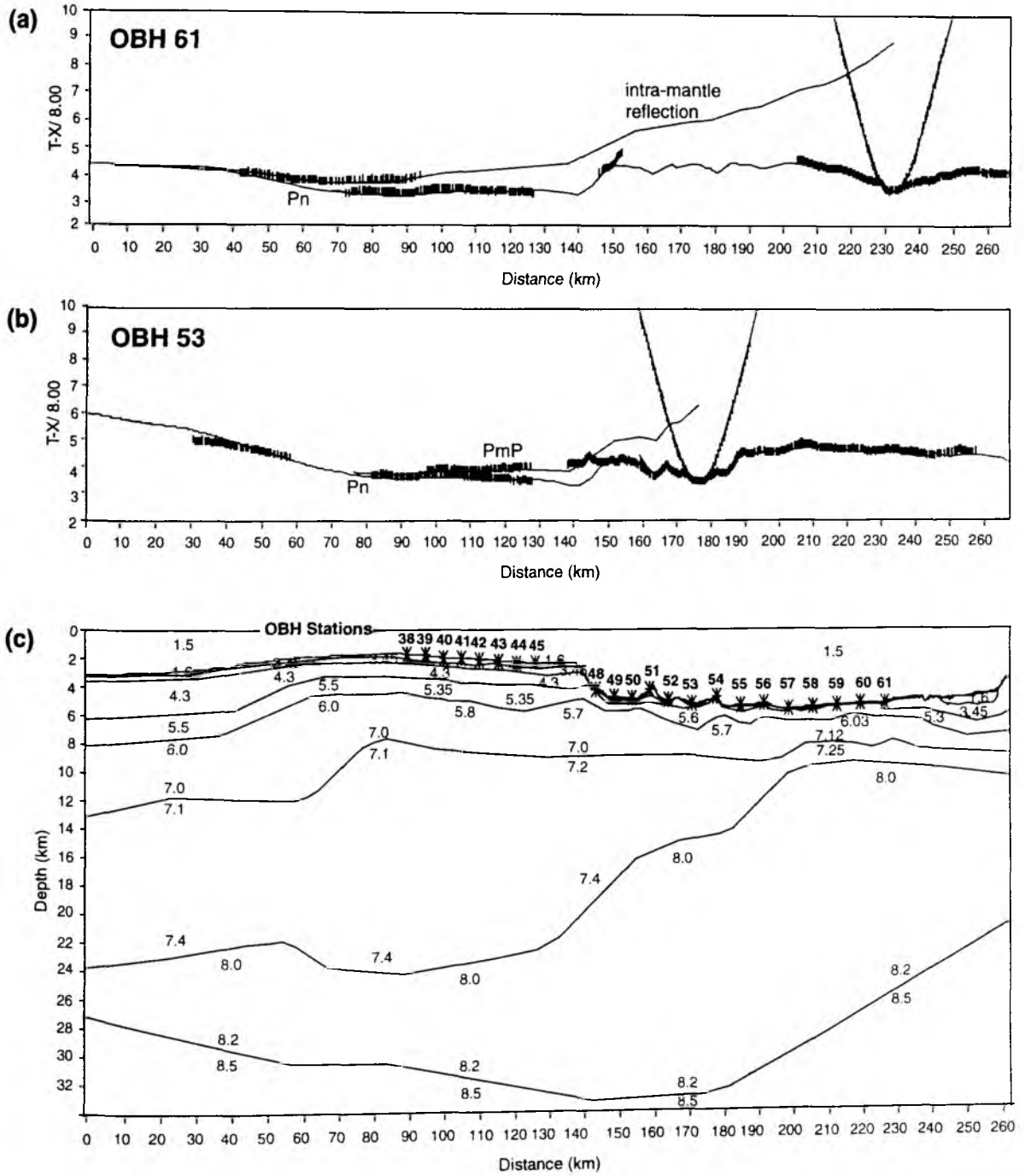

Figure 6.3.4.6.31: Profile SO131-06: Traveltimes of OBH 61(a) and OBH 53 (b), velocity model (c).

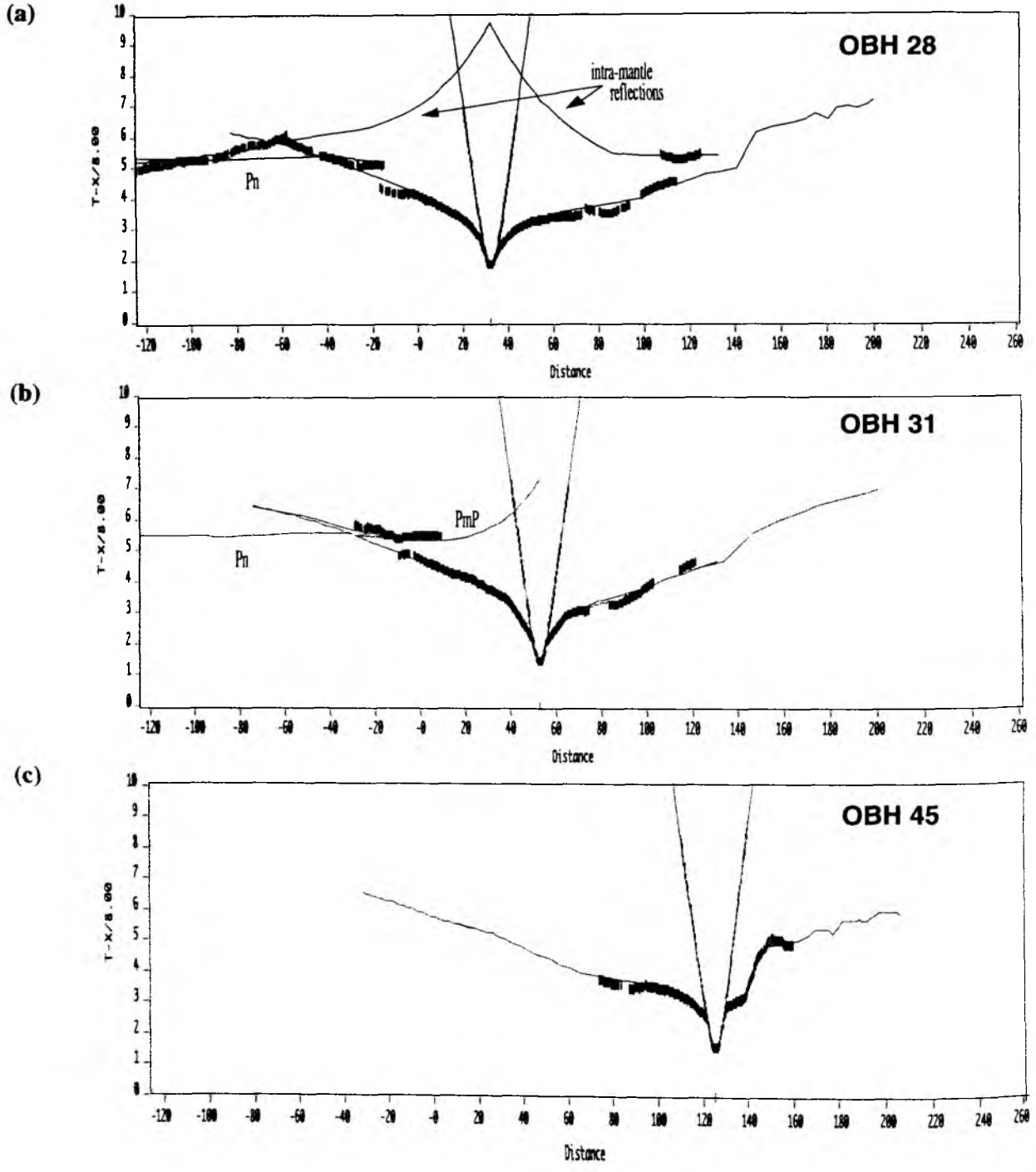

Figure 6.3.4.6.32: Traveltimes of selected OBH-Positions along profiles SO131-05 and So131-06.

6.3.4.7 THE 3-D SEISMIC EXPERIMENT AROUND NERO

(A. Hojka, E. Flueh, M. Perez, H. Borús, J. Bialas, D. Kläschen, U. Domasck)

6.3.4.7.1 GENERAL CONSIDERATIONS

Marine 3-D seismic surveys are generally performed using multiple streamers and sources towed by one or several ships. These techniques were not available to us, so we attempted to use ocean bottom recorders and airgun shots to study the region around NERO.

For 3-D seismic investigations, the common midpoint (CMP) coverage should be great and distributed evenly throughout the survey area. Moreover, for each CMP one would ideally like the offset ranges and the azimuthal orientations within each CMP to be widely spread. In an ideal case with an infinite number of shots and receivers this can be easily achieved.

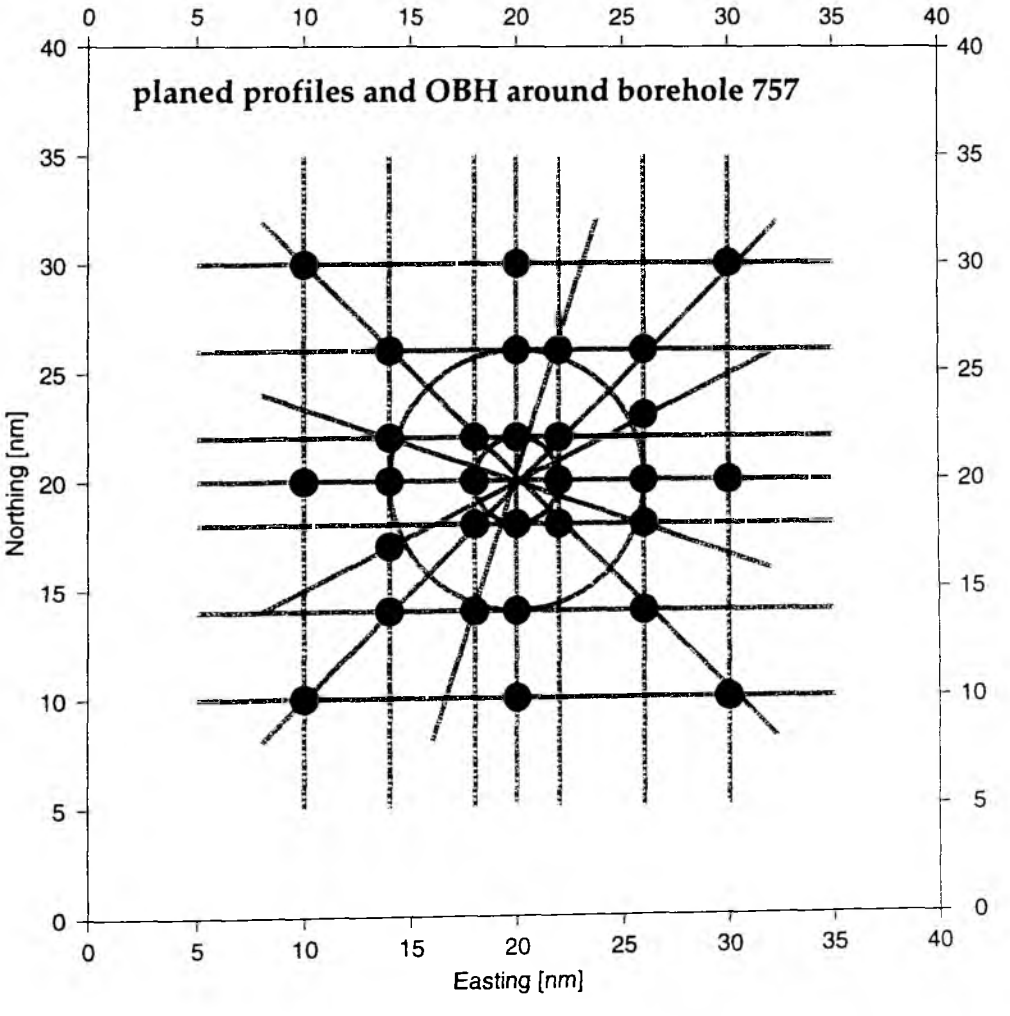

Figure 6.3.4.7.1.1: Receiver (OBH, large dots) and shot points originally planned.

For the SINUS 3-D Experiment we planed to use 30 ocean bottom recorders and a borehole seismometer. We allocated 6 days for shooting within an area of 30nm by 30 nm, centered around the NERO site. The originally planned set up is shown in Figure 6.3.4.7.1.1. The shots are assumed to be fired at 60 s intervals with a ship speed of 5 knots over ground resulting in a 150 m shot spacing. The bin width of each CMP was set to 250 m.

Rays describe the path from the shot point to the receiver, so the ray pattern will be unseparable from the CMP pattern. In the *SINUS* project the computational coverage included 30 OBH locations, fourteen rectangular profiles (30 nm length each, 5192 shots in total), five diagonal striking profiles (1798 shots total) and two circular profiles (2 nm and 6 nm radius, 622 shots total). Thus, nearly 7600 shots for each of the 30 OBH stations have been tested for their CMP and ray coverage behavior, which equals a total of 225000 observations.

The shot lines were composed of three elements: A rectangular grid along which the instruments are placed, augmented by several radial lines and two additional circles. The CMP distribution and selected raypaths of each of these three elements and their combination is shown in Figure 6.3.4.7.1.2. Further details on the distribution from all instruments is shown in Figure 6.3.4.7.1.3. The upper diagrams show on a logarithmic scale the distribution of offsets, fold and azimuthal variations for the entire survey area For clarity the lower diagram displays every 150th ray (light gray), but every CMP.

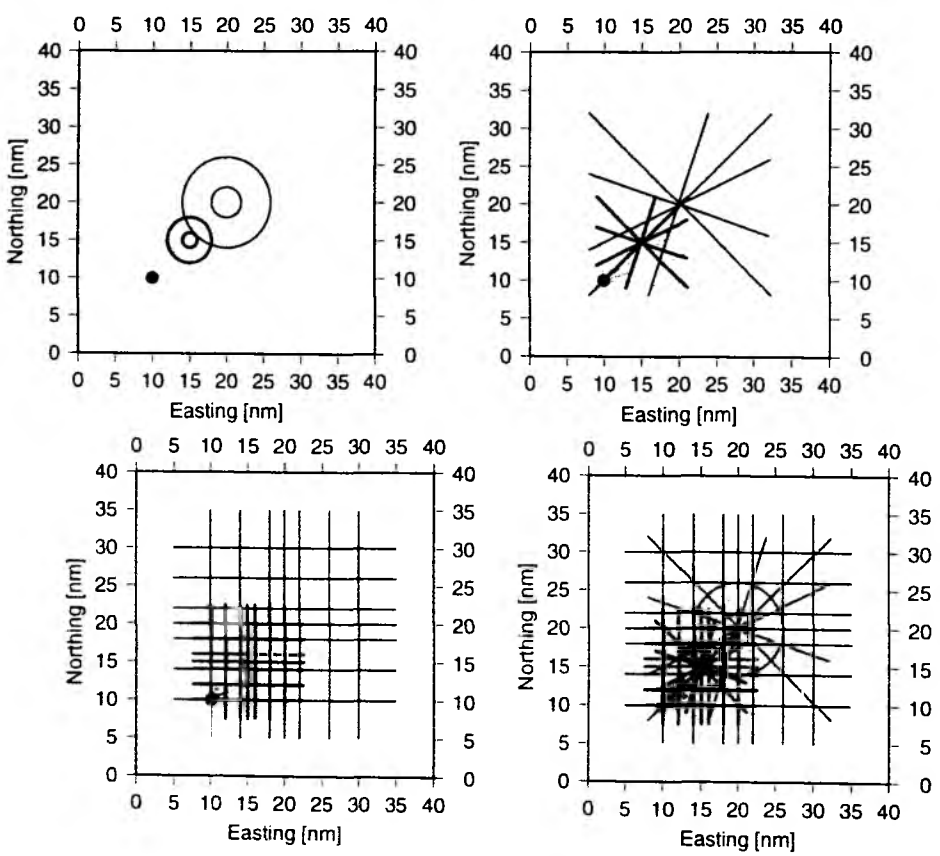

Figure 6.3.4.7.1.2: Different ray and CMP patterns.

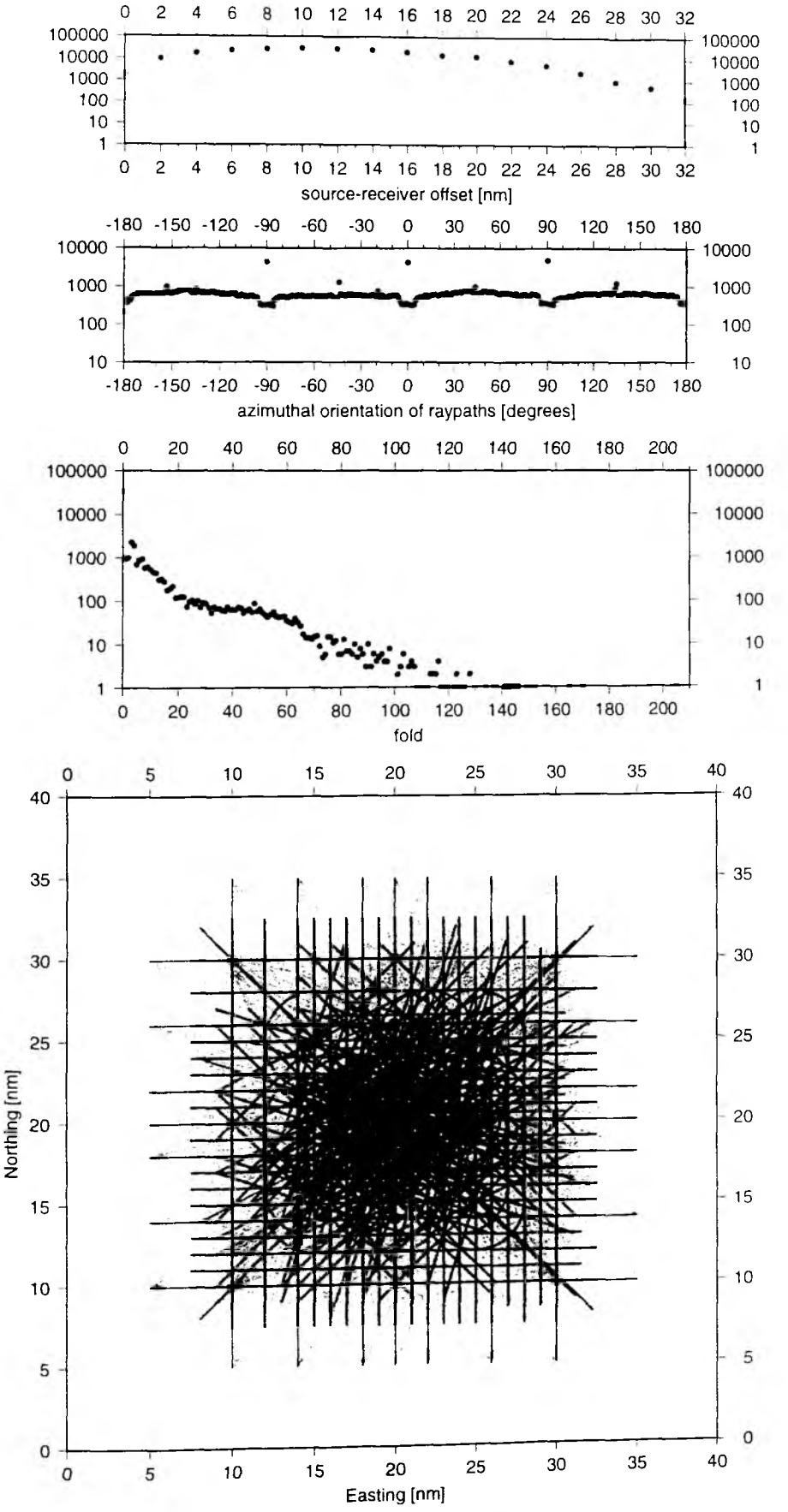

Figure 6.3.4.7.1.3:
Distribution of raypaths and midpoints (bottom), source-receiver offset, azimuthal and fold variation (top).

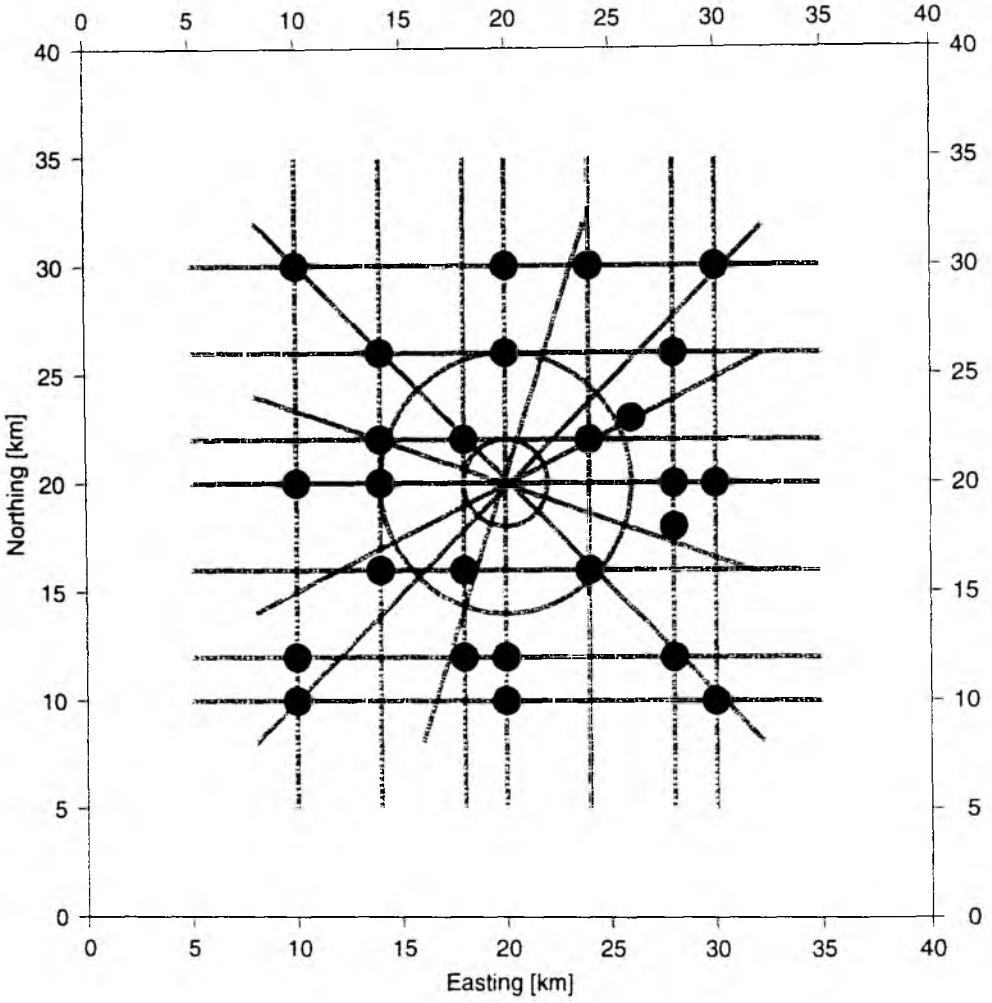

Figure 6.3.4.7.1.4: Chosen profile and receiver setup to improve coverage.

The CMP's are preferentially distributed with an offset between 8 nm and 14 nm. The integral effect summing all azimuths can be seen in the diagram below. All azimuths are equally well represented. However due to the rectagular grid the azimuthal variation with preferences for 0, 90, 180, and 270 degrees dominate. The fold is also unevenly distributed being highest directly above the borehole with a coverage of 205. The outer regions show a gradually decreasing coverage. The regions located beyond 8 nm from the center have a weak CMP coverage.

A moderate coverage (5 - 40) is found within a radius of 6 nm to 8 nm around the borehole, with the best coverage (40 - 205) being found under a 6 nm radius from the centered borehole. It is evident that despite a high coverage in the center, several gaps remain, which imposes problems for the seismic imaging. Also, only the inner 10 square miles have a high fold which quickly diminishes to the sides.

However, besides the imaging conditions, one also has to consider tomographic inversion of the data set to define the velocity field in great

detail. Tomographic inversion critically are dependent upon the starting model (Kissling, 1988). This requires dense observations along selected lines, so that a 3-D velocity model can be derived from a grid of reliable 2-D lines (Zelt, 1994).

For this reason, all receivers were originally placed along the shooting lines. A better compromise between CMP-coverage and detailed inline observation was thought of onboard prior to the experiment. At that time it was also clear that only 26 recorders were available and shooting had to be shortened due to weather downtime. The chosen setup and theoretical coverage is shown in Figure 6.3.4.7.1.4 and Figure 6.3.4.7.1.5. The rectangular grid and instruments were distributed asymetrically about the borehole. But still allowed for several profiles with three or four instruments per line. The reduction in the number of instruments was made by sacrifycing 7 of the 8 instruments originally planned for the center, since their CMP contribution only adds to the center, where fold is already high.

6.3.4.7.2 THE WORK DONE

The twentyfour instruments (OBH38, 39, 62 - 83) were deployed between 21:00 24. May and 12:00 25. May. The instruments at locations 38 and 39 had been deployed previously recorded data of line SO131-06. After an apparently successful test, the 1200 m long vertical array was deployed for the first time. In Figure 6.3.4.7.2.1 the location of the instruments and subsequent shots is given. Since after deployment we encountered force 7 winds, only one array was deployed on a forewind course along profile SO131-07. After reaching the end of the line, recovery of the array was complicated in still degrading weather conditions. Due to this shooting had to be interrupted for 15 hours and resumed at 09:00 26. May along SO131-08, again with only one airgun array. Along SO131-09 the second array was also deployed and shooting continued until 12:00 29. May. During shooting and also during transit times the streamer was deployed and the magnetometer was operated constantly. By this time it became clear that the planned two-ship experiment in conjunction with the JOIDES RESOLUTION could not be performed. And additionally some instruments were running low on power. Therefore 5 OBH (OBH38, 79, 80, 81, and 83) were retrieved and four instruments were redeployed, two of them (OBH86 and 87) in the immediate vicinity of the NERO site. They were intended to substitute the borehole seismometer. The remaining two instruments were redeployed at the locations of OBH80 and 81.

Shooting continued at 22:30 29. May for the circular profiles SO131-18 and 19 and continued until 15:00 01. June. The shooting rate was varied between 30 and 60 s, and portions of profile SO131-16 were reshot because the streamer data was not properly recorded. Early analysis of the data recorded on the retrieved instruments and from profiles SO131-05 and 06 indicated that deep crustal reflections are seen at offset ranges between 50 and 90 km. Therefore some of the remaining lines for the 3-D experiment were extended to larger offsets.

Instrument recovery began at 16:00 01. June with the vertical array. Although the releaser responded and the correct range was measured, it soon became apparent that the array was stuck at the seafloor and did not ascend. We therefore proceeded to pick up all other instruments first, which was successfully completed 10:00 02. June. An attempt was made to dredge for the array during daylight of 02. June. In total 6500 m of wire was laid out in a circle around the array with a large hook attached to the end. The dredge was

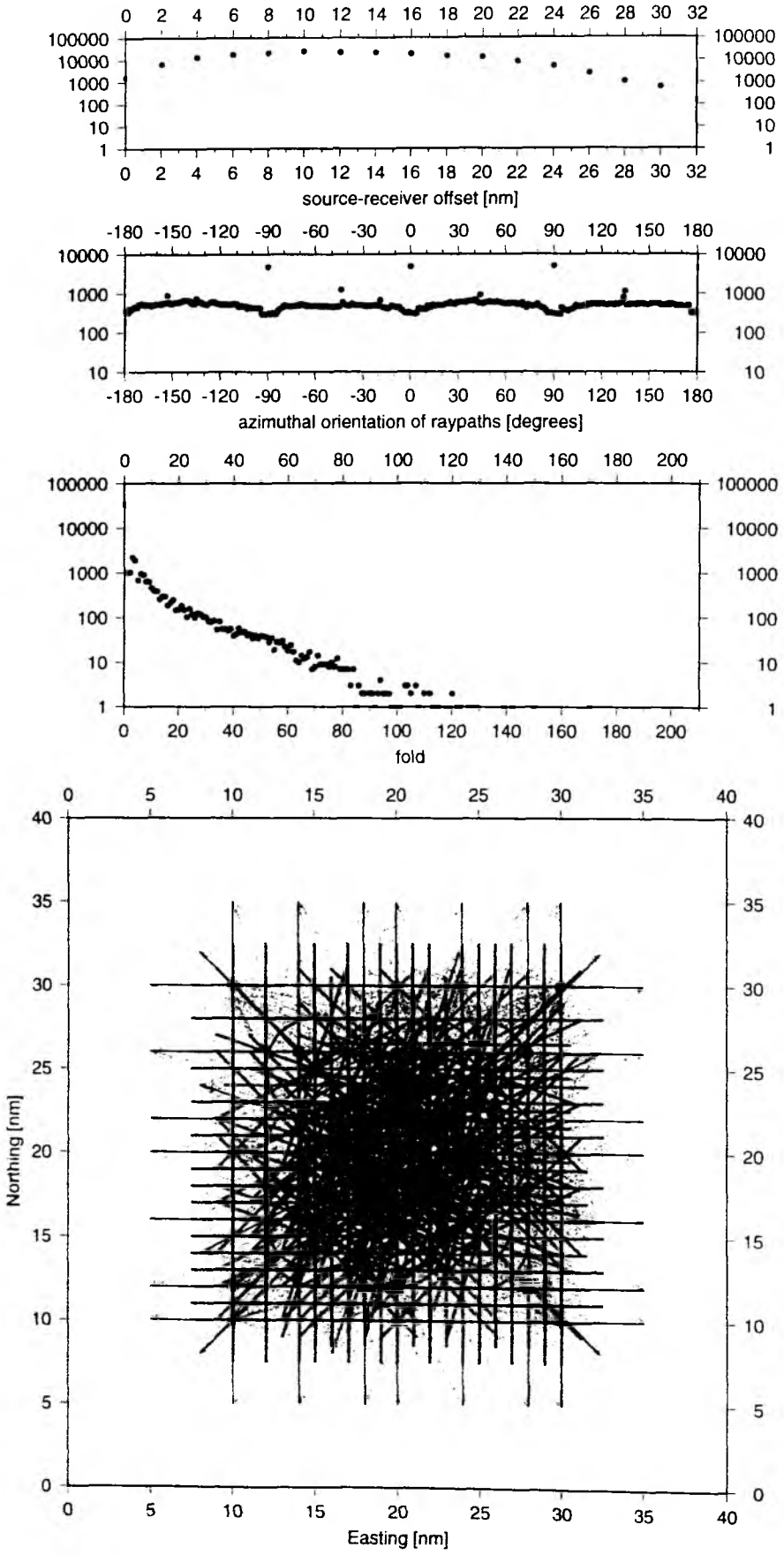

Figure 6.3.4.7.1.5:
Distribution of raypaths and midpoints (bottom), source-receiver offset, azimuthal and fold variation (top).

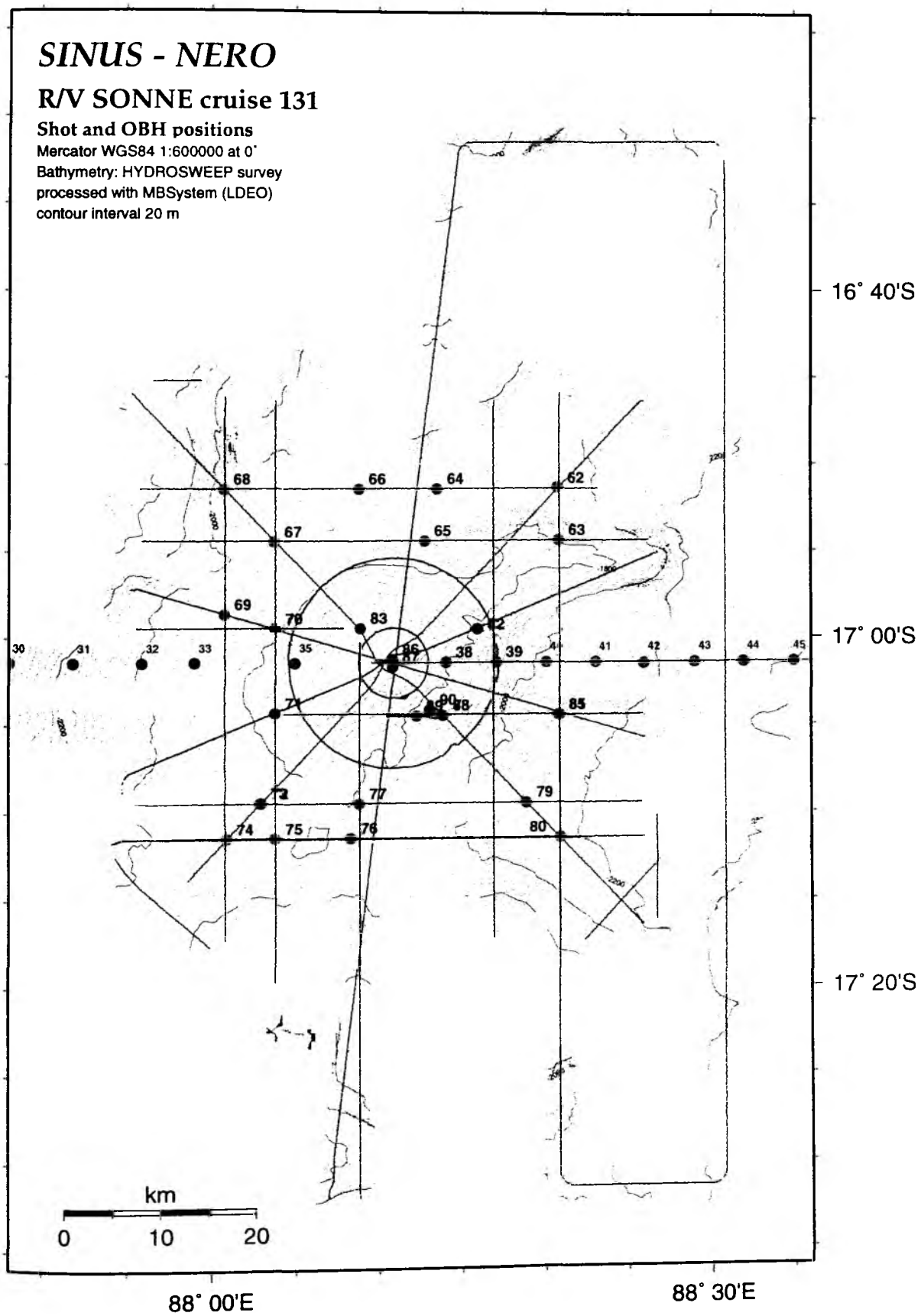

Fig. 6.3.4.7.2.1: NERO - Shot and OBH positions.

successful, and the whole array was recovered on the first attempt without any damage to the system. Later on, between 23:00 02. June and 04:00 03. June parts of profile SO131-15 were also re shot, because the streamer data was poorly recorded during earlier shooting.

Further details about instrumentation and shot locations are summarized in Appendices 9.1.2 and 9.1.7.

6.3.4.7.3 FIRST RESULTS

All data were quickly analyzed onboard for quality control. It turned out that OBH77 had a broken hydrophone which only recorded the direct water wave, therefore no useful data from this instrument are available. Other problems occured at instruments OBH74 and OBH75, which further reduced the coverage. The final possible coverage is shown in Figure 6.3.4.7.3.1, for comparison to Figures 6.3.4.7.1.3 and 6.3.4.7.1.5. Only the CMP's within the 40 by 40 nm grid are considered. In total 10109 shots were fired allowing 226931 seismic traces to be generated. The maximum fold is 92, and the maximum offset within the data set is 48 nm. In addition, data from profiles SO131-05 and 06 can be taken into consideration All data recorded by the streamer along the profiles are shown in Figures 6.3.4.7.3.2 to 6.3.4.7.3.26. Selected record sections are shown in Figures 6.3.4.7.3.27 to 6.3.4.7.3.65.

Within the 3D survey, Profile SO131-13 was chosen for preliminary 2-D modelling. It is 100 km long, and runs diagonally across the Ninetyeast Ridge, across the NERO Site. The profile was shot from NW to SE, the location of instruments and shots is shown in Figure 6.3.4.7.2.1. All instruments recorded well and the record sections are shown in Figures 6.3.4.7.3.57 to 6.3.4.7.3.65.

To obtain a model of the crust along the line SO131-13, forward modelling and inversion of the seismic events were simultaneously carried out. The results of both methods were compared throughout the modelling in order to get a good fit of the travel times. The preliminary model obtained from forward modelling is shown in Figure 6.3.4.7.3.66 and that obtained from inversion in Figure 6.3.4.7.3.67.

For forward modelling, seismic arrivals were picked for every instrument along the line and were modelled by ray tracing with *MacRay* (see section 6.3.3). The seismic sections are quite symmetric on both sides of the OBH, indicating only little variability. Due to the short length of the profile, no refracted arrivals from the Moho were recorded. However, Moho reflection are recorded at OBH68 and OBH80. Preliminary modelling of these reflections indicate that the Moho can be found at approximately 24 km depth, in agreement with the results of profile SO131-06 which crosses the ridge perpendicularly at the same latitude.

The thickness of the sedimentary cover and the vulcanite layer for the starting model were determined from MCS data. The velocity for the sedimentary layer ranges from 1.5 km/s to 1.6 km/s, and its thickness varies between 100 m to 200 m along the profile. In the vulcanite layer velocities range from 2.2 km/s to 3 km/s. The first refracted arrival was modelled with a third layer whose velocity ranges from 4 km/s to 5.5 km/s. The preliminary model shows strong undulations of the layer. The second refracted arrival was modelled with mid-crustal velocities ranging from 6 km/s to 7.5 km/s. This mid- crustal layer deepens at the center of the ridge to a maximum depth of 17 km.

The inversion is based upon a first arrival refraction tomography method. Therefore all available first arrival picks (2524 in total) were taken into

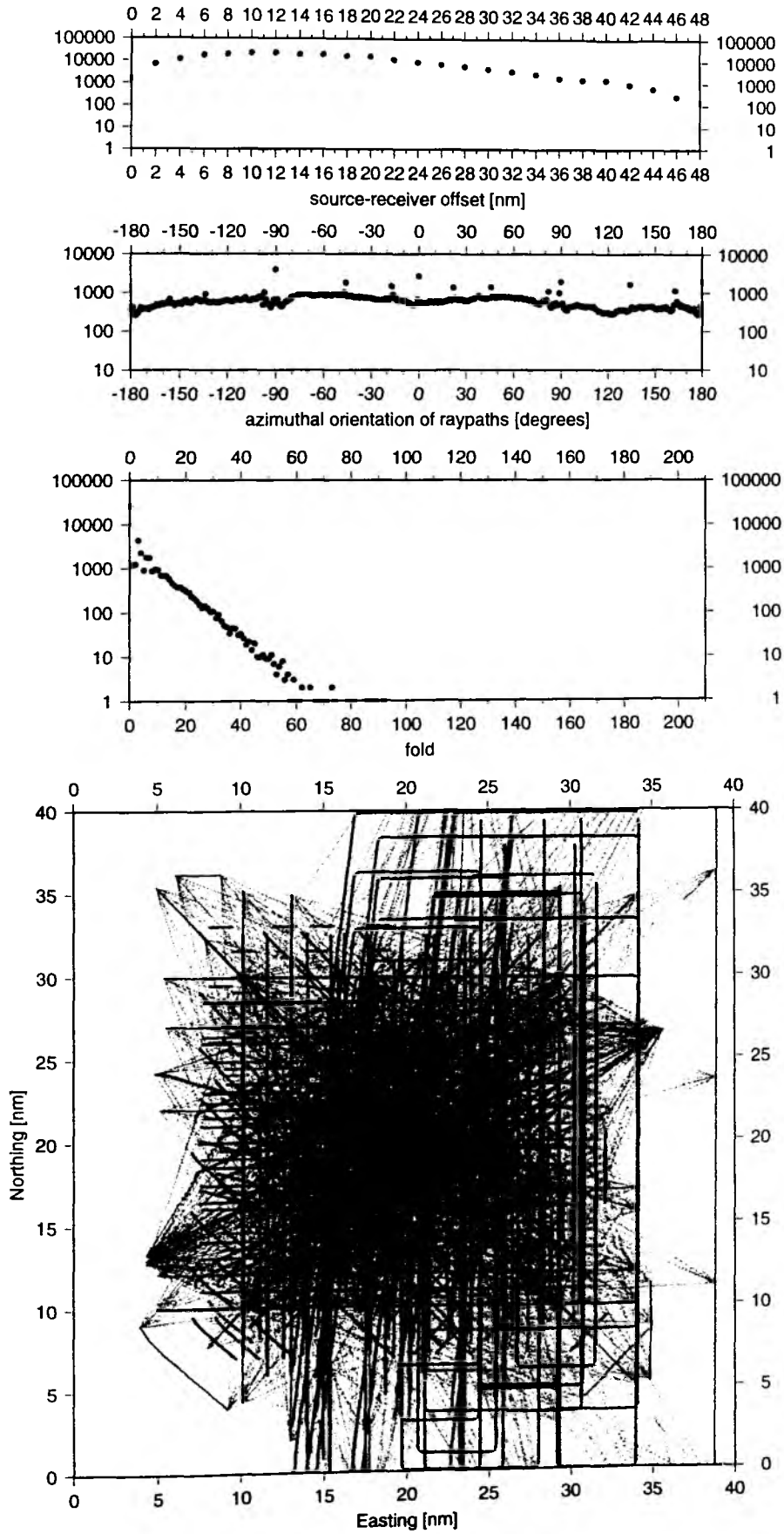

Figure 6.3.4.7.3.1:
Final distribution of raypaths and midpoints (bottom), source-receiver offset, azimuthal and fold variation (top).

account. The result reveals a good overall coverage and a ray penetration down to 13.5 km depth. Because inversion in general strongly depends on the velocity distribution of the starting model, several starting models and smoothing parameters have been tested to find a convergent velocity field. The input from previous forward modelling showed the best traveltime fit. During the last inversion it took 20 iterations to decrease the rms misfit to 60 ms. Figure 6.3.4.7.3.67 shows in the upper diagram the observed and calculated traveltimes and their residuals. Moreover, the whole coverage and final velocity field can be seen in the lower diagrams.

MCS-data around NERO

In the NERO area, seismic reflections traveltimes were picked interactively on the screen in every significant point with the help of Seismic Unix along the 25 profiles. Picks were made at sufficiently dense intervals to follow the variations of the reflections. In this area two prominent horizons could be recognized beneath the seafloor. Traveltime comparison with the ODP site 757 seismic stratigraphy report (Peirce, Weissel, et al., 1989) allows correlation with these events and interpretation from drilling results.

The first horizon is identified as reflector 6. It correlates with a lithology change from nannofossil ooze with foraminifers to calcareous ooze with chalk and ash. It is found at 168.5 mbsf. A P-wave logger aboard the drill ship measured velocities of 1600 m/s at this layer. Age determination of this boundary is middle Eocene (Peirce, Weissel, et al., 1989) which corresponds to 42 My, as described by Newman & Sclater (1988). The second reflector corresponds to reflector no. 10 (Peirce, Weissel, et al., 1989). It was drilled at 390 mbsf and marks a change in all physical properties, and represents the contact of sedimentary layers with basalt flows. The P-wave velocity from the logging tool is reported as 5500 m/s. Reflections from these flows are reported to dip towards the south which agrees with observations made from the SINUS lines (e.g. line 241). Samples from these flows were recovered during leg 121 (Peirce, Weissel, et al., 1989). They show a maximum thickness of 5.5 m to less than 1 m. Their age is questionable, but suggested to be at least late Paleocene age (appr. 59 My) (Peirce, Weissel, et al., 1989; Newman & Sclater, 1988).

The two way traveltime values for these two horizons were measured from sea level for all profiles around the NERO site. They vary between 1971 ms and 3643 ms to the seafloor (Fig. 6.3.4.7.68), from 2270 ms to 3645 ms to the first horizon (Fig. 6.3.4.7.69) and between 2174 and 4021 ms for the basalt horizon (Fig. 6.3.4.7.70). The first layer could not be picked everywhere along the profiles. Either onlap terminates against several highs of the basalt layer, or the layer could not be identified within the sediment layers (e.g. on line 26 at the NE corner of the grid; Fig. 6.3.4.7.3.69). The first horizon has a structure similar to the seafloor. The isochrons differ by some 200 ms TWT. This indicates that layers formed at times younger than middle Eocene are of constant thickness and have not been disturbed by tectonic activities. This corresponds to the tectonic description of Newman and Sclater's upper sediment group (Newman & Sclater, 1988). Variations in layer thicknesses above basement are therefore mainly due to variations below this first horizon. However, there are exeptions to this observation, which are primarily located between 88°:00'E – 88°:30'E at 16°:40'S. Here the difference in TWT between first layer and seafloor increases by 100 ms, to a total of 300 ms. The surface of the second horizon strikes NW -SE, and shows a rough surface with maximum heights along strike. At the positions of the above mentioned anomalies, the traveltime values

decrease to 2600 ms TWT. This means that the basement outcrops above seafloor at these points. This is the area where Sinus and Cosinus volcanos are located. Subtraction of seafloor traveltimes and basement traveltimes results in a map of sediment thicknesses (Fig. 6.3.4.7.3.71). As the traveltime values are not taken at the same positions, previously interpolated values were used for this calculation. As an artifact, minor circular anomalies were found along the picked values. Nevertheless the traveltime variations support the above mentioned observations and are compareable to the sediment thickness map of Newman and Sclater (1988). Even though the maps are given in different units (ms TWT and m), the main structures agree well. These structures represent the increased thicknesses (600 ms TWT) seen in the SW and SE quadrants of the map (Fig. 6.3.4.7.3.71), as well as the outcrop features of the Sinus and Cosinus volcano. This unit is not included in the map by Newman and Sclater, but the south trending tongue can be found on the northern tip of their map. The overall outline of circular isochrons observed just west of the borehole correspond to another thickness anomalie on the Newman & Sclater map. Newman and Sclater report a W to E striking fault between 17°05´S and 17°02`S which crosses the Ninetyeast Ridge just south of the NERO site. However this fault is not directly outlined by the isochron maps derived from the SINUS data. Investigating the reflection lines at the proposed position of the fault resulted in different observations. Hints for a structural unconformity are found on lines 13 (shotpoint(sp) 3025), 18 (sp 5150), 19 (sp 6150), 21 (sp 6660) and 241 (sp 8075). Some of them form small steps in the seafloor topography which could be traced through the sedimentary layers. Others are found as small clusters of diffractions within the sediments. These observations point to recent tectonic activities in the area of the NERO site.

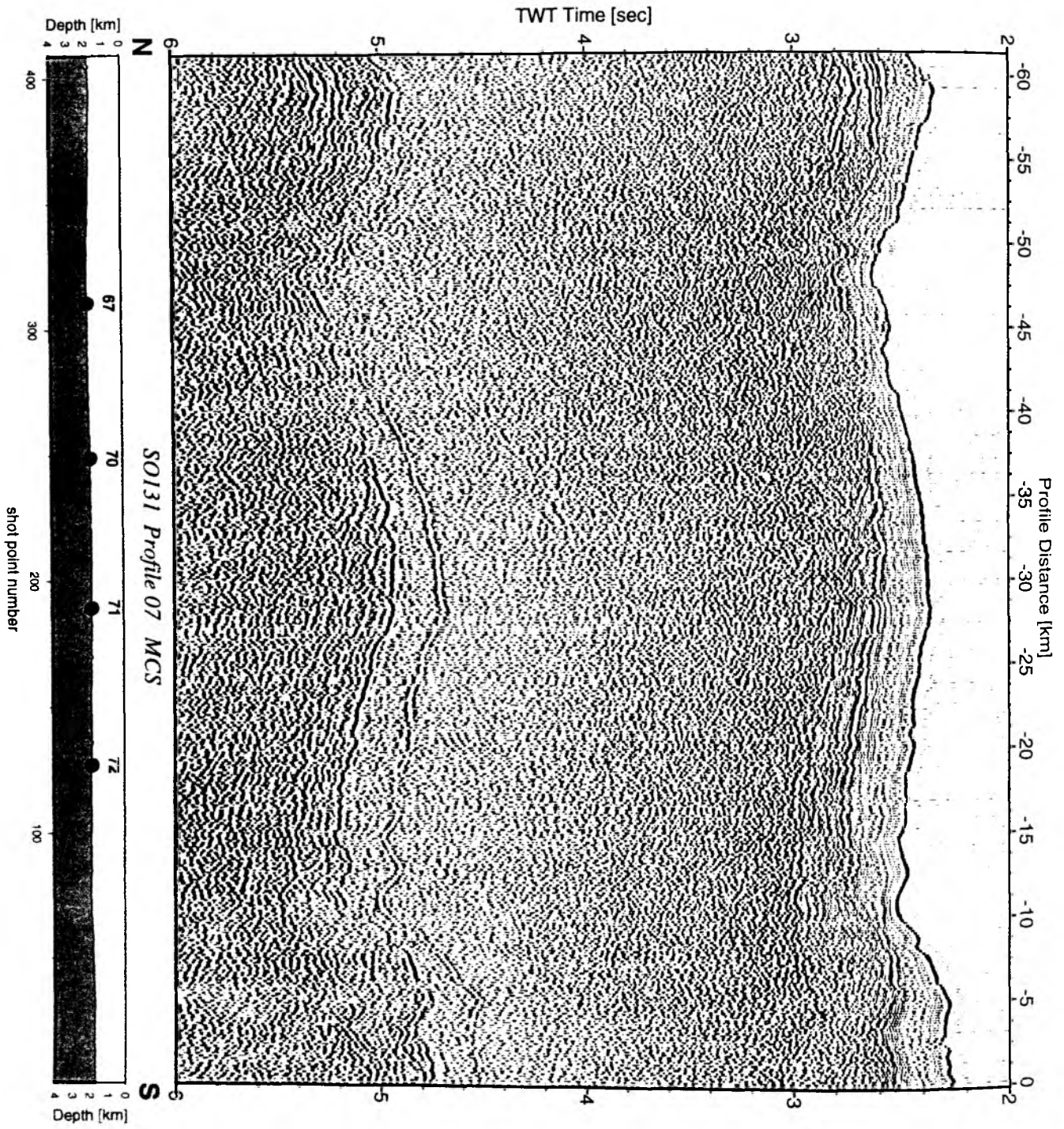

Figure 6.3.4.7.3.2: Seismic section from MCS stack, Profile 07.

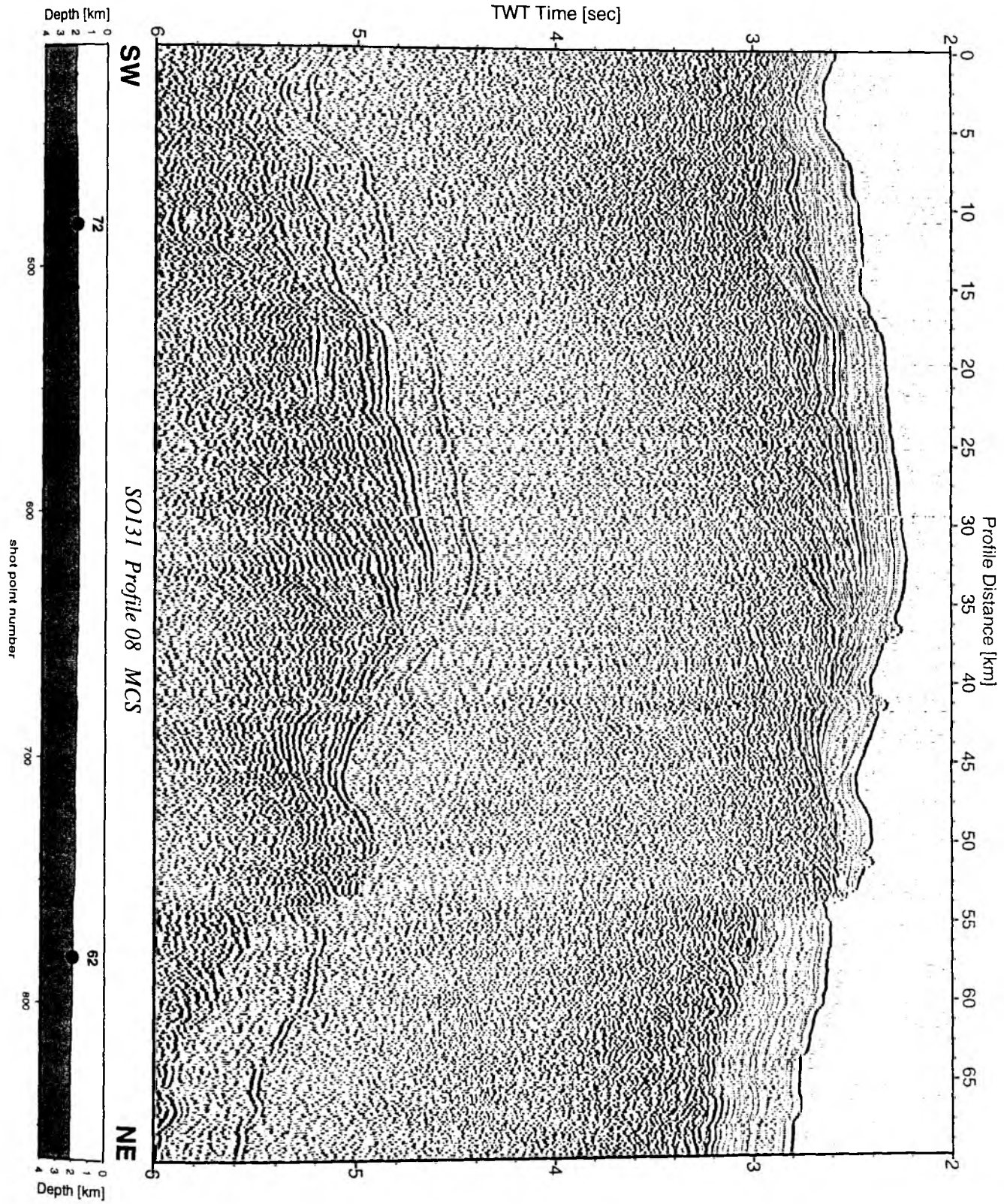

Figure 6.3.4.7.3.3: Seismic section from MCS stack, Profile 08.

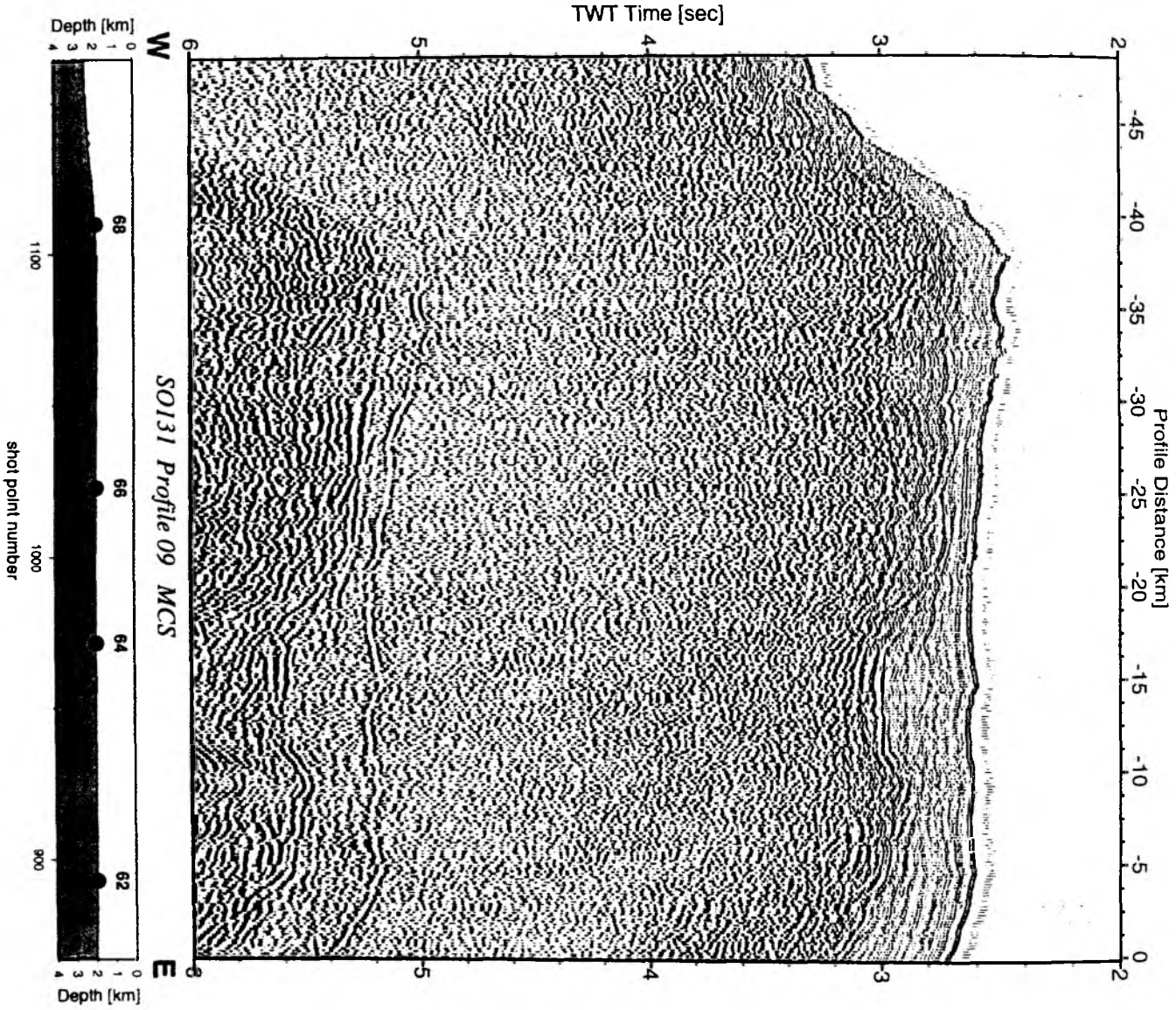

Figure 6.3.4.7.3.4: Seismic section from MCS stack, Profile 09.

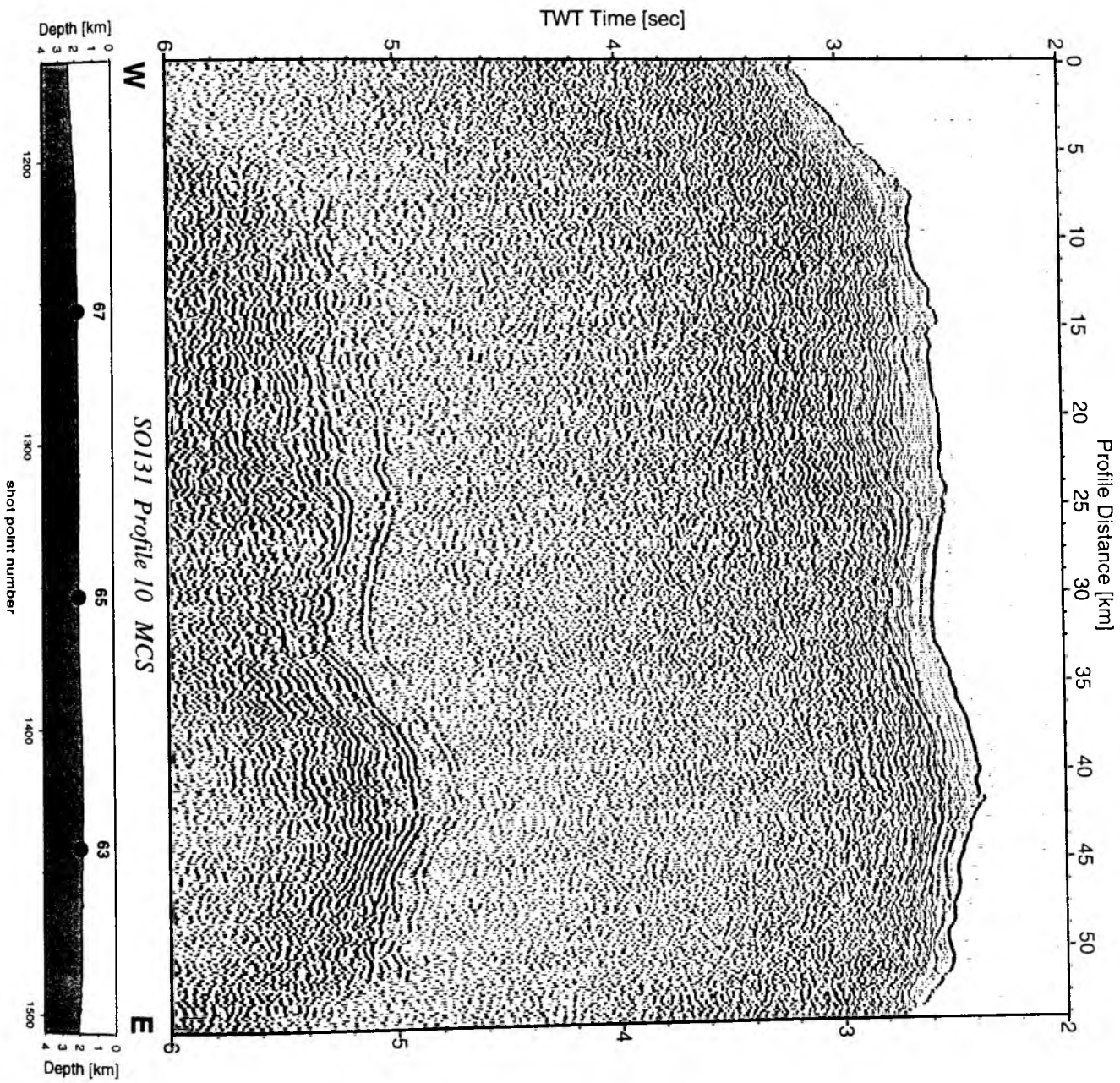

Figure 6.3.4.7.3.5: Seismic section from MCS stack, Profile 10.

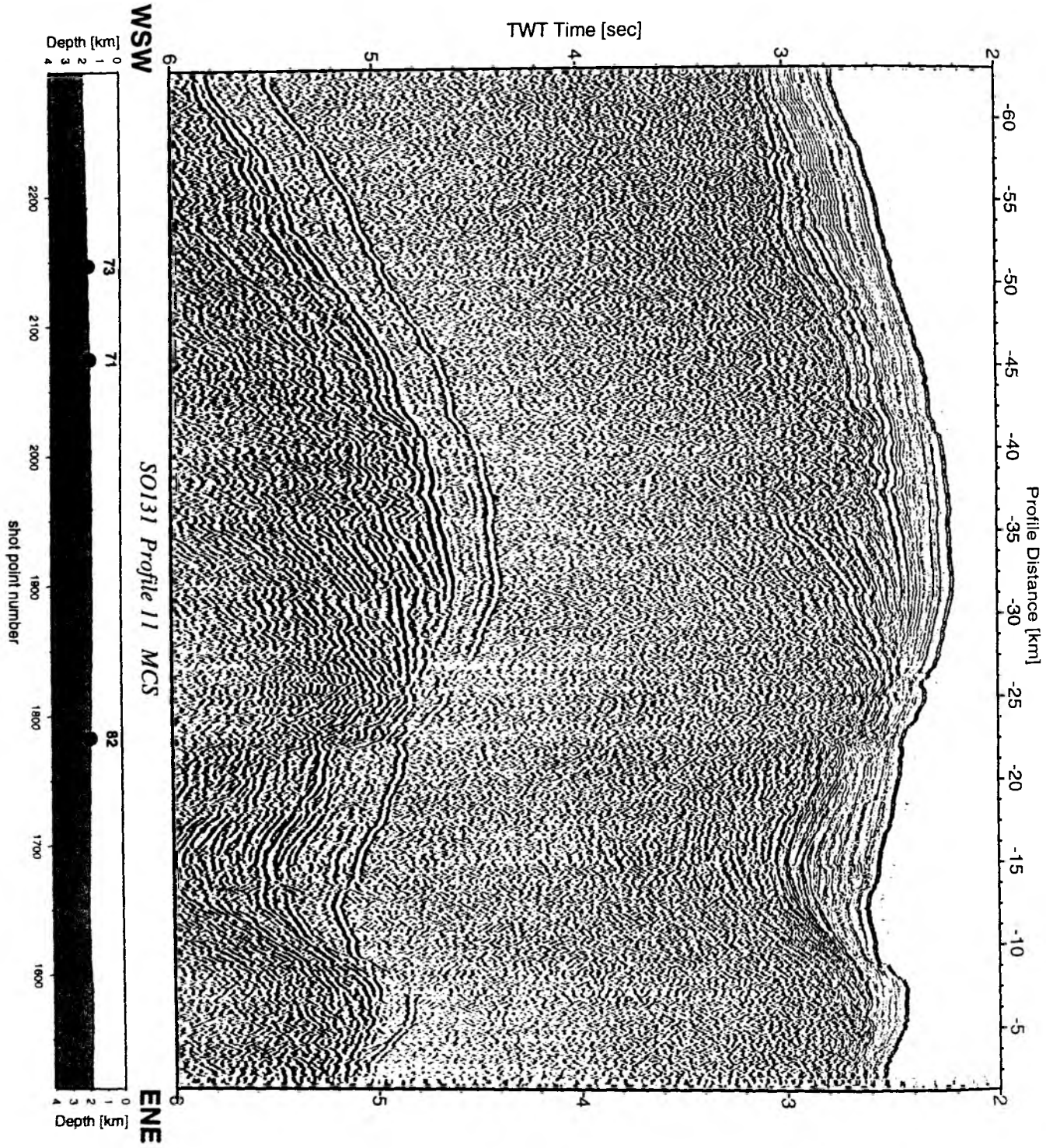

Figure 6.3.4.7.3.6: Seismic section from MCS stack, Profile 11.

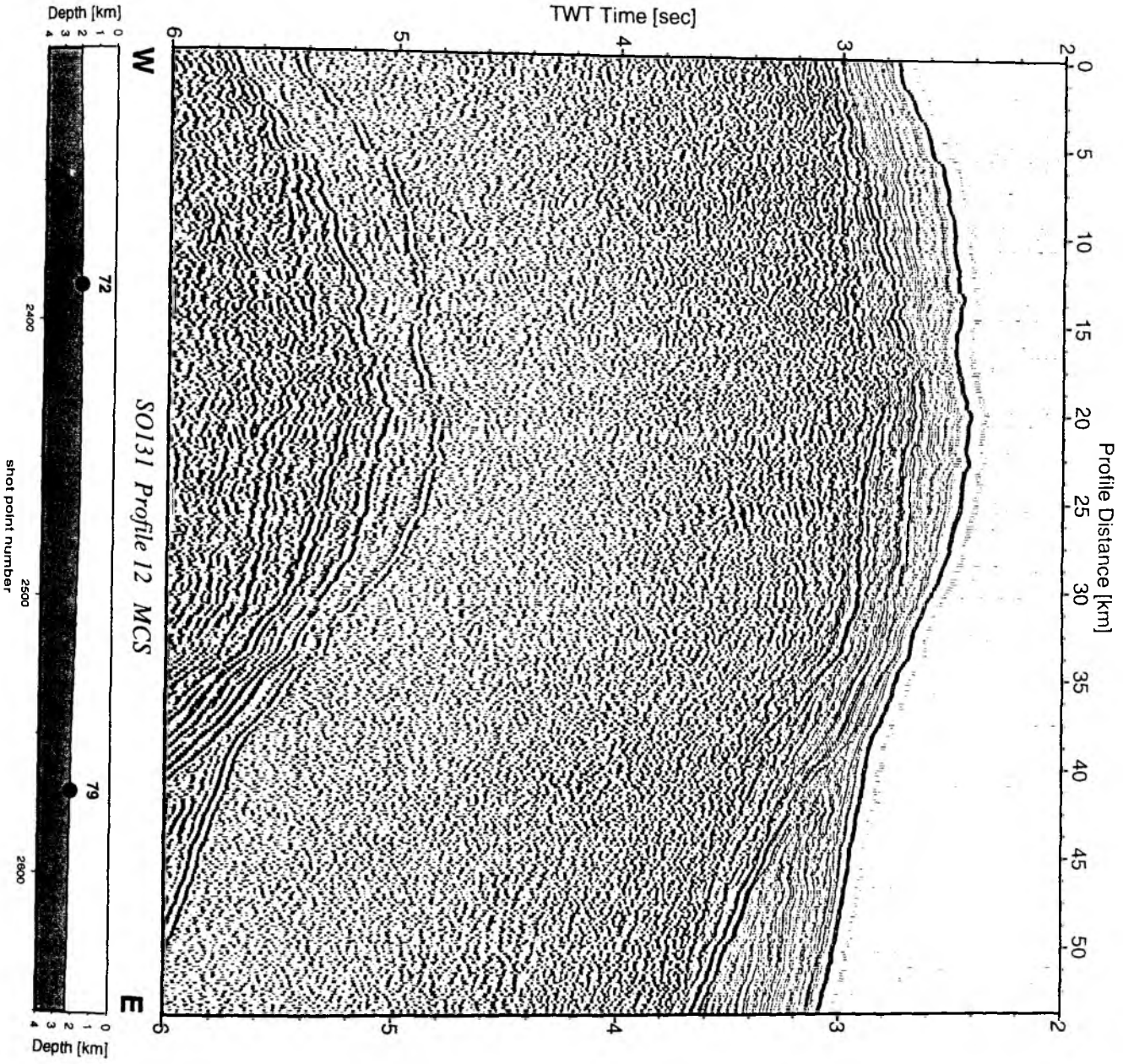

Figure 6.3.4.7.3.7: Seismic section from MCS stack, Profile 12.

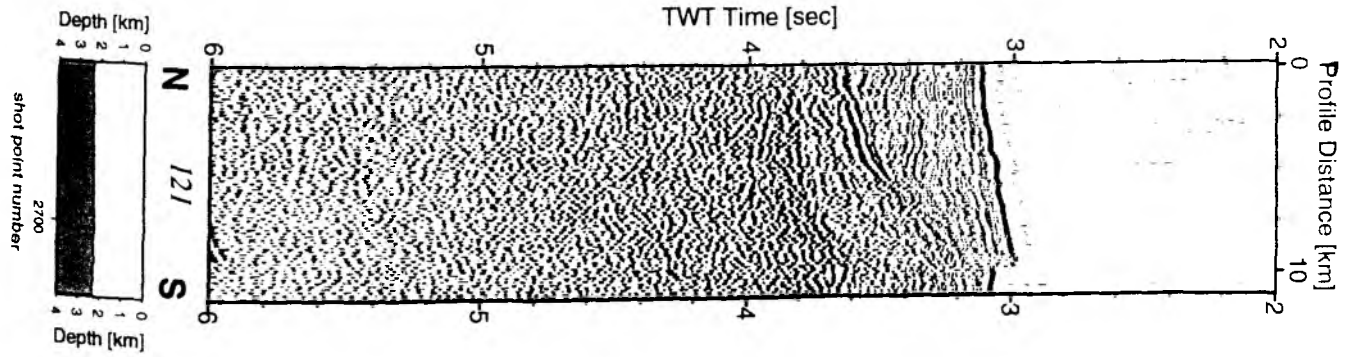

Figure 6.3.4.7.3.8: Seismic section from MCS stack, Profile 121.

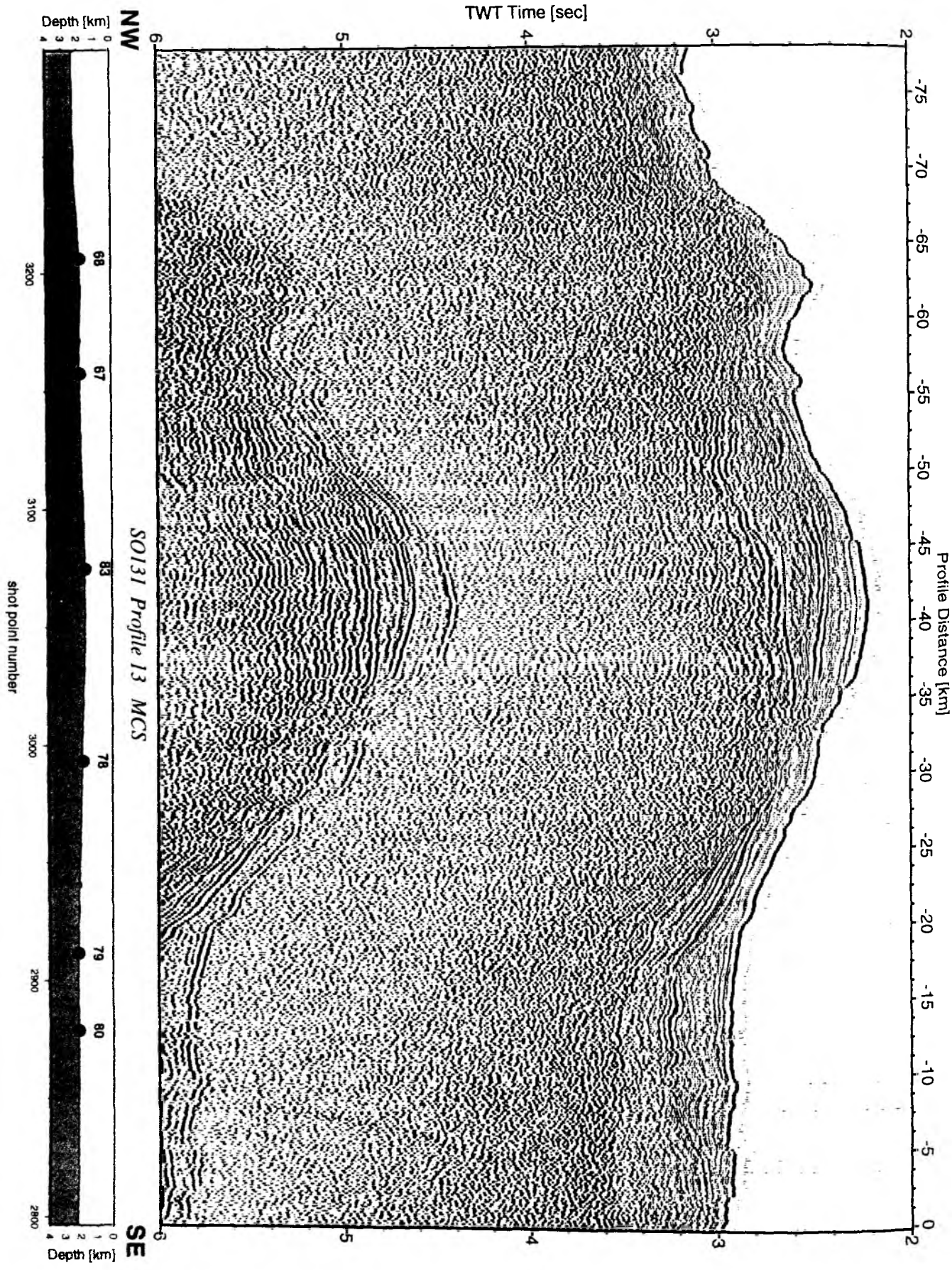

Figure 6.3.4.7.3.9: Seismic section from MCS stack, Profile 13.

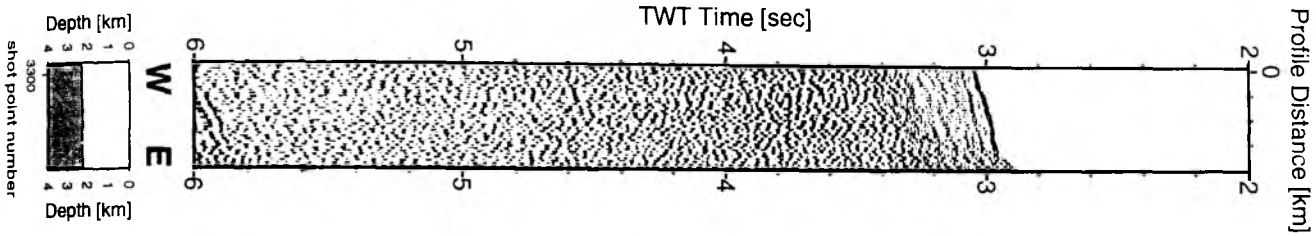

Figure 6.3.4.7.3.9b: Seismic section from MCS stack, Profile 131.

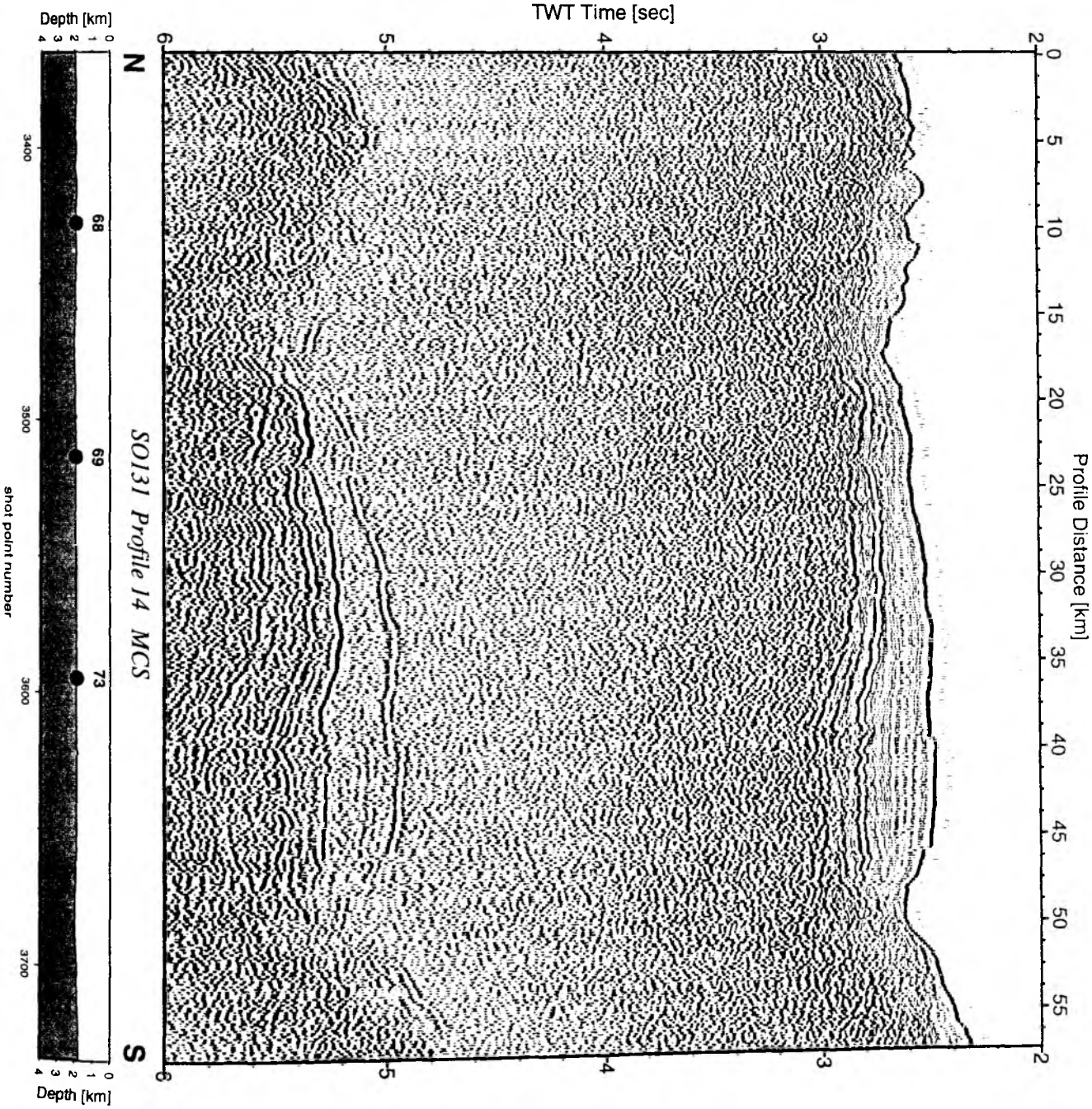

Figure 6.3.4.7.3.10: Seismic section from MCS stack, Profile 14.

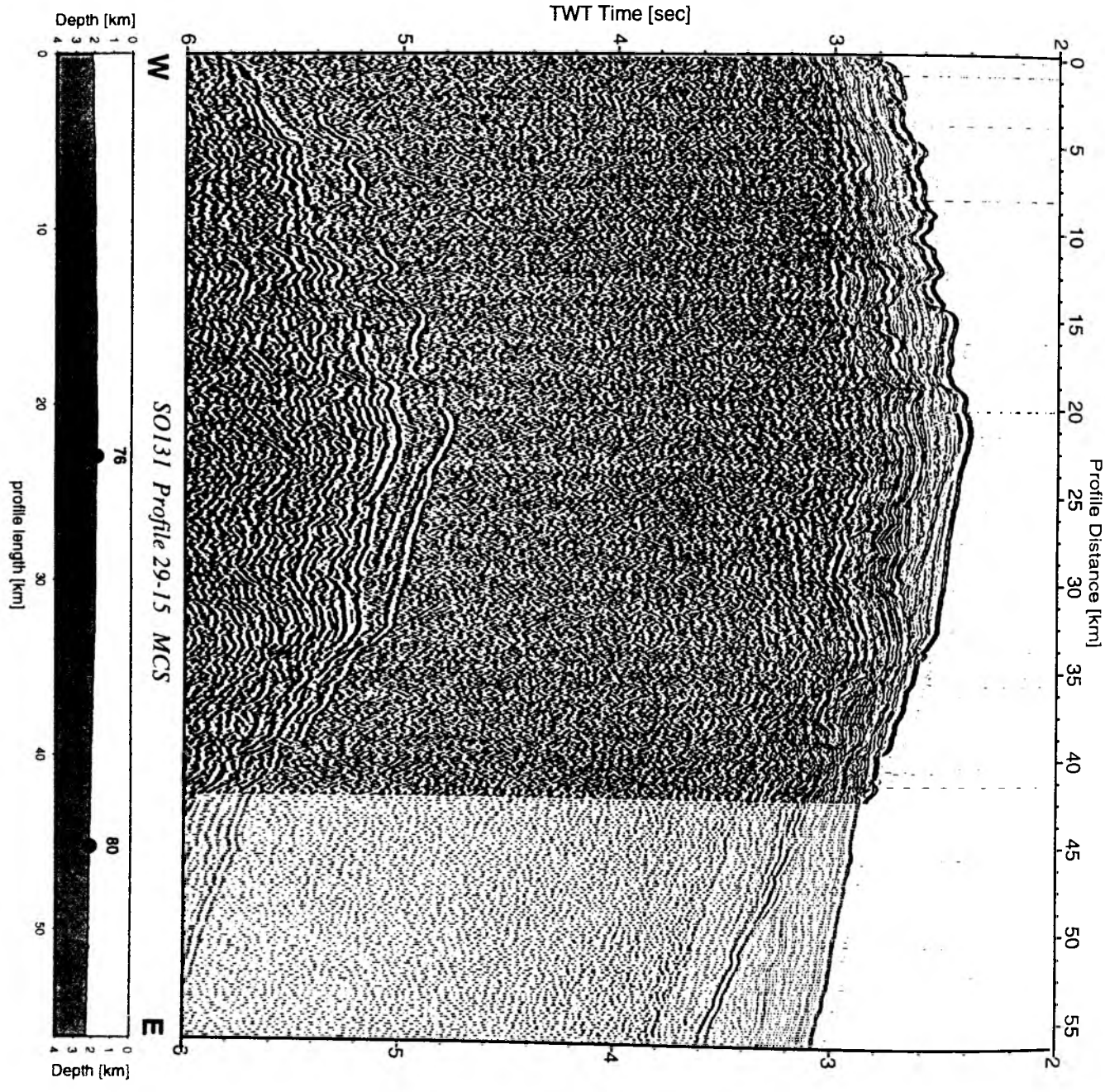

Figure 6.3.4.7.3.11: Seismic section from MCS stack, merge of Profile 29, and 15.

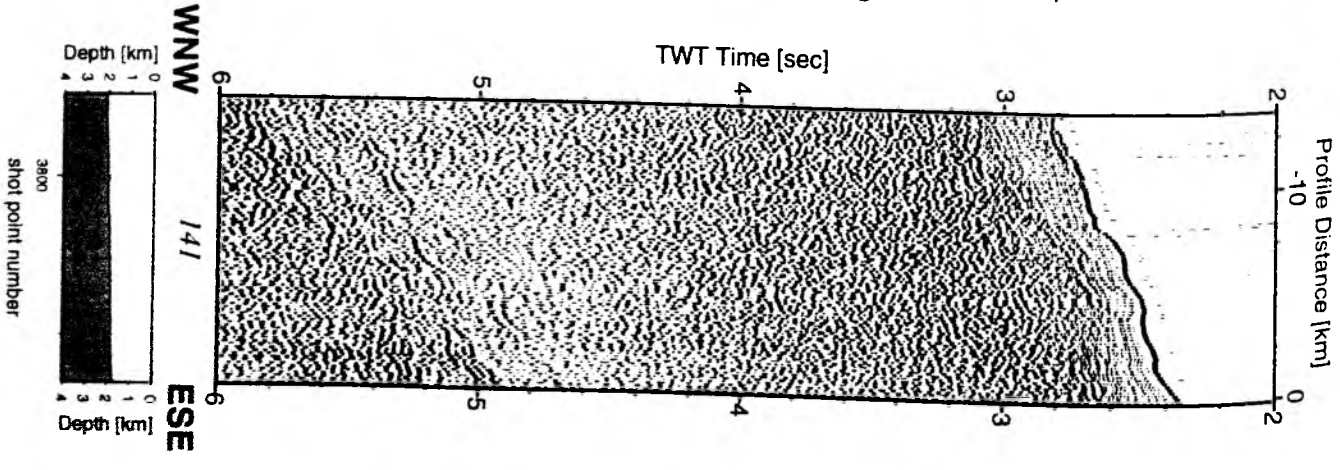

Figure 6.3.4.7.3.12: Seismic section from MCS stack, Profile 141.

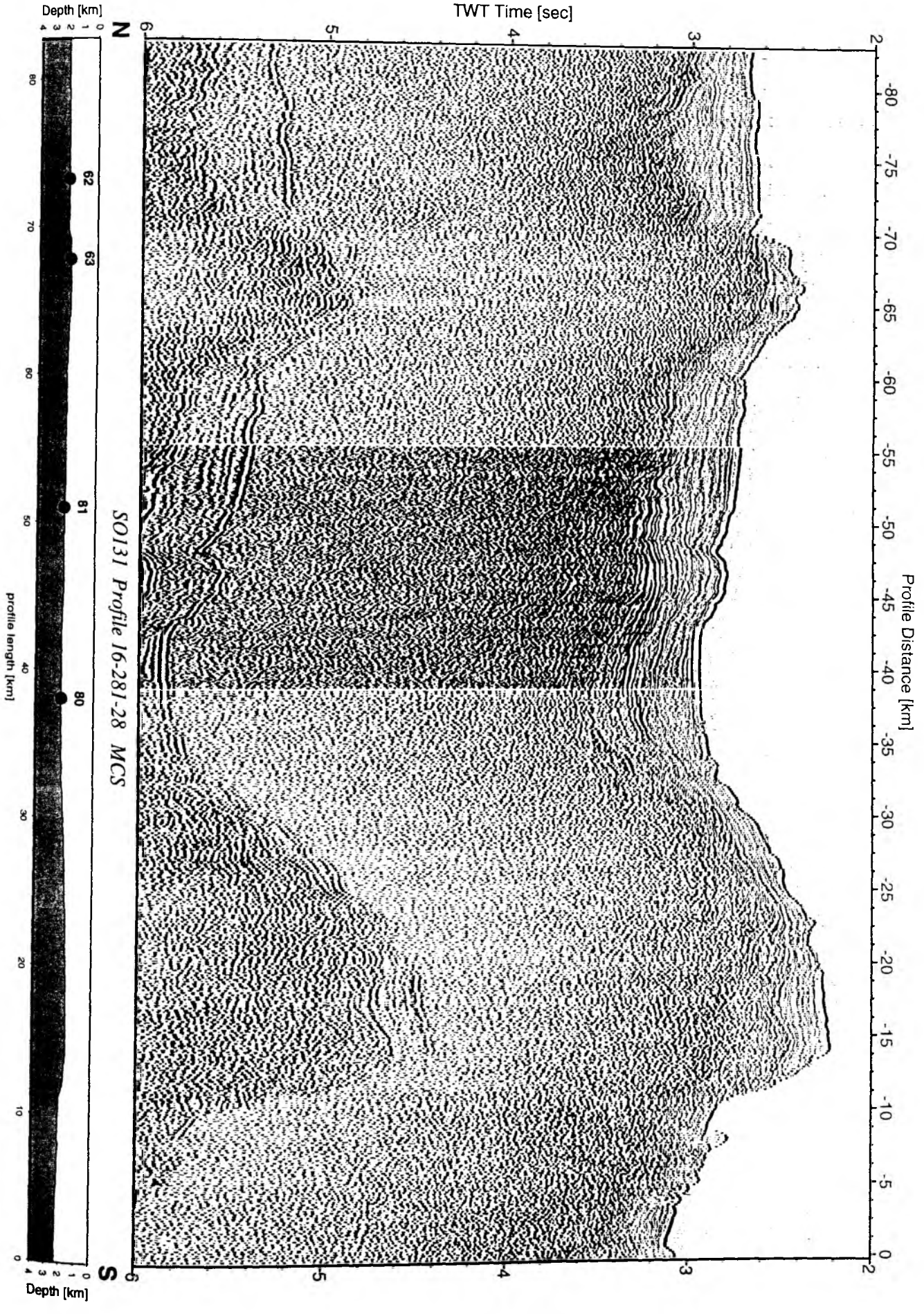

Figure 6.3.4.7.3.13: Seismic section from MCS stack, merge of Profile 16, 281, and 28.

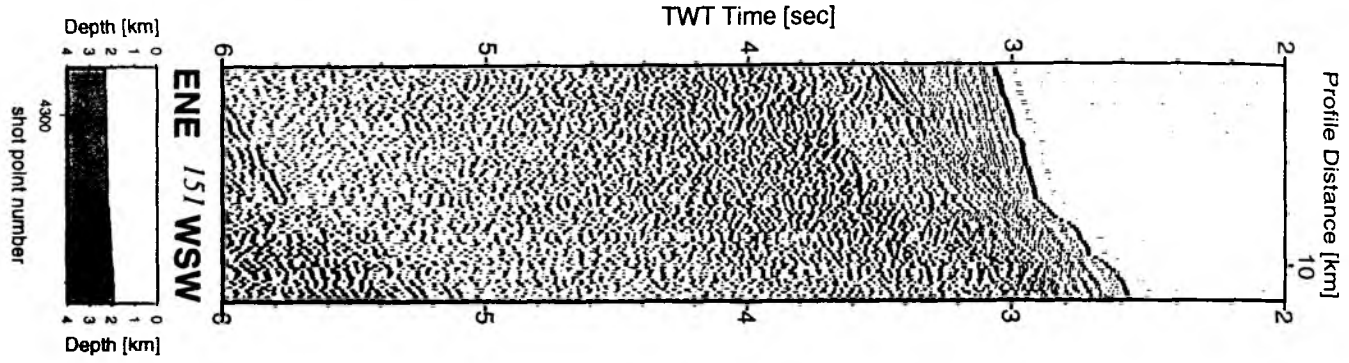

Figure 6.3.4.7.3.14: Seismic section from MCS stack, Profile 151.

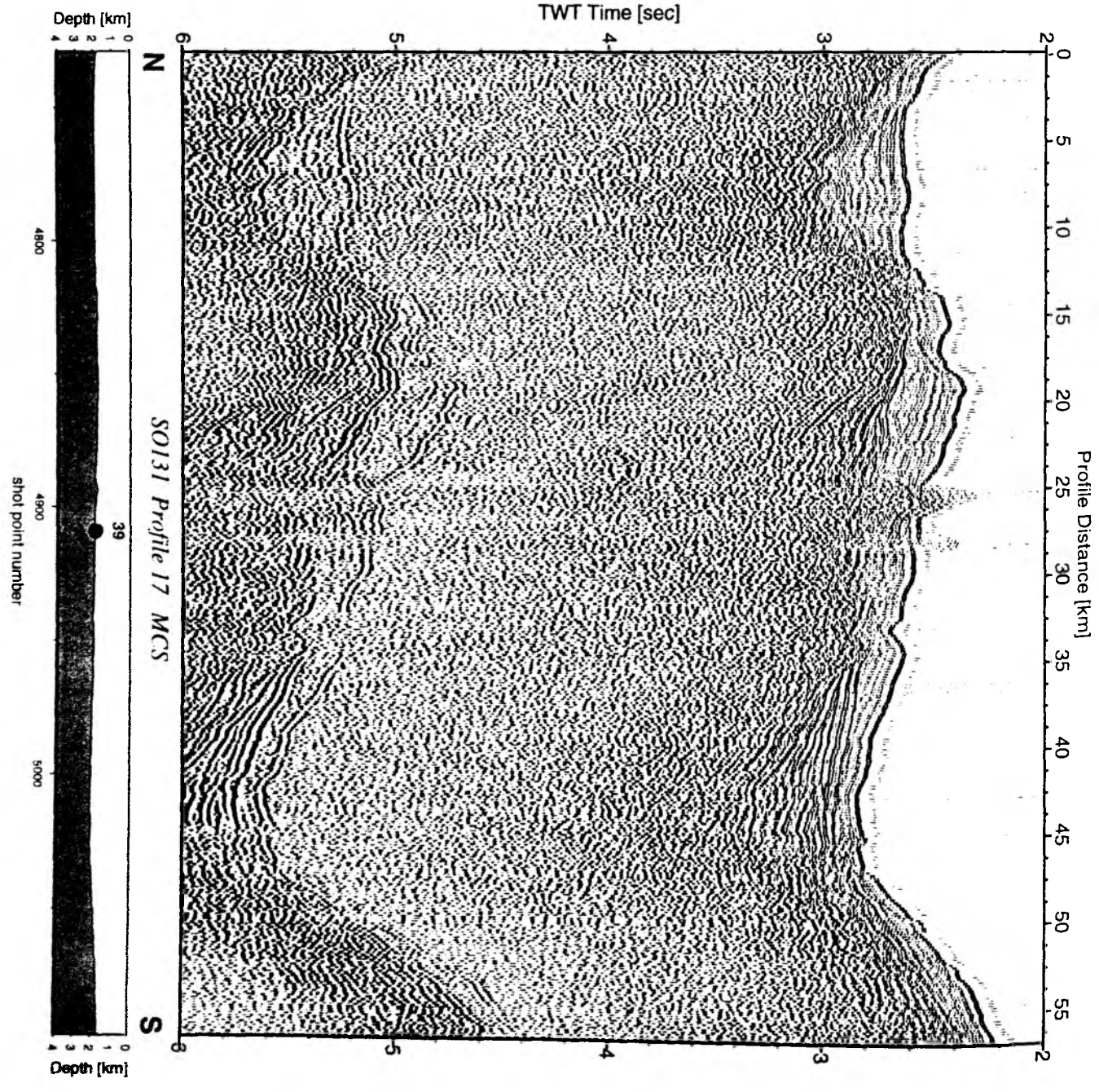

Figure 6.3.4.7.3.15: Seismic section from MCS stack, Profile 17.

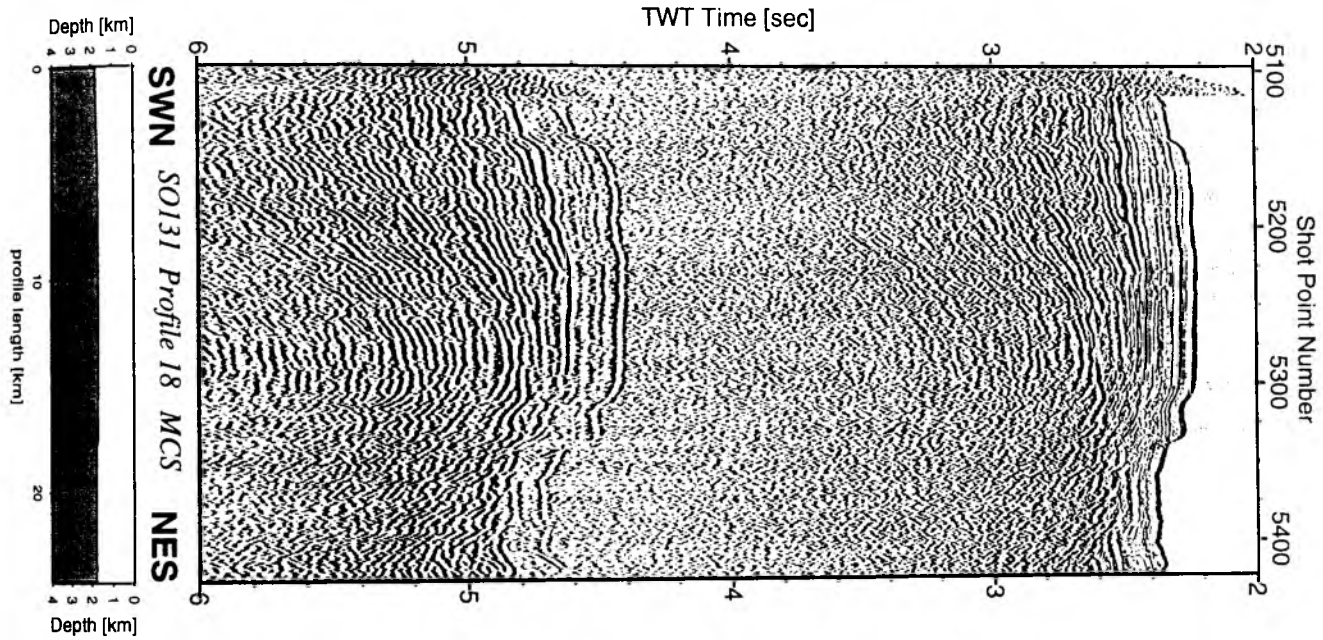

Figure 6.3.4.7.3.16: Seismic section from MCS stack, Profile 18.

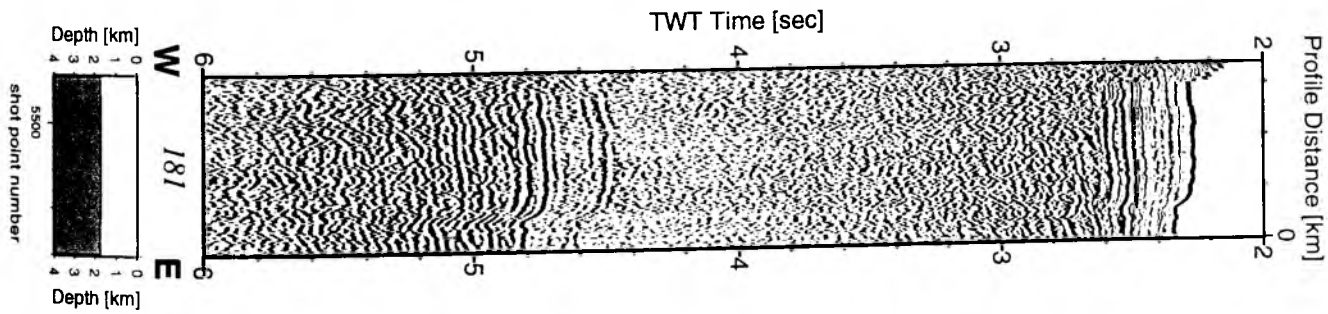

Figure 6.3.4.7.3.17: Seismic section from MCS stack, Profile 181.

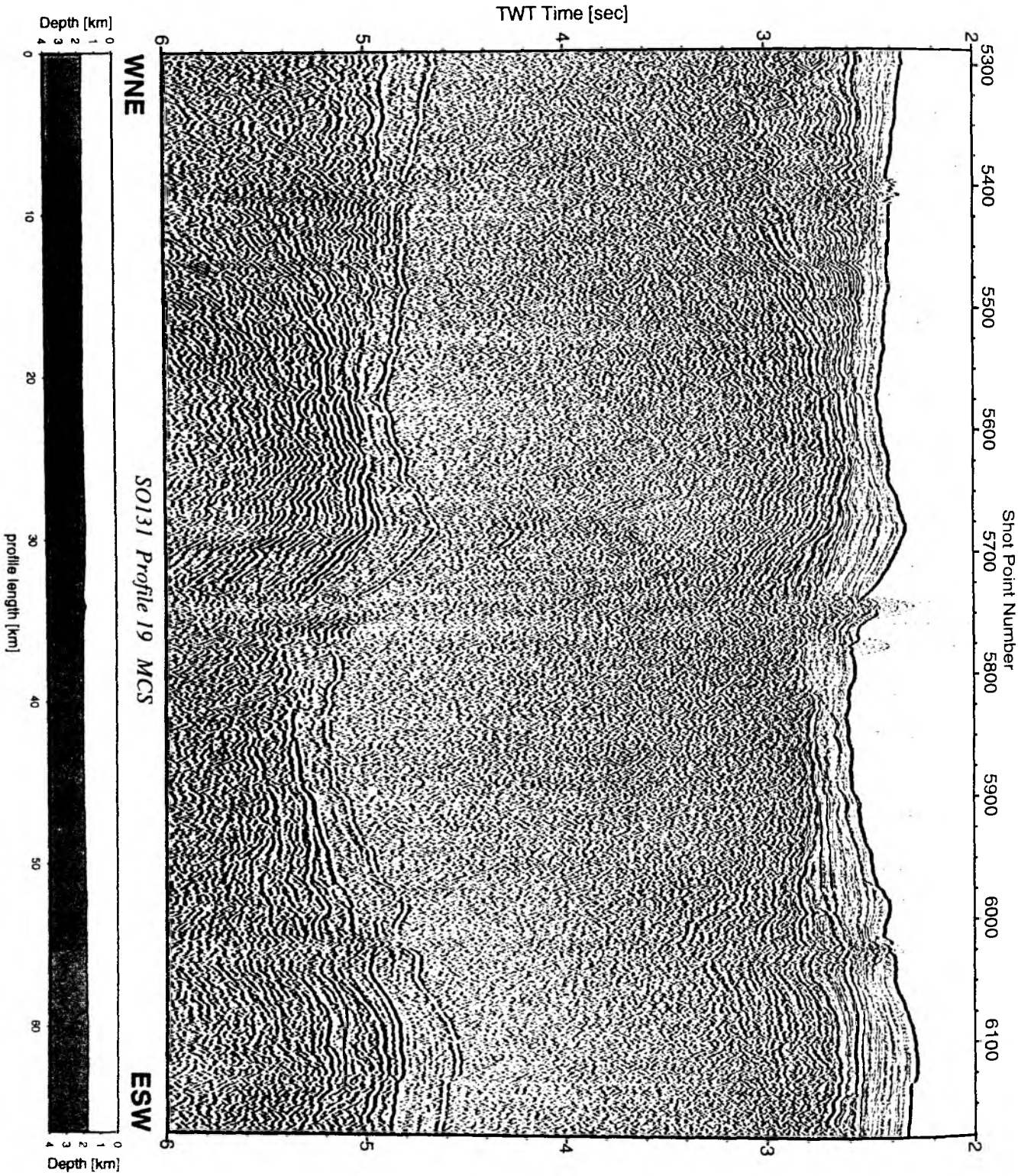

Figure 6.3.4.7.3.18: Seismic section from MCS stack, Profile 19.

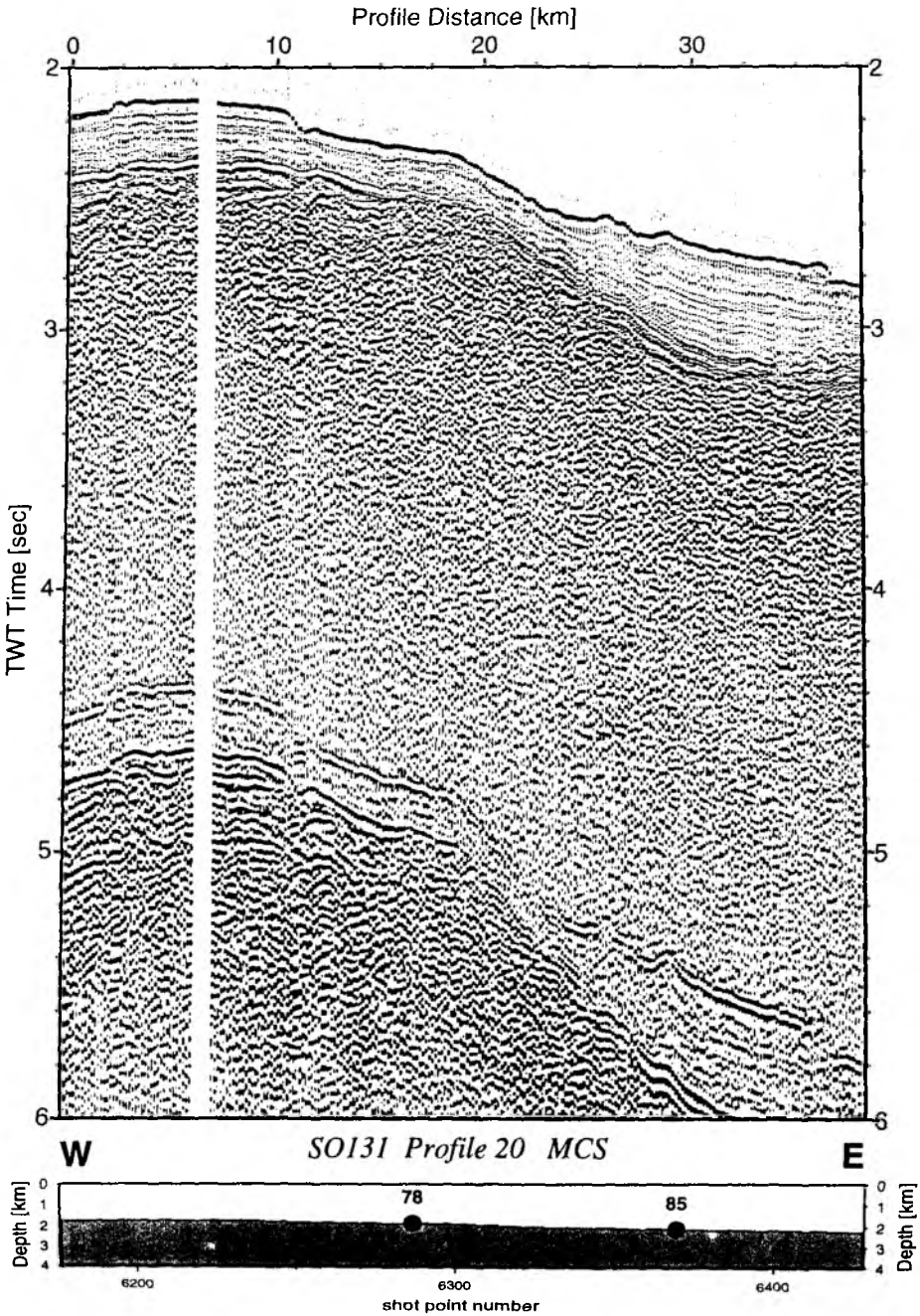
Profile Distance [km]
0
10
20
30
TWT Time [sec]
2
3
4
5
6
W
SO131 Profile 20 MCS
E
Depth [km]
0
1
2
3
4
78
85
6200
6300
6400
shot point number

Figure 6.3.4.7.3.19: Seismic section from MCS stack, Profile 20.

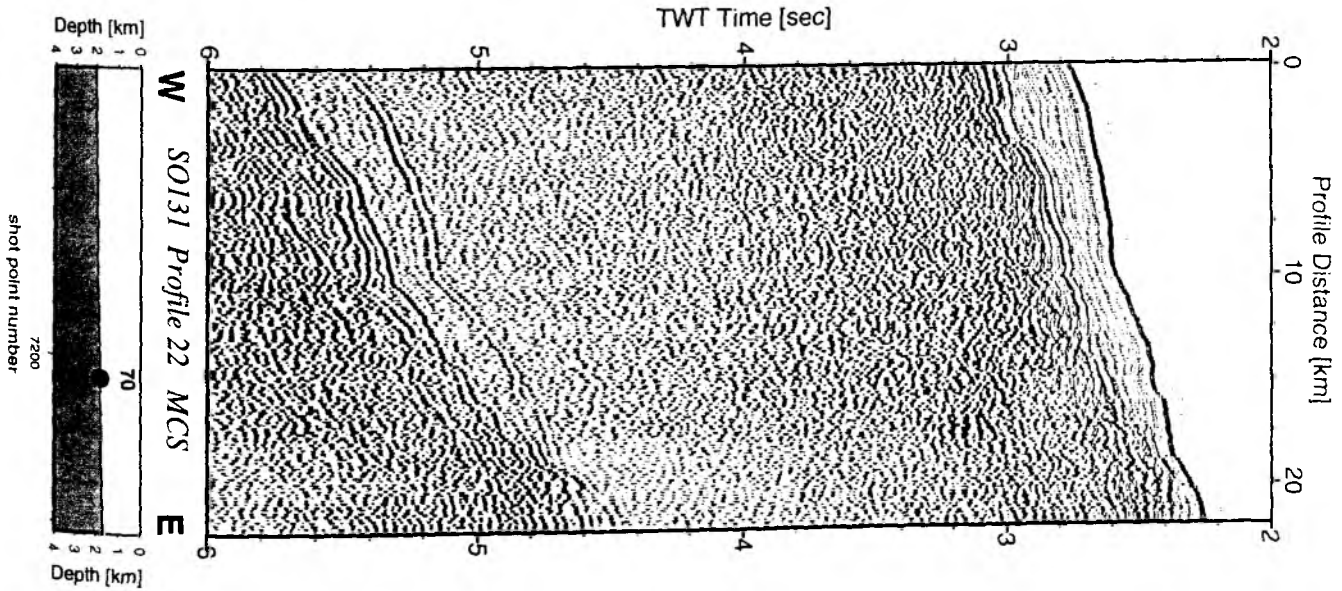

Figure 6.3.4.7.3.20: Seismic section from MCS stack, Profile 22.

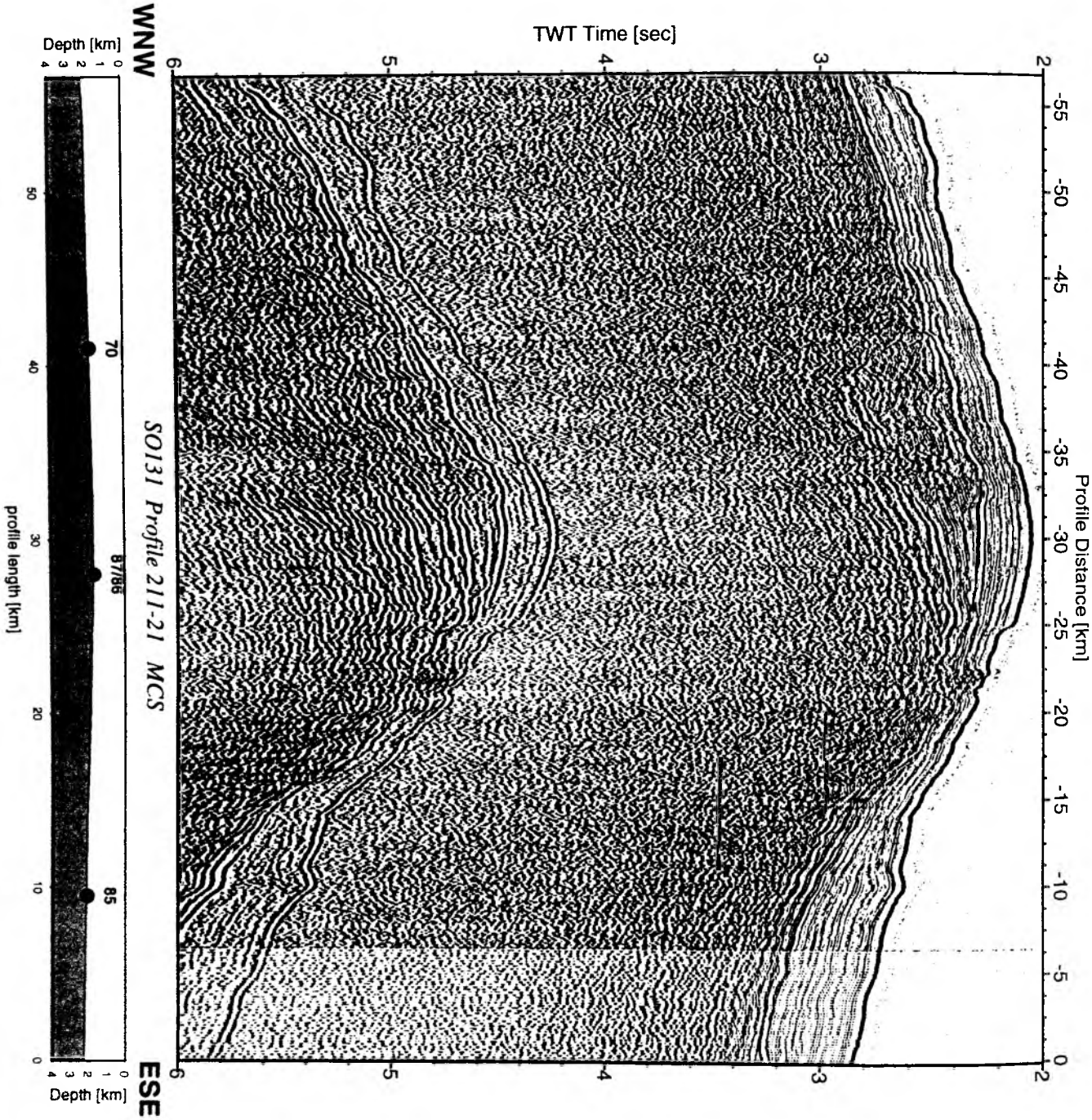

Figure 6.3.4.7.3.21: Seismic section from MCS stack, merge of Profile 211. 21.

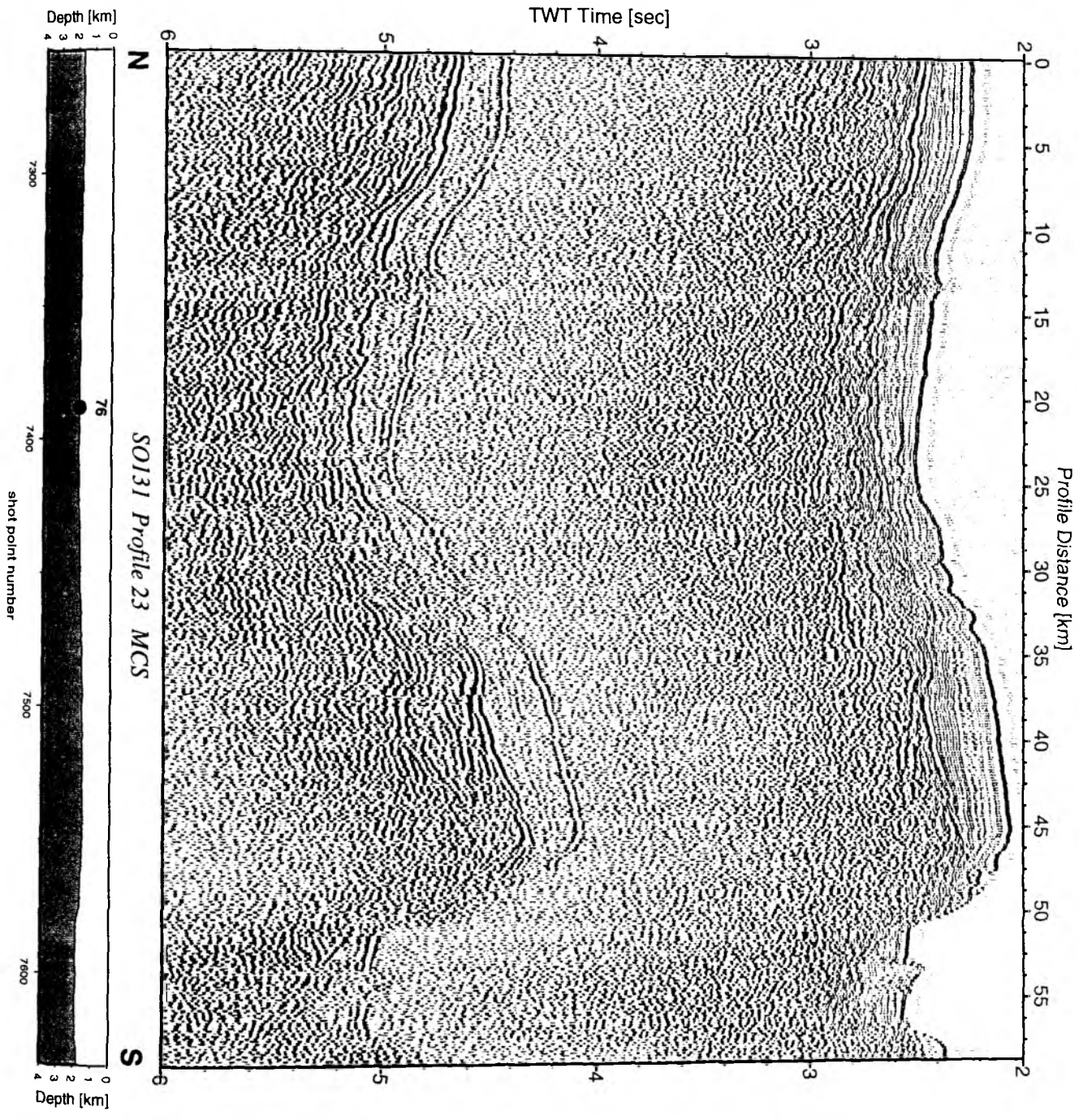

Figure 6.3.4.7.3.22: Seismic section from MCS stack, Profile 23.

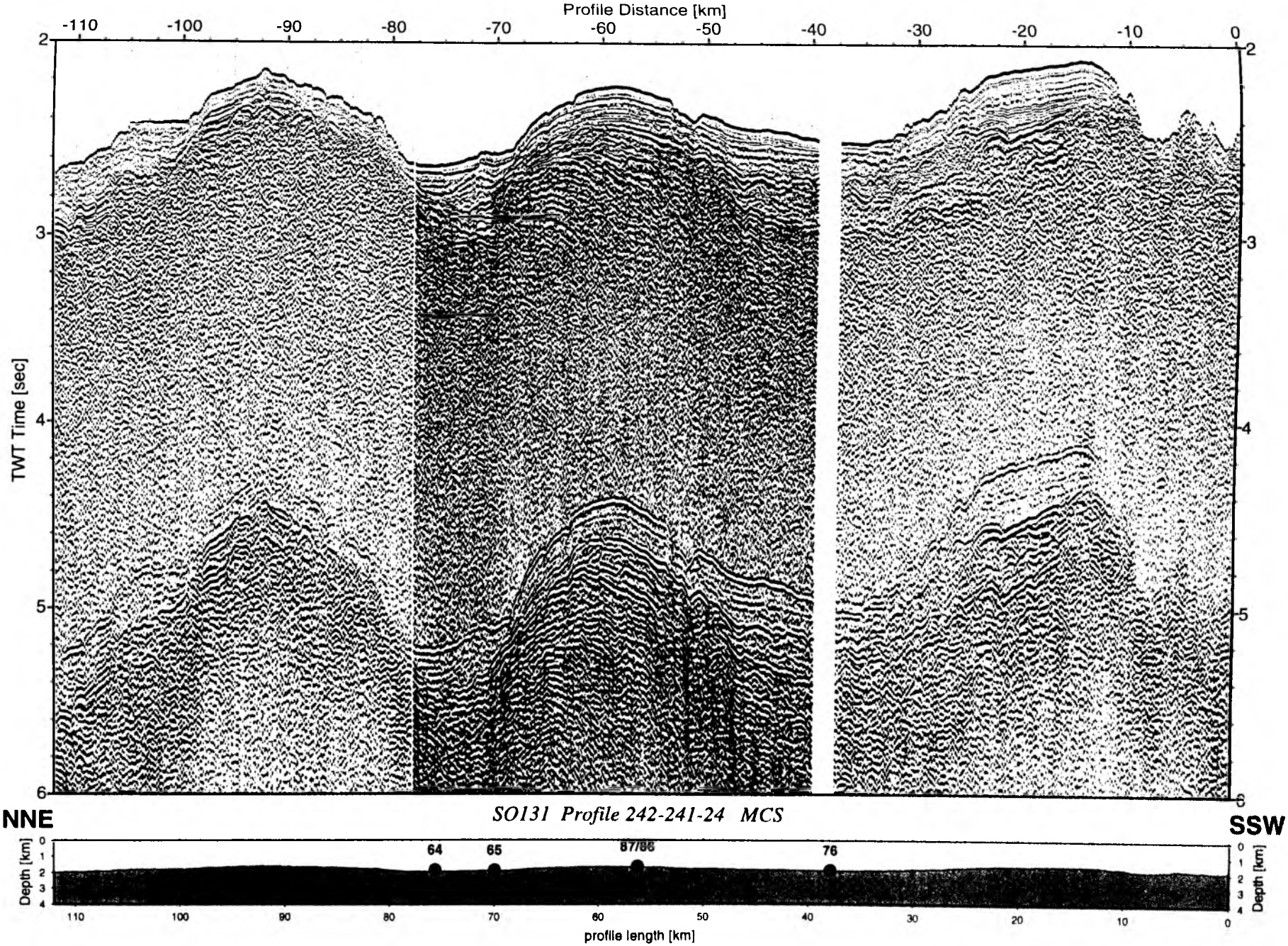

Figure 6.3.4.7.3.23: Seismic section from MCS stack, merge of Profile 242, 241, and 24.

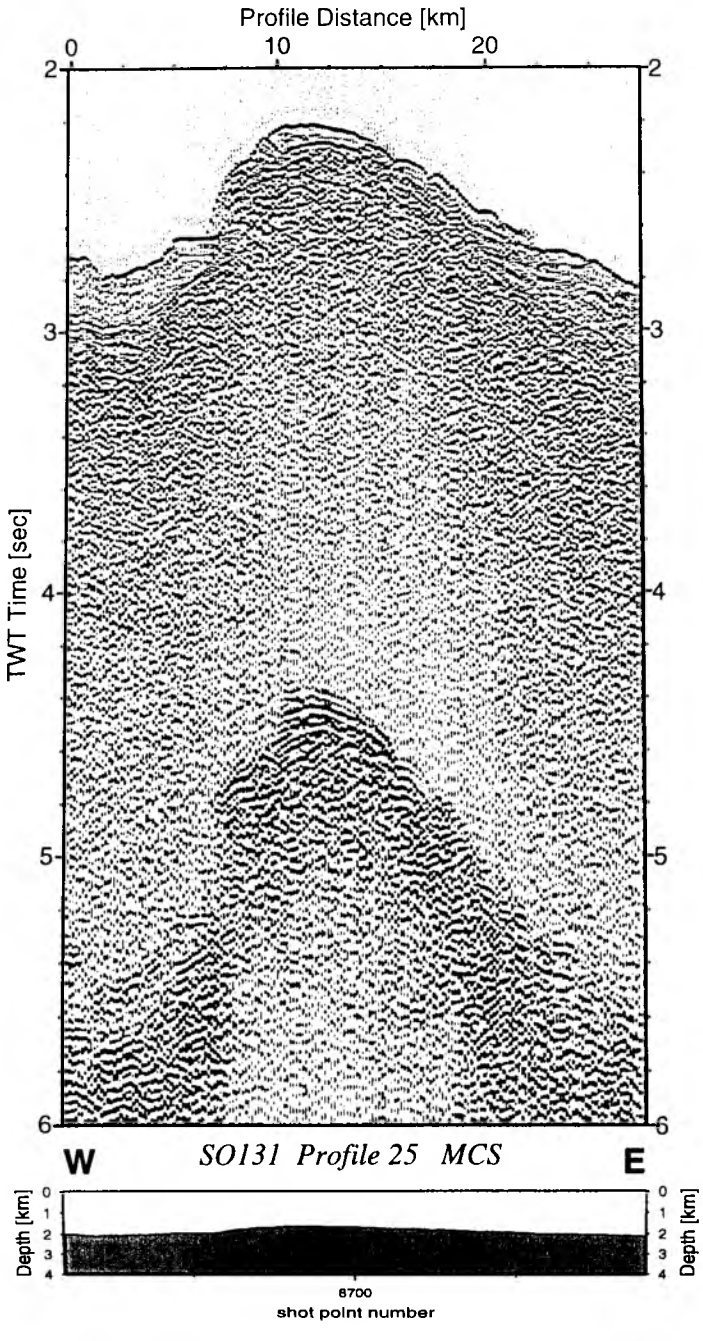
Profile Distance [km]
0
10
20
2
3
4
5
6
TWT Time [sec]
W
SO131 Profile 25 MCS
E
Depth [km]
0
1
2
3
4
6700
shot point number

Figure 6.3.4.7.3.24: Seismic section from MCS stack, Profile 25.

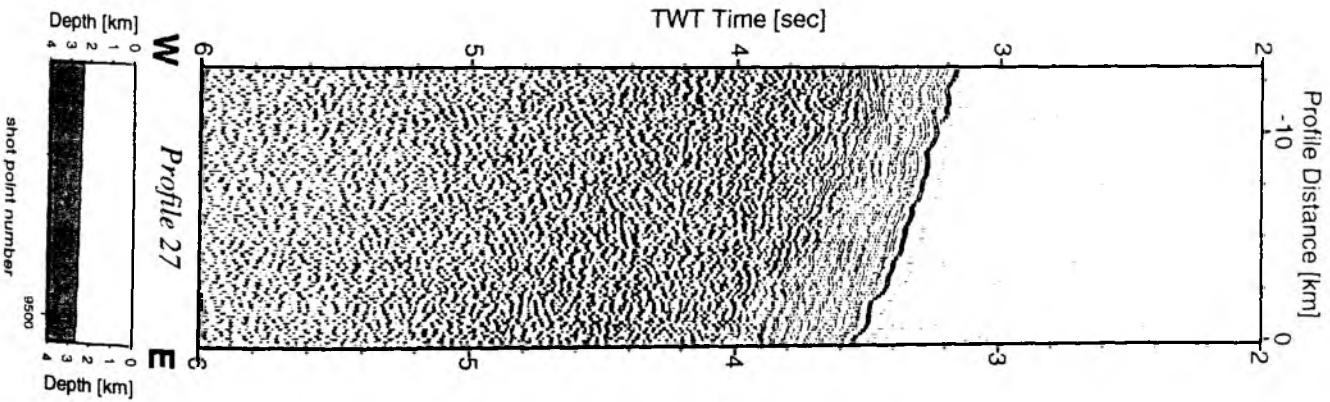

Figure 6.3.4.7.3.25: Seismic section from MCS stack, Profile 27.

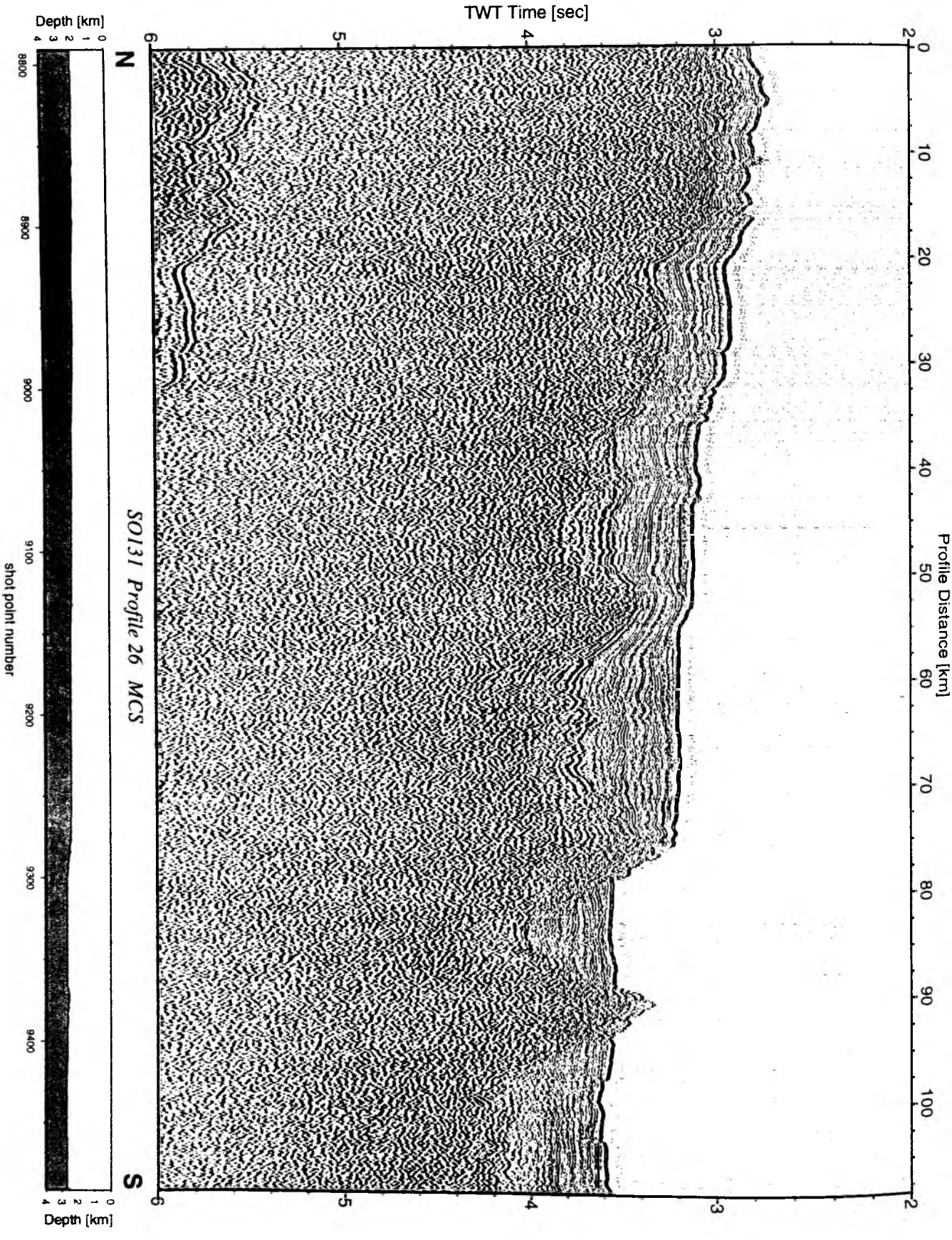

Figure 6.3.4.7.3.26: Seismic section from MCS stack, Profile 26.

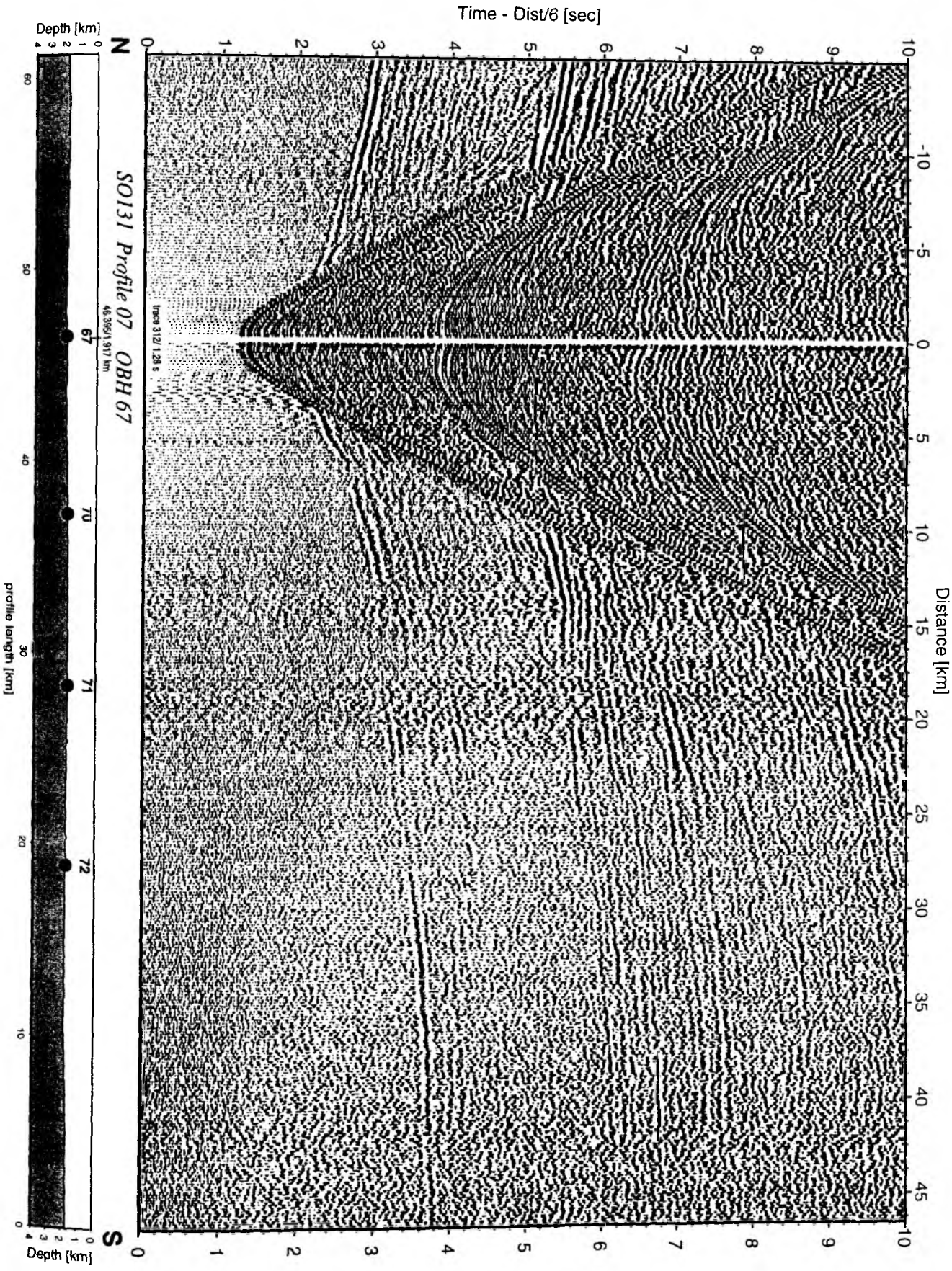

Figure 6.3.4.7.3.27: Record section from OBH 67 , Profile 07.

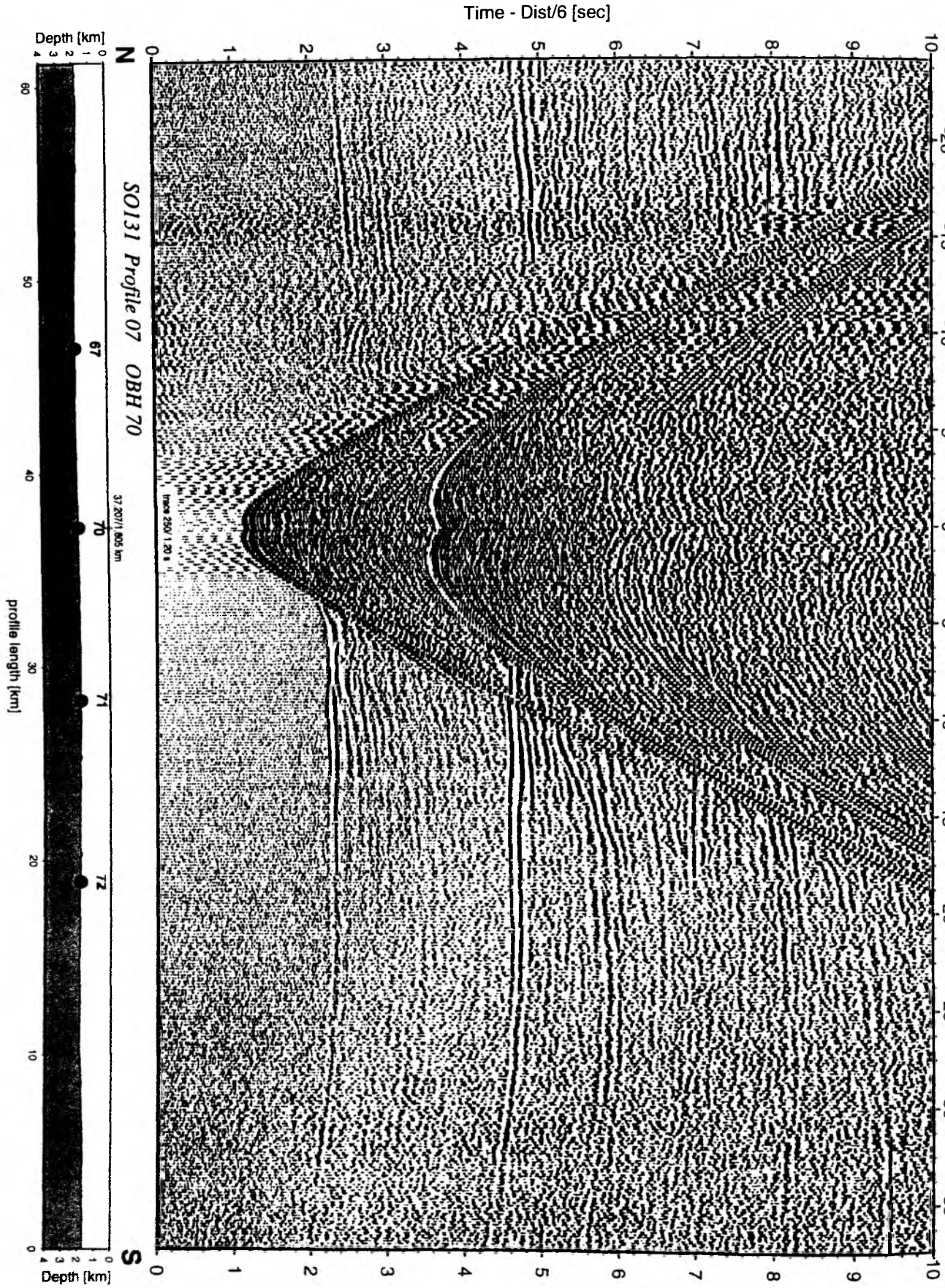

Figure 6.3.4.7.3.28: Record section from OBH 70 , Profile 07.

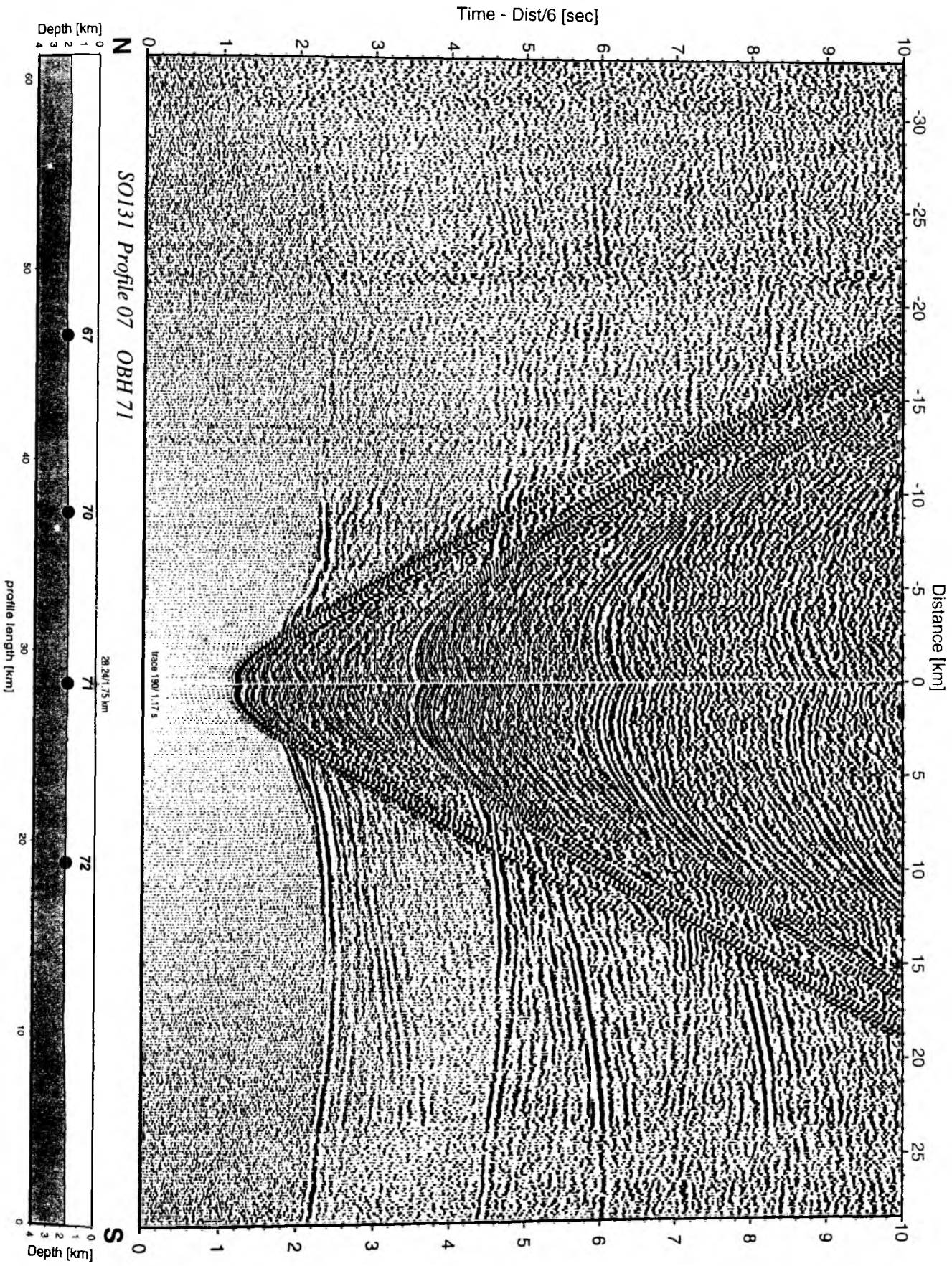

Figure 6.3.4.7.3.29: Record section from OBH 71 , Profile 07.

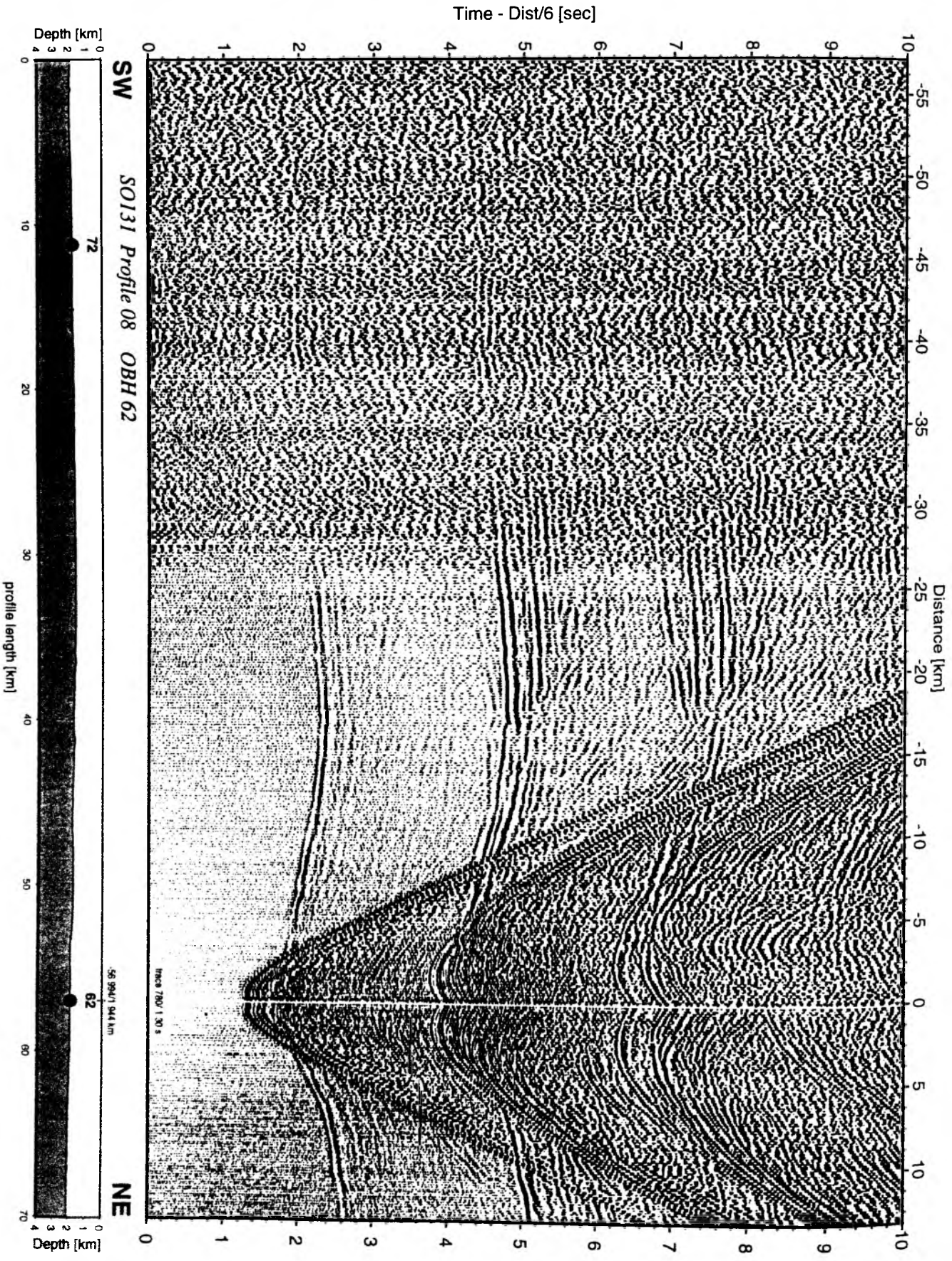

Figure 6.3.4.7.3.30: Record section from OBH 62 , Profile 08.

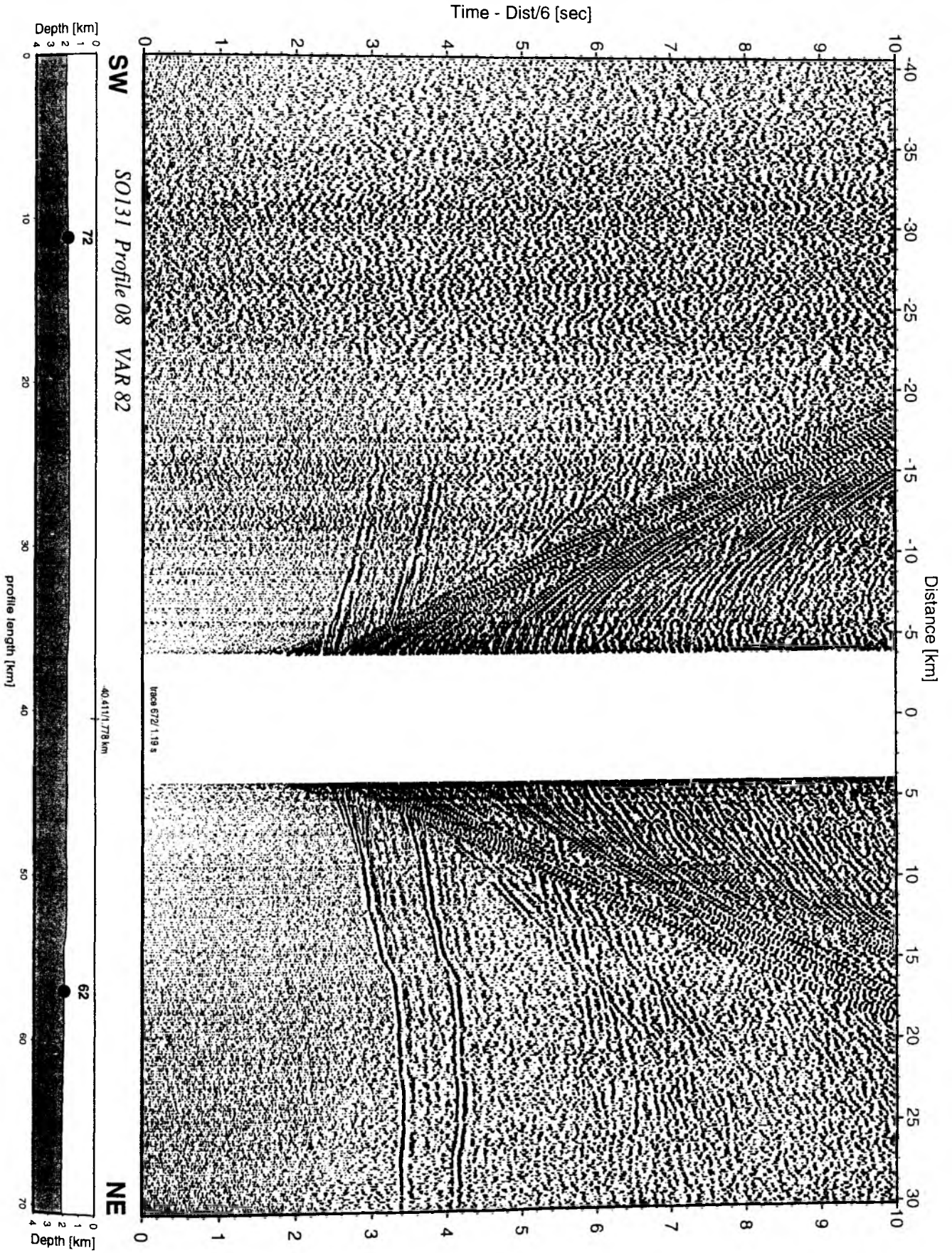

Figure 6.3.4.7.3.31: Record section from VAR 82 channel_1, Profile 08.

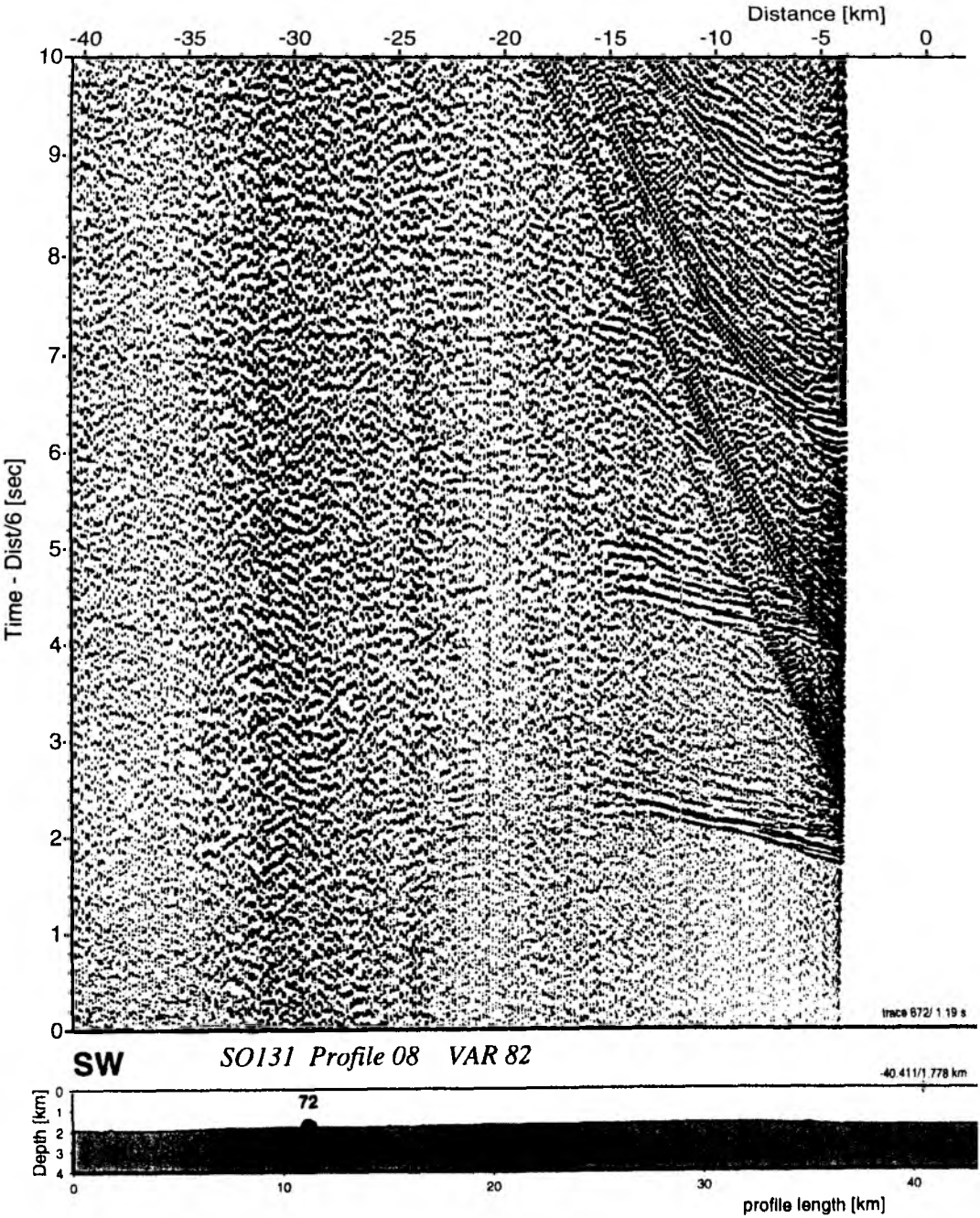
Distance [km]
-40
-35
-30
-25
-20
-15
-10
-5
0
Time - Dist/6 [sec]
10
9
8
7
6
5
4
3
2
1
0
trace 672/ 1.19 s
SW
SO131 Profile 08 VAR 82
-40.411/1.778 km
Depth [km]
0
1
2
3
4
72
0
10
20
30
40
profile length [km]

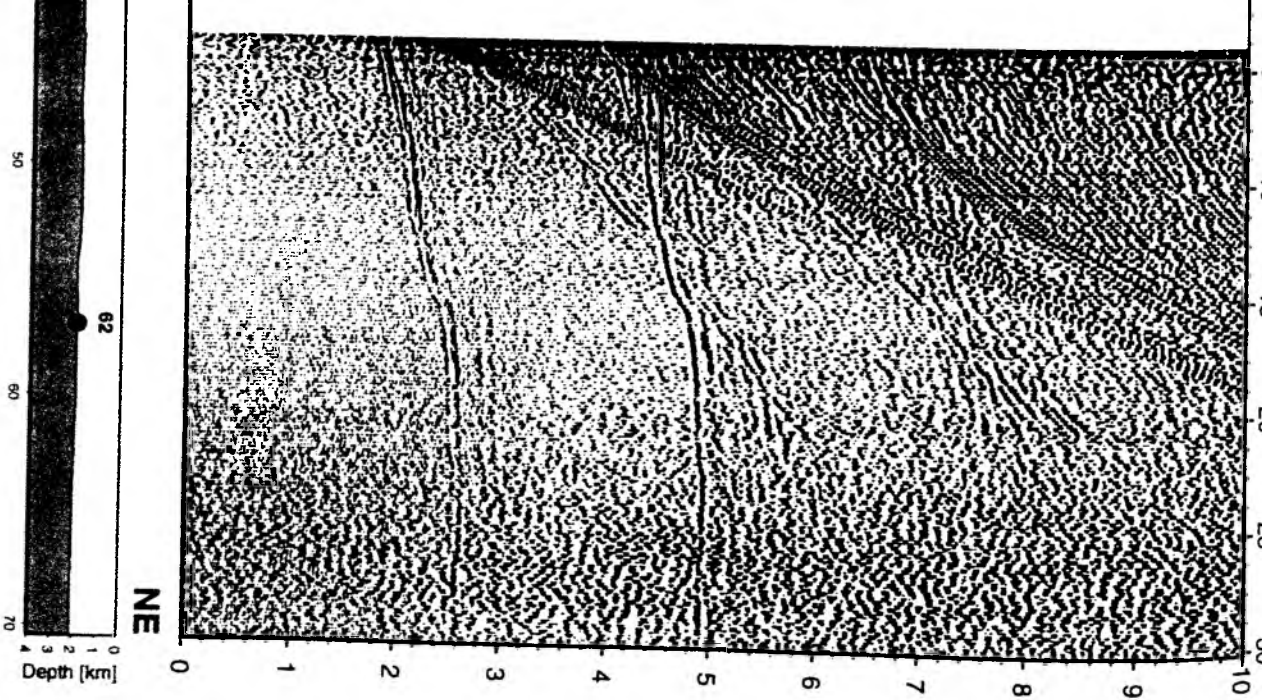

Figure 6.3.4.7.3.32: Record section from VAR 82 channel_3, Profile 08.

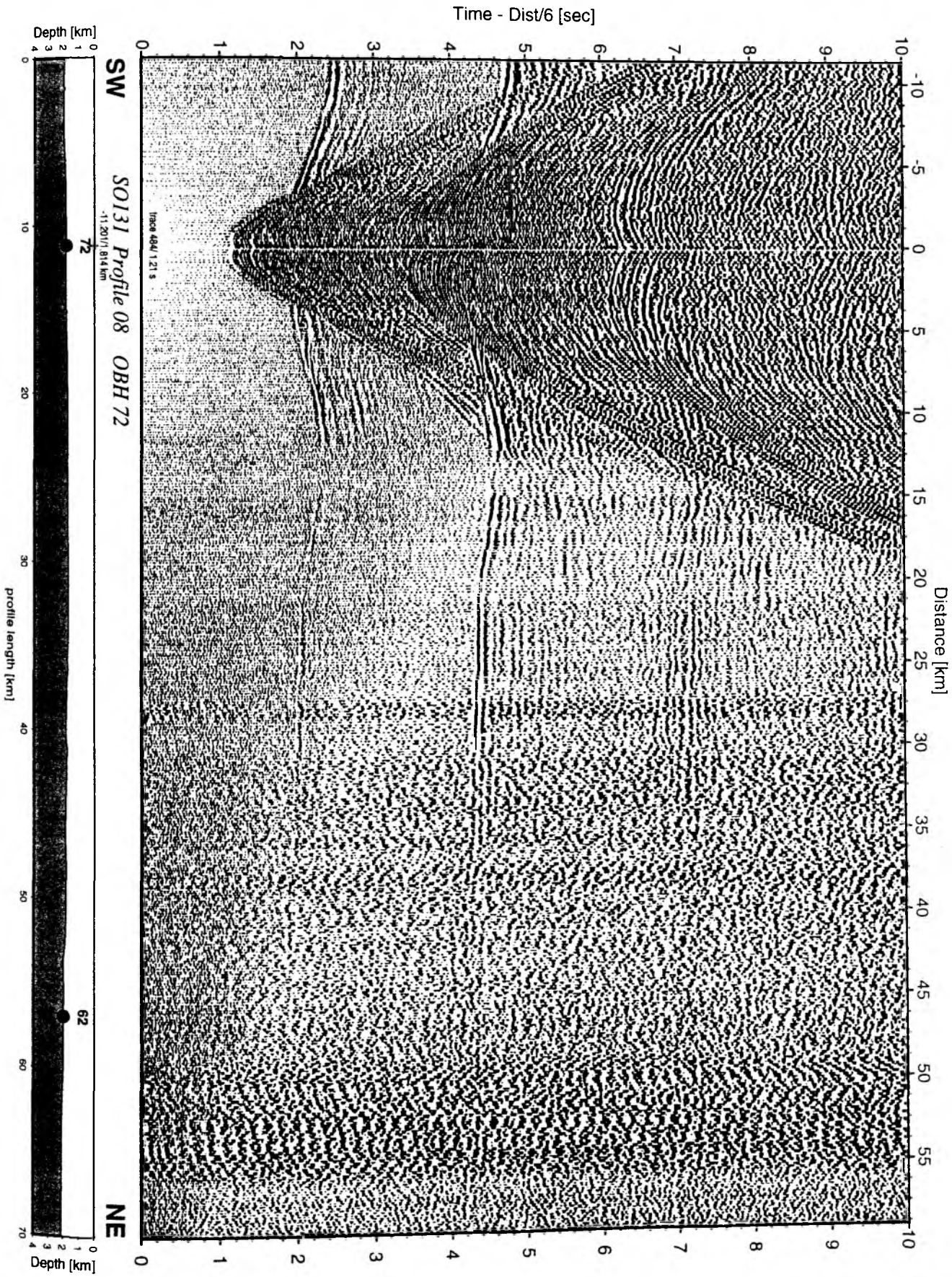

Figure 6.3.4.7.3.33: Record section from OBH 72 , Profile 08.

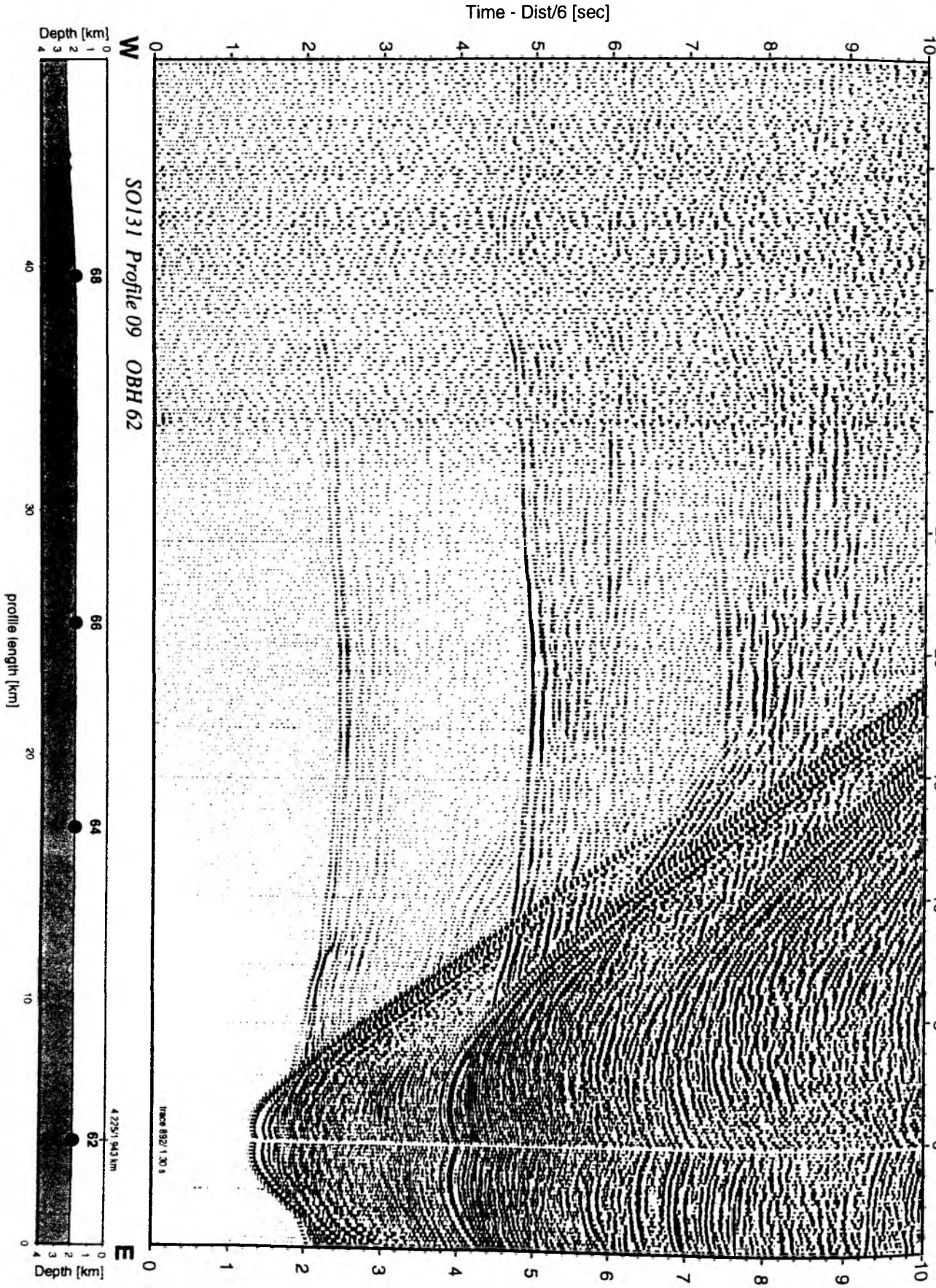

Figure 6.3.4.7.3.34: Record section from OBH 62 , Profile 09.

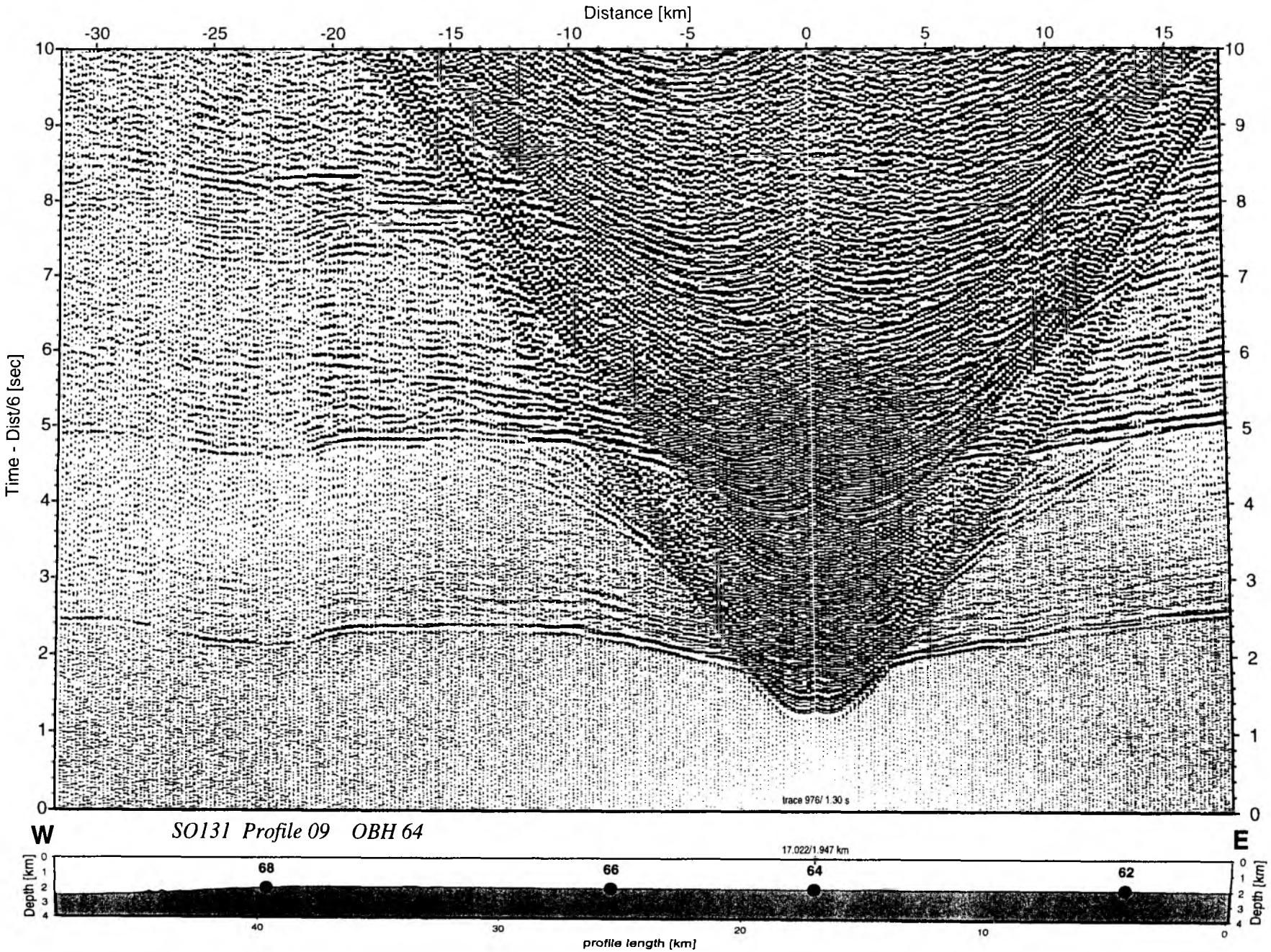

Figure 6.3.4.7.3.35: Record section from OBH 64 , Profile 09.

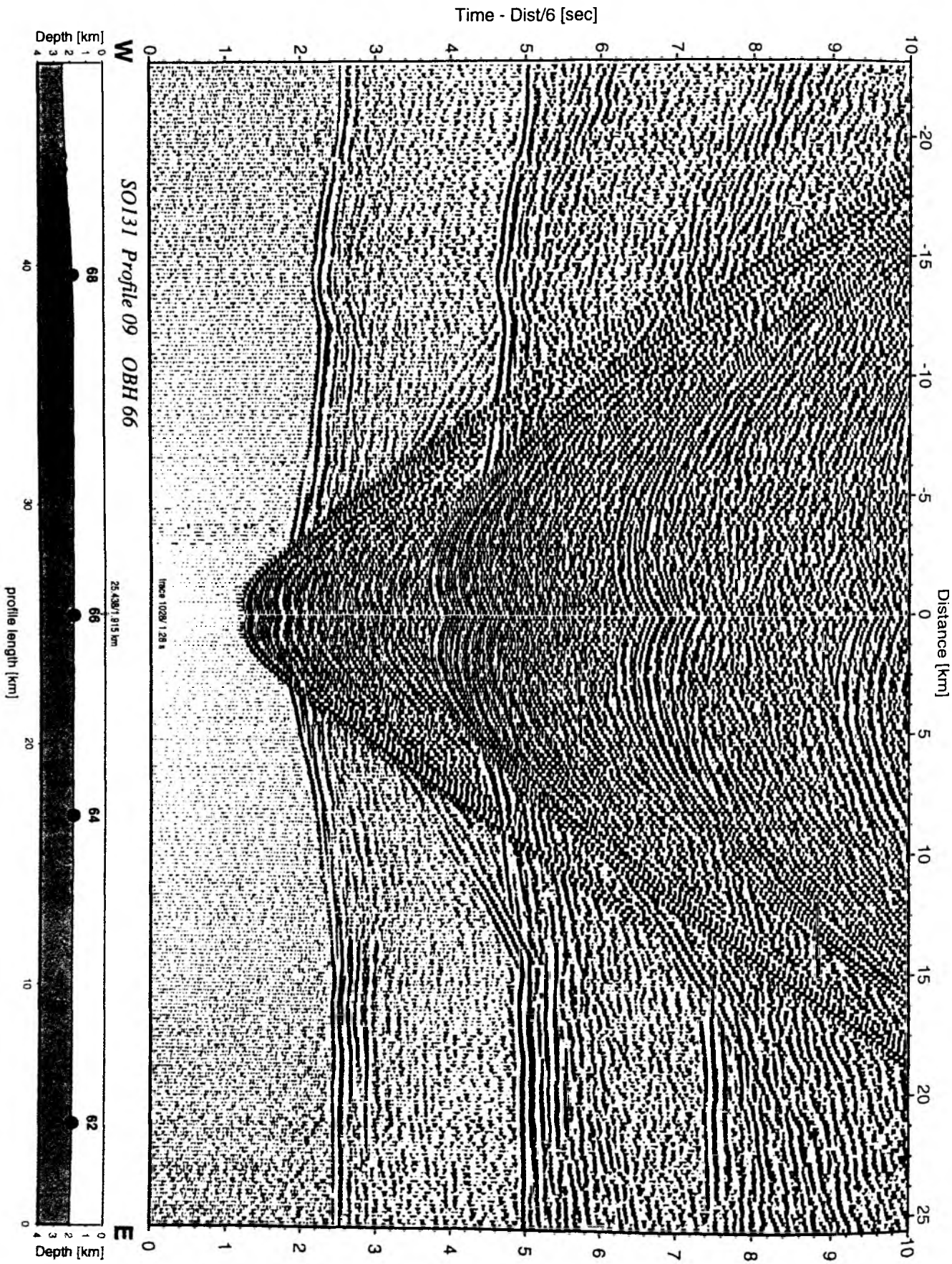

Figure 6.3.4.7.3.36: Record section from OBH 66 , Profile 09.

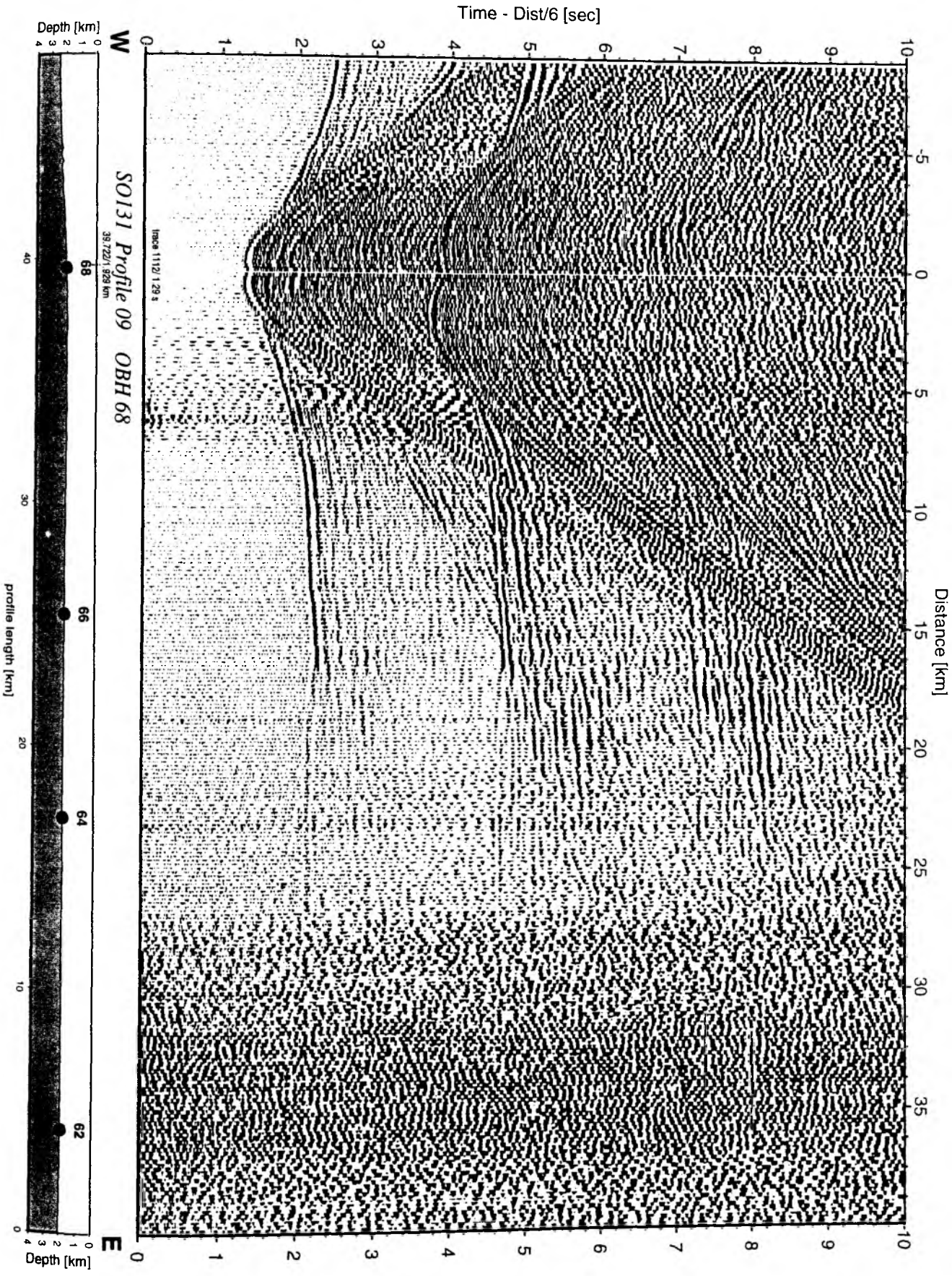

Figure 6.3.4.7.3.37: Record section from OBH 68 , Profile 09.

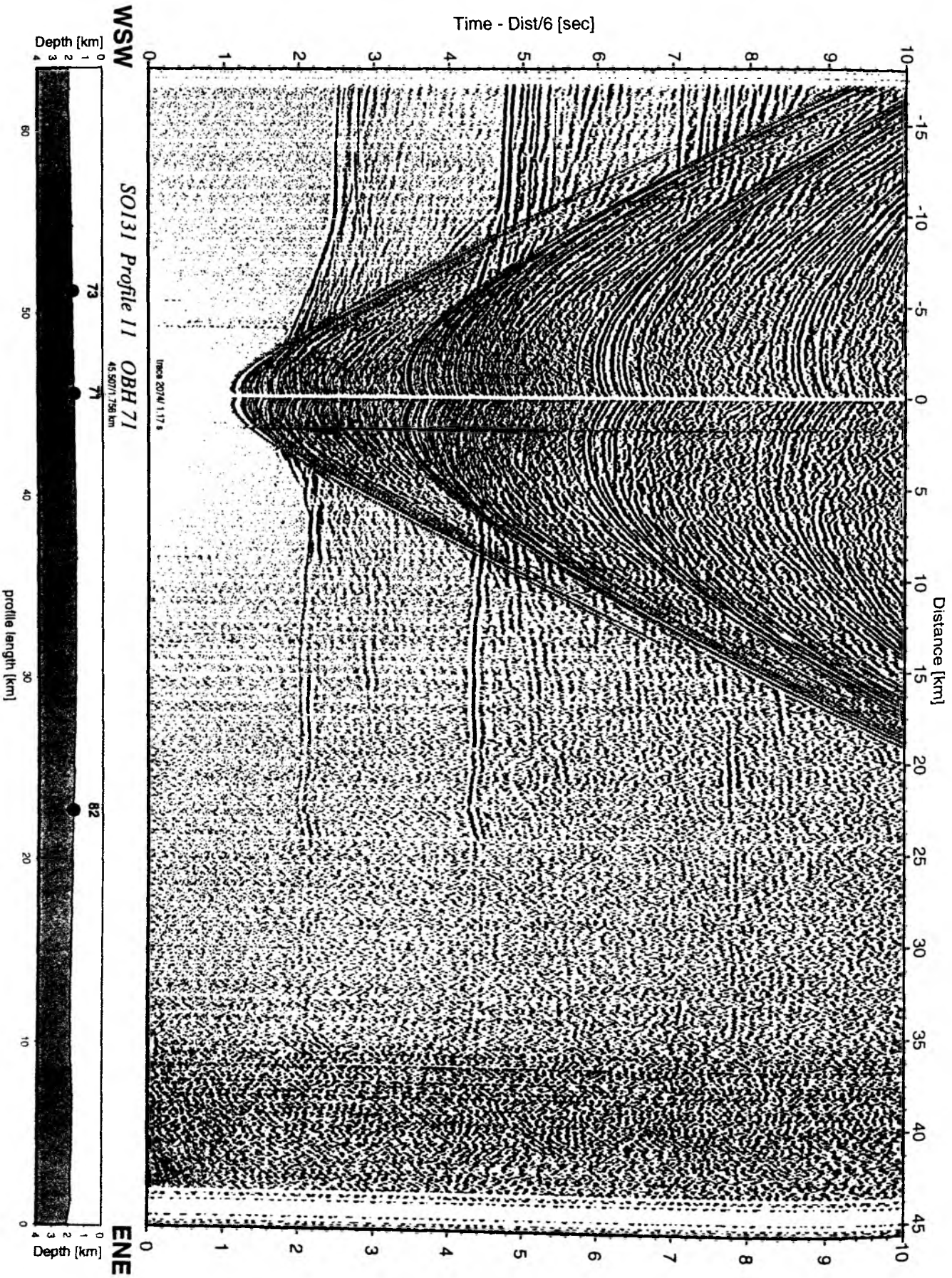

Figure 6.3.4.7.3.38: Record section from OBH 71 , Profile 11.

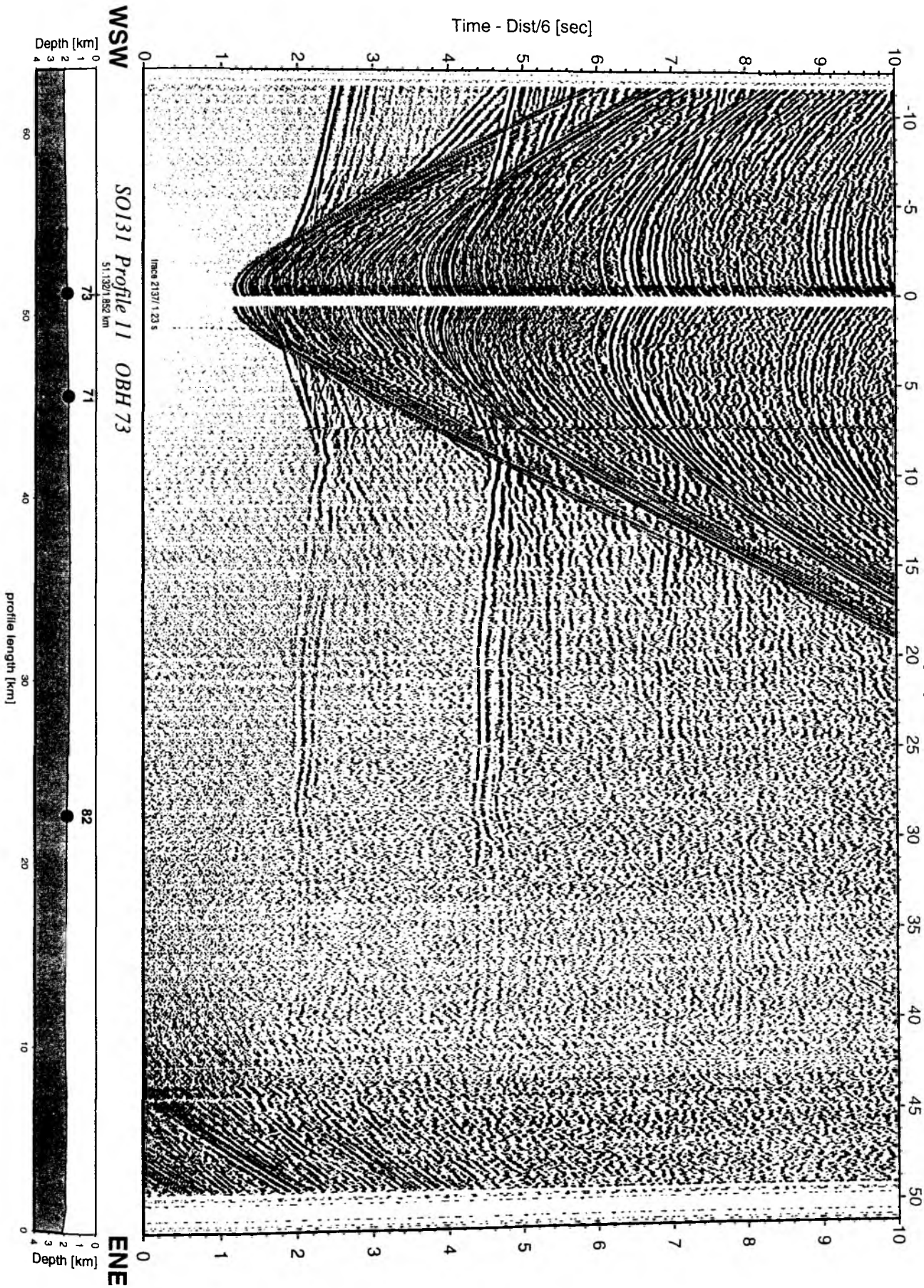

Figure 6.3.4.7.3.39: Record section from OBH 73 , Profile 11.

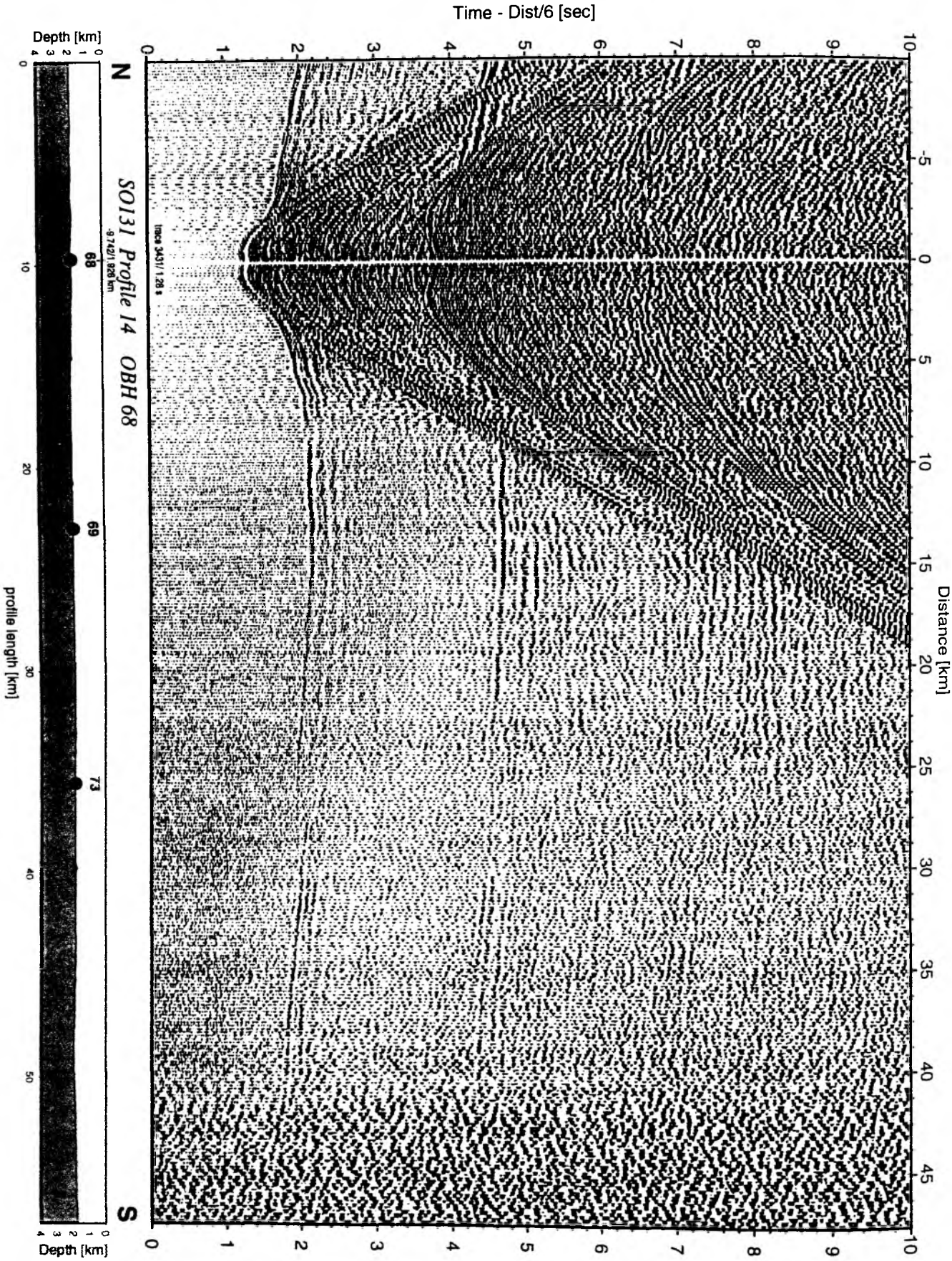

Figure 6.3.4.7.3.40: Record section from OBH 68 , Profile 14.

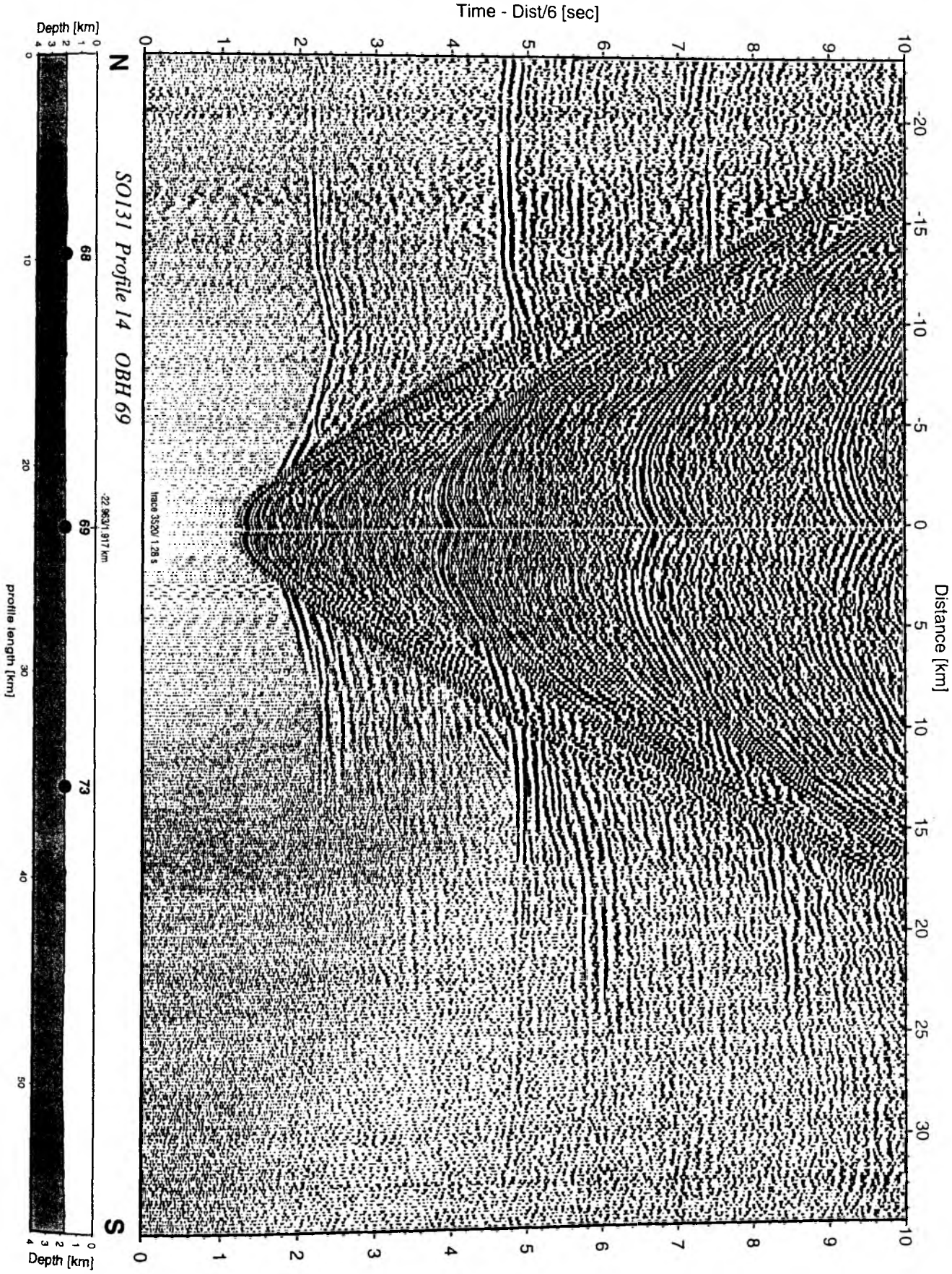

Figure 6.3.4.7.3.41: Record section from OBH 69 , Profile 14.

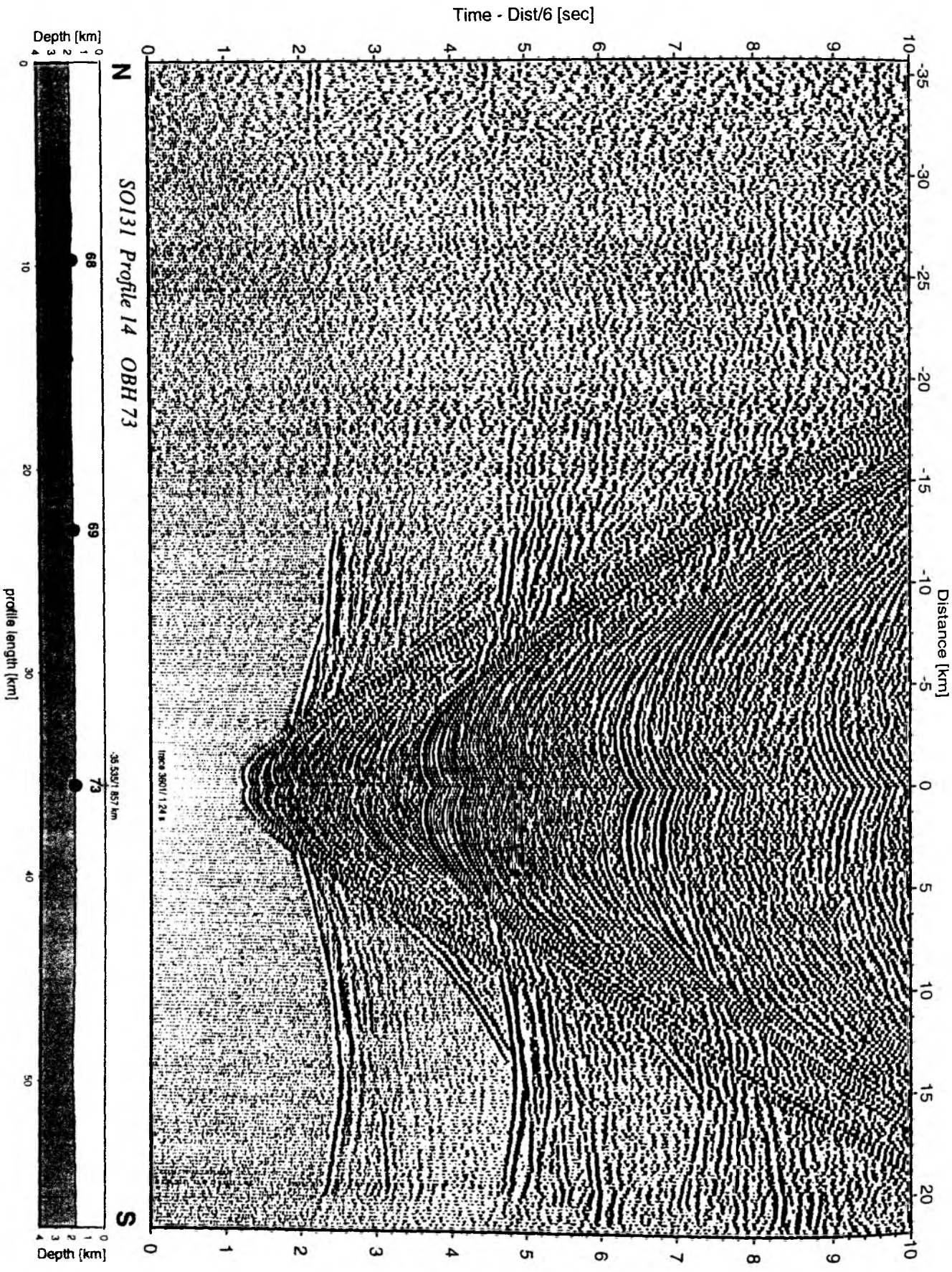

Figure 6.3.4.7.3.42: Record section from OBH 73 , Profile 14.

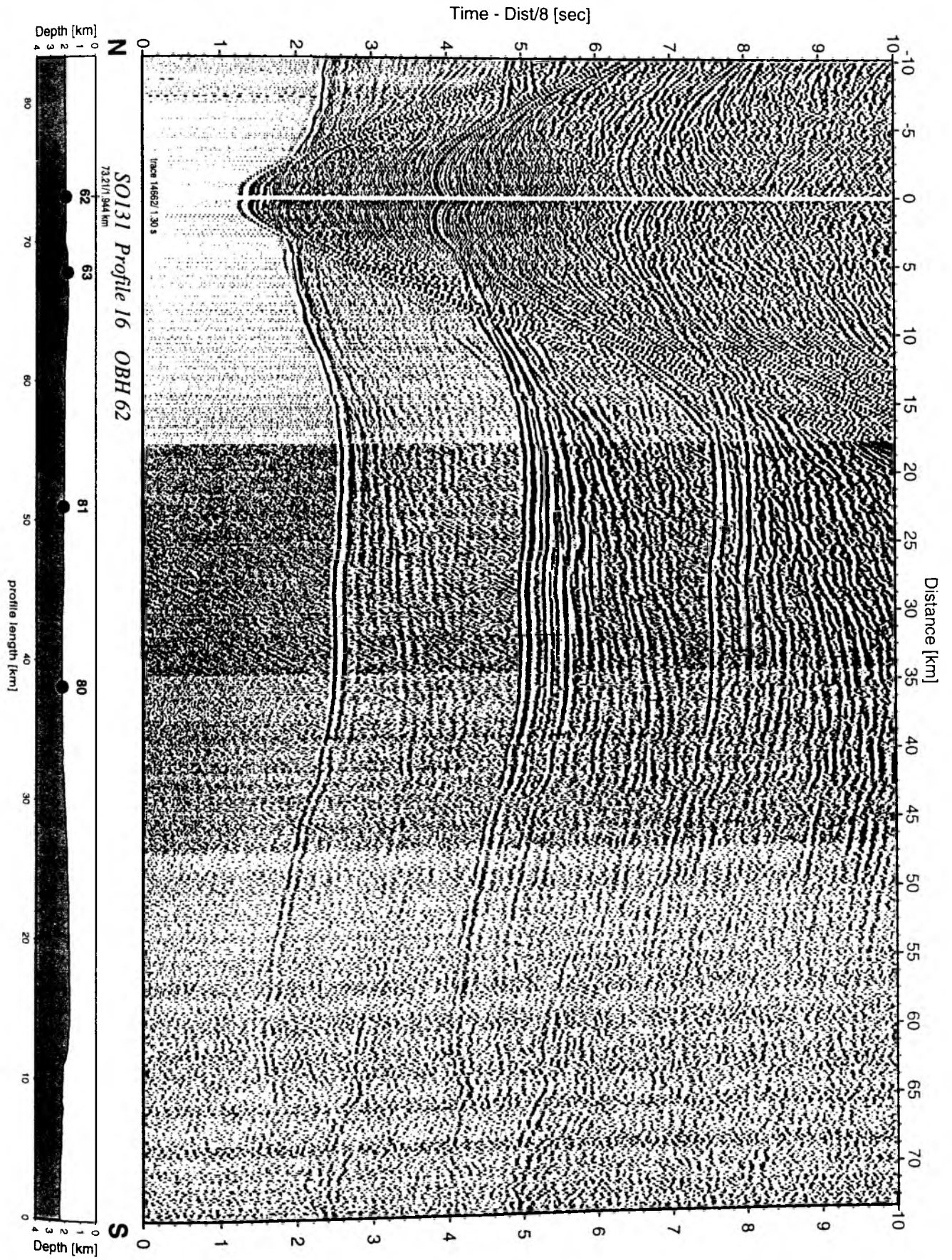

Figure 6.3.4.7.3.43: Record section from OBH 62 , Profile 16.

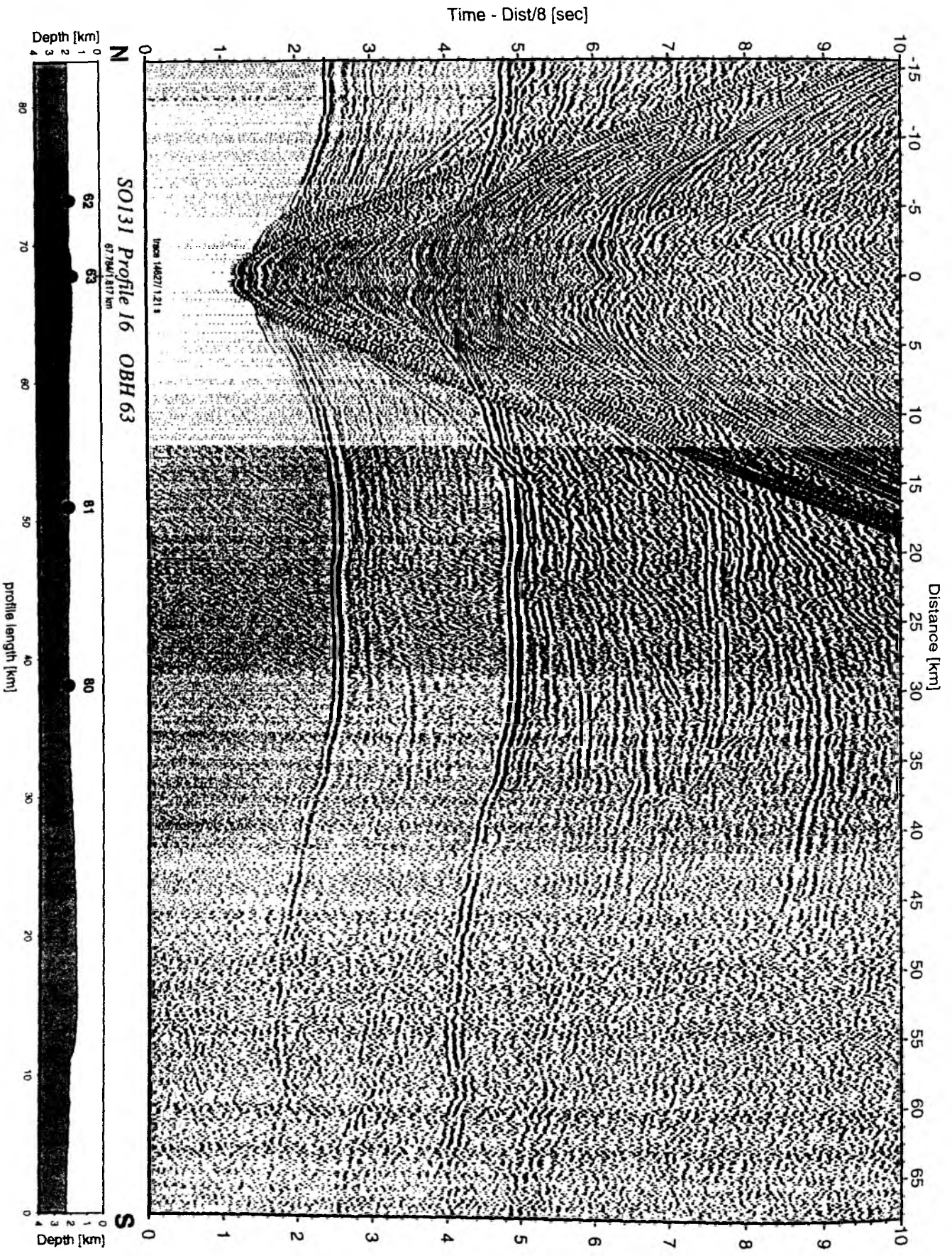

Figure 6.3.4.7.3.44: Record section from OBH 63 , Profile 16.

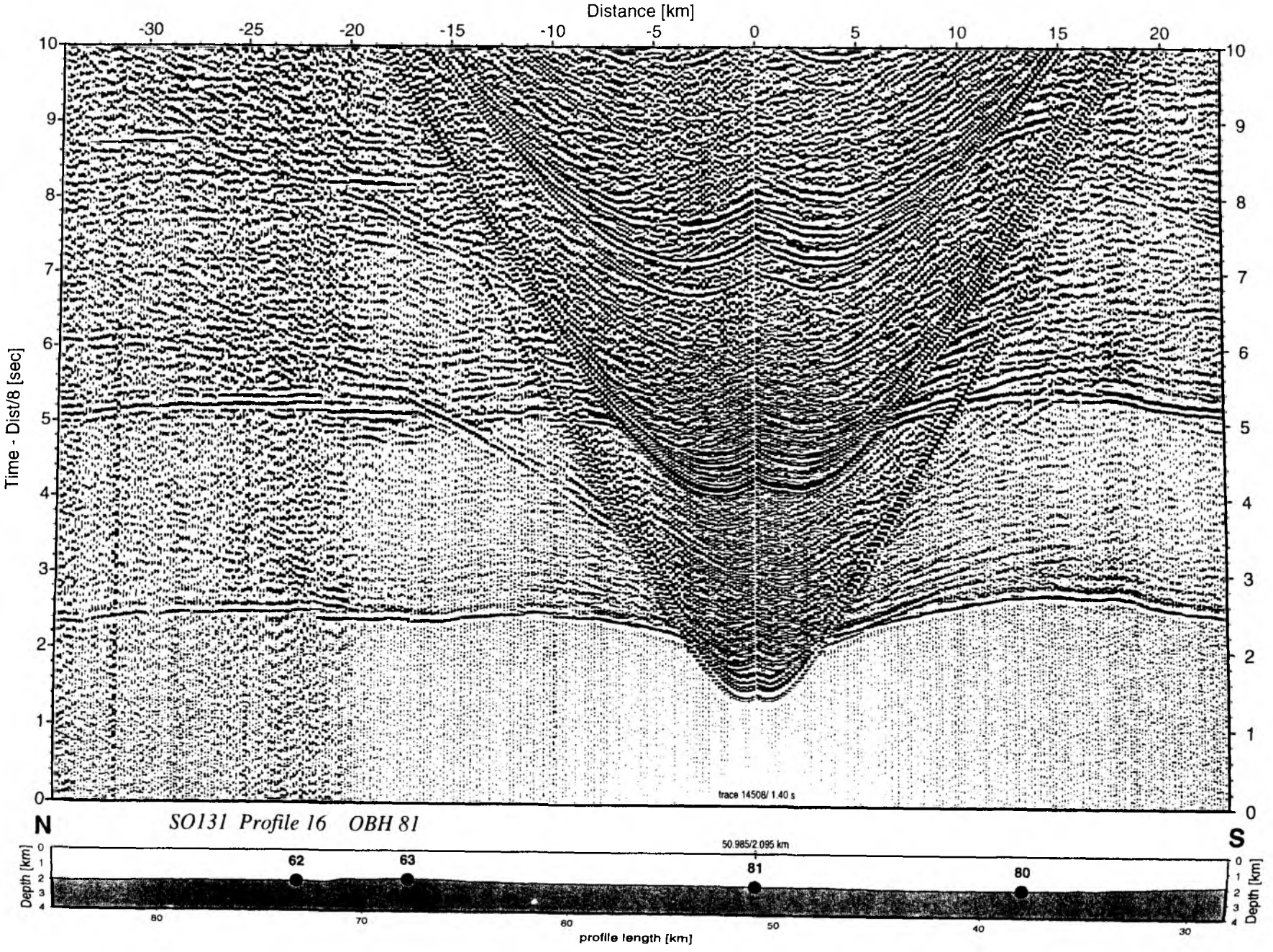

Figure 6.3.4.7.3.45: Record section from OBH 81 , Profile 16.

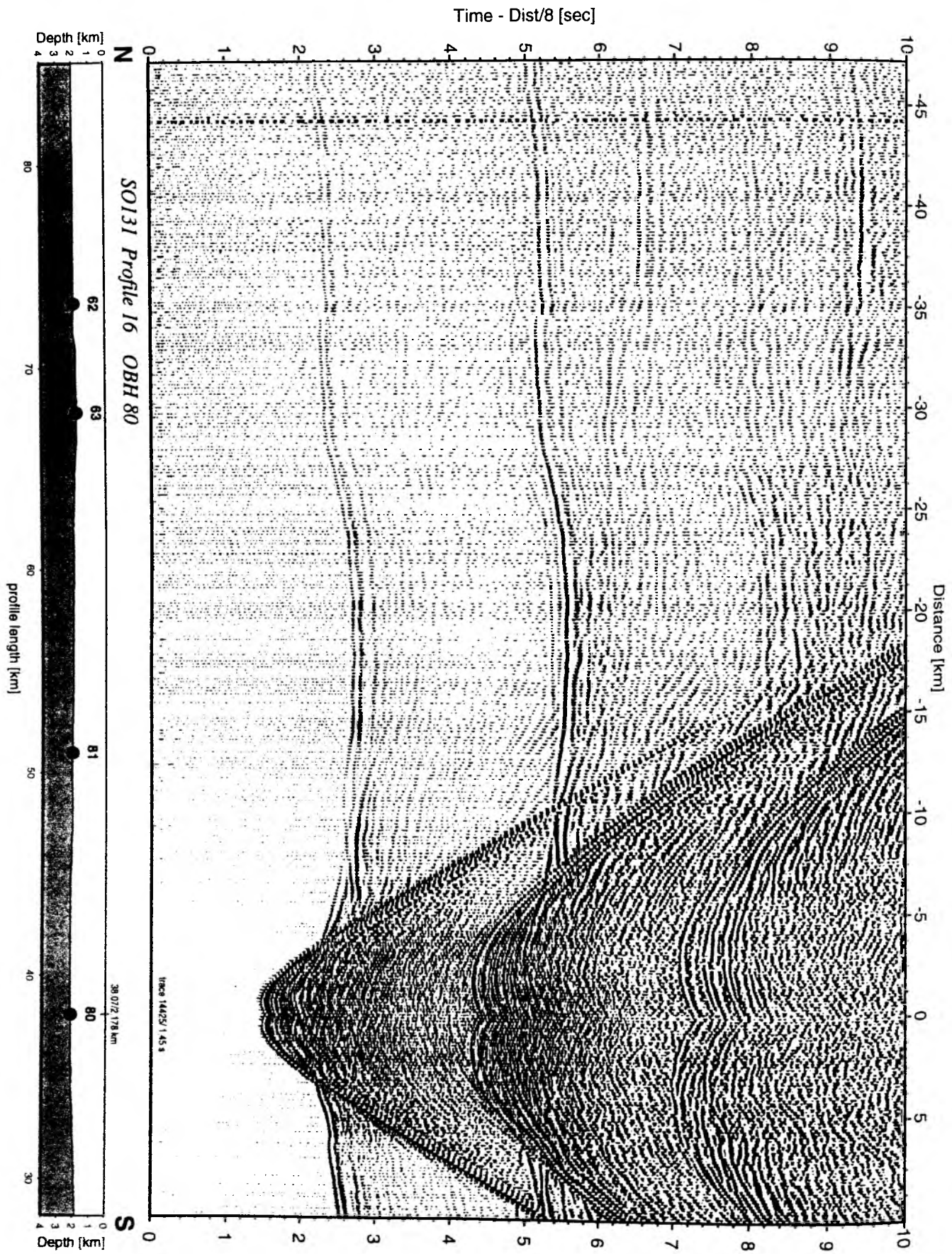

Figure 6.3.4.7.3.46: Record section from OBH 80 , Profile 16.

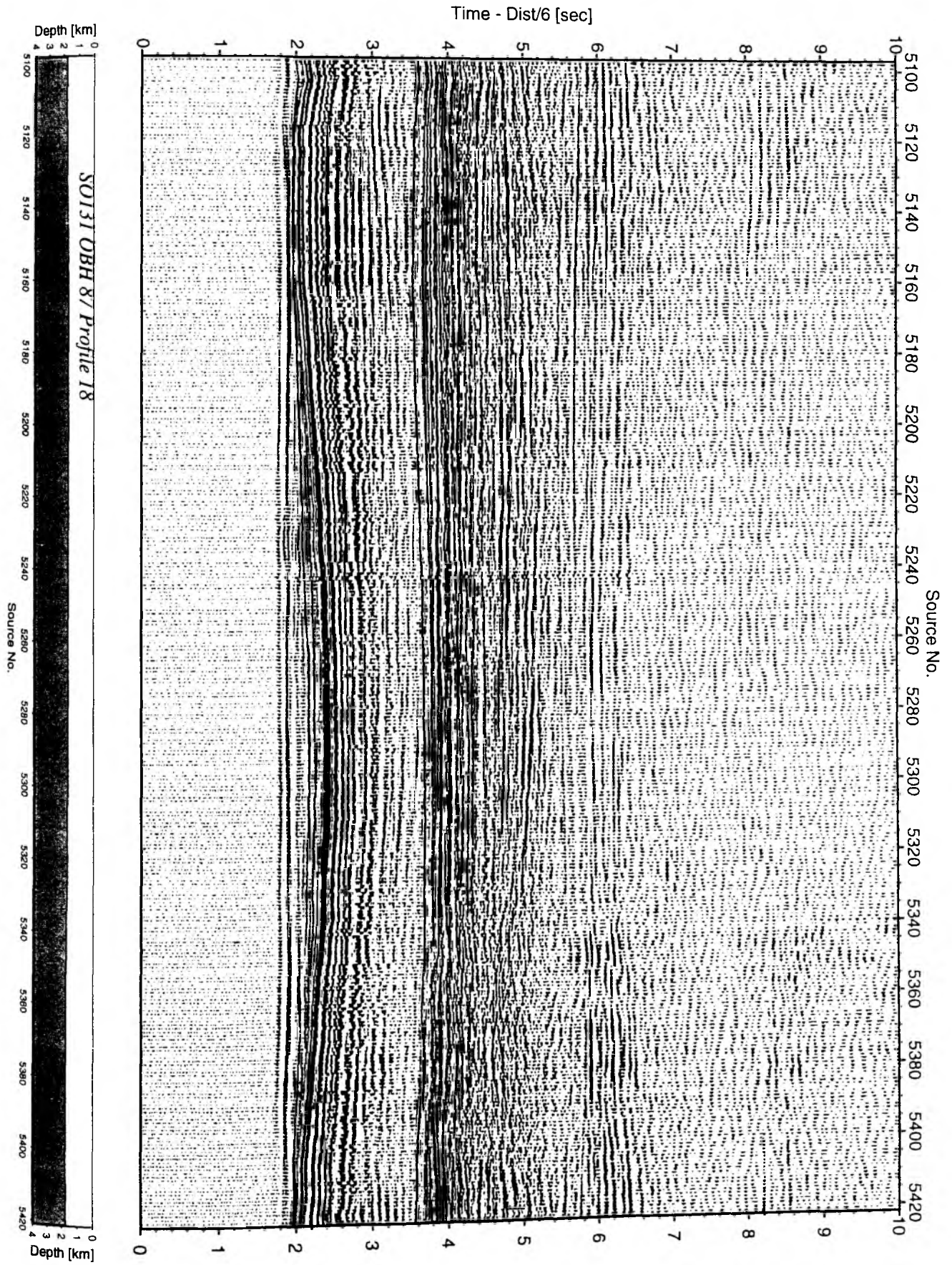

Figure 6.3.4.7.3.47: Record section from OBH 87 , Profile 18.

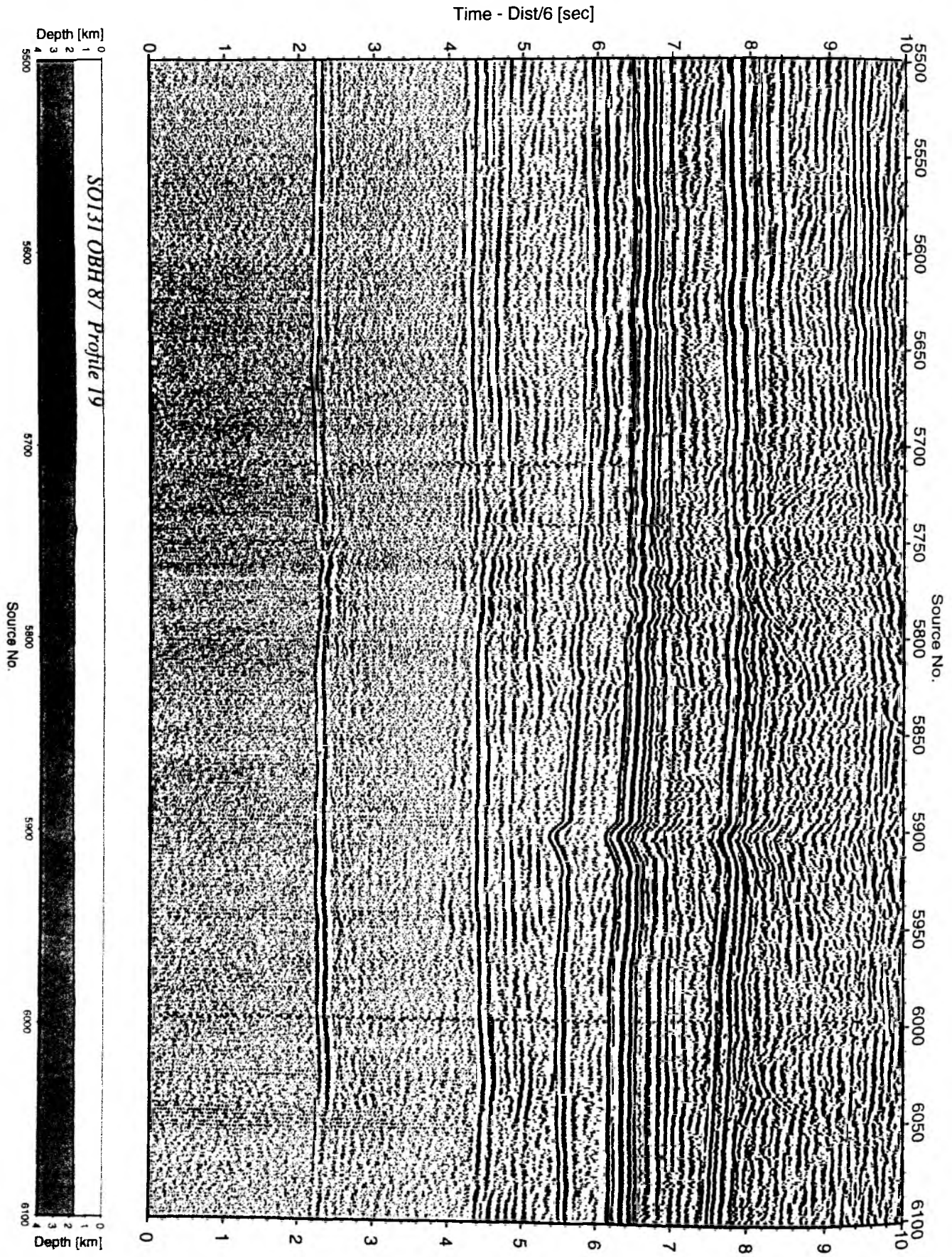

Figure 6.3.4.7.3.48: Record section from OBH 87 , Profile 19.

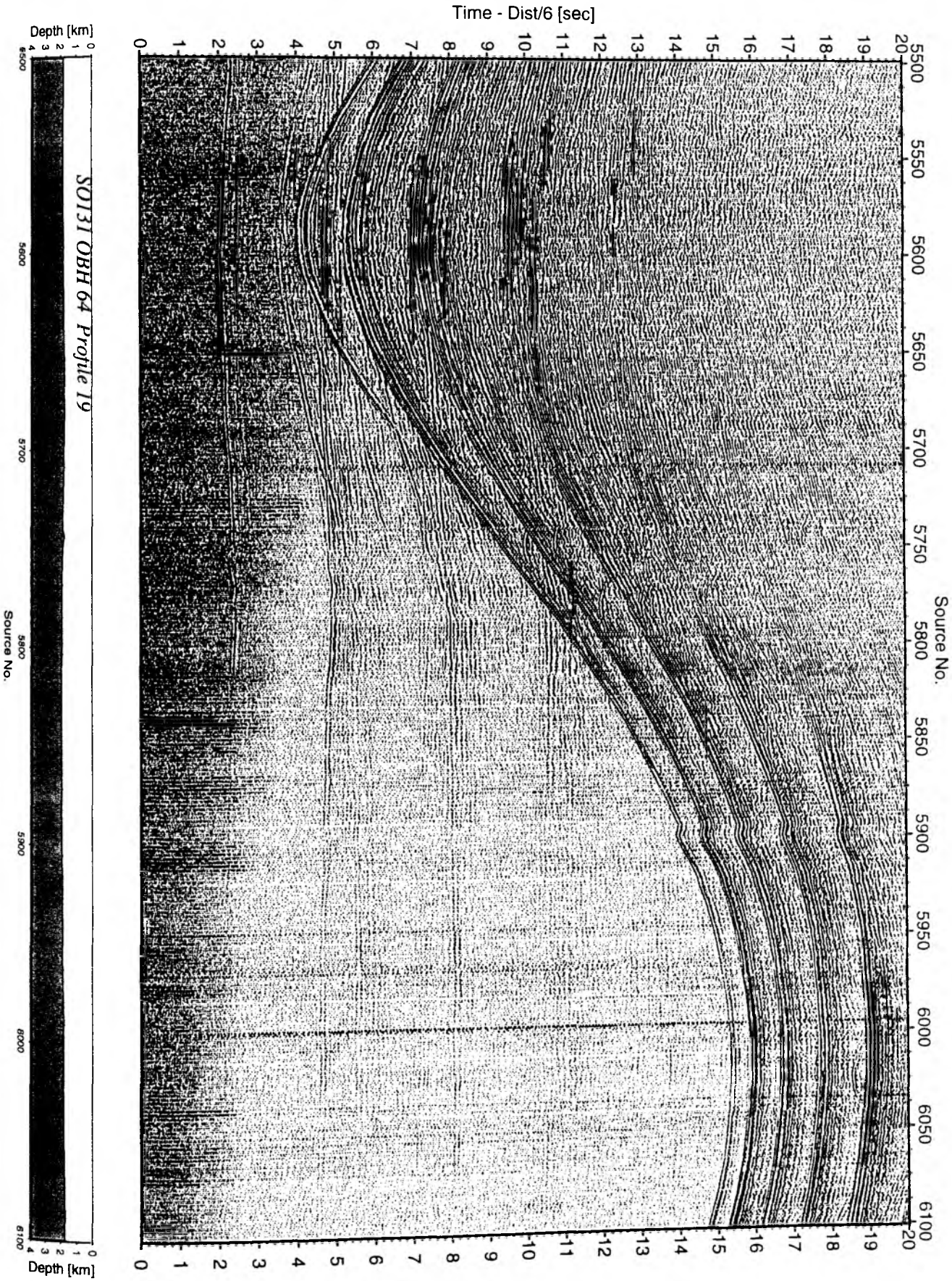

Figure 6.3.4.7.3.49: Record section from OBH 64 , Profile 19.

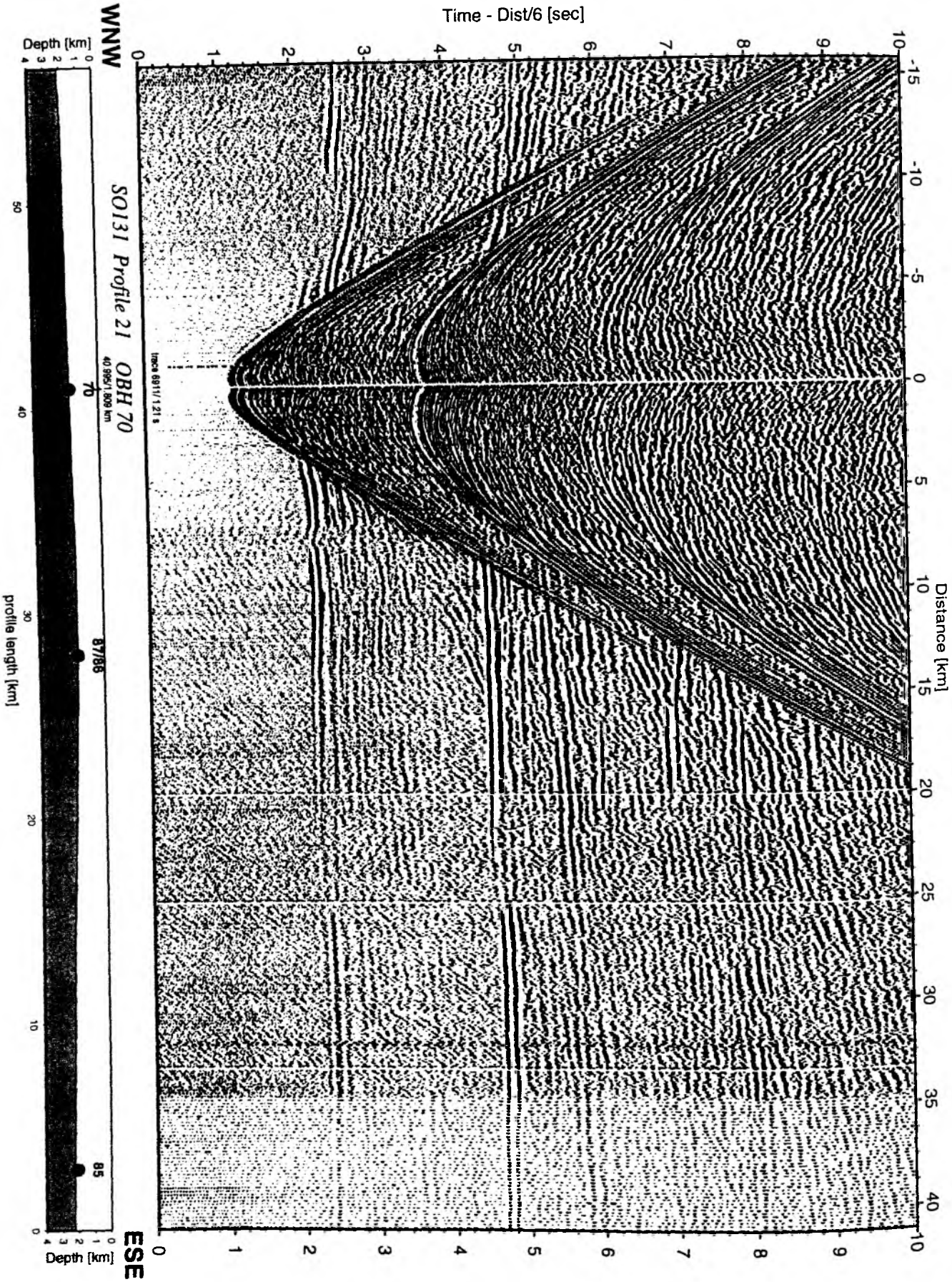

Figure 6.3.4.7.3.50: Record section from OBH 70 , Profile 21.

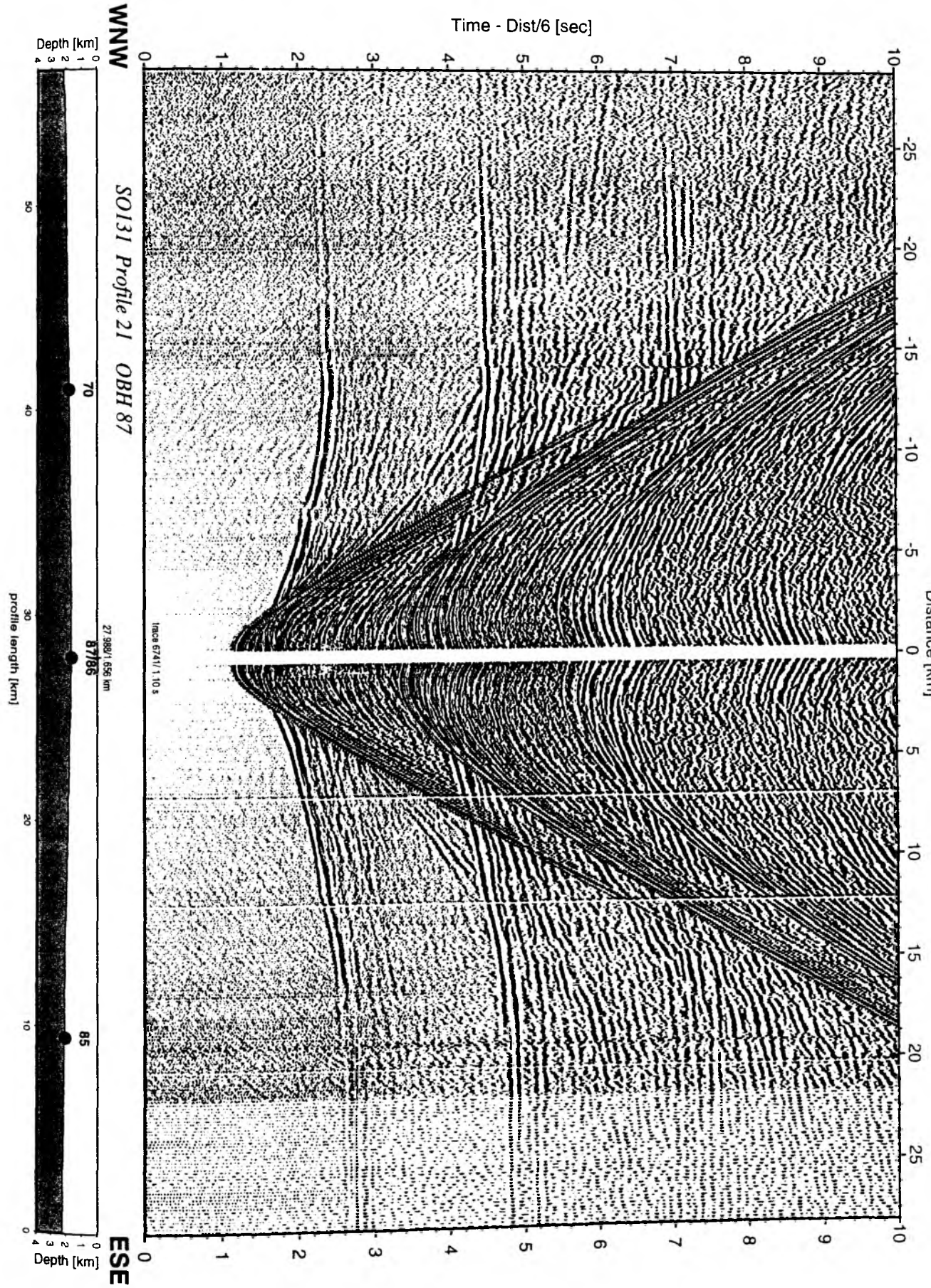

Figure 6.3.4.7.3.51: Record section from OBH 87 , Profile 21.

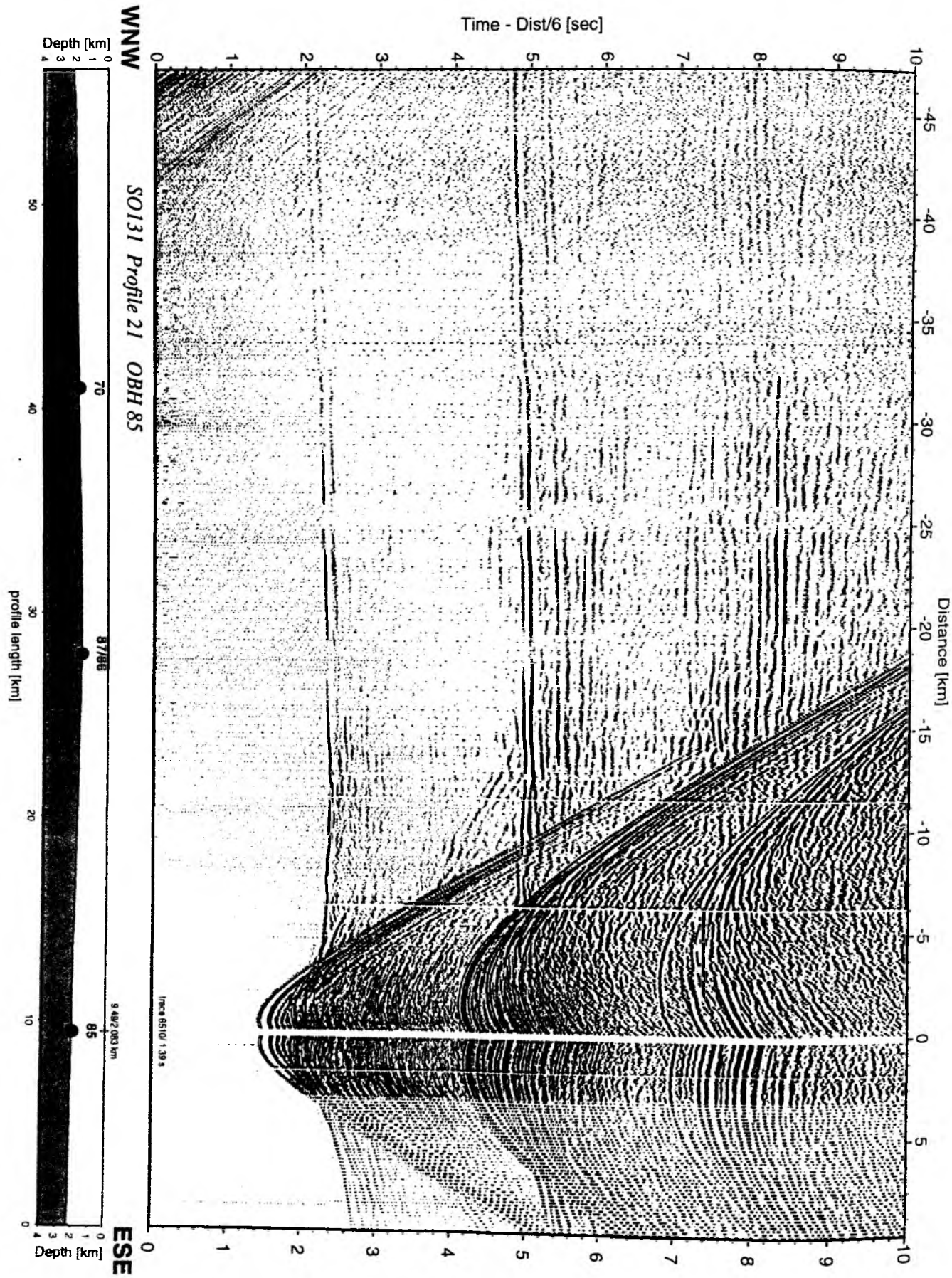

Figure 6.3.4.7.3.52: Record section from OBH 85 , Profile 21.

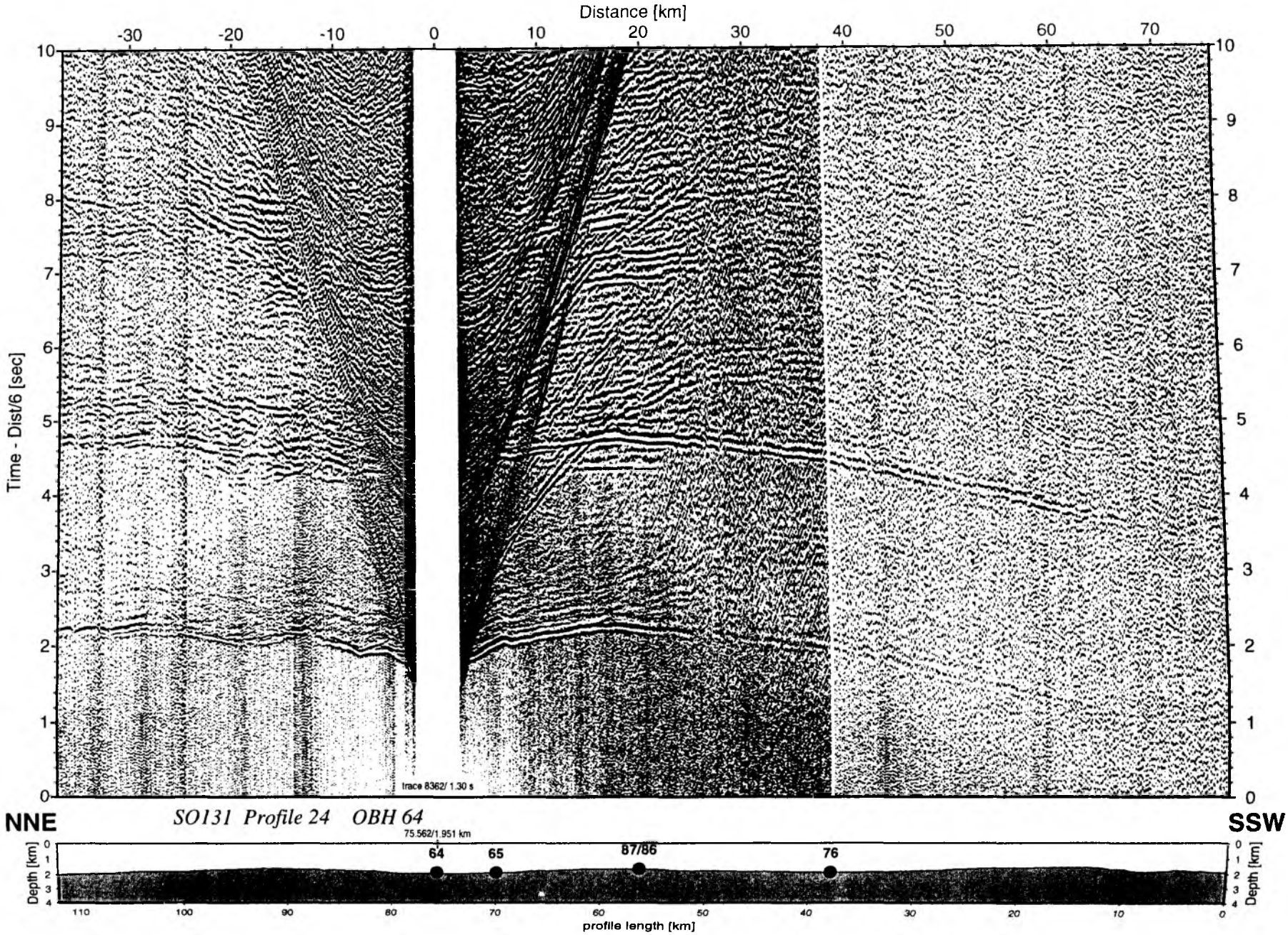

Figure 6.3.4.7.3.53: Record section from OBH 64 , Profile 24.

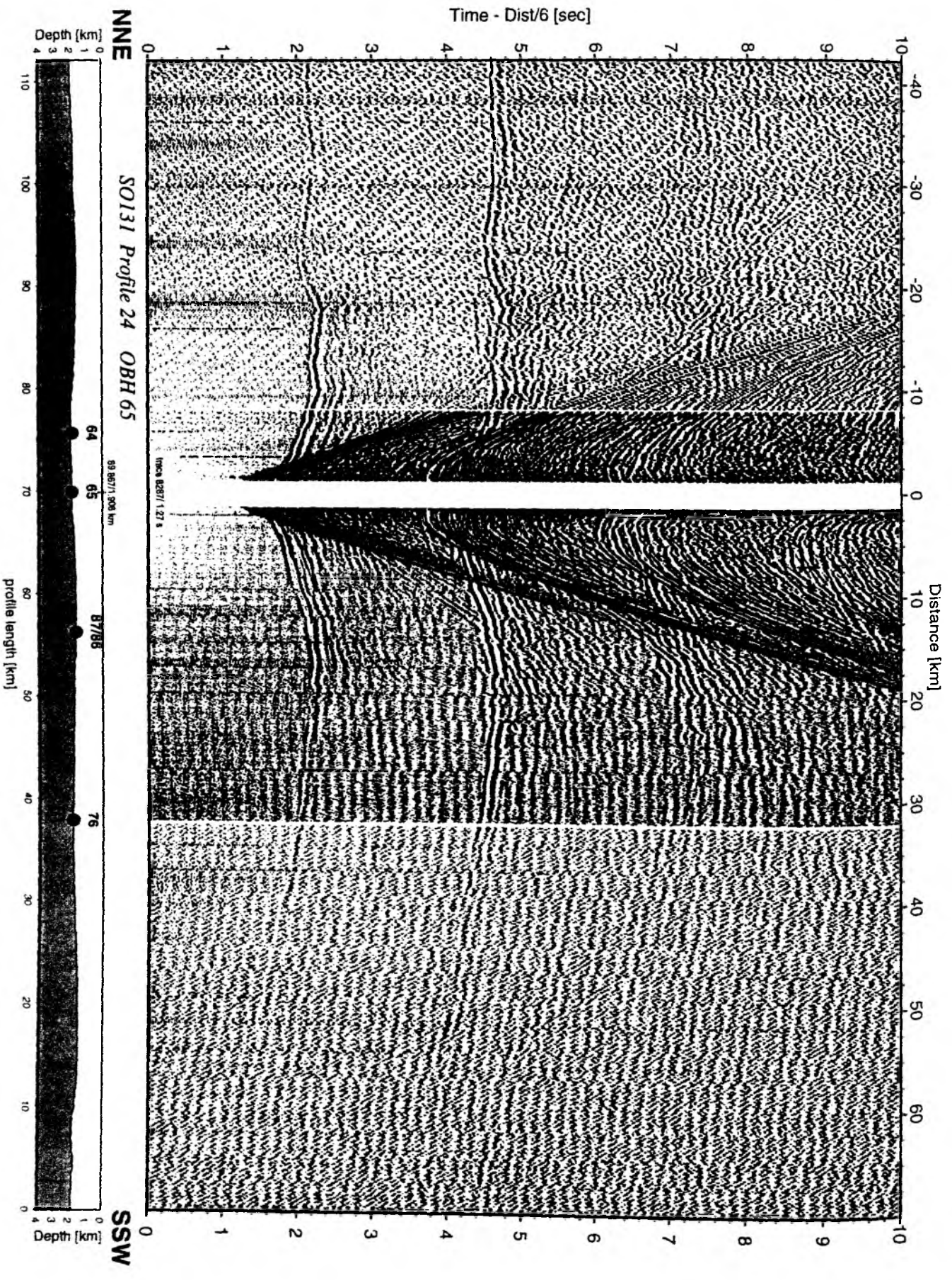

Figure 6.3.4.7.3.54: Record section from OBH 65 , Profile 24.

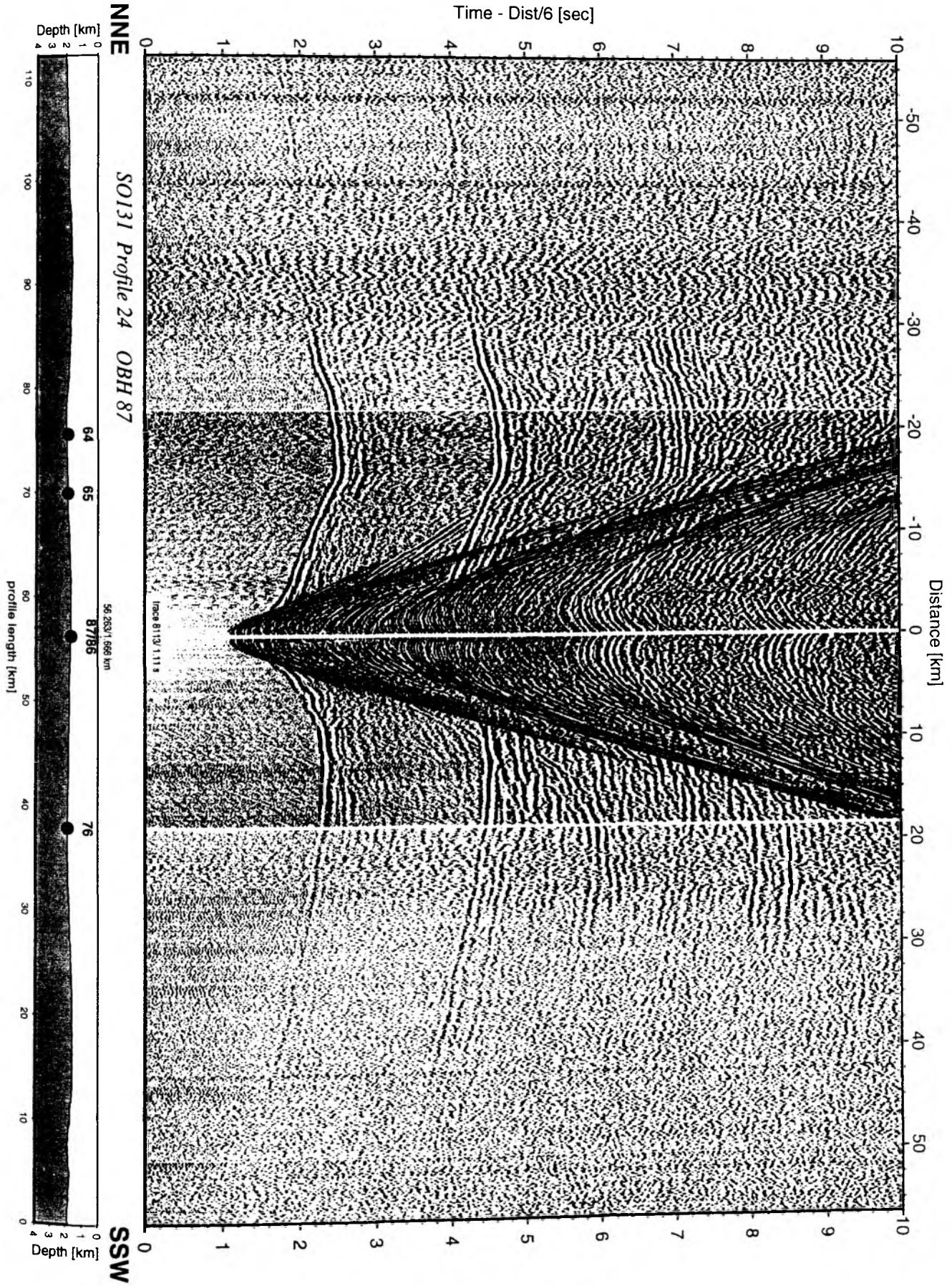

Figure 6.3.4.7.3.55: Record section from OBH 87 , Profile 24.

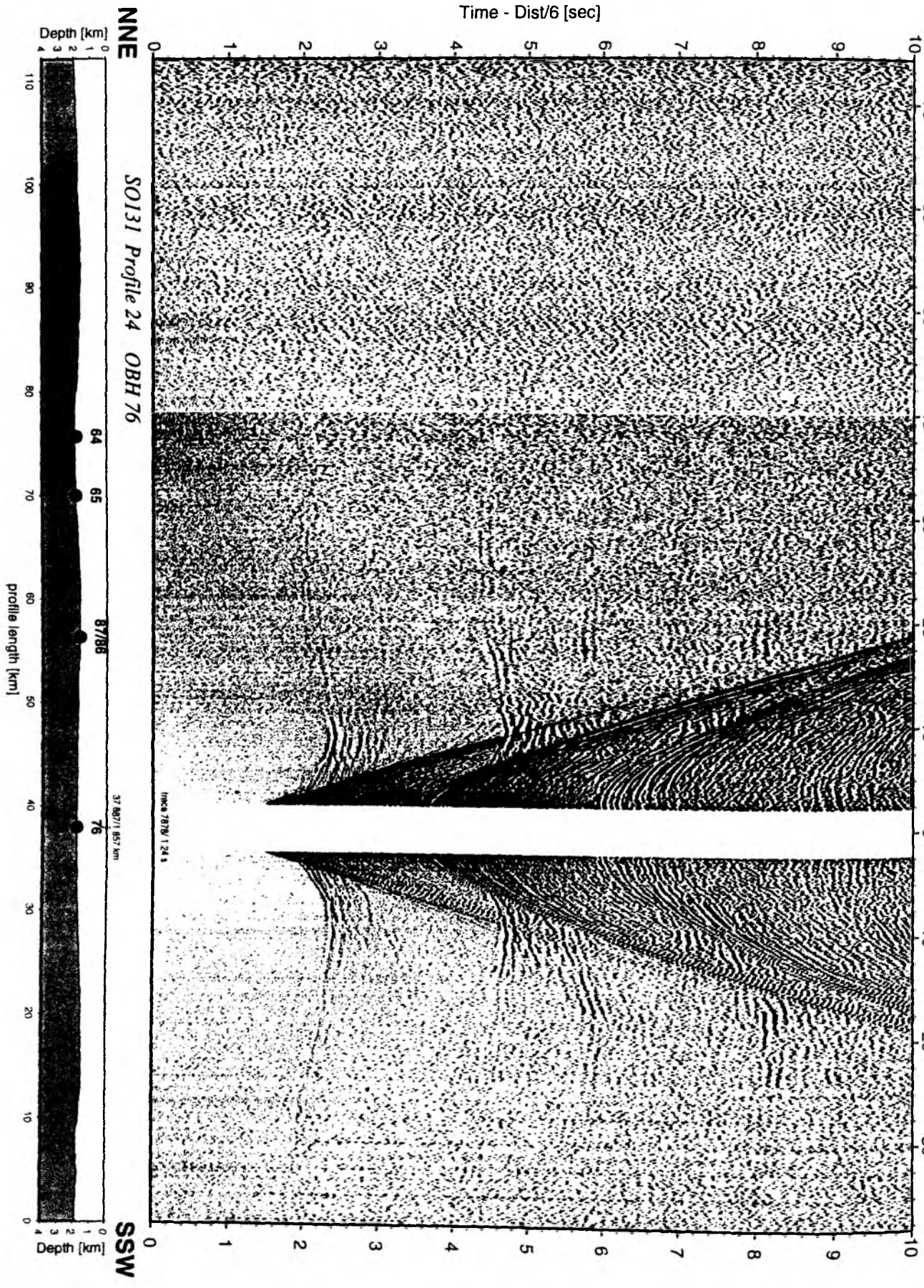

Figure 6.3.4.7.3.56: Record section from OBH 76 , Profile 24.

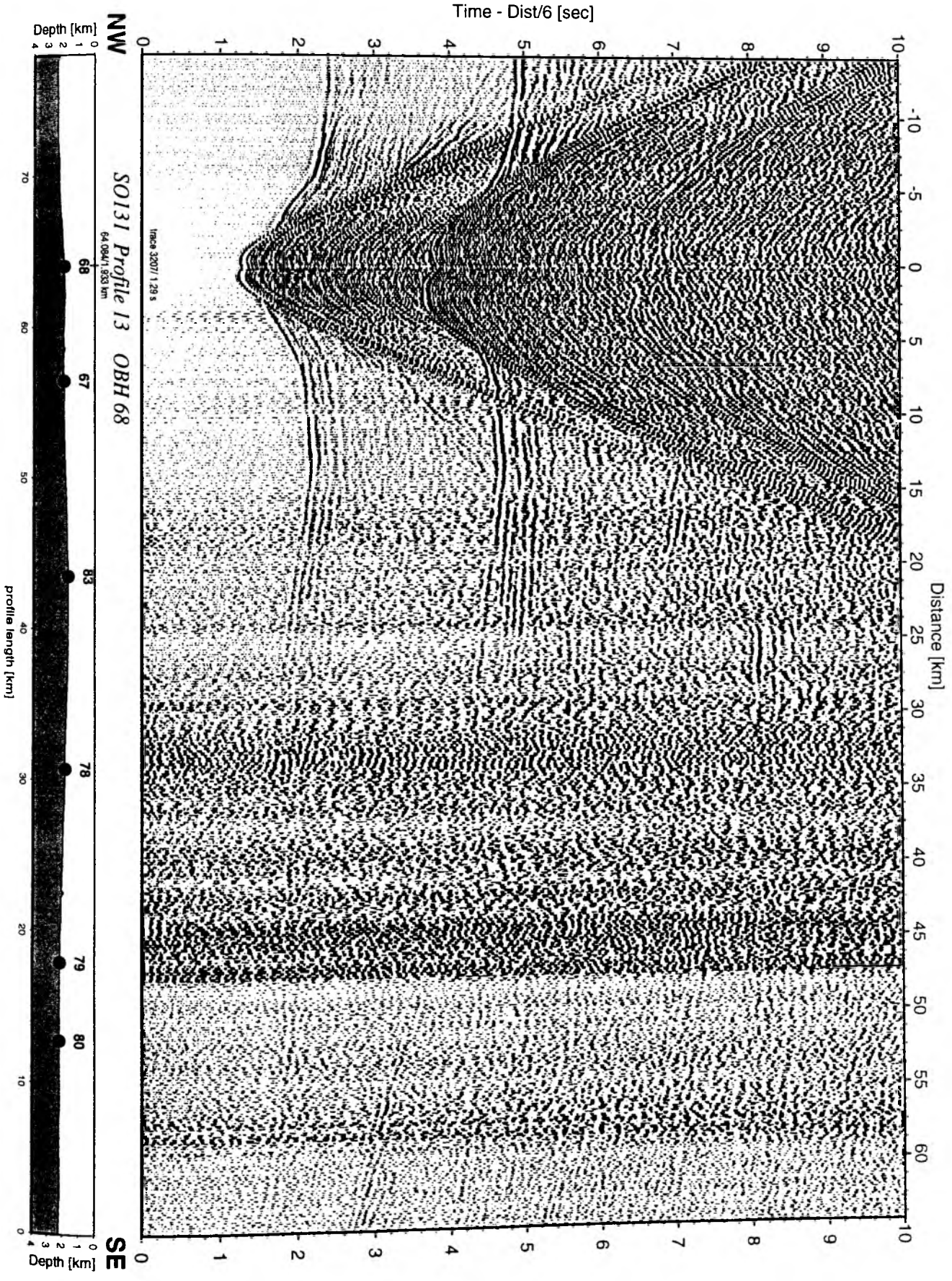

Figure 6.3.4.7.3.57: Record section from OBH 68 , Profile 13.

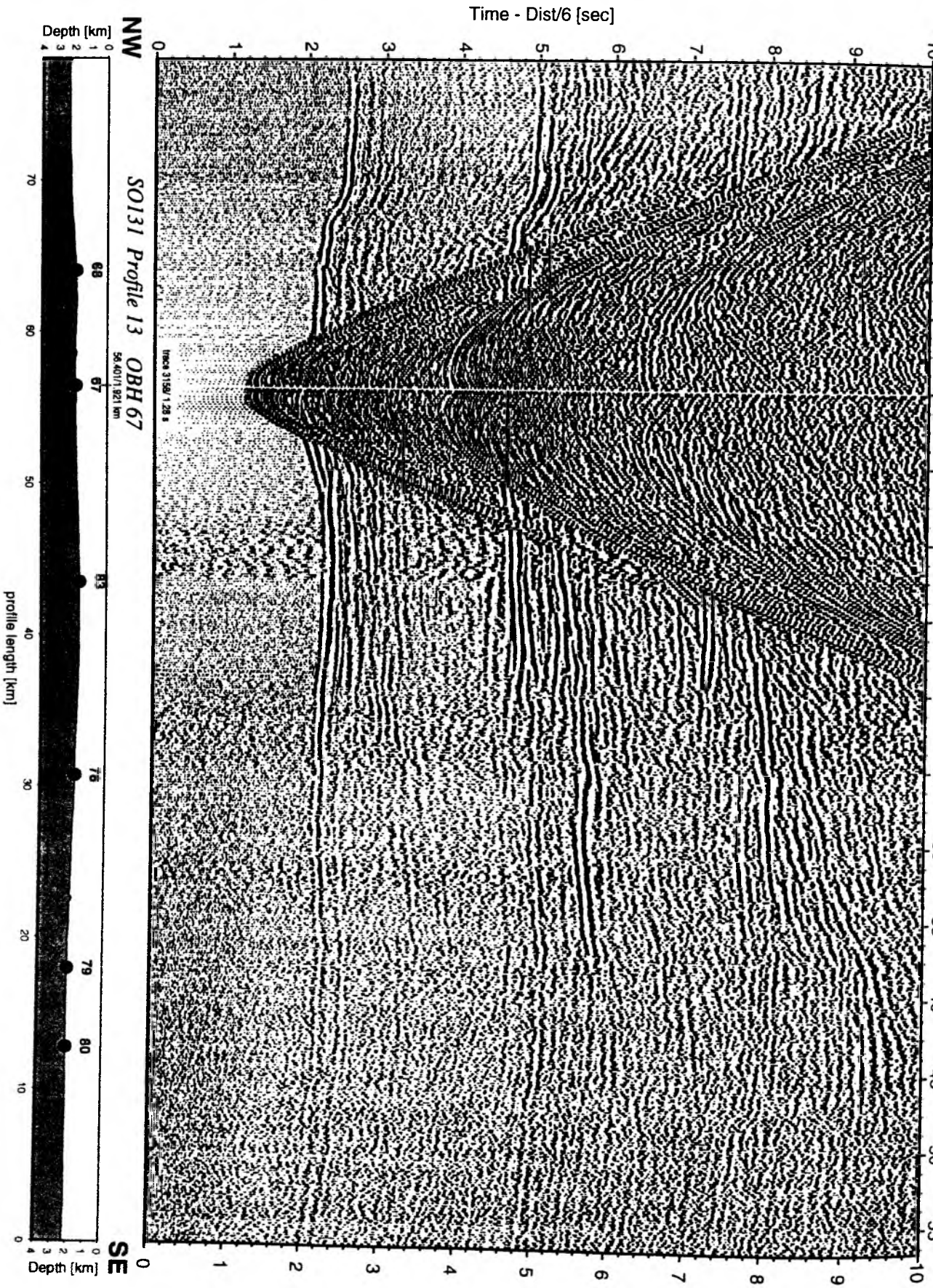

Figure 6.3.4.7.3.58: Record section from OBH 67 , Profile 13.

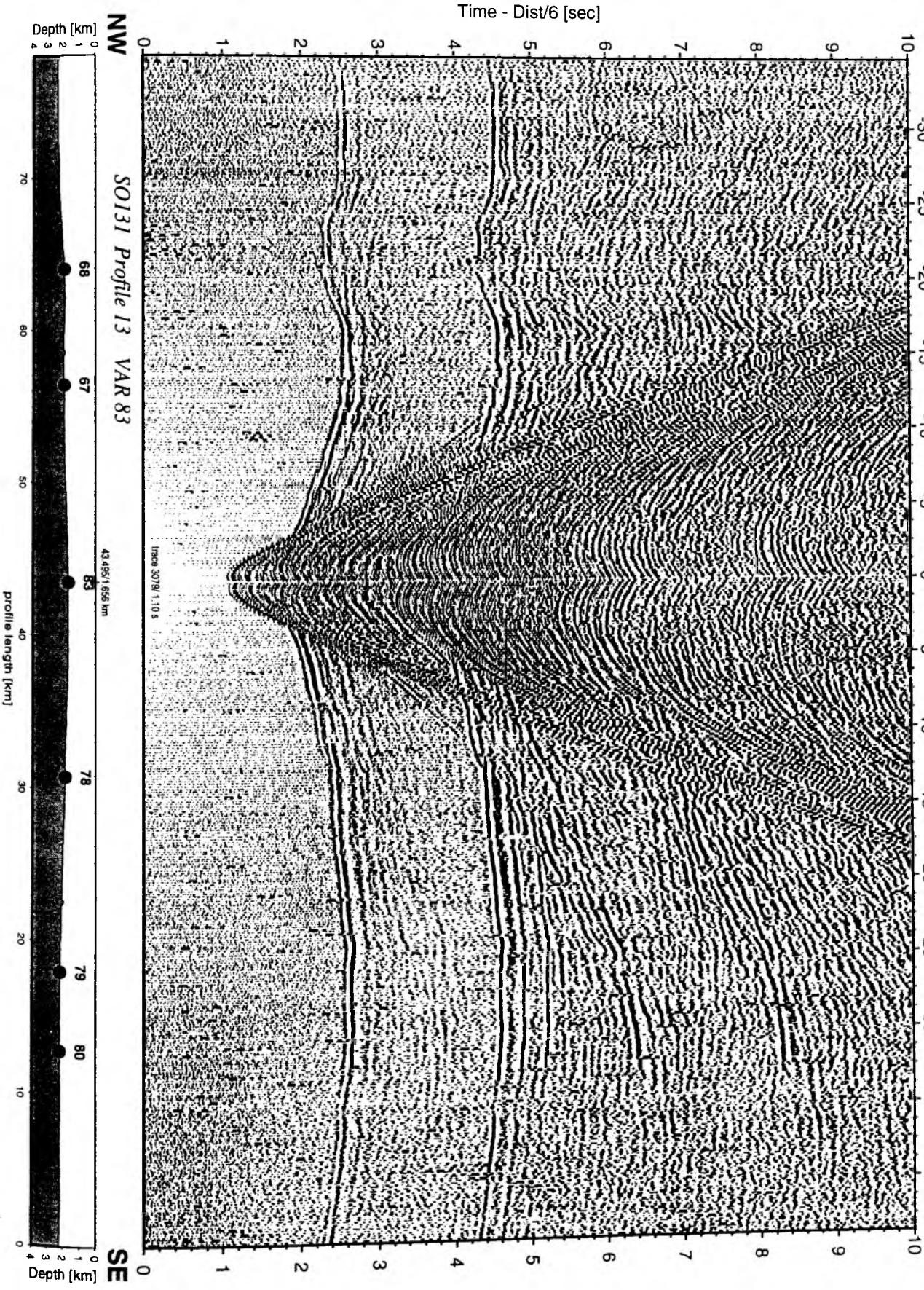

Figure 6.3.4.7.3.59: Record section from VAR 83 , Profile 13.

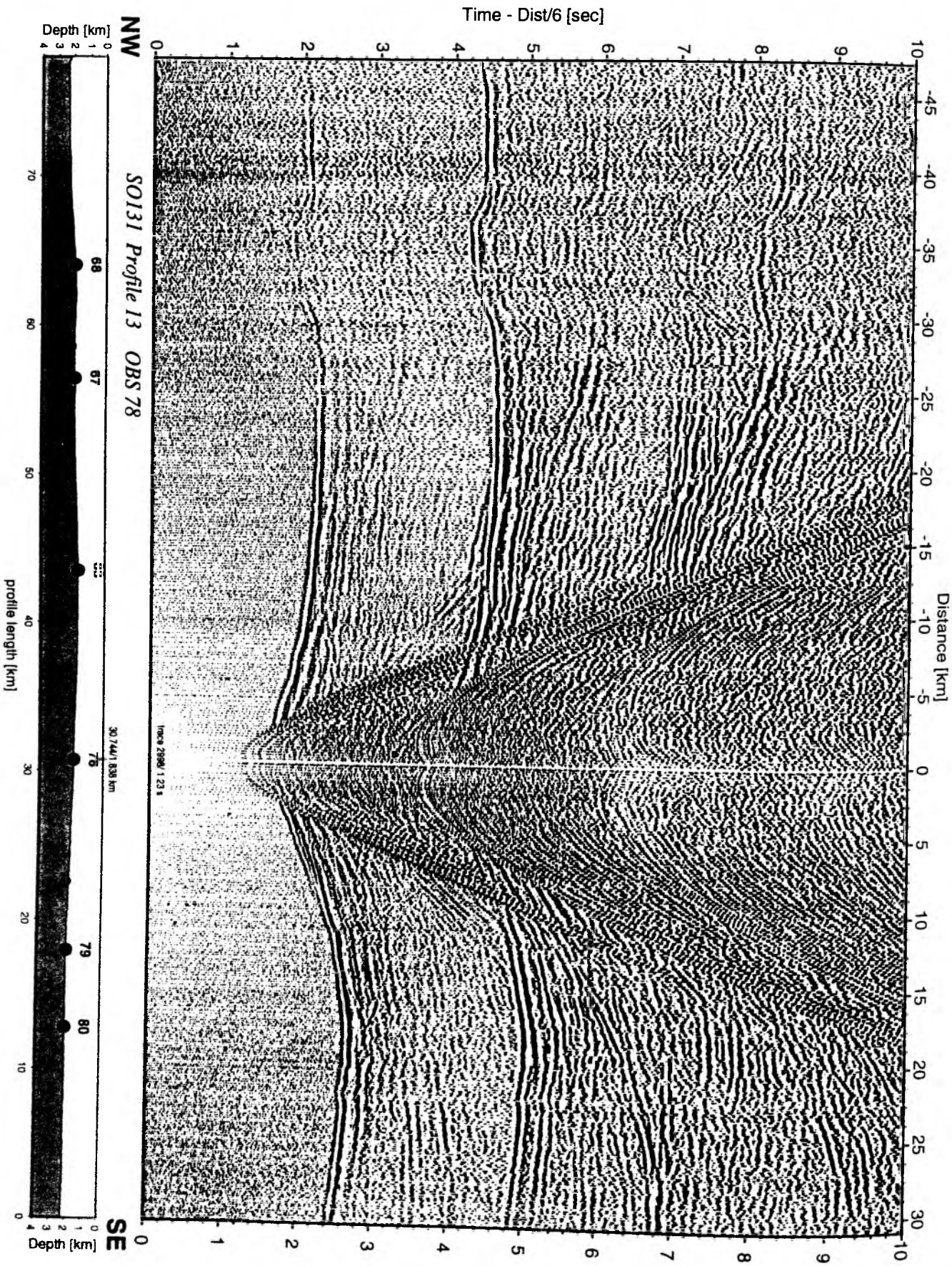

Figure 6.3.4.7.3.60: Record section from OBS 78 hydrophone, Profile 13.

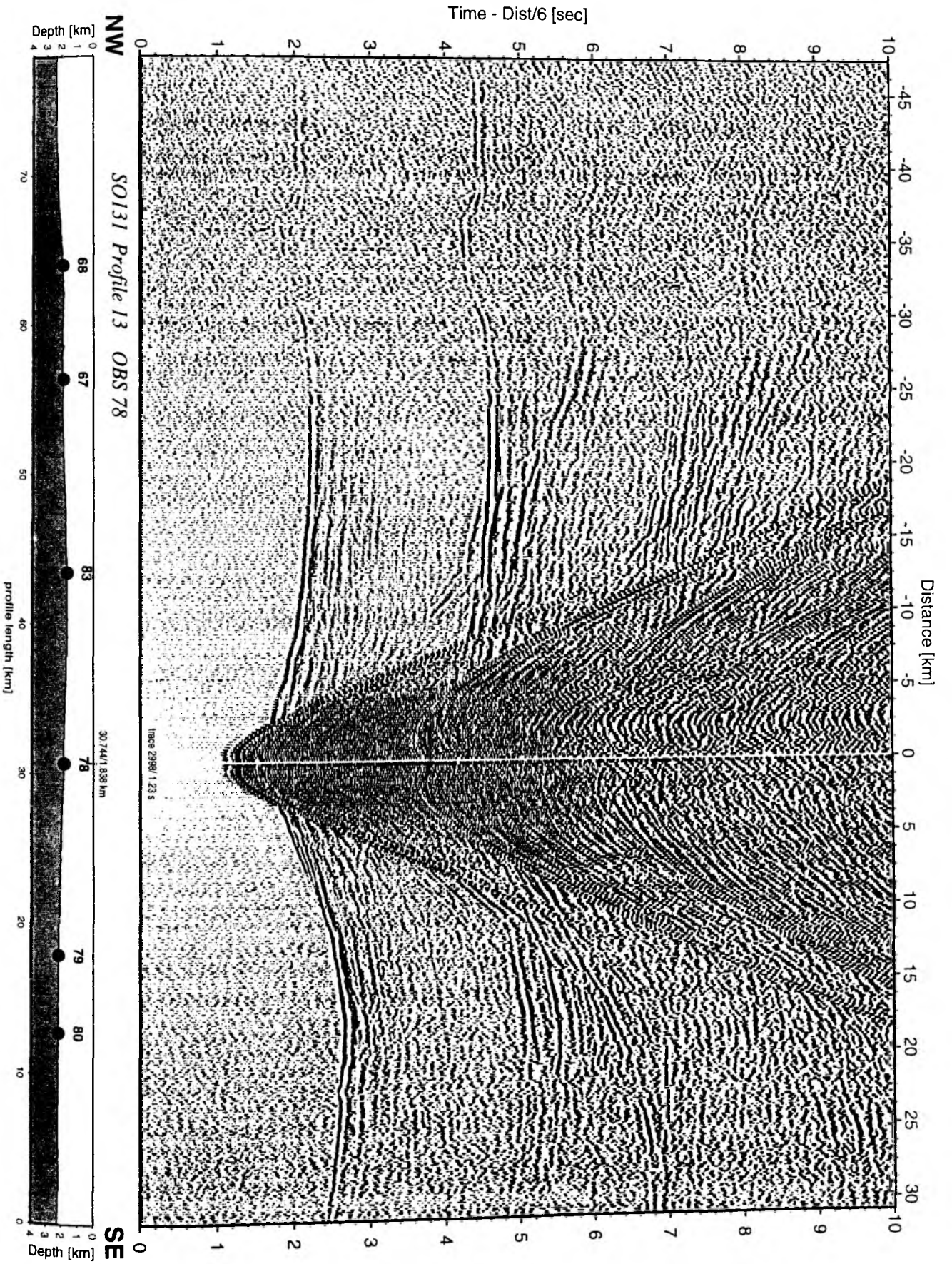

Figure 6.3.4.7.3.61: Record section from OBS 78 vertical component, Profile 13.

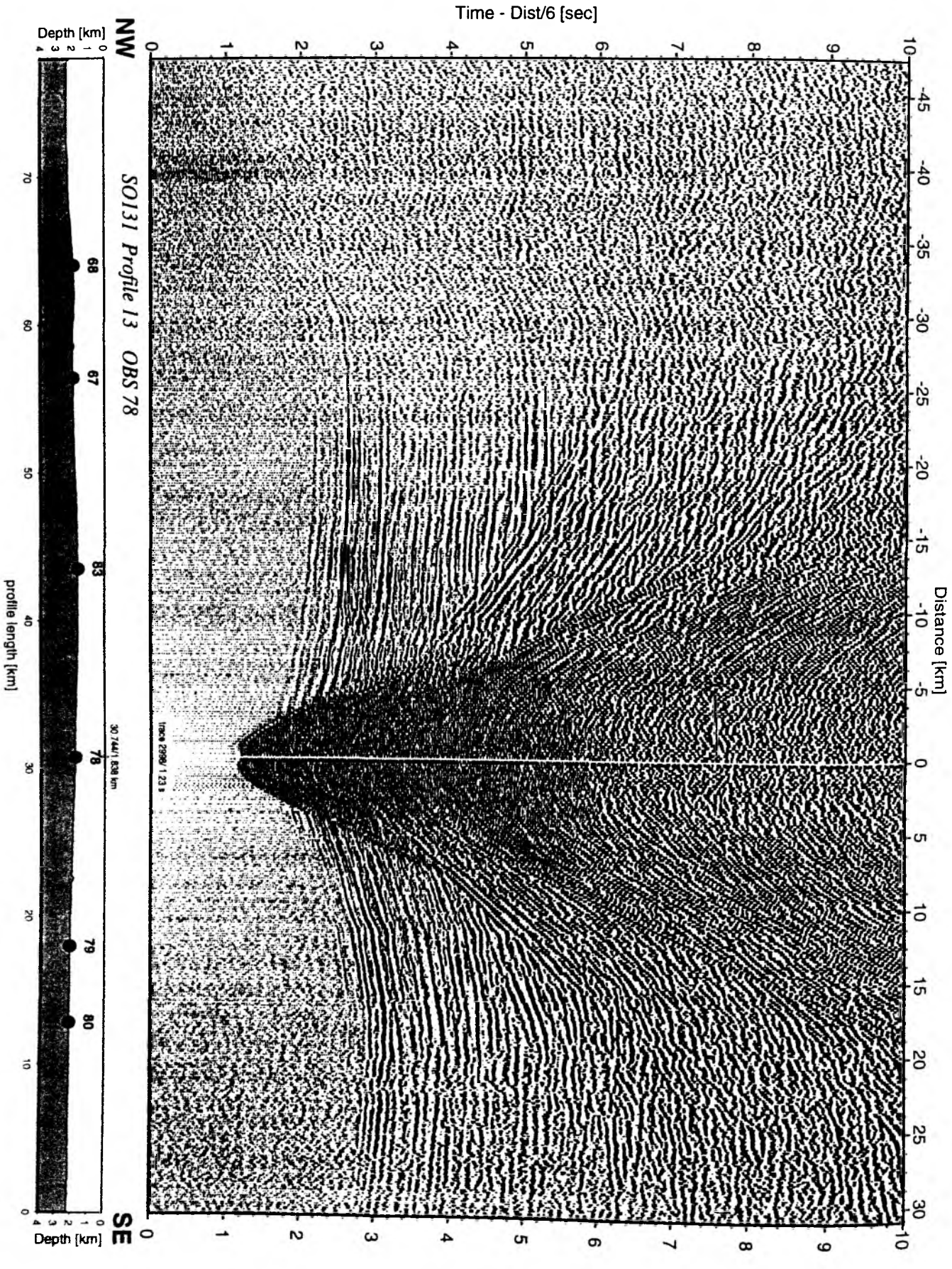

Figure 6.3.4.7.3.62: Record section from OBS 78 horizontal component 1, Profile 13.

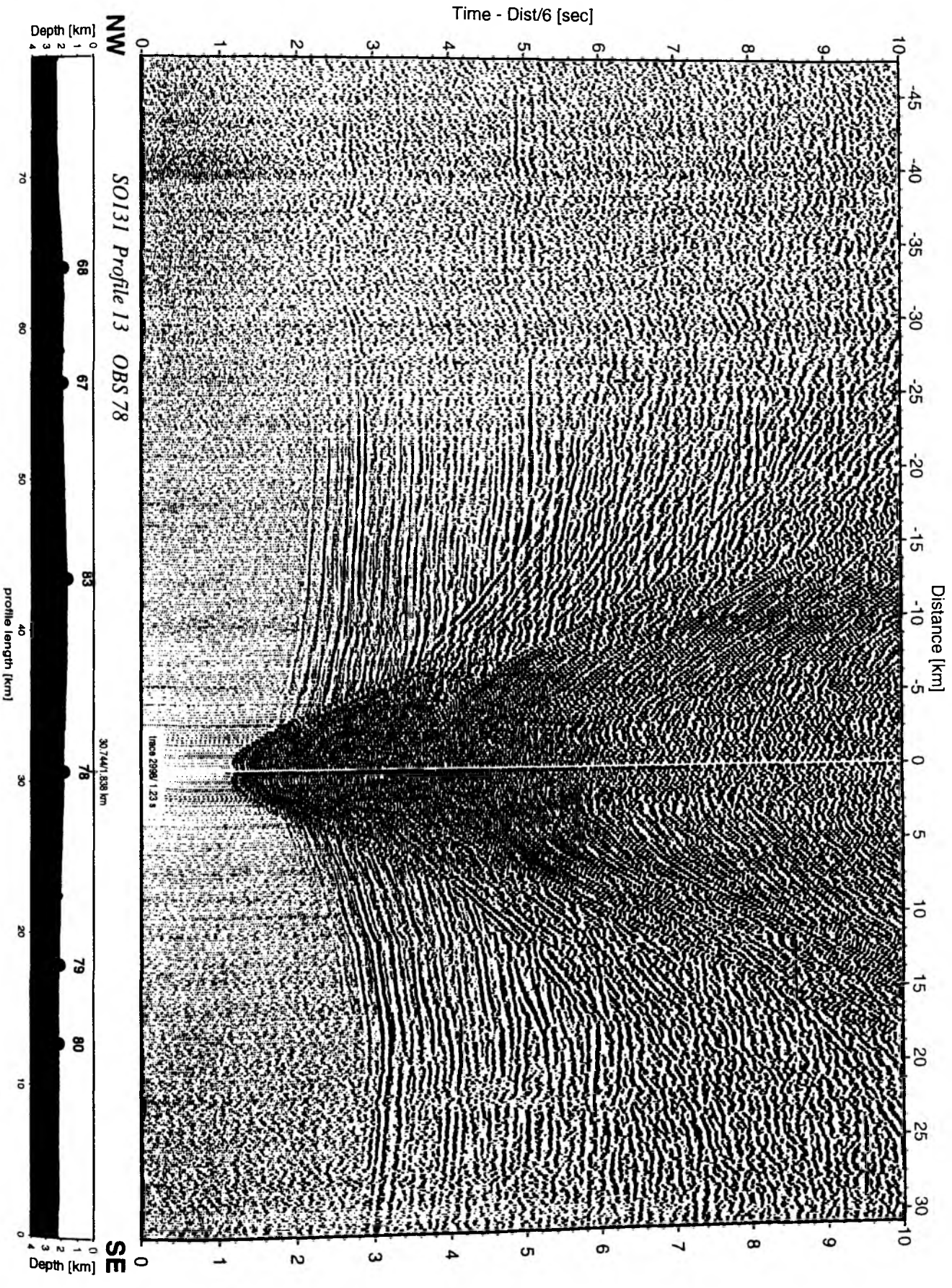

Figure 6.3.4.7.3.63: Record section from OBS 78 horizontal component 2, Profile 13.

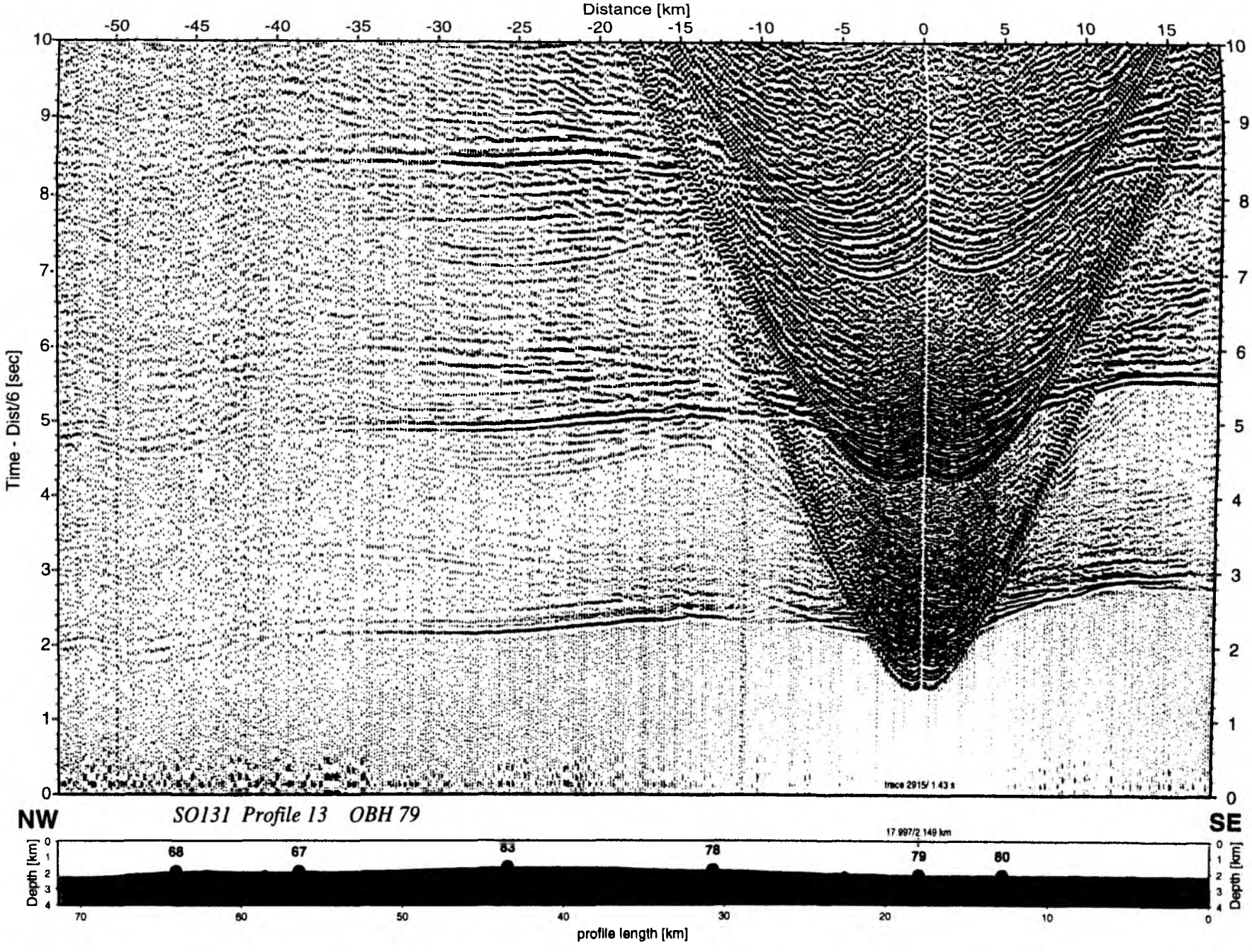

Figure 6.3.4.7.3.64: Record section from OBH 79 , Profile 13.

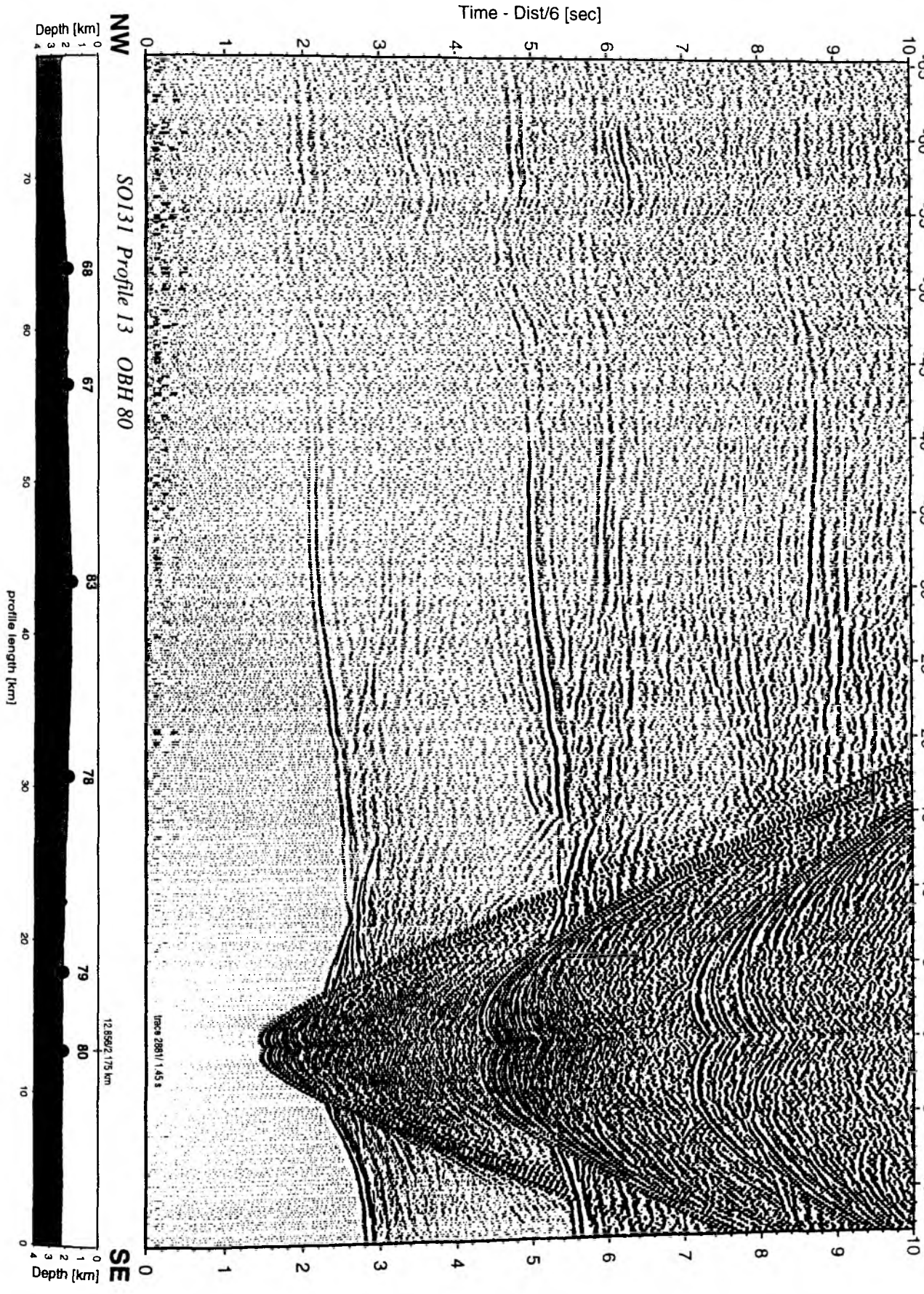

Figure 6.3.4.7.3.65: Record section from OBH 80 , Profile 13.

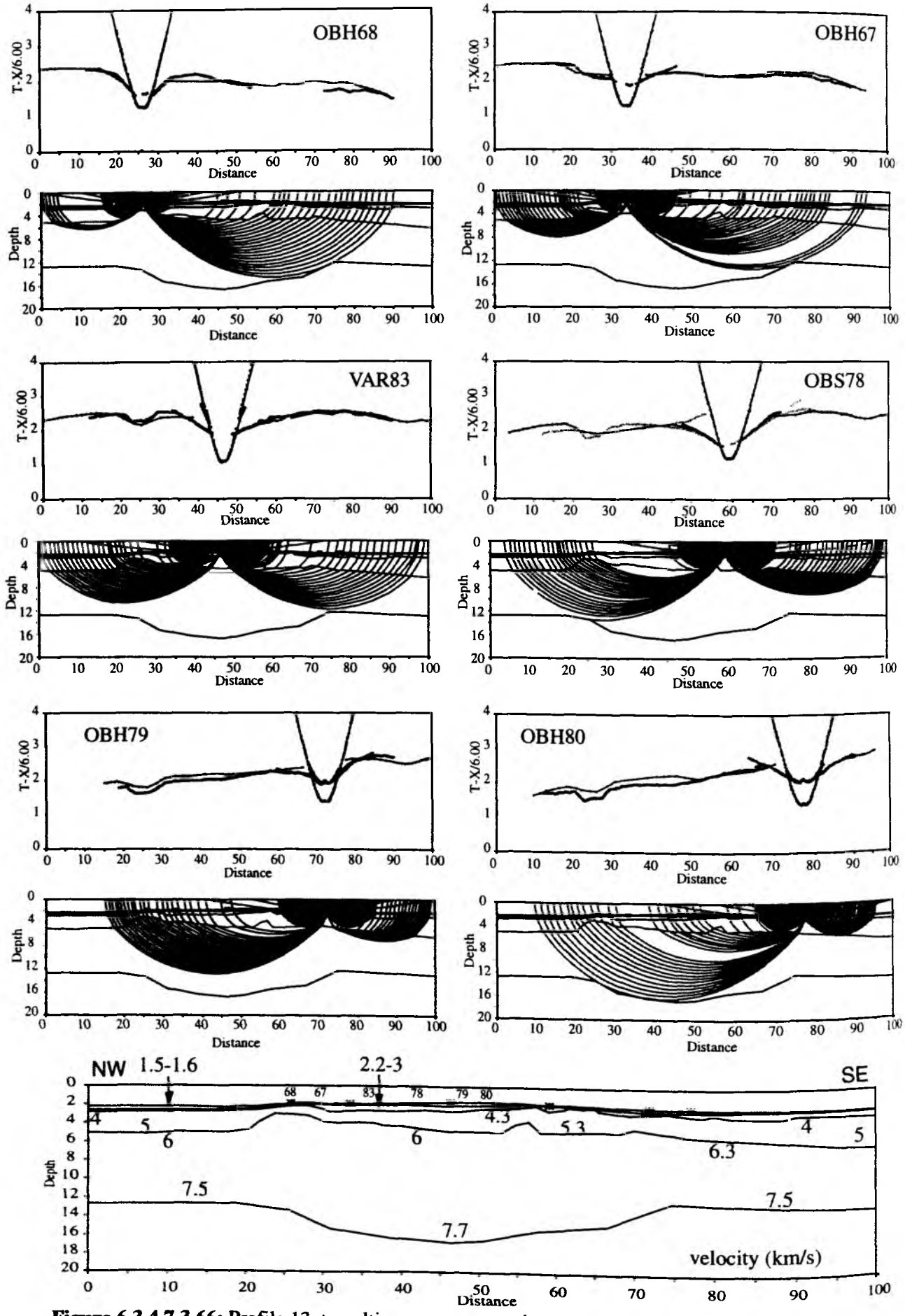

Figure 6.3.4.7.3.66: Profile 13, traveltimes, ray penetration and velocity model after preliminary forward modelling.

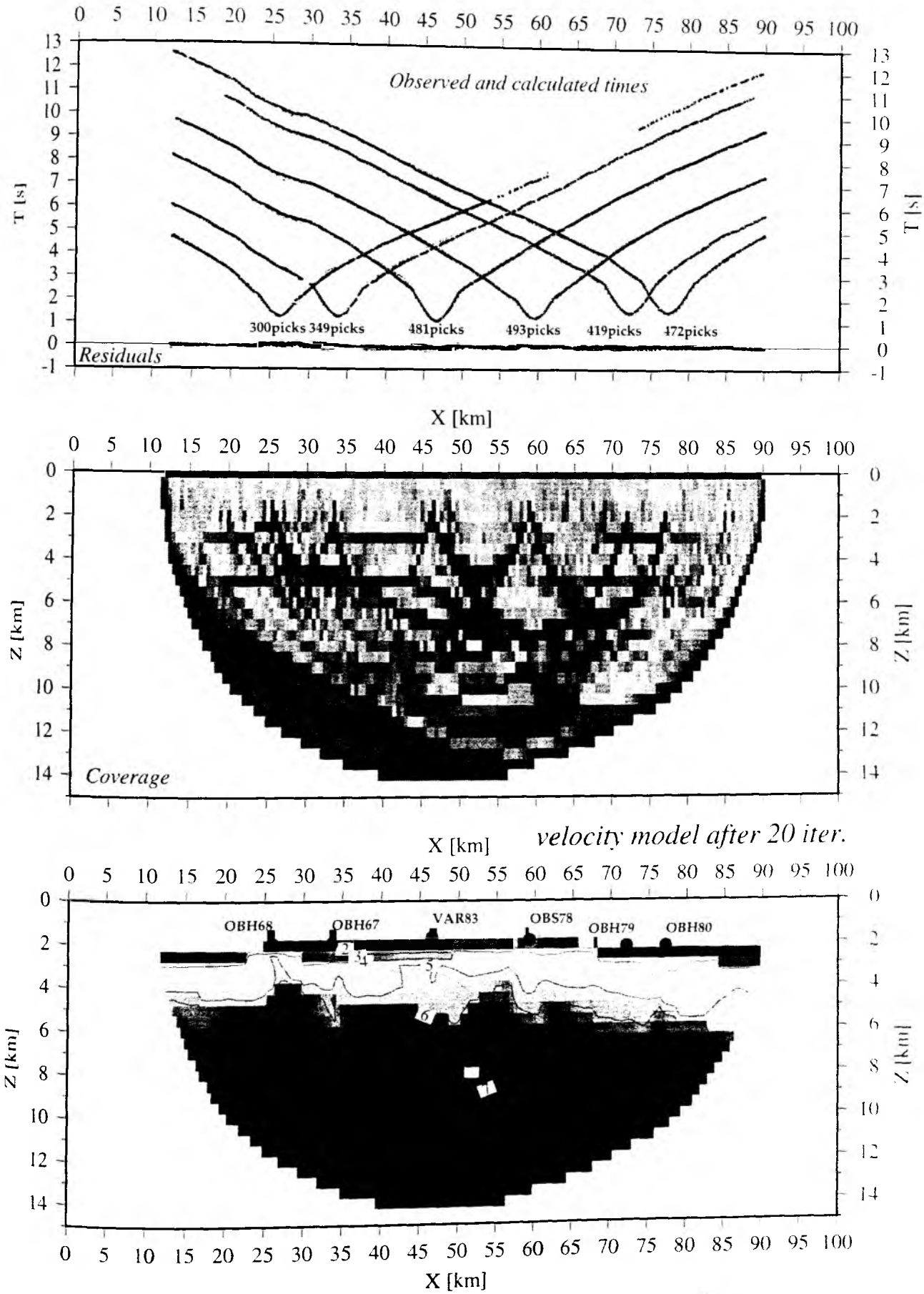

Figure 6.3.4.7.3.67: Results of a first arrival refraction tomography for profile 13.

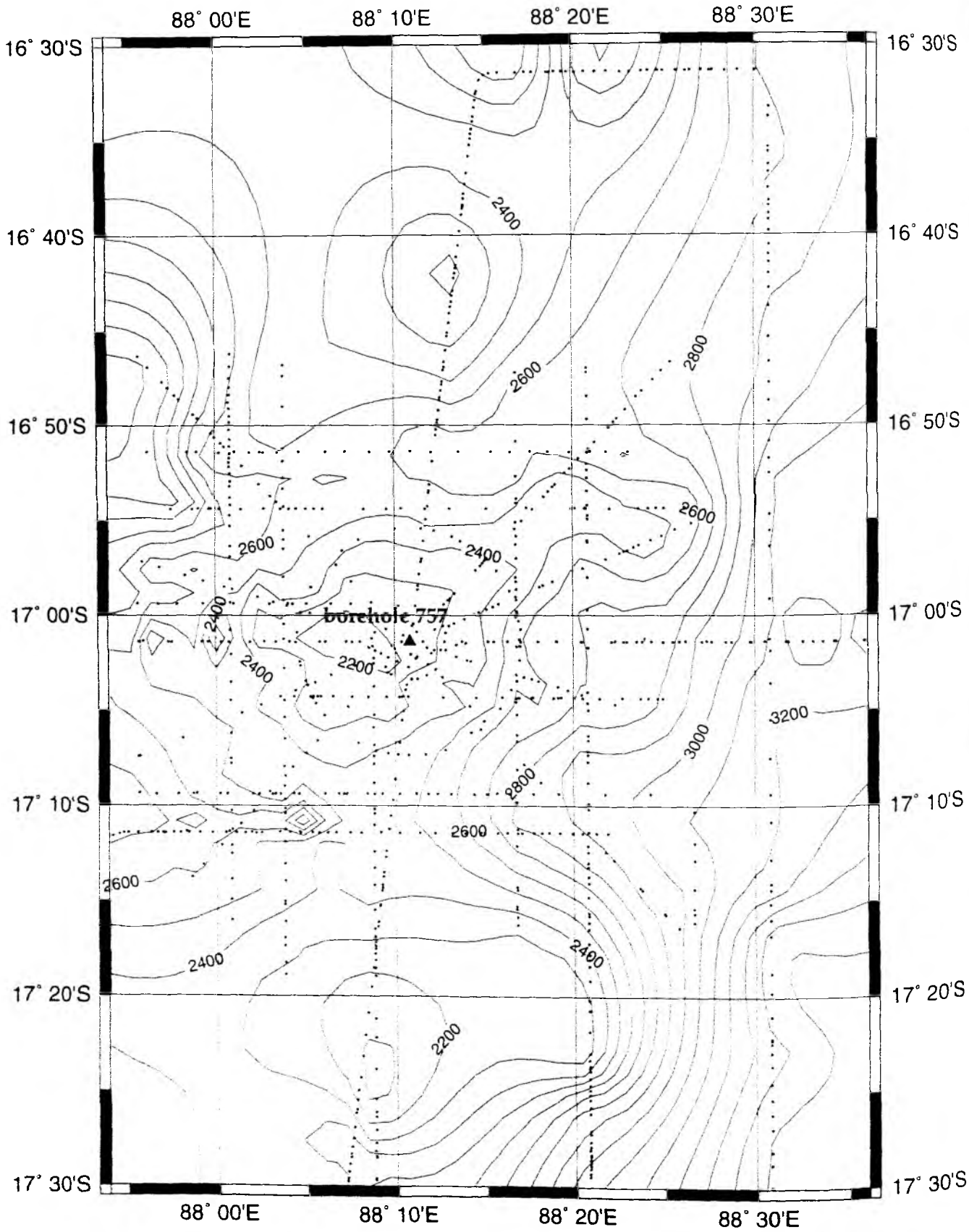

Figure 6.3.4.7.3.68: Depth of the seafloor in TWT [ms] from digitized MCS data.

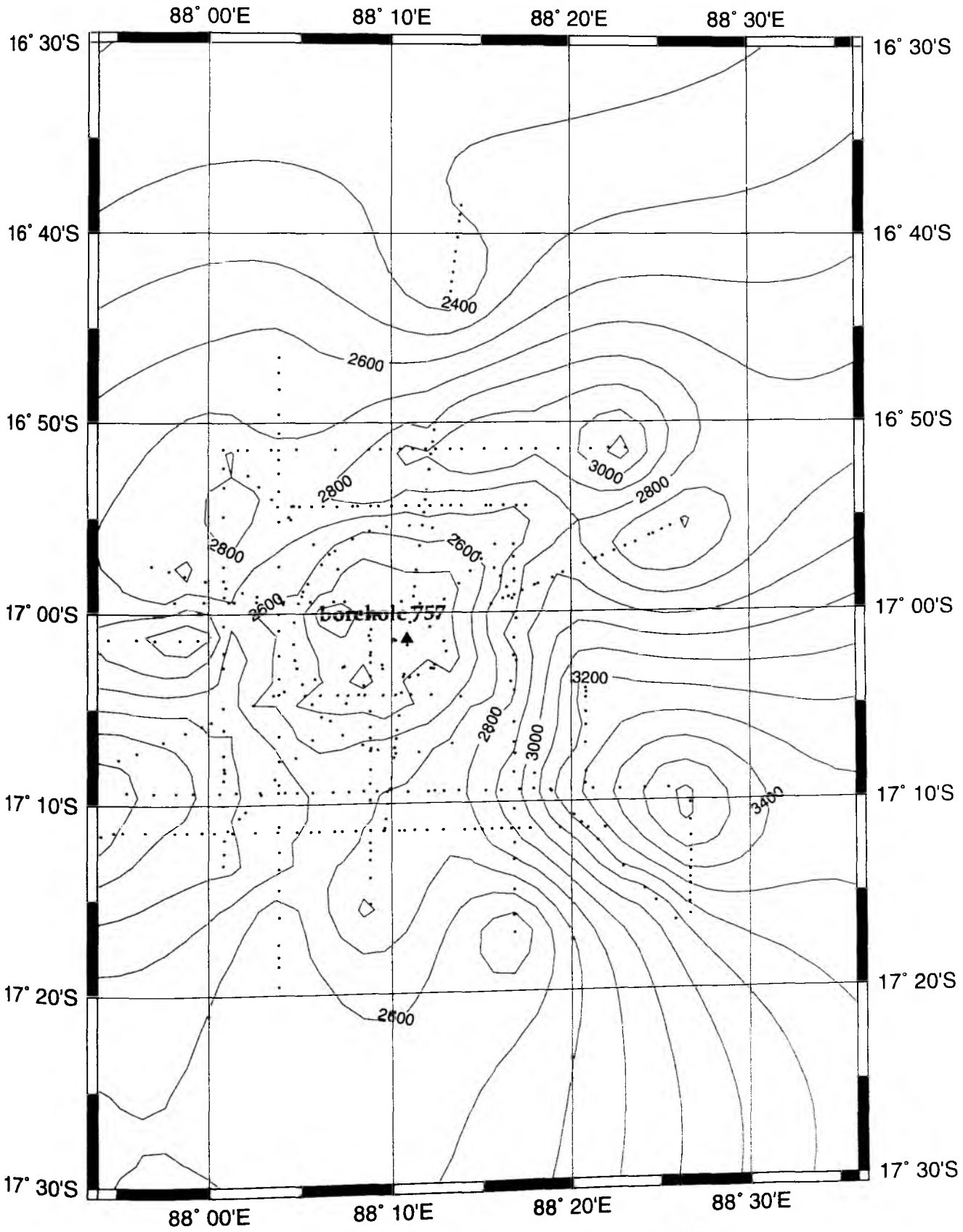

Figure 6.3.4.7.3.69: Depth map of the top of the first layer below sealevel in TWT [ms].

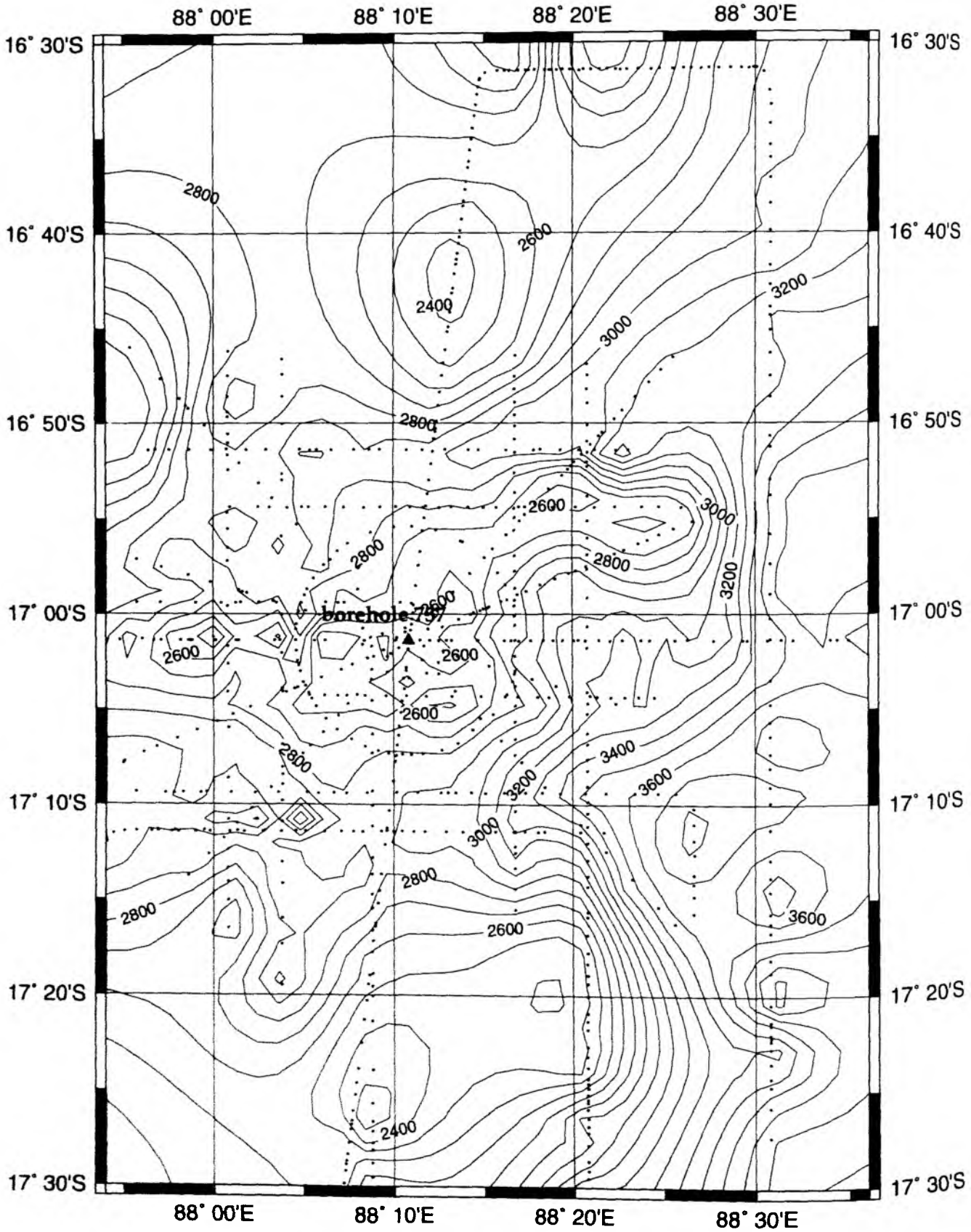

Figure 6.3.4.7.3.70: Depth map of the top of the basement below sealevel in TWT [ms].

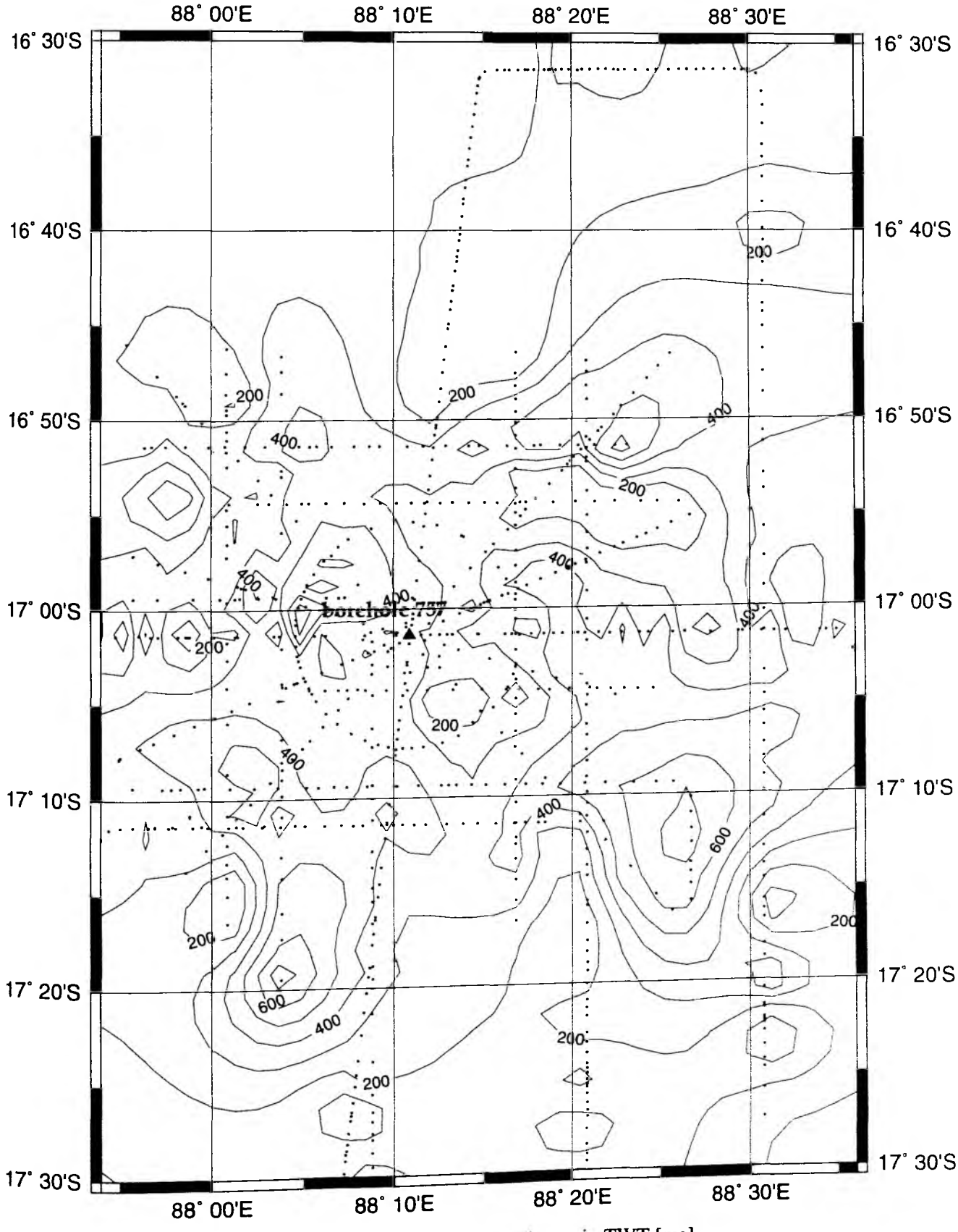

Figure 6.3.4.7.3.71: Isochron thickness map of the sediment in TWT [ms].

6.3.4.8 PROFILE SO131-31

(C. Kopp, I. Grevemeyer, H. Lelgemann, J. Bialas)

Profile SO131-31 completes the east-west oriented dipline across the Ninetyeast Ridge, in prolongation of SO131-05 and 06. It starts imediately east of SO131-06, and 15 instruments (OBH94 to 108) were deployed at 4 nm spacing centered around the Ninetyeast Fracture Zone in the Wharton Basin. Instruments were deployed between 16:00 and 24:00 on 04.06. Shooting started at 05:00 05.06 with 60 s shot interval and was terminated at 15:00 06.06. The location of instruments and shots is shown in Figure 6.3.4.8.1. The streamer was also deployed during shooting and the near vertical data are shown in Figure 6.3.4.8.2. All instruments were recovered between 06:00 and 18:00 07.06. Details on instrumentation can be found in Appendix 9.1.8. All instruments recorded well, and the record sections are shown in Figures 6.3.4.8.3 to 6.3.4.8.20. Most records are of excellent quality, especially those located in deeper waters.

Modelling and interpretation:

As line SO131-31 is the eastern prolongation of line SO131-06, the velocity model shown in Figure 6.3.4.8.21 was taken as basis for the western part of this model. For a better comparison, and to enable a later merging of both models, the same number of interfaces was chosen. This explains the large number of dummi interfaces beneath the seafloor. The velocities in the overlapping areas are kept equal except for some differences discussed later.

Bathymetric mapping of the area revealed the location of the Ninetyeast Fracture Zone to be around km 90 along this profile, where the seafloor shows prominent volcanic structures, particularly two peaks at the western part of the fracture zone. The topography of this area has strong effects on the seismic phases resulting in an unusual changing of high and low apparent velocities (see for example Figure 6.3.4.8.21 a).

Seismic modelling reveals a basement topography which is even rougher than the seafloor, showing several deep sediment troughs. The remarkable basement low at the flank of the eastern peak at km 90 is filled with sediment that has a velocity of about 3.3 km/s, which is observed by OBH 104 and OBH 105 (slow refraction phases at km 90 and km 75 in Figure 6.3.4.8.16). On very short segments the basement depth could be picked from the streamer data, but the reflections on the MCS data are rather scattered on this line.

Sediment phases can be seen on only a few OBH sections, which indicates a generally thin sediment cover. Velocities raise to 5.5 km/s and 6.0 km/s respectively, close to the seafloor in many parts of the model. Underneath the bathymetric high between 130 and 90 km velocities are about 5.5 km/s, which is lower than in the vicinity of this structure. The 6.0 isopach descends beneath the two peaks.

Though interpreted only from the bathymetry it could be explained by a tectonic origin (e.g. thrust zone). This velocity structure confirms rather the interpretation of extrusions forming a volcanic body imposed upon the crust. The interface between 5 km/s and 6 km/s gives strong reflections in refraction as well as in the reflection seismics (Figure 6.3.4.8.2). It is interpreted as the lower boundary of the younger volcanic material.

Crustal and mantle refractions show up very clearly on most of the sections up to a shot distance of 160 km. Far reaching lower crustal refractions at some stations give detailed insight to the velocities in the lower part of the crust

(Figure 6.3.4.8.8). Some mantle reflections additionally confirm the Moho depth (e.g. on OBH 95 and OBH 99 to the west).

Compared to normal oceanic crust, velocities are rather high in the upper crust with 6 km/s at one kilometer beneath seafloor. The high velocities of the lower crust are decreasing from west (7.5 km/s) to east (7.2-7.3 km/s) toward more or less normal lower crust velocities. The gradient does not change significantly compared to the model of profile SO131-06, neither in the upper nor in the lower crust. The dashed line in Figure 6.3.4.8.21 represents no significant change in velocities, but separates the high gradient of the upper crust from the low gradient beneath.

The total thickness of the crust decreases on profile SO131-06 from 22 km to less than normal thickness (at km 210 in Figure 6.3.4.31). This general trend is confirmed by the westernmost stations of profile SO131-31, but the observation on this line reveals a greater thickness of about 7 km with little reduced lower crustal velocities (km 140 - 190 on Figure 6.3.4.8.21). To fix this and some other differences between the two models a combined modeling with all available stations has to be done. However, the general fit between the different observations is acceptable. Between km 60 and 110 the crust thickens again to 9.5 km, which can be seen clearly on several stations. This thickening occurs around the presumed location of the Ninetyeast Fracture and suggests a relation between both. The course of the isopachs shows a crustal downbending rather than a simple thickening, which could be caused by an additional thrust component to the actual strike slip character of the fracture. East of the fracture zone the crust measures only 5.5 km, which could indicate generation by a slow spreading ridge.

The velocities of the upper mantle range between 7.9 and 8.0 km/s which is comparable to the lines in the west. There may also be some hints for intra-mantle reflections like on profile SO131-06, but in any case, they are not that pronounced. It is interesting to note that the Ninetyeast Fracture Zone apparently acts as a barrier to wave propagation. OBH 94 to 101 all show high energy from the westernmost shots to distances of up to 200 km. All instruments located further east receive energy from no further away than the 89° Fracture Zone (max. 100 km).

A compilation of the velocity models from profiles SO131-05, SO131-06, and SO131-31 with a total length of 520 km as discussed separately in the previous sections is given in Figure 6.3.4.22.

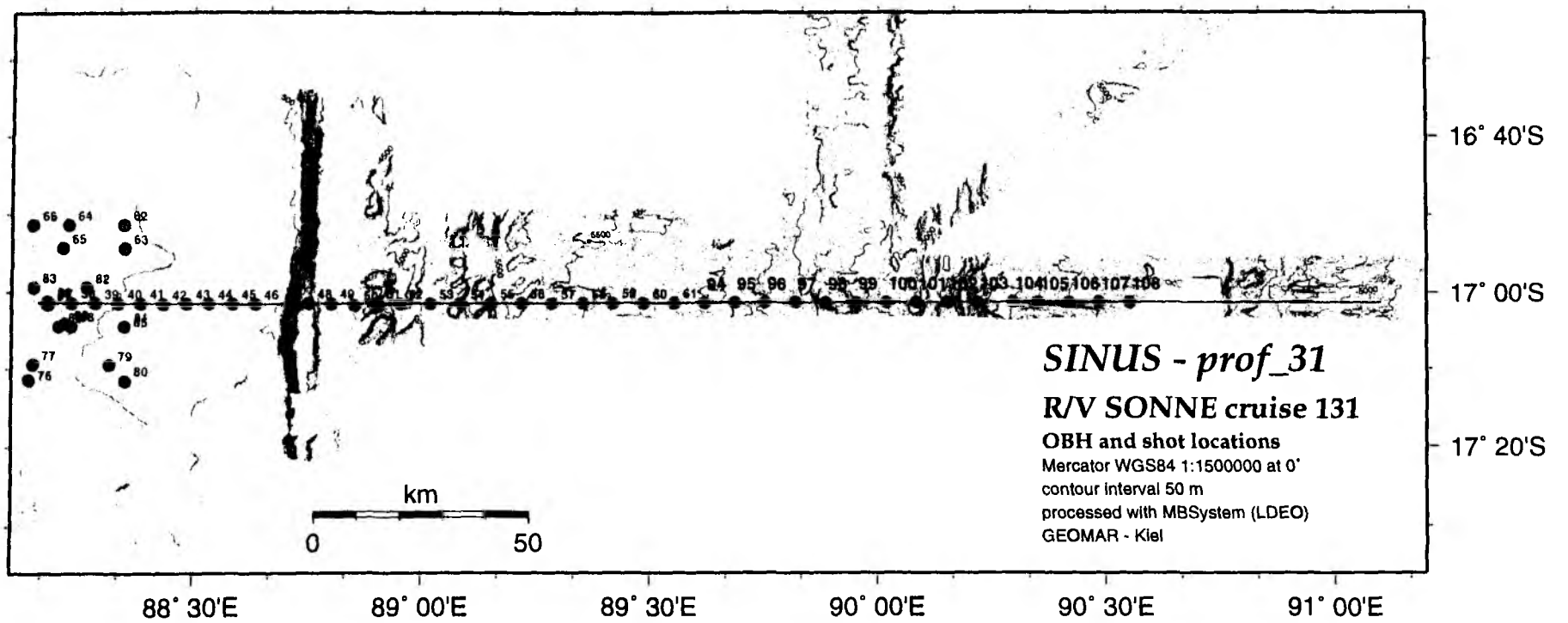

Fig. 6.3.4.8.1: Profile 31 - Shot and OBH positions.

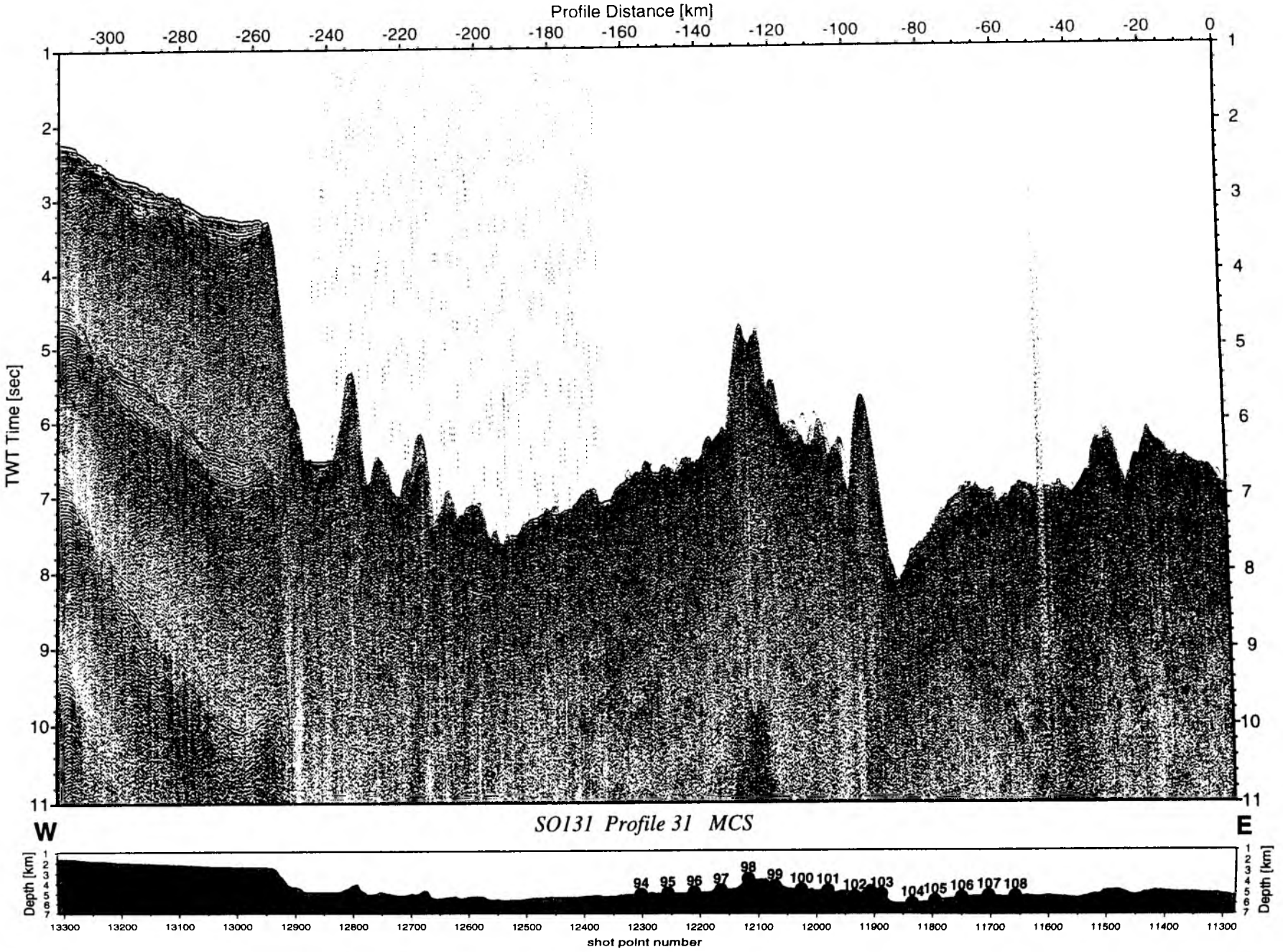

Figure 6.3.4.8.2: Seismic section from MCS stack, Profile 31.

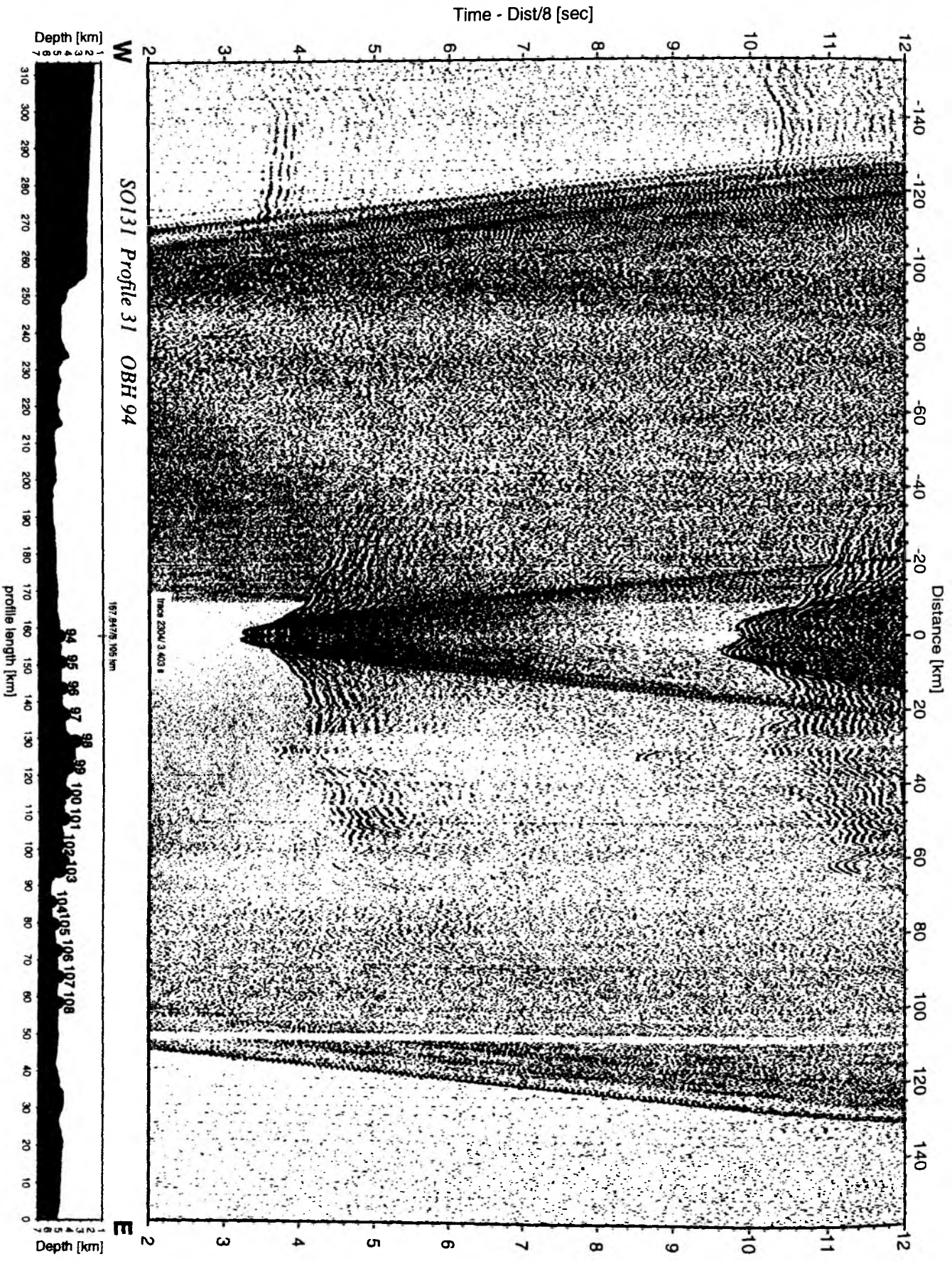

Figure 6.3.4.8.3: Record section from OBH 94 , Profile 31.


Distance [km]
-160
-140
-120
-100
-80
-60
-40
-20
0
Time - Dist/8 [sec]
12
11
10
9
8
7
6
5
4
3
2
trace 2257/ 3.320 s
W
SO131 Profile 31 OBH 95
150.752/4.98 km
Depth [km]
1
2
3
4
5
6
7
94
95
96
310
300
290
280
270
260
250
240
230
220
210
200
190
180
170
160
150
140
profile length [km]

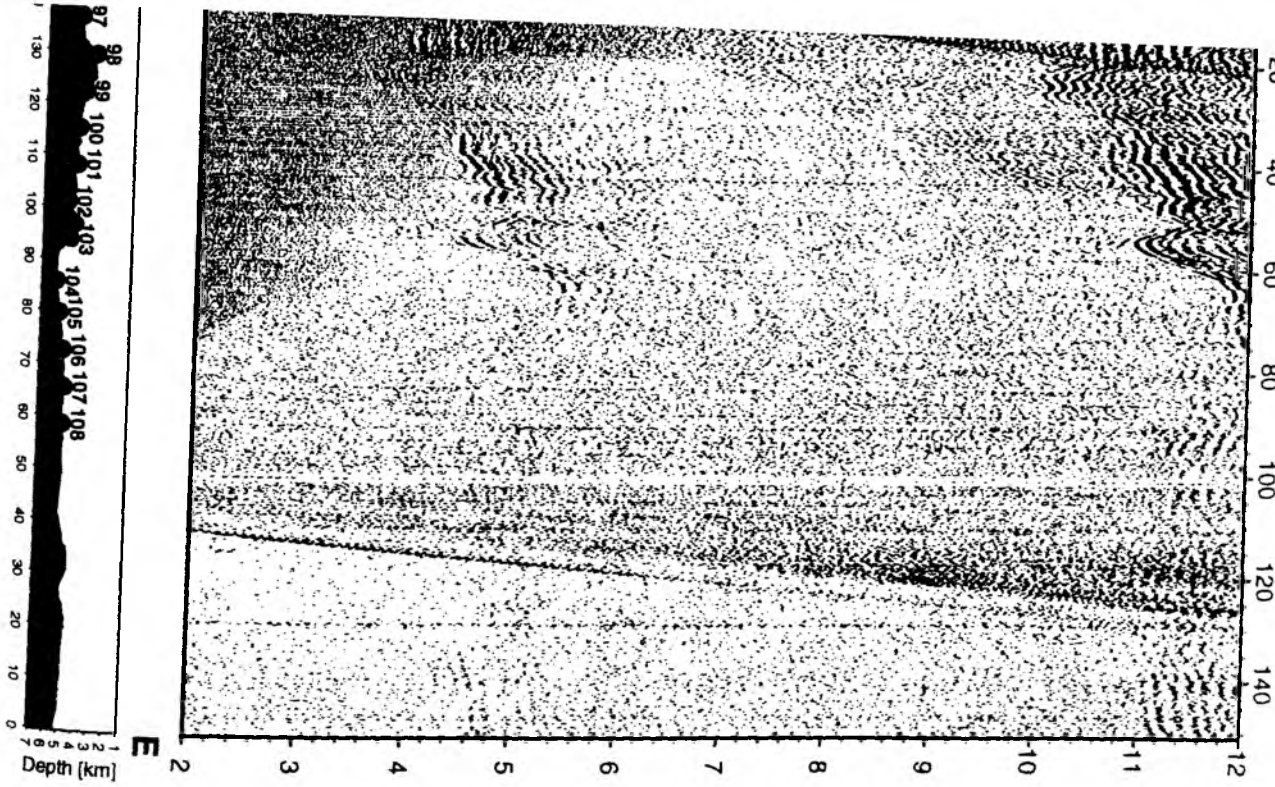

Figure 6.3.4.8.4: Record section from OBH 95 , Profile 31.

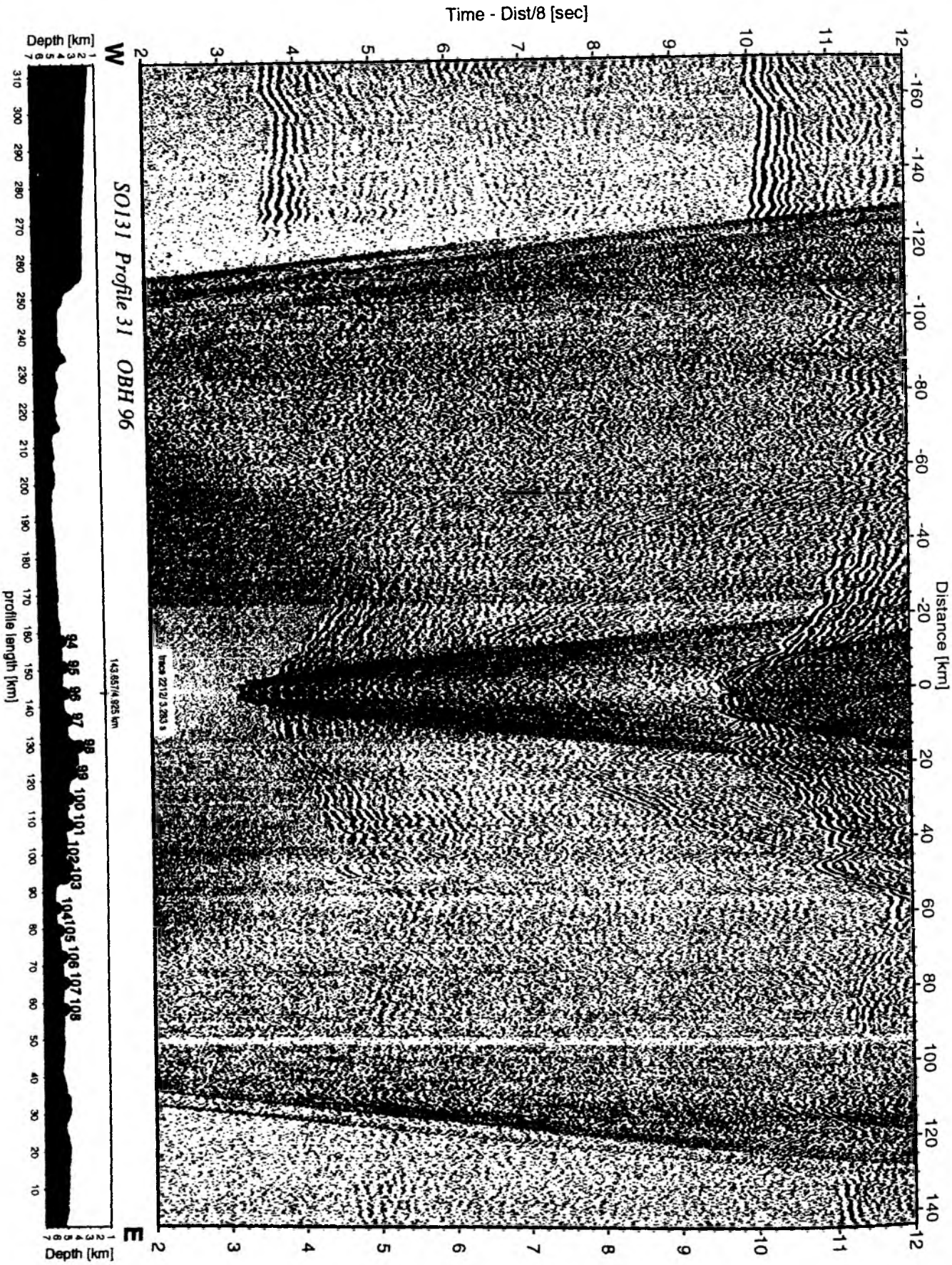

Figure 6.3.4.8.5: Record section from OBH 96 , Profile 31.

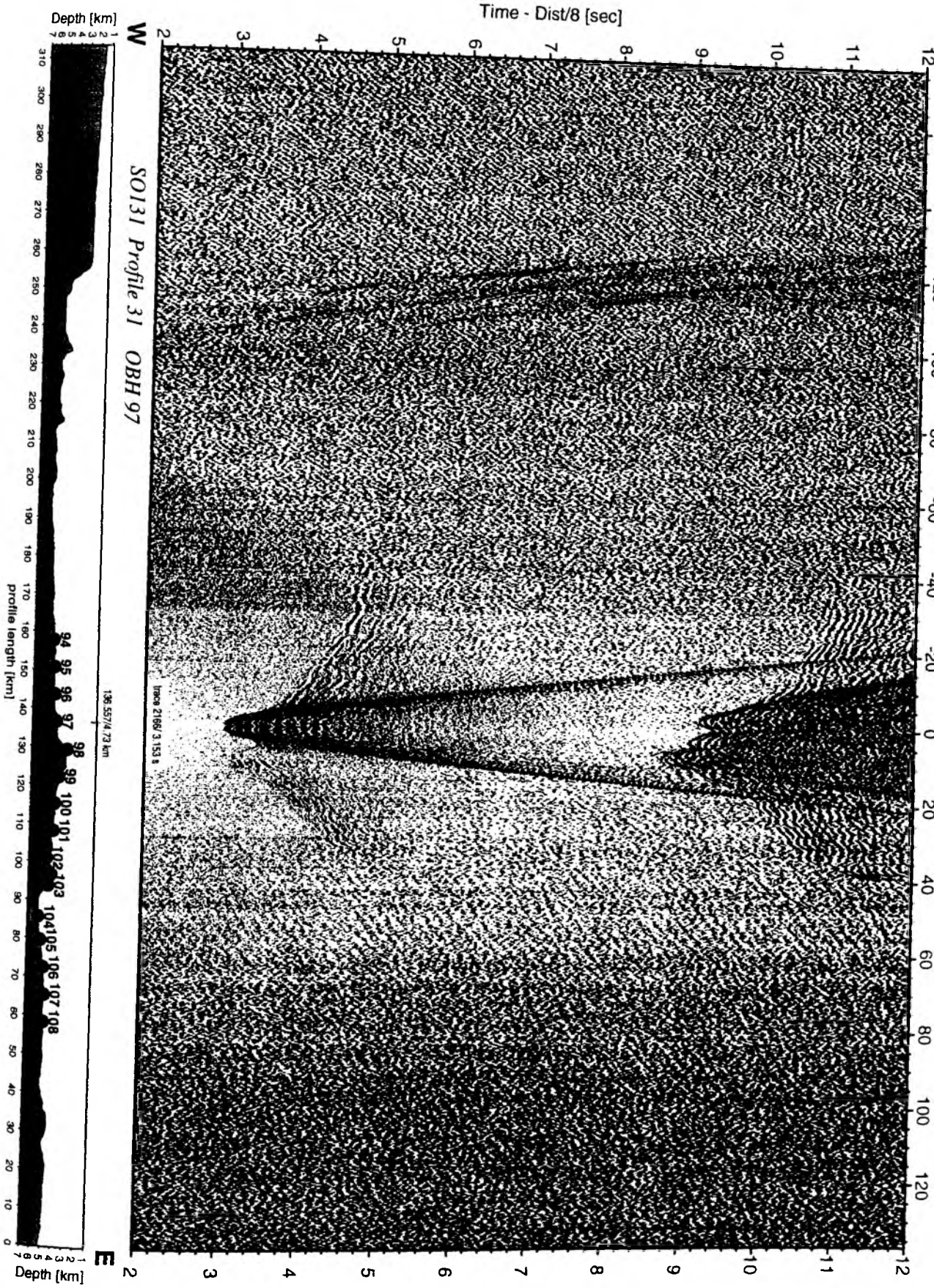

Figure 6.3.4.8.6: Record section from OBH 97 , Profile 31.

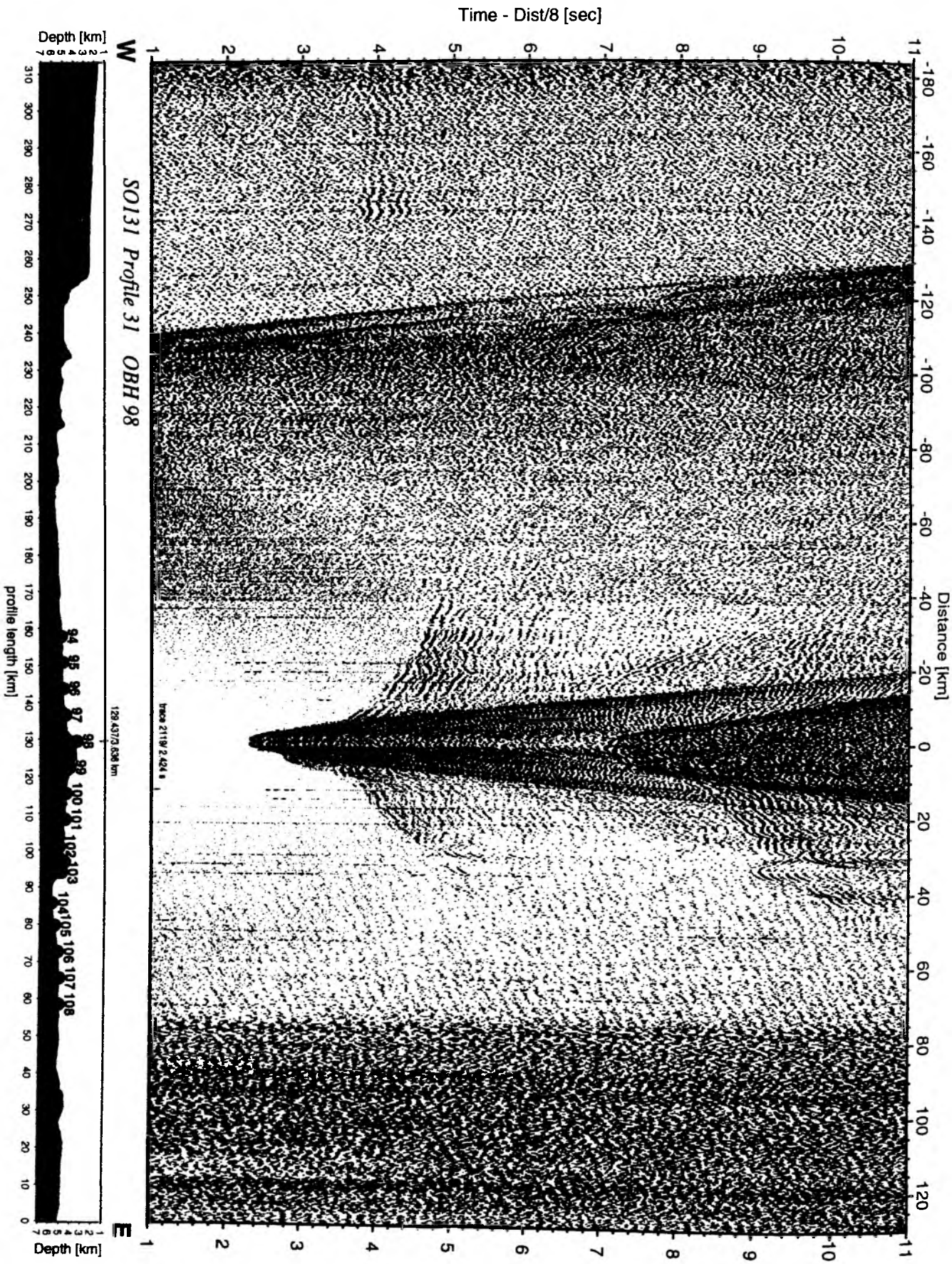

Figure 6.3.4.8.7: Record section from OBH 98 , Profile 31.

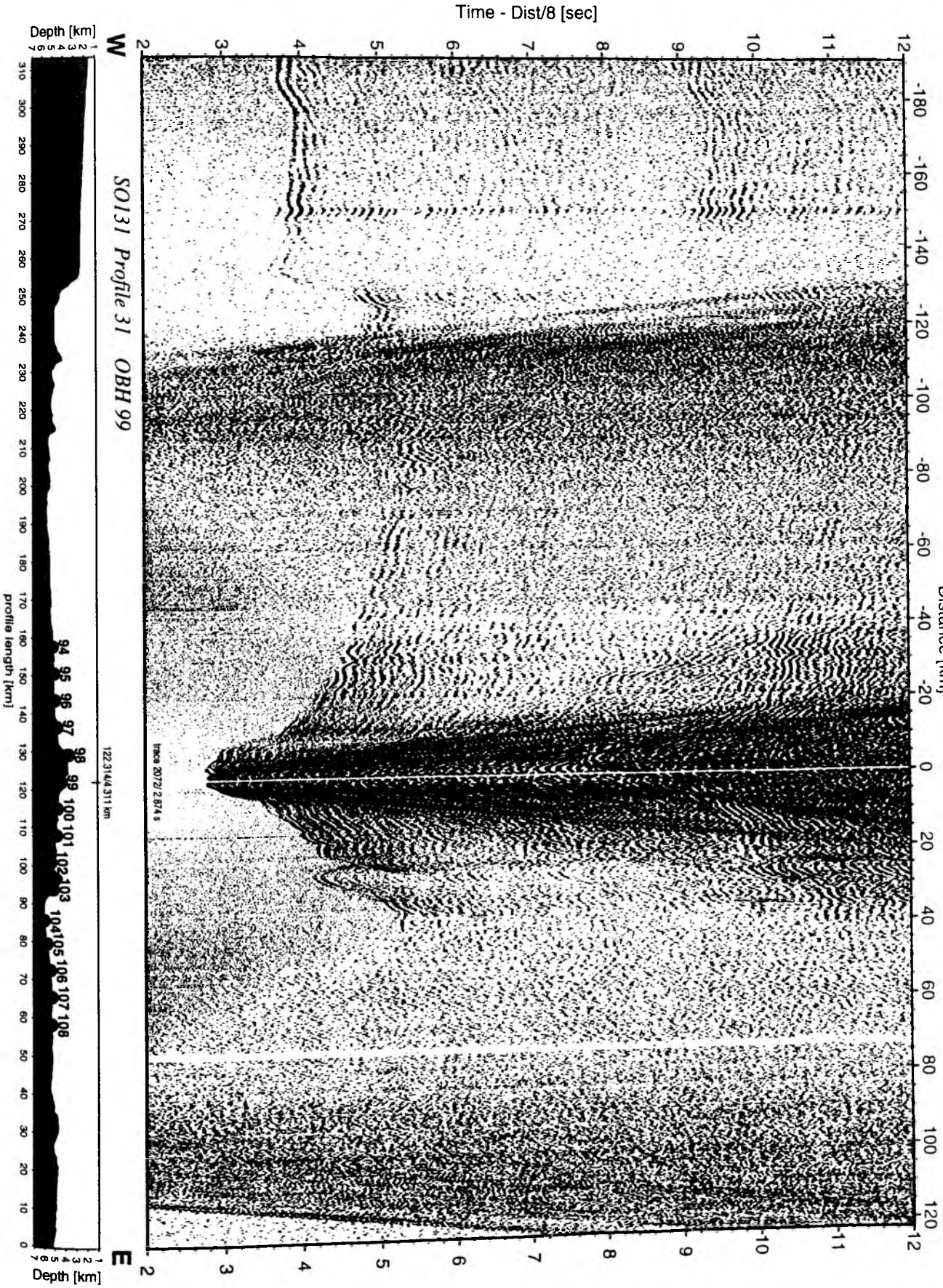

Figure 6.3.4.8.8: Record section from OBH 99 , Profile 31.

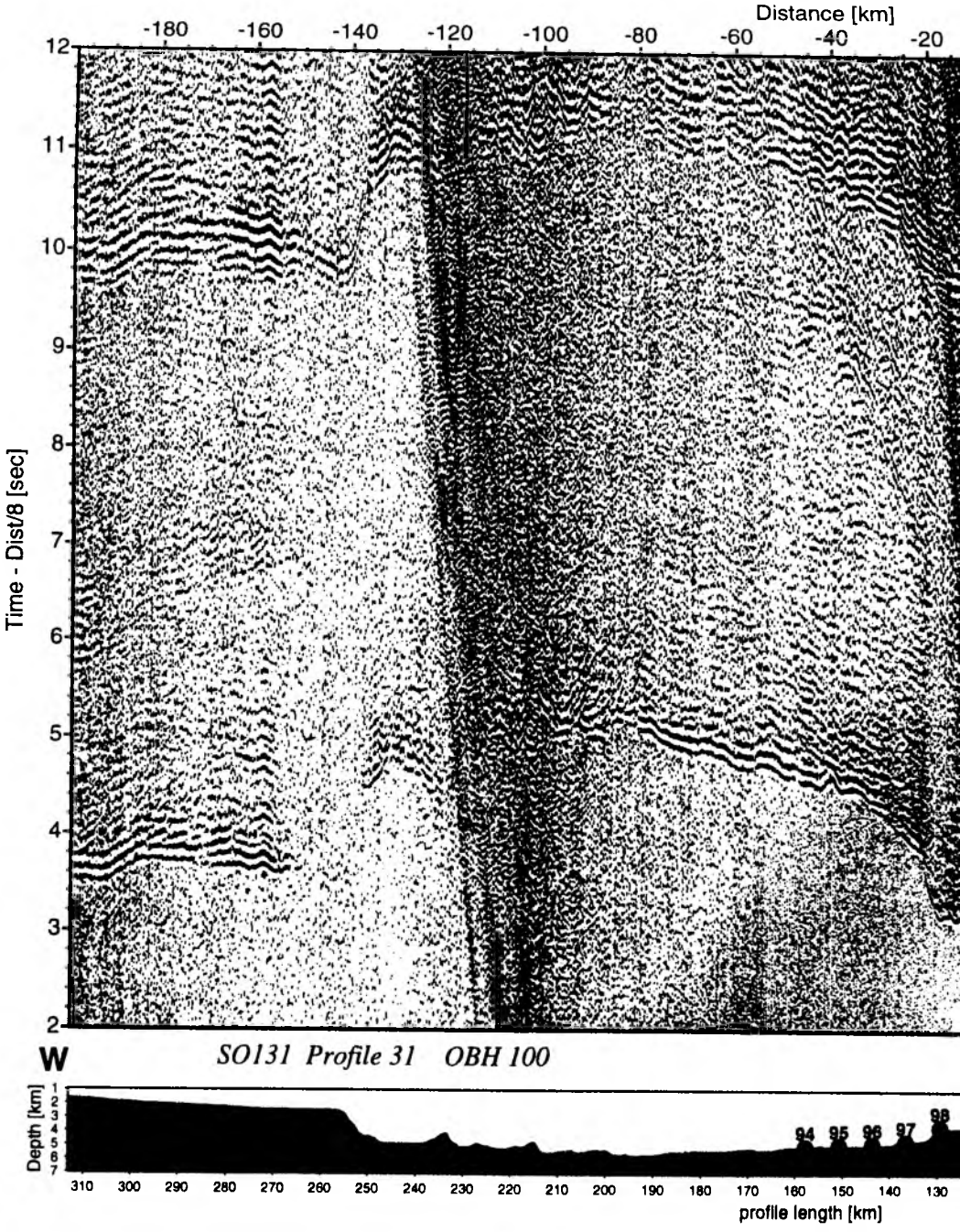
Distance [km]
-180
-160
-140
-120
-100
-80
-60
-40
-20
12
11
10
9
8
7
6
5
4
3
2
Time - Dist/8 [sec]
W
SO131 Profile 31 OBH 100
Depth [km]
1
2
3
4
5
6
7
94
95
96
97
98
310
300
290
280
270
260
250
240
230
220
210
200
190
180
170
160
150
140
130
profile length [km]

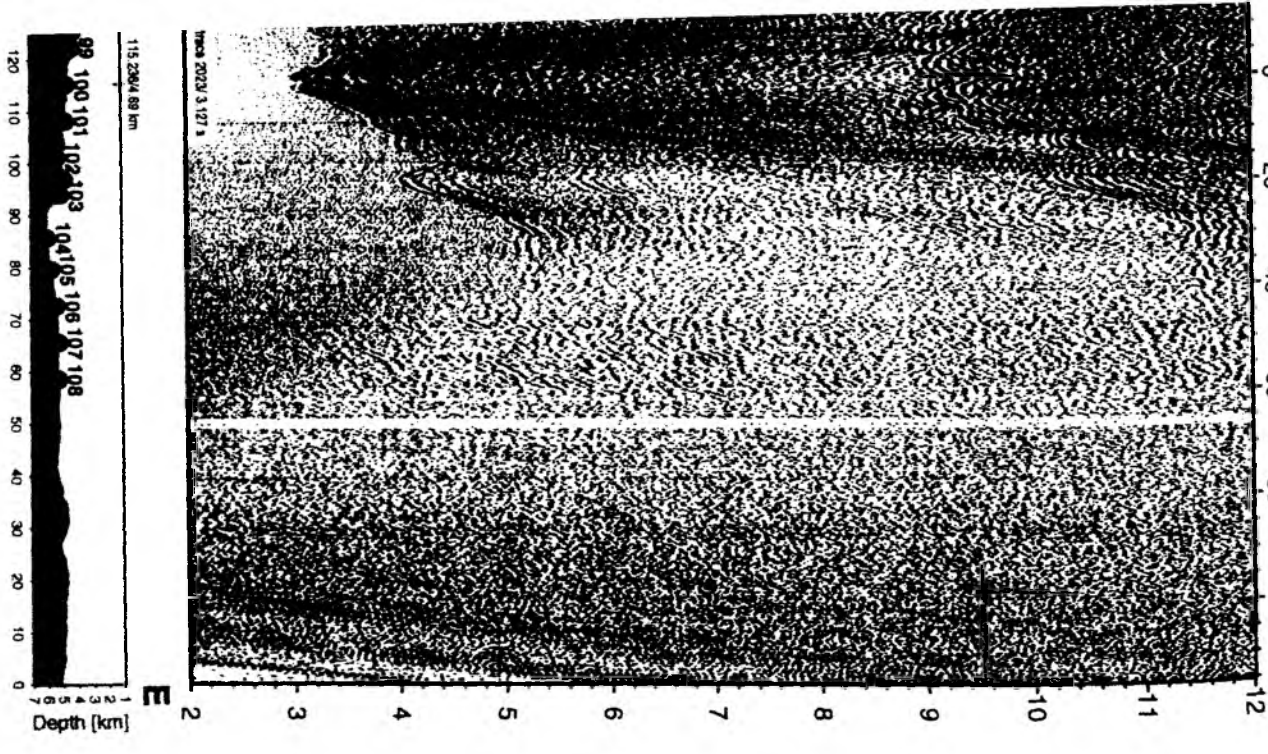

Figure 6.3.4.8.9: Record section from OBH 100 , Profile 31.

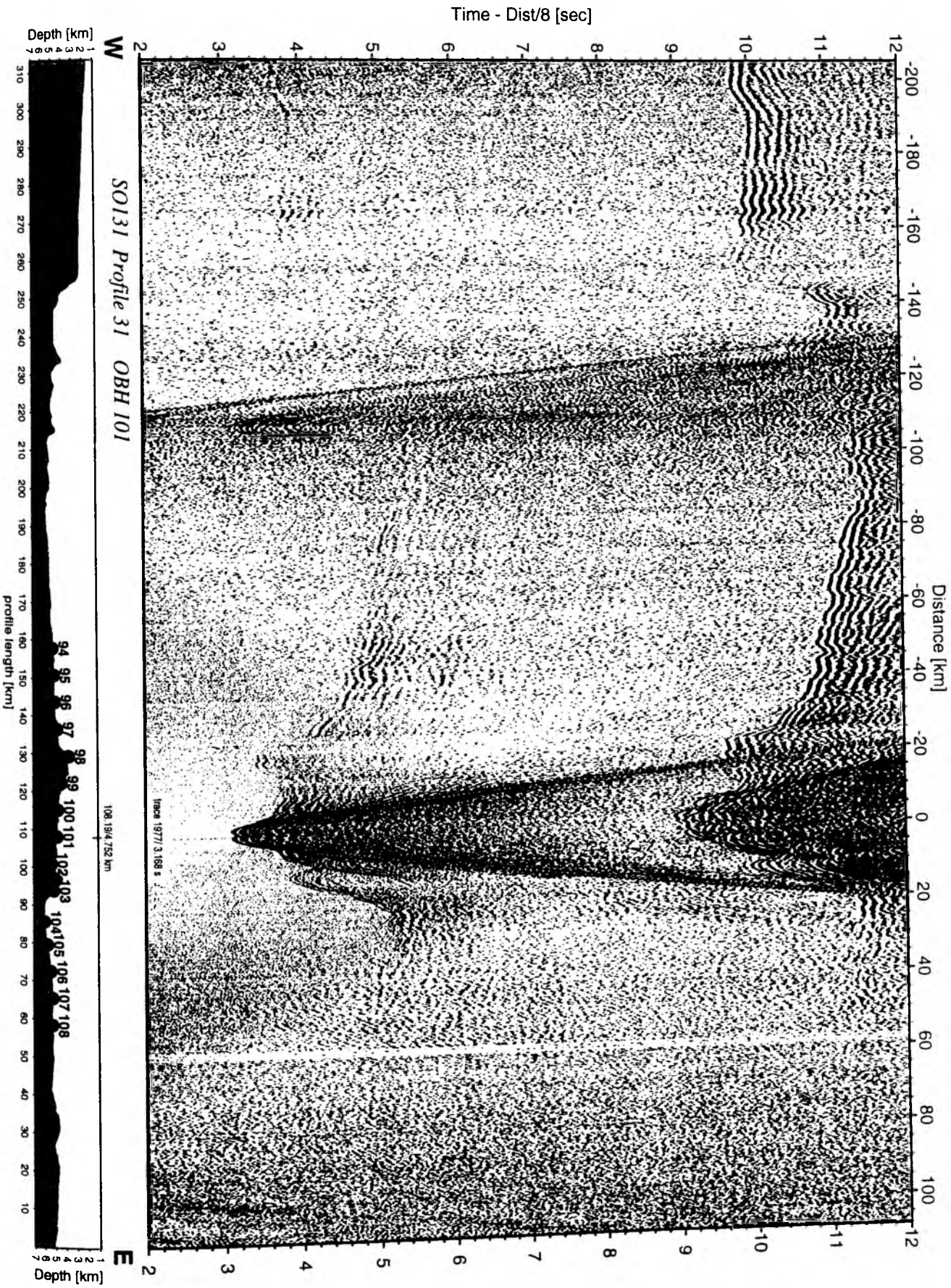

Figure 6.3.4.8.10: Record section from OBH 101 , Profile 31.

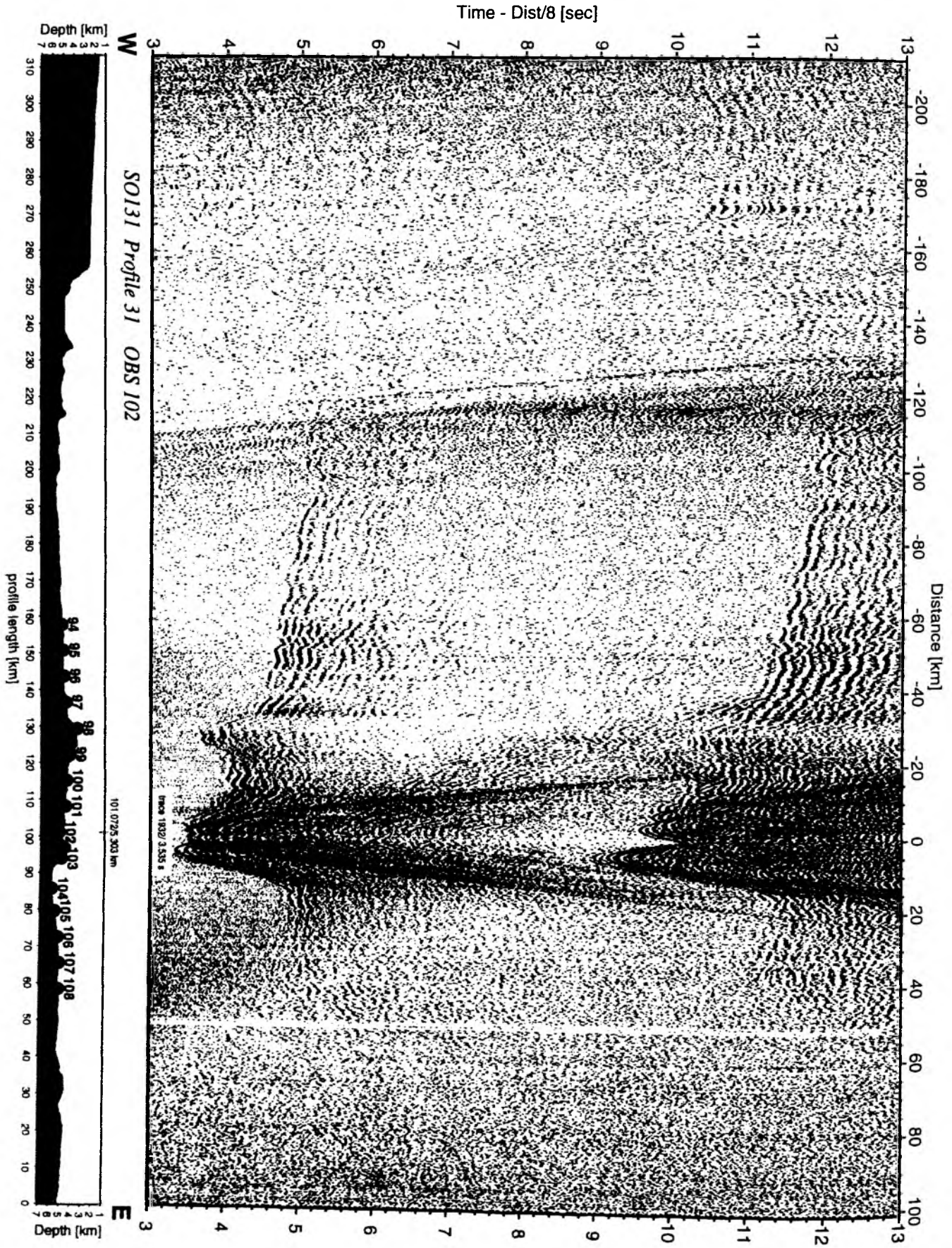

Figure 6.3.4.8.11: Record section from OBS 102 hydrophone, Profile 31.

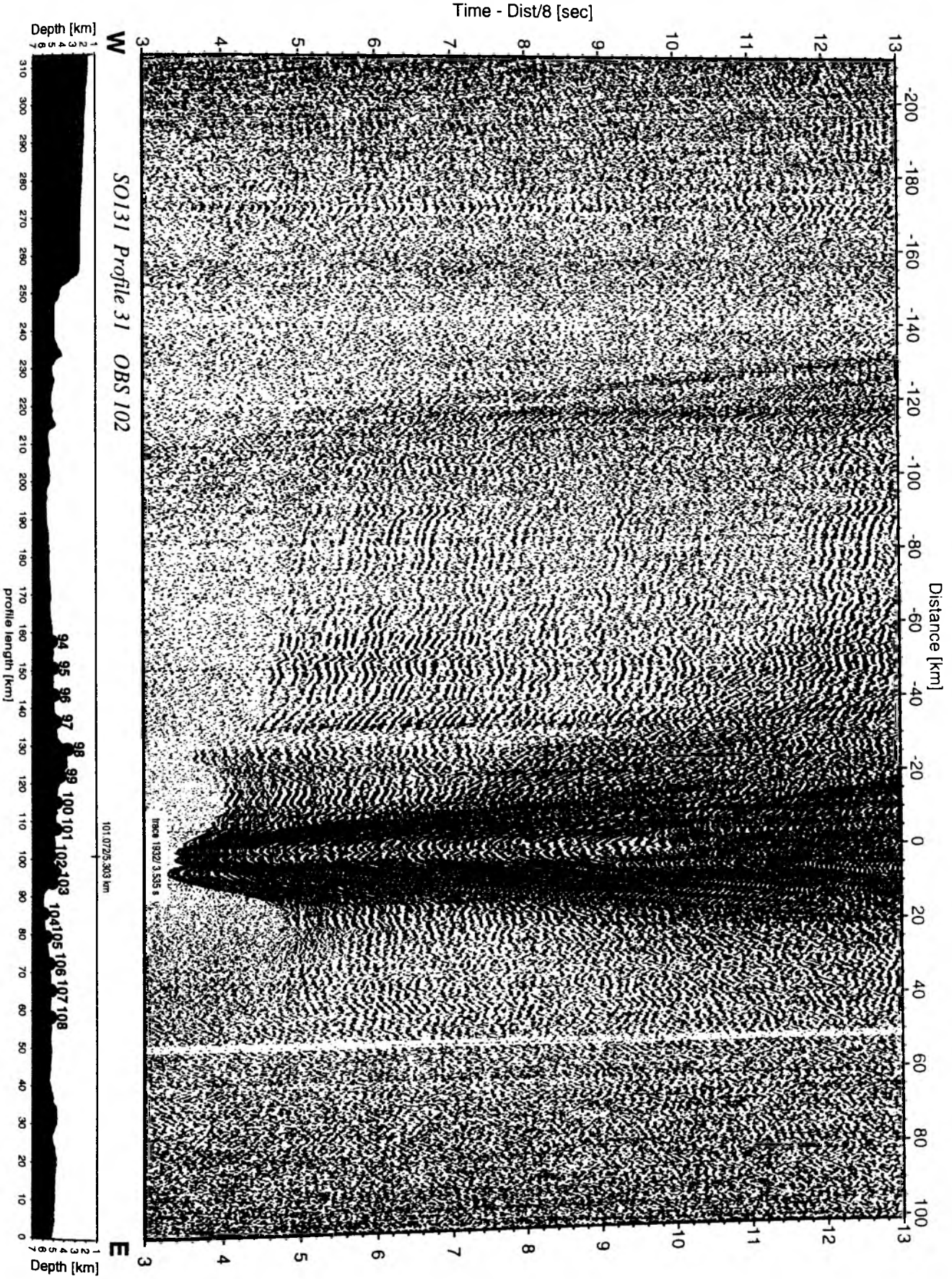

Figure 6.3.4.8.12: Record section from OBS 102 vertical component, Profile 31.

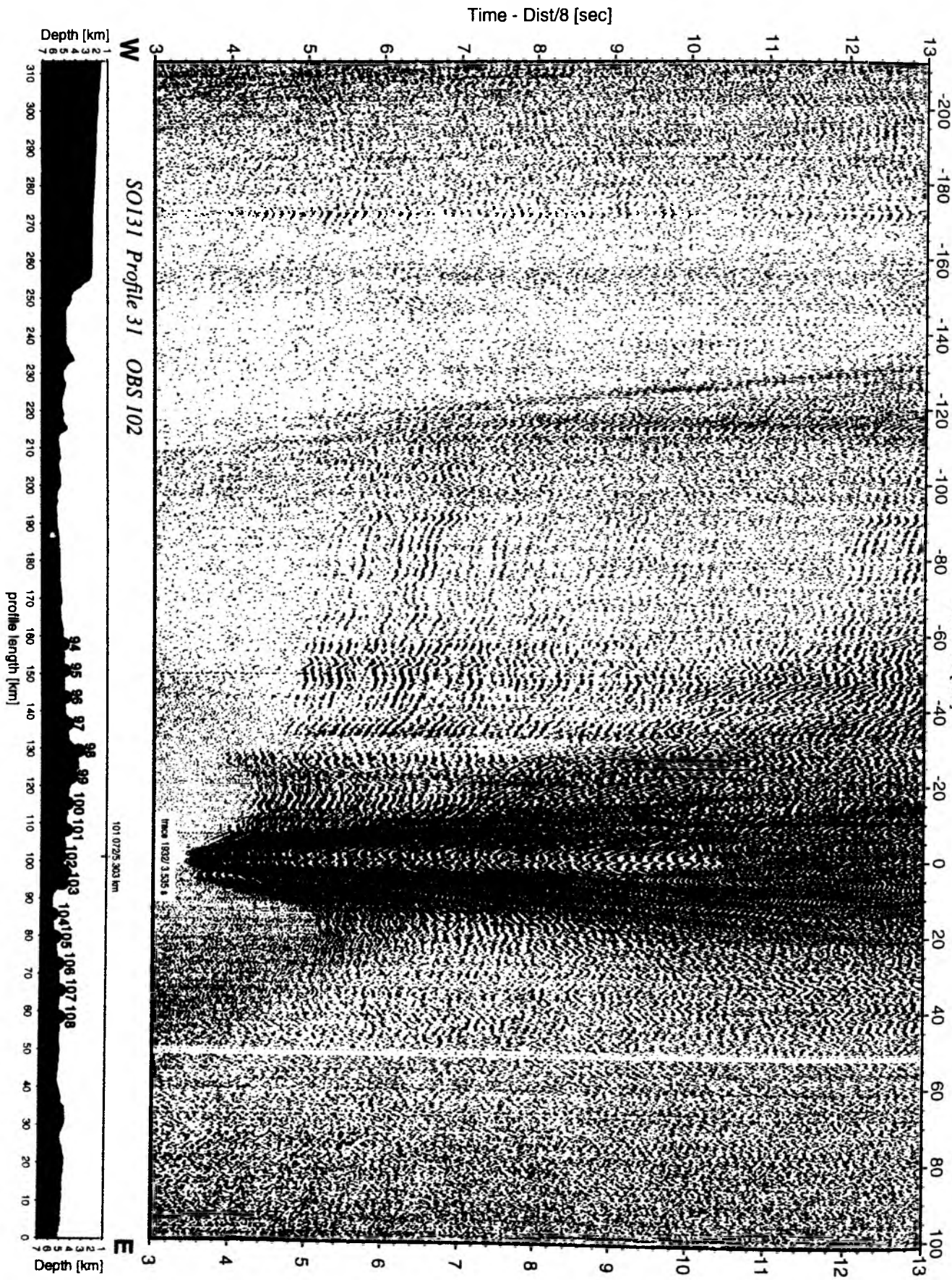

Figure 6.3.4.8.13: Record section from OBS 102 horizontal component 1, Profile 31.

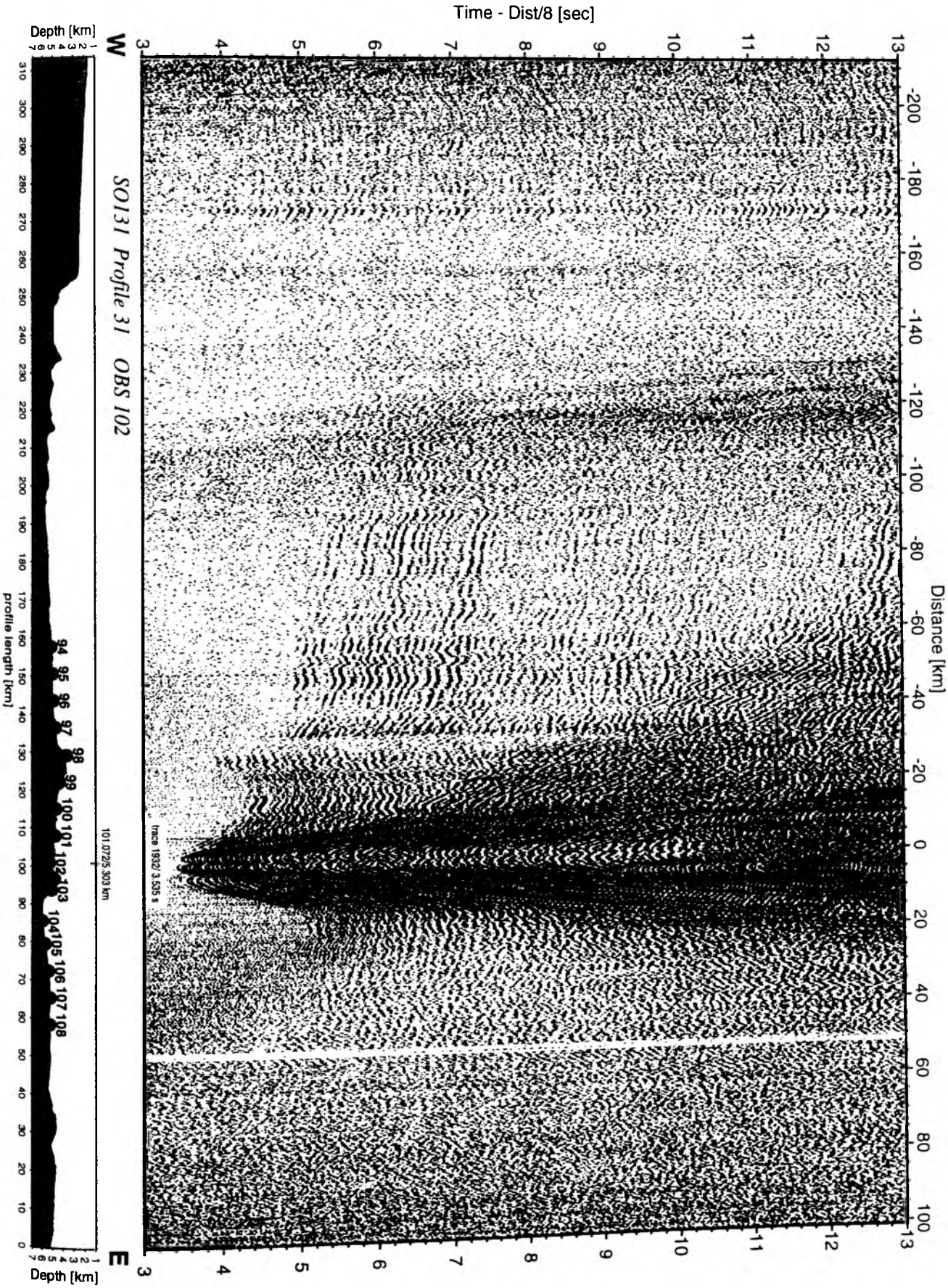

Figure 6.3.4.8.14: Record section from OBS 102 horizontal component 2, Profile 31.

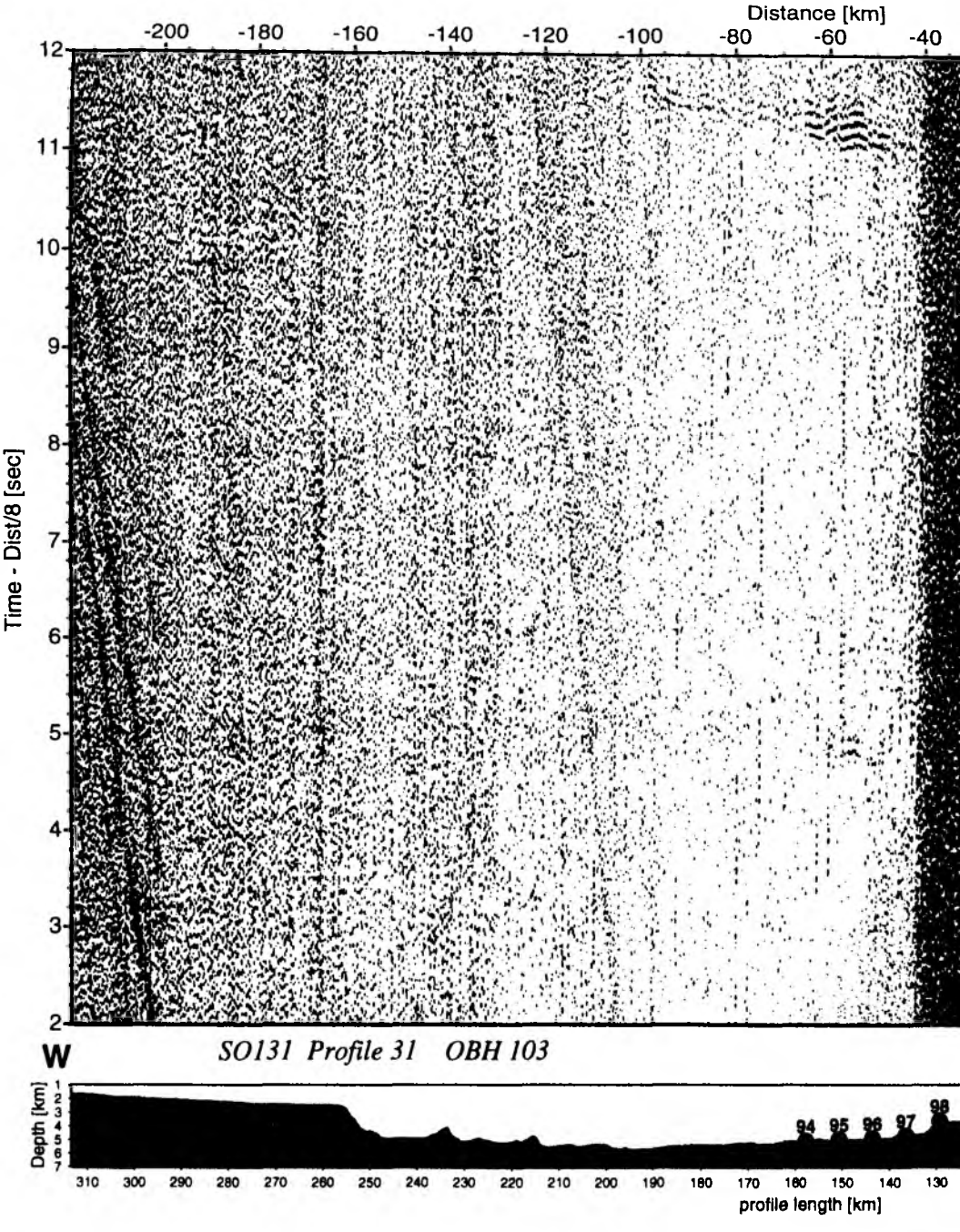
Distance [km]
-200
-180
-160
-140
-120
-100
-80
-60
-40
Time - Dist/8 [sec]
12
11
10
9
8
7
6
5
4
3
2
W
SO131 Profile 31 OBH 103
Depth [km]
1
2
3
4
5
6
7
94
95
96
97
98
310
300
290
280
270
260
250
240
230
220
210
200
190
180
170
160
150
140
130
profile length [km]

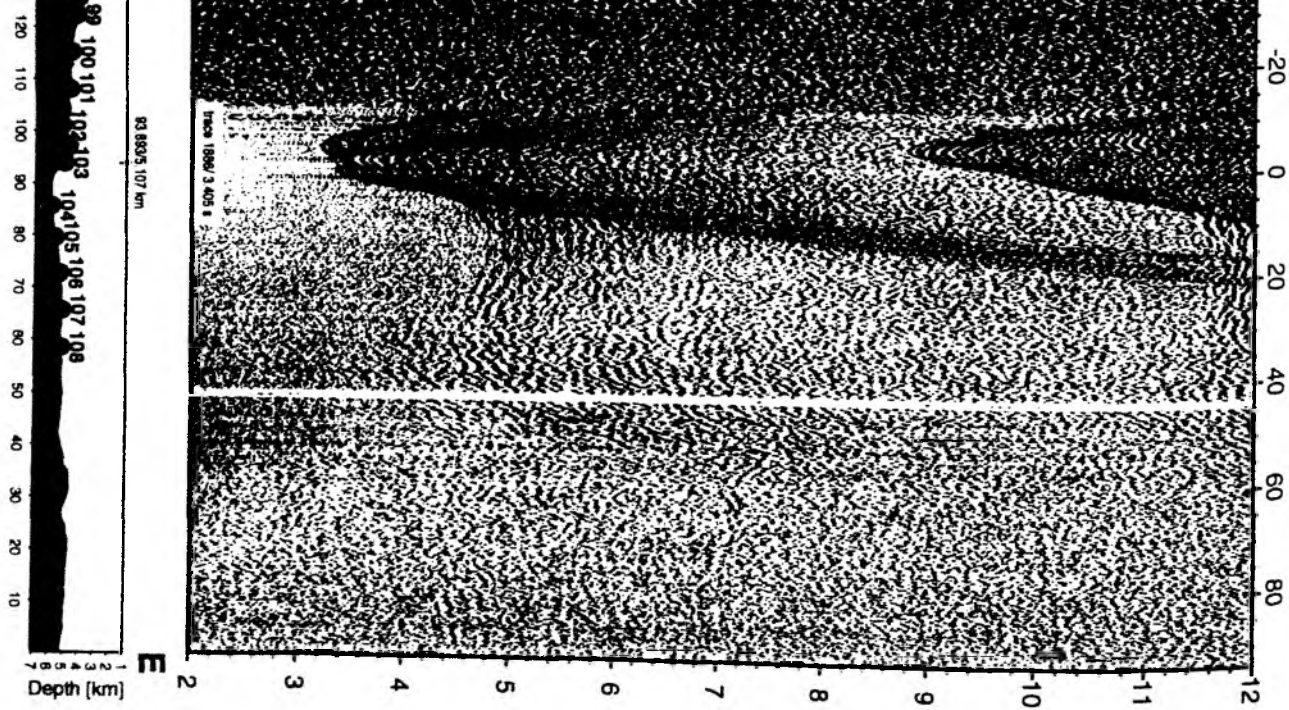

Figure 6.3.4.8.15: Record section from OBH 103 , Profile 31.

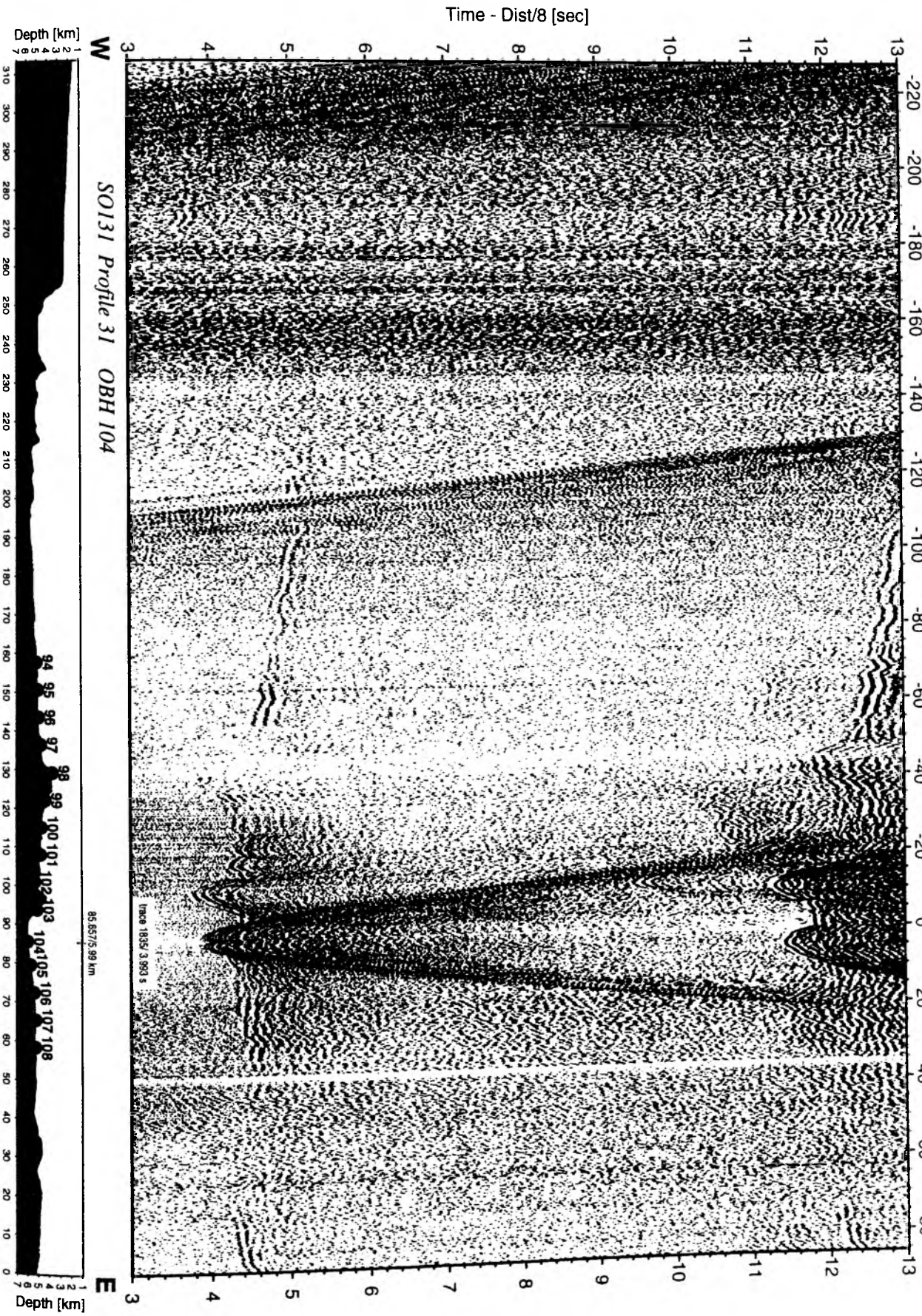

Figure 6.3.4.8.16: Record section from OBH 104 , Profile 31.

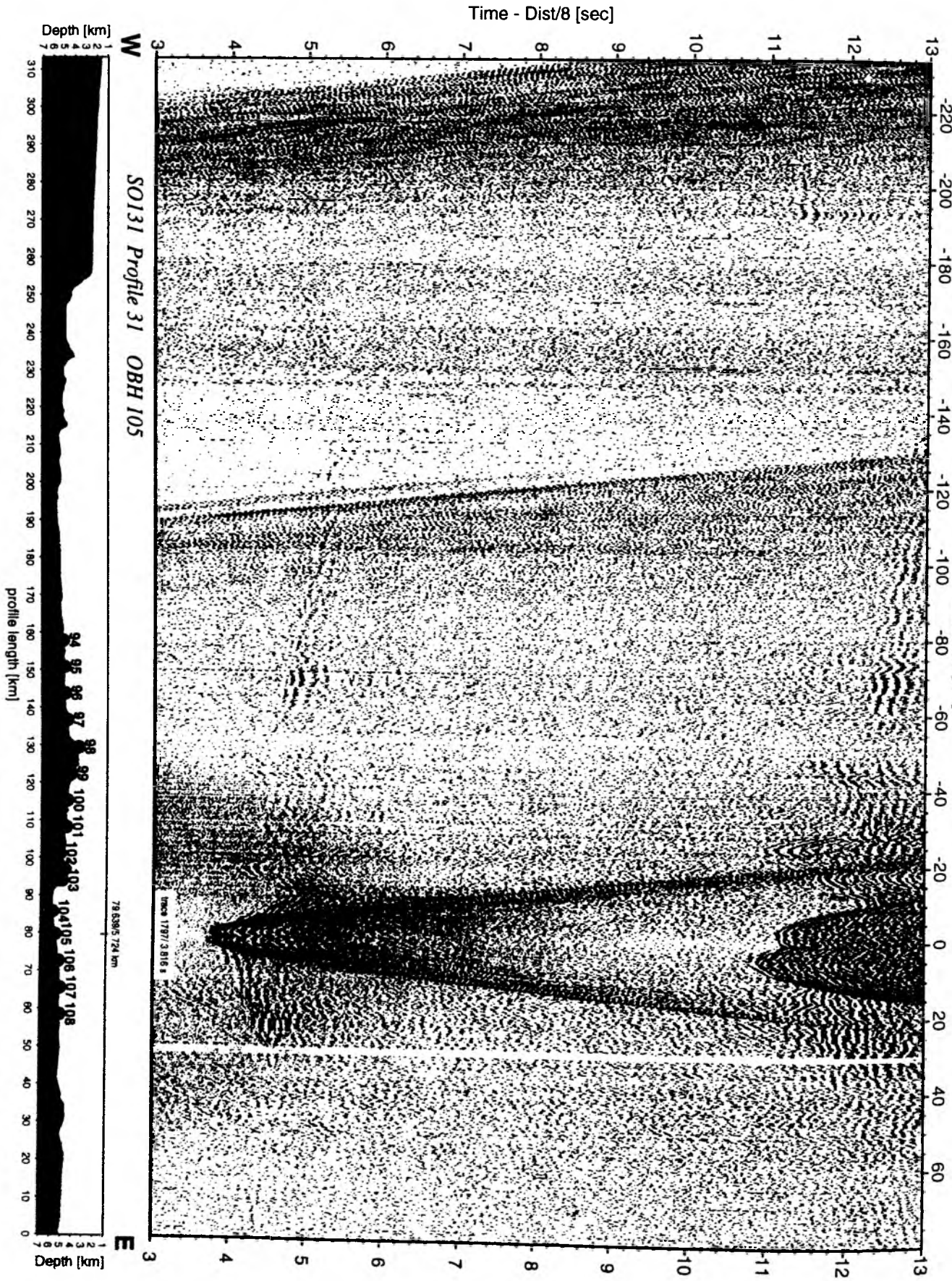

Figure 6.3.4.8.17: Record section from OBH 105 , Profile 31.

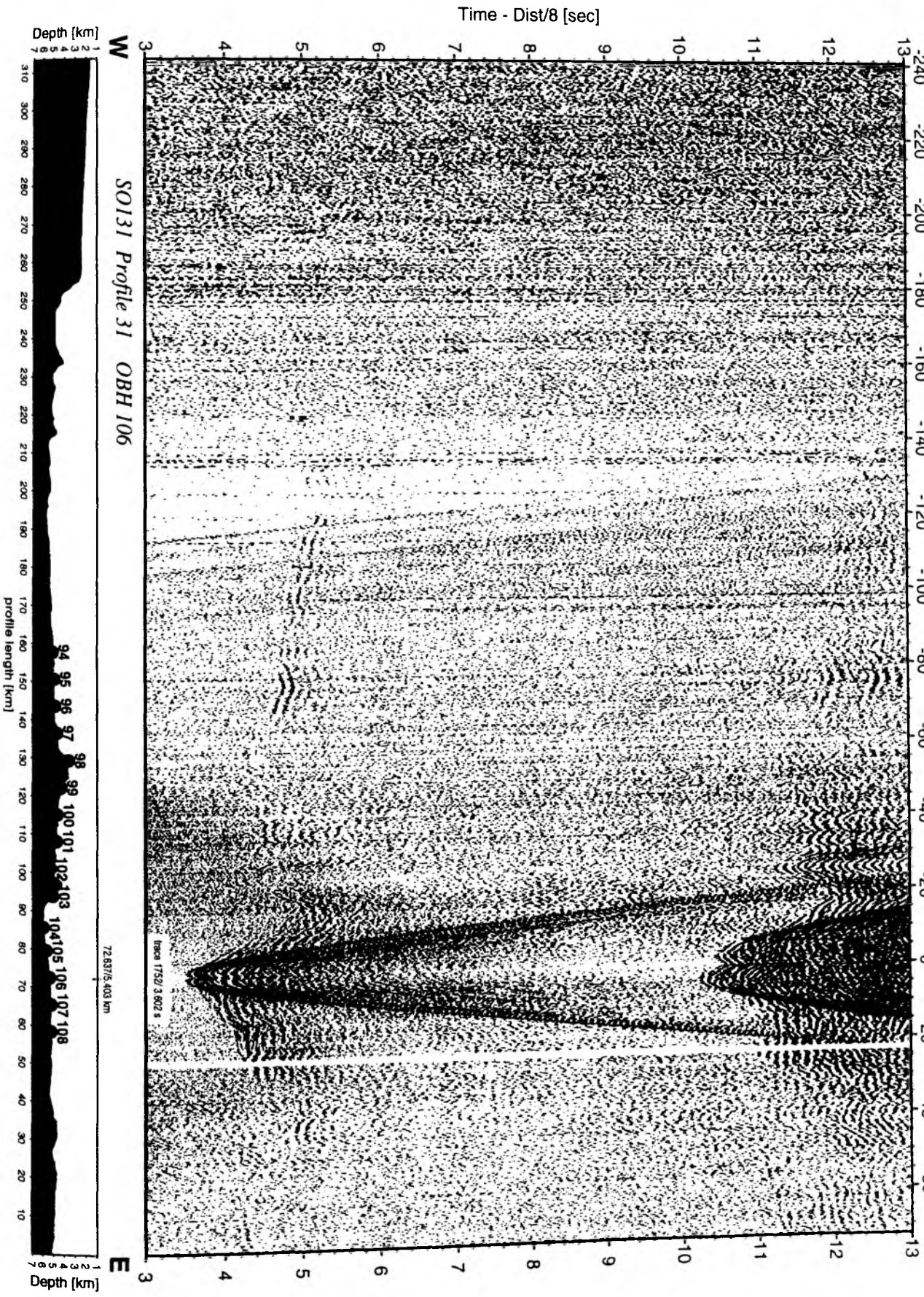

Figure 6.3.4.8.18: Record section from OBH 106 , Profile 31.

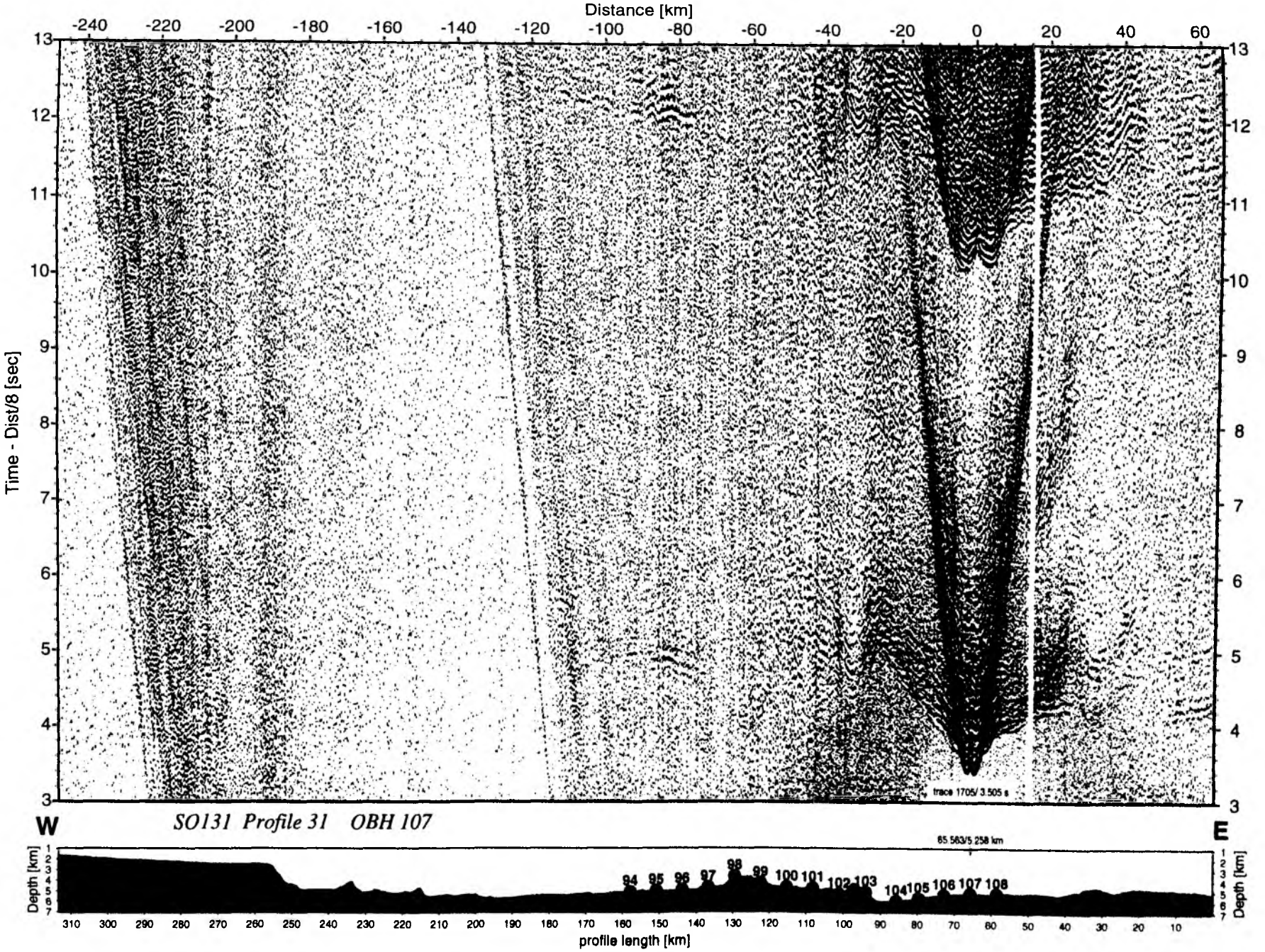

Figure 6.3.4.8.19: Record section from OBH 107 , Profile 31.

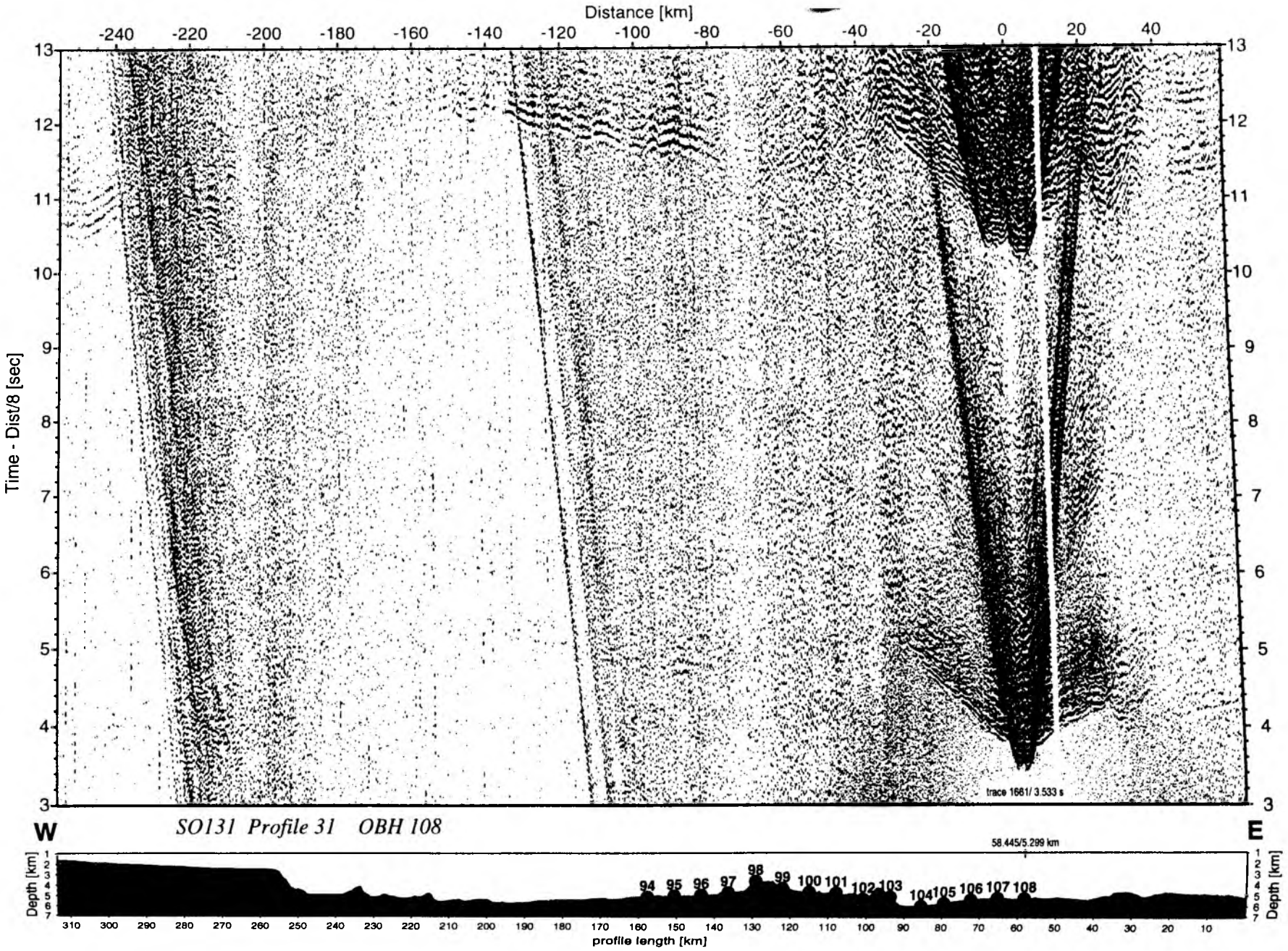

Figure 6.3.4.8.20: Record section from OBH 108 , Profile 31.

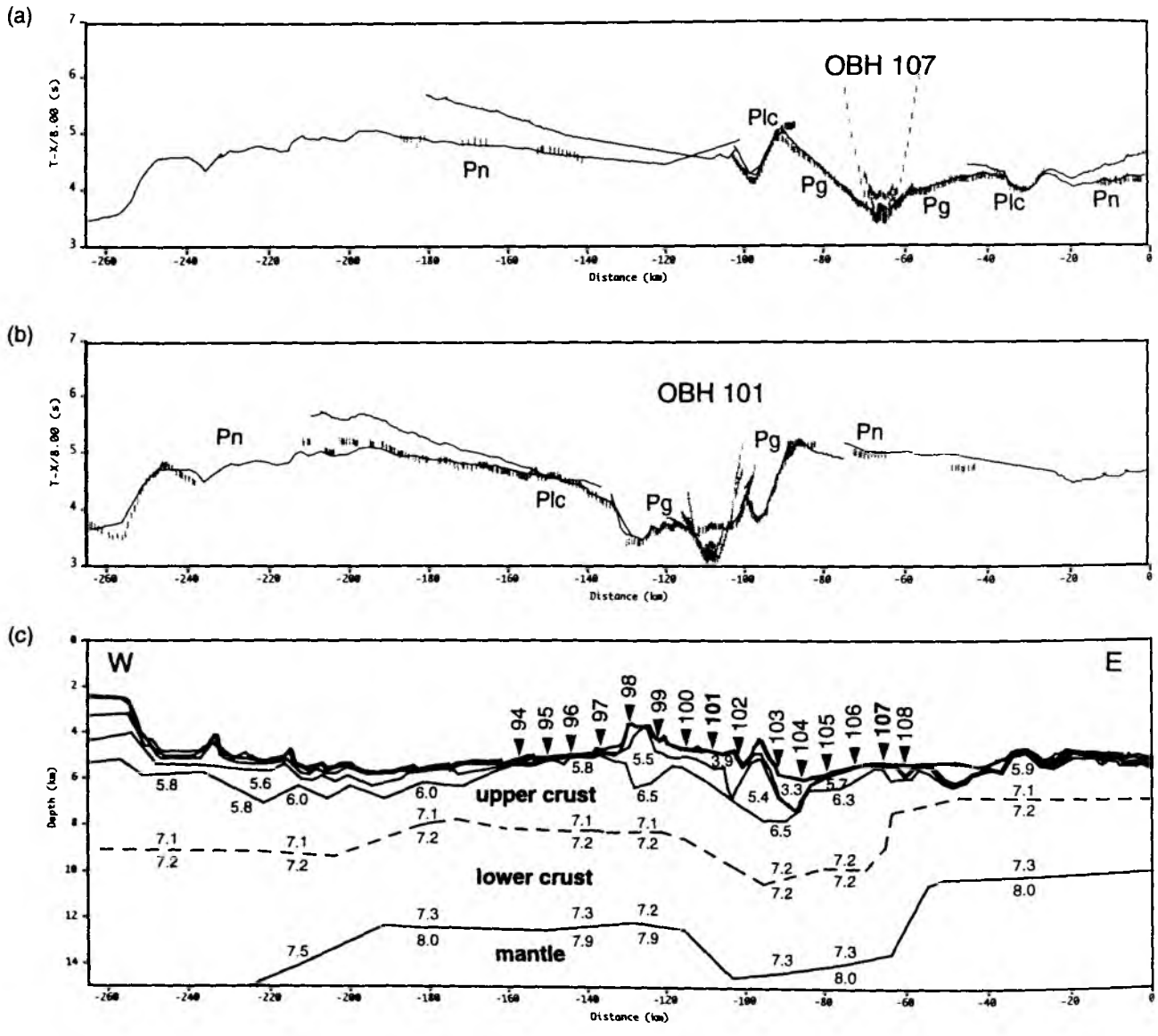

Figure 6.3.4.8.21: Traveltimes for OBH 107 (a) and OBH 101 (b) and velocity model for profile SO131-31 (c). (Pg = upper crust refraction, Plc = lower crust refraction, Pn = mantle refraction).

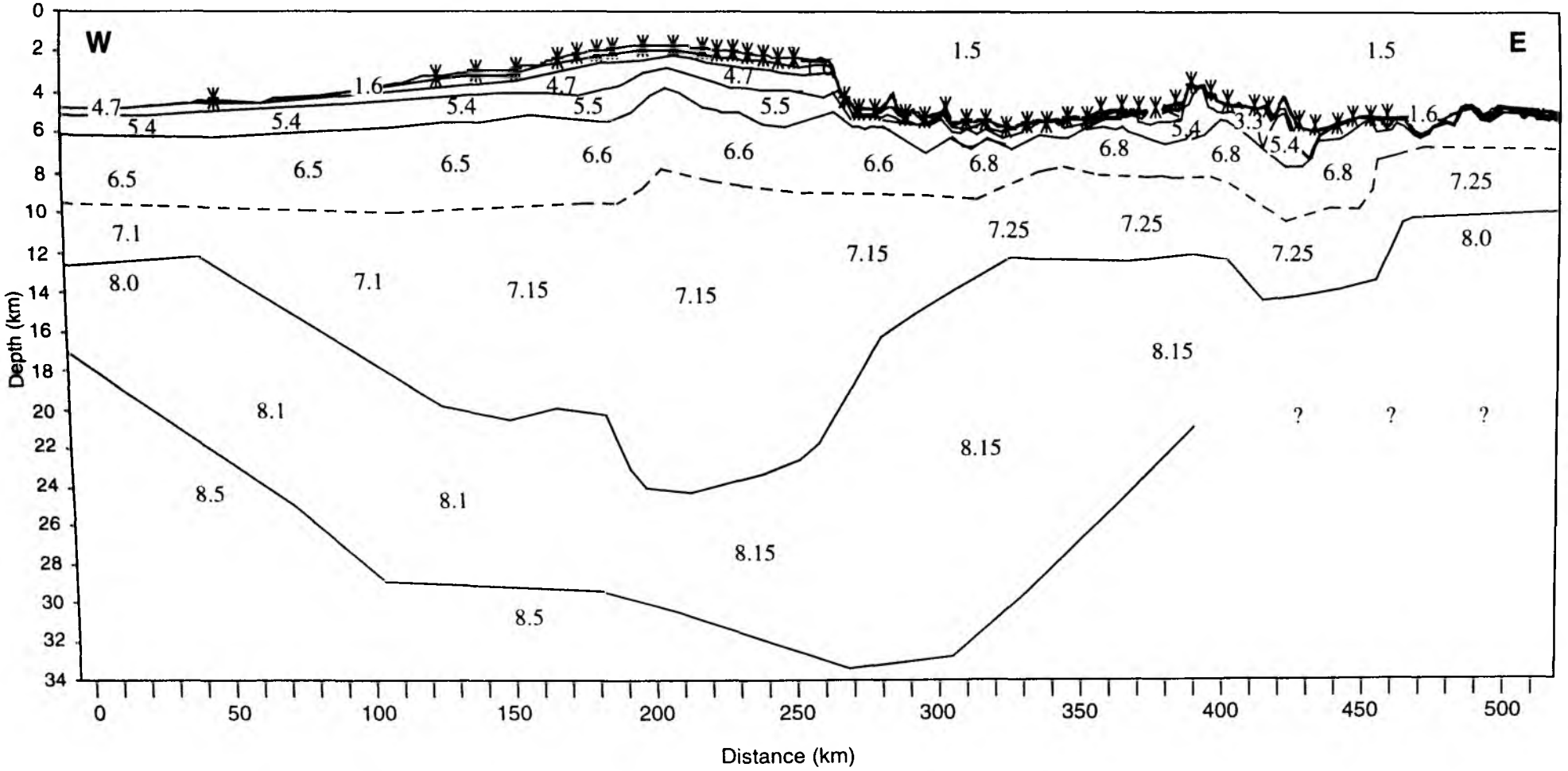

Figure 6.3.4.22 : Combined simplified velocity model of profiles SO131-05, SO131-06, and SO131-31.

6.3.4.9 PROFILE SO131-32: MONTES SINUS AND COSINUS

(W. Weinrebe, D. Kläschen und E. Flueh)

Spurious spikes observed on the Ninetyeast Ridge around NERO were first thought to be erroneous readings from the Hydrosweep System. It was however soon realized, that some of them occured consistently on several profiles at identical locations. Also, on some of the reflection profiles side swipes are evident. Parasound recordings of these features were not available, the slopes being too step

To investigate the nature of these features in detail, a high resolution profile SO131-32 was shot on 06.06., with one array being deployed and a shot rate of 10 s, corresponding to a 25 m shotspacing being choosen. The detailed bathymetry along this profile is shown in Figure 6.3.4.9.1., and several small hills are clearly evident. Two of them are about 150 m high, and their appearence on the Hydrosweep monitor lead us to call them Monte Sinus and Monte Cosinus (Fig. 6.3.4.9.4). A perspective illuminated image of the bathymetry of the area illustrates the steep morphology of these features.

The seismic reflection data were processed in the way described in chapter 6.3.2.1, and the seismic section is shown in Figure 6.3.4.9.2. To move dipping reflectors into their true subsurface position and to collaps diffractions, a time migration was performed. As steeply dipping events were prefered to be imaged the simplest type of a cascaded migration technique was used. The first migration algorithm applied works in the frequency-wavenumber domain for constant velocities and is able to image steeply dipping events. A velocity of 1500 m/s was used. The input for the second migration was the pre-migrated data set. Here a migration algorithm based on the recursive downward extrapolation which is performed in the f-x (frequency, spatial coordinate) domain with a 45 degree operator. This migration alogorithm allows vertical and lateral velocity variations. The migration velocities are based on the forward modelling of Profile SO131-06 (chapter 6.3.4.6), time converted, and reduced by a time variant percentage (vel.perc.) during migration application.

Profile distance (km)	TWT time (s) interval	Velocity (km/s)	vel.perc.
0	2.2	1.5	100
	2.7	1.6	95
	3.1	3.4	90
	3.8	4.7	85
	4.8	5.4	80
7.5	2.3	1.5	100
	2.7	1.6	95
	3.1	3.4	90
	3.8	4.7	85
	4.8	5.4	80
15	2.6	1.5	100
	2.9	1.6	95
	3.3	3.4	90
	4.0	4.7	85
	5.0	5.4	80

A blow up around the Monte Sinus (shot point 13,800) and Monte Cosinus (shot point 13,900) of the time migrated section is shown in Figure 6.3.4.9.3. The origin of these features is still unclear, but it can be seen especially at Monto Sinus, that the strong reflector beneath the sediment strata is not continous or even missing below the bathymetric high. Below Monto Cosinus the sediment strata seems to be tectonically disrupted what indicates, that the origin of these features is related to the deeper subsurface dynamics.

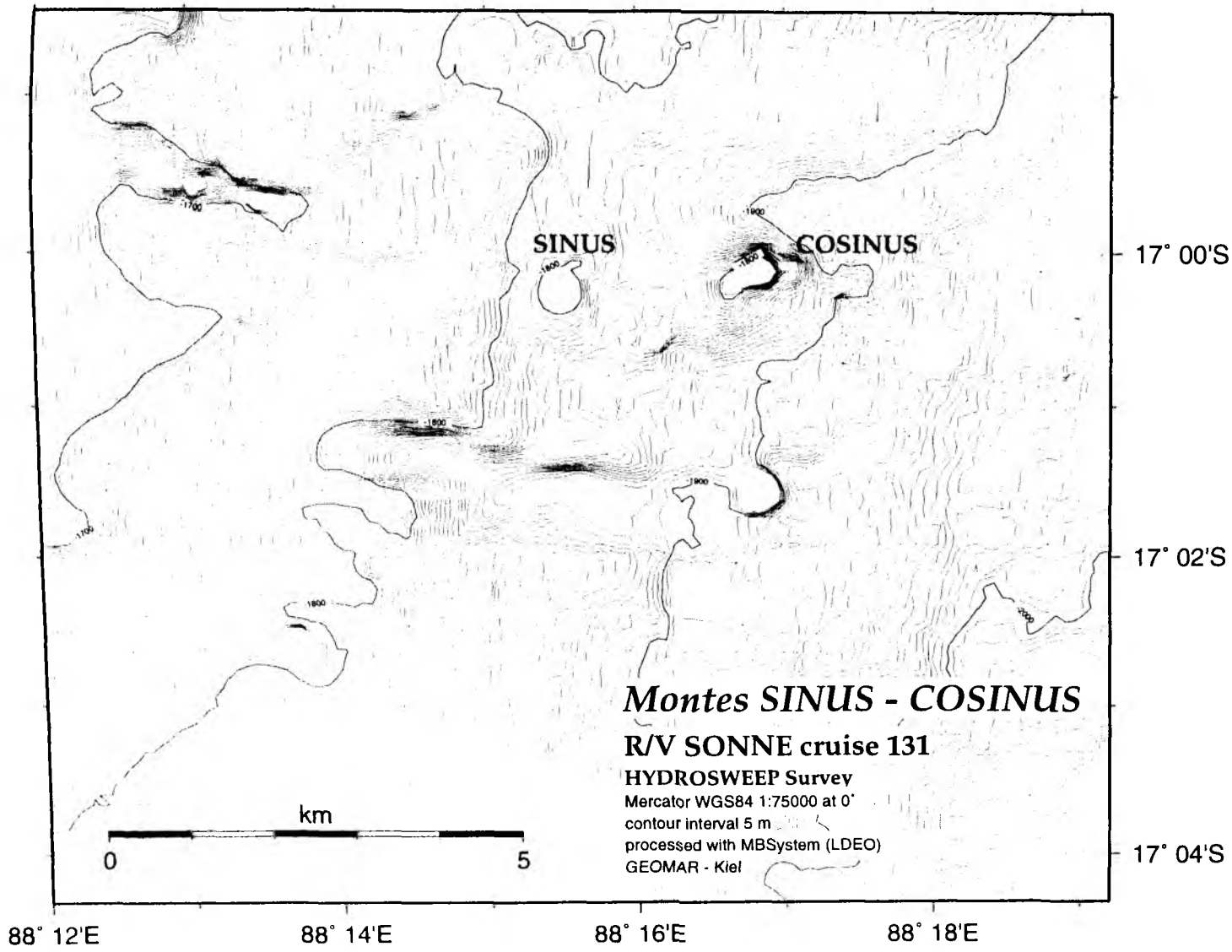

Fig. 6.3.4.9.1: Bathymetry of the area around Mts SINUS and COSINUS.

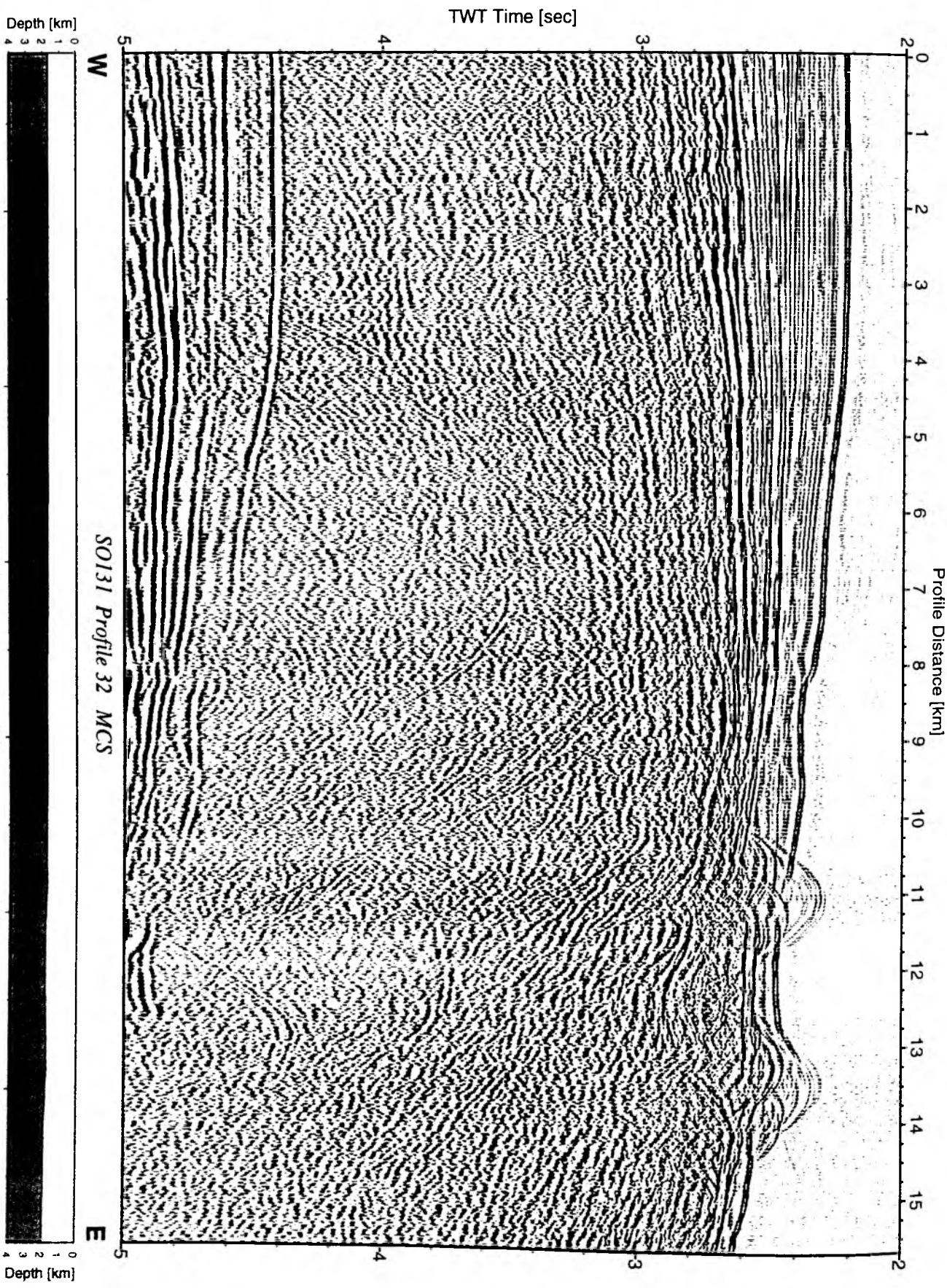

Figure 6.3.4.9.2: Seismic section from MCS stack, Profile 32.

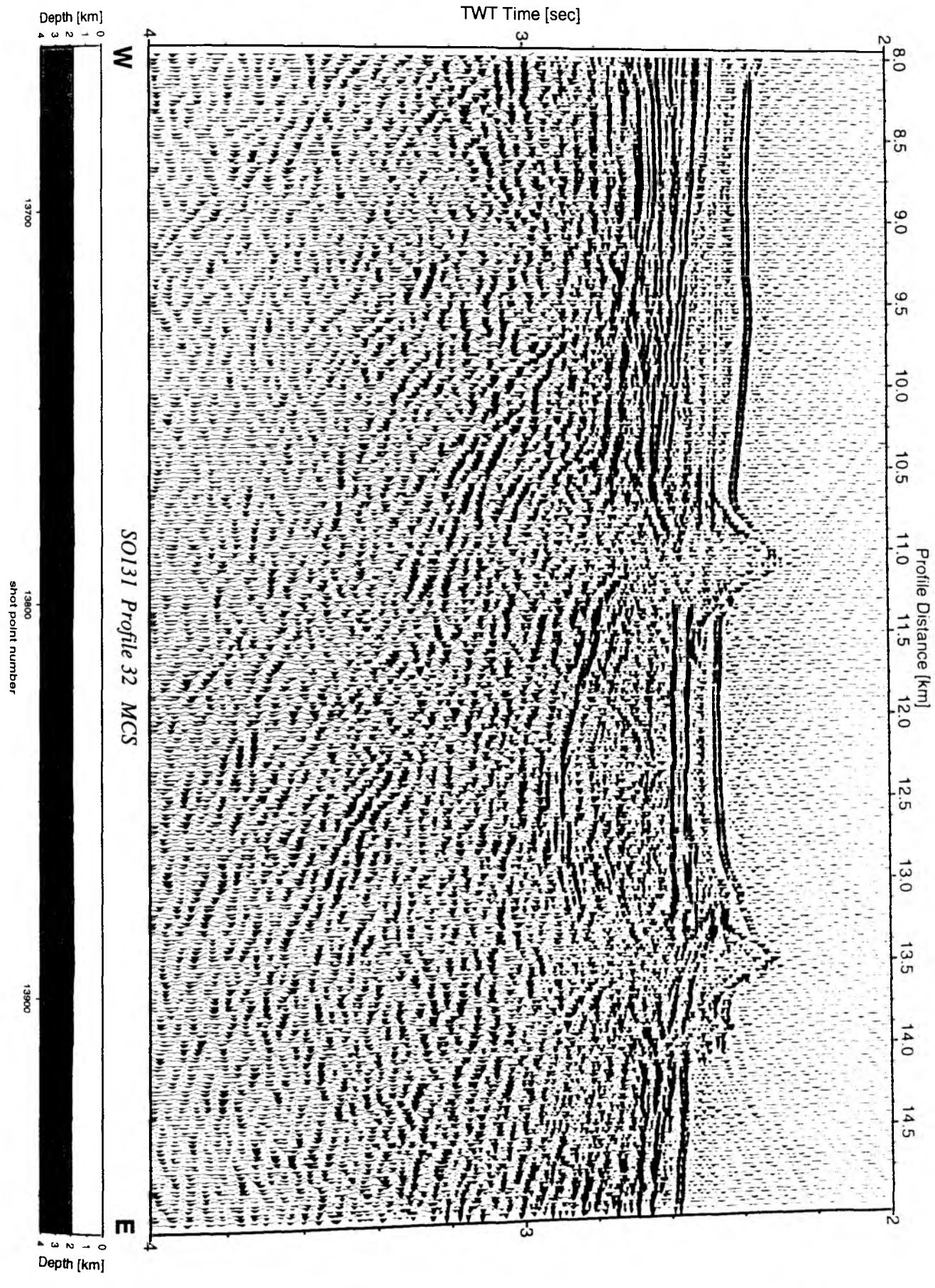

Figure 6.3.4.9.3: Seismic section from MCS post-stack migration, Profile 32.

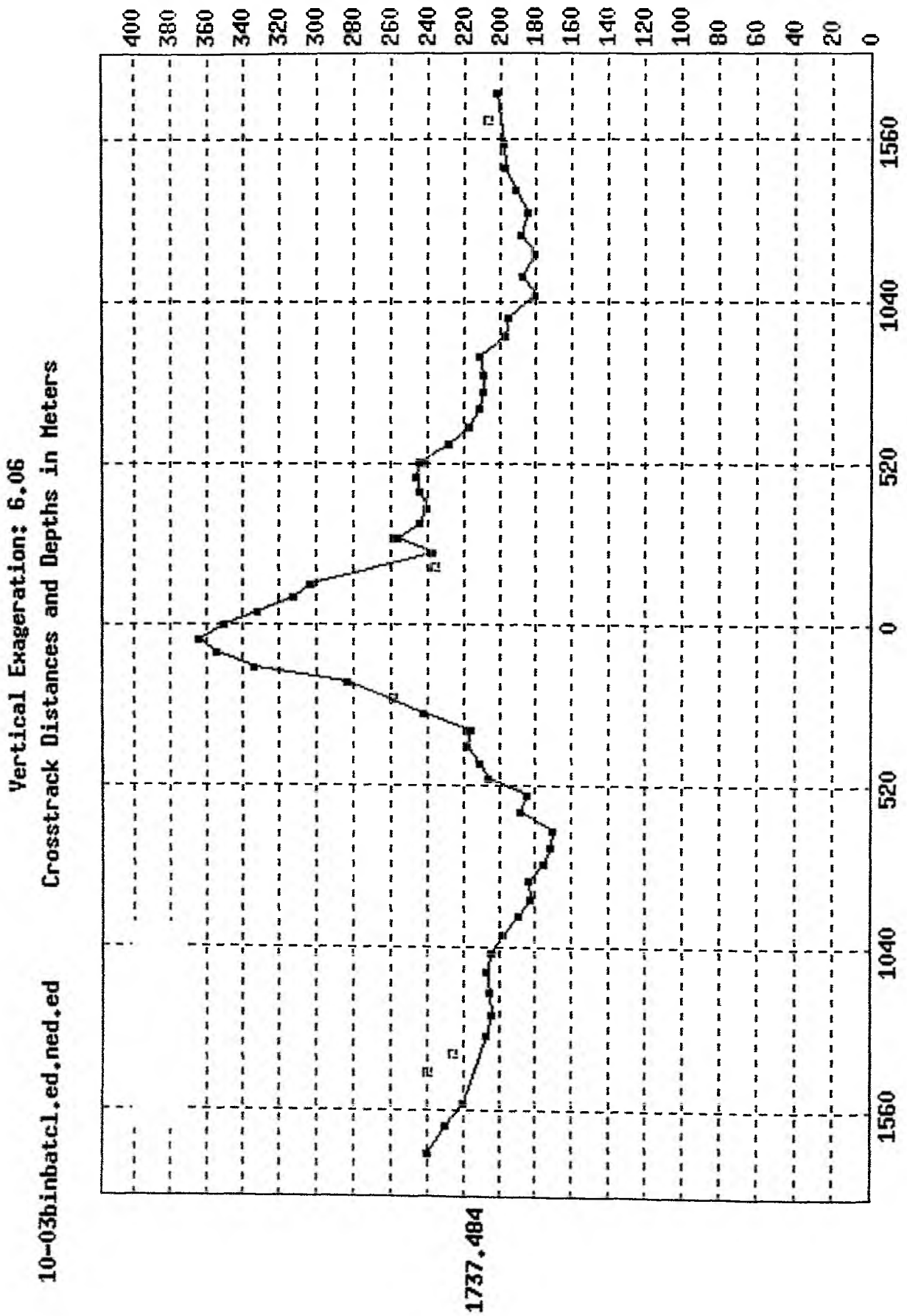

Fig. 6.3.4.9.4: Bathymetric cross-section of Monte Cosinus. Heights and across-track distances in m.

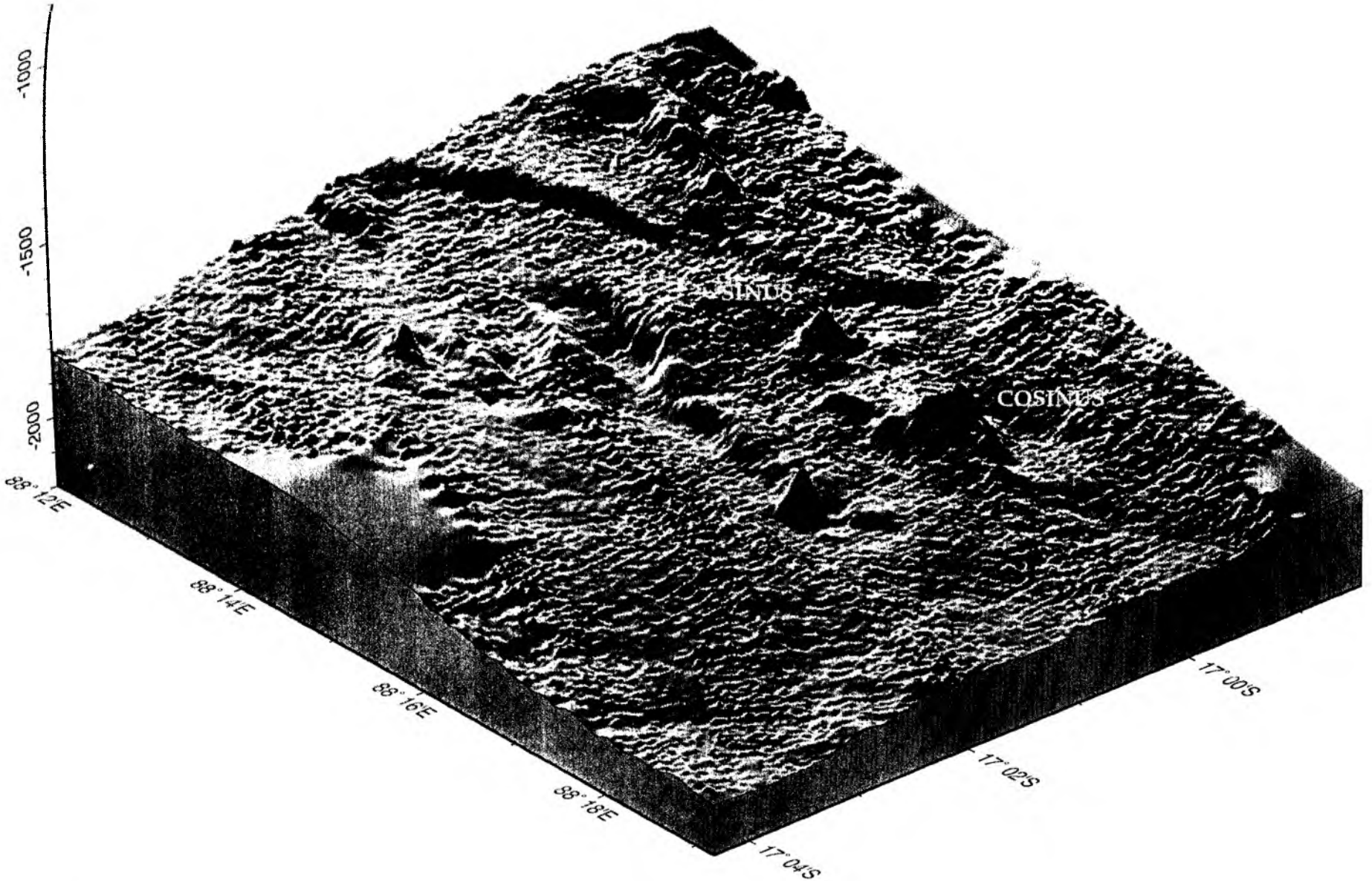

Fig. 6.3.4.9.5: Perspective image of the area around Montes SINUS and COSINUS. View from southeast, illumination from northwest.

6.4 Magnetics

(I. Grevemeyer, and watchstanders)

This trend may reflect the long-wavelength structure of the Earth magnetic Along all seismic lines magnetic total field data were recorded using a proton precession magnetometer towed 250 m astern R/V SONNE. In addition, we carried out two small bathymetric and magnetic surveys in the Wharton Basin. The first survey covered oceanic crust adjacent to Ninetyeast Ridge and the second sampled the magnetic field over the Ninetyeast Fracture Zone. Moreover, transit profiles were used to increase the coverage of both magnetic and swath mapping data. In total ca. 3500 km of magnetic data were aquired. The survey lines of the cruise are shown in Figure 6.4.1.

Marine geophysicists are primarily interested in crustal magnetisation. Magnetic reversals preserved in oceanic crust, for example, can be used to delinate seafloor spreading velocities. At sea, however, magnetic data obtained by a single sensor are inherently affected by the time-dependent nature of the outer magnetic field, where the solar wind interacts with the Earth magnetic field. We therefore carried out a quality check of our measurements. In Figure 6.4.2 we display the magnetic field obtained on parallel running profiles. The correlation of adjacent tracks is reasonable good. Some features, however, indicated lateral variations of upper crustal magnetisation. Figure 6.4.3 has a track segment sampled three times by the lines 05, 06 and 31. Although the correlation of the three surveys is excellent, the data display a considerable degree of deviation. We are confident that the systematic deviations were not caused by a malfunction of the magnetometer, but indicate the impact of the outer field on our measurements.

The location of Ninetyeast Ridge in the central portion of the Indian ocean makes it difficult to quantify the impact of daily variations and magnetic storms, i.e., no reference station is available. A crossover analysis may provide an initial assessment where several intersecting profiles were sampled. This approach would be appropriate for the 3-D seismic survey area. Profiles obtained in the Central Indian Basin and Wharton Basin, however, provided only a few crossovers. Nevertheless, mathematical models of daily variations and the magnetic storm database at the Geophysical Data Center in Japan can be used to assess the time-dependent features of the field. Such an approach generally decreases crossover errors significantly. Afterwards, magnetic anomalies could be calculated more accurately. Therefore, a post-cruise data processing would be appropriate.

Figures 6.4.4 and 6.4.5 present magnetic anomalies and bathymetry along our major seismic lines. In Figure 6.4.6 we show the magnetic field over ODP site 757. The grid contains the data recorded along the seismic lines of the 3-D seismic experiment and some additional magnetic lines. Track data were gridded using continuous curvature splines in tension (Smith and Wessel, 1991). Afterwards, we applied a median filter (radius 750 m) to decrease noise and to remove small anomalies elongated along the profiles, most likely, due to small magnetic storms and/or daily variations. In areas where the data coverage is poor, however, some along track anomalies remain in the grid. The same approach was applied to the Ninetyeast Fracture Zone survey (Figure 6.4.7). Around ODP site 757 magnetic anomalies decrease from south to north. field and may disappear after removal of the IGRF. In addition to this regional trend, the field contains several local anomalies. At 88°00,E/16°50,S, for example, we sampled a prominent anomaly of about 200 nT, which may

represent a fossil eruptive centre. Nevertheless, a detailed interpretation of the magnetic features is beyond the scope of this report.

In the Central Indian Ocean Basin westwards of Ninetyeast Ridge, we obtained a single profile along the flowline of crustal generation. Eastwards, in the Wharton Basin, two surveys sampled the magnetic field in flowline direction. The surveys covered oceanic crust imediately eastwards of Ninetyeast Ridge and the Ninetyeast Fracture Zone. Figure 6.4.8 displays along track anomalies as a wiggle plot. To remove the long-wavelength structure of the field we removed a linear trend from the data. Most profound are sequences of magnetic reversals, which present the famous seafloor spreading anomalies. Within the SINUS survey area, the age of oceanic crust is not well constraint. Therefore, the reversals may help to refine the age of the seafloor in the vicinity of Ninetyeast Ridge near ODP site 757. In turn, new seafloor ages could be a key for plate tectonic reconstructions of the Indian Ocean and the emplacement of Ninetyeast Ridge.

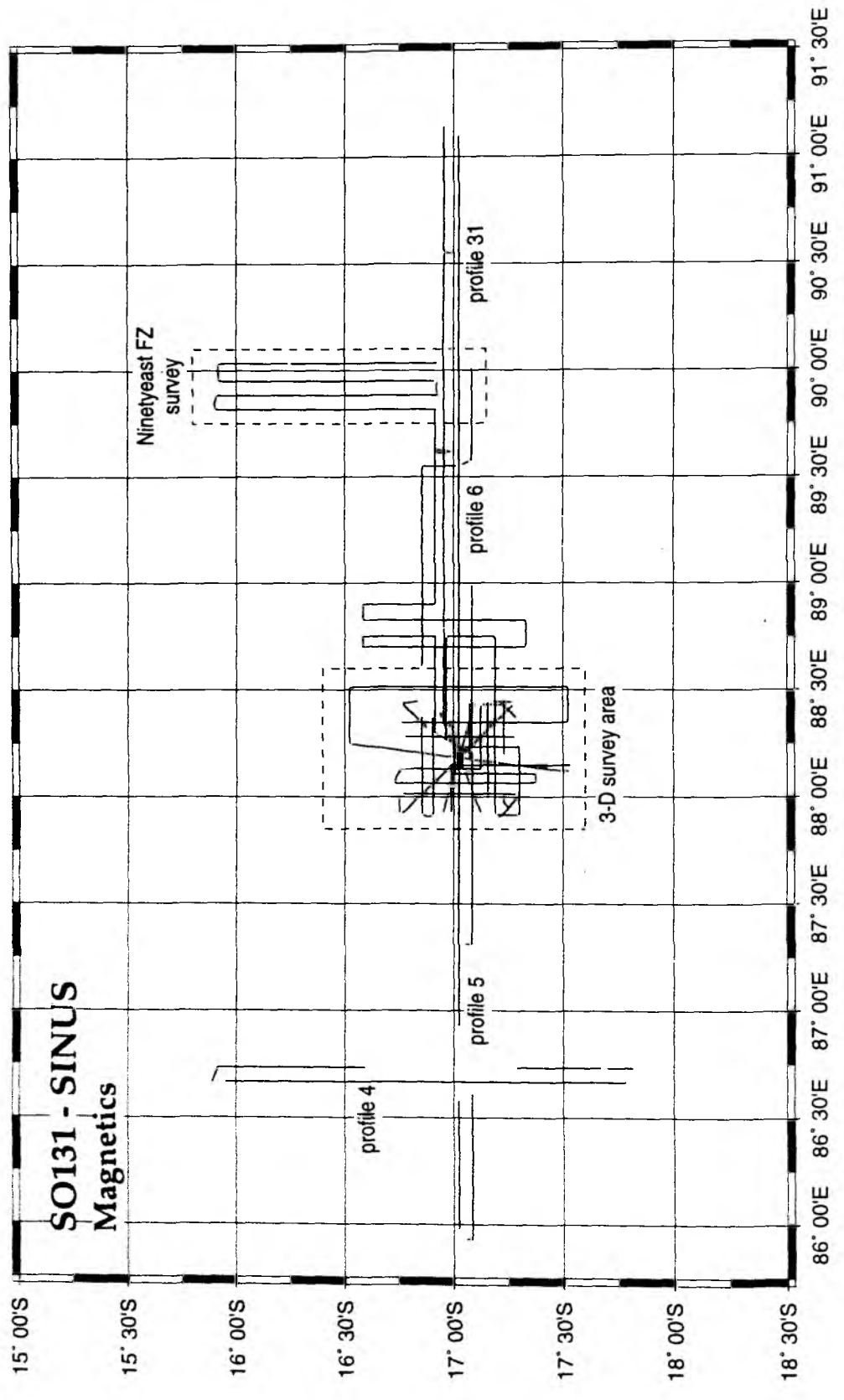

Figure 6.4.1: Location map showing magnetic tracks.

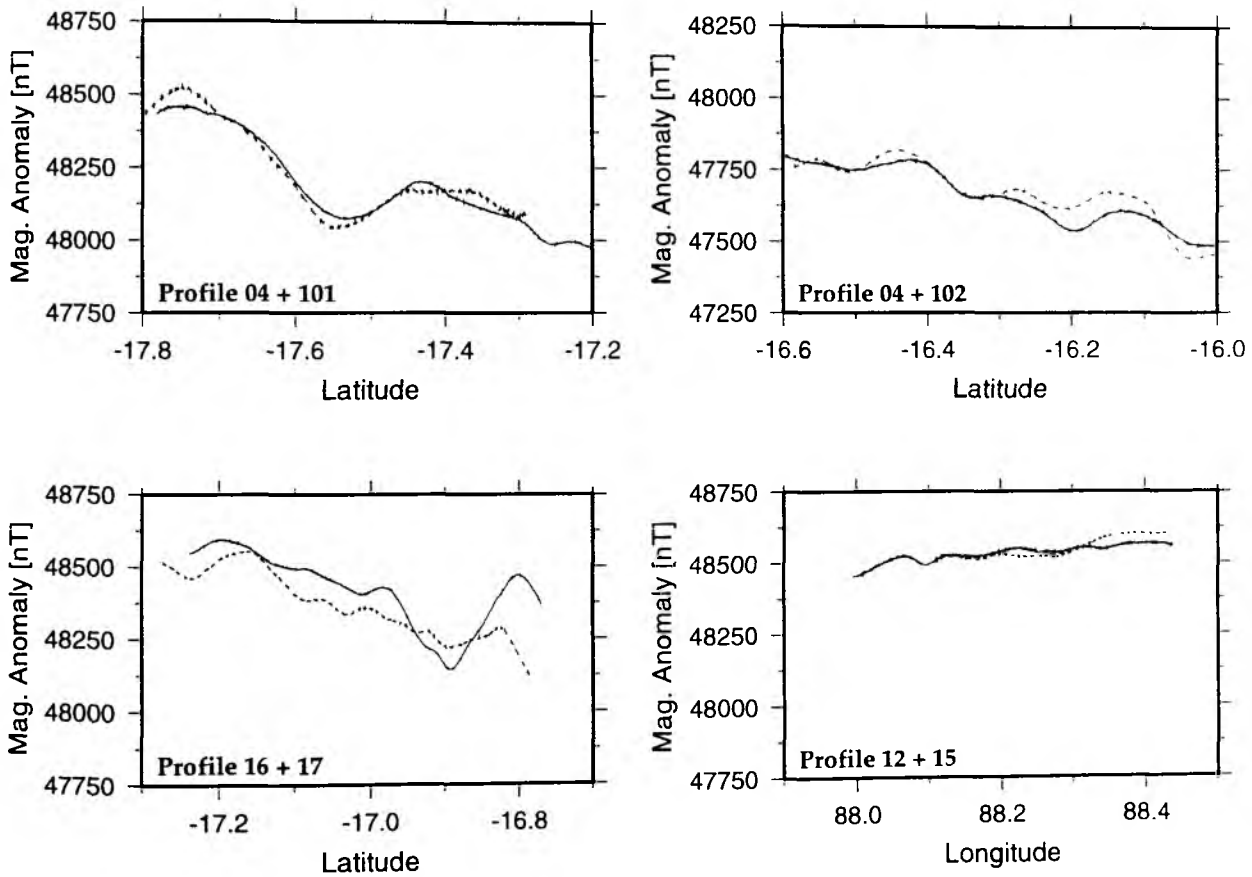

Figure 6.4.2: Magnetic anomalies obtained on parallel running tracks

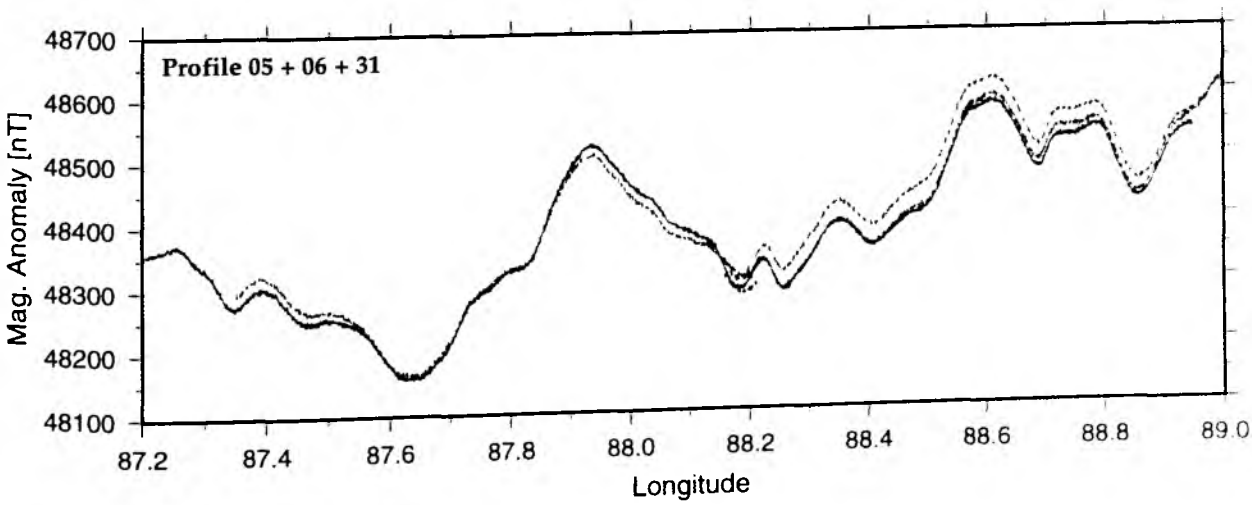

Figure 6.4.3: Magnetic anomalies recorded on the same track segment.

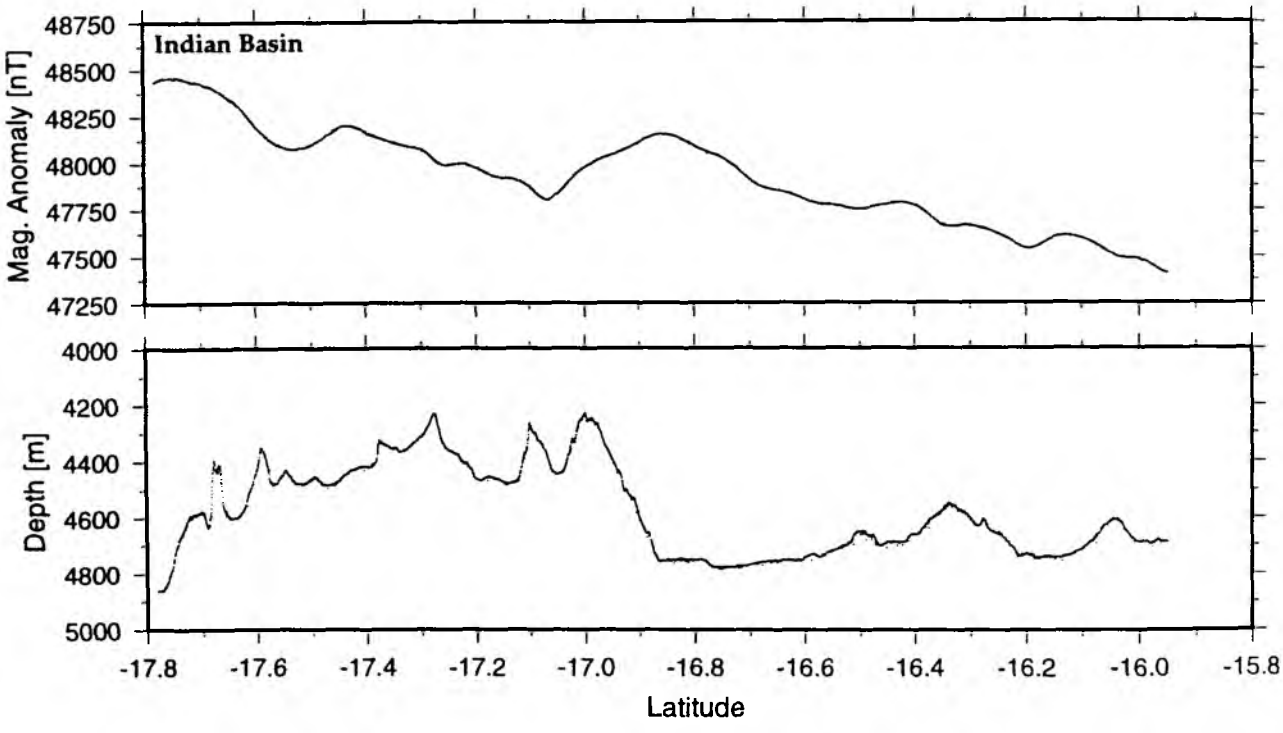

Figure 6.4.4: Along track magnetic anomaly and bathymetry, Profile 04.

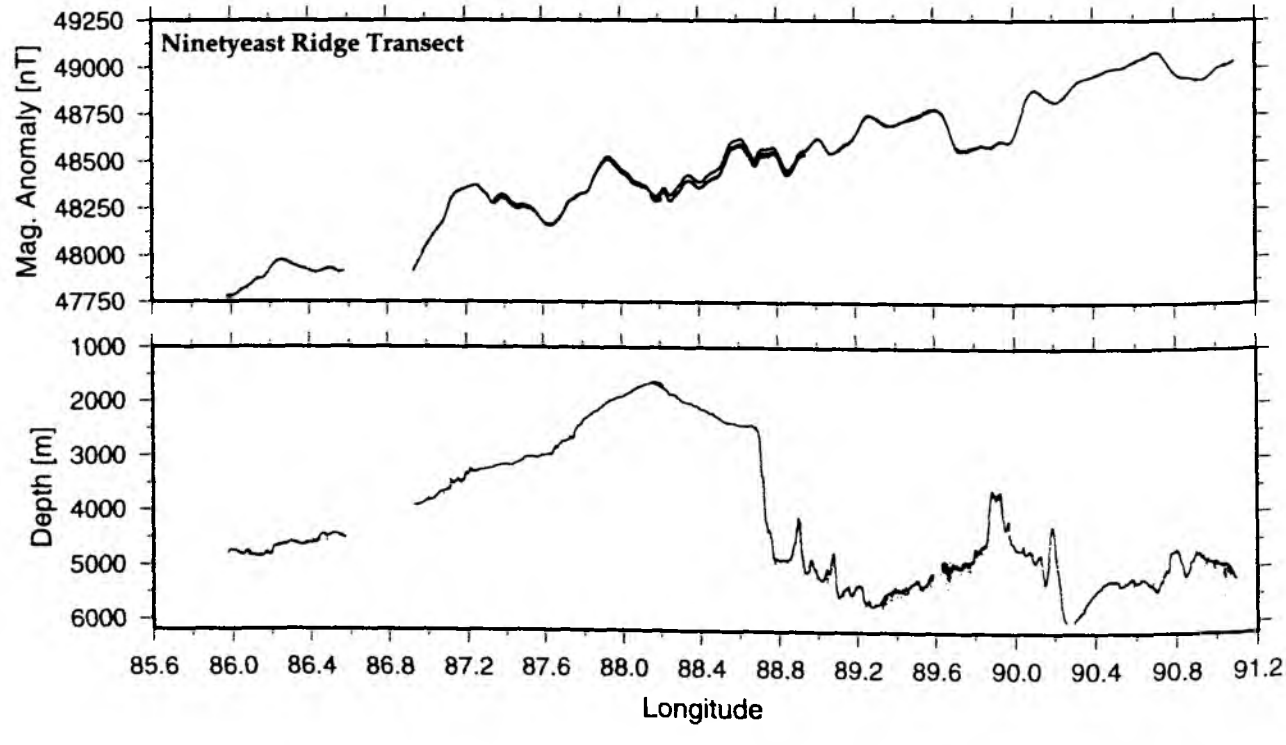

Figure 6.4.5: Along track magnetic anomaly and bathymetry, Profile 05 + 06 + 31.

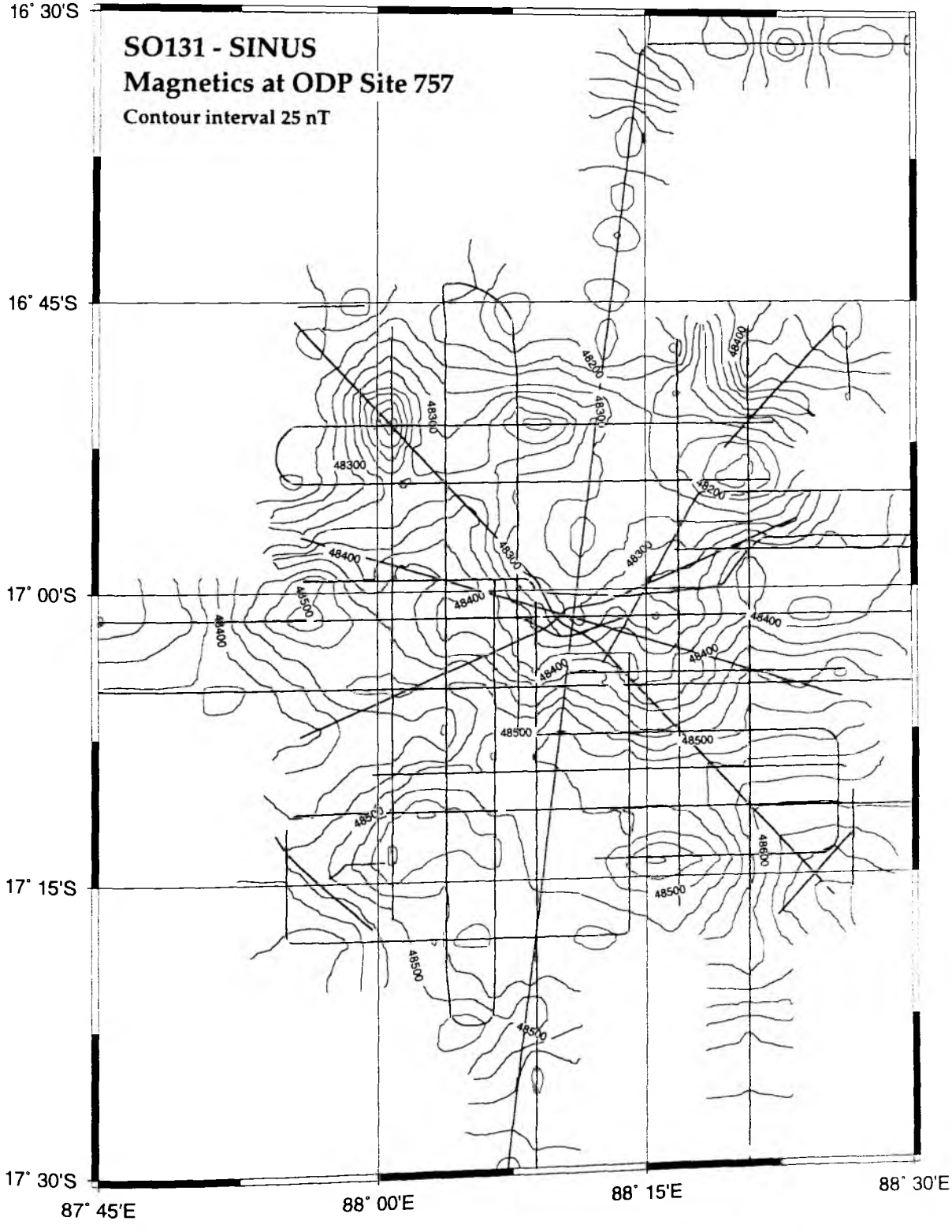

Figure 6.4.6: Magnetic field over ODP Site 757.

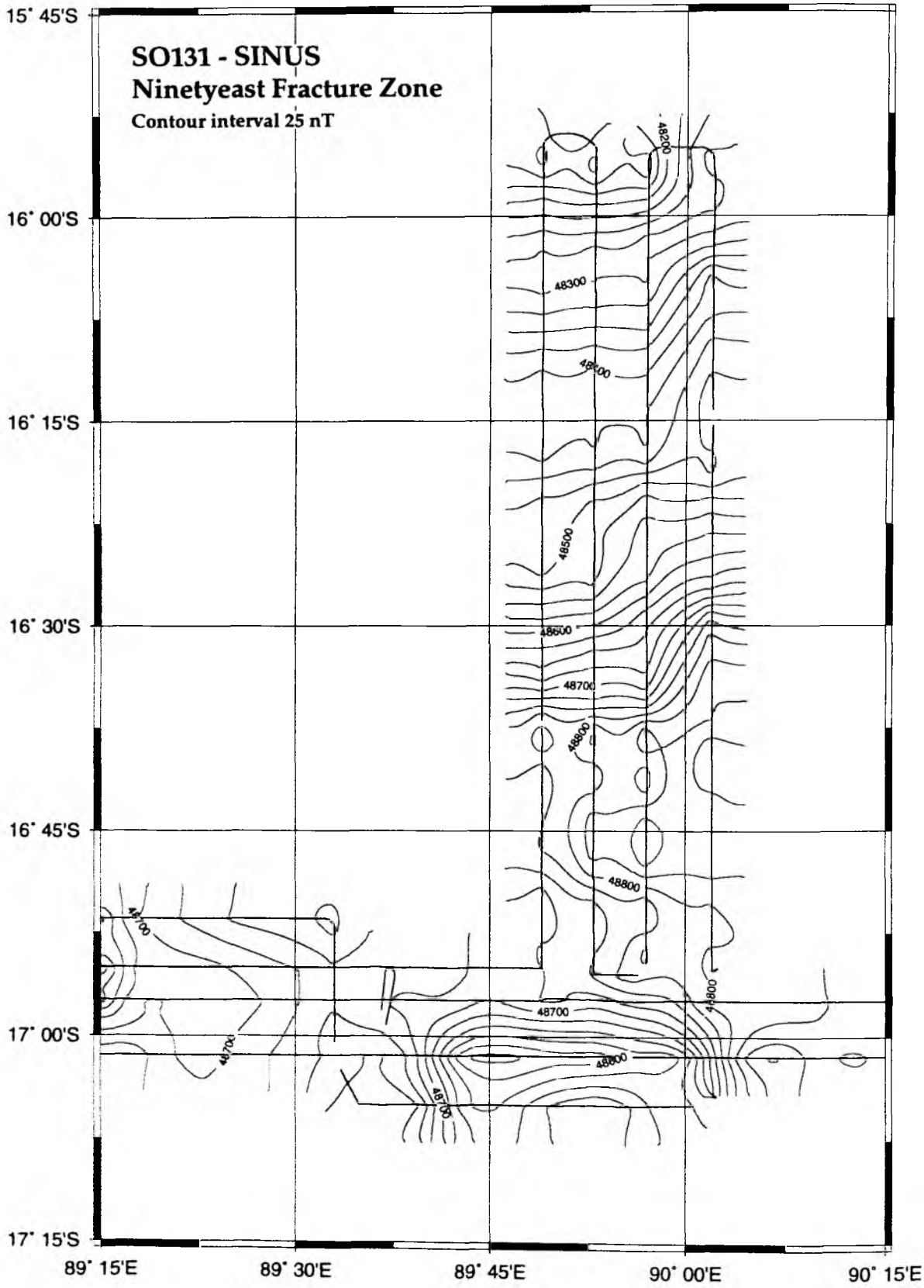

Figure 6.4.7: Magnetic field over the Ninetyeast Fracture Zone.

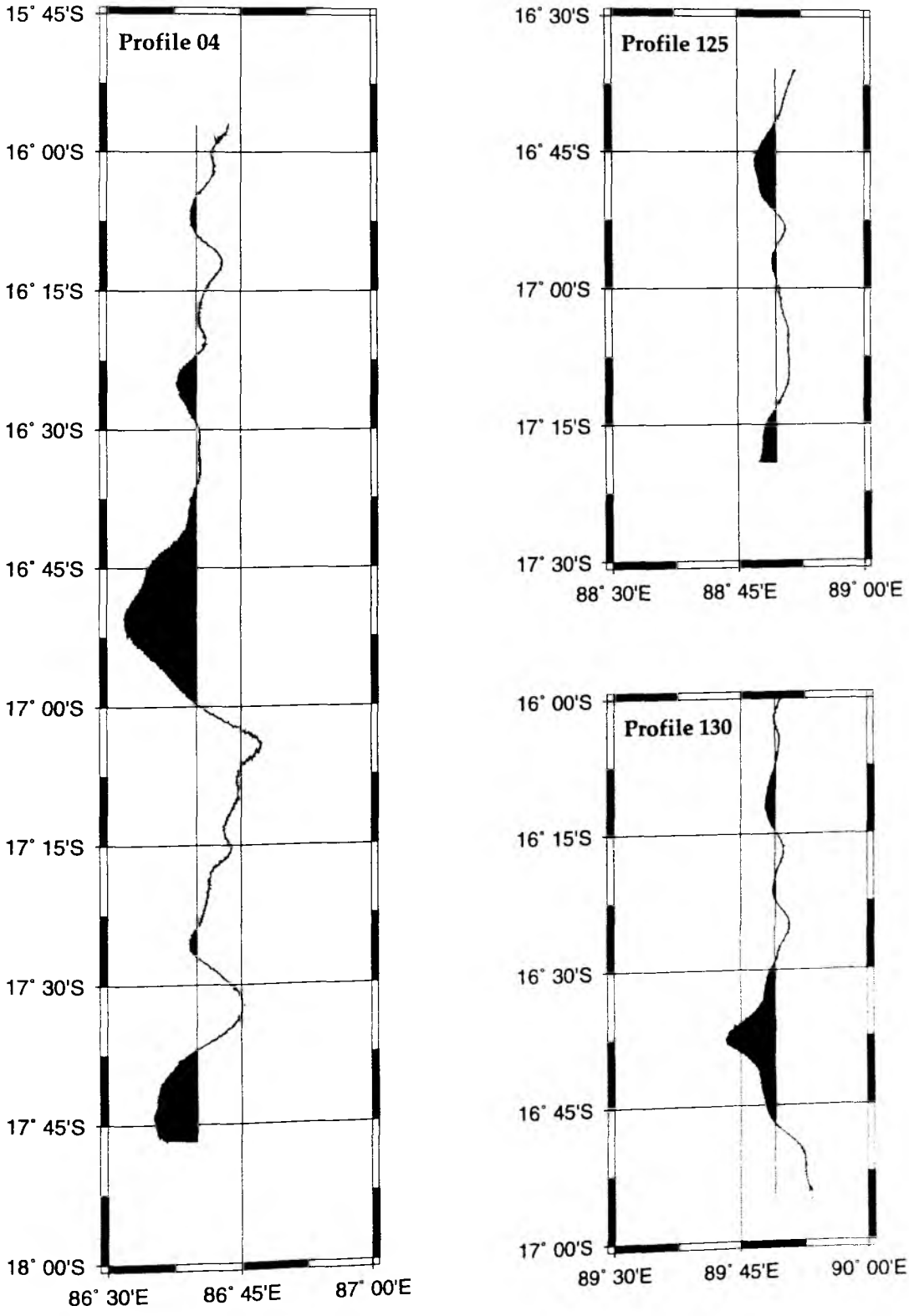

Figure 6.4.8: Magnetic spreading anomalies along Profile 04, 125 and 130.

7. ACKNOWLEDGEMENTS

The cruise SO 131 was funded by the German Ministery of Education, Research, Science, and Technologie (BMBF) under project No. 03 G 0131 to GEOMAR and BGR with the continued and generous most commendable support for marine sciences with an oustanding research vessel such as SONNE. The travel expenses of the BGR staff for SO131 were funded by the BGR budget. The participation of E. Haase was funded by the National Science Foundation (NSF) and O. Exner by the Deutsche Forschungsgemeinschaft (DFG) through grant Vi 133/3-4.

We warmly thank master H. Papenhagen and his crew for the excellent support with all work done and the splendid working atmosphere throughout the entire cruise, despite the length and the adverse weather conditions.

One of the planned highlights of SINUS should have been the two-ship experiment between SONNE and JOIDES RESOLUTION. Organising two ships to meet in the middle of the ocean is difficult by nature, but bringing two of the most prestigious vessels of the international research fleet to meet far from anywhere seemed unachievable. The list of people who helped to make the rendezvous of JOIDES RESOLUTION with SONNE at the Ninetyeast Ridge a reality is endless, and naming some would overlook others. We therefore express our sincere thanks to the organizing offices of ODP and BEO, who together with their advisory boards made this all possible. Although we did meet the JOIDES RESOLUTION and sailed around her several times, the two-ship experiment could not be accomplished due to unforeseen circumstances and complications. The disappointment was great, but it was those people that in the originally planning made this cruise possible who expressed in their many correspondence their own disappointment but also sent us motivation to prevail and try to accomplish the best science possible, despite the circumstances.

8. REFERENCES

Ammon, C.J. and J.E., Vidale, 1993: Tomography without rays, Bull. Seismol. Soc. Am., 83, 509-528.

Blondel, P. and B.J.Murton, 1997: Handbook of Seafloor Sonar Imagery, John Wiley and Sons, Chichester, 314.

Bonatti, E., and Harrison, C.G.A., 1988: Eruption styles of basalts in oceanic spreading ridges and seamounts: Effect of magma temperature and viscosity, J. Geophys. Res., 93, 2967-2980.

Bowin, C., 1973: Origin of the Ninetyeast Ridge from studies near the Equator, J. Geophys. Res., 78, 6029-6043.

Caress, D.W., McNutt, M.K., Detrick, R.S., and Mutter, J.C., 1995: Seismic imaging of hotspot-related crustal underplating beneath the Marquesas islands, Nature, 373, 600-603.

Caress, D.W., and D.N.Chayes, 1996: Improved processing of Hydrosweep DS Multibeam data on the R/V Maurice Ewing Marine Geophysical Researches 18, 631-650.

Chen, Y.J., 1992: Oceanic crustal thickness versus spreading rate, Geophys. Res. Lett., 19, 753-756.

Davis, T.A., B.P. Luyendyk, et al., 1974: Init. Repts. DSDP, 26, (U.S. Gov. Printing Office), Washington.

Detrick, R.S., Collins, J.A., Stephen, R.A., and Swift, S.A., 1994: In situ evidence for the nature of the seismic layer 2/3 boundary in oceanic crust, Nature, 370, 288-290.

Dragoset, W.H., 1990: Airgun array specs: A tutorial, Geophysics: The Leading Edge of Exploration, 24-32.

Duncan, R.A., 1981: Hotspots in the southern oceans – an absolute frame of reference for motion of Gondwana continents, Tectonophysics, 74, 29-42.

Duncan, R.A., 1991: Age distribution of volcanism along aseismic ridges in the eastern Indian ocean, Proc. ODP, Sci. Results, 121, 507-517, College Station, TX (Ocean Drilling Program).

Essen, H.-H., H. Janle, F. Schirmer and J. Siebert, 1981: Propagation of surface waves in marine sediments, J. Geophys., 49, 115-122.

Essen, H.-H., 1994: Scattering from a rough sedimental sea-floor containing shear and layering, J. Acoust. Soc. Am., 95 427-444.

Ewing, J. and G.M. Purdy, 1982: Upper crustalvelocity structure in The ROSE area of the East Pacific Rise, J. Geophys. Res., 87, 8397-8402.

Flueh, E. R, and R. von Huene, 1994: Fahrtbericht SO96 KODIAK-SEIS, GEOMAR-Kiel.

Flueh, E. R., Bialas, J., 1996: A digital, high data capacity ocean bottom recorder for seismic investigations. Int. Underwater Systems Design, 18, 3, 18-20.

Flueh, E. R., and Fisher, M. A., 1996: Cruise report SO108-ORWELL. GEOMAR Report 49, ISSN 0936-5788, 278pp.

Flueh, E. R., and C. Reichert, 1997: Cruise report SO123-MAMUT. GEOMAR Report 62 ISSN 0936-5788, 292pp.

Francis, T.J.G. and R.W. Raitt, 1967: Seismic refraction measurements in the southern Indian ocean, J. Geophys. Res., 72, 3015-3041.

Geller, C.A., J.K. Weissel, and R.N. Anderson, 1983: Heat transfer and intraplate deformation in the central Indian ocean, J. Geophys. Res., 88, 1018-1032.

Grevemeyer, I., and Weigel, W., 1996: Seismic velocities of the uppermost igneous crust versus age, Geophys. J. Int., 124, 631-635.

Grevemeyer, I., and Weigel, W., 1997: Increase of seismic velocities in upper oceanic crust: The "superfast" spreading East Pacific Rise at 14°14'S, Geophys. Res. Lett., 24, 217-220

Grevemeyer, I., Weigel, W., and Jennrich, C., 1998: Structure and aging of oceanic crust at 14°S on the East Pacific Rise, Geophys. J. Int., in press.

Heezen, B.C., and M.Tharp, 1965: Physiographic diagram of the Indian ocean (with descriptive sheet), Geological Society of America, Inc., New York.

Herber, R. Nuppenau, V., and Snoek, M., 1981: An OBS for marine seismic investigations basic requirements and options: The Hamburg OBS, Bull. di Geofis. Teor. ed Appl., 23, 233-242.

Kent, W., A.D. Saunders, P.D. Kempton, and N.C. Ghose, 1997: Rajmahal basalts, eastern India: mantle sources and melt distribution at a volcanic rifted margin, in J.J. Mahoney and M.F. Coffin (eds.), Large Igneous Provinces: continental, oceanic, and planetary flood volcanism, Gophysical Monograph, 100, 145-182, American Geophysical Union, Washington.

Kirk, R.E., K. Robertson, R.B. Whitmarsh and P.R. Miles, 1991: A technique for conducting seismic refraction experiments on the ocean bed using bottom shots, Mar. Geophys. Res., 13, 153-160.

Kissling, E., 1988: Geotomography with local earthquakes, Rev. Geophys., 26, 659-698.

Klein, E.W., 1981: A linear gradient crustal model for south Hawaii, Bull. Seis. Soc. Am. , 71, 1503-1510,

Knickmeyer, E.T., 1996: Hochgenaues Differential-GPS, Proc. 11th Annual Meeting of the German Hydrographic Society, Glücksburg, 3.-5.6 1996.

Koelsch, D.E., W.E. Witzell, J.E. Broda, F.B. Wooding and G.M. Purdy, 1986: A deep Towed explosive source for seismic experiments on the ocean floor. Mar. Geophys. Res., 8, 345-361.

Laws, R.M., L. Hatton, and M. Haarsten, 1990: Computer modelling of clustered airguns, First Break, 8, 331-344.

Le Pichon, X., and J.R. Heirtzler, 1968: Magnetic anomalies in the Indian ocean and sea-floor spreading, J. Geophys. Res., 73, 2101-2117.

Liu, C.-S., J.R. Curray, and J.M. McDonald, 1983: New constraints on the tectonic evolution of the eastern Indian ocean, Earth Planet. Sci. Lett., 65, 331-342.

Luetgert, J., 1992: Interactive Two-Dimensional Seismic Raytracing for the Macintosh, USGS Open File Report, 43.

Luyendyk, B.P., and W. Rennick, 1977: Tectonic history of aseismic ridges in the eastern Indian ocean, Geol. Soc. Am. Bull., 88, 1347-1356.

9. APPENDICES

9.1 DETAILS OF OBH/OBS DEPLOYMENTS AND SEISMIC PROFILES

9.1.1 SINUS-SO131-PROFILE 01 - 03

9.1.2 SINUS-SO131-SOURCES

9.1.3 SINUS SO131 PROFILE 30-SEEBOSEIS

9.1.4 SINUS-SO131.PROFILE 04

9.1.5 SINUS-SO131-PROFILE 05

9.1.6 SINUS-SO131-PROFILE 06

9.1.7 SINUS-SO131-3D-ARRAY

9.1.8 SINUS-SO131-3D-PROFILES

9.1.9 SINUS-SO131-PROFILE 31

9.2 ACTIVITY REPORT FROM JOIDES RESOLUTION

9.3 CAPTAINS REPORT

Appendix 9.1.1 **SINUS-SO131-Profile 01 - 03**

INST.	LAT (N)			LON (E)			DIST. TO	DEPTH	REL.	ANT.	REC.	SKEW	REMARKS
	D	M	S	D	M	S	NEXT (nm)	(m)	CODE	CH.	NO.	(ms)	
OBH01	23	06	10,62	66	27	44,40		811	C454	B	02.96	-1	on profile 01 - 03
Streamer								14			03.97	0	on profile 01 & 03
Streamer								14			971201	0	on profile 02
Trigger											01.95	-2	on profile 01 - 03

Appendix 9.1.2 SINUS-SO131-SOURCES

PRO-FILE	PULSE NO.	DATE	TIME UTC	LAT (S) D	M	S	LON (E) D	M	S	LENGTH (nm)	PULSE INT.	NO./VOL. of GUNS	REMARKS
SO131 01	1	05.05.98	19:47:02	23	05	14,40	66	19	50,28		10 s	1	R; W; HP
	731	05.05.98	21:48:42	23	12	40,38	66	27	33,72	13,00		3 l	
SO131 02	1	05.05.98	21:58:10	23	13	04,02	66	27	24,78		10 s	1	R; W; HP
	440	05.05.98	23:11:20	23	12	19,02	66	20	50,76	6,50		3 l	
SO131 03	1	05.05.98	23:34:09	23	11	59,88	66	21	06,42		10 s	1	R; W; HP
	1219	06.05.98	02:57:08	23	00	14,52	66	34	26,22	17,50		3 l	
SO131 04	1	16.05.98	05:14:00	17	37	37,38	86	40	01,08		60 s	20	R; W; M; HP; TIME + 74 ms due to trigger gun # 5,11,16 leakage
	1190	17.05.98	01:03:00	15	57	57,54	86	40	02,16	99,66		48,2 l	
SO131 05	1	18.05.98	14:51:00	17	01	24,30	88	56	44,46		60 s	20	R; W; M; HP; TIME + 74 ms due to trigger; #7 leak.; #5,11 unsynchr.
	2050	20.05.98	01:00:00	17	01	22,80	85	58	30,42	170,40		51,2 l	
SO131 06	1	21.05.98	17:57:00	17	01	21,78	89	56	37,98		60 s	20	R; W; M; HP
	1752	22.05.98	23:08:00	17	01	23,76	87	21	44,58	148,10		51,2 l	
SO131 07	1	25.05.98	08:36:00	17	20	16,56	88	03	51,72		60 s	10	R; W; M; HP only starboard-array
	409	25.05.98	15:24:00	16	46	19,56	88	03	50,28	34,00		25,6 l	
SO131 08	1	26.05.98	01:56:00	17	13	48,30	87	58	32,34		60 s	10	R; W; M; HP only starboard-array
	540	26.05.98	10:55:00	16	51	22,80	88	24	33,18	37,60		25,6 l	
SO131 09	1	26.05.98	11:10:00	16	51	23,52	88	23	09,90		60 s	20	R; W; M; HP
	299	26.05.98	16:08:00	16	54	22,38	87	55	44,64	26,00		51,2 l	
SO131 10	1	26.05.98	17:09:00	16	54	22,08	87	55	53,16		60 S	20	R; W; M; HP
	344	26.05.98	22:52:00	16	54	17,94	88	26	14,82	29,00		51,2 L	
SO131 11	1	26.05.98	23:28:00	16	55	11,94	88	26	30,30		30 s	20	R; W; M; HP #14 not in use
	779	27.05.98	05:57:00	17	07	52,08	87	54	55,68	32,70		48,9 l	

R = reflec. seism. (3 ch.); W = wide angle/refrac. seism.; M = magn.; HP = hydrosweep parasound

Appendix 9.1.2 SINUS-SO131-SOURCES

PRO-FILE	PULSE NO.	DATE	TIME UTC	LAT (S) D	M	S	LON (E) D	M	S	LENGTH (nm)	PULSE INT.	NO./VOL. of GUNS	REMARKS
SO131 12	1	27.05.98	06:18:00	17	08	01,02	87	54	51,24		60 s	20	R; W; M; HP
	349	27.05.98	12:06:00	17	09	20,28	88	25	38,70	29,50		48,9 l	#14 not in use
SO131 121	1	27.05.98	12:23:00	17	10	04,86	88	26	39,24		60 s	20	R; W; M; HP
	73	27.05.98	13:35:00	17	16	02,88	88	26	41,16	6,00		44,6 l	#4, 11, 14 not in use
SO131 13	1	27.05.98	13:51:00	17	16	27,78	88	25	52,92		60 s	20	R; W; M; HP
	500	27.05.98	22:10:00	16	46	09,18	87	55	36,60	41,90		44,6 l	#4, 11, 14 not in use
SO131 131	1	27.05.98	22:23:00	16	45	15,54	87	55	38,40		60 S	20	R; W; M; HP
	45	27.05.98	23:07:00	16	45	09,54	87	58	54,00	3,10		44,6 l	#4, 11, 14 not in use
SO131 14	1	27.05.98	23:33:00	16	46	04,86	88	00	46,50		60 s	20	R; W; M; HP
	370	28.05.98	05:42:00	17	17	05,52	88	00	43,50	31,00		44,6 l	#4, 11, 14 not in use
SO131 141	1	28.05.98	05:55:00	17	17	38,88	88	00	03,78		60 s	20	R; W; M; HP
	93	28.05.98	07:27:00	17	14	54,60	87	56	43,14	4,20		41,6 l	#4, 9, 11, 14 not in use
SO131 15	1	28.05.98	07:47:00	17	11	34,44	87	55	00,06		60 s	20	R; W; M; HP
	364	28.05.98	13:50:00	17	11	23,10	88	25	48,78	29,40		41,6 l	#4, 9, 11, 14 not in use
SO131 151	1	28.05.98	14:16:00	17	12	40,80	88	26	52,38		60 s	20	R; W; M; HP
	74	28.05.98	15:29:00	17	17	11,10	88	22	23,40	6,20		41,6 l	#4, 9, 11, 14 not in use
SO131 16	1	28.05.98	15:53:00	17	16	52,44	88	20	52,20		60 s	20	R; W; M; HP
	372	28.05.98	22:04:00	16	45	59,70	88	20	50,10	30,90		41,6 l	#4, 9, 11, 14 not in use
SO131 17	1	28.05.98	23:04:00	16	46	18,18	88	16	50,28		60 s	20	R; W; M; HP
	369	29.05.98	05:12:00	17	17	01,62	88	16	50,34	30,70		38,6	#4, 7, 9, 11, 14 not in use
SO131 18	1	29.05.98	11:45:00	17	03	16,68	88	11	39,66		30 s	10	R; W; M; HP
	326	29.05.98	14:27:30	17	03	26,16	88	10	57,30	13,60		25,6 l	**small circle, 2 nm**

R = reflec. seism. (3 ch.); W = wide angle/refrac. seism.; M = magn.; HP = hydrosweep parasound

Appendix 9.1.2 SINUS-SO131-SOURCES

PRO-FILE	PULSE NO.	DATE	TIME UTC	LAT (S) D	M	S	LON (E) D	M	S	LENGTH (nm)	PULSE INT.	NO./VOL. of GUNS	REMARKS
SO131 181	1	29.05.98	14:31:00	17	03	23,70	88	10	37,74		60 s	10	R; W; M; HP
	108	29.05.98	15:24:30	17	03	18,78	88	05	50,34	4,60		25,6 l	
SO131 19	1	29.05.98	15:40:00	17	02	43,26	88	04	45,06		30 s	10	R; W; M; HP
	891	29.05.98	23:05:00	17	02	38,04	88	04	42,36	37,00		25,6 l	**large circle, 6 nm**
SO131 20	1	29.05.98	23:56:00	17	04	15,78	88	04	14,94		60 s	20	R; W; M; HP
	253	30.05.98	04:08:00	17	04	23,04	88	25	45,54	20,60		51,2 l	
SO131 201	1	30.05.98	04:47:00	17	05	42,48	88	26	01,92		60 s	20	R; W; M; HP
	41	30.05.98	05:27:00	17	04	45,60	88	22	35,64	3,40		51,2 l	
SO131 21	1	30.05.98	05:28:00	17	04	44,70	88	22	30,18		30 s	20	R; W; M; HP
	644	30.05.98	10:49:30	16	57	10,38	87	55	16,74	27,10		51,2 l	
SO131 22	1	30.05.98	11:26:00	16	59	27,36	87	55	29,76		60 s	20	R; W; M; HP
	141	30.05.98	13:46:00	16	59	24,60	88	07	47,46	11,80		51,2 l	
SO131 23	1	30.05.98	14:04:00	17	00	08,76	88	08	49,62		60 s	20	R; W; M; HP
	382	30.05.98	20:25:00	17	31	54,90	88	08	49,50	31,80		51,2 l	
SO131 24	1	30.05.98	20:55:00	17	31	57,30	88	06	58,50		60 s	20	R; W; M; HP
	242	31.05.98	00:56:00	17	11	46,56	88	09	33,36	20,30		51,2 l	
SO131 241	1	31.05.98	00:59:00	17	11	31,44	88	09	36,12		30 s	20	R; W; M; HP
	513	31.05.98	05:15:00	16	50	39,24	88	12	18,54	21,00		48,9 l	# 4 leak.
SO131 242	1	31.05.98	05:17:00	16	50	39,24	88	12	18,54		60 s	20	R; W; M; HP
	220	31.05.98	08:56:00	16	31	42,18	88	14	59,22	19,10		48,9 l	# 4 off
SO131 25	1	31.05.98	08:58:00	16	31	37,68	88	15	07,20		60 s	20	R; W; M; HP
	181	31.05.98	11:58:00	16	31	30,66	88	30	23,22	14,60		48,9 l	# 4 off

R = reflec. seism. (3 ch.); W = wide angle/refrac. seism.; M = magn.; HP = hydrosweep parasound

Appendix 9.1.2 SINUS-SO131-SOURCES

PRO-FILE	PULSE NO.	DATE	TIME UTC	LAT (S) D	M	S	LON (E) D	M	S	LENGTH (nm)	PULSE INT.	NO./VOL. of GUNS	REMARKS
SO131 26	1	31.05.98	12:09:00	16	32	24,96	88	30	45,60		60 s	20	R; W; M; HP
	701	31.05.98	23:49:00	17	31	03,72	88	30	39,54	58,60		48,9 l	# 4 off
SO131 27	1	31.05.98	23:52:00	17	31	14,28	88	30	28,08		60 s	20	R; W; M; HP
	112	01.06.98	01:43:00	17	31	12,30	88	21	08,94	8,90		48,9 l	# 4 off
SO131 28	1	01.06.98	01:45:00	17	31	06,78	88	21	03,54		60 s	20	R; W; M; HP
	253	01.06.98	05:57:00	17	10	17,22	88	20	52,62	20,80		46,9 l	# 3, 4 off
SO131 281	1	01.06.98	05:59:00	17	10	03,00	88	20	48,30		30 s	20	R; W; M; HP
	212	01.06.98	07:44:00	17	01	04,74	88	20	48,84	9,00		46,9 l	# 3, 4 off
SO131 29	1	02.06.98	15:57:00	17	11	25,86	88	22	08,10		20 s	10	R; M; HP
	950	02.06.98	21:14:20	17	11	36,42	87	54	16,80	26,60		25,6 l	part of pr. SO131-15
SO131 30	1	03.06.98	07:12:00	17	04	26,28	88	14	20,34		10 s	3	R; W; M; HP
	269	03.06.98	07:56:40	17	04	25,08	88	10	39,42	3,50		6,8 l	SEBOSEIS experiment
SO131 31	1	04.06.98	21:54:00	17	01	23,04	91	06	01,56		60 s	20	R; W; M; HP
	2028	06.06.98	07:41:00	17	01	29,16	88	09	50,28	168,50		51,2 l	second half # 19 off
SO131 32	1	06.06.98	08:15:00	17	00	08,04	88	09	15,48		60 s	10	R; W; M; HP
	679	06.06.98	10:08:10	17	00	02,82	88	18	01,32	8,40		25,6 l	
SUM	21508									1356,56			
										= 2512.35 km			

R = reflec. seism. (3 ch.); W = wide angle refrac. seism.; M = magn.; HP = hydrosweep parasound

Appendix 9.1.3 SINUS-SO131-Profile 30-SEEBOSEIS

INST.	LAT (S)			LON (E)			DIST. TO	DEPTH	REL.	ANT.	REC.	SKEW	REMARKS
	D	M	S	D	M	S	NEXT (nm)	(m)	CODE	CH.	NO.	(ms)	
OBH88	17	04	25,44	88	13	49,08	1.6	1840	D669	D	980401	-1	**OBS**; sampling rate: 1 kHz; not rel.
OBH89	17	04	26,70	88	12	13,08	1	1813	A319	A	971201	0	sampling rate: 62 Hz
OBH90	17	04	06,12	88	13	00,90	0.8	1829	C464	B	980402	0	sampling rate: 500 Hz
OBH91	17	04	26,16	88	12	25,08	0.7	1817	6A24	B	NINA	0	HH Zyl.
OBH92	17	04	17,82	88	13	00,78	0.7	1829	D654	C	MONIKA	0	HH Zyl.; no recording
OBH93	17	04	26,70	88	13	36,96		1839			ELKE	0	HH Zyl.; **OBS**
Streamer								12			971201	0	
Trigger											91.15	-1	

Appendix 9.1.4 SINUS-SO131-Profile 04

INST.	LAT (S)			LON (E)			DIST. TO	DEPTH	REL.	ANT.	REC.	SKEW	REMARKS
	D	M	S	D	M	S	NEXT (nm)	(m)	CODE	CH.	NO.	(ms)	
OBH02	16	46	23,52	86	39	57,48	3.0	4770	6A24	A	02.96	-23	
OBH03	16	49	20,52	86	39	56,58	3.0	4749	D634	B	980401	-3	
OBH04	16	52	21,48	86	39	56,94	3.0	4737	C679	B	05.96	-3	
OBH05	16	55	22,98	86	39	59,46	2.0	4525	D669	D	15.93	-43	OBS
OBH06	16	57	21,84	86	39	58,02	2.0	4376	A319	A	19.96		Battery cable cut upon recovery
OBH07	16	59	22,56	86	39	59,16	2.0	4240	6A34	B	92.06	-6	
OBH08	17	01	22,38	86	39	59,64	2.0	4319	6A29	C	03.94	-29	also Profile 05
OBH09	17	03	21,30	86	39	58,08	2.0	4433	A324	A	98403	5	
OBH10	17	05	22,62	86	39	58,68	2.0	4316	C454	D	91.13	-5	
OBH11	17	07	21,00	86	39	57,96	3.0	4457	D654	A	91.12	3	
OBH12	17	10	22,20	86	39	58,74	3.0	4455	C634	B	1.96	-16	
OBH13	17	13	23,52	86	39	57,84		4414	B214	D	04.96	-37	
Streamer								14			971201	-2	
Trigger											03.97	-9	

Appendix 9.1.5 SINUS-SO131-Profile 05

INST.	LAT (S)			LON (E)			DIST. TO	DEPTH	REL.	ANT.	REC.	SKEW	REMARKS
	D	M	S	D	M	S	NEXT (nm)	(m)	CODE	CH.	NO.	(ms)	
OBH08	17	01	22,38	86	39	59,64	3.8	4319	6A29	C	03.94	-29	also profile 04
OBH14	17	01	24,72	86	43	59,16	3.8	4266	A319	D	19.96	-23	
OBH15	17	01	22,50	86	47	58,98	3.8	4267	6A24	A	05.96	-1	
OBH16	17	01	23,22	86	51	57,90	3.8	4112	C459	B	92.06	-5	
OBH17	17	01	24,12	86	56	00,18	3.8	3910	C464	A	02.96	-34	
OBH18	17	01	20,94	86	59	55,32	3.8	3852	D669	B	15.93	-63	**OBS**
OBH19	17	01	22,92	87	03	59,10	3.8	3670	A314	D	980401	-7	
OBH20	17	01	22,86	87	07	58,50	3.8	3510	B214	A	04.96	-47	
OBH21	17	01	22,74	87	11	58,62	3.8	3331	C634	D	1.96	-18	
OBH22	17	01	22,68	87	15	58,44	3.8	3260	D654	B	91.12	7	
OBH23	17	01	22,14	87	19	59,40	3.8	3220	6A34	D	91.13	-7	
OBH24	17	01	23,70	87	23	57,42	3.8	3155	B219	D	980403	6	
OBH25	17	01	24,66	87	27	58,44	3.8	3117	C676	C	06.96	-28	
OBH26	17	01	22,50	87	31	58,98	3.8	3022	D649	C	91.10		4 resets; not synchronized
OBH27	17	01	22,50	87	35	59,04	3.8	2984	C444	B	92.01	-41	
OBH28	17	01	23,70	87	39	59,46	3.8	2848	C454	C	02.95	-36	
OBH29	17	01	22,50	87	43	58,20	3.8	2651	A324	C	08.94	-46	
OBH30	17	01	29,82	87	48	03,24	3.8	2351	D719	D	01.95	-11	**VA, 100m**
OBH31	17	01	23,52	87	51	57,84	3.8	2174	D634	A	03.96	-45	
OBH32	17	01	23,70	87	55	58,32	3.8	1994	B459	D	03.97	-5	
OBH33	17	01	22,38	87	58	57,18	2.9	1923	B644	D	01.97	-52	OAS and Benthos hydrophones
OBH34	17	01	25,20	88	01	59,94	2.9	1836	B639	B	91.15	-11	no data, data buffer overflow
OBH35	17	01	23,46	88	04	58,62	2.9	1734	B559	B	02.97	16	
OBH36	17	01	23,58	88	07	58,56	2.9	1671	D674	B	91.14	-11	no data, hydroph. not connected
OBH37	17	01	23,16	88	11	00,06		1659	D629	A	971202	-2	
Streamer								14			971201	-2	part I; 18.05., 14:51 UTC
Trigger											971201	-2	till 19.05., 09:40 UTC
Streamer								14			971201	-1	part II; 19.05., 10:27 UTC
Trigger											971201	-1	till 20.05., 00:01 UTC

Appendix 9.1.6 SINUS-SO131-Profile 06

INST.	LAT (S)			LON (E)			DIST. TO	DEPTH	REL.	ANT.	REC.	SKEW	REMARKS
	D	M	S	D	M	S	NEXT (nm)	(m)	CODE	CH.	NO.	(ms)	
OBH38	17	01	22,98	88	13	57,30	2.9	1809	D629	A	03.96	-154	also profile 07 - 28; data buf. overfl.
OBH39	17	01	23,70	88	16	57,42	2.9	1869	D674	B	06.96	-76	also profile 07 - 17
OBH40	17	01	24,00	88	20	00,66	2.9	2017	B559	A	02.97	17	
OBH41	17	01	23,22	88	22	58,26	2.9	2081	B639	B	91.14	-9	
OBH42	17	01	28,38	88	25	49,80	2.9	2164	D719	B	01.95	-7	**VA, 100m**
OBH43	17	01	25,02	88	28	58,02	2.9	2266	B644	D	03.97	-4	hydrophone poor
OBH44	17	01	24,66	88	31	56,22	2.9	2376	B495	A	02.95	-29	
OBH45	17	01	23,40	88	34	59,22	2.9	2406	C444	D	92.01	-36	
OBH46	17	01	25,62	88	37	57,00	2.9	2440	D649	C	91.15	-10	no data, data buffer overflow
OBH47	17	01	21,90	88	41	57,42	2.9	2592	D654	D	980402	0	no data, not activated
OBH48	17	01	22,32	88	44	57,96	2.9	4359	D669	C	15.93	-59	**OBS**
OBH49	17	01	23,04	88	47	56,58	2.9	4882	D634	B	08.94	-39	
OBH50	17	01	22,56	88	50	58,80	2.9	4875	A324	D	91.10	-132	
OBH51	17	01	21,66	88	53	58,74	2.9	4188	C454	B	01.96	-15	
OBH52	17	01	24,06	88	56	58,26	3.8	5097	C679	C	91.13	-6	
OBH53	17	01	23,88	89	00	59,34	3.8	5245	B219	D	91.12	5	
OBH54	17	01	24,60	89	05	01,20	3.8	4967	6A34	A	980403	-17	
OBH55	17	01	23,04	89	09	01,68	3.8	5366	C634	A	02.96	-35	
OBH56	17	01	22,86	89	12	59,40	3.8	5356	B214	C	92.06	-5	
OBH57	17	01	24,12	89	17	00,00	3.8	5723	A314	B	03.94	-18	
OBH58	17	01	23,94	89	21	00,00	3.8	5505	C464	D	04.96	-47	
OBH59	17	01	23,52	89	25	02,94	3.8	5390	C459	C	05.96	-2	
OBH60	17	01	24,30	89	29	01,32	3.8	5291	6A24	D	19.96	-23	
OBH61	17	01	23,52	89	33	04,86		5324	A319	A	980401	-5	
Streamer								14			971201		skew not determined
Trigger											01.97	-3	

INST.	LAT (S)			LON (E)			DEPTH	REL.	ANT.	REC.	SKEW	REMARKS
	D	M	S	D	M	S	(m)	CODE	CH.	NO.	(ms)	
OBH38	17	01	22,98	88	13	57,30	1809	D629	A	03.96	-154	on pr. 06 - 28; data buffer overflow
OBH39	17	01	23,70	88	16	57,42	1869	D674	B	06.96	-76	on pr. 06 - 17
OBH62	16	51	22,74	88	20	47,52	1943	A319	D	02.96	-116	on pr. 07 - 28
OBH63	16	54	23,10	88	20	45,36	1808	6A24	A	01.96	-57	on pr. 07 - 28
OBH64	16	51	23,28	88	13	29,82	1947	D654	C	91.12	18	on pr. 07 - 28
OBH65	16	54	23,64	88	12	41,10	1912	C464	D	91.13	-20	on pr. 07 - 28
OBH66	16	51	22,14	88	08	47,58	1917	D649	C	01.97	-132	Benthos hydrophone; on pr. 07 - 28
OBH67	16	54	22,74	88	03	45,78	1918	C459	A	03.94	-52	on pr. 07 - 28
OBH68	16	51	24,06	88	00	46,92	1928	A314	A	04.96		on pr. 07 - 28; not sync.; one reset
OBH69	16	58	35,16	88	00	46,14	1916	B214	B	19.96		on pr. 07 - 28; not sync.; humid
OBH70	16	59	22,98	88	03	45,78	1812	C634	B	02.95	-102	on pr. 07 - 28
OBH71	17	04	17,28	88	03	45,00	1752	6A34	D	05.96	2	on pr. 07 - 28
OBH72	17	09	21,78	88	02	54,18	1824	B219	C	08.94	-128	on pr. 07 - 28
OBH73	17	05	22,02	88	00	46,26	1857	C679	D	92.06	-12	on pr. 07 - 28
OBH74	17	11	24,24	88	00	53,52	1893	C444	D	92.01		on pr. 07 - 28; not sync.
OBH75	17	11	23,46	88	03	46,20	1853	D634	A	91.10	445	on pr. 07 - 28
OBH76	17	11	22,92	88	08	16,20	1831	B495	C	03.97	-15	on pr. 07 - 28
OBH77	17	09	24,66	88	08	46,86	1812	B644	D	02.97	72	on pr. 07 - 28; hydrophone poor
OBH78	17	04	24,78	88	13	47,16	1839	D669	B	15.93	-185	on pr. 07 - 28; **OBS**
OBH79	17	09	23,76	88	18	47,10	2147	B639	C	980401	-11	on pr. 07 - 17
OBH80	17	11	24,00	88	20	49,14	2175	C454	D	980402	-3	on pr. 07 - 17
OBH81	17	04	24,00	88	20	47,52	2093	B559	B	91.14	-10	on pr. 07 - 17
OBH82	16	59	03,00	88	15	27,60	1836	D719	B	980403	5	on pr. 07 - 28; **VA, 1200m**
OBH83	16	59	24,24	88	08	50,88	1660	D738	A	01.95	-4	on pr. 07 - 17; **VA, 100m**
OBH84	17	11	24,84	88	20	40,80	2177	C454	D	971201	-2	on pr. 18 - 28
OBH85	17	04	18,30	88	20	49,98	2094	B559	B	980402	-2	on pr. 18 - 28
OBH86	17	01	10,50	88	10	46,68	1651	D674	A	06.96	-17	OAS and ITI hydrophones; on pr. 18 - 28
OBH87	17	01	34,74	88	10	46,56	1663	B639	B	980401	-7	on pr. 18 - 28

Appendix 9.1.8 SINUS-SO131-3D-Profiles

PROFILE	BEGIN		END		STREAMER	SKEW	TRIGGER	SKEW	REMARKS
NO.	JUL. DATE	TIME UTC	JUL. DATE	TIME UTC	REC. NO	(ms)	REC. NO	(ms)	
PR07	145	08:36:00	145	15:24:00	971201	-1	91.15	-3	only starboard airgun-array
PR08	146	01:56:00	146	10:55:00	971201	-1	91.15	-3	only starboard airgun-array
PR09	146	11:10:00	146	16:08:00	971201	-1	91.15	-2	
PR10	146	17:09:00	146	22:52:00	971201	-1	91.15	-4	
PR11	146	23:28:00	147	05:57:00	971201	-1	91.15	-2	
PR12	147	06:18:00	147	12:06:00	971201	-1	91.15	-3	
PR121	147	12:23:00	147	13:35:00	971201	-1	91.15	-3	
PR13	147	13:51:00	147	22:10:00	971201	-1	91.15	-3	
PR131	147	22:23:00	147	23:07:00	971201	-1	91.15	-3	
PR14	147	23:33:00	148	05:42:00	971201	-1	91.15	-2	
PR141	148	05:55:00	148	07:27:00	971201	-1	91.15	-2	
PR15	148	07:47:00	148	13:50:00	971201	-1	91.15	-2	
PR151	148	14:16:00	148	15:29:00	971201	-1	91.15	-1	trigger off
PR16	148	15:53:00	148	22:04:00	971201	-1	91.15	-1	trigger off
PR17	148	23:04:00	149	05:12:00	971201	0	91.15	-2	
PR18	149	11:45:00	149	14:27:30	971201	-1	91.15	-5	**small circle, R = 2 nm**
PR181	149	14:31:00	149	15:24:30	971201	-1	91.15	-5	
PR19	149	15:40:00	149	23:05:00	971201	-1	91.15	-5	**large circle, R = 6 nm**
PR20	149	23:56:00	150	04:08:00	971201	-1	91.15	-5	
PR201	150	04:47:00	150	05:27:00	971201	-1	91.15	-5	
PR21	150	05:28:00	150	10:49:00	971201	-1	91.15	-5	
PR22	150	11:26:00	150	13:46:00	971201	-1	91.15	-5	
PR23	150	14:04:00	150	20:25:00	971201	-1	91.15	-3	
PR24	150	20:55:00	151	00:56:00	971201	-1	91.15	-3	
PR241	151	00:59:00	151	05:15:00	971201	-1	91.15	-3	
PR242	151	05:17:00	151	08:56:00	971201	-1	91.15	-3	
PR25	151	08:58:00	151	11:58:00	971201	-1	91.15	-3	
PR26	151	12:09:00	151	23:49:00	971201	-1	91.15	-3	
PR27	151	23:52:00	152	01:43:00	971201	0	91.15	-1	
PR28	152	01:45:00	152	05:57:00	971201	0	91.15	-1	
PR281	152	05:59:00	152	07:44:00	971201	0	91.15	-1	
PR29	153	16:08:00	153	21:33:00	971201	0	91.15	-1	

Appendix 9.1.9 SINUS-SO131-Profile 31

INST.	LAT (S)			LON (E)			DIST. TO	DEPTH	REL.	ANT.	REC.	SKEW	REMARKS
	D	M	S	D	M	S	NEXT (nm)	(m)	CODE	CH.	NO.	(ms)	
OBH94	17	01	23,94	89	36	59,94	3.8	5045	A319	A	02.97	21	
OBH95	17	01	22,86	89	40	59,76	3.8	4983	D654	D	03.97	-4	
OBH96	17	01	22,50	89	44	59,58	3.8	4925	6A24	C	01.96	-15	
OBH97	17	01	22,56	89	48	59,58	3.8	4723	C464	B	02.96	-44	
OBH98	17	01	23,58	89	53	00,24	3.8	3635	A314	D	91.13	-6	
OBH99	17	01	23,04	89	57	01,02	3.8	4303	C459	C	03.94	-16	
OBH100	17	01	23,94	90	01	00,24	3.8	4686	B214	B	08.94	-41	
OBH101	17	01	21,78	90	04	58,44	3.8	4754	C634	D	91.12	2	
OBH102	17	01	22,86	90	08	59,04	3.8	5306	D669	B	980401	-7	OBS
OBH103	17	01	23,28	90	13	01,68	4.0	5108	6A34	A	91.10		not sync.
OBH104	17	01	22,86	90	17	40,08	3.6	5997	B219	B	92.06		not sync.; battery cable cut
OBH105	17	01	24,72	90	21	00,78	3.8	5783	D634	C	02.95	-33	
OBH106	17	01	23,04	90	25	00,18	3.8	5412	C679	A	05.96	3	
OBH107	17	01	22,86	90	28	59,28	3.8	5209	C454	A	06.96	-16	
OBH108	17	01	22,98	90	32	59,88		5296	D674	D	15.93	-57	
Streamer								12			971201	-2	
Trigger											91.15	-9	

Appendix 9.2

Activity Report from JOIDES RESOLUTION

28 May 1998
Hole 1107A
Lat. 17 degrees 1.418' S, Long. 88 degrees 10.850' E. Water Depth: 1650 m

After an eight day transit we arrived on Site 1107 (Prospectus Site 757, NERO). We had hoped to pick up time in transit to ensure completion of the highest priority objectives at Ninetyeast Ridge (establishing the ION borehole and the two-ship offset seismic experiment in collaboration with the Sonne). This was not to be the case, and we actually took several hours longer to reach our location, our speed averaging less than 10 knots. As an additional hinderance to our operations schedule, based on our transit time from the Southwest Indian Ridge and no indication of improvement in speed during our transit to Darwin, the Captain was forced to add an additional day to our long transit in. There was an ambitious program outlined in our prospectus, including establishing a borehole for future installation of a subseafloor observatory, conventional logging and vertical seismic profile experiment, deployment of a test installation of the strainmeter module in preparation for Leg 186, and the NERO offset seismic experiment (NOSE) in conjunction with the continuing expedition of the Seismic Investigation at Ninetyeast Ridge Using the Sonne and JOIDES Resolution during ODP Leg 179 (SINUS). We had originally scheduled 11 days to complete these objectives. However, our extended portcall, lost shipment, and extended transit times all worked to shorten our operational schedule, paring away 17 of our original 26 days of total operational time, and reducing our time on location at NERO from 11 days to less than six days. Our optimistic estimate indicated that even given this radical reduction, if all went extraordinarily well we could still complete the borehole (although to a significantly less depth of penetration than our original target of 100-200 m into basement) and have some time remaining for the two-ship experiment. Our restricted schedule, however, required that we allocate no time for the many other operations we had hoped to complete at NERO.

After we arrived on site, we deployed a beacon and ran to seafloor with 48.82 m of 16 in casing fixed to a reentry cone. This assembly was washed in, and subsequently we reentered the hole with a 14-3/4 in tricone bit to drill a large borehole to allow deployment of 10-3/4 in casing some 30-40 m into basement. We also deployed the ocean bottom seismometers and installed the LDEO sensor sub on the drill string to conduct our second seismic-while-drilling experiment. Based on Leg 121 statistics, we had hoped to drill to basement in 12 or so hours, and to drill at least 30-40 m into basement over the next 10 hours. Drilling the sediment column took longer than we expected, probably due to the size of the hole we were drilling and resistive layers of volcanic breccia and tuff overlying basement as were reported in the Leg 121 Initial Report. Basement drilling also proceeded somewhat slower then we expected, although penetration rates were quite variable in the subaerially emplaced lava flows. At about 410 mbsf, we encountered a relatively hard layer, and ROP slowed to less than 2 m/hr. In light of

the fact the drilling in basement had up to this point proceeded reasonably quickly, we envisioned this hard layer as an ideal position to anchor the bottom of the casing with cement. After drilling to 422 mbsf to ensure that any material wiped off the walls of the borehole during emplacement of the casing would have a place to go and not impede casing operations, we terminated deepening Hole 1107A as we had reached our target depth for casing of approximately 40 m into basement.

In our optimistic schedule developed after recognizing we only had 5.5 days of operational time, we had hoped to set aside about 48 hours of ship time for the two-ship experiment. This time included pipe trips, set up and rig down time, and preparation to get underway (as this was to be our last operation) which resulted in an estimated 29 hours of shooting time for the two-ship experiment. Any additional time was to be allocated to deepening the hole. At this point in our operations, individually minor but collectively significant delays due to handling pipe in heavy seas, slowed ROP, and mechanical difficulties had pared more than 25 hours from our already drastically reduced timetable. We maintained regular (at least daily, often more) updates with the Sonne and ODP/TAMU, to keep them apprised of our rapidly diminishing chances of having sufficient time to complete the two ship experiment.

By the time our last casing operation was completed (10-3/4 in casing set to 414 mbsf), we recognized there would not be sufficient time to clean out the cement shoe in the bottom of the casing, drill through the cement, clean out the rathole underneath and make 10 m of new hole below the casing string. This was the absolute minimum envisioned as necessary for establishing a borehole for the observatory emplacement. In our estimation, completing the borehole and allowing time for even a short two-ship experiment would have resulted in a 24 hour delay in our arrival to Darwin. This was not possible given the program's tight operational schedule and that the leg had already been extended two days beyond the original schedule.

Even with the disappointment we all felt regarding cancellation of the two-ship experiment, we recognized that while we did not have sufficient time to prepare for and rig down after a two-ship experiment (at least 20-24 hours), since we already had a drilling bit in the bottom of the hole, we did have enough operational time to deepen the borehole. We had elected to use a tricone bit rather than a coring bit to ensure we could penetrate through the casing shoe without delay. This bit, although not allowing coring of the material drilled, did allow rapid penetration through the formation in the few hours we had remaining. We continued drilling to a depth of 493.8 mbsf, which is just over 120 m into basement and almost 80 m below the casing shoe. We hope this depth will allow a successful installation of the Ninetyeast Ridge Observatory. Postcruise processing is required to interpret the data collected during our seismic-while-drilling experiment, however our initial inspection of the data indicates this will be possible.

FS SONNE

Stationsprotokoll SO 131

APPENDIX 9.3

R.F. Reedereigemeinschaft
Forschungsschiffahrt GmbH

F.S. "S O N N E"
Kapt. H.Papenhagen

Stationsprotokoll F.S. "S O N N E" Reise SO 131

Gebrauchte Abkürzungen für die eingesetzten Geräte und Anzahl der Einsätze:

CTD/ROS	CTD-Rosette (Seabird)	: 02 Einsätze
OBH	Ocean Bottom Hydrofone	: 108 Einsätze

Eingesetzte Winden:

Winde			RF-Nr.	SO 131 Einsatz	Gesamt Einsatz	SO 131 S`länge	gefierte max.Sl	Gesamt S`länge	Zust
W 1	NSW	18,2	813004	000 h	0488 h	000000 m	3289 m	359640	4
W 2	LWL	18,2	865017	000 h	0816 h	068192 m	4905 m	527460	3
W 4	Roches	11,0	817095	000 h	0000 h	000000 m	0000 m	000000	1
W 5	NSW	11,0	816187	010 h	0189 h	009772 m	5552 m	141798	4
W 6	Drako	18,2	30518	009 h	0618 h	013080 m	6680 m	798772	4

Geräteverluste:

Keine

Abkürzungen im Stationsprotokoll:

z.W.	zu Wasser
a.D.	an Deck
Boko	Bodenkontakt
Bosi	Bodensicht
Slmax.	Seillänge
Lt	Lottiefe nach Hydrosweep
W x	eingesetzte Winde
HS	Hydrosweep
PS	Parasound

Alle Zeiten in : UTC + 5 Stunden

05.05.1998

1425	Beginn Tarierung des streamers, Test einer airgun		24 22,7 N 66 43.6 E
1715	Ende Test		24 10.1 N 66 36.2 E

OBH 1

2243	Beginn Station	LT = 813 m	23 06,2 N 66 27.7 E
2252	OBH z.W.	LT = 811 m	23 06,27 N 66 27.74 E

Profil SO 131-01

2356	Beginn auslegen streamer

06.05.1998

0000	streamer z.W.
0011	Bb-airgun z.W.

FS SONNE Stationsprotokoll SO 131

0104	Beginn Profil	23 06,2 N	66 20,8 E		
0249	Ende Profil	23 12,7 N	66 27,6 E	08 sml	
Profil	SO 131-02				
0258	Beginn Profil	23 13,0 N	66 27,4 E		
0411	Ende Profil	23 12,3 N	66 20,8 E	06 sml	
Profil	SO 131-03				
0434	Beginn Profil	23 11,7 N	66 21,4 E		
0757	Ende Profil	23 00,0 N	66 34,7 E	18 sml	32 sml
0811	streamer und airgun a.D.				
OBH T 1					
0913	OBH ausgelöst				
0923	OBH aufgetaucht				
0926	OBH a.D.	23 06,1 N	66 27,8 E		

07.05.1998

Releasertest W 6			
1800	Beginn Station	LT = 3613 m	16 46,6 N 69 11,6 E
1807	8 Stck releaser z.W,		
	SL = 25 m 3 releaser		
	SL = 60 m 4 releaser		
1910	Slmax = 3200 m Beginn Test		
1945	Ende Test / Beginn hieven		
2030	Alle releaser a.D./ Ende Teststation		

08.05.1998

Draht fetten W 6			
0815	Beginn austecken	LT = 3450 m	14 36,6 N 70 06,0 E
1033	Slmax = 6680 m Beginn hieven		
1236	Draht eingehievt		

11.05.1998

Releaser-Test W 6			
0800	Beginn Station	LT = 4244 m	01 25,6 N 76 38,4 E
0805	Releaser z.W.		
0858	Slmax = 3200 m Hydrofon z.W.		
0858-0912	11 releaser getestet		
0912	Beginn hieven		
0958	Releaser a.D.		
1000	Ende Station		

Alle Zeiten : UTC + 7 Stunden

16.05.1998

Profile	*131- 04 101 / 102*				
0057	OBH 02	z.W.	LT = 4768 m	16 46,39 S	86 40,0 E
0128	OBH 03	z.W.	LT = 4750 m	16 49,35 S	86 39,97 E
0150	OBH 04	z.W.	LT = 4739 m	16 52,35 S	86 39,96 E
0225	OBH 05	z.W.	LT = 4513 m	16 55,39 S	86 40,00 E
0243	OBH 06	z.W.	LT = 4380 m	16 57,37 S	86 39,98 E

0303	OBH 07 z.W.	LT = 4248 m	16 59,37 S 86 39,99 E	
0323	OBH 08 z.W.	LT = 4325 m	17 01,39 S 86 40,00 E	
0344	OBH 09 z.W.	LT = 4442 m	17 03,39 S 86 39,99 E	
0403	OBH 10 z.W.	LT = 4317 m	17 05,38 S 86 39,98 E	
0421	OBH 11 z.W.	LT = 4458 m	17 07,36 S 86 39,97 E	
0446	OBH 12 z.W.	LT = 4455 m	17 10,38 S 86 39,99 E	
0512	OBH 13 z.W.	LT = 4413 m	17 13,39 S 86 39,97 E	
0525	Magnetometer z.W.	KL = 350 m		
0550	Beginn Profil 101		17 16,0 S 86 44,0 E	
0843	Ende Profil 101		17 48,0 S 86 44,0 E	32 sml
0851	Magnetometer vorgehievt			
1007	Bb-airgun-array z.W.			
10014	Magnetometer	KL = 350 m		
1020	Stb-airgun-array z.W.			
1028	Streamer z.W.			
1028	Schuß 1		17 46,3 S 86 40,2 E	
1214	Beginn Registrierung		17 37,62 S 86 40,02 E	
2400			16 38,4 S 86 40,0 E	
17.05.1998				
0803	Schuß 1190 Ende Profil		15 57,8 S 86 40,0 E	99,66 sml
0810	streamer a.D.			
0834	Magnetometer vorgehievt			
0914	Bb-array a.D.			
0934	Stb-array a.D.			
0949	Magnetometer z.W.			
1019	Beginn Profil 102		15 55,0 S 86 44,0 E	
1447	Ende Profil 102		16 44,0 S 86 44,0 E	49 sml
1501	Magnetometer a.D.			
1552	OBH 2 a.D.		16 46,4 S 86 39,6 E	
1631	OBH 3 a.D.		16 49,3 S 86 39,7 E	
1704	OBH 4 a.D.		16 52,3 S 86 39,7 E	
1830	OBH 5 a.D.		16 55,4 S 86 39,7 E	
1858	OBH 6 a.D.		16 57,4 S 86 39,7 E	
1931	OBH 7 a.D.		16 59,4 S 86 39,8 E	
CTD - 1	*W 5*			
1945	CTD z.W.	LT = 4305 m	16 59,4 N 68 39,7 E	
2102	Simax = 4250 m	LT = 4310 m	16 59,3 N 86 39,6 E	
2246	CTD a.D. / Ende Station			
2340	OBH 9 a.D.		17 03,4 S 86 39,6 E	
18.05.199S				
0014	OBH 10 a.D.		17 05,3 S 86 39,7 E	
0111	OBH 11 a.D.		17 07,4 S 86 39,7 E	
0142	OBH 12 a.D.		17 10,4 S 86 39,6 E	
0232	OBH 13 a.D.		17 13,5 S 86 39,7 E	
Profile	*131-05 / 103 / 104*			
0402	OBH 14 z.W.	LT = 4270 m	17 01,38 S 86 43,98 E	
0432	OBH 15 z.W.	LT = 4264 m	17 01,38 S 86 47,98 E	
0502	OBH 16 z.W.	LT = 4112 m	17 01,39 S 86 51,96 E	
0531	OBH 17 z.W.	LT = 3923 m	17 01,40 S 86 56,00 E	
0600	OBH 18 z.W.	LT = 3833 m	17 01,39 S 87 00,00 E	
0636	OBH 19 z.W.	LT = 3672 m	17 01,38 S 87 03,99 E	

0708	OBH 20 z.W.	LT = 3512 m	17 01,38 S 87 08,00 E
0740	OBH 21 z.W.	LT = 3330 m	17 01,38 S 87 11,98 E
0813	OBH 22 z.W.	LT = 3260 m	17 01,39 S 87 15,97 E
0847	OBH 23 z.W.	LT = 3221 m	17 01,37 S 87 19,99 E
0921	OBH 24 z.W.	LT = 3156 m	17 01,39 S 87 23,96 E
0950	OBH 25 z.W.	LT = 3117 m	17 01,40 S 87 28,02 E
1024	OBH 26 z.W.	LT = 3023 m	17 01,38 S 87 31,99 E
1055	OBH 27 z.W.	LT = 2982 m	17 01,38 S 87 36,00 E
1127	OBH 28 z.W.	LT = 2847 m	17 01,40 S 87 40,00 E
1200	OBH 29 z.W.	LT = 2651 m	17 01,38 S 87 43,98 E
1235	OBH 30 z.W. (vertikal-array)		
1239	Kopfboje z.W.	LT = 2341 m	17 01,50 N 87 48,00 E
1310	OBH 31 z.W.	LT = 2174 m	17 01,39 N 87 51,97 E
1339	OBH 32 z.W.	LT = 1995 m	17 01,40 S 87 55,97 E
1405	OBH 33 z.W.	LT = 1923 m	17 01,38 S 87 58,97 E
1432	OBH 34 z.W.	LT = 1841 m	17 01,40 S 88 02,00 E
1456	OBH 35 z.W.	LT = 1734 m	17 01,39 S 88 04,98 E
1518	OBH 36 z.W.	LT = 1671 m	17 01,39 S 88 07,97 E
1556	OBH 37 z.W.	LT = 1659 m	17 01,39 S 88 11,00 E
1608	Magnetometer z.W.		
1631	Beginn Profil 103	17 05,0 S 88 59,0 E	
2037	Ende Profil 103	17 05,0 S 88 59,0 E	43 sml
2048	Magnetometer vorgehievt		
2122	Streamer z.W.		
2134	Bb-airgun-array z.W.		
2142	Stb-airgun-array z.W.		
2151	Magnetometer z.W.		
2151	1. Schuß auf Profil 05	17 01,39 S 88 56,41 E	
20.05.1998			
0800	Magnetometer aufgekürzt		
0800	Ende Profil 05	17 01,40 S 85 58,20 E	171 sml
0814	Bb-Array a.D.		
0824	Stb-Array a.D.		
0830	Streamer a.D.		
0847	Magnetometer ausgesteckt		
0859	Beginn Profil 131-104	17 05,0 S 85 56,0 E	
1247	Ende Profil 131-104	17 05,0 S 86 36,0 E	38 sml
1303	Magnetometer a.D.		
1400	OBH 08a.D.	17 01,4 S 86 39,9 E	
1455	OBH 14a.D.	17 01,4 S 86 43,8 E	
1534	OBH 15a.D.	17 01,3 S 86 47,8 E	
1616	OBH 16a.D.	17 01,4 S 86 51,8 E	
1700	OBH 17a.D.	17 01,3 S 86 55,9 E	
1810	OBH 18a.D.	17 01,3 S 86 59,7 E	
1847	OBH 19a.D.	17 01,4 S 87 03,7 E	
1926	OBH 20a.D.	17 01,4 S 87 07,8 E	
2001	OBH 21a.D.	17 01,4 S 87 11,9 E	
2101	OBH 22a.D.	17 01,4 S 87 15,8 E	
2141	OBH 23a.D.	17 01,3 S 87 19,8 E	
2218	OBH 24a.D.	17 01,3 S 87 23,8 E	

2256	OBH 25a.D.		17 01,3 S 87 27,8 E	
2337	OBH 26a.D.		17 01,4 S 87 31,8 E	
21.05.1998				
0019	OBH 27a.D.		17 01,4 S 87 35,7 E	
0102	OBH 28a.D.		17 01,4 S 87 39,8 E	
0143	OBH 29a.D.		17 01,4 S 87 43,8 E	
0254	OBH 30VA a.D.		17 01,4 S 87 47,7 E	
0333	OBH 31a.D.		17 01,4 S 87 51,7 E	
0413	OBH 32a.D.		17 01,4 S 87 55,7 E	
0457	OBH 33a.D.		17 01,4 S 87 58,7 E	
0538	OBH 34a.D.		17 01,4 S 88 01,7 E	
0609	OBH 35a.D.		17 01,4 S 88 04,8 E	
0654	OBH 36a.D.		17 01,4 S 88 07,7 E	
0726	OBH 37a.D.		17 01,4 S 88 10,7 E	

Profil 131-105 / 06 / 106

0817	OBH 38z.W.	LT = 1808 m	17 01,39 S 88 13,94 E	
0845	OBH 39z.W.	LT = ??	17 01,39 S 88 16,97 E	
0912	OBH 40z.W.	LT = 2017 m	17 01,40 S 88 20,01 E	
0938	OBH 41z.W.	LT = 2081 m	17 01,39 S 88 22,97 E	
1016	OBH 42VA z.W.	LT = 2163 m	17 01,47 S 88 25,82 E	
1044	OBH 43z.W.	LT = ??	17 01,42 S 88 28,98 E	
1113	OBH 44z.W.	LT = 2376 m	17 01,40 S 88 31,94 E	
1143	OBH 45z.W.	LT = 2407 m	17 01,39 S 88 34,99 E	
1215	OBH 46z.W.	LT = 2530 m	17 01,40 S 88 37,90 E	
1254	OBH 47z.W.	LT = 2612 m	17 01,40 S 88 42,00 E	
1326	OBH 48z.W.	LT = 4353 m	17 01,37 S 88 44,97 E	
1353	OBH 49z.W.	LT = 4883 m	17 01,38 S 88 47,94 E	
1421	OBH 50z.W.	LT = 4874 m	17 01,39 S 88 51,00 E	
1446	OBH 51z.W.	LT = 4175 m	17 01,37 S 88 54,00 E	
1510	OBH 52z.W.	LT = 5095 m	17 01,41 S 88 57,00 E	
1543	OBH 53z.W.	LT = 5244 m	17 01,40 S 89 00,98 E	
1613	OBH 54z.W.	LT = 4939 m	17 01,41 S 89 05,02 E	
1643	OBH 55z.W.	LT = 5368 m	17 01,38 S 89 08,98 E	
1711	OBH 56z.W.	LT = 5355 m	17 01,39 S 89 12,99 E	
1740	OBH 57z.W.	LT = 5711 m	17 01,39 S 89 16,98 E	
1810	OBH 58z.W.	LT = ??	17 01,40 S 89 21,00 E	
1841	OBH 59z.W.	LT = ??	17 01,39 S 89 25,01 E	
1910	OBH 60z.W.	LT = 5290 m	17 01,40 S 89 29,00 E	
1940	OBH 61z.W.	LT = 4348 m	17 01,39 S 89 33,03 E	
1954	Magnetometer z.W.			
2018	Beginn Profil 105	Magnetik	17 05,0 S 89 35,0 E	
2330	Ende Profil 105		17 05,0 S 90 00.5 E	
2345	Magnetometer vorgehievt			
22.05.1998				
0023	Streamer z.W.			
0033	Bb-Array z.W.			
0046	Stb-Array z.W.			
0047	1. Schuß	LT = 4247 m	17 01,4 S 89 57,4 E	
0057	Beginn Profil 06	LT = 4099 m	17 01,4 S 89 56,3 E	
23.05.1998				
0608	Ende Profil 06		17 01,4 S 87 21,4 E	148 sml

0619	Magnetometer vorgehievt			
0630	Bb-Array a.D.			
0639	Stb-Array a.D.			
0648	Streamer a.D.			
0657	Magnetometer z.W.			
0712	Beginn Profil	106	Magnetik	17 05,0 S 87 19,3 E
1344	Ende Profil	106		17 05,0 S 88 12,0 E
1400	Magnetometer ein			
1550	OBH 40 ausgelöst			
1621	OBH 40a.D.			17 01,5 S 88 19,97 E
1649	OBH 41a.D.			17 01,5 S 88 22,9 E
1724	OBH 42a.D.	Vertikal-array		17 01,6 S 88 25,8 E
1753	OBH 43a.D.			17 01,6 S 88 28,9 E
1819	OBH 44a.D.			17 01,5 S 88 31,9 E
1850	OBH 45a.D.			17 01,5 S 88 34,9 E
1923	OBH 46a.D.			17 01,5 S 88 37,9 E
1958	OBH 47a.D.			17 01,4 S 88 41,9 E
2146	OBH 48a.D.			17 01,5 S 88 44,9 E
2213	OBH 49a.D.			17 01,5 S 88 47,8 E
2317	OBH 50a.D.			17 01,5 S 88 50,9 E
2356	OBH 51a.D.			17 01,5 S 88 54,0 E
24.05.1998				
0044	OBH 52a.D.			17 01,4 S 88 56,9 E
0141	OBH 53a.D .			17 01,5 S 89 01,0 E
0236	OBH 54a.D.			17 01,4 S 89 05,0 E
0323	OBH 55a.D.			17 01,4 S 89 08,9 E
0421	OBH 56a.D.			17 01,4 S 89 13,0 E
0520	OBH 57a.D.			17 01,4 S 89 17,0 E
0603	OBH 58a.D.			17 01,4 S 89 21,0 E
0712	OBH 59a.D.			17 01,2 S 89 25,1 E
0808	OBH 60a.D.			17 01,4 S 89 29,0 E
0857	OBH 61a.D.			17 01,4 S 89 32,9 E

Profile 107 und 108 Magnetik

0903	Magnetometer z.W.		
0910	Beginn Profil	107	17 00,4 S 89 33,0 E
1005	Profilwechsel	107 / 108	16 51,5 S 89 33,0 E
1520	Ende Profil	108	16 51,5 S 88 37,5 E

Auslegung OBH und Vertikal-arrays i.G. „Joides Resolution"

2101	OBH 62z.W.	LT = 1943 m	16 51,38 S 88 20,79 E
2134	OBH 63z.W.	LT = 1807 m	16 54,38 S 88 20,75 E
2227	OBH 64z.W.	LT = 1946 m	16 51,39 S 88 13,50 E
2257	OBH 65z.W.	LT = 1910 m	16 54,39 S 88 12,68 E
2336	OBH 66z.W.	LT = 1917 m	16 51,37 S 88 08,79 E
25.05.1998			
0022	OBH 67z.W.	LT = 1915 m	16 54,39 S 88 03,76 E
0100	OBH 68z.W.	LT = 1928 m	16 51,40 S 88 00,77 E
0159	OBH 69z.W.	LT =	16 58,59 S 88 00,77 E
0231	OBH 70z.W.	LT = 1817 m	16 59,39 S 88 03,77 E
0318	OBH 71z.W.	LT = 1751 m	17 04,29 S 88 03,75 E
0346	OBH 72z.W.	LT = 1879 m	17 05,38 S 88 00,77 E

0422	OBH 73z.W.	LT =	17 09,37 S	88 02,90 E	
0449	OBH 74z.W.	LT =	17 11,39 S	88 00,91 E	
0513	OBH 75z.W.	LT = 1851 m	17 11,39 S	88 03,77 E	
0548	OBH 76z.W.	LT = 1830 m	17 11,39 S	88 08,27 E	
0607	OBH 77z.W.	LT = 1812 m	17 09,41 S	88 08,78 E	
0700	OBH 78z.W.	LT = 1839 m	17 04,41 S	88 13,79 E	
0755	OBH 79z.W.	LT =	17 09,40 S	88 18,78 E	
0824	OBH 80z.W.	LT =	17 11,40 S	88 20,80 E	
0911	OBH 81z.W.	LT = 2096 m	17 04,40 S	88 20,70 E	
1042	OBH 82z.W. VAla	LT = 1831 m	16 59,44 S	88 16,00 E	
1052	OBH 82abgetaucht		16 59,49 S	88 15,66 E	
1141	OBH 83z.W. Vaku	LT = 1657 m	16 59,41 S	88 08,83 E	

Profil 109 Magnetik

1154	Magnetometer z.W.			
1200	Beginn Profil	16 59,4 S	88 06,4 E	
1448	Ende Profil	17 21,8 S	88 06,4 E	22 sml

Profil 07 Seismik / OBH / Magnetik

1526	Streamer z.W.			
1529	Stb-array z.W.			
1537	Beginn Profil	17 19,4 S	88 03,8 E	
2224	Ende Profil	16 46,2 S	88 03,8 E	33 sml
2240	Stb-array a.D.			
2250	streamer a.D.			

Profile 110 - 113 Magnetik

2335	Beginn Profil 110	16 46,4 S	88 07,8 E	
26.05.1998				
0242	Profilwechsel 110 / 111	17 07,5 S	88 07,8 E	
0445	Profilwechsel 111 / 112	17 07,5 S	88 25,8 E	
0538	Profilwechsel 112 / 113	17 14,0 S	88 25,8 E	
0815	Ende Profil 113	17 14,0 S	87 58,4 E	70 sml
0829	Magnetometer vorgehievt			

Profil 08 Seismik / OBH / Magnetik

0839	Streamer z.W.			
0849	Stb-Array z.W.			
0856	Beginn Profil	17 13,6 S	87 58,7 E	
1435	Magnetometer z.W.			
1627	Ende Profil	16 46,5 S	88 25,6 E	37 sml

Profil 09 Seismik / OBH / Magnetik

1740	Beginn Profil	16 51,4 S	88 25,8 E	
1808	Bb-Array z.W.			
1810	1. Schuß	16 51,4 S	88 22,8 E	
1816	Magnetometer z.W.			
2309	Ende Profil	16 51,4 S	87 55,8 E	26 sml

27.05.1998

Profil 10 Seismik / OBH / Magnetik

0000	Beginn Profil	16 54,4 S	87 55,8 E	
0009	1. Schuß			
0552	Ende Profil	10 54,4 S	88 25,8 E	31 sml

FS SONNE Stationsprotokoll SO 131

0602	Magnetometer vorgehievt		
Profil	*11 Seismik / OBH / Magnetik*		
0621	Schiff auf Profilkurs		
0627	Magnetometer z.W.		
0628	Beginn Profil / 1. Schuß	16 55,4 S 88 26,2 E	
1241	Ende Profil	17 07,3 S 87 56,0 E	31 sml
1251	Magnetometer vorgehievt		
Profil	*12 Seismik / OBH / Magnetik*		
1318	Beginn Profil / 1. Schuß	17 09,4 S 87 55,7 E	
1323	Magnetometer z.W.		
1906	Ende Profil	17 09,4 S 88 25,8 E	31 sml
1916	Magnetometer vorgehievt		
Profil	*12 A Seismik / OBH / Magnetik*		
1923	Beginn Profil / 1. Schuß	17 10,3 S 88 26,7 E	
1928	Magnetometer z.W.		
2036	Magnetometer vorgehievt		
2035	Ende Profil 12 A	17 16,3 S 88 26,6 E	06 sml
Profil	*13 Seismik / OBH / Magnetik*		
2051	Beginn Profil 1. Schuß	17 16,4 S 88 25,7 E	
2102	Magnetometer z.W.		
28.05.1998			
0500	Ende Profil	16 46,52 S 87 55,9 E	41 sml
Profil	*13 A Seismik / OBH / Magnetometer*		
0523	Beginn Profil	16 45,2 S 87 55,7 E	
0607	Magnetometer vorgehievt		
0607	Ende Profil	16 45,2 S 87 59,5 E	05 sml
Profil	*14 Seismik / OBH / Magnetik*		
0633	Beginn Profil 1.Schuß	16 46,3 S 88 00,8 S	
0637	Magnetometer z.W.		
1235	Ende Profil	17 16,4 S 88 00,8 E	30 sml
1242	Magnetometer vorgehievt		
Profil	*14 A Seismik / OBH / Magnetik*		
1255	Beginn Profil	17 17,6 S 87 59,9 E	
1258	Magnetometer z.W.		
1427	hieven Magnetomer ein		
1427	Ende Profil	17 12,3 S 87 55,5 E	06 sml
Profil	*15 Seismik / OBH / Magnetik*		
1447	Beginn Profil	17 11,4 S 87 55,5 E	
1451	Magnetometer z.W.		
2050	Ende Profil	17 11,4 S 88 26,0 E	29 sml
2056	Magnetometer vorgehievt		
Profil	*15 A Seismik / OBH / Magnetik*		
2116	Beginn Profil	17 12,8 S 88 26,7 E	
2120	Magnetometer z.W.		
2229	Magnetometer vorgehievt		

2229	Ende Profil		17 17,4 S 88 22,1 E	06 sml
Profil	*16*	*Seismik / OBH / Magnetik*		
2253	Beginn Profil 1. Schuß		17 16,6 S 88 20,8 E	
2257	Magnetometer z.W.			
29.05.1998				
0505	Ende Profil		16 46,4 S 88 20,8 E	30 sml
0515	Magnetometer vorgehievt			
Profil	*17*	*Seismik / OBH / Magnetik*		
0604	Beginn Profil 1. Schuß		16 46,6 S 88 16,8 S	
0608	Magnetometer z.W.			
1204	Ende Profil		17 16,4 S 88 16,8 E	30 sml
1214	Magnetometer ein			
1226	Bb-Array ein			
1234	Stb-Array ein			
1243	Streamer a.D.			
Aufnahme und Auslegung OBH				
1320	OBH 80	ausgelöst		
1341	OBH 80	aufgetaucht		
1347	OBH 80	a.D.	17 11,4 S 88 20,6 E	
1342	OBH 82	z.W. LT = 2145 m	17 11,41 S 88 20,68 E	
1354	OBH 79	ausgelöst		
1424	OBH 79	a.D.	17 09,4 S 88 18,7 E	
1442	OBH 81	ausgelöst		
1516	OBH 81	a.D.	17 04,4 S 88 20,6 E	
1523	OBH 85	z.W. LT = 2095 m	17 04,31 S 88 20,83 E	
1533	OBH 39	ausgelöst		
1605	OBH 39	a.D.	17 01,4 s 88 16,9 E	
1629	OBH 83 VA	ausgelöst		
1709	OBH 83 VA	a.D.		
1731	OBH 86	z.W. LT = 1652 m	17 01,19 S 88 10,78 E	
1741	OBH 87	z.W. LT = 1662 m	17 01,58 S 88 10,78 E	
Profil 18	*Seismik / OBH*	*Kreis mit Radius = 2 sml um Bohrloch „Joides Resolution"*		
1821	Sreamerz.W.			
1828	Stb-Array z.W.			
1845	Beginn Profil 1. Schuß		17 03,4 S 88 11,5 E	
2128	Ende Profil		17 03,4 S 89 10,6 E	12 sml
Profil	*18 A*	*Anschlußprofil zu Profil19*		
2131	Beginn Profil		17 03,3 S 88 10,3 E	
2224	Ende Profil		17 03,3 S 88 05,5 E	05 sml
Profil	*19*	*Seismik / OBH Radius um Bohrloch = 12 sml*		
2240	Beginn Profil		17 02,6 S 88 04,7 E	
30.05.1998				
0605	Ende Profil		17 02,6 S 88 04,7 E	38 sml
Profil	*20*	*Seismik / OBH / Magnetik*		
0653	Bb-Array z.W.			
0701	Magnetometer z.W.			
0656	Beginn Profil 1.Schuß		17 04,3 S 88 04,5 E	

FS SONNE Stationsprotokoll SO 131

0701	Magnetometer z.W.			
1108	Ende Profil	17 04,4 S	88 26,8 E	21 sml
1120	Magnetometer vorgehievt			

Profil 21 Seismik / OBH / Magnetik

1147	Beginn Profil	17 05,7 S	88 25,7 E	
1157	Magnetometer z.W.			
1740	Ende Profil	16 57,2 S	87 55,9 E	30 sml
1749	Magnetometer vorgehievt			

Profil 22 Seismik / OBH / Magnetik

1828	Magnetometer z.W.			
1826	Beginn Profil 1. Schuß	16 59,4 S	87 55,8 E	
2046	Ende Profil	16 59,4 S	88 08,0 E	13 sml

Profil 23 Seismik / OBH / Magnetik

2104	Beginn Profil 1. Schuß	17 00,3 S	88 08,8 E	
31.05.1998				
0318	Ende Profil	17 31,4 S	88 08,8 E	31 sml
0325	Magnetometer vorgehievt			

Profil 24 Seismik / OBH / Magnetik

0359	Magnetometer z.W.			
0401	Beginn Profil	17 31,4 S	88 07,0 E	
1555	Ende Profil	16 32,0 S	88 14,7 E	60 sml

Profil 25 Seismik / OBH / Magnetik

1602	Beginn Profil	16 31,5 S	88 15,5 E	
1858	Ende Profil	16 31,6 S	88 30,5 E	15 sml

Profil 26 Seismik / OBH / Magnetik

1909	Beginn Profil 1. Schuß	16 32,6 S	88 30,8 E	
01.06.1998				
0643	Ende Profil	17 30,7 S	88 30,8 E	60 sml

Profil 27 Seismik / OBH / Magnetik

0652	Beginn Profil 1. Schuß	17 31,4 S	88 30,2 E	
0840	Ende Profil	17 31,2 S	88 21,2 E	09 sml

Profil 28 Seismik / OBH / Magnetik

0846	Beginn Profil	17 30,0 S	88 20,9 E	
1442	Magnetometer a.D.			
1444	Ende Profil	17 01,0 S	88 20,8 E	
1456	Bb-Array a.D.			
1507	Stb-Array a.D.			
1507	Streamer a.D.			

Aufnahme OBH / OBS und Vertikalarrays

1510	OBH 82VA lang ausgelöst
1535	Verankerung taucht nicht auf
1543	OBH 86ausgelöst
1610	OBH 87ausgelöst

1629	OBH 86a.D.	17 01,2 S	88 10,6 E
1638	OBH 87a.D.	17 01,6 S	88 10,6 E
1700	OBH 82VA lang nochmals eingemessen		
1716	OBH 38ausgelöst		
1746	OBH 38a.D.	17 01,4 S	88 13,8 E
1758	OBH 78ausgelöst		
1828	OBH 78a.D.	17 04,4 S	88 13,7 E
1903	OBH 85ausgelöst		
1939	OBH 85a.D.	17 04,3 S	88 20,6 E
2000	OBH 84ausgelöst		
2039	OBH 84a.D.	17 11,4 S	88 20,5 E
2130	OBH 77ausgelöst		
2154	OBH 76ausgelöst		
2201	OBH 77a.D.	17 09,4 S	88 08,8 E
2227	OBH 76a.D.	17 11,3 S	88 08,2 E
2236	OBH 75ausgelöst		
2305	OBH 74ausgelöst		
2307	OBH 75a.D.	17 11,3 S	88 03,7 E
2335	OBH 73ausgelöst		
2337	OBH 74a.D.	17 11,4 S	88 00,8 E
02.06.1998			
0009	OBH 73a.D.	17 09,3 S	88 02,8 E
0024	OBH 72ausgelöst		
0055	OBH 72a.D.	17 05,4 S	88 00,8 E
0103	OBH 71ausgelöst		
0133	OBH 71a.D.	17 04,3 S	88 03,7 E
0150	OBH 70ausgelöst		
0218	OBH 70a.D.	16 59,4 S	88 03,6 E
0227	OBH 69ausgelöst		
0254	OBH 69a.D.	16 58,6 S	88 00,7 E
0311	OBH 67ausgelöst		
0345	OBH 67a.D.	16 54,4 S	88 03,6 E
0354	OBH 68ausgelöst		
0502	OBH 68a.D.	16 51,4 S	88 00,5 E
0544	OBH 66ausgelöst		
0642	OBH 66a.D.	16 51,4 S	88 08,7 E
0645	OBH 65ausgelöst		
0750	OBH 65a.D.	16 54,4 S	88 12,5 E
0755	OBH 64ausgelöst		
0843	OBH 64a.D.	16 51,4 S	88 13,3 E
0907	OBH 62ausgelöst		
0933	OBH 63ausgelöst		
0938	OBH 62a.D.	16 51,4 S	88 20,7 E
1002	OBH 63a.D.	16 54,4 S	88 20,6 E

Bergung OBH 83 mit Vertikal-Array 1200 m W 6

Vermutete Position des VA	LT = 1822 m	16 59,49 S	88 15,66 E
1052	Suchdraggen z.W.		
1124	SL = 1819 m	16 59,25 S	88 16,13 E
	dampfen mit 1,5 kn und Fiergeschw. 1,1 m/sec im Radius von 700 m um die VA-Position		
1250	Simax = 6500 m Beginn hieven		
1430	SL = 70 m VA an der Oberfläche		
1527	Kopfboje abgerissen		

1548	Verankerung komplett bis auf Kopfboje a.B.			
1603	Kopfboje a.D. / Ende Station			
Profil	*114*	*Magnetik*		
1622	Magnetometer z.W.			
1627	Beginn Profil		16 58,0 S 88 16,0 E	
1911	Ende Profil		16 58,0 S 88 43,9 E	13 sml
Profil	*115*	*Magnetik*		
1921	Beginn Profil		16 59,0 S 88 45,0 E	
2027	Ende Profil		17 10,7 S 88 45,0 E	13 sml
Profil 116		Magnetik		
2034	Beginn Profil		17 11,4 S 88 44,2 E	
2215	Ende Profil		17 11,4 S 88 25,6 E	22 sml
Profil	*29*	*Seismik / OBH / Magnetik*		
2236	Streamer z.W.			
2248	Bb-Array z.W.			
2257	Beginn Profil		17 11,4 S 88 21,8 E	
03.06.1998				
0404	Ende Profil		17 11,4 S 87 55,0 E	
0432	Bb-Array und Streamer a.D.			
Profile	*117 / 118 / 119*	*Magnetik*		
0508	Beginn Profil 117		17 11,4 S 87 55,0 E	
0544	Profilwechsel 117 / 118		17 18,0 S 87 55,0 E	
0731	Profilwechsel 118 / 119		17 17,9 S 88 13,8 E	
0846	Ende Profil 119		17 04,0 S 88 14,0 E	
0857	Magnetometert a.D.			
Profil	*30*	*Seismik / OBH / OBS / imlodierende Glaskugeln*		
0922	OBH 89 z.W.	LT = 1814 m	17 04,44 S 88 12,22 E	
0936	OBH 91 z.W.	LT = 1817 m	17 04,44 S 88 12,42 E	
0950	OBH 92 z.W.	LT = 1829 m	17 04,30 S 88 13,01 E	
1008	OBH 90 z.W.	LT = 1829 m	17 04,10 S 88 13,02 E	
1025	Beginn Auslegung OBH 93			
1106	Kopfboje z.W.	LT = 1837 m	17 04,44 S 88 13,56 E	
1121	OBH 88 z.W.	LT = 1840 m	17 04,42 S 88 13,83 E	
1147	1. Glaskugel z.W.		17 04,38 S 88 12,62 E	
1205	2. GK z.W.		17 04,44 S 88 12,82 E	
1213	3. GK z.W.		17 04,44 S 88 13,02 E	
1220	4. GK z.W.		17 04,44 S 88 13,22 E	
1237	5. GK z.W.		17 04,44 S 88 13,33 E	
1257	Streamer z.W.			
1312	Stb-Array z.W.			
1412	Beginn Profil 30		17 04,44 S 88 14,6 E	
1453	Ende Profil 30		17 04,44 S 88 10,62 E	
1508	Stb-Array a.D.			
1517	Streamer a.D.			
1555	OBH 93 angepickt			
1600	OBH 88 ausgelöst			
1635	OBH 90 ausgelöst			
1637	OBH 93 a.D.		17 04,3 S 88 13,4 E	
1647	OBH 88 a.D.		17 04,4 S 88 13,7 E	

1707	OBH 90	a.D.	17 04,1 S 88 12,8 E	
1712	OBH 92	ausgelöst		
1744	OBH 92	a.D.	17 04,3 S 88 12,9 E	
1742	OBH 91	ausgelöst		
1757	OBH 89	ausgelöst		
1803	OBH 91	a.D.	17 04,4 S 88 12,3 E	
1821	OBH 89	a.D.	17 04,4 S 88 12,2 E	

Profile	*120 / 121 / 122 /*		*Magnetik*	
1830	Beginn Profil		17 04,4 S 88 12,1 E	
1836	Magnetometer	z.W.		
1936	Profilwechsel	120 / 121	16 55,0 S 88 18,0 E	
2209	Profilwechsel	121 / 122	16 55,0 S 88 44,9 E	
2400	Ende Profil	122	16 35,2 S 88 45,0 E	57 sml

04.06.1998

Profile	*123 / 124 / 125 / 126*		*Magnetik*	
0017	Beginn Profil	123	16 35,0 S 88 42,0 E	
0436	Ende Profil	123	17 20,0 S 88 42,0 E	45 sml
0517	Beginn Profil	124	17 20,0 S 88 49,5 E	
0926	Ende Profil	124	16 35,7 S 88 49,5 E	45 sml
0958	Beginn Profil	125	16 35,4 S 88 54,1 E	
1149	Profilwechsel	125 / 126	16 54,7 S 88 54,2 E	
1555	Ende Profil	126	16 55,0 S 89 37,0 E	
1628	Magnetometer ein			

Auslegung von OBH und OBS

1648	OBH 094	z.W.		LT = 5029 m	17 01,39 S 89 36,99 E
1717	OBH 095	z.W.		LT = 4982 m	17 01,38 S 89 41,00 E
1747	OBH 096	z.W.		LT = 4925 m	17 01,38 S 89 44,99 E
1818	OBH 097	z.W.		LT = 4724 m	17 01,38 S 89 49,00 E
1851	OBH 098	z.W.		LT = 3632 m	17 01,39 S 89 53,00 E
1919	OBH 099	z.W.		LT = 4310 m	17 01,38 S 89 57,02 E
1946	OBH 100	z.W.		LT = 4679 m	17 01,40 S 90 01,00 E
2015	OBH 101	z.W.		LT = 4754 m	17 01,36 S 90 04,98 E
2047	OBH 102	z.W.	OBS	LT = 5308 m	17 01,38 S 90 08,98 E
2117	OBH 103	z.W.		LT = 5101 m	17 01,39 S 90 13,03 E
2155	OBH 104	z.W.		LT = 5398 m	17 01,38 S 90 17,69 E
2222	OBH 105	z.W.		LT = 5728 m	17 01,41 S 90 21,01 E
2253	OBH 106	z.W.		LT = 5388 m	17 01,38 S 90 25,00 E
2324	OBH 107	z.W.		LT = 5226 m	17 01,38 S 90 28,99 E
2355	OBH 108	z.W.		LT = 5234 m	17 01,38 S 90 33,00 E

05.06.1998

Profil	*127*	*Magnetik*		
0004	Magnetometer	z.W.		
0020	Beginn Profil		16 57,7 S 90 33,5 E	
0348	Ende Profil		16 57,4 S 91 10,0 E	35 sml

Profil	*31*	*Seismik / OBH / Magnetik*
0423	Streamer	z.W.
0437	Bb-Array	z.W.

0447	Stb-Array z.W.		
0449	Beginn Profil	17 01,4 S 91 06,4 E	
06.06.1998			
1435	Ende Profil	17 01,4 S 88 10,0 E	173 sml
1441	Magnetometer vorgehievt		
1452	Stb-Array a.D.		

Profil 31 Seismik / OBH / Magnetik

1515	Beginn Profil	17 00,2 S 88 09,4 E	
1520	Magnetometer z.W.		
1707	Ende Profil	17 00,5 S 88 18,0 E	08 sml
1722	Bb-Array a.D.		

Profil 128 Magnetik

1746	Beginn Profil	16 57,4 S 88 22,0 E	
07.06.1998			
0534	Ende Profil	16 57,4 S 90 33,0 E	
600	Magnetometer ein		

Aufnahme von 14 OBH und 1 OBS

0517	OBH 108 ausgelöst		
0620	OBH 107 ausgelöst		
0632	OBH 108 a.D.	17 01,3 S 90 33,0 E	
0657	OBH 106 ausgelöst		
0730	OBH 107 a.D.	17 01,3 S 90 29,0 E	
0744	OBH 105 ausgelöst		
0805	OBH 106 a.D.	17 01,3 S 90 25,0 E	
0814	OBH 104 ausgelöst		
0843	OBH 103 ausgelöst		
0859	OBH 105 a.D.	17 01,4 S 90 21,00 E	
0928	OBH 102 OBS ausgelöst		
0951	OBH 104 a.D.	17 01,3 S 90 17,6 E	
1025	OBH 103 a.D.	17 01,4 S 90 13,1 E	
1048	OBH 101 ausgelöst		
1235	OBH 102 a.D.	17 01,1 S 90 08,9 E	
1250	OBH 100 ausgelsöt		
1311	OBH 101 a.D.	17 00,4 S 90 04,3 E	
1317	OBH 099 ausgelsöt		
1353	OBH 100 a.D.	17 01,2 S 90 00,9 E	
1410	OBH 098 ausgelöst		
1443	OBH 099 a.D.	17 01,3 S 89 56,8 E	
1455	OBH 097 ausgelsöt		
1512	OBH 098 a.D.	17 01,4 S 89 52,7 E	
1530	OBH 096 ausgelöst		
1559	OBH 097 a.D.	17 01,5 S 89 49,0 E	
1611	OBH 095 ausgelöst		
1630	OBH 096 a.D.	17 01,4 S 89 45,0 E	
1625	OBH 094 ausgelöst		
1801	OBH 095 a.D.	17 01,4 S 89 421,0 E	
1830	OBH 095 a.D.	17 01,0 S 89 36,5 E	

Magnetikprofile 129 – 134

1840	Beginn Profil	129	17 00,6 S 89 36,4 E	
1844	Magnetometer	z.W.		
1912	Profilwechsel	129 / 130	16 55,0 S 89 37,0 E	
2021	Profilwechsel	130 / 131	16 55,0 S 89 49,0 E	
08.06.1998				
0202	Ende Profil	131	15 55,0 S 89 49,0 E	78 sml
0232	Beginn Profil	132	15 55,0 S 89 53,0 E	
0839	Ende Profil	132	16 55,0 S 89 53,0 E	60 sml
0905	Beginn Profil	133	16 55,0 S 89 57,0 E	
1439	Ende Profil	133	15 55,0 S 89 57,0 E	60 sml
1509	Beginn Profil	134	15 55,0 S 90 02,0 E	
2100	Ende Profil	134	16 55,0 S 90 02,0 E	60 sml
2120	Magnetometer an Bord			

12.06.1998

Testprofil GEOMAR

0908	Streamer	z.W.
0914	Bb-Array	z.W.
1037	Bb-Array	a.D.
1043	Streamer	a.D.

CTD 2 W 5

1345	Beginn Station		LT = 6219 m	07 44 S 103 14 E
1352	CTD z.W.			
1551	Slmax = 5522 m			
2035	CDT a.D.	/	Ende Station	

Insgesamt vermessen	3800	km	Magnetik / Hydrosweep / Parasound
Davon	2527	km	Seismik / HS / PS / Magnetik
Mit	21688		Schüssen
Mit	108	mal	OBH-Einsätzen